OFFSHORE HYDROMECHANICS

First Edition

J.M.J. Journée and W.W. Massie

Delft University of Technology

January 2001

Contents

PREFACE

This text book is an attempt to provide a comprehensive treatment of hydromechanics for offshore engineers. This text has originally been written for students participating in the Interfaculty Offshore Technology curriculum at the Delft University of Technology. Offshore Hydromechanics forms the link in this curriculum between earlier courses on Oceanography and (regular as well as irregular) Ocean Waves on the one hand, and the design of Fixed, Floating and Subsea Structures on the other.

Topics have been selected for inclusion based upon their applicability in modern offshore engineering practice. The treatment of these selected topics includes both the background theory and its applications to realistic problems.

The book encompasses applied hydrodynamics for the seas outside the breaker zone. Popularly, one can say that this book uses information on wind, waves and currents to determine external forces on all sorts of structures in the sea as well as the stability and motions of floating structures and even of the sea bed itself. Only a short period of reflection is needed to conclude that this covers a lot of ocean and quite some topics as well! Indeed the following application examples illustrate this.

The notation used in this book is kept as standard as possible, but is explained as it is introduced in each chapter. In some cases the authors have chosen to use notation commonly found in the relevant literature - even if it is in conflict with a more universal standard or even with other parts of this text. This is done to prepare students better to read the literature if they wish to pursue such maters more deeply. In some other cases, the more or less standard notation and conventions have been adhered to in spite of more common practice. An example of this latter disparity can be found in chapter 14; conventions and notation used there do not always agree with those of the coastal engineers.

One will discover that many equations are used in the explanation of the theories presented in this book. In order to make reader reference easier, important theoretical results and equations have been enclosed in boxes. A few appendices have been used to collect relevant reference information which can be useful for reference or in more than one chapter.

Modular Structure of the Book

An Offshore Hydromechanics course based upon this text can be built up from four related modules. Each module has its own content and objectives; each module represents approximately the same amount of (student) work. Within certain limitations, readers can choose to work only with one or more from these modules relevant to their own needs:

1. Hydrostatics, Constant Flow Phenomena and Surface Waves.
   Upon completion of this segment students will understand hydrostatics as it relates to all forms of structures. Compressive buckling of free-hanging drill strings is explained Constant potential as well as real flows and the forces which they can exert on structures complete this module along with a review of wave theory and wave statistics.

---

[0] J.M.J. Journée and W.W. Massie, *"OFFSHORE HYDROMECHANICS"*, First Edition, January 2001, Delft University of Technology. For updates see web site: http://www.shipmotions.nl.

Module 1 covers chapter 1, a small part of chapter 2 and chapters 3, 4 and 5. It provides basic knowledge for all the succeeding modules; every course should include this module. Module 1 can be succeeded by modules 2 and/or 4.

2. Static Floating Stability, Principles of Loads and Motions and Potential Theories.
   Upon completion of this segment students will become experienced with stability computations for all sorts of floating structures - including those with partially filled water ballast tanks, etc. They will understand the basic application of linear potential theory to ships and other floating structures for the computation of external and internal forces, as well as the principle of motions of bodies in waves.
   Module 2 covers chapters 2, 6, and 7. It should be scheduled directly after module 1 and prepares the student for the further development of this topic in module 3.

3. Loads and Motions in Waves, Nonlinear Hydrodynamics, Station Keeping and Operability.
   Students completing this segment will be able to predict the behavior of floating or sailing bodies more completely. They will be familiar with first order ship motions in waves, as well as nonlinear phenomena such as mean and second order drift forces. Applications such as station keeping and the determination of offshore workability will be familiar.
   Module 3 covers the chapters 8, 9, 10 and 11. It should follow module 2 in the scheduling.

4. Slender Cylinder Hydrodynamics and Sea Bed Morphology.
   Students completing this segment will be familiar with the Morison equation and its extensions as well as with methods to determine its coefficients and approximate methods for predicting the survival loads on an offshore tower structure. The computation of forces on pipelines as well as the morphological interaction between the sea bed and pipelines and other small objects will be familiar too.
   Module 4 covers chapters 12, 13 and 14. It can be scheduled directly after module 1 and parallel with modules 2 and 3, if desired.

These modules are listed below and shown in the figure 0.1 as well.
Each of the following module combinations can be appropriate for specific groups of students; each path can be completed via a contiguous series of classes if desired.

Modules	Objective	Suited for
1,2,3,4	Complete Course	Offshore Technology and any others optionally
1,2,3	Complete Ship Motions	Marine Technology Dredging Technology
1,2	Limited Ship Motions	Dredging Technology, Civil and Mechanical Engineering
1,4	Slender Structure Loads	Civil and Mechanical Engineering

The overall objective of this text is to use theory where necessary to solve practical offshore engineering problems. Some sections which become rather mathematical contain a warning

1. INTRODUCTION
Hydrostatics
Constant potential and real flows; forces
Wave mechanics and wave statistics

2. SHIP MOTIONS I
Floating stability
Potential Theory for
   ship hydromechanics
Fundamentals of ship motions

**4. SLENDER BODIES AND
SEA BED MORPHOLOGY**
Morison equation and forces
   on slender structures
Survival loads on tower structures
Forces on pipelines

3. SHIP MOTIONS II
Ship motion applications
Higher order forces
Station keeping
Offshore operability

Figure 0.1: Offshore Hydromechanics Study Paths

such as "The result of this section is more important that the road leading to it". Even in such sections, however, the theory is summarized so that students can use and apply it for other purposes without excessive difficulty.

Separate exercise materials are used in several of the TU Delft classes. Much of this is available in a companion publication: *Exercises on Offshore Hydromechanics*. This includes various problems - including many old examination questions - along with solutions to many of the problems posed in the publication *Solutions of Exercises on Offshore Hydromechanics*. Both publications can be obtained from the Internet as freely downloadable files at web site http://dutw189.wbmt.tudelft.nl/~johan.

References to Other Books

References are listed by first author and year date in the text. More complete bibliographic data is included in an appendix. A few books and other materials provide such generally used information or insight that they are not repeatedly listed always in the various chapters. Instead, this section lists them with a short description of each.

Many are (or were when published) what could be considered classic works:

- J. Gerritsma, retired Professor of Maritime Technology at the Delft University of Technology, wrote Lecture Notes on *Waves, Shipmotions and Manoeuvring I* (in Dutch), Report 563-K, 1989, Ship Hydromechanics Laboratory, Maritime Technology Department, Delft University of Technology, Delft, The Netherlands. In particular, the sections on waves give just that information (and not more) that is of real importance here.

- G. Kuiper, Professor of Maritime Technology at the Delft University of Technology, wrote Lecture Notes on *Resistance and Propulsion of Ships*, Report 847-K, 1997, Ship Hydromechanics Laboratory, Maritime Technology Department, Delft University of Technology, Delft, The Netherlands.

- A.R.J.M. Lloyd published in 1989 his book on ship hydromechanics, *Seakeeping, Ship Behaviour in Rough Weather*, ISBN 0-7458-0230-3, Ellis Horwood Limited, Market Cross House, Cooper Street, Chichester, West Sussex, P019 1EB England.

- O.M. Faltinsen, Professor of Marine Technology at the Norwegian University of Science and Technology is the author of *Sea Loads on Ships and Offshore Structures,* published in 1990 in the Cambridge University Press Series on Ocean Technology.

- J.N. Newman, Professor of Marine Engineering at Massachusetts Institute of Technology, authored *Marine Hydrodynamics* in 1977. It was published by the MIT Press, Cambridge, Massachusetts, USA. It is standard work, especially in the area of ship hydromechanics.

- B. Kinsman wrote *Wind Waves - Their Generation and Propagation on the Ocean Surface* while he was Professor of Oceanography at The Johns Hopkins University in Baltimore, Maryland. The book, published in 1963 was complete for its time; the wit scattered throughout its contents makes is more readable than one might think at first glance.

- T. Sarpkaya and M. St. Dennis Isaacson are the authors of *Mechanics of Wave Forces on Offshore Structures* published in 1981 by Van Nostrand Reinhold Company. Sarpkaya, Professor at the U.S. Naval Postgraduate School in Monterey, California has been a leader in the experimental study of the hydrodynamics of slender cylinders for a generation.

- *Hydromechanics in Ship Design* was conceived by a retired United States Navy Captain, Harold E. Saunders with the assistance of a committee of the Society of Naval Architects and Marine Engineers. His work appeared in three volumes: Volume I was published in 1956; volume II followed in 1957, and volume III did not appear until 1965 - after Captain Saunders death in 1961. This set of books - especially volumes I and II - is a classic in that it was written before computers became popular. His explanations of topics such as potential theory seem therefore less abstract for many readers.

- *Fluid Mechanics - An Interactive Text* is a new publication at the most modern end of the publishing spectrum; it is a CD-ROM that can only be read with the aid of a computer! This work - covering much of basic fluid mechanics - was published in 1998 by the American Society of Civil Engineers. It includes a number of animations, and moving picture clips that enhance the visual understanding of the material presented.

Acknowledgments

Although more restricted Lecture Notes by the authors on Offshore Hydromechanics already existed, this book was little more than an idea in the minds of the authors until the spring of 1997. It goes without saying that many have contributed the past three years in a less direct way to what is now this text:

- The books given in the previous reference list were a very useful guide for writing lecture notes on Offshore Hydromechanics for students in the "Delft-Situation".

- Tristan Koempgen - a student from Ecole Nationale Superieure de Mechanique et d'Aeortechnique, ENSMA in Portiers, France - worked on first drafts of what has become parts of several chapters.

- Prof.dr.ir. G. Kuiper provided segments of his own Lecture Notes on "Resistance and Propulsion of Ships" for use in this text in Chapter 4.

- Lecture Notes by prof.ir. J. Gerritsma on waves and on the (linear) behavior of ships in waves have been gratefully used in Chapters 5 and 6.

- Many reports and publications by prof.dr.ir. J.A. Pinkster on the 3-D approach to the linear and nonlinear behavior of floating structures in waves have been gratefully used in Chapter 9 of this text.

- Drafts of parts of various chapters have been used in the classroom during the past three academic years. Many of the students then involved responded with comments about what was (or was not) clear to them, the persons for whom all this effort is primarily intended.

- In particular, Michiel van Tongeren - a student-assistant from the Maritime Technology Department of the Delft University of Technology - did very valuable work by giving his view and detailed comments on these lecture notes from a "student-point-of-view".

Last but not least, the authors are very thankful for the patience shown by their superiors at the university, as well as their families at home. They could not have delivered the extra but very intellectually rewarding effort without this (moral) support.

Authors

The author team brings together expertise from a wide variety of fields, including Naval Architecture as well as Civil and Mechanical Engineering. They have tried to demonstrate here that a team can know more. More specifically, the following two Delft University of Technology faculty members have taken primarily responsibility for producing this book:

- **Ir. J.M.J. Journée**, Associate Professor,
  Ship Hydromechanics Laboratory, Maritime Technology Department,
  Delft University of Technology, Mekelweg 2, 2628 CD Delft, The Netherlands.
  Tel: +31 15 278 3881
  E-mail: J.M.J.Journee@wbmt.tudelft.nl
  Internet: http://www.shipmotions.nl

- **W.W. Massie, MSc, P.E.**, Associate Professor,
  Offshore Technology, Civil Engineering Faculty,
  Delft University of Technology, Stevinweg 1, 2628 CN Delft, The Netherlands.
  Tel: +31 15 278 4614
  E-mail: Massie@offshore.tudelft.nl

Feel free to contact them with positive as well as negative comments on this text.

Both authors are fortunate to have been educated before the digital computer revolution. Indeed, FORTRAN was developed only after they were in college. While they have both used computers extensively in their career, they have not become slaves to methods which rely exclusively on 'black box' computer programs.

The authors are aware that this first edition of Offshore Hydromechanics is still not complete in all details. Some references to materials, adapted from the work of others may still be missing, and an occasional additional figure can improve the presentation as well. In some ways a book such as this has much in common with software: It never works perfectly the first time it is run!

Chapter 1

INTRODUCTION

The development of this text book has been driven by the needs of engineers working in the sea. This subsection lists a number of questions which can result from very practical general offshore engineering situations. It is the intention that the reader will become equipped with the knowledge needed to attack these problems during his or her study of this book; problems such as:

- How do I determine the design (hydrodynamic) loads on a fixed offshore tower structure?

- Can a specified object be safely loaded and carried by a heavy lift float-on float-off vessel?

- What is the opimum speed of a given supply boat under the given sea conditions?

- How should a semi-submersible platform be ballasted to survive an extreme storm?

- Under what conditions must a floating drilling rig stop work as a result too much motion?

- How important is the heading of a drilling ship for its behavior in waves?

- What dynamic positioning power is needed to keep a given drilling ship on station under a given storm condition?

- How will the productivity of a marine suction dredge decline as the sea becomes rougher?

- What sea conditions make it irresponsible to tranfer cargo from a supply boat to a fixed or another floating platform?

- How does one compute the wave and current forces on a large truss-type tower structure in the sea?

- How can the maximum wave and current loads on a truss-type tower structure be estimated efficiently?

- What sea bed changes can be expected near a pipeline or small subsea structure?

In contrast to some other books, this one attempts to prevent a gap from occurring between material covered here and material which would logically be presented in following texts. For example, after the forces and motions of a ship have been determined in chapter 8, the treatment continues to determine the internal loads within the ship. This forms a good link to ship structures which will then work this out even further to yield local stresses, etc.

1.1   Definition of Motions
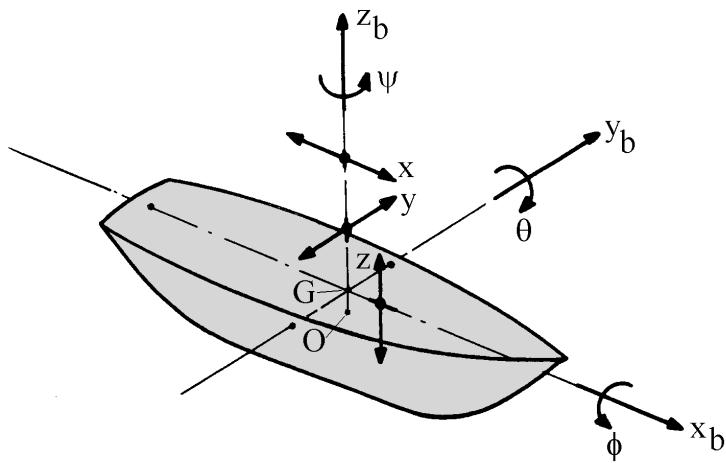
Figure 1.1: Definition of Ship Motions in Six Degrees of Freedom

The six ship motions in the steadily translating system are defined by:

- three translations of the ship's center of gravity (**CoG** or G) in the direction of the x-, y- and z-axes:

  - surge in the longitudinal x-direction, positive forwards,
  - sway in the lateral y-direction, positive to port side, and
  - heave in the vertical z-direction, positive upwards.

- three rotations about these axes:

  - roll about the x-axis, positive right turning,
  - pitch about the y-axis, positive right turning, and
  - yaw about the z-axis, positive right turning.

These definitions have been visualised in figure 1.1.

Any ship motion is build up from these basic motions. For instance, the vertical motion of a bridge wing is mainly build up by heave, pitch and roll motions.

Another important motion is the vertical relative motion, defined as the vertical wave elevation minus the local vertical motion of the ship. This is the motion that one observe when looking over thee rail downwards to the waves.

1.2 Problems of Interest

This section gives a brief overview of fixed and mobile offshore units, such as dredgers, pipe laying vessels, drilling vessels, oil production, storage and off-loading units and several types of support and transportation vessels. Their aspects of importance or interest with respect to the hydromechanical demands are discussed. For a more detailed description of offshore structure problems reference is given to a particular Lecture on Ocean Engineering by [Wichers, 1992]. Some relevant knowledge of that lecture has been used in this section too.

1.2.1 Suction Dredgers

Dredging is displacement of soil, carried out under water. The earliest known dredging activities by floating equipment took place in the 14th century in the harbor of the Dutch Hanze city of Kampen. A bucket-type dredging barge was used there to remove the increasing sand deposits of the rivers Rhine and IJssel.

Generally, this work is carried out nowadays by cutter suction dredgers or trailing suction hopper dredgers. The cutter suction dredger is moored by means of a spud pile or mooring lines at the stern and by the ladder swing wires at the bow. These dredgers are often used to dredge trenches for pipe lines and approach channels to harbors and terminals in hard soil. The trailing suction hopper dredger is dynamically positioned; the dredger uses its propulsion equipment to proceed over the track.

The environmental sea and weather conditions determine:

- the available working time in view of:
  - the necessity to keep the digging tools in contact with the bottom, such as dippers, grabs, cutters, suction pipes and trail heads,
  - the anchorage problems in bad weather, such as breaking adrift from anchors and bending or breaking of spud piles,
  - the stability of the discharge equipment, such as floating pipelines and conveyor belts,
  - the mooring and stability of barges alongside in the event of currents and/or high wind velocities and waves and
  - the overloading of structural elements associated with dredging such as bucket-ladders or cutter arms,

- maneuverability, especially at strong side winds and strong currents entering at a specific angle, which is important for the dredging slopes,

- problems on slamming of bottom doors of sea-going hopper barges and on jumping suction pipes of hopper suction dredgers and

- hopper overflow losses due to excessive rolling of the vessel.

Cutter suction dredgers are moored by means of a spud pile or radially spread steel wires. An important feature of spud pile mooring (see figure 1.2) is the relative high stiffness, compared to other mooring systems. One of the reasons for this high stiffness is the required accurate positioning of the cutter head in the breach. This is necessary for a good dredging efficiency. Another reason is to avoid to high loads on the cutter head and on the ladder. Since the spud pile can only take a limited load, the workability limit in waves is at significant wave heights between 0.5 and 1.0 m depending on the size of the dredger, the wave direction and the water depth.
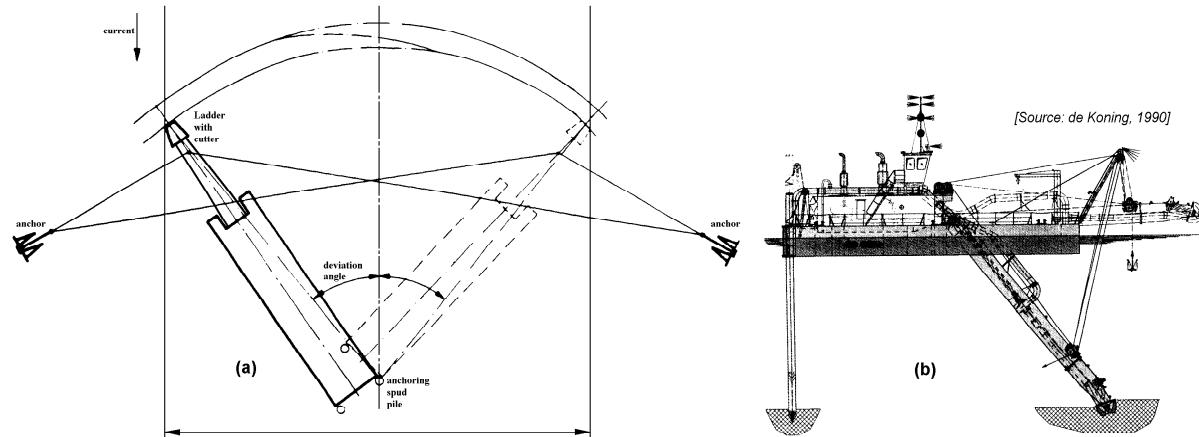
Figure 1.2: Cutter Suction Dredger with Fixed Spud Piles

Cutter suction dredgers may also be equipped with a softer mooring system. In this case the spud pile is replaced by three radially spread steel wires attached to the spud keeper. This so-called 'Christmas tree' mooring results in lower loads but larger wave induced motions of the dredger. Thus, larger workability has to be traded off against lower cutting efficiency. Other components of the dredging equipment - such as the floating pipe line to transport the slurry, its connection to the dredger and the loads in the ladder - may also be limiting factors to the workability of the dredger in waves.

Aspects of importance or interest of cutter suction dredgers are:
  - a realistic mathematical modelling of the soil characteristics for simulations,
  - the loads in the spud pile, the cutter head and the ladder hoist wires,
  - the motions of the dredger and the cutter head in the breach and
  - the loads in the swing wires.

Trailing suction hopper dredgers are used for maintenance work (removal of deposits in approach channels) and dredging of trenches or approach channels in softer soils. It is a ship-shape vessel with hopper type cargo holds to store the slurry. At each side of the ship is a suction arm, which consists of a lower and a higher part, connected through cardanic joints. The connection to the ship is through upper joints and stringers. On modern suction dredgers, the support wire connected to the lower part of the suction pipe near the suction head is provided with a constant tension device for compensation of heave motions. Figure 1.3 shows an example of the increased size of these vessels between 1962 and 1997. This type of dredgers sail along a track during the dredging operation. For manoeuvering, the main propeller(s), the rudder(s) and a combination with bow and/or stern thrusters are used. For that purpose the helmsman manually controls the vessel by using a monitor
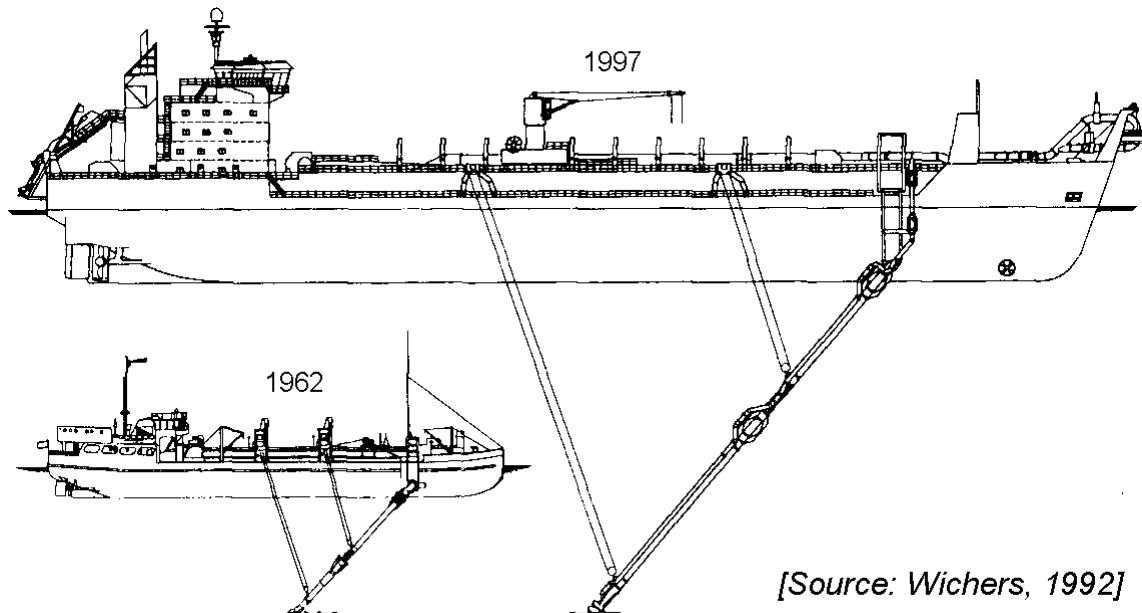
Figure 1.3: Trailing Cutter Suction Hoppers

showing the actual position of the master drag head and the desired track. Operating in near-shore areas, the vessel will be exposed to waves, wind and current and manual control of the vessel may be difficult. An option is an automatic tracking by means of DP systems. Aspects of importance or interest of trailing suction hopper dredgers are:
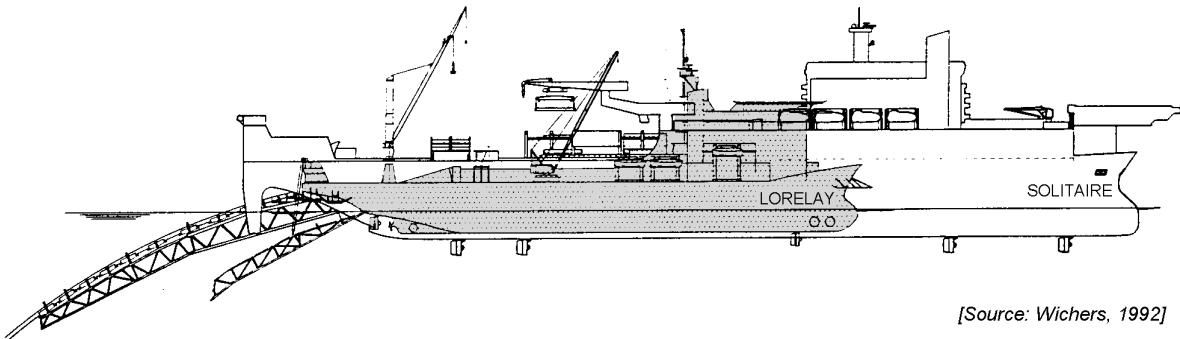
- the motions of the vessel in waves,
- the current forces and the wave drift forces on the vessel,
- the low speed tracking capability,
- the motions of the suction arms,
- the loads in the suction arm connections to the vessel,
- the effect and interactions of the thrusters and
- the avoidance of backward movements of the suction head at the sea bed.

1.2.2 Pipe Laying Vessels

One of the problems of laying pipes on the sea bed lies in the limited capacity of the pipe to accept bending stresses. As a result, it is necessary to keep a pipe line under considerable axial tension during the laying operation otherwise the weight of the span of the pipe between the vessel and the point of contact of the pipe on the sea bed will cause the pipe to buckle and collapse. The tension in the pipe line is maintained using the anchor lines of the pipe laying vessel. The tension is transferred to the pipe by means of the pipe line tensioner located near the point where the pipe line leaves the vessel. The pipe tensioner is designed to grip the pipe without damaging the pipe coating (concrete) and ease the pipe aft while retaining pipe tension as the vessel is hauled forward by the anchor winches. Forward of the tensioner, additional sections of the pipe line are welded to the already existing part. Aft of the tensioner, part of the free span of the pipe line is supported by a so-called stinger.

Pipe laying vessels can consist of semi-submersibles or ship-shaped hulls. Semi-submersibles have the advantage of better motion characteristics in waves which is beneficial for the pipe laying operation. On the other hand, ship-shaped vessels have a higher variable load capacity and a much higher transit speed.

Pipe laying vessels are usually moored by means of anchor systems which are continually being relocated as the laying operation progresses. A new development is a pipe laying vessels kept in position and deriving the pipe line tension by using a dynamic positioning (DP) system instead of anchor lines; for instance pipe laying vessel 'Solitaire', operated since 1998 by Allseas Marine Contractors. Figure 1.4 shows a comparison of this vessel with the much smaller 'Lorelay' of this company, operated since 1986. The considerable increase of size is obvious here.

[Source: Wichers, 1992]

Figure 1.4: Pipe Laying Vessels 'Lorelay' (1986) and 'Solitaire' (1998)

With respect to the combined effect of vessel and pipe motions and the dynamic positioning performance, analyses have to be carried out to find the sea state that can be regarded as the maximum operational condition. In order to determine the most critical wave direction, these analyses have to be run for a number of wave directions. As an indication for this sea state can be found: $H_{1/3}^{\max} = 3.0$ m for the 150 m length pipe laying vessel 'Lorelay' and $H_{1/3}^{\max} = 4.0$ m for the 250 m vessel 'Solitaire'. In many cases, bow-quartering environmental conditions will be found as the most critical operational condition with regard to vessel motions, pipe movements at the stinger and the DP performance. In order to establish whether the DP system of a pipe laying vessel is still redundant or close to its maximum capability as a result of forces exerted by the environment and the pipe tension, a DP analysis should be performed which forms an integral part of the dynamic analyses. The results of these analyses have to be used to determine nominal and maximum stinger tip clearance values. This information is required to assist offshore personnel in determining nominal lay tension during pipe laying operations with changing environmental conditions. If moored by means of anchor systems, the ability to lay pipes in severe sea conditions is determined by:
  - the stiffness of the mooring system,
  - the forces in the mooring lines,
  - the holding capacity of the anchors,
  - the possibility for anchor handling,
  - the wave frequency motions of the vessel,
  - the low frequency horizontal (surge, sway and yaw) motions of the vessel,
  - the forces exerted by the stinger on the stinger-vessel connections and

- the buckling and bending stresses in the pipe line.

In case of dynamic positioning, the accuracy of the low speed tracking capability is an important aspect too.

After laying the pipe, it has - in many cases - to be buried in the sea bed or to be covered by gravel stone. Another possibility is to tow a trencher along the pipe, which acts as a huge plow. The trencher lifts the pipe, plows a trench and lowers the pipe trench behind it. The sea current takes care of filling the trench to cover the pipe, as will be discussed in chapter 14.

In very extreme conditions the pipe is plugged and lowered to the sea bed, still keeping sufficient tension in the pipe in order to avoid buckling. After the pipe is abandoned, the vessel rides out the storm. The ship has to survive a pre-defined extreme sea state, for instance a 100-years storm in the North Sea.

1.2.3 Drilling Vessels

When geological predictions based on seismic surveys have been established that a particular offshore area offers promising prospects for finding oil, a well is drilled to examine these predictions. These drilling operations are carried out from barges, ships, semi-submersibles or jack-up rigs; see figure 1.5.
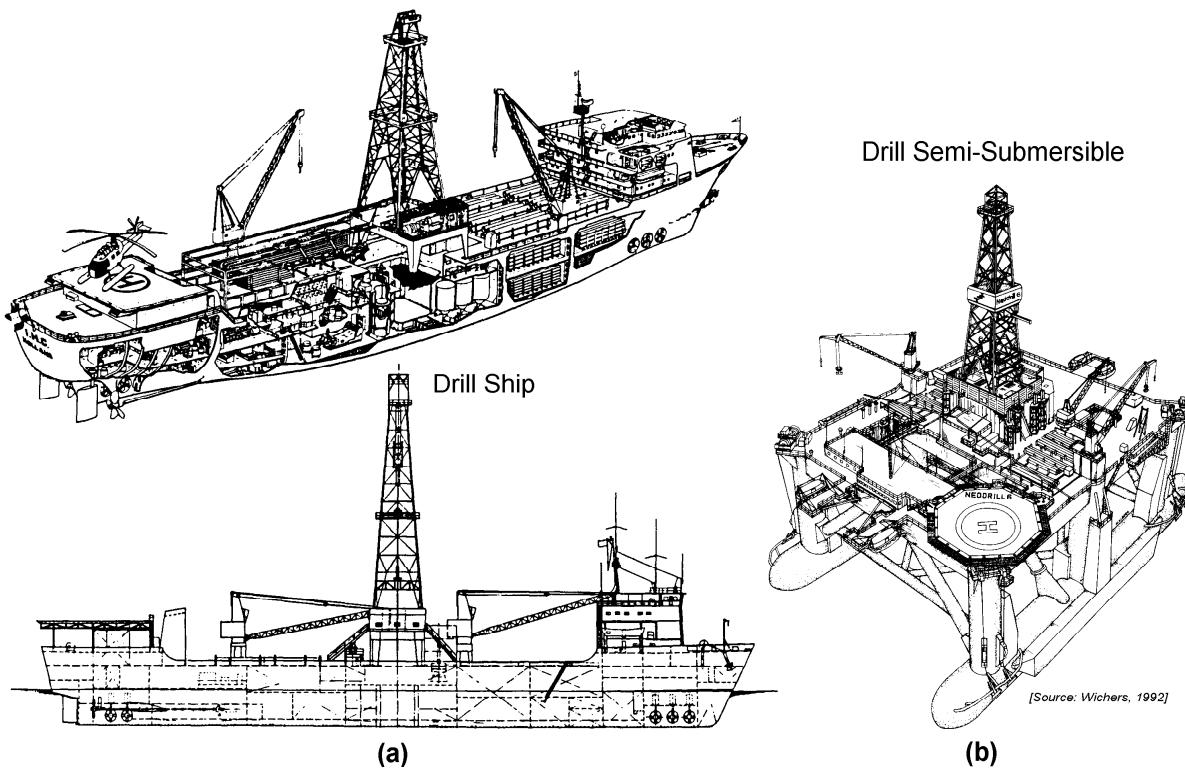
Figure 1.5: Ship and Semi-Submersible Type of Drilling Vessel

For floating drilling units it is important that they can work in high sea conditions. Generally, semi-submersibles will have the least vertical motions and hence the highest workability. In order to enhance further the workability of drilling vessels, the vertical motions of the vessel at the location of the drill string are compensated for by a so-called heave

compensator. This device is essentially a soft spring by means of which the drill string is suspended from the drilling tower on the vessel. In this way, the drill string can be maintained under the required average tension, while the vertical motions of the vessel - and hence of the suspension point of the drill string in the drilling tower - do not result in unduly high drill string tension variations or vertical movement of the drill bit. Also the marine riser is kept under constant tension by means of a riser tensioning system.

Horizontal motions are another factor of importance for drilling vessels. As a rule of thumb, the upper end of the drill string may not move more to one side of the center of the drill than approximately 5 % of the water depth. This places considerable demands on the mooring system of the vessels. Semi-submersible drilling vessels are generally moored by means of 8 to 12 catenary anchor legs. Drill ships can be moored by means of a spread mooring system which allows a limited relocation of the vessel's heading or a by means of a dynamic positioning (DP) system. The latter system of mooring is also used for semi-submersible drilling vessels for drilling in water exceeding 200 m depth.

Summarized, aspects of importance or interest of drilling vessels are:
 - the wave frequency vertical motions at the drill floor,
 - the horizontal motions at the drill floor,
 - the deck clearance of the work deck of a semi-submersible above a wave crest (air gap),
 - the vertical relative motions of the water in the moonpool of drill ships,
 - the damage stability of a drilling semi-submersible,
 - the forces in the mooring lines,
 - the mean and low frequency horizontal environmental forces on DP ships and
 - the thruster effectivity in high waves and currents.

As an example, some limiting criteria for the ship motions - used for the design of the 137 m length drilling ship 'Pelican' in 1972 - were:
 - ship has to sustain wind gusts up to 100 km/hour,
 - maximum heel angle: 3 degrees,
 - roll: 10 degrees in 10 seconds,
 - pitch: 4 degrees in 10 seconds and
 - heave: 3.6 meter in 8 seconds.

1.2.4   Oil Production and Storage Units

Crude oil is piped from the wells on the sea bed to the production platform where it is separated into oil, gas, water and sand. After purification, the water and sand returns to the sea. Gas can be used for energy on the platform, flared away or brought to shore by means of a pipe line. In some cases the produced gas or water is re-injected in the reservoir, in order to enhance the production of crude oil. Crude oil is piped to shore or pumped temporarily into storage facilities on or near the platform.

Jackets

Fixed platforms for oil and gas production are used at water depths ranging to about 150 m. In most cases they consist of a jacket, a steel frame construction piled to the sea bed; see figure 1.6. The jacket supports a sub-frame with production equipment and accommodation deck on top of it.

The jacket has to be transported on a barge to its installation site at sea. During transport, the aspects of importance or interest of a jacket are:

[Source: Wichers, 1992]
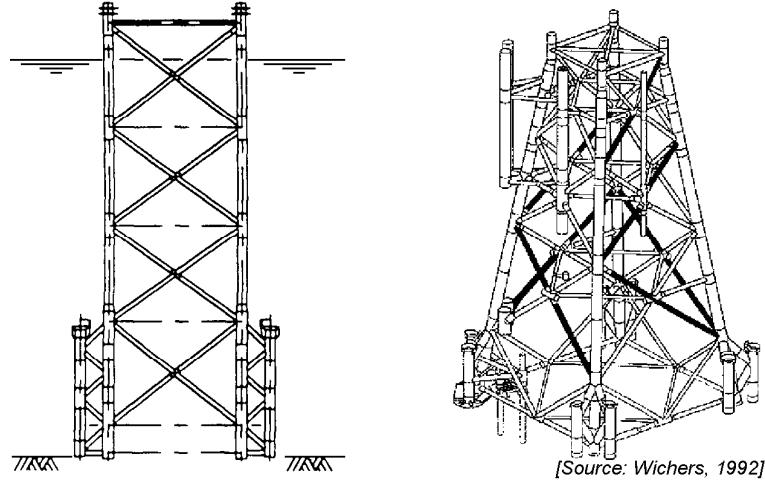
Figure 1.6: Jackets

- the accelerations and motions of the jacket,
- the forces exerted by the sea-fastenings on the jacket and
- the wave impacts on overhanging parts of the structure.

During the installation phase of the jacket, it has to be launched from its transportation barge; see figure 1.7. Then, the jacket is temporally a floating structure.
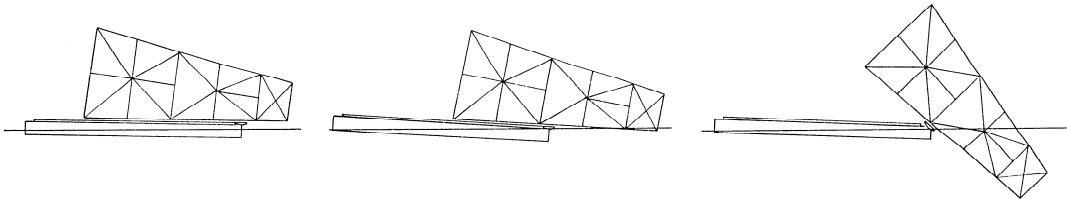
Figure 1.7: Schematic View of Launching a Jacket from a Barge

During launching, the aspects of importance or interest of the jacket are:
- the motions of the jacket on the transportation barge in waves,
- the forces exerted on the jacket by the launchways and rocker arm beams,
- the maximum depth to which the jacket dives and
- the static as well as the dynamic stability of the jacket.

Then, the free-floating jacket has to be up-ended before it can be put on the sea bed. During this installation phase, the aspects of importance or interest of a jacket are:
- the flooding sequence of the ballast tanks,
- the hydrostatic stability of the jacket,
- the current forces on the jacket and
- the internal stresses in the jacket.

When the jacket is ballasted to stand on the sea bed, in some cases it will have to be positioned over the pre-drilled template; see figure 1.6. The guiding pins have to enter the receiver cans on the template. In many cases this operation is carried out with help of a crane vessel. During this installation phase, the aspects of importance or interest of a jacket are:

- the motions in waves,
- the current forces,
- the internal stresses in the jacket,
- the loads in the guiding pins and
- hoist wave loads in case of crane assisted positioning.

Finally, the jacket will be anchored to the sea bed by means of long steel pipes which are lowered through the pile sleeves and hammered into the sea bed. This can be done by a crane vessel, which also installs the top-side modules.

Jack-Ups

A jack-up is a mobile drilling unit that consists of a self-floating, flat box-type deck structure supporting the drilling rig, drilling equipment and accommodation; see figure 1.8. It stands on 3 or 4 vertical legs along which the platform can be self-elevated out of the water to a sufficient height to remain clear of the highest waves. Drilling operations take place in the elevated condition with the platform standing on the sea bed. This type of platform is used for drilling operations in water depths up to about 100 m. Jack-ups spend part of their life as floating structures. This is when such platforms are towed to a new location by means of ocean-going tugs. In this mode, the legs are lifted up and extend upwards over the platform.

[Source: Internet]
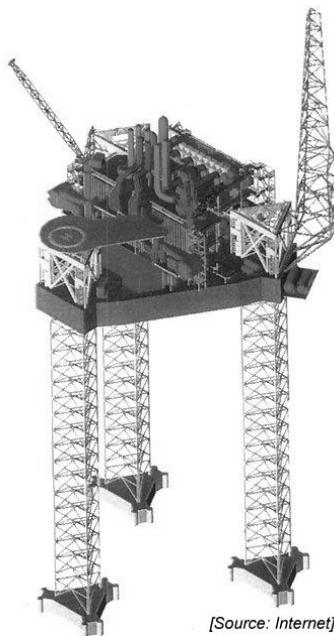
Figure 1.8: Jack-Up
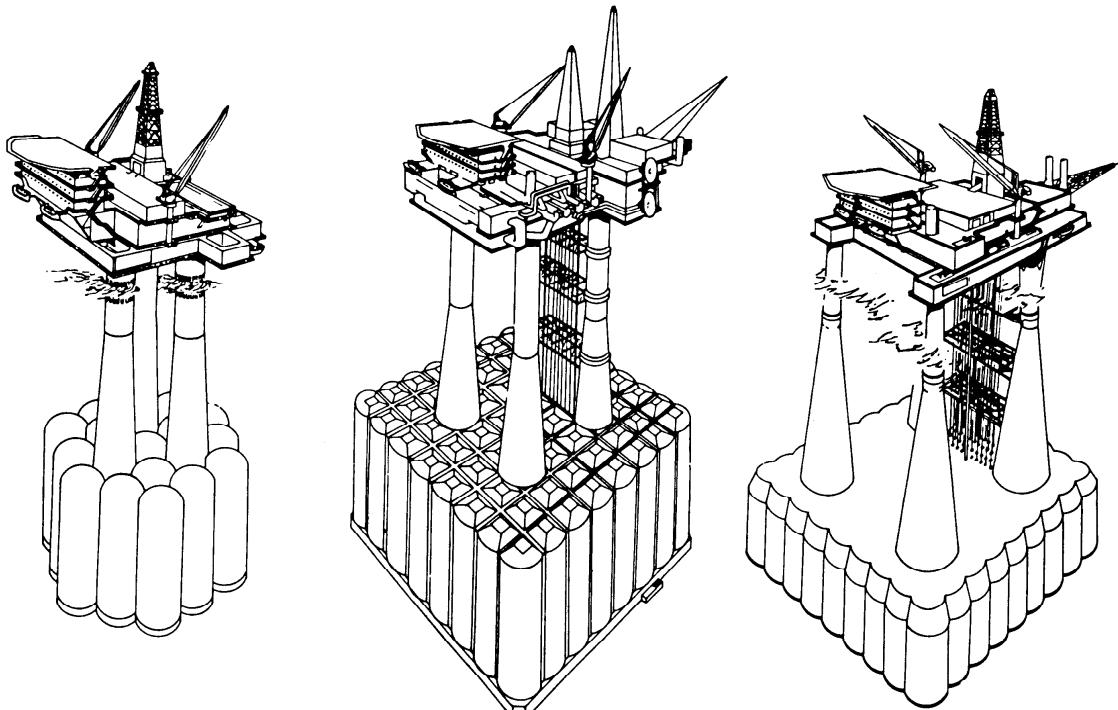
Aspects of importance or interest in the towing condition of a jack-up are:
- the towing resistance,
- the course stability under tow and
- the bending stresses in the legs at the point of connection to the deck structure.

These bending stresses are adversely affected by the wave induced roll and pitch motions of the vessel. In some cases the highest sections of the legs are removed for the towing operation in order to reduce the bending stresses to acceptable levels.

Gravity Base Structures

Gravity Base Structures (GBS) are applied to remote fields in deep and harsh waters in the central and northern part of the North Sea. They consist of a combination of a number of large diameter towers, placed on top of a large area base which contains also storage capacity. Piling to the sea bed is not required because of the large size of the base and the mass of the structure, but the sea bed has to be leveled. The towers support a sub-frame with a production equipment and accommodation deck on top of it. Figure 1.9 shows some examples of large gravity base structures.

[Source: Coppes, 1996]

Figure 1.9: Some Gravity Base Structures

After construction inshore, the unit is mated with the top-side structure in relatively sheltered waters. Aspects of importance or interest during this mating phase of a GBS are:
  - the positioning of the top-side relative to the main structure and
  - the impact loads between the top-side structure and the main platform structure.
Both these aspects require very mild environmental conditions during the actual mating. Then the complete platform is towed out to the work location by 4 to 6 tugs. Aspects of importance or interest during this towing phase of a GBS are:
  - the towing force,
  - the course stability under tow,
  - the 'keel' clearance at restricted water depths, influenced by vertical platform motions,
  - the wave induced motions,
  - the motions due to vortex shedding and flow separation around slender columns and
  - the current loads.
At the work location, the platform is being ballasted down to the sea bed. Aspects of importance or interest during this ballasting down phase of a GBS are:

- the positioning accuracy,
- the vertical motions on setting down and
- the horizontal wave, wind and current forces.

Floating Production Units

Floating Production units (FP) are used for oil production at smaller fields. In very deep water they are also economically attractive for large oil fields. The production equipment and accommodation is placed on a floating structure, permanently moored to the sea bed. They have no storage capacity. The oil is off-loaded to a Floating Storage and Off-loading unit (FSO). Figure 1.10 shows an overview of this.
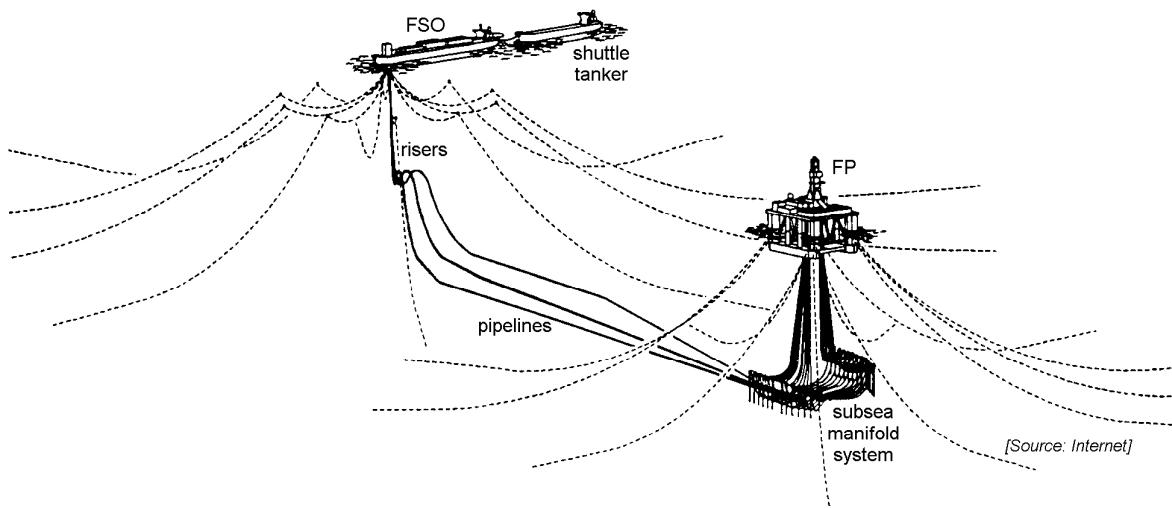
Figure 1.10: Floating Production Unit with External Storage Facilities

Two types of floating production platforms without storage capacity can be distinguished: the semi-submersible and the tension leg platform (TLP). Production on a TLP in remote areas - so that a pipe line is uneconomical - requires external storage capacity, for instance by using a storage tanker moored nearby.

A Semi-Submersible Platform consists of a rectangular deck structure supported by 4 to 8 surface-piercing vertical columns standing on submerged horizontal floaters. These vessels have good motion characteristics and do not require the heading changed as the predominant direction of the weather changes. The vessels are moored by means of 8 to 12 catenary mooring lines consisting of chains or combinations of chain and wire. Parts of the pipe lines transporting the oil to the floater have to be flexible to allow for the wave induced motions of the floater. These flexible pipe lines have to be sufficiently strong and resilient to withstand high pressures and temperatures of the crude oil as well as the continual flexing due to the floater motions; see figure 1.11.

The aspects of importance or interest are generally the same as those for drilling semi's. However, the production semi-submersible will be permanently moored which means that - consequently - more stringent demands are placed on the design. Additional aspects of importance or interest of semi-submersible production platforms are:

- the behavior of bundles of flexible flow lines and risers and

[Source: Wichers, 1992]
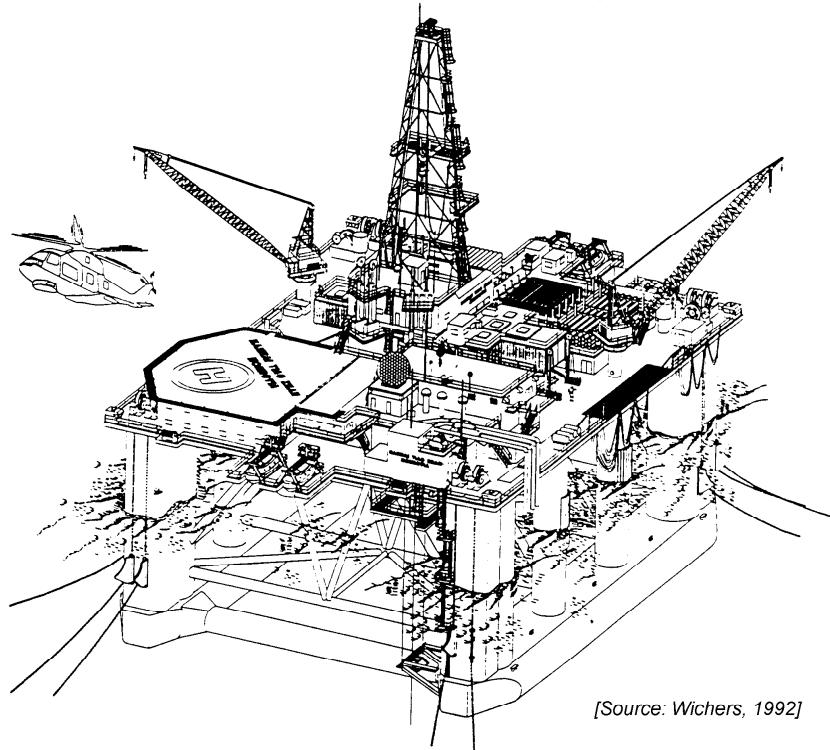
Figure 1.11: Semi-Submersible Production Platform

  - the stresses in the individual flexible flow lines.

A Tension Leg Platform (TLP) consists of a semi-submersible type hull with for instance four vertical surface-piercing columns standing on underwater floaters and supporting a large rectangular deck; see figure 1.12. At each of the four corners of the floater, pre-tensioned tethers extend vertically downwards to foundation templates which are piled into the sea bed. Due to the vertical tendons, which are pre-tensioned to such a degree that they never become slack, any vertical motion of the TLP will be eliminated. This allows for steel pipe line connections between the wells and the floater, without the need for flexible sections of pipe lines. As a result, it is possible to install the well head control valves on the deck of the floater instead of on the sea bed. This represents a considerable advantage from the point of view of ease of maintenance and investment.

The installation phases consist of construction of the floaters in a dry dock inshore, float out, deck mating, tow out to the production field and the final installation. Aspects of importance or interest during the installation phase of a TLP are:

  - the avoidance of vessel impact loads during the deck mating operation,
  - the horizontal positioning accuracy during deck mating and hook-up of the tethers and
  - the towing resistance.

Aspects of importance or interest in the installed condition of a TLP are:

  - the avoidance of wave impacts on the under side of the deck,
  - the wave and low frequency horizontal forces and motions,
  - the wave and current induced vortices,
  - the avoidance of slack tethers,
  - the maximum tether tensions,
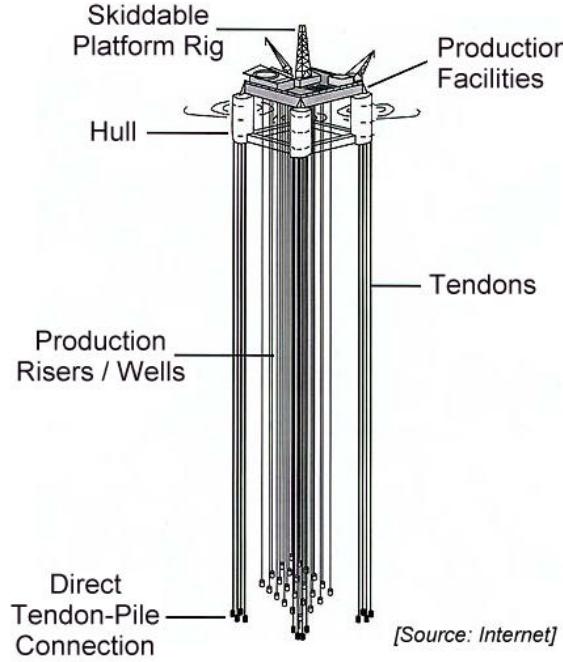
Figure 1.12: Tension Leg Platform

- the behavior of the bundles of the tethers,
- the super-harmonics in tether tensions (springing) and
- the current and wind forces.

Floating Storage and Off-loading Units

Permanently moored Floating Storage and Off-loading vessels (FSO's) are used to store the produced crude oil. Periodically, the oil is collected and transported to shore by means of shuttle tankers. For the off-loading operation, the shuttle tanker is often moored either in tandem with the storage vessel or alongside.

Sometimes the stored oil is piped to a Single Point Mooring system (SPM) some distance away, to which the shuttle tanker is temporarily moored. A Spar buoy mooring system is an example of this combined offshore storage and mooring facility; see figure 1.13.

Generally, due to costs aspects, existing tankers - with sizes ranging from 80 to 200 kDWT - have been used as storage vessels, permanently moored in the neighborhood of a production platform or a group of platforms. When converting oil tankers for this purpose, special attention has to be paid to the remaining fatigue life of this older vessel. Nowadays, the number of suitable tankers on the market is relatively small and a trend toward purpose built storage vessels is discernible.

A factor of prime importance for the operation of these vessels is the continued integrity of the mooring system and of the pipe line carrying the crude to the storage vessel. Another important aspect is the operational limit of the crude oil transfer operation between the storage vessel and the shuttle tanker. Both these design requirements are mainly determined by the wind, wave and current induced motions, the mooring forces of the storage vessel and those of the shuttle tanker.

Aspects of importance or interest of an FSO are:
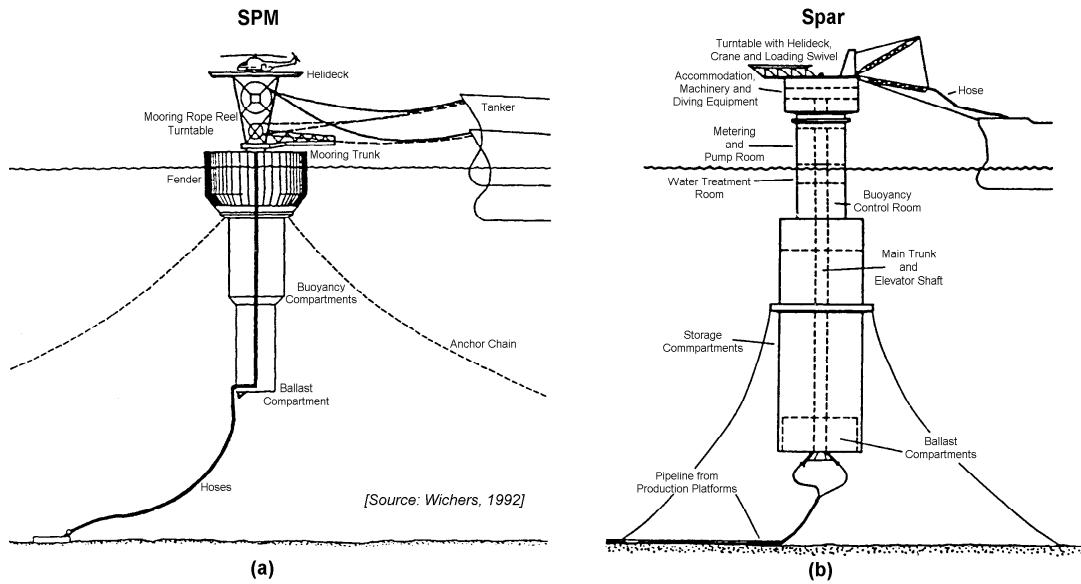
Figure 1.13: Mooring to an SPM and a Spar Buoy

- design loads of the mooring system for extreme sea conditions (100-year storm),
- the environmental loads on and fatigue aspects of mooring system components,
- the loads in the shuttle-to-storage vessel mooring lines,
- the mean and low frequency environmental forces on the storage vessel,
- the operational limits with respect to shuttle tanker loading,
- the approach manoeuvre of the shuttle tanker,
- the installation aspects of the storage vessel mooring and
- the behavior of (flexible) flowlines in extreme conditions.

Floating Production, Storage and Off-loading Vessel

A Floating Production, Storage and Off-loading vessel (FPSO) is generally based on the use of a tanker hull, which has been converted for the purpose. Such vessels have a large storage capacity and deck area to accommodate the production equipment and accommodation; see figure 1.14. When converting old tankers for this purpose, special attention has to be paid to the fatigue life of the vessel.

Motion characteristics of such vessels are acceptable as long as the vessel can 'weathervane' with the predominant direction of the wind and the waves. This requires that a single point mooring system be used by means of which the vessel is effectively held at the bow or stern by the mooring system and allowed to rotate freely around that point. A complicating factor of the SPM system is the need to include fluid swivel systems in the oil transport system to and from the vessel.

In some sheltered locations it is not necessary to apply an SPM type mooring system. In such cases a spread mooring system which holds the vessel in a fixed mean heading direction is the preferred solution since no swivels are required in the oil transport lines to and from the vessel. Due to the wave induced motions of the FPSO, the oil transportation lines to the vessel have to be flexible.
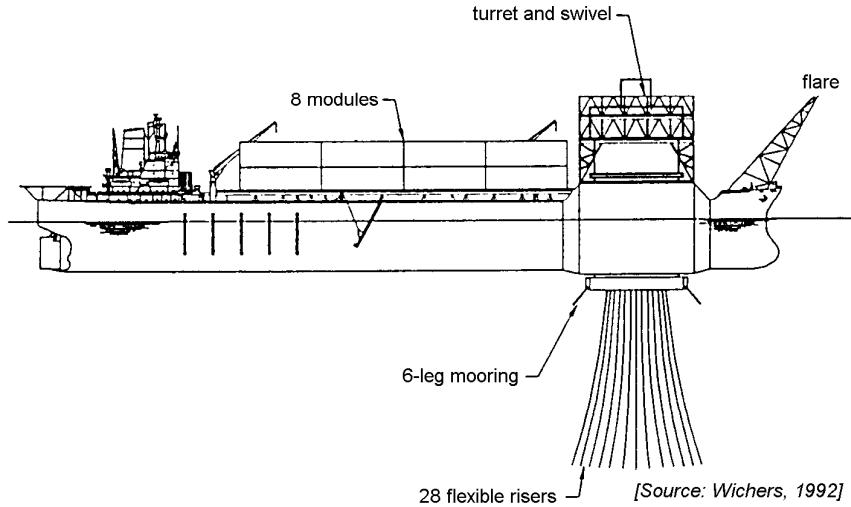
Figure 1.14: Floating Production, Storage and Off-loading Unit (FPSO)

Aspects of importance or interest are mainly similar to those for an FSO system, discussed before. However, two additional aspects for FPSO's are:

- the effect of the vessel motions on the production process and

- the vertical relative motions between the waves and the deck edges (deck wetness).

1.2.5   Support Vessels

Some requirements on support vessels - such as seismic and survey vessels, stand-by vessels, anchor handling vessels, well maintenance vessels, diving support vessels and crane vessels - are briefly described here.

Seismic and Survey Vessels

The decision to drill at a given location is based on the result of seismic and geological surveys of the structure underlying the sea bed. Some seismic survey systems are shown in figure 1.15.

Whereas in earlier days of the offshore industry existing utility vessels were used as a base for carrying out such surveys, nowadays purpose built vessels extensively equipped with sophisticated seismic data gathering and analysis systems are appearing on the market. The success rate of finding oil and gas fields has increased considerably since the introduction in recent years of three-dimensional seismic survey method. Aspects of importance or interest of this type of vessels are:

  - the wave frequency motions and accelerations,

  - the vertical relative motions between the waves and the deck edges (deck wetness),

  - the low speed tracking capability,

  - the station keeping ability and

  - the workability of the specialists onboard..
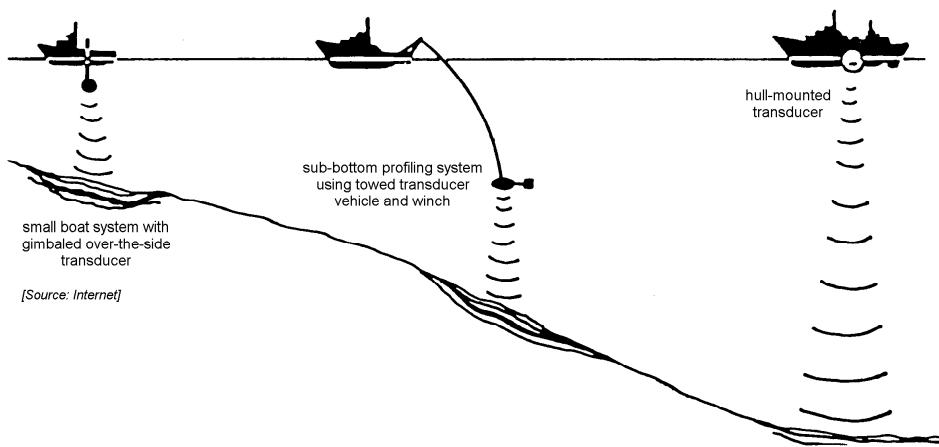
Figure 1.15: Seismic Survey Vessel Systems

Well Maintenance Vessels

Throughout the productive life of an oil or gas well, maintenance of the well plays an important role. Well maintenance generally requires that a so-called 'work-over unit' be brought overhead of the wellhead. The well is entered and tools are lowered into the well. In the past, use was generally made of drilling vessels since these were fitted with the necessary equipment for carrying out the positioning operation, the entering of the well and the lowering of the tools into the well. In recent years, however, there is a trend to using smaller, more cost effective vessels for this work. These vessels, while possessing the required equipment in the form of a drilling tower etc., do not need to have other facilities which are specifically needed for drilling operations, such as a large load carrying capacity for the purpose of the storage of large amounts of drill string or well casing or for drilling fluids. Maintenance vessels can therefore be smaller and less expensive. At present a number of smaller semi-submersibles are in use for this purpose. Well maintenance has also been carried out from the decks of larger supply vessels which have been fitted with the necessary work-over equipment.

Aspects of importance or interest are the same as mentioned for the semi-submersible drilling rigs. An increasing number of this type of vessels is being fitted with DP systems. This type of mooring system is very flexible and avoids the complications involved in deploying anchor lines over a sea bed that may have several pipe lines situated on it.

Diving Support Vessels

Diving support vessels are intended as a base for diving operations offshore. Many of the subsea activities require the presence of divers subsea, as the development of robot techniques has not yet progressed far enough to be applicable to all activities. The offshore industry moves into deeper waters in its search for oil and gas, so diving operations must be carried out in ever deeper water. Safe diving operations in deep water require even more sophisticated support systems, such as large pressure vessels and diving bells to allow the divers to remain under deep water pressure while on board. This makes deep water diving practical, since it is not necessary to depressurize in between working spells. Diving support vessels are fitted with all equipment necessary for safe deep water diving operations,

involving a number of divers simultaneously. Besides sophisticated diving equipment, such vessels are often equipped with DP systems. Since the divers operating on the sea bed depend on the vessel, high demands are placed on the integrity of the DP systems and on the motion characteristics of such vessels in waves.

Aspects of importance or interest of diving support vessels are:
  - the horizontal wind, wave and current loads,
  - the wave frequency motions and accelerations,
  - the vertical relative motions in the moonpool,
  - the effect of current and wave frequency motions on the thruster performances and
  - the station keeping ability.

Crane Vessels

Offshore construction - such as involved in building a fixed offshore production platform - requires a large number of crane lifts in which the construction elements (so-called modules) are lifted off a transportation barge or a supply vessel onto the platform; see figure 1.16. It has long been recognized that it is beneficial - from the point of view of the overall construction time and costs of a platform - to be able to reduce the number of modules to be connected up offshore to the smallest possible number. This has resulted in a tremendous escalation in the lifting capacity of floating cranes.

[Source: Heeremac, 1995]
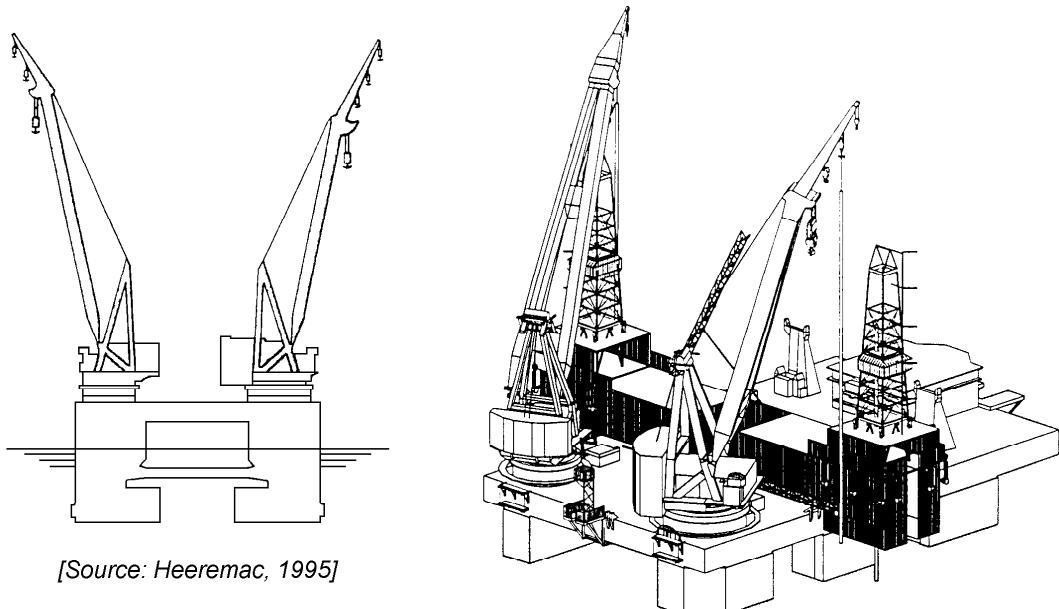
Figure 1.16: Semi-Submersuble Crane Vessel

Until the mid-sixties, the heavy lift vessels for the offshore industry were either converted tankers fitted with a revolving crane at the bow or conventional flat barges with a fixed gantry type crane. Their lifting capacity amounted a few hundred tons. After the mid seventies, a new breed of heavy lift vessels was introduced, which consists of Semi-Submersible Crane Vessels (SSCV's) with a large displacement. They were fitted with two revolving cranes, which could work independently or in tandem depending on the work required. At present, crane vessels are in service which can lift masses of over 10 thousand tons by

using the two cranes simultaneously. Due to the superior motion behavior of the semi-submersible hull form in waves, the workability with respect to crane operations increased tremendously.

Subjects of prime importance for crane operations offshore are the impact load that can occur as a load is taken off a transportation barge, because of the different vertical velocities of the two vessels. In an environment with waves the barge and the heavy lift crane vessel carry out wave frequency motions. As the lift is taken off the barge, it will carry out vertical motions which are dictated by the crane vessel motion characteristics. The barge, on the other hand, also carries out wave frequency motions which - in general - will not be in phase with the motions of the load in the hook. When the load is just clearing the barge, this will result in impacting of the load on the barge. This may lead to damage of the load, the barge or the crane vessel or even all three of them. The prime concern then is to reduce the risk that a critical impact occurs. This can be influenced by the design of the crane vessel, for instance by including the ability to transport the load on the deck of the crane vessel, but also by operational procedures and aids such as quick de-ballasting systems. Besides the occurrence of impact loads which are mainly affected by the vertical motion response to waves, the horizontal motions of the crane vessel are of importance with respect to the feasibility of accurate positioning of the load onto the platform under construction. These motions are affected by environmental loads due to wind, waves and current acting on the crane vessel, by the design and layout of the mooring or positioning system and by the dynamics of the load hanging in the crane.

Thus, aspects of importance or interest of crane vessels are:
  - the vertical crane hook motions in waves,
  - the horizontal positioning accuracy of the hook load,
  - the impacts on lift-off and set-down of the load,
  - the deck load capacity,
  - the transit speed and
  - the mooring forces.

For the DP system extensive investigations have been carried out into the following aspects of the station keeping ability:
  - the thruster-hull, thruster-thruster and thruster-current interactions,
  - the drift forces due to waves,
  - the current forces and
  - the wind forces.

1.2.6 Transportation Vessels

Some types of transportation vessels are discussed here: shuttle tankers, heavy lift transportation vessels, launch barges, ocean-going tugs, supply vessels and personnel transfer vessels.

Shuttle Tankers

From the storage facilities the oil is transported to shore by means of pipelines or shuttle tankers. These shuttle tankers are temporarily moored close to the storage system by means of a single point mooring (SPM) system, mooring in tandem (see figure 1.17) or alongside the storage vessel or by means of a DP system.
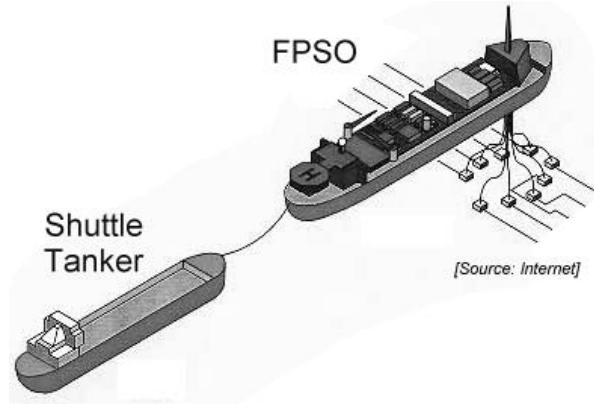
Figure 1.17: Mooring in Tandem

It may be noted that seamen on a shuttle tanker don't like mooring in tandem behind an FPSO. Weather vaning of both vessels causes that their ship is in the smoke of the FPSO continuously.

Heavy Lift Transportation Vessels

Heavy lift transportation vessels are towed or self-propelled heavy and voluminous cargo barges which are used to transport large volume heavy lifts over long distances. The cargo is taken aboard by either roll-on from ashore or float-on by submerging the cargo deck.

Self-propelled heavy lift transportation vessels have been developed; firstly based on the conversion of conventional bulk cargo vessels or tankers and later by purpose built vessels; see figure 1.18. Some of these vessels can even transport dry-docks in which they can dock themselves. The advantage of these vessels is that they can be used to transport drilling semi-submersibles and jack-ups over long distances in a relatively short time, with speeds in a seaway up to about 13 knots. The alternative would be a relatively slow process of towing such structures by means of conventional ocean-going tugs. During the voyage, often use will be made of advises of weather routing offices.

Aspects of importance or interest of heavy lift transportation vessels are:
  - the transit speed,
  - the motion behavior of the vessel with large heavy cargo on its deck,
  - the sea-fastenings to secure the cargo to the vessel and
  - the wave impact loads on the cargo, which often overhangs the deck edge of the vessel.

Careful assessment of the motions and accelerations of the vessel in laden condition can lead to considerable savings in the sea-fastenings.

Launch Barges

Launch barges are very large flat top barges which transport the jacket structures and other construction elements of a platform which have been built onshore; see figure 1.19. The barge is towed out to the work location.

Aspects of interest during towing of a launch barge are:
  - the towing resistance of the barge,
  - the course stability under tow,

[Source: Dove and Johnson, 1995]
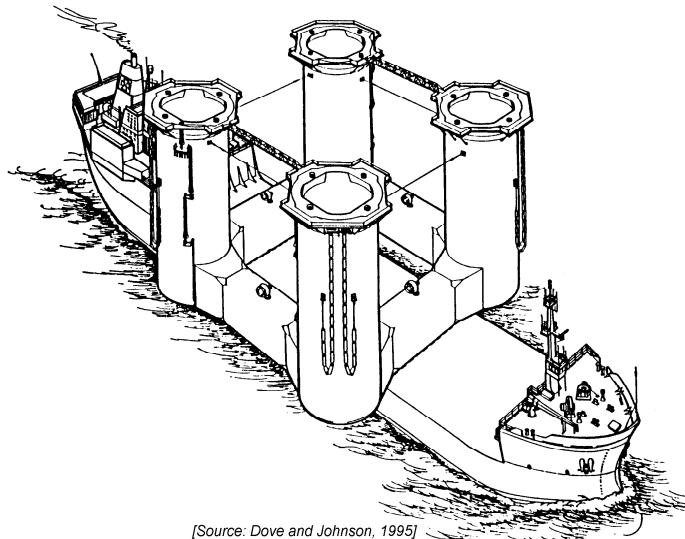
Figure 1.18: Heavy Lift Float-On Float-Off Vessel

- the motions and accelerations of the barge and
- the forces on sea-fastenings holding the jacket on the barge.

At the work location, the barge is held stationary, while the jacket structure is end-launched off the barge. During this launching operation - see figure 1.7 - the barge is not tightly held by the tugs since, as the jacket is launched, the barge will carry out relatively violent motions and be pushed away over quite a distance. The launching operation is initiated after the sea-fastenings have been cut loose and the jacket is only resting on the launchways. By ballasting the barge to the specified trim angle and with initial winch pulling, the jacket will start to slide over the launchways.

Aspects of importance or interest for the barge during launching are:
- the maximum depth of submergence of the aft end of the barge,
- the ballast distribution,
- the friction of the launchways,
- the angle of rotation of the rocker beams,
- the rocker beam forces and
- the stability during the launch.

Very slender structures are sometimes side-launched. Some jackets have been designed to be crane-lifted off the barge by a crane barge or a crane vessel. Then the impact loads on jacket and barge at the moment of lift-off is an aspect of importance.

Tugs and Supply Vessels

Tugs and supply vessels are the 'workhorses' of the offshore industry.

Tugs are used to tow all types of floating offshore equipment out to the work location and are in many cases a permanent 'companion'; see figure 8.32. Large deep-sea tugs are used for long distance towing and smaller tugs are employed for short range towing operations. A special type of tug is the so-called anchor handling tug. This vessel is used to position and re-position the anchors of drilling rigs and in stand-by mode it is used for a pipe laying vessel as it proceeds along the pipe line trajectory.
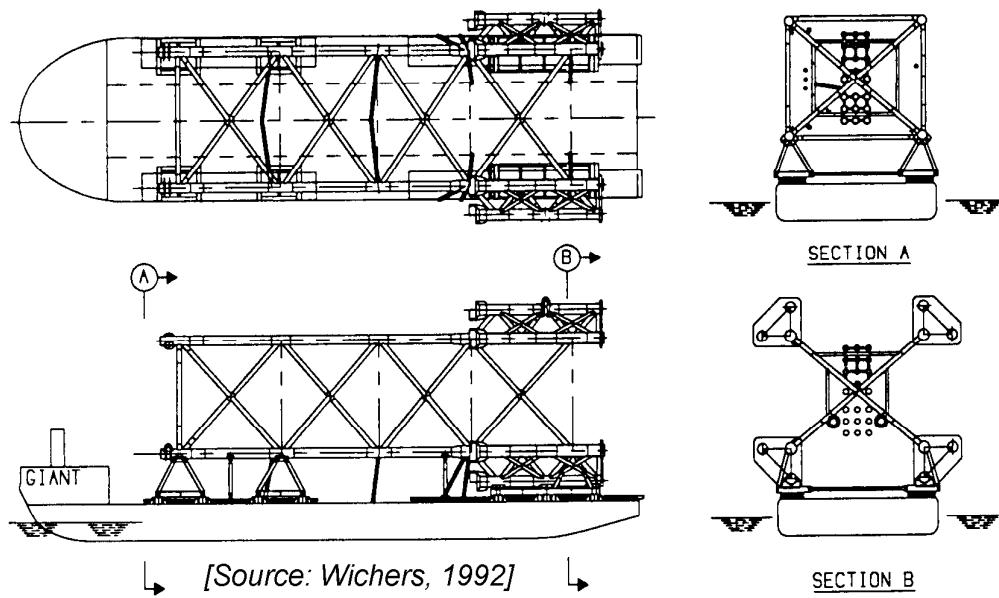
Figure 1.19: Transport of a Jacket on a Barge
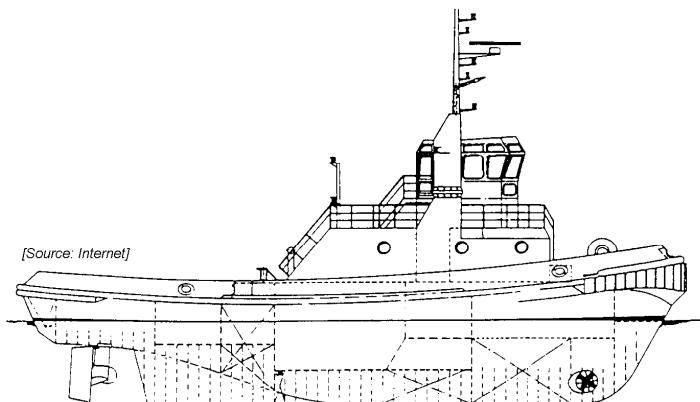
Figure 1.20: Tug

Supply vessels do as their name implies; they are used primarily to transport equipment necessary for the execution of work offshore. This can mean, for instance, drill pipes and drilling muds for a drilling vessel or pipe sections for a pipe laying vessel. The design of supply vessels reflect that they are often dedicated to operations in a particular area. A typical aspect of the design of a supply vessel is the forward location of the deck house with the large open space aft. All equipment to be transported is located on the aft deck; see figure 1.21.

The seakeeping characteristics of these vessels are very important. Aspects of importance or interest of supply vessels and anchor handling tugs are:

  - the motions and accelerations on the work deck and on the bridge,
  - the vertical relative motions between the waves and the deck edges (deck wetness),
  - the effect of shipped water in pipes transported on the open deck of supply vessels,
  - the slamming of waves against horizontal hull surfaces and overhanging cargo and
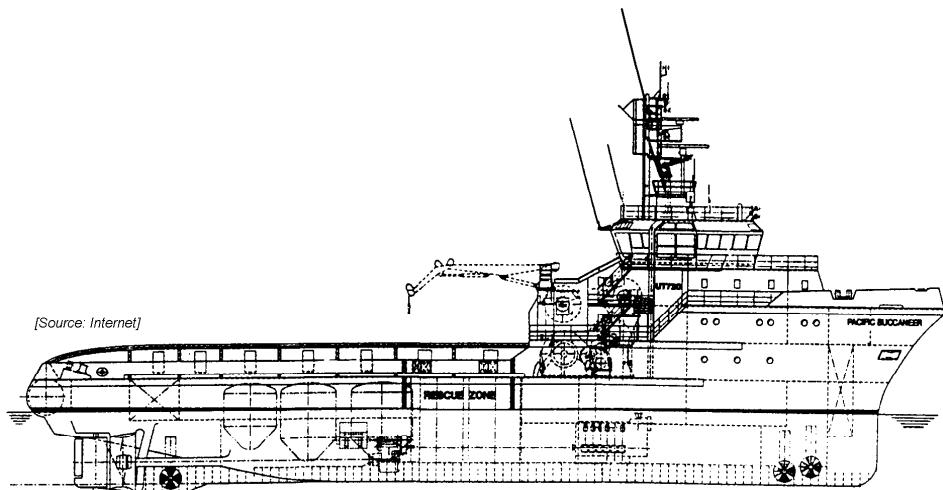
Figure 1.21: Supply Vessel

- the station keeping near platforms during (un)loading and anchor handling operations.

Personnel Transfer Vessels

Helicopters are the most important means to transfer personnel safely and quickly from and to offshore units and ships. For this, these structures have to be equipped with a helicopter deck. Also, supply vessels are still used to tranfer personnel. Figure 1.22 shows a special crew boat for personnel transfer, with a length of 31 meter, which can transport 55 passengers with a cruising speed of 20 knots. However, in the North Sea areas, the helicopter is the most common vehicle for personnel transfer.
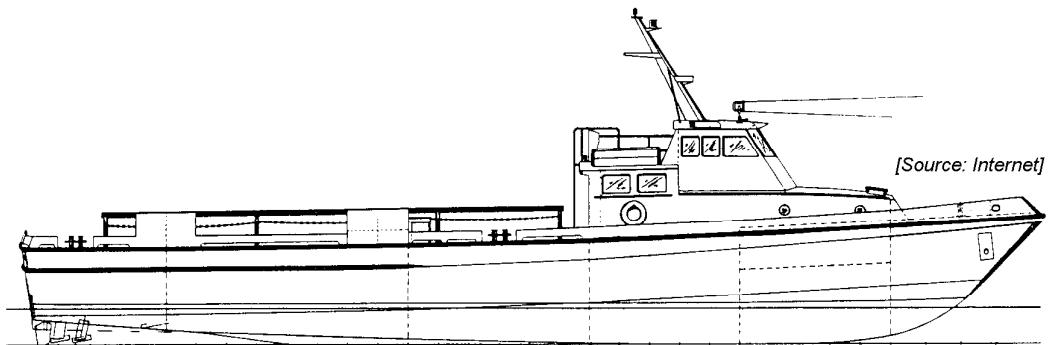
Figure 1.22: Crew Boat

For long distances, helicopters are used to transfer pilots to and from ships too. Pilot vessels are used generally for short distances. Conventional types of pilot vessels operate with service speeds under 20 knots. Generally, they are operating safely in weather conditions up to sea states defined by Beaufort 9 or 10. Figure 1.23 shows some modern types of these vessels: a planing hull ship and small waterplane area twin hull (SWATH) ship, with maximum speeds of about 28 knots. At a reduced speed, they can operate safely in weather conditions up to Beaufort 8.

planing hull type

SWATH type

[Source: Internet]

(a)   **(b)**
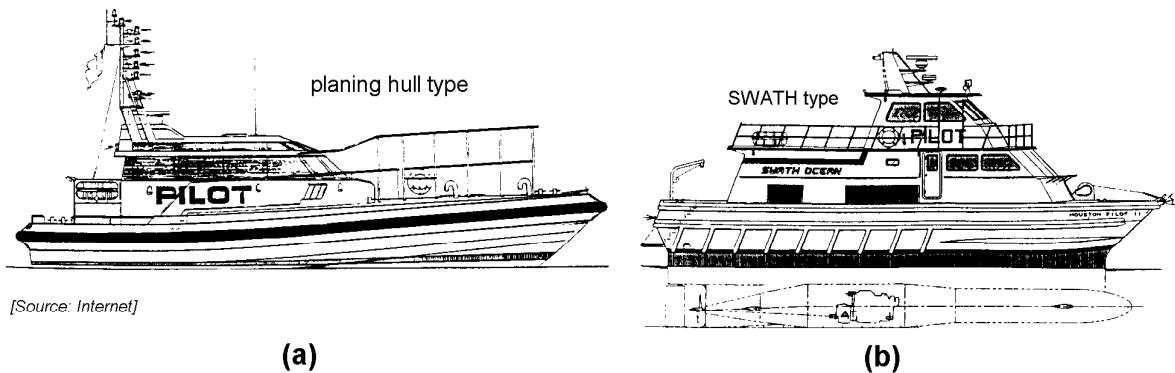
Figure 1.23: Pilot Vessels

Aspects of importance or interest during sailing of these vessels are:
  - the vertical accelerations of the vessel,
  - the wave-induced vibrations in the vessel and
  - the slamming behavior of the vessel at high speeds.
The wave-induced vibrations and the slamming forces at high speeds can cause considerable
(fatigue) damage to these vessels and be dangerous to people.
Aspects of importance or interest during (dis)embarkation a vessel are:
  - the maneuverability of the vessel,
  - the vertical and horizontal motions and
  - the safety of crew and pilots during (dis)embarkation.

Chapter 2

HYDROSTATICS

2.1 Introduction

This chapter discusses only the static properties of a structure. It is assumed here that any disturbance to the equilibrium state will be brought about so slowly that all dynamic effects can be ignored.

First, the hydrostatic pressure, Archimedes' law, the resulting internal forces in a structure and the concept of effective tension will be considered. The effective tension is a fictitious internal force or stress, acting within submerged bodies. It is referred to as effective tension here in order to distinguish it from effective stress as used in soil mechanics - a somewhat different entity.

Static floating stability will be considered later in this chapter. One often takes for granted that a floating structure will float in a proper (desired or upright) position. This will happen only if it is correctly designed, however. A "good" example is the Swedish sailing vessel *VASA*, see [Franzen, 1962], which capsized in 1628 on her maiden voyage which lasted less than two hours; she sank in calm water while still in view of the people of Stockholm.

In service a ship or other floating structure will experience many external loads (e.g. from wind and waves) as well as "internal" loads (from cargo, for example) trying to turn it over. It must be able to resist these, via what is termed its **static stability**. Too little stability is obviously not desirable; this was the case with the *VASA*. Too much stability can be undesirable as well because stability affects a ship's natural roll frequency; excessive and unpleasant motions in a seaway can be the result. Too much stability can be costly too. Thus, as with so many other design features, stability is often a compromise. Because a floating structure will meet varied conditions during its life, its ability to survive should ideally be expressed in statistical terms with stability standards set accordingly. Indeed, no floating structure can be guaranteed to remain stable under all conditions. Even though it **is** possible to design a boat - such as a motor lifeboat used by a coastal rescue team - to be self-righting; this does not guarantee that it always remains upright!

2.2   Static Loads

2.2.1   Hydrostatic Pressure

In any body of fluid, hydrostatic pressure results from the weight of the fluid column above the point at which that pressure is measured. At a free water surface, the pressure will normally be zero relative to the atmospheric pressure (which is nearly always neglected in offshore hydromechanics). In equation form:

$$\boxed{p = \rho g h} \tag{2.1}$$

in which:

$$
\begin{array}{rcl}
g & = & \text{acceleration of gravity} \\
h & = & \text{distance below the fluid surface} \\
p & = & \text{pressure } (= \text{force/area}) \\
\rho & = & \text{mass density of the fluid}
\end{array}
$$

For sea water, the mass density, ρ, is in the order of 1025 kg/m^3; one may remember from oceanography that this density is a function of temperature and salinity, by the way.

2.2.2   Archimedes Law and Buoyancy

Archimedes - who lived from 285 until 212 BC - is reported to have run naked through the streets after making his discovery that a body **submerged** in a fluid experiences an upward buoyant force, F_∇, equal to:

$$\boxed{F_\nabla = \rho g \nabla} \tag{2.2}$$

in which:

$$
\begin{array}{rcl}
F_\nabla & = & \text{buoyant force} \\
\nabla \text{ (nabla)} & = & \text{volume of the submerged part of the object}
\end{array}
$$

This approach views buoyancy as a distributed mass force, completely analogous to the gravity force on (or weight of) the mass of an object.

One can look at buoyancy in another way, however. Since the hydrostatic pressure at any chosen point on the underside of a submerged body will be higher than the pressure on the upper surface directly above that point, one can expect there to be a net upward force on that body. Indeed, an equivalent way of determining $\rho g \nabla$ is to take the vertical component of the pressure times area and to integrate this function over the entire surface of the body. This buoyant force is also equal (or equivalent) to the integral of the hydrostatic pressure vector over the surface of the body.

2.2.3   Internal Static Loads

The two different ways of looking at the buoyant force on a body lead to two different approaches to static internal loads on a structure as well. This is best illustrated by considering a steel drilling pipe hanging in an oil well as shown schematically in figure 2.1.
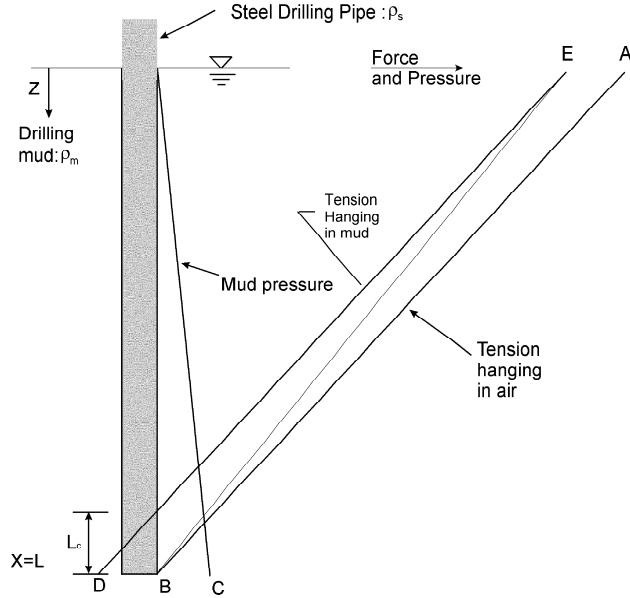
Figure 2.1: Forces and Pressures on A Vertical Drill String

The string is hanging with its lower end above the bottom of the vertical well which is further filled only with air (for this intellectual exercise). Because its own weight - the gravity force - is a distributed force (along the length in this case), the tension force in the drill string will depend upon location along its length as well. The tension will be maximum at the top of well ($z = 0$) and will reduce linearly to zero at the bottom end of the string ($z = L$). In equation form, this tension is given by:

$$T = \rho_s g A (L - z) \tag{2.3}$$

in which:

$$
\begin{array}{rcl}
L & = & \text{Length of the pipe hanging in the well (m)} \\
g & = & \text{Acceleration of gravity (m/s}^2\text{)} \\
A & = & \text{Cross section area of steel in the pipe (m}^2\text{)} \\
z & = & \text{Coordinate measured downward from the top} \\
  &   & \quad \text{in this special case! (m)} \\
\rho_s & = & \text{Mass density of steel (kg/m}^3\text{)}
\end{array}
$$

This tension is shown graphically as line $\overline{AB}$ in the figure and should be quite straightforward; confusion can result after the well is filled with a liquid such as drilling mud.

If the buoyant force caused by the mud is treated as a distributed force just as did Archimedes, then one could conclude that there is a distributed buoyant force acting on the entire body equal to the weight of drilling mud displaced by the drill string.
Starting at the bottom (considering only a thin (horizontal) slice of the string first), the buoyant force on this slice will be (nearly) zero simply because its volume is so small. As one considers an ever-increasing string slice length, this buoyant force will increase to:

$$\rho_m g A L \tag{2.4}$$

at the top of the string. Since this buoyant force acts in a direction opposite to the gravity force, one finds:

$$T_e = (\rho_s - \rho_m)gA(L - z) \tag{2.5}$$

Since $\rho_s > \rho_m$, T_e will be generally be greater than zero as well, but will be less than T, above. T_e is often referred to as the **effective tension**. It, too, varies linearly from a maximum value at $z = 0$ to zero at $z = L$ and indicated by line $\overline{EB}$ in the figure. In general the effective tension is based upon the **submerged weight** of the body. This is the weight of the body in air minus the buoyant force acting on it. It can be computed for homogeneous bodies in water using a density of $(\rho_b - \rho)$, where ρ_b is the mass density of the body.

If, on the other hand, one treats the buoyant force as the resultant of pressures acting on the surface of the body - the drill string in this case, then one finds first that the pressures on the (vertical) drill string walls are in equilibrium and contribute no vertical force. The drill string does experience a vertical force at its bottom end which is equal to:

$$F_z = \rho_m gAL \tag{2.6}$$

This concentrated vertical upward force combines with the distributed weight of the drill string by shifting line $\overline{AB}$ in the figure to position $\overline{DE}$. One discovers now that the lower section of the drill string is in compression instead of tension! The length that is in compression can be computed:

$$L_c = \frac{\rho_m}{\rho_s}L \tag{2.7}$$

One can also conclude that there will be no axial force in the drill string at an elevation L_c above its bottom end and that the entire length below that point will be in compression. This does not agree with what was found when the buoyant force was treated as Archimedes had done, above.

It is easiest to resolve this apparent dilemma by examining a slightly different situation. Consider a solid body which has the same density as water; an atheletic swimmer is a reasonable approximation of this. Considering buoyancy as a distributed force (in the Archimedian sense) would now yield an effective tension in this swimmer's body that would be zero, independent of the depth to which he or she might happen to dive. As anyone who has suddenly plunged into a pool has probably discovered, this is not the case. Indeed, as one dives rapidly deeper into the water the external pressure trying to crush one's body only gets larger. This observation supports the external pressure form of buoyancy argument rather than Archimedes' approach. Apparently, the external pressure form is better for revealing the actual true stress in the submerged body, just as with the rapidly diving swimmer.

On the other hand, the effective tension - resulting from the distributed force approach to buoyancy - also has its uses even though the effective tension will not be measured by a strain gauge mounted on the submerged object. Consider a given length of metal chain hanging between two fixed points in air. The tension at any point in that chain is dependent upon the chain's weight per unit length. If the chain were hung in the same configuration under water, one would expect the tension to be lower. That will indeed be the case; the tension force between adjacent links of the chain now becomes the effective tension.

2.2.4 Drill String Buckling

Returning to the hanging drill string problem posed above, an important structural engineering question involves the buckling behavior of its lower part. It was shown above that the actual axial force in the lower L_c meters of the drill string is compressive. Since the mud surrounding this string provides no lateral support, a structural engineer would feel very justified in applying the Euler column buckling formula:

$$\frac{P_{cr}}{A} = \frac{\pi^2 E}{(L_c/r)^2} \tag{2.8}$$

in which:

$$
\begin{array}{lll}
P_{cr} & = & \text{Critical buckling load (N)} \\
A & = & \text{Cross section area of the column (m}^2) \\
E & = & \text{Material elastic modulus (N/m}^2) \\
L_c/r & = & \text{Column slenderness ratio (-)}
\end{array}
$$

to determine that if L_c is long enough, the drill string segment should buckle.
Another structural engineer can argue that the effective tension in this drill string segment is positive over its entire length; a structure in tension will not buckle.

An independent approach is needed to resolve this discussion. An independent theoretical approach follows from potential energy changes. How does the potential energy of the mud plus drill string change as the drill string buckles? Considering first the drill string steel, if it buckles, then the bottom end of the drill string will move up very slightly, thus raising its center of gravity and thereby increasing the total potential energy of the string. The mud, on the other hand, loses a minute amount of potential energy as it compensates for this drill string movement. Since the drill string has a higher density than the mud, the string gains more potential energy than the mud loses. Potential energy is thus created if the drill string buckles! Any type of engineer should recognize that this cannot happen; One cannot expect the drill string to buckle when it is hanging freely in the mud-filled well.
Apparently two conditions must be met before a long slender submerged object will buckle:
    - it must actually be under compression and
    - its effective tension must be negative.
These criteria can be checked by considering a chain instead of the drill string hanging in the well. The positive weight minus buoyant force of each link will cause there to be a positive effective tension between each link. However, since each link is also essentially surrounded by drilling fluid exerting an external pressure on its surface, it should be equally obvious that the material in each of the deepest links (at least) will be experiencing a compressive force, just like the diving swimmer, above.
Another check can be made by considering - at least intellectually - a drilling string with a density which is less than that of the drilling mud. One can see immediately from equation 2.5 that the effective tension will now be negative. Indeed, the sting will buckle as soon as a long enough segment is lowered into the drilling mud.

Of course the force situation in the drill string changes as soon as a point of a drill bit tooth is lowered to the hole bottom. From that moment on, an extra upward force is exerted on the base of the drill string so that the effective tension becomes negative in the lowest part

of the string. This negative effective tension segment gets longer in direct proportion to the well bottom contact force. If this contact force gets big enough, then the lower segment of the drill string will obviously buckle.

An experimental test of drill string buckling has been carried out by D. Brussmann in Germany. Unfortunately, his work is not reported in the open literature, but one of the authors has seen photos of his test. The photos show - *in contrast to the conclusions above* - that the drill string will buckle even before it touches the bottom of the well. This obviously makes the confusion complete and can initiate an interesting discussion of what to believe of all this.

More than a century ago, a famous hydraulic engineer (in his time), C.M. Allen is reported to have remarked: ”When the theory and the experiment do not agree, then take a good hard look at the theory.” In any case, a safe conclusion to all this is that new - confirmatory tests are needed. These are being carried out at the Delft University of Technology.

2.2.5   Pipeline on Sea Bed

Consider the horizontal force balance on an isolated segment of a horizontal pipe submerged in (and completely surrounded by) a fluid; the fluid pressure acting at the depth of the center line of the pipe is p. The mathematics is simplest if one makes two simplifications:

1. The pipe has a rectangular cross section with height 1; this makes all forces either horizontal or vertical.

2. The pressure change between the top and bottom of the pipe - at least that on the vertical surfaces of the pipe - can be neglected. This is not acceptable if the vertical equilibrium is considered; it is the pressure difference the top and bottom surfaces which yields the buoyant force. These vertical forces have no effect on the horizontal equilibrium of interest here, however.

Consider first a straight pipe. The pressure forces on each side of the pipe will be opposite, equal and have identical lines of action; they will cancel. The same will be true of the hydrostatic pressure forces on the pipe ends. Of course, all these external pressures will cause compressive loadings within the pipe wall, but there is no resultant horizontal force and no (internal) moment in a straight segment of an isolated horizontal pipe (or bar). This means that no matter how long the structure is, and even though it is obviously subjected to a potentially large compressive load, no moments are generated. This is quite like the case with the vertical drill string. The effective tension in this pipe is now zero and it does not buckle. This is in agreement with the two 'rules' given above.

Even if the pipe has an initial curvature, one can work out the pressure force balance to discover that there is still no resulting moment in the pipe; it still will not buckle! Instead, just as one might expect when the limit $T_e = 0$ is reached in the above 'rules', the pipe has come to a neutral state of equilibrium.

2.3   Static Floating Stability

The static stability of a floating structure encompasses the up-righting properties of the structure when it is brought out of equilibrium or balance by a disturbance in the form

of a force and/or moment. As a result of these (extra) loads, the structure will translate and/or rotate about its center of gravity. Formally, dynamic as well as static properties of the structure play a role in this. In this chapter - as mentioned above - only the static properties of the structure will be considered. Dynamic effects are considered in later chapters of this book, however.

2.3.1 Definitions

The body axes and the notations, as used here in static stability calculations, are presented in figure 2.2.
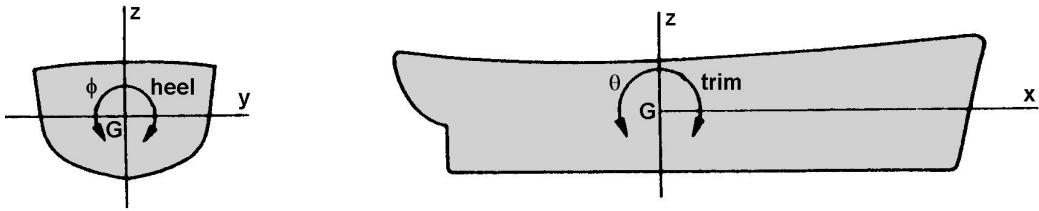
Figure 2.2: Body Axes and Notations

Planes have been defined here as they are generally used in ship hydrostatics. Most ships have only one plane of symmetry, called the **middle line plane** (x, z); this vertical plane is the principal plane of reference. The **design water plane** or **load water plane** (simply called **water plane** here) is a plane perpendicular to the middle line plane, chosen at the still water surface. The **base plane** of the structure is a plane perpendicular to the middle line plane through the keel or the bottom of the ship. It may or may not be parallel to the water plane in the longitudinal direction. Planes perpendicular to both the middle line plane and the water plane are called **transverse planes**. A transverse plane at half the length of the ship is called the **amidships section** of the ship.

So-called hydrostatic forces and moments, caused by the surrounding water, will act on a structure in still water. It is known from above that the **buoyancy** of a structure immersed in a fluid is the vertical upthrust that the structure experiences due to the displacement of the fluid.
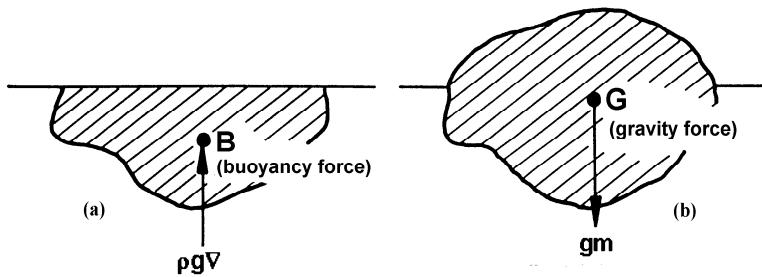
Figure 2.3: Definition of Centers and Forces

The center of the volume of the fluid displaced by a floating structure is known as the **center of buoyancy** B, see figure 2.3-a. The first moment of the under water volume about the center of buoyancy is zero.

The projections of the center of buoyancy B of a ship in the plan and in the section are known as the longitudinal center of buoyancy (LCB) and the vertical center of buoyancy (VCB). If the structure is not symmetrical below the water plane, then the center of buoyancy will not be situated in the middle line plane. Its projections in plan may then be referred to as the transverse center of buoyancy (TCB).

Defining it formally: The **center of gravity, G,** of a structure is that point through which, for static considerations, the whole weight of the structure may be assumed to act, see figure 2.3-b. The first moment of mass or weight about the center of gravity is zero. The center of volume of its immersed part also defines the center of buoyancy, B.

For the sake of simplicity and understanding, the disturbances and the hydrostatic forces and moments are considered (in this text) only to act in the plane of the drawing. The structure is considered to be a floating cylinder with a constant but arbitrarily shaped cross section. The center of gravity G and the center of buoyancy B of the structure are assumed to be positioned in the plane of drawing.

Rotations in the plane of drawing are defined here as **heel**, a rotation about the structure's longitudinal horizontal axis. The same principles holds as well for **trim**, a rotation about the body's transverse horizontal axis. Superposition can be used for combinations of heel and trim - at least if the angles of rotation are not too large.

2.3.2   Equilibrium

In figure 2.3, m is the mass of the floating structure. Often in literature on ship and offshore hydromechanics, this displacement mass:

$$\boxed{m = \rho \nabla} \qquad \text{(Archimedes' Law)} \tag{2.9}$$

is denoted sometimes by the symbol Δ (delta).

A floating structure is said to be in a **state of equilibrium** or **balance** when the resultant of all the forces acting on it is zero and the resulting moment of these forces is also zero.

Three different states of equilibrium or types of stability can be distinguished for a structure which is subject to a small disturbance from an equilibrium position (see figure 2.4):

1. If, following the disturbance, the structure tends to return to the equilibrium position it is said to be in a state of **stable** equilibrium or to possess **positive** stability.

2. If, following the disturbance, the structure remains in its new position, then it is said to be in a state of **neutral** equilibrium or to possess **neutral** stability.

3. If, following the disturbance, the excursion from the equilibrium position tends to increase, the structure is said to be in a state of **unstable** equilibrium or to possess **negative** stability.

If a structure is floating freely in rest in a fluid, the following equilibrium or balance conditions in the plane of the drawing in figure 2.3 are fulfilled:

1. **Horizontal equilibrium:** the sum of the horizontal forces equals zero.

2. **Vertical equilibrium:** the sum of the vertical forces equals zero.

3. **Rotational equilibrium:** the sum of the moments about G - or any other point - equals zero.
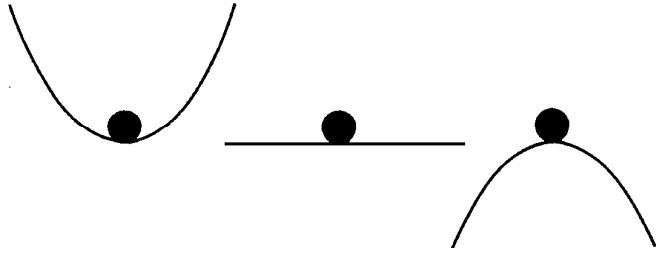
Figure 2.4: Stable, Neutral and Unstable Balance

Horizontal Equilibrium

A translation in a horizontal direction leads to no resultant hydrostatic force, so that unless other external influences - such as moorings are involved - the structure is in neutral equilibrium for this type of disturbance. This equilibrium is of no further interest here.

Vertical Equilibrium

For a floating structure, a vertical downward movement (sinking deeper) results in an increase of the buoyant force which will tend to force the structure back upwards; it tends to return the structure to its original state of equilibrium so that the structure is stable for this type of disturbance.

Archimedes' principle holds for the vertical equilibrium between buoyancy and gravity forces:

$$\boxed{\rho g \nabla = g m} \tag{2.10}$$

If an additional mass, p, is placed on this structure, its original equilibrium will be disturbed. The structure will sink deeper and heel until a new state of equilibrium has been reached. The new vertical equilibrium is given by:

$$\rho g \cdot (\nabla + \Delta \nabla) = g \cdot (m + p) \tag{2.11}$$

in which $\Delta \nabla$ is the increase of the volume of displacement of the floating structure.

If the mass p has been placed on the structure in such a manner that it only sinks deeper parallel to the water plane without heel, the change of draft ΔT follows from:

$$\Delta \nabla = \Delta T \cdot A_{WL} = \frac{p}{\rho} \quad \text{or:} \quad \boxed{\Delta T = \frac{p}{\rho \cdot A_{WL}}} \tag{2.12}$$

Here, A_{WL} is the area of the water plane and it is assumed that this area is constant over the draft interval ΔT.

Rotational Equilibrium

A moment acting on the structure results in a rotation about G, or heel. The structure may display a stable, a neutral or even an unstable equilibrium.

If an external heeling moment acts on the structure as given in figure 2.5, it follows from the rotational equilibrium:

$$M_H = \rho g \nabla \cdot y = g m \cdot y \tag{2.13}$$
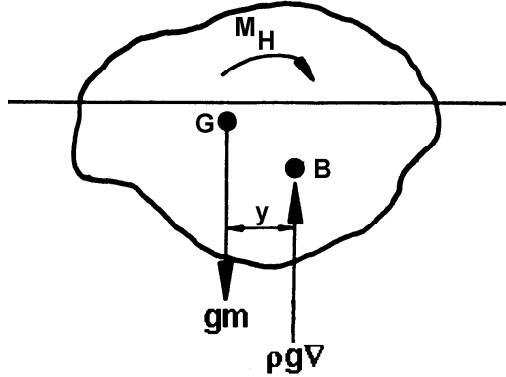
Figure 2.5: Heeling Moment

From this follows too that if no external moment acts on the structure, the lever arm y should be zero:

$$M_H = 0 \quad \text{which results in:} \quad y = 0 \tag{2.14}$$

This means that for any floating structure at rest, the center of buoyancy B and the center of gravity G will be situated on the same vertical line. If this is not so, the structure will heel or trim until they do become vertically aligned. This means too that the longitudinal position of the center of gravity can be found easily from the longitudinal position of the center of buoyancy, which can be derived from the under water geometry of the structure.

2.3.3   Shifting Masses and Volumes

Static stability problems are mainly related to an addition, a removal or a shift of masses and/or volumes (of displacement). The principal effects of these actions are a shift of the total center of gravity, G, and/or of the center of buoyancy, B. These effects will be treated here first.

Consider a structure with a mass m. This mass includes a mass p, placed somewhere on the structure. When this mass, p, will be shifted now over a certain distance, c, as shown in figure 2.6, the original overall center of gravity G_0 will be shifted to G_1 - parallel to this displacement - over a distance equal to:

$$\boxed{\left| \overline{G_0 G_1} = \frac{p \cdot c}{m} \right|} \tag{2.15}$$

This can be seen easily by writing the first moments of the masses with respect to the x- and y-axes, respectively:

$$
\begin{aligned}
m \cdot x_{G_1} &= m \cdot x_{G_0} + p \cdot (x_{p_1} - x_{p_0}) \\
m \cdot y_{G_1} &= m \cdot y_{G_0} + p \cdot (y_{p_1} - y_{p_0}) \\
new &= old + change
\end{aligned}
\tag{2.16}
$$

Then, the shift of the center of gravity of the structure from G_0 to G_1 is given by:
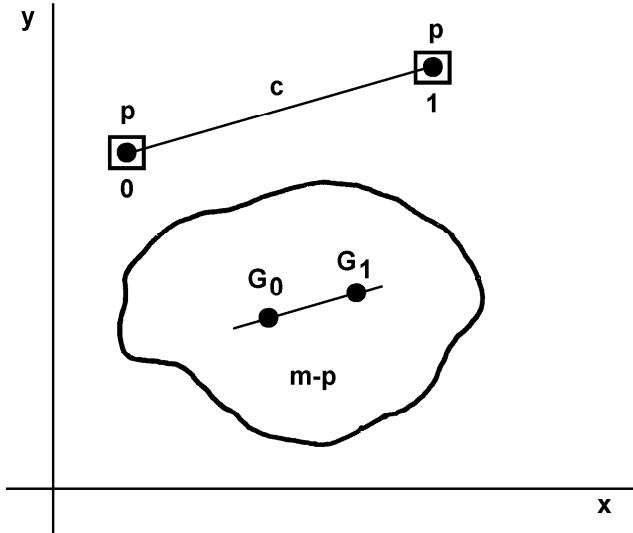
Figure 2.6: Shifting Mass on a Structure

$$x_{G_1} - x_{G_0} = \frac{p \cdot (x_{p_1} - x_{p_0})}{m}$$

$$y_{G_1} - y_{G_0} = \frac{p \cdot (y_{p_1} - y_{p_0})}{m} \tag{2.17}$$

Combining these two equations provides equation 2.15 above.
From these two equations follows too that:

$$\frac{x_{G_1} - x_{G_0}}{y_{G_1} - y_{G_0}} = \frac{x_{p_1} - x_{p_0}}{y_{p_1} - y_{p_0}} \tag{2.18}$$

which means that the shift of G_0 to G_1 will be **parallel** to the shift of the mass p.

In case of a freely suspended mass, p, (cargo hanging in a crane of a ship is a good example) this mass p should be considered as being concentrated at the suspension point of the crane hoisting rope. This becomes the case immediately after hoisting the cargo (assuming that the suspended cargo is not horizontally restrained in any way). The vertical elevation of the cargo above or beneath the deck or a horizontal displacement of the mass by a changed angle of heel of the ship is of no importance at all on the ship's center of gravity. At each angle of heel, the cargo acts as a vertical force acting downwards at the suspension point in the crane.

One can also discover that the center of buoyancy shifts parallel to a line through the centers of the volumes of the emerged and the immersed water displacement wedges when a floating body heels by an external moment only. The volume of the emerged wedge, in fact, has been shifted to the immersed wedge; see figure 2.7.

Because these two volumes are equal, two succeeding water planes with a small mutual difference in angle of heel intersect each other on a line with respect to which the first moments of volume of the two wedges are zero. This is a line through the center of the water plane. This means that the structure heels and/or trims about a line through the center of the water plane, the **center of floatation**. In case of a heeling ship (with symmetric water planes) this is a line at half the breadth of the water plane.
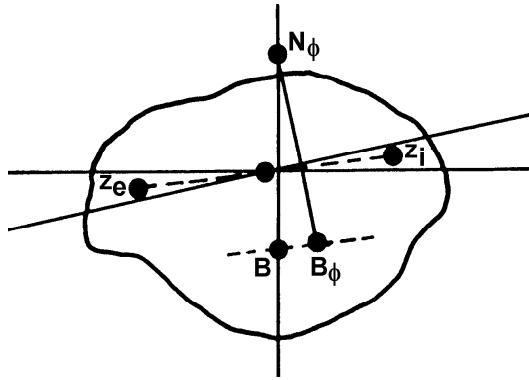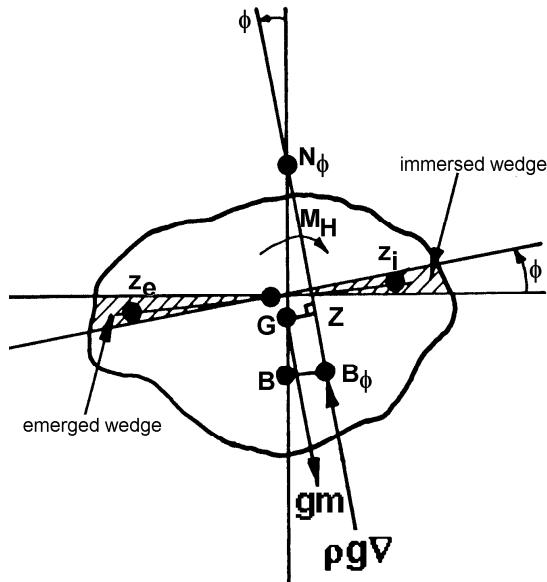
Figure 2.7: Shifting Buoyancy of a Structure

2.3.4   Righting Moments

A structure is floating at rest. Because of the rotational equilibrium, the center of gravity, G, is positioned on a vertical line through the center of buoyancy, B. If one adds an (external) heeling moment M_H to this structure, it will heel with an angle ϕ; see figure 2.8.

Figure 2.8: Rotational Equilibrium at an Angle of Heel ϕ

As a result of this heeling, the shape of the under water part of the structure will change; the center of buoyancy shifts from B to B_ϕ on a line parallel to the line through the centers of the emerged and immersed wedges $\overline{z_e z_i}$. An equilibrium will be achieved when the righting stability moment M_S equals the (external) heeling moment M_H:

$$M_S = M_H \tag{2.19}$$

in which the righting stability moment, M_S, is defined by:

$$M_S = \rho g \nabla \cdot \overline{GZ} \tag{2.20}$$

The righting stability lever arm , $\overline{GZ}$, can be written as:

$$\overline{GZ} = \overline{GN_\phi} \cdot \sin\phi \tag{2.21}$$

With this, the righting stability moment, M_S, becomes:

$$\boxed{M_S = \rho g \nabla \cdot \overline{GN_\phi} \cdot \sin\phi} \tag{2.22}$$

The so-called **metacenter,** N_ϕ, is the point of intersection of the lines through the vertical buoyant forces at a zero angle of heel and at an angle of heel, ϕ. The position of this metacenter N_ϕ depends on the new position of the center of buoyancy, B_ϕ; so on the shape of the structure at and near its water plane. This zone is sometimes referred to as the "zone between water and wind". The angle of heel ϕ and the shape of the emerged and immersed wedges control the shift of the center of buoyancy from B to B_ϕ and thereby also the position of N_ϕ.

2.3.5 Metacenter

This metacenter, N_ϕ, will be explained here in detail for the case of a rectangular barge. When using this barge - with length L, breadth B and draft T - the volume of displacement, ∇, and the center of buoyancy, B, can be determined easily. Then, the emerged and immersed wedges in the cross sections are bounded by vertical lines so that these wedges are right angle triangles and the position of its centroids can be calculated easily too.

The barge is floating in an upright even keel condition. An external heeling moment, M_H, causes the pontoon to heel to a relatively large angle, ϕ. The position of the metacenter N_ϕ can be calculated easily in such a special case; see figure 2.9.
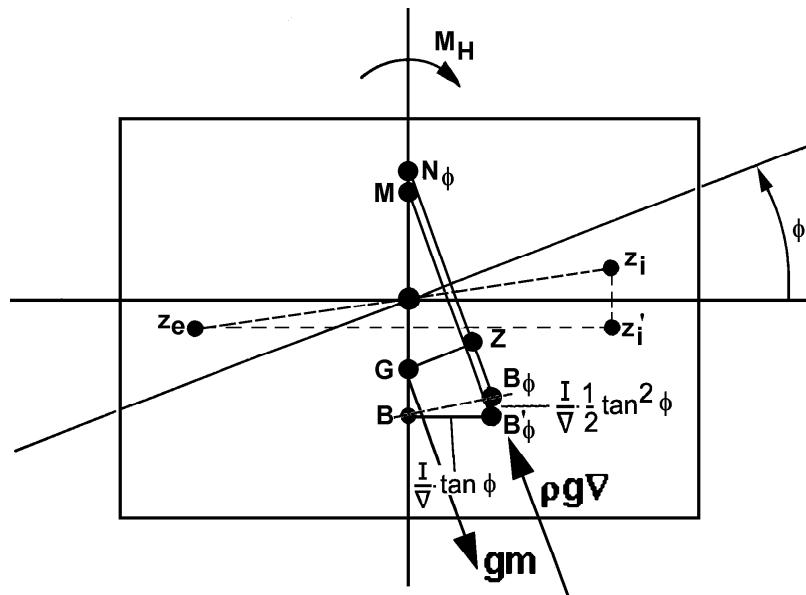
Figure 2.9: Rectangular Barge Stability

The shift of z_e of the emerged wedge to z_i of the immersed wedge can be split in two parts:

1. A **horizontal** shift $\overline{z_e z_i'}$.
   This horizontal shift causes a horizontal displacement of the center of buoyancy from B to B_ϕ':

$$\overline{BB_\phi'} = \overline{BM} \cdot \tan\phi \tag{2.23}$$

and the vertical buoyancy force, $\rho g \nabla$, intersects the vertical buoyancy force at $\phi = 0°$ at the **initial metacenter** M.
The first moment of volumes with respect to the middle line plane of the barge in the heeled condition is given by:

$$\{LBT\} \cdot \{\overline{BM} \tan\phi\} = \{LBT\} \cdot \{0\} + 2 \cdot \left\{ L\frac{1}{2}\frac{B}{2}\frac{B}{2} \tan\phi \right\} \cdot \left\{ \frac{2}{3}\frac{B}{2} \right\}$$
$$new \qquad = \qquad old \quad + \qquad change \tag{2.24}$$

so that:

$$\overline{BM} = \frac{\frac{1}{12} \cdot L \cdot B^3}{L \cdot B \cdot T} \tag{2.25}$$

or expressed in terms of the moment of inertia (second moment of areas) of the water plane, I_T, and the displacement volume of the barge ∇:

$$\boxed{\overline{BM} = \frac{I_T}{\nabla}} \tag{2.26}$$

2. A **vertical** shift $\overline{z_i' z_i}$.
   This vertical shift causes a vertical displacement of the center of buoyancy from B_ϕ' to B_ϕ:

$$\overline{B_\phi' B_\phi} = \overline{MN_\phi} \tag{2.27}$$

and the vertical buoyancy force, $\rho g \nabla$, intersects the vertical buoyancy force at $\phi = 0°$ at the **metacenter** N_ϕ.
The first moment of volumes with respect to a plane parallel to the not heeled water plane through the center of buoyancy B of the barge in the not heeled condition is given by:

$$\{LBT\} \cdot \{\overline{MN_\phi}\} = \{LBT\} \cdot \{0\} + 2 \cdot \left\{ L\frac{1}{2}\frac{B}{2}\frac{B}{2} \tan\phi \right\} \cdot \left\{ \frac{1}{3} \cdot \frac{B}{2} \cdot \tan\phi \right\}$$
$$new \qquad = \qquad old \quad + \qquad change \tag{2.28}$$

so that:

$$\overline{MN_\phi} = \frac{\frac{1}{12} \cdot L \cdot B^3}{L \cdot B \cdot T} \cdot \frac{1}{2} \tan^2\phi \tag{2.29}$$

or again expressed in terms of the moment of inertia of the water plane, I_T, the displacement volume of the barge ∇ and the angle of heel ϕ:

$$\boxed{\overline{MN_\phi} = \frac{I_T}{\nabla} \cdot \frac{1}{2} \tan^2\phi} \tag{2.30}$$

Now the position of the metacenter N_ϕ follows from a superposition of equations 2.26 and 2.30:

$$\overline{BN_\phi} = \overline{BM} + \overline{MN_\phi}$$
$$= \frac{I_T}{\nabla} \cdot \left(1 + \frac{1}{2}\tan^2\phi\right) \tag{2.31}$$

or:

$$\boxed{\overline{BN_\phi} = \overline{BM} \cdot \left(1 + \frac{1}{2}\tan^2\phi\right)} \tag{2.32}$$

The term $\overline{BM} \cdot 1$ represents the effect of the horizontal part of the shift of z_e to z_i and the term $\overline{BM} \cdot \frac{1}{2}\tan^2\phi$ represents the effect of the vertical part of this shift. Note that the angle of heel, ϕ, has no effect on M; but it has effect on N_ϕ.

2.3.6   Scribanti Formula
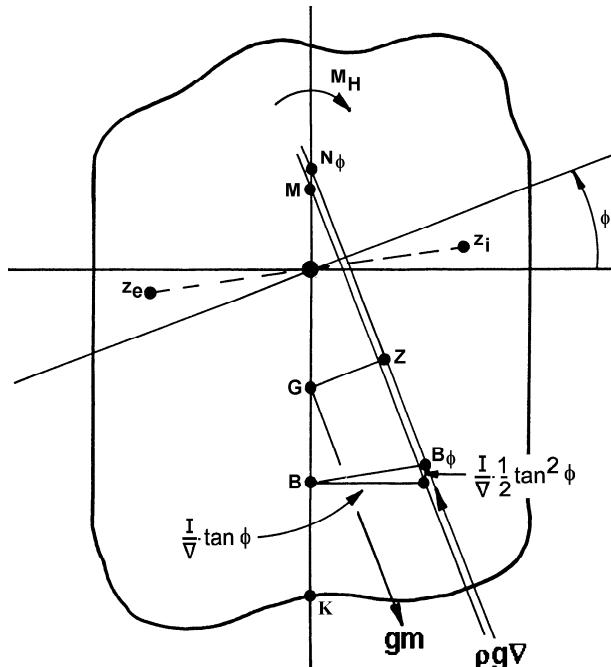
Figure 2.10: Wall Sided Structure

A floating structure is said to be **wall-sided** if, for the angles of heel to be considered, those portions of the hull covered or uncovered by the changing water plane are vertical when the structure is floating upright; see figure 2.10. The wedges in the cross sections are bounded by vertical lines - as is the case for the barge - so that the emerged and immersed wedges are right angle symmetrical triangles and the position of the metacenter N_ϕ can be calculated easily in such a special case.

It can be found that - regardless the under-water geometry of a structure - equation 2.30 is valid for **all wall-sided structures**:

$$\boxed{\overline{BN_\phi} = \frac{I_T}{\nabla} \cdot (1 + \frac{1}{2}\tan^2\phi)} \quad \textbf{Scribanti Formula} \tag{2.33}$$

in which I_T is the transverse moment of inertia (second moment of areas) of the not heeled water plane about the axis of inclination for both half water planes.

This is a fairly good approximation for ships that have vertical sides over a great part of the length and which are not so far heeled that the deck enters the water or the bottom comes above the water level.

At **small angles of heel** (up to about 10 degrees), the effect of the vertical shift of the center of buoyancy, $\overline{B'_\phi B_\phi} = \overline{MN_\phi}$, can be ignored. This can be seen in the Scribanti formula too, because in that case $\frac{1}{2}\tan^2\phi$ is very small compared to 1.0. The work line of the vertical buoyancy force, $\rho g \nabla$, intersects the work line of the vertical buoyancy force for $\phi = 0°$ at the initial metacenter, M, which location is defined by equation 2.26, useful for $\phi < \pm 10°$. Up to angles of heel of about 10 degrees, this is a fairly good approximation of the metacenter of the ships that are almost wall-sided at the "zone between water and wind" over a relatively large part of the length. Sailing yachts for instance, do not fulfil this requirement.

At **larger angles of heel**, the effect of the vertical shift of the center of buoyancy must be taken into account. The work line of the vertical buoyancy force, $\rho g \nabla$, intersects the work line of the vertical buoyancy force for $\phi = 0°$ at the metacenter, N_ϕ, which location is defined by equation 2.32, useful for $\phi > \pm 10°$. Use of this formula yields sufficiently accurate results for "non-Scribanti" ships until heel angles of heel of about 20 to 25 degrees. Keep in mind that this formula is not longer valid when the angle of heel gets so large that the water plane changes rapidly. This is the case when the bilge or chine (the "corner" where the sides of a ship meet its bottom) comes out of the water or the deck enters the water, for example. This possibility always has to be checked, when carrying out stability calculations!

It has been shown above that the metacenter is defined by the intersection of lines through the vertical buoyant forces at a heel angle ϕ and a heel angle $\phi + \Delta\phi$. Depending on the magnitude of ϕ and the increment $\Delta\phi$, two different metacenter definitions have been distinguished here, as tabled below.

metacenter point	symbol	ϕ	$\Delta\phi$
initial metacenter	M	0	very small
metacenter	N_ϕ	0	larger

Note that - for symmetrical under water forms like ships - both the metacenters M and N_ϕ are situated in the middle line plane ($\phi = 0$).

The stability lever arm $\overline{GZ} = \overline{GN_\phi} \cdot \sin\phi$ is determined by the hydrostatic properties of the submerged structure (form and heel dependent) and the position of the center of gravity of this structure (mass distribution dependent). This is the reason why the following expression for $\overline{GN_\phi}$ has been introduced:

$$\boxed{\overline{GN_\phi} = \overline{KB} + \overline{BN_\phi} - \overline{KG}} \tag{2.34}$$

Here, K is the keel point of the structure; see figure 2.10.

The magnitude of $\overline{KB}$ follows from the under water geometry of the structure and the magnitude of $\overline{KG}$ follows from the mass distribution of the structure.

If - within the range of considered angles of heel - the shape of the water plane does not change very much (wall-sided structure), a substitution of equation 2.32 in equation 2.34 results in:

$$\overline{GN_\phi} \;=\; \overline{KB} + \overline{BM} \cdot \left(1 + \frac{1}{2}\tan^2\phi\right) - \overline{KG}$$

$$=\; \overline{GM} + \frac{1}{2}\overline{BM} \cdot \tan^2\phi \tag{2.35}$$

For small angles of heel, the stability lever arm becomes $\overline{GZ} = \overline{GM}\cdot\sin\phi$ and $\overline{GM}$ becomes:

$$\boxed{\overline{GM} = \overline{KB} + \overline{BM} - \overline{KG}} \tag{2.36}$$

Submerged Structures
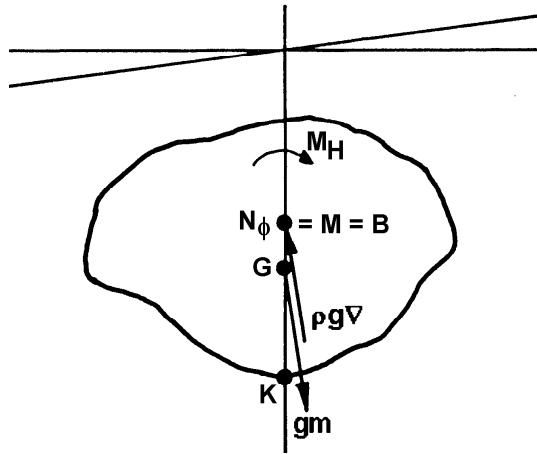
Figure 2.11: Submerged Floating Structure

Fully submerged structures, such as tunnel segments during installation or submarines (see figure 2.11), have no water plane. The definitions of $\overline{BM}$ and $\overline{BN_\phi}$ show that these values are zero, which means that the metacenter coincides with the center of buoyancy. In this case the previous equations reduce to:

$$\boxed{\overline{GN_\phi} = \overline{GM} = \overline{KB} - \overline{KG}} \qquad \text{(for fully submerged bodies only)} \tag{2.37}$$

2.3.7 Stability Curve

If a floating structure is brought under a certain angle of heel ϕ, see figure 2.12, then the righting stability moment is given by:

$$\begin{aligned}
M_S \;&=\; \rho g \nabla \cdot \overline{GZ} \\
&=\; \rho g \nabla \cdot \overline{GN_\phi} \cdot \sin\phi \\
&=\; \rho g \nabla \cdot \left\{\overline{GM} + \overline{MN_\phi}\right\} \cdot \sin\phi
\end{aligned} \tag{2.38}$$

In these relations:

$$\boxed{\overline{GZ} = \overline{GN_\phi} \cdot \sin\phi = \left\{\overline{GM} + \overline{MN_\phi}\right\} \cdot \sin\phi} \qquad \text{(stability lever arm)} \tag{2.39}$$
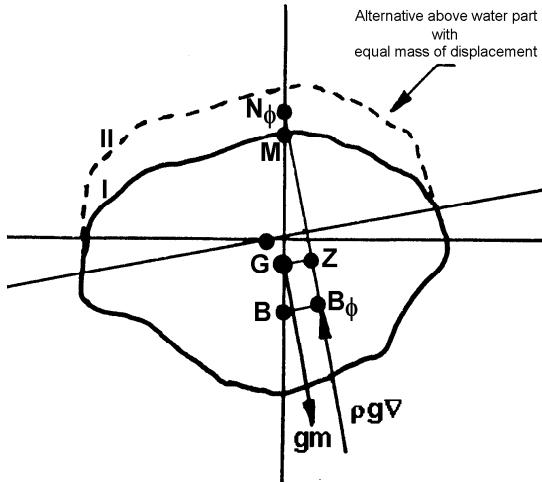
Figure 2.12: Stability Lever Arm

The value $\overline{GZ}$ determines the magnitude of the stability moment.

For practical applications it is very convenient to present the stability in the form of righting moments or lever arms about the center of gravity G, while the floating structure is heeled at a certain displacement,ϕ. This is then expressed as a function of ϕ. Such a function will generally look something like figure 2.13 and is known as the **static stability curve** or the **GZ-curve**.
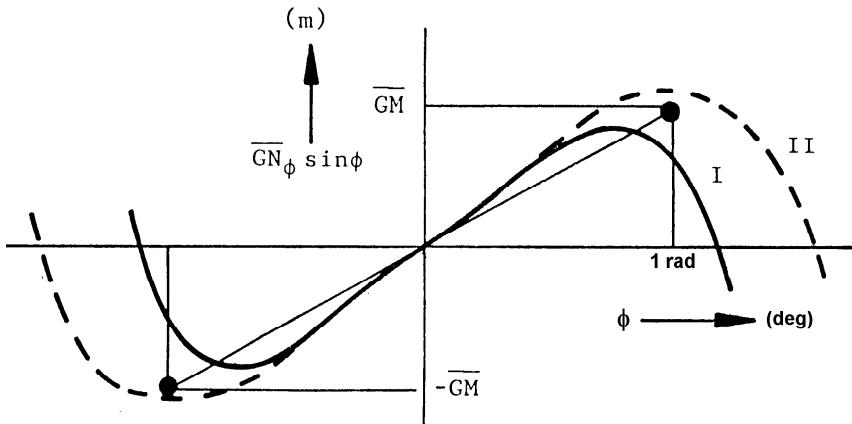
Figure 2.13: Static Stability Curves

Because the stability lever arm is strongly dependent on the angle of heel, ϕ, a graph of $\overline{GZ}$, as given in figure 2.13 is very suitable for judging the stability. For an arbitrarily (non symmetric) floating structure form, this curve will not be symmetrical with respect to $\phi = 0$, by the way.

For symmetric forms like ships however, the curve of static stability will be symmetric with respect to $\phi = 0$. In that case, only the right half of this curve will be presented as in figure 2.14.

The heel angle at point A in this figure, at which the second derivative of the curve changes sign, is roughly the angle at which the increase of stability due to side wall effects (Scribanti
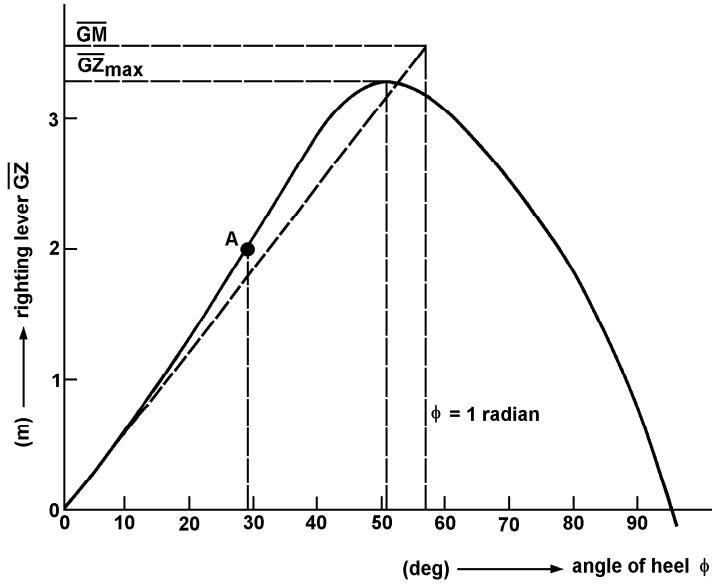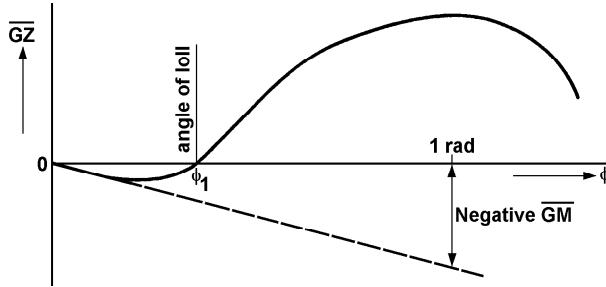
Figure 2.14: Ship Static Stability Curve

formula) starts to be counteracted by the fact that the deck enters the water or the bilge comes above the water.

Figure 2.15 shows the static stability curve when the initial metacentric height, $\overline{GM}$, is negative while $\overline{GZ}$ becomes positive at some reasonable angle of heel ϕ_1, the so-called **angle of loll**.

Figure 2.15: Static Stability Curve with a Negative $\overline{GM}$

If the floating structure is momentarily at some angle of heel less than ϕ_1, the moment acting on the structure due to $\overline{GZ}$ tends to increase the heel. If the angle is greater than ϕ_1, the moment tends to reduce the heel. Thus the angle ϕ_1 is a position of stable equilibrium. Unfortunately, since the $\overline{GZ}$ curve is symmetrical about the origin, as ϕ_1 is decreased, the floating structure eventually passes through the upright condition and will then suddenly lurch over towards the angle $-\phi_1$ on the opposite side and overshoot this value (because of dynamic effects) before reaching a steady state. This causes an unpleasant rolling motion, which is often the only direct indication that the heel to one side is due to a negative $\overline{GM}$ rather than a positive heeling moment acting on the structure.

Characteristics of Stability Curve

Some important characteristics of the static stability curve can be summarized here:

1. **Slope at The Origin**
   For small angles of heel, the righting lever arm is proportional to the curve slope and the metacenter is effectively a fixed point. It follows, that the tangent to the $\overline{GZ}$ curve at the origin represents the metacentric height $\overline{GM}$. This can be shown easily for the case of a wall-sided structure:

$$
\begin{aligned}
\frac{d}{d\phi}\left\{\overline{GZ}\right\} &= \frac{d}{d\phi}\left\{\overline{GN_\phi}\cdot\sin\phi\right\} \\
&= \frac{d}{d\phi}\left\{\left(\overline{GM}+\frac{1}{2}\overline{BM}\cdot\tan^2\phi\right)\cdot\sin\phi\right\}
\end{aligned}
\qquad (2.40)
$$

   This derivative becomes $\overline{GM}$ for zero heel. This means that the initial metacentric height $\overline{GM}$ can be of great importance for the further form of the curve, especially at smaller angles of heel, and for the area under the curve (see item 5 below).

2. **Maximum $\overline{GZ}$ Value**
   The maximum $\overline{GZ}$ value is rules the largest steady heeling moment that the floating structure can resist without capsizing. Its value and the angle at which it occurs are both important. The shape of the above-water part of the floating structure is of great importance for the maximum attainable value of the stability lever arm.

3. **Range of Stability**
   At some angle of heel (sometimes even greater than 90 degrees) the $\overline{GZ}$ value decreases again to zero and even becomes negative for larger inclinations. This angle is known as the **angle of vanishing stability**. The range of angles for which $\overline{GZ}$ is positive is known as the **range of stability**. This range is of great importance for the maximum attainable area under the stability curve and thereby also on the maximum potential energy that the structure can absorb via a roll motion. The shape of the above-water part has a large influence on the angle of vanishing stability; compare curves I and II in figures 2.12 and 2.13. For angles within the range of stability, a floating structure will return to the upright state when the heeling moment is removed.

4. **Angle of Deck Edge Immersion**
   For most floating structures, there is a point of inflection in the stability curve, corresponding roughly to the angle at which the deck edge becomes immersed. This point is not so much of interest in its own right as in the fact that it provides guidance to the designer upon the possible effect of certain design changes on stability. The shape of the above water part of the structure can have a large influence on its static stability. More or less the same statement can be made when the bilge or the bottom chine emerges, because of the decrease of the breadth of the water line. Keep in mind that for wall-sided structures, when the deck enters the water or the bottom chine comes above the water level, the immersed and emerged wedges are no longer nice triangles; calculations become much more cumbersome!

5. **Area Under The Static Stability Curve**

An important parameter when judging the stability properties of a structure floating upright is the work that has to be done to reach a chosen heel angle, ϕ^*:

$$P_{\phi^*} = \int_0^{\phi^*} M_S \cdot d\phi$$

$$= \rho g \nabla \cdot \int_0^{\phi^*} \overline{GN_\phi} \cdot \sin\phi \cdot d\phi \qquad (2.41)$$

This means that the area under the static stability curve is an important quantity for the evaluation of the stability properties. It represents the ability of the floating structure to absorb roll energy imparted to it by winds, waves or any other external effect.

2.3.8 Eccentric Loading

When a load is added at an arbitrarily place on a floating structure, its static response can be split into two components: It will sink deeper parallel to the original water plane and it will rotate (heel and/or trim) as well.

The parallel sinkage is caused by an increase of the total mass of the structure which requires a corresponding increase in displacement.

Heel or trim after a parallel sinkage will be caused by the generation of a moment. This moment is caused by a shift of the center of gravity and of the center of buoyancy. Both, they have been displaced from their originally vertical colinear positions.

Now, suppose a floating structure initially has a mass m, a displacement volume ∇_0, a center of gravity G_0 and a center of buoyancy B_0, as given in figure 2.16. Then a mass p, placed on this structure, will result in a new volume of displacement $\nabla = \nabla_0 + \Delta\nabla_0$, a new center of gravity G and a new center of buoyancy B.

No moment will be generated when the centers of gravity and buoyancy shift horizontally over equal distances. Using the first moment of masses, it can be seen that this is true whenever the mass p has been placed above, at or under the center of the added displacement $\Delta\nabla_0$ caused by parallel sinkage.
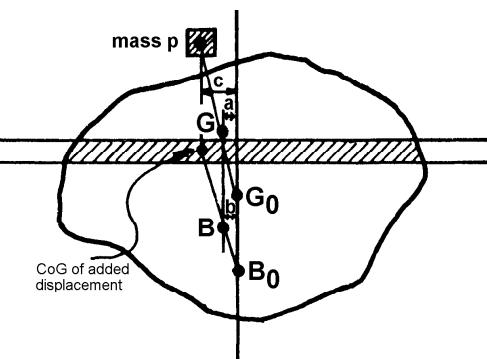
Figure 2.16: Parallel Sinkage

The first moments of the masses of the structure and the masses of displacement are defined here with respect to a line through G_0 and B_0:

$$
\begin{aligned}
\{m + p\} \cdot a &= \{m\} \cdot 0 + \{p\} \cdot c \\
\{\rho \nabla_0 + \rho \cdot \Delta \nabla_0\} \cdot b &= \{\rho \nabla_0\} \cdot 0 + \{\rho \cdot \Delta \nabla_0\} \cdot c \\
new &= old \quad + \quad change
\end{aligned}
\tag{2.42}
$$

Because $p = \rho \cdot \Delta \nabla_0$, it follows that $a = b$. This means that the new center of buoyancy B and the new center of gravity G are situated on one vertical line; no additional heeling moment remains.

The equilibrium after placing a load at an arbitrarily place on the structure, can be determined in two steps:

1. Place the mass p in the required horizontal plane vertically above or under the increased volume due to parallel sinkage, ΔT_0, of the structure. When the water plane does not change very much during this draft increase, one can write:

$$
\boxed{\Delta T_0 = \frac{p}{\rho \cdot A_{WL}}}
$$

The center of this added displacement lies a distance $\Delta T_0/2$ directly above this original water plane. The center of buoyancy B_0 shifts to B because of the added
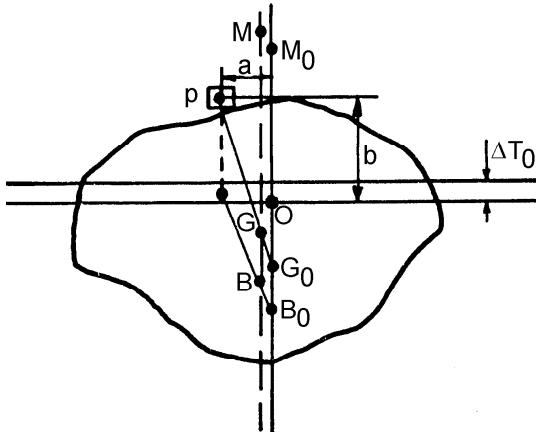
Figure 2.17: Load Above Waterline Centre

volume of displacement $\Delta \nabla_0 = p/\rho = \Delta T_0 \cdot A_{WL}$. The center of gravity shifts from G_0 to G because of the increase of the mass of the structure with $p = \rho \cdot \Delta \nabla_0$. These two shifts can be calculated easily with the first moments of masses and volumes, especially when the shape of the water plane does not change very much during the draft increase ΔT_0:

$$
\begin{aligned}
\text{horizontal part of } \overline{G_0 G} &= \frac{a \cdot m}{m + p} \\
\text{horizontal part of } \overline{B_0 B} &= \frac{a \cdot \nabla_0}{\nabla_0 + \Delta \nabla_0} = \frac{a \cdot m}{m + p}
\end{aligned}
\tag{2.43}
$$

See figure 2.17 for the meaning of the symbols used here.

When the structure hull is symmetric with respect to a plane through the points G_0, B_0 and M_0, then the center of the water plane lies in that symmetry plane, too. Then, we can place p above both, the center of buoyancy and the center of gravity. Because $a = 0$, both the horizontal part of $\overline{G_0G}$ and the horizontal part of $\overline{B_0B}$ are zero. The metacenters are given by:

$$\overline{B_0M_0} = \frac{I_T}{\nabla_0} \qquad \text{and} \qquad \overline{BM} = \frac{I_T}{\nabla_0 + \Delta\nabla_0} \tag{2.44}$$

Finally, the vertical shifts of G_0 and B_0 are given by:

$$\text{vertical part of } \overline{G_0G} = \frac{\left(\overline{GO} + b\right) \cdot m}{m + p}$$

$$\text{vertical part of } \overline{B_0B} = \frac{\left(\overline{BO} + \Delta T_0/2\right) \cdot \nabla_0}{\nabla_0 + \Delta\nabla_0} = \frac{\left(\overline{BO} + \Delta T_0/2\right) \cdot m}{m + p} \tag{2.45}$$

2. Replace the resulting moment, caused by a movement of the mass p horizontally over a distance c to its desired position, by a heeling moment M_H; see figure 2.18. The
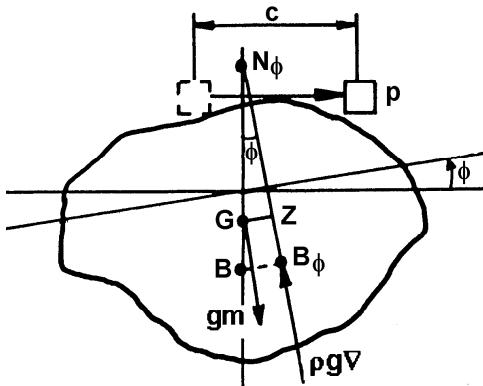
Figure 2.18: Shifting a Load

displacement mass, $\rho\nabla$, includes the mass p:

$$\nabla = \nabla_0 + \Delta\nabla_0 = \nabla_0 + \frac{p}{\rho} \tag{2.46}$$

The heeling moment M_H must be equal to the righting stability moment M_S:

$$M_H = M_S$$
$$g \cdot p \cdot c \cdot \cos\phi = g \cdot \rho\nabla \cdot \overline{GN_\phi} \cdot \sin\phi \tag{2.47}$$

The heel angle, ϕ, follows from this moment equilibrium:

$$\boxed{\phi = \arccos\left\{\frac{\rho\nabla \cdot \overline{GN_\phi} \cdot \sin\phi}{p \cdot c}\right\}} \tag{2.48}$$

If the static stability curve lever arms $\overline{GZ} = \overline{GN_\phi} \cdot \sin\phi$ are known as functions of ϕ, then ϕ can be determined iteratively.

For **wall-sided structures** one can substitute equation 2.35 in equation 2.48 and get:

$$\phi = \arccos\left\{\frac{\rho\nabla\cdot\left\{\overline{GM}+\frac{1}{2}\overline{BM}\cdot\tan^2\phi\right\}\cdot\sin\phi}{p\cdot c}\right\} \tag{2.49}$$

or using $\tan\phi$:

$$\frac{1}{2}\overline{BM}\cdot\tan^3\phi+\overline{GM}\cdot\tan\phi=\frac{p\cdot c}{\rho\nabla} \tag{2.50}$$

This third degree equation in $\tan\phi$ can be solved iteratively using the Regula-Falsi method by calculating the Left Hand Side (LHS) of the equation as a function of ϕ until a value equal to the value of the Right Hand Side (RHS) has been found.

For small angles of heel and when the shape of the water plane does not change very much, the expression for ϕ can be simplified to become:

$$\phi = \arctan\left\{\frac{p\cdot c}{\rho\nabla\cdot\overline{GM}}\right\} \tag{2.51}$$

so that ϕ can be found directly in this situation.

2.3.9　Inclining Experiment

Much of the data used in stability calculations depends only on the geometry of the structure. The total mass of the structure m follows from the displacement volume, ∇. The longitudinal position of the center of gravity, G, follows simply from the longitudinal position of the center of buoyancy, B, which can be determined from the under water geometry of the structure. The vertical position of the center of gravity must be known before the stability can be completely assessed for a given loading condition. Since the vertical position of the center of gravity, $\overline{KG}$, sometimes can be 10 times greater than the initial metacentric height $\overline{GM}$, $\overline{KG}$ must be known very accurately if the metacentric height is to be assessed with reasonable accuracy. $\overline{KG}$ can be calculated for a variety of loading conditions, provided it is accurately known for one precisely specified loading condition.

The displacement volume, ∇ can be calculated, given the geometry of the structure, in combination with measured drafts fore and aft (at both ends) in the upright condition ($\phi = \phi_0 \approx 0°$). With this displacement and the measured angle of heel ($\phi = \phi_1$) after shifting a known mass p on the structure over a distance c, the vertical position of the center of gravity can be found easily by writing equation 2.51 in another form:

$$\overline{GM} = \frac{p\cdot c}{\rho\nabla\cdot\tan\left(\phi_1-\phi_0\right)} \qquad \text{with: } \phi_0 \ll \phi_1 \text{ and } \phi_1 < \pm10° \tag{2.52}$$

The known underwater geometry of the structure and this "measured" $\overline{GM}$ value yields the vertical position of the center of gravity G.

An experiment to determine the metacentric height in this way is called an **inclining experiment**. The purposes of this experiment are to determine the displacement, ∇, and the position of the center of gravity of the structure under a precisely known set of conditions. It is usually carried out when construction is being completed (afloat) before leaving the construction yard. An additional inclining experiment may be carried out following an extensive modernization or a major refit. Keep in mind that ∇ and G have to be corrected when the mass p is removed from the structure, again.

2.3.10 Free Surface Correction

Free surfaces of liquids inside a floating structure can have a large influence on its static stability; they reduce the righting moment or stability lever arm.
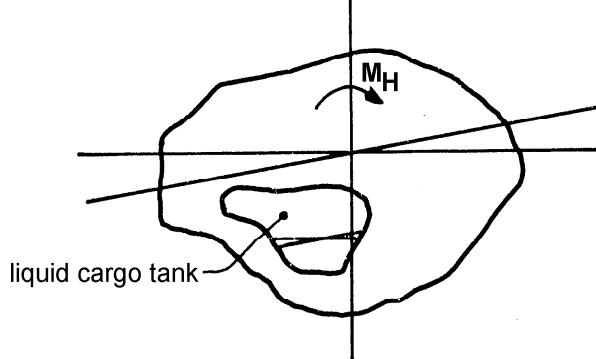
Figure 2.19: Floating Structure with a Tank Partially Filled with Liquid

When the structure in figure 2.19 heels as a result of an external moment M_H, the surface of the fluid in the tank remains horizontal. This means that this free surface heels relative to the structure itself, so that the center of gravity of the structure (including liquid) shifts. This shift is analogous to the principle of the shift of the center of buoyancy due to the emerged and immersed wedges, as discussed above. Of course, the under water geometry of the entire structure and the boundaries of the wedges at the water plane as well as in the tank play a role. They determine, together with the angle of heel, the amount by which the centers of buoyancy and of gravity now shift.

In case of a vertical wedge boundary, (a wall-sided tank) as given in figure 2.20, this shift can be calculated easily with the first moment of volumes with triangular cross sections. In this figure, ρ' is the density of the liquid in the tank, v is the volume of the liquid in the
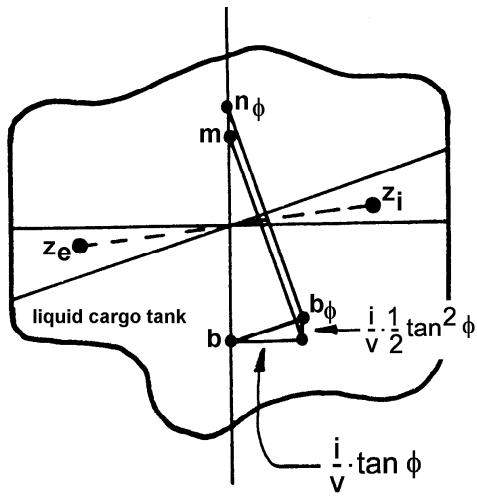
Figure 2.20: Effect of a Liquid Free Surface in a Wall Sided Tank

tank and i is the transverse moment of inertia (second moment of areas) of the surface of

the fluid in the tank ($\phi = 0$). The center of gravities are marked here by b and not by g, to avoid confusions with the acceleration of gravity.

The influence of the movement of the mass $\rho' v$ from b to b_ϕ on the position of the overall center of buoyancy can also be determined using the first moment of volumes with triangular cross sections:

direction	shift of center of gravity of fluid	shift of center of gravity of total structure
horizontal	$\frac{i}{v} \cdot \tan \phi$	$\frac{\rho' i}{\rho \nabla} \cdot \tan \phi$
vertical	$\frac{i}{v} \cdot \frac{1}{2} \tan^2 \phi$	$\frac{\rho' i}{\rho \nabla} \cdot \frac{1}{2} \tan^2 \phi$

The amount of fluid in the tank, v, does not matters, only the transverse moment of inertia of the surface of the fluid in the tank, i, counts. This has been made more clear in figure 2.21.
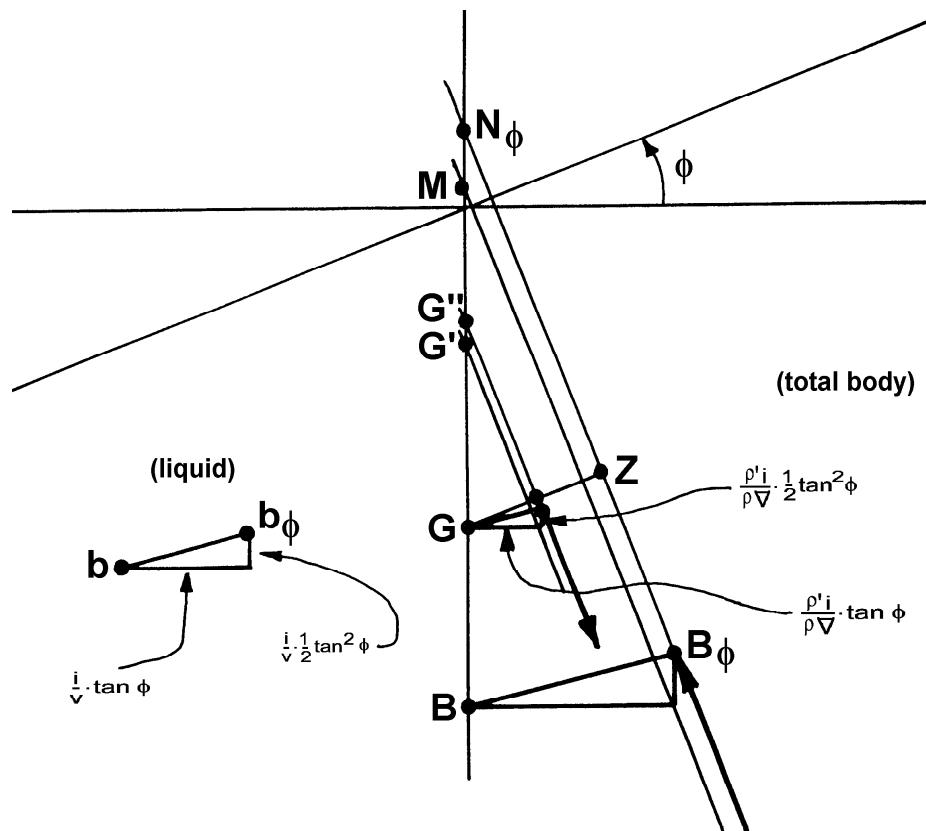
Figure 2.21: Metacentric Height Reduction Caused by Free Surfaces in Wall Sided Tanks

This means that the righting stability lever arm will be reduced by $\overline{GG''} \cdot \sin \phi$, with:

$$\overline{GG''} = \frac{\rho' i}{\rho \nabla} \cdot \left(1 + \frac{1}{2} \tan^2 \phi \right) \qquad (2.53)$$

The magnitude $\overline{GG''}$ is called the **free surface correction** or the **reduction of the metacentric height**.

For small angles of heel for which $\frac{1}{2}\tan^2\phi$ is small relative to 1.0, one can write for the reduction of the metacentric height:

$$\overline{GG''} \approx \overline{GG'} = \frac{\rho' i}{\rho \nabla} \tag{2.54}$$

For more free surfaces (more tanks) the reduction of the metacentric height becomes:

$$\boxed{\overline{GG''} = \frac{\sum \{\rho' i\}}{\rho \nabla} \cdot \left(1 + \frac{1}{2}\tan^2\phi\right)} \tag{2.55}$$
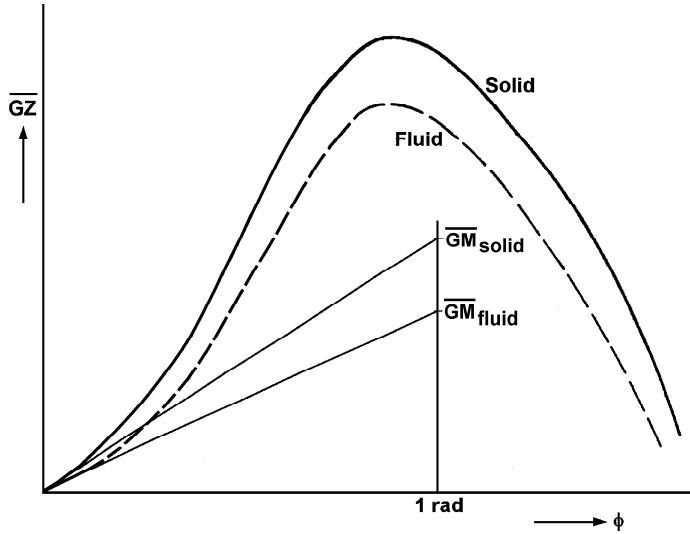
Figure 2.22: $\overline{GZ}$-Curve, Corrected for Free Surface

Note that the effect of the free surface on the stability lever arm (see figure 2.22) is independent of the position of the tank in the floating structure; the tank can be at any height in the structure and at any position in its length or breadth.

The effect is also independent of the amount of liquid in the tank, provided that the moment of inertia (second moment of areas) of the free surface remains substantially unchanged when inclined. The moment of inertia of the free surface of a tank which is almost empty or almost full can change significantly during an inclining experiment. This is why tanks which cannot be completely full or empty during an inclining experiment are specified to be half full.

It is common practice to treat the free surface effect as being equivalent to a virtual rise of the center of gravity of the structure. One should appreciate that this is merely a convention which has no factual basis in reality.

A similar free surface effect can arise from movements of granular cargo such as grain which is stowed in bulk. Here, however, there is no simple relation between the angle of inclination of the ship and the slope of the surface of the grain. At small angles of heel the grain is not likely to shift, so there is no influence on initial stability. When the heel

angle becomes great enough, a significant shift can take place very abruptly; its effect can be equally abrupt!

.

Chapter 3

CONSTANT POTENTIAL FLOW PHENOMENA

3.1   Introduction

This chapter introduces hydrodynamics by treating the simplest of flows: constant, incompressible, potential flows; time is therefore unimportant. These flows obey reasonably simplified laws of fluid mechanics and mathematics as will be explained in this chapter. In spite of its limitations, potential flow is widely used in fluid mechanics. It often gives at least a qualitative impression of flow phenomena. Discrepancies between real and idealized flows are often accommodated via experimentally determined coefficients.

The concepts introduced in this chapter will be extended and applied in later chapters for a wide variety of solutions including those involving waves. Indeed, potential theory can very easily be extended to time dependent flows as well. This chapter starts by defining a potential flow field and its properties in a very general way. The power of the method will become more obvious as it is applied to constant flow situations later in this chapter. Much of the information in this chapter may be well-known to the reader; it can be seen as a quick review. In any case, this chapter introduces the notation used in many of the remaining chapters as well.

3.2   Basis Flow Properties

All flows are treated here as being **non-viscous, incompressible, continuous and homogeneous.** There are no cavitation holes or gas bubbles in the fluid.

3.2.1   Continuity Condition

Consider first a differential element of fluid within a larger body of a compressible flow. This block has edges with dimensions dx by dy by dz oriented parallel to the axes of a right-handed (x, y, z)-axis system as shown in figure 3.1 (only the y-component of velocity is shown).
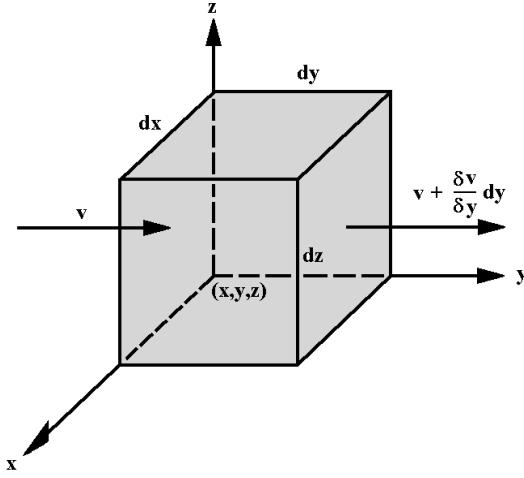
Figure 3.1: Basic Element for Continuity Definition

In the most general situation, the increase of mass per unit of time of the fluid with density ρ in this block is given by:

$$\frac{\partial m}{\partial t} = -\frac{\partial}{\partial t}\left(\rho \cdot dx\,dy\,dz\right) = -\frac{\partial \rho}{\partial t} \cdot dx\,dy\,dz \qquad (3.1)$$

The minus sign comes from the fact that if the mass transport increases across the block, then there will be a net loss of mass from within it.

The continuous and homogeneous flow will have a velocity, $\vec{V}$, defined in terms of velocity components, $u(x, y, z)$, $v(x, y, z)$, $w(x, y, z)$ along the three axes, respectively. This is here still a compressible flow, so the density of the fluid in the flow is a function of x, y and z; $\rho(x, y, z)$. Note that only a flow component perpendicular to a face of the block will cause a mass transport in (or out) through that face of the block.

Looking first along the x-axis, the mass flow through plane $dy\,dz$ during a unit of time dt <u>in-to</u> the block at x is:

$$m_{\text{in along } x\text{-axis}} = \rho \cdot u \cdot dy\,dz\,dt$$

and the mass flow through plane $dy\,dz$ during a unit of time dt <u>out-of</u> the block at $x + dx$ is:

$$m_{\text{out along } x\text{-axis}} = \left[\rho\,u + \frac{\partial\,(\rho\,u)}{\partial\,x} \cdot dx\right] \cdot dy\,dz\,dt$$

Then the net mass flow through the block per unit of time is the mass flow out per unit of time at $x + dx$ minus the mass flow in per unit of time at x:

$$\left(\frac{\partial m}{\partial t}\right)_{\text{along } x\text{-axis}} = \left[\rho\,u + \frac{\partial\,(\rho\,u)}{\partial\,x} \cdot dx\right] \cdot dy\,dz - \rho\,u \cdot dy\,dz \qquad (3.2)$$

$$= \frac{\partial\,(\rho\,u)}{\partial\,x} \cdot dx\,dy\,dz \qquad (3.3)$$

Similarly, along the y and z directions:

$$\left(\frac{\partial m}{\partial t}\right)_{\text{along } y\text{-axis}} = \left[\rho\,v + \frac{\partial\,(\rho\,v)}{\partial\,y}\cdot dy\right]\cdot dx\,dz - \rho\,v\cdot dx\,dz$$

$$= \frac{\partial\,(\rho\,v)}{\partial y}\cdot dx\,dy\,dz \tag{3.4}$$

$$\left(\frac{\partial m}{\partial t}\right)_{\text{along } z\text{-axis}} = \left[\rho\,w + \frac{\partial\,(\rho\,w)}{\partial\,z}\cdot dz\right]\cdot dx\,dy - \rho\,w\cdot dx\,dy$$

$$= \frac{\partial\,(\rho\,w)}{\partial\,z}\cdot dx\,dy\,dz \tag{3.5}$$

Combining equations 3.1 through 3.5 provides the **Continuity Equation**:

$$\frac{\partial\,m}{\partial\,t} = -\frac{\partial\rho}{\partial t}\cdot dx\,dy\,dz = \left\{\frac{\partial\,(\rho\,u)}{\partial\,x} + \frac{\partial\,(\rho v)}{\partial y} + \frac{\partial\,(\rho\,w)}{\partial\,z}\right\}\cdot dx\,dy\,dz \tag{3.6}$$

or:

$$\boxed{\frac{\partial\,\rho}{\partial\,t} + \frac{\partial\,(\rho\,u)}{\partial\,x} + \frac{\partial\,(\rho v)}{\partial y} + \frac{\partial\,(\rho\,w)}{\partial\,z} = 0} \tag{3.7}$$

In a more elaborate vector notation this equation becomes:

$$\frac{\partial\rho}{\partial t} + div\cdot\left(\rho\cdot\vec{V}\right) = 0 \qquad \text{or} \qquad \frac{\partial\rho}{\partial t} + \nabla\cdot\left(\rho\cdot\vec{V}\right) = 0 \tag{3.8}$$

In the above equation, div or ∇ (nabla) denotes the sum of the partial derivatives:

$$div = \nabla\;(\text{nabla}) = \frac{\partial}{\partial x} + \frac{\partial}{\partial y} + \frac{\partial}{\partial z} \tag{3.9}$$

Note that nabla will refer to the displacement volume of a floating body in chapter 2 and later on; this is an entirely different quantity!

Now, the fluid will be treated as incompressible; the density ρ is considered to be constant. This can be done in many cases in hydrodynamics. This allows equation 3.7 to be simplified by cancelling ρ:

$$\boxed{\frac{\partial\,u}{\partial\,x} + \frac{\partial\,v}{\partial\,y} + \frac{\partial\,w}{\partial\,z} = 0} \tag{3.10}$$

or in a more elaborate vector notation:

$$div\cdot\vec{V} = 0 \qquad \text{or} \qquad \nabla\cdot\vec{V} = 0 \tag{3.11}$$

If one is working with only two dimensions, then the third dimension above (usually z) can be neglected; all terms in that direction are set to zero.

It is left to the reader to verify that in a two-dimensional homogeneous incompressible flow the continuity condition in equation 3.10 can be written in polar coordinates (see figure 3.2) as:

$$\frac{1}{r}\left(\frac{\partial\,(r\cdot v_r)}{\partial\,r} - \frac{\partial\,v_\theta}{\partial\,\theta}\right) = 0 \qquad \text{or:} \qquad \boxed{\frac{v_r}{r} + \frac{\partial\,v_r}{\partial\,r} + \frac{1}{r}\cdot\frac{\partial\,v_\theta}{\partial\,\theta} = 0} \tag{3.12}$$
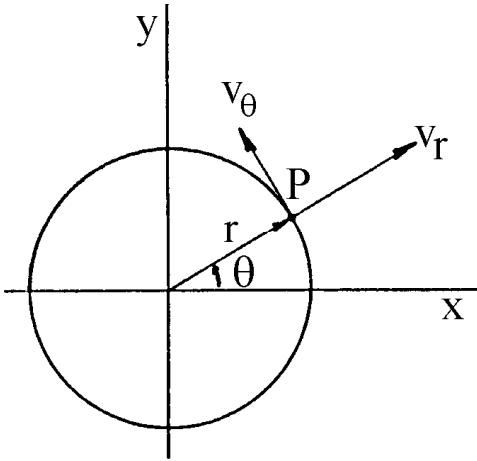
Figure 3.2: Rectangular and Polar Coordinates

Another very simple form of the continuity equation is:

$$Q = A \cdot V \tag{3.13}$$

in which Q is the volume flow rate (m^3/s), A is the cross section area perpendicular to the velocity (m^2) and V is the velocity component perpendicular to the area (m/s) averaged over the cross section area.

3.2.2 Deformation and Rotation

The stresses in the fluid will now be related to deformations and rotations of the fluid particle. The cube, considered before, will be deformed and rotated by forces on its sides. Mathematically, the velocity components $u(x, y, z, t)$, $v(x, y, z, t)$ and $w(x, y, z, t)$ can be expanded in a Taylor series. That series for $u(x, y, z, t)$, for example, would become:

$$u + \Delta u = u + \frac{\partial u}{\partial x} \cdot \Delta x + \frac{\partial u}{\partial y} \cdot \Delta y + \frac{\partial u}{\partial z} \cdot \Delta z + \frac{\partial u}{\partial t} \cdot \Delta t + ... \text{ higher order terms...} \tag{3.14}$$

The higher order terms can be ignored as $\Delta u \to 0$ and u can be cancelled in both sides of the equation. Tthen equation 3.14 reduces to:

$$du = \frac{\partial u}{\partial x} \cdot dx + \frac{\partial u}{\partial y} \cdot dy + \frac{\partial u}{\partial z} \cdot dz + \frac{\partial u}{\partial t} \cdot dt \tag{3.15}$$

which can - after ordering terms - be written as:

$$du = \frac{\partial u}{\partial x} \cdot dx \quad + \frac{1}{2}\left(\frac{\partial u}{\partial y} + \frac{\partial v}{\partial x}\right) \cdot dy + \frac{1}{2}\left(\frac{\partial u}{\partial y} - \frac{\partial v}{\partial x}\right) \cdot dy$$

$$+ \frac{1}{2}\left(\frac{\partial u}{\partial z} + \frac{\partial w}{\partial x}\right) \cdot dz + \frac{1}{2}\left(\frac{\partial u}{\partial z} - \frac{\partial w}{\partial x}\right) \cdot dz + \frac{\partial u}{\partial t} \cdot dt \tag{3.16}$$

$$= stretch \quad + \quad dilatation \quad + \quad rotation$$

$$+ \quad translation$$

For simplicity only two dimensions will be considered now, a cross section of the fluid particle in the (x, y)-plane as shown in figure 3.3. The velocity components in the other planes can be found in a similar way.
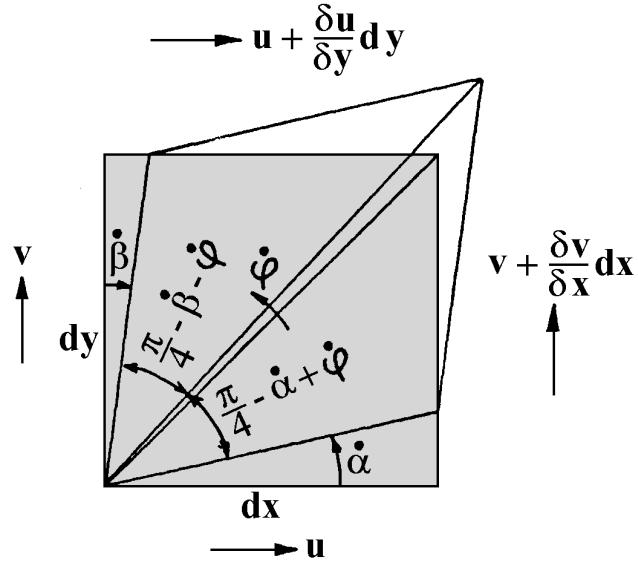
Figure 3.3: Deformation and Rotation

2-D Deformation

From figure 3.3 follows the **deformation**:

$$\frac{\partial v}{\partial x} = \tan \dot{\alpha} \approx \dot{\alpha} \qquad \text{and} \qquad \frac{\partial u}{\partial y} = \tan \dot{\beta} \approx \dot{\beta} \tag{3.17}$$

2-D Dillatation

The deformation velocity (or **dilatation**) becomes:

$$\boxed{\frac{\dot{\alpha} + \dot{\beta}}{2} = \frac{1}{2}\left(\frac{\partial v}{\partial x} + \frac{\partial u}{\partial y}\right)} \tag{3.18}$$

2-D Rotation

In case of a small square surface element $(dx = dy)$, the diagonal rotates over an angle:

$$\dot{\varphi} = \frac{1}{2}\left(\dot{\alpha} - \dot{\beta}\right) \qquad \text{because:} \qquad \frac{\pi}{4} - \dot{\alpha} + \dot{\varphi} = \frac{\pi}{4} - \dot{\beta} - \dot{\varphi} \tag{3.19}$$

Thus, the angular velocity (or **rotation**) of the diagonal is:

$$\boxed{\dot{\varphi} = \frac{1}{2}\left(\frac{\partial v}{\partial x} - \frac{\partial u}{\partial y}\right)} \tag{3.20}$$

which is zero by definition in potential theory, as will be treated in the next section.

3.3   Potential Flow Concepts

A velocity potential of a flow is simply a mathematical expression, which has the property that the velocity component in a point in the fluid in any chosen direction is simply the derivative of this potential function in that point to that chosen direction. This will be explained in more detail in the next sections.

3.3.1   Potentials

If u, v and w are velocity components along the x-, y- and z-axes respectively, the increase of the so-called potential value between two points A and B in the fluid - see figure 3.4 - is defined as:

$$
\begin{aligned}
\Delta\Phi_{A\to B} &= \int_A^B \vec{V} \cdot d\vec{s} = \int_A^B (u \cdot dx + v \cdot dy + w \cdot dz) \\
&= \int_A^B \left(\frac{\partial\Phi}{\partial x}dx + \frac{\partial\Phi}{\partial y}dy + \frac{\partial\Phi}{\partial z}dz \right) = \int_A^B d\Phi = \Phi\left(B\right) - \Phi\left(A\right) \quad (3.21)
\end{aligned}
$$

In fact, this follows from the definition of the potential value itself.
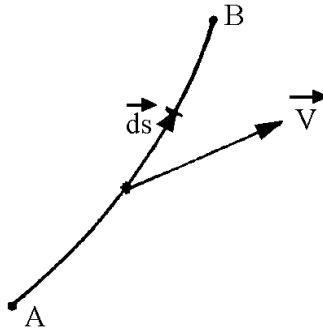
Figure 3.4: Definition of Velocity Potential

This means that the increase of the potential value from A to B is independent of the chosen integration route between those points.

Potential Lines

Equation 3.21 also means that potential lines are curves defined in such a way that:

$$\Phi = constant \quad (3.22)$$

Using the definitions above, this implies in 3-D rectangular coordinates that:

$$d\Phi = u \ dx + v \ dy + w \ dz \quad (3.23)$$

or in 2-D polar coordinates:

$$d\Phi = v_r \ dr + r \ v_\theta \ d\theta \quad (3.24)$$

Potential Function

Equation 3.23 includes a very convenient definition of the potential function: A **potential function,** Φ, associated with a potential flow field is a mathematical expression having the convenient property that at any point in the flow, the velocity component in any chosen direction is simply the derivative of this potential function in that chosen direction:

$$u = \frac{\partial \Phi}{\partial x} \qquad v = \frac{\partial \Phi}{\partial y} \qquad w = \frac{\partial \Phi}{\partial z} \qquad (3.25)$$

While potential functions can be defined (in theory) in any number of dimensions, it is easiest to understand them in a two-dimensional situation; this will be used here. In 2-D polar coordinates - see figure 3.2 - the potential functions are given by:

$$v_r = \frac{\partial \Phi}{\partial r} \qquad \text{and} \qquad v_\theta = \frac{1}{r} \cdot \frac{\partial \Phi}{\partial \theta} \qquad (3.26)$$

All potential theory solutions must fulfill the following two conditions:

1. **Laplace Equation**
   Applying the continuity condition (equation 3.10) to the velocities in equation 3.25 provides the **Laplace equation** for an incompressible fluid:

$$\frac{\partial^2 \Phi}{\partial x^2} + \frac{\partial^2 \Phi}{\partial y^2} + \frac{\partial^2 \Phi}{\partial z^2} = 0 \qquad \text{or:} \qquad \nabla^2 \Phi = 0 \qquad (3.27)$$

2. **Rotation Free**
   This condition - see also equations 3.16 and 3.20 - follows from the potential theory itself. One can write for the (x, y)-plane:

$$u = \frac{\partial \Phi}{\partial x} \qquad \text{so:} \qquad \frac{\partial u}{\partial y} = \frac{\partial}{\partial y}\left(\frac{\partial \Phi}{\partial x}\right) = \frac{\partial^2 \Phi}{\partial y \partial x}$$

$$v = \frac{\partial \Phi}{\partial y} \qquad \text{so:} \qquad \frac{\partial v}{\partial x} = \frac{\partial}{\partial x}\left(\frac{\partial \Phi}{\partial y}\right) = \frac{\partial^2 \Phi}{\partial x \partial y} \qquad (3.28)$$

Because:

$$\frac{\partial^2 \Phi}{\partial y \partial x} = \frac{\partial^2 \Phi}{\partial x \partial y} \qquad \text{one can write:} \qquad \frac{\partial v}{\partial x} - \frac{\partial u}{\partial y} = 0 \qquad (3.29)$$

This can be applied similarly to the other planes as well so that:

$$\frac{\partial v}{\partial x} - \frac{\partial u}{\partial y} = 0 \qquad \text{in the } (x, y)\text{-plane}$$

$$\frac{\partial w}{\partial y} - \frac{\partial v}{\partial z} = 0 \qquad \text{in the } (y, z)\text{-plane}$$

$$\frac{\partial u}{\partial z} - \frac{\partial w}{\partial x} = 0 \qquad \text{in the } (x, z)\text{-plane} \qquad (3.30)$$

or in 2-D polar coordinates:

$$\frac{v_\theta}{r} + \frac{\partial v_\theta}{\partial r} - \frac{1}{r} \cdot \frac{\partial v_r}{\partial \theta} = 0 \qquad (3.31)$$

In vector notation, the velocity can be written in component form in a rectangular coordinate system as:

$$\vec{V}(x,y,z) = u(x,y,z)\,\vec{x} + v(x,y,z)\,\vec{y} + w(x,y,z)\,\vec{z} \tag{3.32}$$

or in 2-D polar coordinates - see figure 3.2 with $\vec{x}$, $\vec{y}$, $\vec{e}_r$, and $\vec{e}_\theta$ as unit vectors - as:

$$\vec{V}(r,\theta) = v_r\,\vec{e}_r + v_\theta\,\vec{e}_\theta \tag{3.33}$$

Because $\partial v/\partial x$, $\partial u/\partial y$ and $\partial w/\partial z$ are the three rotation components in a Cartesian axes system, equations 3.30 mean that any potential fluid flow is free of rotation. This condition can be tested easily in a real flow with a free surface. Sprinkle some short wooden toothpicks on the flow. If these do not turn as they pass a body in this flow, then (that portion of) the flow is rotation-free. Of course, if these floats come very close to the body they will turn in the (viscous) boundary layer near the body; this potential flow condition is not fulfilled there.

3.3.2   Euler Equations

In 1755, **Leonard Euler** applied Newton's second law ($force = mass$ x $acceleration$) to **non-viscous and incompressible** fluids. Doing this in the x-direction for a fluid mass element dm - as given in figure 3.1 - yields:

$$dm \cdot \frac{Du}{Dt} = \rho \cdot dxdydz \cdot \frac{Du}{Dt} = -\frac{\partial p}{\partial x}dx \cdot dydz \tag{3.34}$$

so that the instationary Euler equation in the x-direction becomes:

$$
\begin{aligned}
\frac{Du}{Dt} &= \frac{\partial u}{\partial t} + \frac{\partial u}{\partial x}\frac{dx}{dt} + \frac{\partial u}{\partial y}\frac{dy}{dt} + \frac{\partial u}{\partial z}\frac{dz}{dt} \\[1mm]
&= \frac{\partial u}{\partial t} + u\frac{\partial u}{\partial x} + v\frac{\partial u}{\partial y} + w\frac{\partial u}{\partial z} \\[1mm]
&= -\frac{1}{\rho} \cdot \frac{\partial p}{\partial x} \qquad \text{with: } u = u(x,y,z,t)
\end{aligned}
\tag{3.35}
$$

In the same way, one can write the instationary Euler equations in the other two directions:

$$
\begin{aligned}
\frac{Dv}{Dt} &= \frac{\partial v}{\partial t} + \frac{\partial v}{\partial x}\frac{dx}{dt} + \frac{\partial v}{\partial y}\frac{dy}{dt} + \frac{\partial v}{\partial z}\frac{dz}{dt} \\[1mm]
&= \frac{\partial v}{\partial t} + u\frac{\partial v}{\partial x} + v\frac{\partial v}{\partial y} + w\frac{\partial v}{\partial z} \\[1mm]
&= -\frac{1}{\rho} \cdot \frac{\partial p}{\partial y} \qquad \text{with: } v = v(x,y,z,t)
\end{aligned}
\tag{3.36}
$$

$$
\begin{aligned}
\frac{Dw}{Dt} &= \frac{\partial w}{\partial t} + \frac{\partial w}{\partial x}\frac{dx}{dt} + \frac{\partial w}{\partial y}\frac{dy}{dt} + \frac{\partial w}{\partial z}\frac{dz}{dt} \\[1mm]
&= \frac{\partial w}{\partial t} + u\frac{\partial w}{\partial x} + v\frac{\partial w}{\partial y} + w\frac{\partial w}{\partial z} \\[1mm]
&= -\frac{1}{\rho} \cdot \frac{\partial p}{\partial z} \qquad \text{with: } w = w(x,y,z,t)
\end{aligned}
\tag{3.37}
$$

Thus, the **Euler equations** for a non-viscous and incompressible flow are given by:

$$\left| \frac{\partial u}{\partial t} + u\frac{\partial u}{\partial x} + v\frac{\partial u}{\partial y} + w\frac{\partial u}{\partial z} = -\frac{1}{\rho} \cdot \frac{\partial p}{\partial x} \right| \qquad \text{in } x\text{-direction}$$

$$\left| \frac{\partial v}{\partial t} + u\frac{\partial v}{\partial x} + v\frac{\partial v}{\partial y} + w\frac{\partial v}{\partial z} = -\frac{1}{\rho} \cdot \frac{\partial p}{\partial y} \right| \qquad \text{in } y\text{-direction}$$

$$\left| \frac{\partial w}{\partial t} + u\frac{\partial w}{\partial x} + v\frac{\partial w}{\partial y} + w\frac{\partial w}{\partial z} = -\frac{1}{\rho} \cdot \frac{\partial p}{\partial z} \right| \qquad \text{in } z\text{-direction} \qquad (3.38)$$

3.3.3 Bernoulli Equation

A flow can have kinetic, pressure and potential energy. Since there is **no friction** within the potential flows being discussed in this chapter, energy is conserved along a stream line. In 1738, **Daniel Bernoulli**, one of several members of this illustrious Swiss family - published treatises on fluid flow. This led to the development of an equation for the energy relation which bears his name; it is valid along any stream line.

Instationary or Unsteady Flow

All properties of an instationary flow vary (at all locations) as a function of time. The velocity terms in the Euler equations 3.38 can be written in terms of the velocity potential Φ by:

$$\begin{aligned}
u\frac{\partial u}{\partial x} &= \frac{\partial \Phi}{\partial x} \cdot \frac{\partial^2 \Phi}{\partial x^2} = \frac{1}{2} \cdot \frac{\partial}{\partial x}\left(\frac{\partial \Phi}{\partial x}\right)^2 \\
v\frac{\partial u}{\partial y} &= \frac{\partial \Phi}{\partial y} \cdot \frac{\partial^2 \Phi}{\partial x \partial y} = \frac{1}{2} \cdot \frac{\partial}{\partial x}\left(\frac{\partial \Phi}{\partial y}\right)^2 \\
w\frac{\partial u}{\partial z} &= \frac{\partial \Phi}{\partial z} \cdot \frac{\partial^2 \Phi}{\partial x \partial z} = \frac{1}{2} \cdot \frac{\partial}{\partial x}\left(\frac{\partial \Phi}{\partial z}\right)^2 \quad \text{etc., etc.}
\end{aligned} \qquad (3.39)$$

Substituting this in equations 3.38 provides:

$$\begin{aligned}
\frac{\partial}{\partial x}\left\{ \frac{\partial \Phi}{\partial t} + \frac{1}{2}\left[\left(\frac{\partial \Phi}{\partial x}\right)^2 + \left(\frac{\partial \Phi}{\partial y}\right)^2 + \left(\frac{\partial \Phi}{\partial z}\right)^2 \right] + \frac{p}{\rho} \right\} &= 0 \\
\frac{\partial}{\partial y}\left\{ \frac{\partial \Phi}{\partial t} + \frac{1}{2}\left[\left(\frac{\partial \Phi}{\partial x}\right)^2 + \left(\frac{\partial \Phi}{\partial y}\right)^2 + \left(\frac{\partial \Phi}{\partial z}\right)^2 \right] + \frac{p}{\rho} \right\} &= 0 \\
\frac{\partial}{\partial z}\left\{ \frac{\partial \Phi}{\partial t} + \frac{1}{2}\left[\left(\frac{\partial \Phi}{\partial x}\right)^2 + \left(\frac{\partial \Phi}{\partial y}\right)^2 + \left(\frac{\partial \Phi}{\partial z}\right)^2 \right] + \frac{p}{\rho} \right\} &= 0
\end{aligned} \qquad (3.40)$$

Differentiation of the expressions between braces $\{...\}$ with respect to x, y or z gives zero. So these expressions are functions of only time, $C(t)$, which provides the **Bernoulli equation** for an instationary flow:

$$\boxed{\frac{\partial \Phi}{\partial t} + \frac{1}{2}V^2 + \frac{p}{\rho} + gz = C\left(t\right)} \tag{3.41}$$

in which:

$$V^2 = u^2 + v^2 + w^2 = \left(\frac{\partial \Phi}{\partial x}\right)^2 + \left(\frac{\partial \Phi}{\partial y}\right)^2 + \left(\frac{\partial \Phi}{\partial z}\right)^2 \tag{3.42}$$

Stationary or Steady Flow

In a stationary flow the derivative of the potential, $\partial \Phi / \partial t$, becomes zero and the function of time, $C\left(t\right)$, becomes a constant, C; all time functions are now absent. In this case, the Bernoulli equation becomes:

$$\boxed{\frac{1}{2}V^2 + \frac{p}{\rho} + gz = C} \qquad \text{(along a stream line)} \tag{3.43}$$

Often, the Bernoulli equation for a stationary flow is written in other forms:

$$\boxed{\frac{V^2}{2g} + \frac{p}{\rho g} + z = Constant} \text{ (a)} \qquad \text{or} \qquad \boxed{\frac{1}{2}\rho V^2 + p + \rho gz = Constant} \text{ (b)} \tag{3.44}$$

The Bernoulli equation for stationary flow in 3.44(a) results in units of length (often called head of fluid) and is often favoured by civil engineers, whereas the form of equation 3.44(b) results in pressure and is often favoured by mechanical engineers and naval architects.

3.3.4   2-D Streams

Physically, a **streamline** is a 'line which follows the flow'; if a thin stream of dye were to be added to the flow, it would follow and physically define a streamline.
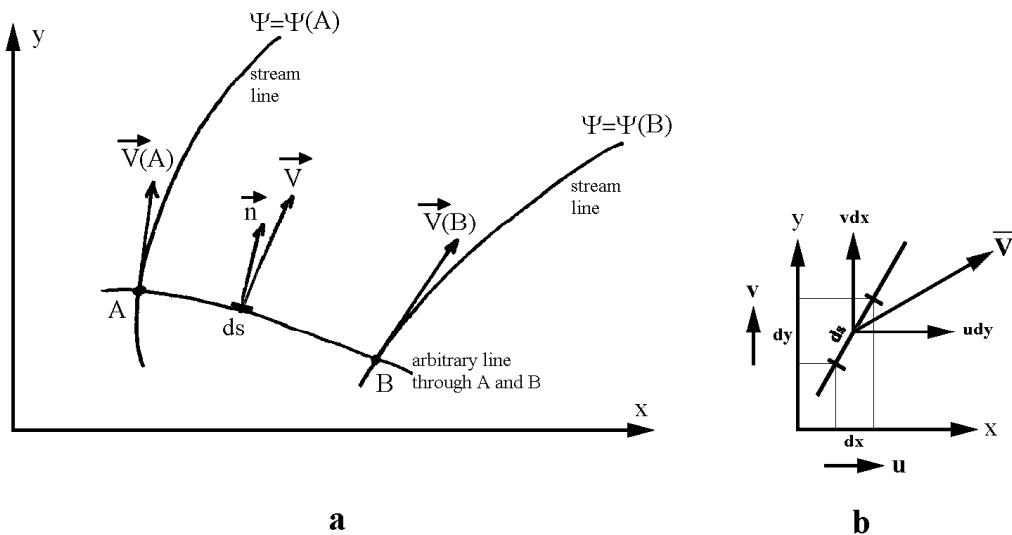
Figure 3.5: Streamlines

The vector $\vec{n}$ in figure 3.5 is the normal vector on an arbitrary line through a point A on the left stream line and a point B on the right stream line.

The rate of flow between two streamlines in the (x, y)-plane (see figures 3.5-a and 3.5-b) is given by:

$$
\begin{aligned}
\Delta \Psi_{A \to B} &= \int_A^B \left(\vec{V} \cdot \vec{n} \right) \cdot ds = \int_A^B (u \cdot dy - v \cdot dx) \\
&= \int_A^B \left(\frac{\partial \Psi}{\partial y} dy + \frac{\partial \Psi}{\partial x} dx \right) = \int_A^B d\Psi = \Psi(B) - \Psi(A)
\end{aligned}
\tag{3.45}
$$

in which $\Delta \Psi_{A \to B}$ is the volume of flow per unit of time between two streamlines through A and B.

2-D Stream Lines

This rate of flow remains constant when A and B follow their streamlines. The volume of flow between any two streamlines is therefore directly proportional to the difference between the - to be defined - stream function values of those two stream lines. Furthermore, the velocity must increase as the streamlines come closer together and decrease as they diverge while following a stream path. This follows from continuity of the incompressible flow Mathematically, a streamline is simply a curve for which:

$$
\Psi = constant
\tag{3.46}
$$

Since no flow takes place across streamlines, then in 2-D rectangular coordinates:

$$
d\Psi = u \ dy - v \ dx
\tag{3.47}
$$

or in 2-D polar coordinates:

$$
d\Psi = v_r \ r \ d\theta - v_\theta \ dr
\tag{3.48}
$$

Just like the potential function has a stream function no direct physical meaning; its derivatives however are very useful.

2-D Stream Function

Much like the potential function defined above, the **stream function**, Ψ, is a mathematical expression such that:

$$
\boxed{u = \frac{\partial \Psi}{\partial y}} \text{ (a)} \qquad \text{and} \qquad \boxed{v = -\frac{\partial \Psi}{\partial x}} \text{ (b)}
\tag{3.49}
$$

or in polar coordinates:

$$
\boxed{v_r = \frac{1}{r} \cdot \frac{\partial \Psi}{\partial \theta}} \text{ (a)} \qquad \text{and} \qquad \boxed{v_\theta = -\frac{\partial \Psi}{\partial r}} \text{ (b)}
\tag{3.50}
$$

3.3.5   Properties

A few basic additional principles are reviewed in this section before continuing with the more classical potential flow mechanics and mathematics.

Orthogonality

The velocity components, u and v, can be expressed in two different but equivalent ways:

$$\boxed{u = \frac{\partial \Phi}{\partial x} = +\frac{\partial \Psi}{\partial y}} \text{ (a)} \qquad \text{and} \qquad \boxed{v = \frac{\partial \Phi}{\partial y} = -\frac{\partial \Psi}{\partial x}} \text{ (b)} \tag{3.51}$$

Since $\partial \Phi / \partial y$ is the negative reciprocal of $\partial \Psi / \partial x$, the stream lines and potential lines must be **orthogonal**; the stream lines and potential lines always cross each other at right angles. This fact can be handy when sketching flow patterns using stream lines and potential lines. In 2-D polar coordinates, the velocity components, v_r and v_θ, are:

$$\boxed{v_r = +\frac{\partial \Phi}{\partial r} = \frac{1}{r} \cdot \frac{\partial \Psi}{\partial \theta}} \text{ (a)} \qquad \text{and} \qquad \boxed{v_\theta = \frac{1}{r} \cdot \frac{\partial \Phi}{\partial \theta} = -\frac{\partial \Psi}{\partial r}} \text{ (b)} \tag{3.52}$$

Impervious Boundary

There is no flow across a streamline so that any **impervious flow boundary**, therefore, must also be a streamline. This means that:

$$\left. \begin{array}{l} \frac{\partial \Phi}{\partial n} = 0 \\[2ex] \Psi = constant \end{array} \right\} \quad \text{at any impervious boundary} \tag{3.53}$$

in which n is the normal to the (impervious) surface.
These are important relations which will be used repeatedly.

Conditions far from a Disturbance

It is usually assumed that nothing special happens as one moves far away from the area of interest. In mathematical terms, this means that:

$$\text{if} \quad x \gg 0 \quad \text{and/or} \quad y \gg 0 \qquad \text{then:} \qquad \Psi \to \Psi_\infty \quad \text{and} \quad \Phi \to \Phi_\infty \tag{3.54}$$

The subscript $_\infty$ denotes a condition which exists far away from the location of primary interest.

Steady and Unsteady Flow

Steady flow means that at any chosen location - thus also at a point on any given streamline - the velocity is constant and independent of time. This means that:

$$\frac{\partial \vec{V}}{\partial t} = 0 \qquad \text{(steady flow)} \tag{3.55}$$

Obviously, **unsteady flow** is any flow condition which does not satisfy this relation. Waves are a good example of unsteady flow, by the way.

Uniform Flows

One speaks of **uniform flow** when the velocity does not change as one progresses along a streamline at any instant in time. This means that:

$$\frac{\partial \vec{V}}{\partial s} = 0 \qquad \text{(uniform flow)} \tag{3.56}$$

in which s is a distance measured along the streamline.

3.4 Potential Flow Elements

Potential flows - described via convenient mathematical formulas - can also be superposed. This means that a series of simple flow situations can be added in order to produce a more complex flow. If these elements fulfil the Laplace equation, the sum of these elements does this too.
This section describes the basic building blocks used in this process; superposition comes later in this chapter.
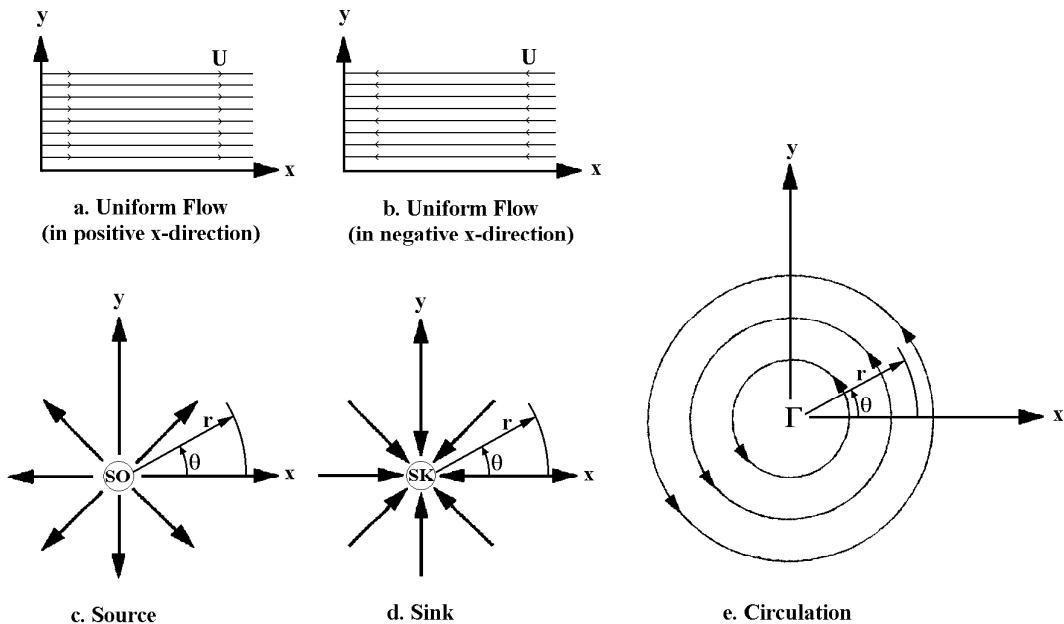
Figure 3.6: Potential Flow Elements

3.4.1 Uniform Flow Elements

The simplest solution of the Laplace equation is:

$$\Phi = U \cdot x \tag{3.57}$$

Its second derivative in the x-direction is zero and all derivatives in the y- and z-directions are also zero; so this potential satisfies the Laplace equation. The meaning of this potential

is a uniform steady flow in the x-direction, since the only velocity component is $u(x,y) = U$. This flow has a series of equally spaced parallel stream lines parallel to the x-axis, as shown in figure 3.6-a. Its stream function follows from:

$$u = \frac{\partial \Psi}{\partial y} = U \qquad \text{so that} \qquad \Psi = U \cdot y \tag{3.58}$$

The flow rate (in m^3/s for example - or actually in m^2/s because only a unit thickness in the z-direction is being considered) between any two stream lines separated by an amount $\Delta \Psi$ is constant and is proportional to $\Delta \Psi$ (or Δy as well in this case). Thus for a uniform flow in the positive x-direction, the potential and stream functions are given by:

$$\boxed{\Phi = +U \cdot x} \text{ (a)} \qquad \text{and} \qquad \boxed{\Psi = +U \cdot y} \text{ (b)} \tag{3.59}$$

If the flow is in the negative x-direction (see figure 3.6-b), the potential and stream functions will change sign:

$$\boxed{\Phi = -U \cdot x} \text{ (a)} \qquad \text{and} \qquad \boxed{\Psi = -U \cdot y} \text{ (b)} \tag{3.60}$$

3.4.2   Source and Sink Elements

A **source** is a point from which flow radiates **outward** in all directions as shown in figure 3.6-c. Its location is often denoted by a small circle enclosing the letters SO or a plus sign. Its potential and stream functions are given most easily in polar coordinates:

$$\boxed{\Phi = +\frac{Q}{2\pi} \cdot \ln r} \text{ (a)} \qquad \text{and} \qquad \boxed{\Psi = +\frac{Q}{2\pi} \cdot \theta} \text{ (b)} \tag{3.61}$$

in which Q is the strength of the source (or flow rate) with units of m^2/s for a two-dimensional flow.

It requires some algebra to show that this potential satisfies the Laplace equation. The potential lines are circles centered at the source location: $r = $ constant; its stream lines are radial lines: $\theta = $ constant.

The Cartesian expression of the potential and stream functions looks like:

$$\Phi = +\frac{Q}{2\pi} \cdot \ln \sqrt{x^2 + y^2} \text{ (a)} \qquad \text{and} \qquad \Psi = +\frac{Q}{2\pi} \cdot \arctan \left(\frac{y}{x} \right) \text{ (b)} \tag{3.62}$$

The velocity in the radial direction can be found from the derivative of the potential function with respect to r, so:

$$v_r = \frac{\partial \Phi}{\partial r} = \frac{1}{r} \cdot \frac{\partial \Psi}{\partial \theta} = \frac{Q}{2\pi r} \tag{3.63}$$

There is no flow in the tangential direction, because:

$$v_\theta = \frac{1}{r} \cdot \frac{\partial \Phi}{\partial \theta} = -\frac{\partial \Psi}{\partial r} = 0 \tag{3.64}$$

This flow is called a source flow because the amount of fluid passing through a circle at radius r is always Q. The fluid is free of rotation, because the source strength, Q, is constant in the fluid. However, the origin, $r = \sqrt{x^2 + y^2} = 0$, is a singular point; the

velocities go to infinity at this point. Therefore, the potential theory is not valid there and this point has to be excluded when carrying out integrations in the fluid.

A **sink** is a **negative source** and thus has an **inward** radial flow. It is denoted by a circle enclosing the letters SK or a minus sign as shown in figure 3.6-d. In polar coordinates it can be expressed as:

$$\boxed{\Phi = -\frac{Q}{2\pi} \cdot \ln r} \text{ (a)} \qquad \text{and} \qquad \boxed{\Psi = -\frac{Q}{2\pi} \cdot \theta} \text{ (b)} \tag{3.65}$$

and in Cartesian coordinates as:

$$\Phi = -\frac{Q}{2\pi} \cdot \ln \sqrt{x^2 + y^2} \text{ (a)} \qquad \text{and} \qquad \Psi = -\frac{Q}{2\pi} \cdot \arctan\left(\frac{y}{x}\right) \text{ (b)} \tag{3.66}$$

3.4.3 Circulation or Vortex Elements

A circulation or a vortex, Γ, is a tangential flow (circular path) around a point as is shown in figure 3.6-e. The potential and stream functions are in this case:

$$\boxed{\Phi = +\frac{\Gamma}{2\pi} \cdot \theta} \text{ (a)} \qquad \text{and} \qquad \boxed{\Psi = -\frac{\Gamma}{2\pi} \cdot \ln r} \text{ (b)} \tag{3.67}$$

or in Cartesian coordinates:

$$\Phi = +\frac{\Gamma}{2\pi} \cdot \arctan\left(\frac{y}{x}\right) \text{ (a)} \qquad \text{and} \qquad \Psi = -\frac{\Gamma}{2\pi} \cdot \ln \sqrt{x^2 + y^2} \text{ (b)} \tag{3.68}$$

The velocities are now in a tangential **counter-clockwise direction**:

$$v_\theta = \frac{1}{r} \cdot \frac{\partial \Phi}{\partial \theta} = -\frac{\partial \Psi}{\partial r} = \frac{\Gamma}{2\pi r} \tag{3.69}$$

There is no velocity in radial direction, because:

$$v_r = \frac{\partial \Phi}{\partial r} = \frac{1}{r} \cdot \frac{\partial \Psi}{\partial \theta} = 0 \tag{3.70}$$

One should remember that the circulation strength, Γ, can be found from:

$$\Gamma = \oint v_\theta \cdot ds = 2\pi r \cdot v_\theta = constant \tag{3.71}$$

The fluid is free of rotation, because the circulation, Γ, is constant in the fluid. However, the origin, $r = \sqrt{x^2 + y^2} = 0$, is a singular point; the velocities go to infinity at this point. Therefore, potential theory is not valid there and this point has to be excluded when carrying out integrations in the fluid.

The potential and stream functions of a circulation with tangential velocities in a **clockwise direction** are given by:

$$\boxed{\Phi = -\frac{\Gamma}{2\pi} \cdot \theta} \text{ (a)} \qquad \text{and} \qquad \boxed{\Psi = +\frac{\Gamma}{2\pi} \cdot \ln r} \text{ (b)} \tag{3.72}$$

or in Cartesian coordinates by:

$$\Phi = -\frac{\Gamma}{2\pi} \cdot \arctan\left(\frac{y}{x}\right) \text{ (a)} \qquad \text{and} \qquad \Psi = +\frac{\Gamma}{2\pi} \cdot \ln \sqrt{x^2 + y^2} \text{ (b)} \qquad (3.73)$$

Note that a circulation flow is a counterpart of a source or sink flow; Φ and Ψ have similar forms but they are exchanged.

3.5 Superposition of Basic Elements

While each of the flow patterns from the four potential flow elements treated above can be quite easily visualized, they are not all that common, and a lot of interesting flow patterns are much more complex as well. The 'power' of potential theory lies in the fact that because of its linearity **superposition** (or 'adding up') of flow pattern components may be used to generate more complex flow patterns. This section concentrates on producing some of these more complex and interesting flow patterns.

3.5.1 Methodology

Superposition may be carried out 'by hand' using the following 5 steps; they are then most suited for simple cases. Superposition of only a few elements can be carried out by hand.

A. Place each potential flow element at its desired x, y location.

B. Draw the flow pattern from each element individually - without regard to the others.

C. Assign appropriate numerical values to each (independent) stream line.

D. The resulting stream function value at any point x, y can be found by adding the stream function values from each of the components at that point. (This is easiest at locations where streamlines from the various elements cross each other. Otherwise, a certain amount of interpolation may be needed to carry this out.) This yields a field of resulting stream function values, each associated with a particular location, x, y.

E. Lines can now be sketched which connect locations having the same stream function values. This is much like drawing contour lines in map-making or a dot-to-dot drawing as in elementary school! Interpolation may again be necessary in this sketching process, however.

These steps are illustrated in figure 3.7 in which a uniform flow (from left to right) is combined with source flow. Parts A and B of the figure show half-planes of the two independent potential flow elements. These are superposed in part C of the figure thus completing the first three steps above. The results of the addition work are shown in part D; part E of the figure shows the resulting set of streamlines.

Whenever a larger number of elements are to be combined, the interpolation work involved in carrying out the above summations becomes too cumbersome for 'handwork'. A slightly different approach is most appropriate for computer processing.

Choose a single, X, Y coordinate system.
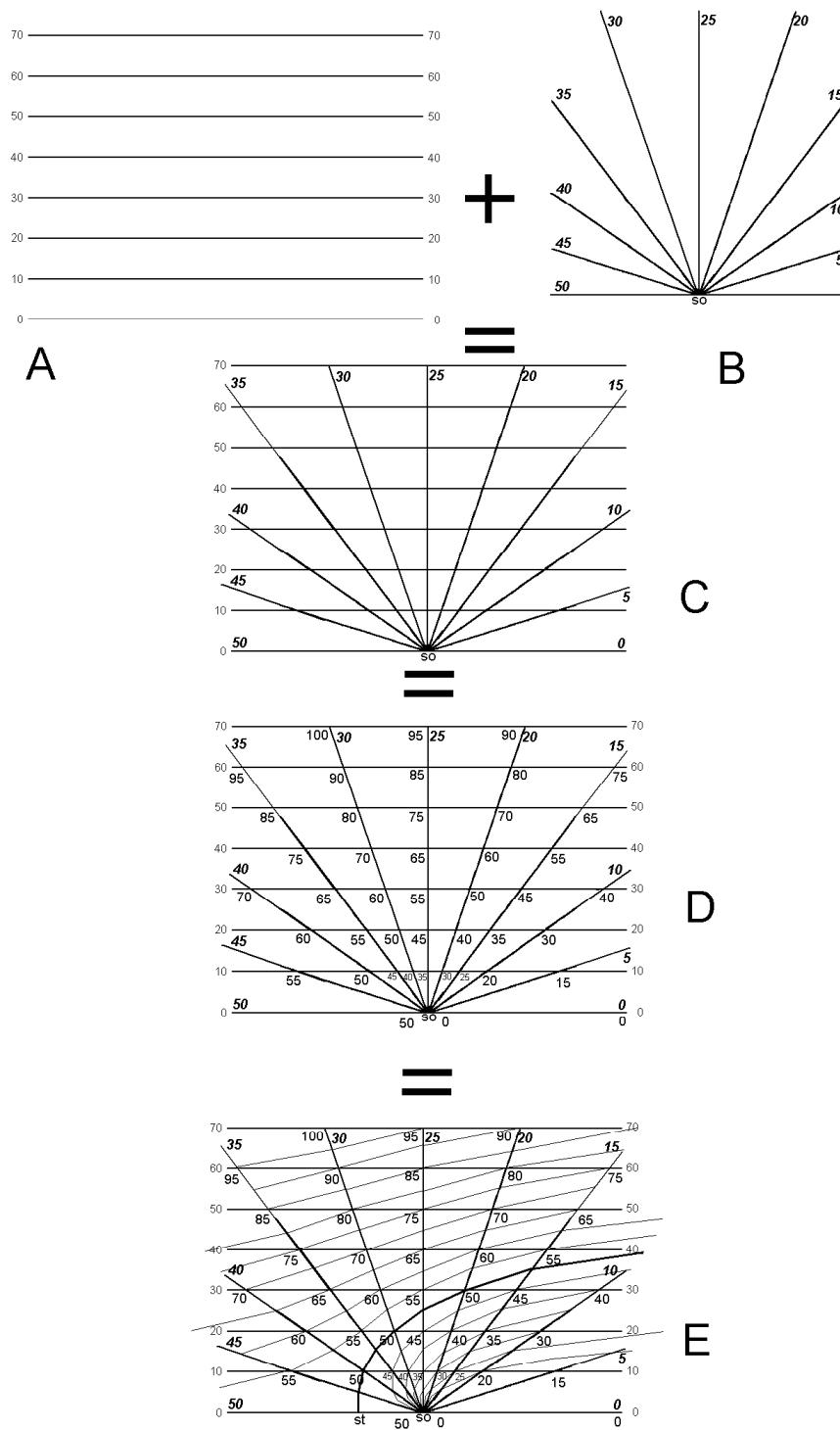
Figure 3.7: Superposition Steps Carried out by Hand

Place each of the potential flow elements at its desired X, Y location. Formulas are available to express each element's stream and potential function in terms of its own (local) x, y coordinates.

Transform the coordinates for each flow element so that its contribution is expressed in terms of X and Y coordinates. These formulas will be used in step 5, below.

Choose a rectangular grid of points in the X, Y coordinate system at which the functions are to be evaluated. The area covered by these points should be the area for which the stream and potential lines are to be plotted.

A computer program - even a spreadsheet program will do - can be used to compute the relevant function value at each grid point. Even a modest, but modern PC can quickly generate values on a grid of 50 by 50 points.

The resulting data table can then be transferred to a 3-D plotting program to generate contour lines of stream or potential values as a function of X and Y. These are the desired product.

Obviously, this method is not really hindered by the number of flow elements to be included; the formulas only become a bit longer in the program. Because the plotting program will interpolate anyway, it is no longer important that the computed grid point data have 'convenient' values.

The rest of this section details a number of simple and useful potential flow element combinations.

3.5.2   Sink (or Source) in Uniform Flow

This first example - still a bit simple - could represent the flow of oil to a well drilled into a reservoir through which the oil is flowing slowly. This situation has the opposite sense of the one used to illustrate the method, above; now, the flow pattern is determined by adding a sink to a uniform flow which goes from right to left. Using equations 3.52 and 3.66:

$$\Psi = -\frac{Q}{2\pi} \cdot \arctan\left(\frac{y}{x}\right) - U_\infty \cdot y \qquad (3.74)$$

Figure 3.8 shows the curve separating the flow going to the sink from that passing (or 'escaping') the sink. All flow originating between the two asymptotes gets 'caught' by the sink.

Obviously, if the sink were to be replaced by a source, the flow coming from the source would then remain within the asymptotes as well.

3.5.3   Separated Source and Sink

Consider next a source and a sink with equal and opposite intensity, $\frac{Q}{2\pi}$, separated by a distance of $2s$.

Once again, superposition is used to yield - using equations 3.66:

$$\Psi_{\text{source}} = \frac{Q}{2\pi} \cdot \theta_1 = \frac{Q}{2\pi} \cdot \arctan\left(\frac{y}{x_1}\right) \qquad \text{for the source} \qquad (3.75)$$

$$\Psi_{\text{sink}} = -\frac{Q}{2\pi} \cdot \theta_2 = -\frac{Q}{2\pi} \cdot \arctan\left(\frac{y}{x_2}\right) \qquad \text{for the sink} \qquad (3.76)$$
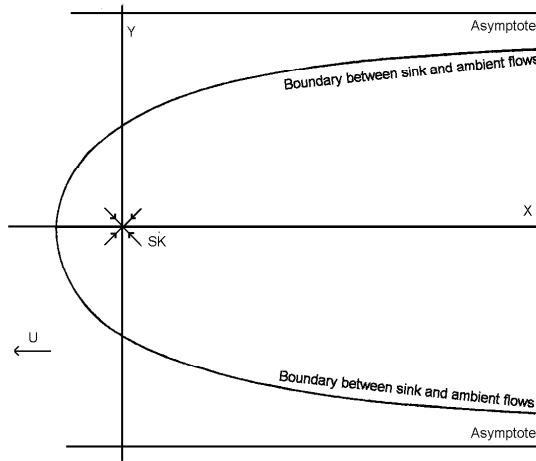
Figure 3.8: Sink in a Uniform Flow

The resulting stream lines are then (in polar coordinates for a change) lines with:

$$\Psi = \frac{Q}{2\pi} \cdot \theta_1 - \frac{Q}{2\pi} \cdot \theta_2 = constant \tag{3.77}$$

These stream lines are a set of circles, all centered on the y axis, and all passing through source and sink; see figure 3.9.
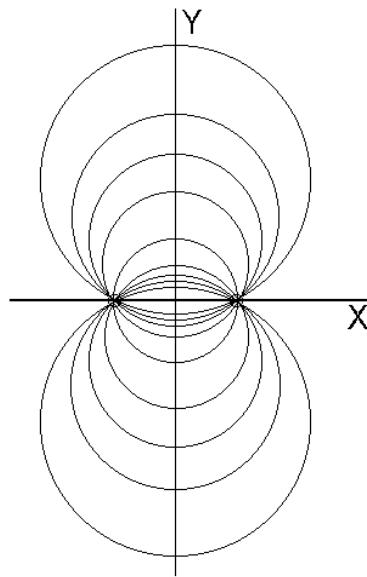
Figure 3.9: Separated Source and Sink

One can also write the resultant stream function in Cartesian coordinates as:

$$\Psi = \frac{Q}{2\pi} \cdot \arctan\left(\frac{2\,y\,s}{x^2 + y^2 - s^2}\right) \tag{3.78}$$

3.5.4   Source and Sink in Uniform Flow

The stream function is, in this case:

$$\Psi = \frac{Q}{2\pi} \cdot \arctan\left(\frac{2\,y\,s}{x^2 + y^2 - s^2}\right) + U_\infty\,y \tag{3.79}$$

The stream lines that one obtains now are shown in figure 3.10. Notice that the ellipse which surrounds the source and the sink (drawn a bit heavier in the figure) is a stream line; no flow takes place through that ellipse. The flow from source to sink stays inside; the constant current flow stays outside and passes around the form.

The physical interpretation of this is that one could obtain the same flow by replacing that ellipse with an impermeable object in a uniform flow.
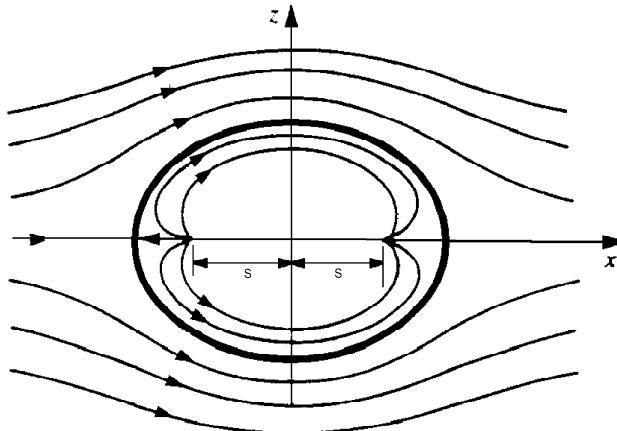
Figure 3.10: Source and Sink in Uniform Flow

This approach can be extended even further as explained in the next section.

3.5.5   Rankine Ship Forms

The Englishman W.J.M. Rankine extended the above-mentioned approach about 1870. He did this by including additional, matched pairs of sources and sinks along the x axis in the uniform flow. They were always located symmetrically about the coordinate origin. By giving each matched source-sink pair its own spacing and strength (relative to the uniform flow), he was able to generate a fatter or thinner, or more blunt or pointed shape; it was always symmetric with respect to both the x and y axes, however. Use of relatively weaker source-sink pairs near the ends of the shape make it more 'pointed'. Since these forms can be made to somewhat resemble a horizontal slice of a ship (neglecting the fact that the stern has a bit different shape from the bow), they came to be know as **Rankine ship forms**. Flow computations with such forms are quite simple to carry out - and have been done for more than a century!

3.5.6   Doublet or Dipole

Suppose, in the discussion of a separate source and sink, above, one were to let the distance $2s$ between them approach zero. This produces what is called a **doublet** or **di-**

pole. The corresponding stream function is found by letting s approach zero in equation 3.78:

$$\Psi = \lim_{s \to 0} \left\{ \frac{Q}{2\pi} \cdot \arctan\left(\frac{2\,y\,s}{x^2 + y^2 - s^2} \right) \right\} \tag{3.80}$$

As $x \to 0$ then $\arctan(x) \to x$, so that:

$$\Psi = \lim_{s \to 0} \left\{ \frac{Q}{\pi}\, s \cdot \left(\frac{y}{x^2 + y^2 - s^2} \right) \right\} \tag{3.81}$$

One must keep the term $\frac{Q}{\pi} s$ (that is renamed the doublet strength, μ) constant and non-zero (otherwise there won't be anything left; the origin is a singular point anyway!). On the other hand, s^2 becomes small even faster so that it can be neglected relative to $x^2 + y^2$. After a bit of algebra, the above stream function becomes:

$$\boxed{\Psi = \mu \cdot \frac{y}{x^2 + y^2} = \frac{\mu \cdot \sin\theta}{r}} \tag{3.82}$$

and similarly:

$$\boxed{\Phi = \mu \cdot \frac{x}{x^2 + y^2} = \frac{\mu \cdot \cos\theta}{r}} \tag{3.83}$$

In figure 3.11, both the stream (solid) and equipotential (dashed) lines are circles centered on the y and x axes respectively. All the circles pass through the origin, too.
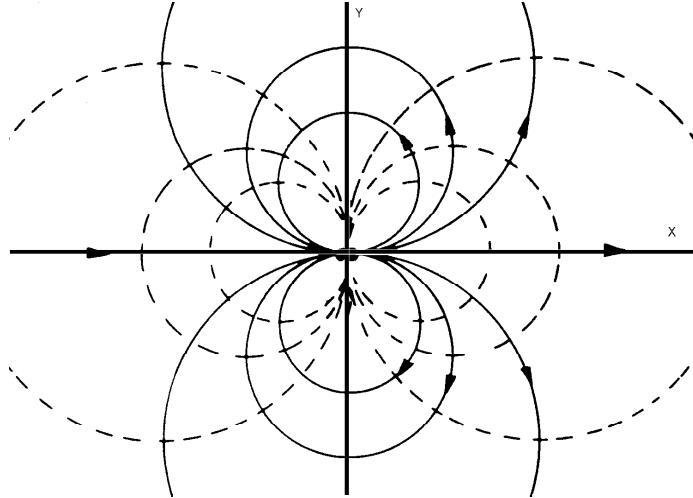
Figure 3.11: Doublet or Dipole Flow

3.5.7 Doublet in Uniform Flow

The next step is to add a uniform flow to the doublet just discussed. If the flow goes along the negative x-axis, this yields:

$$\Psi = \frac{\mu \cdot y}{x^2 + y^2} - U_\infty\, y \tag{3.84}$$

and:

$$\Phi = \frac{\mu \cdot x}{x^2 + y^2} - U_\infty \ x \tag{3.85}$$

In polar coordinates this can be written as:

$$\Psi = \frac{\mu . \sin \theta}{r} - U_\infty \ r \sin \theta \tag{3.86}$$

and:

$$\Phi = \frac{\mu . \cos \theta}{r} - U_\infty r \cos \theta \tag{3.87}$$

It can be interesting to set $\Psi = 0$ in equation 3.84. This means that:

$$\Psi = y \cdot \left[\frac{\mu}{x^2 + y^2} - U_\infty \right] = const. = 0 \tag{3.88}$$

This condition is true when:

1. • $y = 0$

    This means the x axis is a streamline. This can be expected because of the symmetry with respect to this axis.

    • $\frac{\mu}{x^2+y^2} - U_\infty = 0$ or, since $x^2 + y^2 = R^2$: $R^2 = \frac{\mu}{U_\infty} = constant$

    This corresponds to a **circle**! Its radius is:

$$R = \sqrt{\frac{\mu}{U_\infty}} \quad \text{or:} \quad \mu = R^2 \ U_\infty \tag{3.89}$$

The radius of the cylinder and the undisturbed current velocity, U_∞, thus, determines the necessary doublet strength value, μ.

Substituting this value for μ then yields for the general equations in polar coordinates:

$$\boxed{\Psi = \frac{R^2 \ U_\infty \sin \theta}{r} - U_\infty \ r \ \sin \theta = R \ U_\infty \left[\frac{R}{r} - \frac{r}{R} \right] \sin \theta} \tag{3.90}$$

for the stream function and for the potential function:

$$\boxed{\Phi = \frac{R^2 \ U_\infty \cos \theta}{r} - U_\infty \ r \ \cos \theta = R \ U_\infty \left[\frac{R}{r} - \frac{r}{R} \right] \cos \theta} \tag{3.91}$$

The hydrodynamics of a circular cylinder is obviously *very significant* for offshore engineering! The relevant flow pattern is shown in figure 3.12.

It is worthwhile to 'play' with equation 3.84 a bit more. This leads to the following discoveries:

• Far from the cylinder, when $x^2 + y^2$ is large, the stream lines becomes $\Psi_\infty = U_\infty \cdot y$.
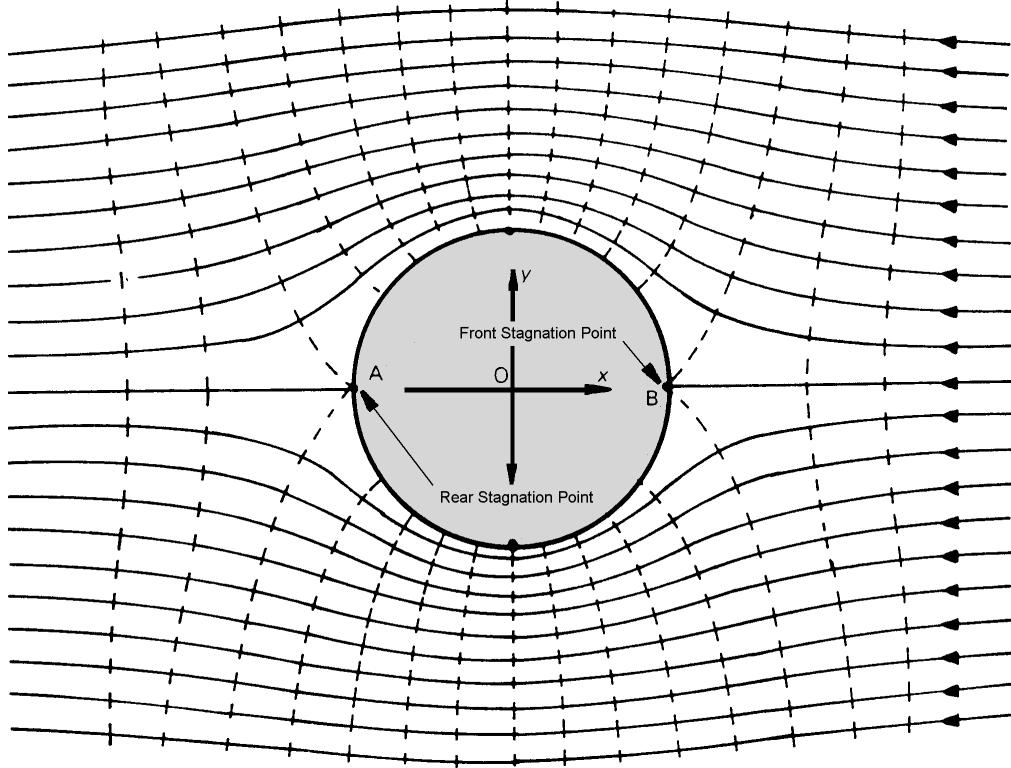
Figure 3.12: Doublet in Uniform Flow Yielding Impervious Cylinder

- One also has to check that there is no radial velocity on the cylinder surface. This implies that the following relationship is satisfied - see 3.52-b:

$$v_r = -\frac{1}{r}\frac{\partial \Psi}{\partial \theta}\bigg|_{r=R} = 0 \tag{3.92}$$

This gives no problems, either.

- One can also check that the potential function fulfills the Laplace equation $(\nabla^2 \Phi = 0)$.

Further details of the flow around a cylinder will be discussed later in this chapter. One additional application of superposition is discussed here first.

3.5.8   Pipeline Near The Sea Bed

Figure 3.12 shows the flow around a single cylinder. Superposition can be used to simulate (approximately) the flow around a cylinder near the (flat) sea bed. The reason why this is approximate will become clear later in this secton. Since the sea bed is flat and impervious, it must be a straight streamline. A straight streamline parallel to the x axis at some given distance from the cylinder axis, y_0 from the cylinder is needed.

This can be achieved (approximately) by building up a symmetrical pattern involving two cylinders, one at a distance y_0 *above* the x axis and one at a distance y_0 *below* that axis as shown in figure 3.13. The lower half of the flow pattern is just 'thrown away' by ignoring it. The sea bed will be the x axis with the y axis positive upward passing through the

cylinder center. This special form of superposition is often referred to as **reflection** (about the sea bed, in this case). Reflection is commonly used for other applications with the sea surface or even a vertical plane of symmetry as the reflection plane.
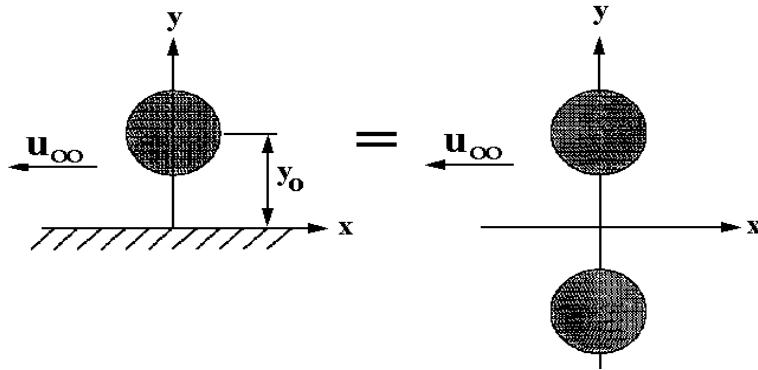
Figure 3.13: Use of Reflection to Get Pipeline Near Sea Bed

This is solved by superposing the solutions for a doublet in a uniform flow above the bed with one below the bed. All of this yields (after transforming coordinates):

$$\Psi = \mu \cdot \frac{y - y_0}{x^2 + (y - y_0)^2} + \mu \cdot \frac{y + y_0}{x^2 + (y + y_0)^2} - U_\infty \, y \tag{3.93}$$

By letting y equal zero (at the sea bed) in this equation, one can check that Ψ remains constant and equal to zero in order to prove that the sea bed is indeed a streamline; this is left to the reader.

A more interesting (and more complicated) check is to see if the surface of the pipeline $R^2 = x^2 + (y - y_0)^2$ is still a streamline and thus is (still) impermeable. A quick way to *disprove* this can be to check the value of Ψ at a few convenient points on the circle representing the pipeline. If the values of Ψ computed at these points on the circle are not identical, then the circle can no longer be a stream line. It can be convenient to select locations such as the top, bottom, front and back of the pipe for this check as is done in the table below.

Location	x	y	Ψ
Top	0	$y_0 + R$	$\mu \cdot \left(\frac{1}{R} + \frac{1}{2y_0 + R} \right) - U_\infty \cdot (y_0 + R)$
Front	$+R$	y_0	$\mu \cdot \left(\frac{2y_0}{R^2 + 4y_0^2} \right) - U_\infty \cdot y_0$
Bottom	0	$y_0 - R$	$\mu \cdot \left(-\frac{1}{R} + \frac{1}{2y_0 - R} \right) - U_\infty \cdot (y_0 - R)$
Back	$-R$	y_0	$\mu \cdot \left(\frac{2y_0}{R^2 + 4y_0^2} \right) - U_\infty \cdot y_0$

One can quickly see from this table that the pipeline's circular surface is no longer a streamline. Why should this be so? The answer lies in the fact that the influence from each potential flow element extends (theoretically) to infinity. Since it has been shown above that *a single* doublet pair in a uniform flow *does* yield a perfect circular section, then it is only to be expected that this circular streamline will be disturbed a bit by the influence of the second doublet introduced in order to make a symmetric pattern with respect to the sea bed. This is why the word 'approximate' was used so rigorously at the beginning of this discussion.

3.6 Single Cylinder in a Uniform Flow

A cylinder is such an important element in offshore structures that its hydrodynamics will be studied in more detail in this section.

3.6.1 Flow

Velocity along Cylinder Wall

It is easiest to determine the tangential velocity along the wall of a cylinder using polar coordinates. Using equation 3.52, one finds that:

$$v_\theta = -\left[\frac{\partial \Psi}{\partial r}\right]_{r=R} = -\frac{\partial}{\partial r}\left\{\frac{\mu \sin\theta}{r} + U_\infty \, r \, \sin\theta\right\}_{r=R} \tag{3.94}$$

which, with $\mu = U_\infty R^2$, yields:

$$\boxed{v_\theta = -2\,U_\infty \sin\theta} \tag{3.95}$$

Observe that:

$$v_\theta = 0 \quad \text{for: } \theta = n\pi \tag{3.96}$$

The tangential velocity where the cylinder wall crosses the x axis is zero. Also:

$$v_\theta = 2U_\infty \quad \text{for: } \theta = (n+\frac{1}{2})\pi \tag{3.97}$$

The tangential velocity at the 'sides' of the cylinder (where the wall crosses the y axis) is exactly twice the undisturbed ambient flow velocity. Note also that this ratio $\frac{u}{U_\infty}$ is independent of the cylinder radius. In theory, the velocity adjacent to a human hair would be just as big as that adjacent to a large circular pile; significant development of micro-scale velocity measurement techniques will be needed before this can be proven, however!
In the two above equations:

$$
\begin{aligned}
U_\infty &= \text{Undisturbed ambient flow velocity magnitude } (m/s) \\
v_\theta &= \text{Velocity component along the cylinder wall } (m/s) \\
n &= \text{Any integer value}
\end{aligned}
$$

Velocity Profile Adjacent to Cylinder

It can be instructive to examine the velocity distribution along the y axis ($x \equiv 0$):

$$\boxed{u = \left[\frac{\partial \Psi}{\partial y}\right]_{x=0} = U_\infty \cdot \left[\frac{R^2}{y^2} + 1\right]} \tag{3.98}$$

u decreases to U_∞ inversely with $\left[\frac{y}{R}\right]^2$. It is equal to $2\,U_\infty$ for $y = R$ just as was found above; this value is worth remembering by the way!

Influence of Circulation

If a circulation is added to the flow, then v_θ along the cylinder wall comes directly from the superposition of equations 3.95 and 3.69:

$$v_\theta = 2\,U_\infty\,\sin\theta + \frac{\Gamma}{2\pi\,R} \tag{3.99}$$

again at the cylinder surface. Notice that v_θ is no longer symmetric with respect to the x axis, as shown in figure 3.14. In this case, a clockwise circulation has been added to a flow from left to right. This, too, will be important for the hydrodynamic force discussion in the next main section of this chapter. A discussion of how this circulation is generated comes up later in this chapter.
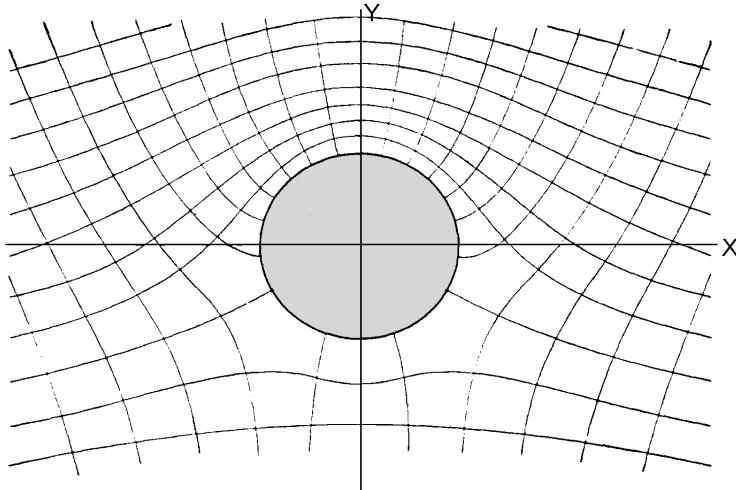
Figure 3.14: Cylinder in Uniform Flow with added Circulation

3.6.2   Pressures

Now that the potential flow around the cylinder is known, it is appropriate to discuss pressures and the forces which result from them. This treatment starts, again, with a single isolated cylinder in an infinite flow; there is no circulation.

Stagnation Points

It has already been pointed out via equation 3.96 that the tangential velocity component at the two locations where the cylinder wall and the x axis cross is identically equal to zero. Since the cylinder wall is impervious, the radial velocity component, v_r, at this location is also zero. There is therefore no velocity at these two **stagnation points**. These points were labeled in figure 3.12.

Stagnation pressures are generally defined in terms of the ambient flow velocity so that:

$$p_s = \frac{1}{2}\,\rho U_\infty^2 \tag{3.100}$$

Pressure Distribution on Cylinder Wall

The next step is to predict the complete pressure distribution along the entire circumference of the cylinder. This is done using the Bernoulli equation 3.44 and the known pressure and velocity at the stagnation point:

$$\frac{1}{2}\rho U_\infty^2 + 0 = p + \frac{1}{2}\rho v_\theta^2 = const. \tag{3.101}$$

The elevation is left out of this balance because it is constant here. Equation 3.95 can be substituted for v_θ here and equation 3.101 can be solved for the pressure, p, along the cylinder wall. This yields:

$$p = \frac{1}{2}\rho U_\infty^2 \cdot \left[1 - 4\sin^2\theta\right] \tag{3.102}$$

This (dimensionless) pressure distribution (the term in brackets above) is shown in figure 3.15 in polar coordinates. It is also plotted in a rectangular coordinate form in chapter 4, by the way.
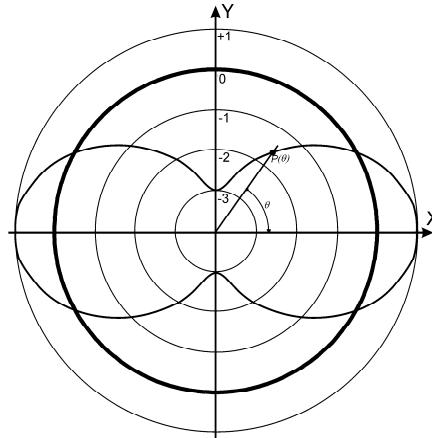
Figure 3.15: Pressure Distribution on a Cylinder in a Potential Flow

3.6.3 Resulting Forces

The next step is to determine the forces from the pressure distribution.

Force Computation Principle

The procedure used to compute the x and y components of the resulting force on the cylinder is illustrated for the x direction using figure 3.16.

This figure shows a 'slice' which extends from front to back across the cylinder; it isolates an arc length $ds = R\,d\theta$ of the cylinder wall. The pressure on each end of this slice is directed normal to the surface (radially) so that its x-component is then $dF_x = p \cdot ds\cos\theta$. Now, one only has to integrate this over the angle θ to get the total force F_x.
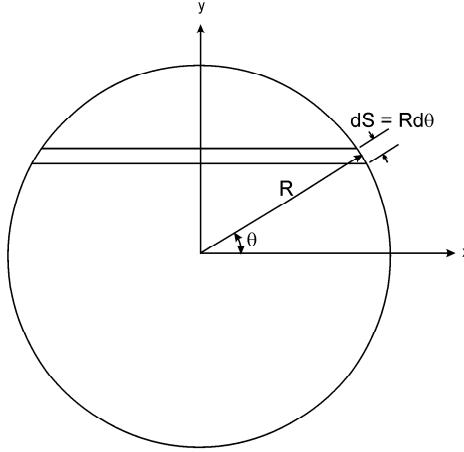
Figure 3.16: Typical Slice used for Computing Resulting Force in X Direction

D'Alembert's Paradox

The French mathematician Jean LeRond D'Alembert who died in 1783, is credited with having carried out the above computation and with discovering that $F_x = 0$ and - from an analogous computation in the y direction - $F_y = 0$ for a circular cylinder placed in a constant, uniform, potential flow! This is **D'Alembert's paradox** - a trap into which most every beginner falls. It could have been avoided by observing - beforehand! - that the pressure distribution in figure 3.15 is completely symmetric about both the x and y axes so that any forces must cancel out in each of these directions. The conclusion should be very clear: *There are no hydrodynamic forces on a circular cylinder in a constant uniform, potential flow.*

Circulation and Lift

If a circulation is added to the flow used in these computations, a force *will be generated*. This comes about because the circulation will increase the tangential flow velocity on one side of the cylinder - say the $+y$ side - while it decreases the flow velocity on the opposite - in this case $-y$ side; see figure 3.14. This is often referred to as the **Magnus effect**. This extra flow will obviously unbalance the symmetry of the flow with respect to the x-axis; one could expect the pressure to be disturbed, too, so that a resultant force in the y direction will result.

The tangential velocity will now be as given in equation 3.99. By letting

$$C = -\frac{\Gamma}{4\pi R U_\infty} = constant \tag{3.103}$$

then 3.99 becomes:

$$v_\theta = 2U_\infty \cdot (\sin\theta - C) \tag{3.104}$$

and the equation for the pressure distribution, 3.102, now becomes:

$$p = \frac{1}{2}\rho U_\infty^2 \left\{ 1 - 4(\sin\theta - C)^2 \right\} \tag{3.105}$$

The drag force can be evaluated just as was done above; this still yields a zero resultant, independent of the value of C.

The resulting force crosswise to the flow can be found by integrating the y-component of the pressure force as follows:

$$F_y = R \int_0^{2\pi} p \sin\theta \ d\theta \qquad (3.106)$$

After a bit of substitution and algebra one should find that:

$$F_y = 4\pi \ R \ \rho \ U_\infty^2 \ C \qquad (3.107)$$

This resultant force is called **lift**; it is directed perpendicular to the direction of the undisturbed approaching flow. Notice that the lift force is only present when $C \neq 0$.

Lift forces are responsible for keeping aircraft airborne. The necessary tangential velocity differential is achieved by making the flow path over the top of a wing or helicopter rotor longer than the flow path on the underside so that the flow over the top must travel faster to pass the object in the same time interval. This same phenomenon is important with ship's propellers, too; see chapter 4.

Lift is largely responsible for driving a sailboat forward when it is sailing 'close-hauled'. The necessary low pressure 'behind' the main sail is now created by the jet caused by the jib or foresail. In tennis or with a baseball pitch, a spinning ball will curve one way or another. Now the ambient air remains stationary while the ball speeds through it. The necessary circulation is created by friction between the spinning ball and the air. Since friction is involved in this case, discussion will have to be delayed until the next chapter.

.

Chapter 4

CONSTANT REAL FLOW PHENOMENA

4.1   Introduction

Now that the basics of constant idealized potential flows have been discussed in the previous chapter, the next step is to consider more realistic - but still constant - flows. The facts that there is no drag force in a potential flow and that a circulation is required to generate a lift force is true only for a potential (non-viscous) flow. The results from this chapter with real flows which include viscous effects will be more realistic.

The initial discussion of some basic concepts motivates attention for two common dimensionless numbers, Rn and Fn, which are handled more generally in Appendix B. These are used to characterize constant flows abound cylinders and ships - and the resultant forces - discussed in the latter part of the chapter. Propulsion systems are handled toward the end of the chapter.

4.2   Basic Viscous Flow Concepts

This section discusses a few basic principles of constant viscous flows. These supplement the discussion on potential flows given in the first parts of chapter 3.

4.2.1   Boundary Layer and Viscosity

In 1883, Osborne Reynolds, an English investigator, observed the flow of water through a glass pipe which drained a container water as shown somewhat schematically in figure 4.1. He first filled the tank with the drain closed so that the water could come to rest.

After opening the drain valve, he found that the flow and streamlines - visualized by a stream of ink:

- The streamlines were straight and parallel in the first segment of the pipe just downstream from its entrance.
- The flow velocity near the pipe wall was less than that near the axis of the pipe.
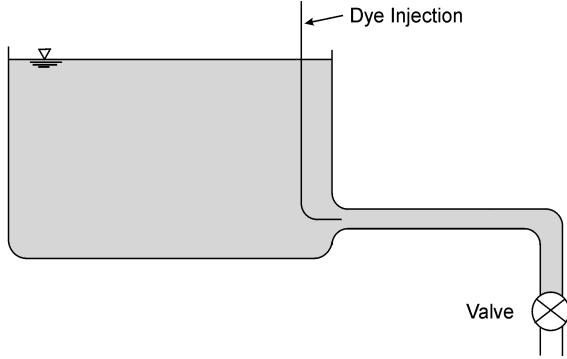
Figure 4.1: Schematic of Reynolds' Experiments

- The streamlines eventually became irregular as the flow progressed further along the pipe. This first happened nearer the mouth of the pipe for flow near its walls and further downstream for flow along the pipe center line.

Further, he observed that if he kept the valve nearly closed (so that all velocities were low) the above development process (as a function of distance in this case) was less abrupt. The flow progressed further before the entire flow became irregular. If the flow velocity was higher, then the whole process took place in a shorter length of pipe.

By repeating the experiments with other fluids and with other pipe diameters, Reynolds discovered that similar phenomena were observed when the following dimensionless parameter had a constant value:

$$Rn = \frac{V \cdot D}{\nu} \tag{4.1}$$

in which:

$$
\begin{array}{rcl}
Rn & = & \text{Reynolds number (-)} \\
V & = & \text{flow velocity (m/s)} \\
D & = & \text{pipe diameter (m)} \\
\nu & = & \text{kinematic viscosity of the fluid (m}^2\text{/s)}
\end{array}
$$

The kinematic viscosity is a fluid property usually quite dependent upon temperature. For water at room temperature, its value is about $1 \cdot 10^{-6}$ m^2/s. This value can be reduced by a factor of two or so simply by heating the water - see appendix A.

The Reynolds number is usually interpreted physically as the ratio of $\frac{\text{Inetia Forces}}{\text{Viscous Forces}}$. Viscous forces are most important, therefore, when the Reynolds number is small.

4.2.2   Turbulence

The breakup of the nice neat streamlines far enough downstream in Reynolds' experimental pipeline was caused by what is called **turbulence**. Turbulence is a result of small eddies or vortices which form in most any viscous flow. Turbulence manifests itself in a flow measurement by causing time-dependent fluctuations in the velocity measured at one point, but in such a way that the average velocity remains unchanged.

Turbulent eddies can have many scales and occur in all sorts of flows. In the atmosphere, a sensitive wind speed meter (anemometer) can register rather quick turbulent fluctuations in the flow. On a larger scale, a wind gust can be seen as a larger scale of turbulence. On a global scale, even a whole hurricane can be considered to be turbulence, relative to the even larger global atmospheric circulation.

4.2.3   Newton's Friction Force Description

Reynolds did not study fluid forces in his experiments. Newton had already done this for fluids as well as for solids; although he is most well-known for his work in solid mechanics. Newton's postulated a fluid friction law based upon the following model. Consider two parallel plates, each of unit area, and separated by a fluid filling a width y between the plates as shown in figure 4.2.
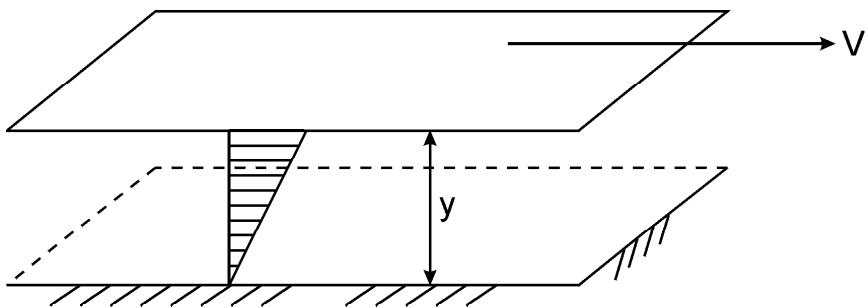
Figure 4.2: Newton's Friction Postulation

If the upper plate is moved with a velocity, V, with respect to the other, then Newton postulated that the velocity profile between the plates was linear, and that the force needed to sustain the movement was proportional to:

$$\tau = \eta \cdot \frac{V}{y} \quad \text{or} \quad \tau = \eta \cdot \frac{dV}{dy} \tag{4.2}$$

in which:

$$
\begin{array}{rcl}
\eta & = & \text{Dynamic viscosity of the fluid } (\frac{\text{kg}}{\text{m·s}}) \\
\tau & = & \text{Shear force per unit area or shear stress } (\text{N/m}^2) \\
\frac{dV}{dy} & = & \text{Velocity gradient } (1/\text{s})
\end{array}
$$

Equation 4.2 works well for viscous fluids and for low velocities and thus Reynolds numbers smaller than about 2000. Other formulations for the fluid friction force under more realistic situations are given in chapter 14.

There is a straightforward relationship between the dynamic viscosity, η, and kinematic viscosity, ν :

$$\nu = \frac{\eta}{\rho} \tag{4.3}$$

in which ρ (kg/m^3) is the mass density of the fluid.

4.3   Dimensionless Ratios and Scaling Laws

One dimensionless ratio - the Reynolds number - has already been introduced above. This section discusses this and one additional common dimensionless number: the Froude number. These are both commonly found in offshore hydromechanics.

Dimensionless ratios are used to characterize families of different conditions in an efficient way. Reynolds used a single number above to characterize flows of different fluids through different diameter pipes and at different velocities. His Reynolds number conveniently combined the three independent variables to form a single one. As long as a consistent set of units is used - it makes no difference if the velocity has been measured in meters per second, feet per minute, or even leagues per fortnight!

For example, by using the Reynolds number to characterize the flow in a pipeline, it is possible to calibrate a venturi or orifice meter using a flow of water even though the meter may later be used to measure a flow of something more exotic like supercritical steam or even molten sodium.

A second use of dimensionless numbers is to correlate (or convert) measurements made on small physical models to equivalent values for a *full-sized* or *prototype* situation. This allows experiments to be carried out on a series of relatively inexpensive *physical models* rather than having to build as many full-sized ships (or other objects) instead.

Dimensionless numbers will be used for both purposes later in this chapter. The remainder of this section is concerned primarily with physical models, however.

4.3.1   Physical Model Relationships

Physical model experiments require some form of similarity between the prototype and the model:

- **Geometric similarity:** The model must have physical dimensions which are uniformly proportional to those of the prototype; it must have the same shape.

- **Kinematic similarity:** Velocities in the model must be proportional to those in the prototype.

- **Dynamic similarity:** Forces and accelerations in the model must be proportional to those in the prototype.

These three similarities require that all location vectors, velocity vectors and force vectors in the coincident coordinates of the scaled model and the prototype have the same direction (argument) and that the magnitude of these vectors (modulus) must relate to each other in a constant proportion.

If α - a number larger than 1 - is used to denote the ratio between the prototype (subscript p) quantity and the model (subscript m) quantity, then:

Item	Scale Factor	Relationship
Length	α_L	$L_p = \alpha_L \cdot L_m$
Velocity	α_V	$V_p = \alpha_V \cdot V_m$
Acceleration of gravity	α_g	$g_p = \alpha_g \cdot g_m$
Density of fluid	α_ρ	$\rho_p = \alpha_\rho \cdot \rho_m$
Fluid viscosity	α_η	$\eta_p = \alpha_\eta \cdot \eta_m$

With these, the scale factors for the areas S, the volumes ∇, the masses M and the mass moments of inertia I, are respectively:

$$
\begin{aligned}
\alpha_S &= \alpha_L^2 \qquad \alpha_\nabla = \alpha_L^3 \qquad \alpha_I = \alpha_\rho \cdot \alpha_L^5 \\
\alpha_M &= \alpha_\rho \cdot \alpha_\nabla = \alpha_\rho \cdot \alpha_L^3
\end{aligned}
\tag{4.4}
$$

The velocity of a body or a water particle is defined as a displacement per unit of time, so the scale factor for the time becomes:

$$
\alpha_T = \frac{\alpha_L}{\alpha_V}
\tag{4.5}
$$

The acceleration of a body or a water particle is defined as an increase of the velocity per unit of time, so the scale factor for the acceleration becomes:

$$
\alpha_A = \frac{\alpha_V}{\alpha_T} = \frac{\alpha_V^2}{\alpha_L}
\tag{4.6}
$$

According to Newton's law, the inertia forces are defined as a product of mass and acceleration, so the scale factor for the inertia forces (and the resulting pressure forces) works out to be:

$$
\begin{aligned}
\alpha_F &= \alpha_M \cdot \alpha_A = \left(\alpha_\rho \cdot \alpha_L^3\right) \cdot \left(\frac{\alpha_V^2}{\alpha_L}\right) = \\
&= \alpha_\rho \cdot \alpha_V^2 \cdot \alpha_L^2
\end{aligned}
\tag{4.7}
$$

Then, the relation between the forces F_p on the prototype and the forces F_m on the model is:

$$
\begin{aligned}
F_p &= \alpha_F \cdot F_m \\
&= \alpha_\rho \cdot \alpha_V^2 \cdot \alpha_L^2 \cdot F_m
\end{aligned}
\tag{4.8}
$$

or:

$$
\alpha_F = \frac{F_p}{F_m} = \frac{\rho_p \cdot V_p^2 \cdot L_p^2}{\rho_m \cdot V_m^2 \cdot L_m^2}
\tag{4.9}
$$

From this, it is obvious that one can write for these forces:

$$
F_p = C \cdot \frac{1}{2}\rho_p V_p^2 \cdot L_p^2 \qquad \text{and} \qquad F_m = C \cdot \frac{1}{2}\rho_m V_m^2 \cdot L_m^2
\tag{4.10}
$$

in which the constant coefficient, C, does not depend on the scale of the model nor on the stagnation pressure term $\frac{1}{2}\rho V^2$.

Viscous forces can be expressed using Newton's friction model as being proportional to:

$$F_v \quad \alpha \quad \eta \frac{V}{L} L^2 \tag{4.11}$$

while the inertia forces (from above) are proportional to:

$$F_i \quad \alpha \quad \rho L^3 \frac{V^2}{L} = \rho L^2 V^2 \tag{4.12}$$

The ratio of these two forces is then - after cancelling out some terms:

$$\frac{F_i}{F_v} = \frac{\rho}{\eta} V \cdot L = \frac{V \cdot L}{\nu} = Rn \tag{4.13}$$

The Reynolds number is thus a measure of the ratio of these forces. Viscous forces are predominant when the Reynolds number is small.

Gravity forces are simply proportional to the material density, the acceleration of gravity and the volume:

$$F_g \quad \alpha \quad \rho g L^3 \tag{4.14}$$

The above information can be used to help design physical models. One can deduce that various forces are represented to different scales. It is therefore impossible to represent all model forces with the same relative importance as in the prototype. A choice is therefore often made, instead, to maintain the ratio between the two most important forces in the prototype when a physical model is built. This can result in several scaling laws as outlined in appendix B. Two of the more important forms are discussed here, however.

4.3.2   Reynolds Scaling

Reynolds scaling is used when inertia and viscous forces are of predominant importance in the flow. This is the case for pipe flow (under pressure) and for wake formation behind a body in a flow. Reynolds scaling requires that the Reynolds number in the model be identical to that in the prototype. Using the basic relations above:

$$\frac{V_m L_m}{\nu_m} = \frac{V_p L_p}{\nu_p} \tag{4.15}$$

or, expressed another way:

$$\frac{\alpha_V \cdot \alpha_L}{\alpha_\nu} = 1. \tag{4.16}$$

Since $\alpha_V = \alpha_L/\alpha_T$, then this becomes:

$$\alpha_T = \frac{\alpha_L^2}{\alpha_\nu} \tag{4.17}$$

Since the fluids in the model and in the ocean are about the same, α_ν (and even α_ρ for that matter) is very close to 1.0, so that:

$$\alpha_T \approx \alpha_L^2 \tag{4.18}$$

This last result, that the time scale is the square of the length scale, would mean that time would pass quite rapidly in the model. Also, one can make further substitutions to discover that α_F is equal to unity; forces in the model would be just as big as in the prototype - again very impractical!

4.3.3   Froude Scaling

Gravity forces become important when a free surface of a liquid is involved. This will be true, whenever a water surface or waves are present. Since inertia and pressure forces are nearly universally important, this makes it appropriate to keep the ratio of $\frac{\text{inertia or pressure forces}}{\text{gravity forces}}$ the same in the model as in the prototype. Scaling based upon the square root of this ratio is called Froude scaling, after **Robert Edmund Froude** (as distinct from his father William Froude from the model resistance extrapolation to full scale, treated in a following section) who has first used it.

Working this out from the basic information above and in a way very analogous to that used for Reynolds scaling yields:

$$
Fn \; = \; \sqrt{\frac{\text{inertia or pressure forces}}{\text{gravity forces}}}
$$

$$
= \; \sqrt{\frac{\alpha_\rho \cdot \alpha_V^2 \cdot \alpha_L^2}{\alpha_\rho \cdot \alpha_L^3 \cdot \alpha_g}} = \frac{\alpha_V}{\sqrt{\alpha_g \cdot \alpha_L}} = \frac{V}{\sqrt{gL}} \tag{4.19}
$$

Since it is especially difficult (or at least very costly) to change the acceleration of gravity for a model involving free liquid surfaces, one may safely set $\alpha_g = 1$. Continuing as was done above, one finds that:

$$
\alpha_T = \sqrt{\alpha_L} \tag{4.20}
$$

This is a lot more convenient to handle than Reynolds scaling!

4.3.4   Numerical Example

As an example, suppose a ship with a length $L_s = L_{pp} = 100$ meter, which sails with a forward ship speed V of 20 knots in still seawater with a temperature of 15°C. Resistance and propulsion tests will be carried out in a towing tank with a 1:40 scale physical model ($\alpha_L = 40$). The temperature of the fresh water in the tank is 20ºC.

The density and the kinematic viscosity of fresh water, salt water and dry air as a function of the temperature are listed in appendix A. Values needed here are for sea water: $\rho = 1025.9$ kg/m^3 and $\nu = 1.19 \cdot 10^{-6}$ m^2/s. The relevant values for fresh water are now: $\rho = 998.1$ kg/m^3 and $\nu = 1.05 \cdot 10^{-6}$ m^2/s.

The length of the ship model is:

$$
L_m = \frac{L_s}{\alpha_L} = \frac{100}{40} = 2.50 \text{ m} \tag{4.21}
$$

The speed V_s of the ship is:

$$
V_s = 0.5144 \cdot V = 0.5144 \cdot 20 = 10.29 \text{ m/s} \tag{4.22}
$$

For practical reasons, the speed of the model will be obtained using Froude scaling:

$$V_m = \frac{V_s}{\sqrt{\alpha_L}} = \frac{10.29}{\sqrt{40}} = 1.63 \text{ m/s} \tag{4.23}$$

As a consequence, the Froude numbers for the ship and model are obviously identical and equal to 0.329.

A consequence of this scaling is that the Reynolds numbers will differ:

$$
\begin{aligned}
Rn_s &= \frac{V_s \cdot L_s}{\nu_{salt}} = \frac{10.29 \cdot 100}{1.19 \cdot 10^{-6}} = 865 \cdot 10^6 \\
Rn_m &= \frac{V_m \cdot L_m}{\nu_{fresh}} = \frac{1.63 \cdot 2.50}{1.05 \cdot 10^{-6}} = 3.88 \cdot 10^6
\end{aligned}
\tag{4.24}
$$

so that:

$$\alpha_{Rn} = 223 \tag{4.25}$$

In order to obtain equal Reynolds numbers, the "model water" needs a kinematic viscosity which is 1/223 times its actual value; this liquid is not available!

Reynolds versus Froude scaling will be picked up again later in this chapter. First, however, the next sections of this chapter will discuss the flow around and hydrodynamic forces on a slender cylinder in a constant current.

4.4   Cylinder Flow Regimes

This figure below summarizes the various forms of flow around a cylinder. A more complete discussion can be found in [Schlichting, 1951]. The Reynolds number (listed on the left, below the flow pattern name) is used in figure 4.3 to characterize each type of flow. The significance of the Cd values listed there will become clear in a later section of this chapter, by the way. The right hand column in figure 4.3 gives a short comparative description of the flow pattern.

4.5   Drag and Lift

Now that the flow patterns near a circular cylinder have been determined, attention can be shifted to the forces that result from the flow.

4.5.1   Drag Force and Drag Coefficient

The pressure variation near a cylinder wall was given in chapter 3. Applying this now in a slightly different way to reveal the pressure difference, relative to an undisturbed flow pressure, yields:

$$
\begin{aligned}
\Delta p &= p - p_0 \\
&= \frac{1}{2} \cdot \rho \cdot U_\infty^2 \cdot \left(1 - 4 \cdot \sin^2\theta\right)
\end{aligned}
\tag{4.26}
$$

in which:
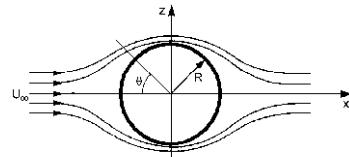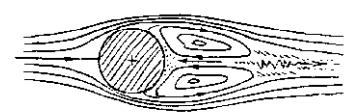
Flow and Parameters	Flow Patern	Flow Description
1. Viscous *Rn < 1* $C_D > 12$		Flow is symmetric about both axes. Friction dominates.
2. Hele-Shaw *1 < Rn < 5* *12 > C_D > 4.5*		Slight separation downstream. Symmetry about flow axis only. Inertia becomes important.
3. Symmetric Vortices *5 < Rn < 65* *4.5 > C_D > 1.6*		First separation and vortices downstream. Wake unstable (turbulent) farther downstream.
4. Precritical *65 < Rn < 5 000* *1.6 > C_D > 1.2*		Vortices become unstable and alternately separate forming a Von Karman vortex street.
5. Subcritical *5K < Rn < 200K* *C_D about 1.2*		Turbulent mixing between vortices downstream. Laminar boundary layer on front of cylinder.
6. Critical *200K < Rn < 500K* *1.2 > C_D > 0.3*		Turbulent wake behind cylinder. Separation and re-attachment of boundary layer upstream of wake.
7. Supercritical *500K < Rn < 4M* *0.3 < C_D < 0.7*		Separation 'bubble' gone. Cylinder boundary layer begins to be turbulent. Wake becomes wider.
8. Postcritical *Rn > 4M* *Cd about 0.7*		Turbulence reaches the boundary layer on the upstream side.

Figure 4.3: Flow Regiems and Descriptions

$$
\begin{aligned}
\Delta p &= \text{pressure difference } (\tfrac{\text{N}}{\text{m}^2}/\text{m} = \text{N/m}) \\
p &= \text{local pressure at the cylinder wall (N/m)} \\
p_0 &= \text{ambient pressure in the undisturbed flow (N/m)} \\
U_\infty &= \text{undisturbed flow velocity (m/s)} \\
\rho &= \text{mass density of the fluid (kg/m}^3) \\
\theta &= \text{angle measured from approaching flow direction (rad)}
\end{aligned}
$$

Since the term $\frac{1}{2} \cdot \rho \cdot U_\infty^2$ also has units of pressure (it is in fact the **stagnation pressure**), it can be convenient to make Δp dimensionless by dividing it by this value. This defines the dimensionless pressure coefficient, C_p. In potential flow theory this coefficient has a value of:

$$
\begin{aligned}
C_p &= \frac{\Delta p}{\frac{1}{2} \cdot \rho \cdot U_\infty^2} \\
&= \left(1 - 4 \cdot \sin^2 \theta\right)
\end{aligned} \tag{4.27}
$$

Experimental and theoretical C_p values are compared in figure 4.4 for smooth cylinders. (The theoretical value of C_p was plotted in polar coordinates in chapter 3, by the way.)
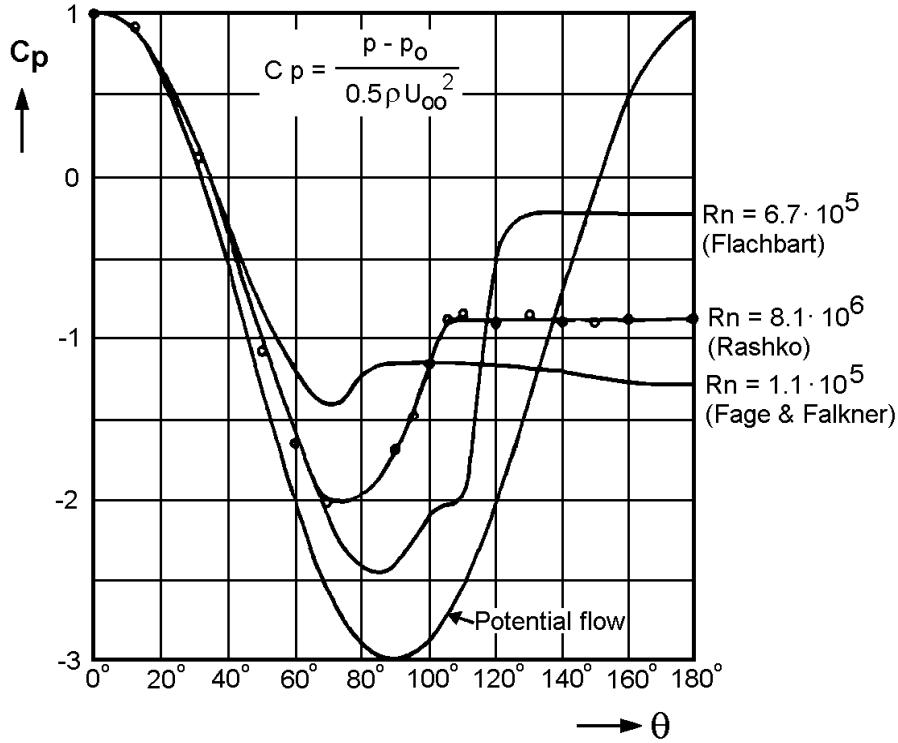
Figure 4.4: Comparison of Theoretical and Experimental Pressure Coefficients

The experimental results compare well to the theory only for small values of θ (on the upstream side). C_p remains approximately constant for θ values greater than about 80 to 120 degrees depending on the Reynolds number. The disagreement between experiments and theory is an indication that the flow has at least been disturbed and generally has separated. The flow disturbance results in a **drag force** - by definition parallel to the flow

direction - on the cylinder. This force (on a unit length of cylinder) can be written as a function of the (undisturbed) stagnation pressure:

$$F_D = \frac{1}{2}\rho\, U^2\, C_D\, D \tag{4.28}$$

in which:

$$
\begin{array}{rcl}
F_D &=& \text{drag force per unit length of cylinder (N/m)}\\
\rho &=& \text{mass density of the fluid (kg/m}^3\text{)}\\
C_D &=& \text{dimensionless coefficient (-)}\\
D &=& \text{cylinder diameter (m)}\\
U &=& \text{undisturbed flow velocity (m/s)}
\end{array}
$$

The drag force is the product of the stagnation pressure, $\frac{1}{2}\rho\, U^2$, an area, D times a unit length, and a dimensionless coefficient, C_D.
This equation thus defines the **drag coefficient** as:

$$C_D = \frac{F_D}{\frac{1}{2}\rho\, U^2 \cdot D} \tag{4.29}$$

The drag coefficient depends on Rn, the cylinder's roughness and the turbulence of the incident flow. The resulting drag coefficients for a fixed smooth cylinder in a constant velocity flow have already been included in figure 4.3.

Fall Velocity

One of the simplest applications of the drag force concept is for the determination of the fall velocity of an object. This is the maximum speed with which an object will fall through the medium which surrounds it. A parachute jumper soon reaches his or her fall velocity (of about 7 m/s) after jumping out of an aircraft, for example. Attention in offshore engineering focuses instead on the speed at which sand grains or gravel or even ropes and chains fall through sea water.
The **fall velocity** in any of these cases is determined by an equilibrium between the **submerged weight** (see chapter 2) of the object on the one hand and the **drag force** from its environment on the other. In equation form:

$$W_{sub} = C_D\, D \cdot \frac{1}{2}\rho\, V_f{}^2 \tag{4.30}$$

in which W_{sub} is the submerged weight of the object (N) and V_f is the fall velocity of the object (m/s).
If one is considering an isolated particle - such as a stone, then the drag coefficient, C_D ,used in equation 4.30 will be for the three-dimensional object. If, on the other hand, a long object such as a rope (fall crosswise) is being considered, then W_{sub} and C_D relate to the two dimensional object.
C_D in equation 4.30 is dependent upon the Reynolds number which depends in turn upon the velocity, V_f . One must iterate (a simple trial-and-error approach is sophisticated enough) to find the proper combination of these two unknowns. This is illustrated here for a steel wire rope such as is used as the main tow rope on the *Smit Rotterdam*, one of

the largest tugboats in the world. The basic data is that the segment of wire rope is 3 inches (76 mm) in diameter and has a submerged weight of 196 N/m. Because the surface of the rope is rough, (it is made from twisted strands of wire) it will have a drag coefficient which is about 30% higher than that listed above for a smooth cylinder. The iteration is indicated in the following table.

$V_{f\ \text{guess}}$ (m/s)	Rn (-)	C_D (-)	$V_{f\ \text{calc}}$ (m/s)
5.0	375 000	1.2	2.05
2.0	150 000	1.6	1.78
1.78	131 250	1.6	1.78

The computation converges quite easily. The numerical value may surprise some; even a seemingly heavy steel wire rope will not fall all that fast in water!

The order of magnitude of the fall velocities for other materials is summarized in the table below.

Quantity→ Object ↓	D (mm)	W_{sub} (N)	Rn (-)	V_f (m/s)
sand grain	0.2	$0.07 \cdot 10^{-6}$	≈ 2	0.02
gravel	20	0.07	20 000	1.00
stone	100	8.38	235 000	2.35
1 m wire rope	76	196	131 250	1.78
1 m chain	76	1079	396000	3.00

Common Fall Velocities

This data for sand, gravel and stones will be handy later when sea bed morphology is discussed in chapter 14. The diameter used for chain is based upon its mass per unit length. Its drag coefficient is about 50% higher than that of a smooth cylinder.

Of course some objects can fall much faster than the values given here. A 400 ton pile was dropped by accident in the Gulf of Mexico when it was hanging in a vertical position. A crude under water measurement, made before it would have reached its terminal fall velocity, indicated a speed of about 11 m/s. When it hit the sea bed - luckily next to the platform it was originally intended for - its impact caused it to penetrate 75 meters into the sea bed.

4.5.2   Lift Force and Strouhal Number

A **lift force** is defined as a force component acting perpendicular to the undisturbed flow velocity. It is therefore also perpendicular to the drag force component. As explained

in chapter 3, there is no lift force when the cylinder is placed in a completely symmetric potential flow. Since the flow pattern remains symmetric in a real flow for Reynolds numbers below about 65, there will be no lift force under these conditions either. However, from the time that vortices are (alternately) shed behind the cylinder, a cyclic pressure variation will occur in the wake. At the location where the vortex is closest to the cylinder the local velocities in the wake will be highest and the local pressures will be lowest. This leads to a resulting force directed toward the vortex; its component in the flow direction is the drag force discussed above, its component perpendicular to the flow direction is the lift. See figure 4.5.
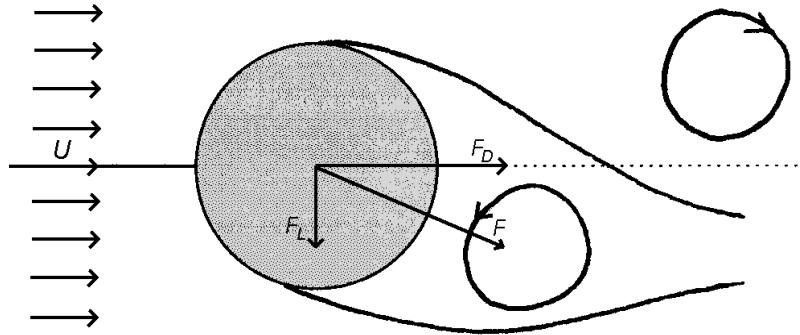
Figure 4.5: Lift, Drag and Resultant Forces

Because vortices are shed alternately, this lift force will alternate in direction as well. Its magnitude will vary more or less sinusoidally with a frequency corresponding to the vortex shedding frequency, f_v, so that:

$$F_\ell = \frac{1}{2} \rho \, U^2 \cdot D \cdot C_L \cdot \sin\left(2\pi \, f_v \, t + \varepsilon_{Ft}\right) \tag{4.31}$$

in which:

$$
\begin{array}{rcl}
F_\ell & = & \text{lift force per unit cylinder length (N/m)} \\
f_v & = & \text{vortex shedding frequency (Hz)} \\
D & = & \text{cylinder diameter (m)} \\
U & = & \text{undisturbed flow velocity (m/s)} \\
C_L & = & \text{dimensionless lift coefficient (-)} \\
t & = & \text{time (s)} \\
\varepsilon_{Ft} & = & \text{phase shift (rad)}
\end{array}
$$

Given the vortex shedding frequency, one can define the dimensionless **Strouhal number** as:

$$St = \frac{f_v \cdot D}{U} \tag{4.32}$$

where St depends on the Reynolds number, Rn, as shown in figure 4.6 taken from reference [Lienhard, 1966] for circular cylinders. It is valid for a circular cylinder with its axis perpendicular to the flow.

Notice that for $10^2 < Rn < 2 \cdot 10^5$ the Strouhal number, St, is approximately 0.2. For $Rn > 2 \cdot 10^5$ the Strouhal number, St, increases a little bit; the vortices and thus the lift force fluctuations are no longer regular and its frequency becomes harder to define.
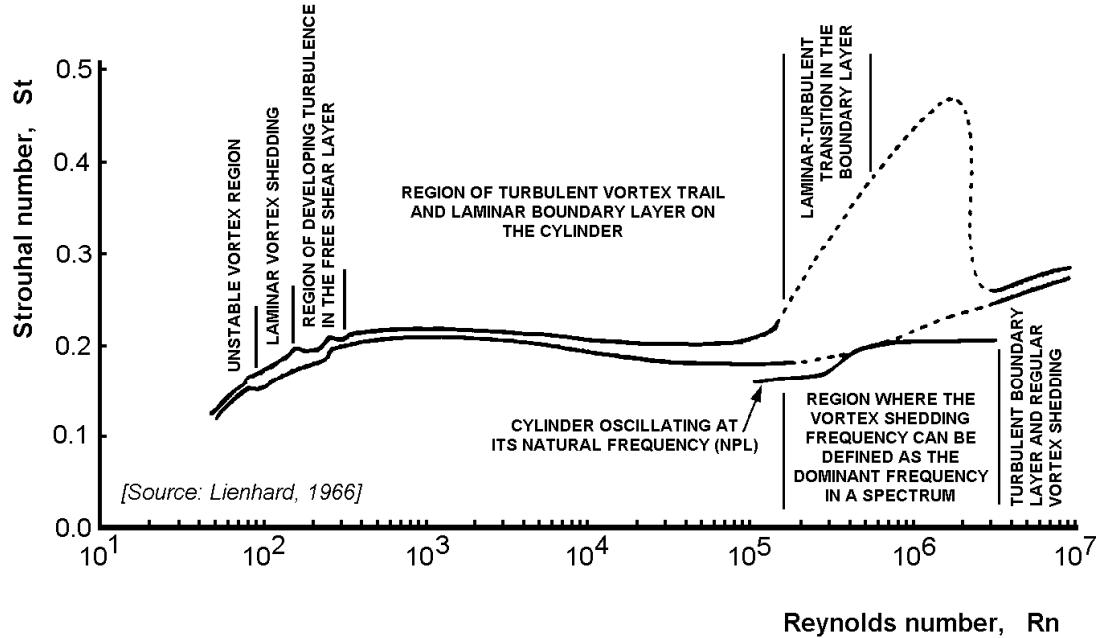
Figure 4.6: Strouhal Number as Function of Reynolds Number

Figure 4.7 schematically shows the vortex street behind a cylinder at four consecutive time instants during a constant flow from left to right.

A. In the initial vortex configuration (at the top of figure 4.7), there is a vortex close behind the cylinder and above the flow axis. Velocities are high in the vortex so that pressures are low; both the upward lift force and the drag force (always to the right) will be maximum.

B. In the second image, the vortices have separated from the cylinder a bit. At this instant the pressure field directly along the cylinder will be rather uniform and less pronounced. The lift force will be zero and the drag force will be slightly lower than in the first situation.

C. The third image is a reflection (about the flow axis) of the first. The lift force is now directed downward and is maximum; the drag force is again maximum as well.

D. The fourth image is a reflection of the second one; the lift force is again zero and the drag is again a bit lower.

This pattern keeps on repeating itself. One sees that the lift force oscillates back and forth with a frequency f_v; the drag force varies only slightly - a fact that is often neglected completely, by the way - and with a frequency of $2 f_v$. This behavior of both the lift and drag will be important for vortex induced vibrations later in this chapter.

While the magnitude of the lift force on a unit length of a cylinder can be of the same order of magnitude as the drag force, one is usually not too concerned about lift forces on offshore structures. This is the case because the drag forces always act in the direction of the current. the elemental drag forces on all cylinder elements add up nicely when integrated over the entire structure to yield a very significant resulting total drag force.
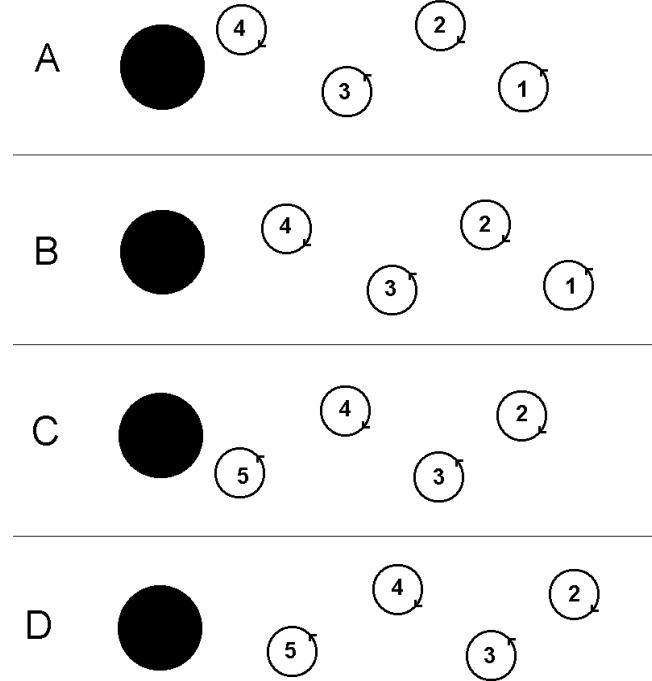
Figure 4.7: Vortex Street Behind Cylinder at 4 Sequential Moments

In contrast to this, the lift force direction on each cylinder segment is entirely dependent on the position of the local vortex at that instant. These vortices will be more or less randomly distributed in the wake of the structure at any time. The lift force on one cylinder segment may be acting in one direction, while at that same time the lift force nearby may be acting in the opposite direction. Integration of these elemental forces over the entire structure leads to a resultant which is much smaller than the resultant drag force.

4.6 Vortex Induced Oscillations

There is one condition, however, which can lead to concern about dynamic lift forces: This concern stems from the fact that if the natural frequency of vibration of the structure - think of an umbilical cable to a remote controlled vehicle for example - happens to coincide with the Strouhal frequency at which vortices are shed, then spectacular things can happen. These are discussed here.

To get an idea of some numerical values - assume $D = 1$ m and $U = 1$ m/s - the corresponding Reynolds number is about $1 \cdot 10^6$. For this value of Rn one finds that the Strouhal number, St, is about 0.2 so that the vortex shedding period is $T_v = 1/f_v \approx 5$ s.

If the natural oscillation frequency of the structure is f_n, then the so-called **reduced velocity** (a dimensionless value) can be defined as:

$$U_r = \frac{U}{f_n \cdot D} \tag{4.33}$$

The **reduced velocity** can be seen as an indicator of resonance. Resonance occurs when

the vortex shedding frequency f_v approaches the natural frequency, f_n:

$$f_v = \frac{St \cdot U}{D} \rightarrow f_n \tag{4.34}$$

so that the reduced velocity is then approximately:

$$U_r = \frac{1}{St} \approx 5 \tag{4.35}$$

Thus, once the natural oscillation frequency of a structure (long risers, or umbilical cables are fine examples) is known, one can determine U_r and use it to predict a danger from resonant vortex-induced oscillations.

4.6.1 Crosswise Oscillations

To understand what is happening, consider the situation as one slowly increases the flow velocity, U, past a cylinder. When the velocity is low enough (but still high enough to cause alternating vortex shedding), the cylinder will remain relatively still in the flow and the vortices will be randomly distributed along the cylinder length in its wake. As U increases, f_v will increase too. As U_r approaches a value of about 5 one observes that the cylinder begins to oscillate significantly in a direction *crosswise to the flow*. A significant effect of this cylinder oscillation is that it distorts the local flow pattern, making it more attractive for vortices to be shed 'behind' the cylinder (seen from the perspective of both the cylinder motion and the flow). Since each adjacent segment of the cylinder is moving in more or less the same way at any instant in time, this in turn stimulates the vortices to become more coherent along the cylinder length. The more or less randomly distributed lift forces on different cylinder or cable segments now start working in phase with one another. The cable responds to this more coherent lift force excitation by oscillating with a larger amplitude - thus reinforcing the entire process; this is called **lock-in**.

As the ambient flow velocity continues to increase, lock-in will ultimately stop (usually after U_r reaches a value of about 7) and the cable comes more or less to rest again. People are still trying to explain and accurately predict these phenomena.

Influence on Drag

A secondary effect of transverse cylinder oscillations can be an increased drag force. There are two "popular and pragmatic" approaches to explain this.

Remembering first that the drag force is:

$$F_D = \frac{1}{2}\rho\, U^2 \cdot C_D \cdot D \tag{4.36}$$

Then:

- Because the cylinder is oscillating (crosswise to the flow), its wake becomes wider. This has an effect similar to that of increasing D; which would increase F_D. This is usually expressed by increasing the value of C_D , instead..
- Since the cylinder now also moves with speed dY/dt, the instantaneous incident flow velocity relative to cylinder becomes:

$$\vec{U}_i = -\frac{dY}{dt}\,\vec{y} + U\ \vec{x} \tag{4.37}$$

So that:

$$U_i^2 = \left[\frac{dY}{dt}\right]^2 + U^2 \tag{4.38}$$

This also increases F_D.

Note that in this latter approach the drag force will no longer (strictly speaking) be directed along the x-axis, parallel to U. Instead, its direction oscillates in phase with dY/dt.

It has been reported that hoisting cables from cranes used to install objects in deep water of at least several hundred meters depth can oscillate in this way. The results have been dramatic at times - with drag coefficients becoming as much as three times the values associated with a fixed wire rope.

The above discussion of forces on an oscillating cylinder is not yet complete. The cylinder oscillation also leads to inertia forces, but these are outside the scope of this chapter; they are discussed in chapter 12.

4.6.2   In-Line Oscillations

The slight time-varying oscillating component of the drag force - superposed on a much more important constant component - has already been mentioned. The amplitude of the "ripple" is usually only a few percent of the total force, and its frequency is twice the Strouhal frequency. Oscillations of the cylinder - if they occur - will now appear for lower values of U_r. Indeed, a cable will sometimes begin a small resonant vibration in the in-line (parallel to the flow) direction when the ambient velocity is only about half that needed to cause a crosswise oscillation.

4.7   Ship Still Water Resistance

This section on the resistance of ships moving in still water is partly based on a text by [Kuiper, 1997] on resistance and propulsion of ships. This text is a good reference for those who wish to know more than is presented here about still water resistance.

The most common purpose of a ship is to transport cargo. The displacement hull form is the most appropriate concept for such ships. The weight of the cargo, stores and fuel is called the **deadweight**. This deadweight and the weight of the empty ship together are equal to the **displacement** of the ship. The movement of such a displacement ship requires relatively little power in comparison to other means of transport, at least at low speed. This is because the friction of the water is low and, as long as the waves generated by the moving ship are small, the required amount of power remains small.

A characteristic feature of a displacement ship is that a large amount of cargo is moved at low speeds with low power. As an indication: the power consumption per ton-km cargo transport of a 90 meters length ship at sea is about 1/3 of the power needed for the same transport at land, but the average sustained sea speed of 12 knots is also only about 1/3 of the speed during road transport (assuming there are no excessive traffic jams).

The low speed restriction for a ship is very important; at increasing speeds the required power increases rapidly due to wave generation. At low speeds, the speed-dependent skin friction drag is the major part of the resistance. For an extrapolation from ship model data

to prototype data, this part mainly depends on the Reynolds number. At higher speeds, one observes an increasing radiation of waves by the hull, which means the appearance of a speed-dependent second type of resistance; wave making resistance. For an extrapolation from ship model data to prototype data, this part mainly depends on the Froude number. In the second part of the 19th century **William Froude**, 1810 - 1879, (as distinct from his son **Robert Edmund Froude** from the Froude number) proposed the British Admiralty to build what would become the world's first towing tank at Torquay in England. He had recently developed scaling laws for predicting the resistance of ships from tests on ship models and he intended to use this tank for the required scale model experiments. The British Admiralty accepted Froude's proposal on the condition that he also used the tank to investigate the ways of reducing the rolling motion of ships. That was when sails were being replaced by steam driven propulsion systems and roll was becoming more of a problem. On March 3 1872, the first indoor professional model test in the world was carried out in a basin of 85 x 11 x 3 meter, as shown in figure 4.8. About half a century later, Froude's towing tank was pulled down.

Froude's Tank (1872)   Denny Tank (1883)

Figure 4.8: The World's First Towing Tanks

In 1883, the world's first privately owned towing tank, the Denny tank as shown in figure 4.8 too, was built at Dumbarton in Scotland, using the original design of Froude's tank in Torquay. The Denny tank - with dimensions 93.00 x 6.80 x 2.75 meter - was closed in 1983, but it was re-opened in 1986 under the umbrella of the Scottish Maritime Museum. The tank testing and museum parts are separate. Since 1989, the tank testing facility operates under the management of Strathclyde University's Department of Ship and Marine Technology.

It has been the merit of William Froude to distinguish the components of the **total hull resistance, R_t,** and to relate them to scaling laws; he distinguished between:
    - a **frictional resistance** component, R_f, and
    - a **residual resistance** component, R_r.
Then he made a very drastic simplification, which has worked out remarkably well: **Froude's first hypothesis** was that these two components of the resistance are independent of each other. The determination of these two components was a second problem, but he found a simple way out of this problem. **Froude's second hypothesis** was that the frictional part

of the resistance can be estimated by the drag of a flat plate with the same wetted area and length as the ship or model. In principle, a flat plate (towed edgewise) has no wave resistance and can therefore be investigated over a range of Reynolds numbers ($Rn = VL/\nu$) without influence of the wave-related Froude number ($Fn = V/\sqrt{gL}$).

4.7.1 Frictional Resistance

To determine the frictional resistance coefficient, William Froude's approach yielded that the frictional resistance coefficient was related to the resistance coefficient of a flat plate with the same length and wetted surface as the ship or model hull:

$$\boxed{C_f = \frac{R_f}{\frac{1}{2}\rho V^2 S}} \qquad \text{or:} \qquad \boxed{R_f = \frac{1}{2}\rho V^2 \cdot C_f \cdot S} \tag{4.39}$$

in which:

$$
\begin{array}{rcl}
C_f & = & \text{frictional resistance coefficient (-)} \\
R_f & = & \text{frictional resistance (N)} \\
\rho & = & \text{density of water (kg/m}^3\text{)} \\
V & = & \text{ship or model speed (m/s)} \\
S & = & \text{wetted surface of ship or model hull (m}^2\text{)}
\end{array}
$$

He did numerous experiments to determine the resistance coefficients of a flat plate as a function of the Reynolds number. He himself did not find a single relationship as a function of the Reynolds number due to laminar flow and edge effects in his measurements. His results not only depended on the Reynolds number but also on the length of the plate. Several friction lines based only on the Reynolds number were developed later, both theoretically using boundary layer theory and experimentally.

For **laminar** flows, the resistance coefficient was formulated from boundary layer theory by Blasius:

$$\text{Blasius:} \quad C_f = 1.328 \cdot \sqrt{Rn} \tag{4.40}$$

So-called **plate lines** were developed for **turbulent** boundary layer flows from the leading edge. These plate lines were extended to include full scale Reynolds numbers. They have relatively simple formulations, such as the **Schoenherr Mean Line** or the **ITTC-1957 Line**, which are defined as:

$$\text{Schoenherr:} \qquad \frac{0.242}{\sqrt{C_f}} = \log_{10}\left(Rn \cdot C_f\right) \tag{4.41}$$

$$\text{ITTC-1957:} \qquad C_f = \frac{0.075}{\left(\log_{10}\left(Rn\right) - 2\right)^2} \tag{4.42}$$

The latter one is accepted as a standard by the International Towing Tank Conference (ITTC).

As a matter of fact it is not too important that a flat plate with a certain length and wetted surface has a resistance coefficient exactly according to one of the mentioned lines. The Froude hypothesis is crude and correlation factors are required afterwards to arrive at correct extrapolations to full scale values. These correlation factors will depend on the plate line which is used.

4.7.2 Residual Resistance

The determination of the resistance components of a ship's hull can be illustrated with the results of resistance tests with a series of models at various scales, the "Simon Bolivar" family of models. Resistance tests were carried out over a certain speed range for each of the models. Each model had a different scale factor, α. The total resistance (in non-dimensional form) is shown in figure 4.9.
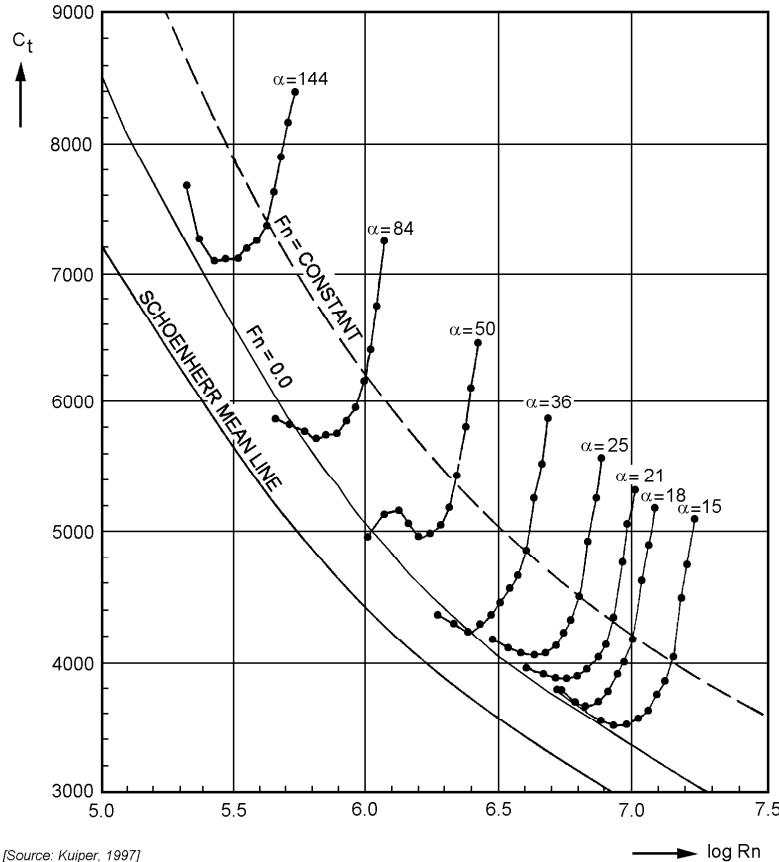
Figure 4.9: Resistance Coefficients of the "Simon Bolivar" Model Family

The **total resistance** force on a ship is made non-dimensional in the same way as the frictional resistance above:

$$\boxed{C_t = \frac{R_t}{\frac{1}{2}\rho V^2 S}} \qquad \text{or:} \qquad \boxed{R_t = \frac{1}{2}\rho V^2 \cdot C_t \cdot S} \qquad (4.43)$$

in which:

$$
\begin{aligned}
C_t &= \text{total resistance coefficient (-)} \\
R_t &= \text{total resistance (N)} \\
\rho &= \text{density of water (kg/m}^3\text{)} \\
V &= \text{ship or model speed (m/s)} \\
S &= \text{wetted surface of ship or model hull (m}^2\text{)}
\end{aligned}
$$

C_t is plotted as a function of the logarithm of the Reynolds number, $Rn = V \cdot L_{WL} / \nu$, in which $\mathbf{L}_{WL}$ is **the length at the water plane**. Each curve of data points has been made with a model of the given scale. The Schoenherr Mean Line follows from equation 4.41; the other two curves connect the points for Fn is zero and for Fn is another constant, respectively.

Similar lines can be drawn for other Froude numbers. Such a line of constant Froude number is approximately parallel to this plate line. If all scaling laws could be satisfied, the resistance curves at all model scales would coincide. Because the Reynolds number is not maintained, this is not the case and each model has a separate curve.

The **residual resistance** coefficient, C_r, at a certain Froude number is now the vertical distance between the plate line and the line for that Froude number. When the plate line and the line of constant Froude number are parallel, this means that the residual resistance component is indeed independent of the Reynolds number. This is assumed to be always the case in Froude's method and the residual resistance at each Froude number is determined by subtracting the calculated frictional resistance coefficient of a flat plate according to equations 4.41 or 4.42 from the measured total resistance.

The assumption that the residual resistance is approximately independent of the Reynolds number is not accurate in many cases. This means that the lines of constant Froude number in figure 4.9 are not exactly parallel. The residual resistance in that case contains a component which depends on the Reynolds number.

To determine this component, the line for $Fn \to 0$ has been determined in figure 4.9. When the Froude number becomes sufficiently small the generated waves will disappear and the difference between the total resistance coefficient and the plate line can only be associated with the longer distance of water particles to travel along the (not flat) hull form and some small viscous effects. Thus the difference between the plate line and the line $Fn \to 0$ has to do with the form of the hull and is therefore called **form resistance**. The line $Fn \to 0$ is now assumed to be always parallel to the lines for other Froude numbers, so that the difference between the total resistance coefficient and the line $Fn \to 0$ is independent of the Reynolds number. This difference is now called **wave resistance**.

In this way the total resistance is split up into:
  - the frictional resistance (from the plate line),
  - the form resistance and
  - the wave resistance.
Form resistance and wave resistance together constitute Froude's residual resistance.

Form Resistance.

Several hypotheses have been made about the relation between the form resistance and the frictional resistance. As already mentioned, Froude assumed that the form resistance was independent of the Reynolds number. He therefore included it as a part of the residual resistance. Hughes in 1953 assumed that the form drag was proportional to the viscous resistance and multiplied the viscous resistance coefficient, C_f, by a constant factor, k, as shown in figure 4.10.

The Reynolds-dependent component of the resistance thus becomes $(1 + k) \cdot C_f$. The factor $(1 + k)$ is called the **form factor**. Froude's method is still used, but Hughes' approach of is the most widely adopted one and is the accepted standard by the ITTC.
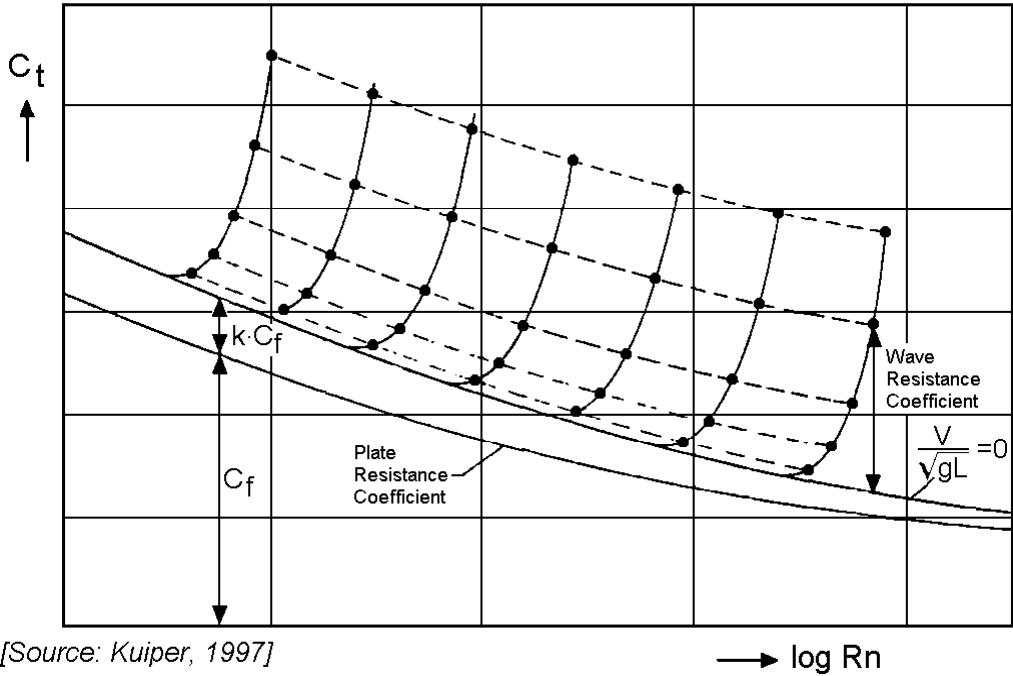
Figure 4.10: Hughes Extrapolation Method

The form factor is influenced primarily by the shape of the after part of the ship but it is often given as a function of the block coefficient, C_B, of the ship as a whole. The **block coefficient** is the ratio between the ship's displacement volume and that of a rectangular box in which the ship's underwater volume "just fit".

Form factors associated with typical block coefficients are listed below.

C_B	$1 + k$
<0.7	1.10-1.15
0.7-0.8	1.15-1.20
>0.8	1.20-1.30

Wave Resistance.

The wave resistance coefficient of the model, C_w, over the speed range of the model is now found by subtracting the frictional and form resistance coefficients from the measured total resistance coefficient:

$$C_w = C_t - (1 + k) \cdot C_f \tag{4.44}$$

4.7.3   Extrapolation of Resistance Tests

Given the components of the total resistance of the model, one must extrapolate this data to full scale. The resistance of the model is generally measured from a low speed up to the design speed. The model design speed is set by maintaining the full scale Froude number. Equation 4.43 is used to express the total resistance in dimensionless form.

The wetted surface, S, is taken as the wetted length from keel to still water line of the frames, integrated over the ship length and multiplied by two, to account for both sides

of the ship. Note that the ship length is measured directly along the center line and not along the water line.

The Froude number is maintained during the model test. This means that the wave resistance coefficient, C_w, at model scale and at full scale are the same. The total resistance coefficient of the ship, $C_{t\,\text{ship}}$, can therefore be found from:

$$\boxed{C_{t\,\text{ship}} = (1+k) \cdot C_{f\,\text{ship}} + C_w + C_a}$$ (4.45)

The form factor, k, and the wave resistance coefficient, C_w, are found directly from the model test. The frictional resistance coefficient at full scale, $C_{f\,\text{ship}}$, can be read from the plate line using the full scale Reynolds number.

The additional resistance coefficient, C_a, is a new element. This coefficient is a correlation coefficient based on experience at full scale. It accounts both for extrapolation errors due to the various assumptions made and for effects at full scale which are not present at the model. Such effects include the relatively rough surface at full scale in relation to the boundary layer thickness. Moreover, C_a contains a correction for the difference in air resistance of the above water part of the hull of model and prototype. [Holtrop and Mennen, 1982] give a simple formula for C_a as a fraction of the length of the ship:

$$C_a = 0.006 \cdot (L_{WL} + 100)^{-0.16} - 0.00205$$ (4.46)

in which L_{WL} is the length of the water plane in meters.

The additional resistance coefficient decreases in this formula with increasing length and this can be attributed, at least partly, to roughness effects. The effect of surface roughness in general requires special attention.

4.7.4 Resistance Prediction Methods

Thus, the total resistance of the ship follows from:

$$\boxed{R_{t\,\text{ship}} = \frac{1}{2}\rho V^2 \cdot C_{t\,\text{ship}} \cdot S}$$ (4.47)

and the resistance coefficient, C_{ts}, has to be determined.

A number of methods to determine the still water resistance coefficients of ships, based on (systematic series of) model test data, are given in the literature. A very well known method, developed at MARIN, is described by [Holtrop, 1977], [Holtrop and Mennen, 1982] and [Holtrop, 1984]. The method is based on the results of resistance tests carried out by MARIN during a large number of years and is available in a computerized format. The reader is referred to these reports for a detailed description of this method, often indicated by the "**Holtrop and Mennen" method**. An example for a tug of the correlation between the results of this "Holtrop and Mennen" method and model test results is given in figure 4.11.

4.8 Wind Loads

Like all environmental phenomena, wind has a stochastic nature which greatly depends on time and location. It is usually characterized by fairly large fluctuations in velocity and
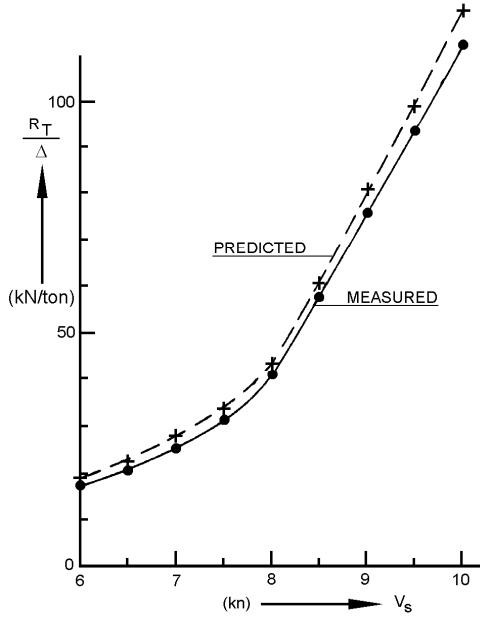
Figure 4.11: Comparison of Resistance Prediction with Model Test Results

direction. It is common meteorological practice to give the wind velocity in terms of the average over a certain interval of time, varying from 1 to 60 minutes or more.

Local winds are generally defined in terms of the average velocity and average direction at a standard height of 10 meters above the still water level. A number of empirical and theoretical formulas are available in the literature to determine the wind velocity at other elevations. An adequate vertical distribution of the true wind speed z meters above sea level is represented by:

$$\frac{V_{tw}(z)}{V_{tw}(10)} = \left(\frac{z}{10}\right)^{0.11} \qquad \text{(at sea)} \qquad (4.48)$$

in which:

$$
\begin{array}{lll}
V_{tw}(z) & = & \text{true wind speed at } z \text{ meters height above the water surface} \\
V_{tw}(10) & = & \text{true wind speed at 10 meters height above the water surface}
\end{array}
$$

Equation 4.48 is for sea conditions and results from the fact that the sea is surprisingly smooth from an aerodynamic point of view - about like a well mowed soccer field.

On land, equation 4.48 has a different exponent:

$$\frac{V_{tw}(z)}{V_{tw}(10)} = \left(\frac{z}{10}\right)^{0.16} \qquad \text{(on land)} \qquad (4.49)$$

At sea, the variation in the mean wind velocity is small compared to the wave period. The fluctuations around the mean wind speed will impose dynamic forces on an offshore structure, but in general these aerodynamic forces may be neglected in comparison with the hydrodynamic forces, when considering the structures dynamic behavior. The wind will be considered as steady, both in magnitude and direction, resulting in constant forces and a constant moment on a fixed floating or a sailing body.

The wind plays two roles in the behavior of a floating body:

- Its first is a direct role, where the wind exerts a force on the part of the structure exposed to the air. Wind forces are exerted due to the flow of air around the various parts. Only local winds are needed for the determination of these forces.

- The second is an indirect role. Winds generate waves and currents and through these influence a ship indirectly too. To determine these wind effects, one needs information about the wind and storm conditions in a much larger area. Wave and current generation is a topic for oceanographers; the effects of waves and currents on floating bodies will be dealt with separately in later chapters.

Only the direct influence of the winds will be discussed here.

Forces and moments will be caused by the speed of the wind relative to the (moving) body. The forces and moments which the wind exerts on a structure can therefore be computed by:

$$X_w = \frac{1}{2}\rho_{air}V_{rw}^2 \cdot C_{Xw}(\alpha_{rw}) \cdot A_T$$

$$Y_w = \frac{1}{2}\rho_{air}V_{rw}^2 \cdot C_{Yw}(\alpha_{rw}) \cdot A_L$$

$$N_w = \frac{1}{2}\rho_{air}V_{rw}^2 \cdot C_{Nw}(\alpha_{rw}) \cdot A_L \cdot L \tag{4.50}$$

in which:

X_w	=	steady longitudinal wind force (N)
Y_w	=	steady lateral wind force (N)
N_w	=	steady horizontal wind moment (Nm)
$\rho_{air} \approx \rho_{water}/800$	=	density of air (kg/m^3)
V_{rw}	=	relative wind velocity (m/s)
α_{rw}	=	relative wind direction (-), from astern is zero
A_T	=	transverse projected wind area (m^2)
A_L	=	lateral projected wind area (m^2)
L	=	length of the ship (m)
$C_{*w}(\alpha_{rw})$	=	α_{rw}-dependent wind load coefficient (-)

Note that it is a "normal" convention to refer to the true **wind direction** as the direction from which the wind comes, while waves and currents are usually referred to in terms of where they are going. A North-West wind will cause South-East waves, therefore!

4.8.1   Wind Loads on Moored Ships

For moored ships, only the true wind speed and direction determine the longitudinal and lateral forces and the yaw moment on the ship, as given in figure 4.12. Because of the absence of a steady velocity of the structure, the relative wind is similar to the true wind:

$$\boxed{V_{rw} = V_{tw}} \qquad \text{and} \qquad \boxed{\alpha_{rw} = \alpha_{tw}} \tag{4.51}$$

The total force and moment experienced by an object exposed to the wind is partly of viscous origin (pressure drag) and partly due to potential effects (lift force). For blunt

[Source: Remery and van Oortmerssen, 1973]
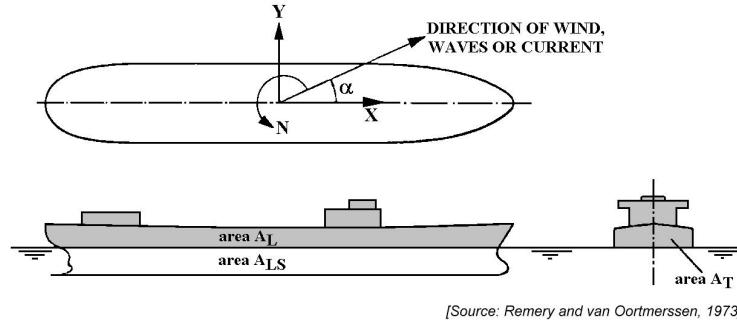
Figure 4.12: Definitions Used here for Forces and Moments

bodies, the wind force is regarded as independent of the Reynolds number and proportional to the square of the wind velocity.

[Remery and van Oortmerssen, 1973] collected the wind data on 11 various tanker hulls. Their wind force and moment coefficients were expanded in Fourier series as a function of the angle of incidence. From the harmonic analysis, it was found that a fifth order representation of the wind data is sufficiently accurate, at least for preliminary design purposes:

$$
\begin{aligned}
C_{Xw} &= a_0 + \sum_{n=1}^{5} a_n \sin(n \cdot \alpha_{rw}) \\
C_{Yw} &= \sum_{n=1}^{5} b_n \sin(n \cdot \alpha_{rw}) \\
C_{Nw} &= \sum_{n=1}^{5} c_n \sin(n \cdot \alpha_{rw})
\end{aligned}
\tag{4.52}
$$

with wind coefficients as listed below.

Tanker No.	1	2	3	4	5	6	7	8	9	10	11
Length L_{pp}					225 m	225 m	225 m	225 m	172 m	150 m	150 m
Condition	loaded	ballast	loaded	ballast	loaded	ballast	loaded	ballast	loaded	loaded	ballast
Bridge Location	at $\frac{1}{2}L$	at $\frac{1}{2}L$	aft	aft	at $\frac{1}{2}L$	at $\frac{1}{2}L$	aft	aft	aft	aft	aft
a_0	-0.131	-0.079	-0.028	0.014	-0.074	-0.055	-0.038	-0.039	-0.042	-0.075	-0.051
a_1	0.738	0.615	0.799	0.732	1.050	0.748	0.830	0.646	0.487	0.711	0.577
a_2	-0.058	-0.104	-0.077	-0.055	0.017	0.018	0.031	0.034	-0.072	-0.082	-0.058
a_3	0.059	0.085	-0.054	-0.017	-0.062	-0.012	0.012	0.024	0.109	0.043	0.051
a_4	0.108	0.076	0.018	-0.018	0.080	0.015	0.021	-0.031	0.075	0.064	0.062
a_5	-0.001	0.025	-0.018	-0.058	-0.110	-0.151	-0.072	-0.090	-0.047	-0.038	0.006
b_1	0.786	0.880	0.697	0.785	0.707	0.731	0.718	0.735	0.764	0.819	0.879
b_2	0.039	0.004	0.036	0.014	-0.013	-0.014	0.032	0.003	0.037	0.051	0.026
b_3	0.003	0.003	0.018	0.014	0.028	0.016	0.010	0.004	0.052	0.023	0.014
b_4	0.034	-0.004	0.028	0.015	0.007	0.001	-0.001	-0.005	0.016	0.032	0.031
b_5	-0.019	-0.003	-0.023	-0.020	-0.044	-0.025	-0.040	-0.017	-0.003	-0.032	-0.029
$10 \cdot c_1$	-0.451	-0.338	-0.765	-0.524	-0.216	-0.059	-0.526	-0.335	-1.025	-0.881	-0.644
$10 \cdot c_2$	-0.617	-0.800	-0.571	-0.738	-0.531	-0.730	-0.596	-0.722	-0.721	-0.681	-0.726
$10 \cdot c_3$	-0.110	-0.080	-0.166	-0.175	-0.063	-0.035	-0.111	-0.090	-0.345	-0.202	-0.244
$10 \cdot c_4$	-0.110	-0.096	-0.146	-0.089	-0.073	-0.017	-0.113	-0.047	-0.127	-0.145	-0.076
$10 \cdot c_5$	-0.010	-0.013	0.021	-0.021	0.024	-0.013	0.099	0.067	-0.022	0.039	0.024

Figure 4.13 shows, as an example, the measured wind forces and moment together with their Fourier approximation, for one of the tankers.
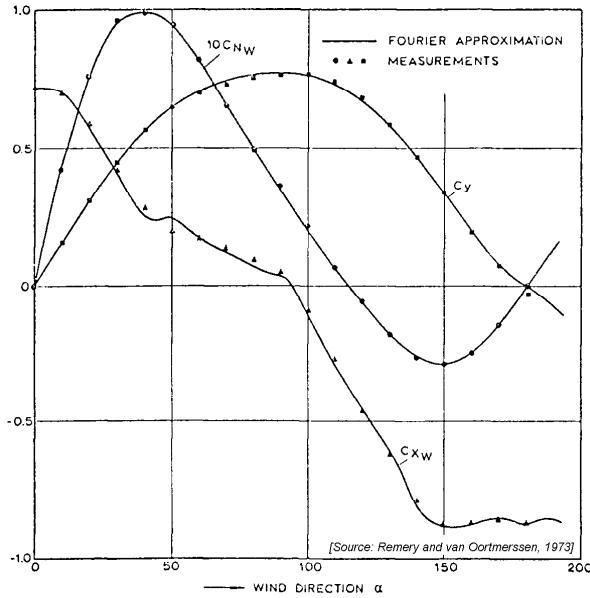
Figure 4.13: Example of Wind Load Coefficients

4.8.2 Wind Loads on Other Moored Structures

The wind forces on other types of structures, as for instance semi-submersible platforms, can be approximated by dividing the structure into a number of components, all with a more or less elementary geometry, and estimating the wind force on each element. Drag coefficients are given in the literature for a lot of simple geometrical forms, such as spheres, flat plates and cylinders of various cross sectional shapes. [Hoerner, 1965] and [Delany and Sorensen, 1970] are good sources of this information. The total wind load on the structure is found by adding the contributions of all the individual component parts. The fact that one element may influence the wind field of another element is neglected in this analysis.

4.8.3 Wind Loads on Sailing Ships

For sailing merchant ships and tankers, only the longitudinal wind resistance, $X_w = R_w$, is of importance for determining a sustained sea speed.

The relative wind speed, V_{rw}, and the relative wind direction, α_{rw}, have to be determined from this true wind speed, V_{tw}, and the true wind direction, α_{tw}, together with the forward ship speed, V_s, and the heading of the ship, see figure 4.14.

As opposed to the hydromechanical notation, for seamen head wind has a direction equal to zero. The effect of the lateral force and the yaw moment on the ship will be corrected via a small course correction. Then the relative wind speed and the relative wind direction (so head wind has a direction equal to zero) follows from:

$$\boxed{V_{rw} = \sqrt{V_s^2 + V_{tw}^2 + 2 \cdot V_s \cdot V_{tw}}}$$

$$\boxed{\alpha_{rw} = \arctan\left(\frac{V_{tw} \cdot \sin\alpha_{tw}}{V_s + V_{tw} \cdot \cos\alpha_{tw}}\right)} \tag{4.53}$$
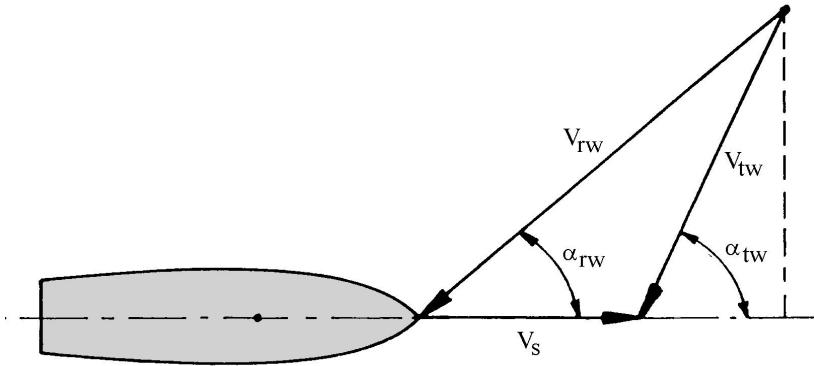
Figure 4.14: Relative Wind

[Isherwood, 1973] published a reliable method for estimating the wind resistance. He analyzed the results of wind resistance experiments carried out at different laboratories with models covering a wide range of merchant ships. He determined empirical formulas for the two horizontal components of the wind force and the wind-induced horizontal moment on any merchant ship form for a wind coming from any direction.

The longitudinal wind resistance is defined by:

$$X_w = \frac{1}{2}\rho_{air}V_{rw}^2 \cdot C_{X_w} \cdot A_T \qquad (4.54)$$

with for the longitudinal wind resistance coefficient C_{X_w}:

$$C_{X_w} = A_0 + A_1 \cdot \frac{2A_L}{L_{oa}^2} + A_2 \cdot \frac{2A_T}{B^2} + A_3 \cdot \frac{L_{oa}}{B} + A_4 \cdot \frac{S}{L_{oa}} + A_5 \cdot \frac{C}{L_{oa}} + A_6 \cdot M \qquad (4.55)$$

in which:

$$
\begin{array}{lll}
L_{oa} & = & \text{length over all (m)} \\
B & = & \text{beam (m)} \\
S & = & \text{length of perimeter of lateral projection excluding water line} \\
& & \text{and slender bodies such as masts and ventilators (m)} \\
C & = & \text{distance from bow of centroid of lateral projected area (m)} \\
A_L & = & \text{lateral projected wind area (m}^2) \\
A_T & = & \text{transverse projected wind area (m}^2) \\
M & = & \text{number of distinct groups of masts or kingposts seen in lateral} \\
& & \text{projection (-); kingposts close against the bridge are not included}
\end{array}
$$

The coefficients for equation 4.55 are listed below.

α_{rw}	A_0	$A_1/10$	A_2	A_3	A_4	$A_5/10$	A_6
0°	2.152	-0.500	0.243	-0.164	0.000	0.000	0.000
10°	1.714	-0.333	0.145	-0.121	0.000	0.000	0.000
20°	1.818	-0.397	0.211	-0.143	0.000	0.000	0.033
30°	1.965	-0.481	0.243	-0.154	0.000	0.000	0.041
40°	2.333	-0.599	0.247	-0.190	0.000	0.000	0.042
50°	1.726	-0.654	0.189	-0.173	0.348	0.000	0.048
60°	0.913	-0.468	0.000	-0.104	0.482	0.000	0.052
70°	0.457	-0.288	0.000	-0.068	0.346	0.000	0.043
80°	0.341	-0.091	0.000	-0.031	0.000	0.000	0.052
90°	0.355	0.000	0.000	0.000	-0.247	0.000	0.018
100°	0.601	0.000	0.000	0.000	-0.347	0.000	-0.020
110°	0.651	0.129	0.000	0.000	-0.582	0.000	-0.031
120°	0.564	0.254	0.000	0.000	-0.748	0.000	-0.024
130°	-0.142	0.358	0.000	0.047	-0.700	0.000	-0.028
140°	-0.677	0.364	0.000	0.069	-0.529	0.000	-0.032
150°	-0.723	0.314	0.000	0.064	-0.475	0.000	-0.032
160°	-2.148	0.256	0.000	0.081	0.000	0.127	-0.027
170°	-2.707	0.397	-0.175	0.126	0.000	0.181	0.000
180°	-2.529	0.376	-0.174	0.128	0.000	0.155	0.000

Similar polynomials for the lateral force and the horizontal moment are given in the paper by [Isherwood, 1973].

4.9   Current Loads

There are several independent phenomena responsible for the occurrence of current: the ocean circulation system resulting in a steady current, the cyclical change in lunar and solar gravity causing tidal currents, wind and differences in sea water density. The steady wind velocity at the water surface is about 3 per cent of the wind velocity at 10 meters height. Tidal currents are of primary importance in areas of restricted water depth and can attain values up to 10 knots. However, such extreme velocities are rare; a 2-3 knots tidal current speed is common in restricted seas. The prediction of tidal currents is left for the oceanographers.

Although surface currents will be the governing ones for floating structures; the current distribution as a function of depth below the surface may also be of importance. For the design of a mooring system of a floating structure, the designer is especially interested in the probability that a particular extreme current velocity will be exceeded during a certain period of time. Observations obtained from current speed measurements are indispensable for this purpose. It may be useful to split up the total measured current in two or more components, for instance in a tidal and a non-tidal component, since the direction of the various components will be different, in general. The variation in velocity and direction of the current is very slow, and current may therefore be considered as a steady phenomenon.

The forces and moment exerted by a current on a floating object is composed of the following parts:

- A viscous part, due to friction between the structure and the fluid, and due to pressure drag. For blunt bodies the frictional force may be neglected, since it is small compared to the viscous pressure drag.

- A potential part, with a component due to a circulation around the object, and one from the free water surface wave resistance. In most cases, the latter component is small in comparison with the first and will be ignored.

The forces and moments, as given in figure 4.12, exerted by the current on a floating structure can be calculated from:

$$X_c = \frac{1}{2}\rho \cdot V_c^2 \cdot C_{Xc}(\alpha_c) \cdot A_{TS}$$

$$Y_c = \frac{1}{2}\rho \cdot V_c^2 \cdot C_{Yc}(\alpha_c) \cdot A_{LS}$$

$$N_c = \frac{1}{2}\rho \cdot V_c^2 \cdot C_{Nc}(\alpha_c) \cdot A_{LS} \cdot L \tag{4.56}$$

in which:

X_c	=	steady longitudinal current force (N)
Y_c	=	steady lateral current force (N)
N_c	=	steady yaw current moment (Nm)
ρ	=	density of water (kg/m^3)
V_c	=	current velocity (m/s)
α_c	=	current direction, from astern is zero (rad)
$A_{TS} \approx B \cdot T$	=	submerged transverse projected area (m^2)
$A_{LS} \approx L \cdot T$	=	submerged lateral projected area (m^2)
L	=	length of the ship (m)
B	=	breadth of the ship (m)
T	=	draft of the ship (m)
$C_{-c}(\alpha_c)$	=	α_c-depending current load coefficient (-)

Results of model tests are given in the literature for various types of structures and vessels.

4.9.1   Current Loads on Moored Tankers

[Remery and van Oortmerssen, 1973] published current loads on several tanker models of different sizes, tested at MARIN. The coefficients C_{Xc}, C_{Yc} and C_{Nc} were calculated from these results. A tanker hull is a rather slender body for a flow in the longitudinal direction and consequently the longitudinal force is mainly frictional. The total longitudinal force was very small for relatively low current speeds and could not be measured accurately. Moreover, extrapolation to full scale dimensions is difficult, since the longitudinal force is affected by scale effects.

For mooring problems the longitudinal force will hardly be of importance. An estimate of its magnitude can be made by calculating the flat plate frictional resistance, according to the ITTC skin friction line as given in equation 4.42:

$$X_c = \frac{0.075}{\left(\log_{10}\left(Rn\right) - 2\right)^2} \cdot \frac{1}{2}\rho V_c^2 \cdot \cos\alpha_c \cdot |\cos\alpha_c| \cdot S \tag{4.57}$$

while:

$$Rn = \frac{V_c \cdot |\cos\alpha_c| \cdot L}{\nu} \tag{4.58}$$

with:

$$
\begin{aligned}
S \approx L \cdot (B + 2T) \quad &= \quad \text{wetted surface of the ship (m}^2) \\
L \quad &= \quad \text{length of the ship (m)} \\
B \quad &= \quad \text{breadth of the ship (m)} \\
T \quad &= \quad \text{draft of the ship (m)} \\
V_c \quad &= \quad \text{current velocity (m/s)} \\
\alpha_c \quad &= \quad \text{current direction (-), from astern is zero} \\
\rho \quad &= \quad \text{density of water (ton/m}^3) \\
Rn \quad &= \quad \text{Reynolds number (-)} \\
\nu \quad &= \quad \text{kinematic viscosity of water (m}^2\text{s)}
\end{aligned}
$$

Extrapolation of the transverse force and yaw moment to prototype values is no problem. For flow in the transverse direction a tanker is a blunt body and, since the bilge radius is small, flow separation occurs in the model in the same way as in the prototype. Therefore, the transverse force coefficient and the yaw moment coefficient are independent of the Reynolds number.

The coefficients for the transverse force and the yaw moment were expanded by MARIN in a Fourier series, as was done for the wind load coefficients as described in a previous section:

$$
\begin{aligned}
C_{Yc}(\alpha_c) \quad &= \quad \sum_{n=1}^{5} b_n \cdot \sin(n \cdot \alpha_c) \\
C_{Nc}(\alpha_c) \quad &= \quad \sum_{n=1}^{5} c_n \cdot \sin(n \cdot \alpha_c) \quad\quad\quad (4.59)
\end{aligned}
$$

The average values of the coefficients b_n and c_n for the fifth order Fourier series, as published by [Remery and van Oortmerssen, 1973], are given in the table below.

n	b_n	$10 \cdot c_n$
1	0.908	-0.252
2	0.000	-0.904
3	-0.116	0.032
4	0.000	0.109
5	-0.033	0.011

These results are valid for deep water. For shallow water, the transverse current force and moment coefficients have to be multiplied by a coefficient, which is given in figure 4.15.

The influence of the free surface is included in the data given on the coefficients b_n and c_n in the previous table. This influence, however, depends on the water depth and on the Froude number, and consequently changes if the current velocity or the tanker dimensions change. For the condition to which these data apply, deep water and a prototype current speed in the order of 3 knots, the effect of the free surface is very small. For the case of a small clearance under the keel and a current direction of 90 degrees, damming up of the water at the weather side and a lowering of the water at the lee side of the ship occurs.

4.9.2   Current Loads on Other Moored Structures

Current loads on other types of floating structures are usually estimated in the same way as is used for wind loads.
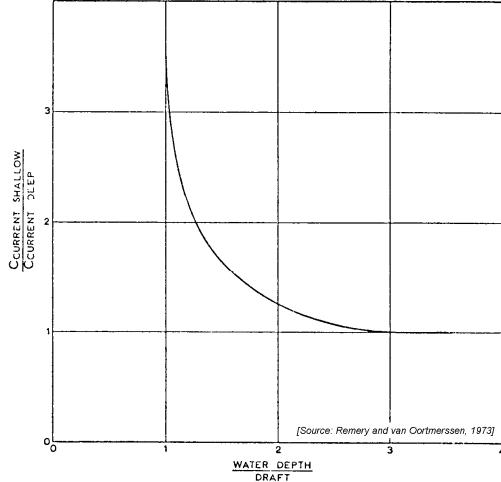
Figure 4.15: Influence of Water Depth on Transverse Current Load on a Tanker

4.9.3   Current Loads on Sailing Ships

For sailing ships, generally it is assumed that the ship is moving with the current. So the forward ship speed is not the ground speed but the speed relative to the water. Then there is no current load; the current itself is a navigation problem only.

4.10   Thrust and Propulsion

Now that the resistance of a ship or other floating objects moving through still water has been discussed, it is appropriate to approach this phenomena from the other side by discussing the propulsion systems needed to overcome the resistance. This section on that topic is partly based on a text by [Kuiper, 1997] on resistance and propulsion of ships. This text is a good reference for those who wish to know more than is presented here about thrust and propulsion.

The basic action of propulsors like propellers is to deliver thrust. In fact, a propulsor is an **energy transformer**, because **torque and rotation**, delivered to the propulsor, will be transformed into **thrust and translation**, delivered by the propulsor. A consequence is that the propulsor also generates water velocities in its wake, which represent a loss of kinetic energy. It is obvious that this will effect the **efficiency** of the propulsor, defined by:

$$\boxed{\eta = \frac{P_{out}}{P_{in}}} = \frac{P_E}{P_D} = \frac{T \cdot V_e}{Q \cdot 2\pi n} \tag{4.60}$$

in which:

η =   propulsive efficiency (-)
P_D =   **delivered power**, delivered **to** the propulsor (Nm/s = W)
P_E =   **effective power**, delivered **by** the propulsor (Nm/s = W)
Q =   torque delivered **to** the propulsor (Nm)
n =   number of revolutions (1/s)
T =   thrust delivered **by** the propulsor (N)
V_e =   mean entrance speed of water in propeller disk,
          also called advance velocity with notation V_a (m/s)

The efficiency varies widely between various types of propulsors, but the **screw propeller** has not yet been equalled in most cases and is therefore the most commonly used propulsor. The propulsor is generally mounted behind the hull. This is because of efficiency; the water which is brought into motion by the friction along the ship is reversed by the propeller action and as a result less energy is left behind in the water.

A risk for every propulsor operating at high rotational velocities is **cavitation**. This occurs when the local pressure, associated with high local velocities in the fluid, is lower than the vapor pressure. As a result the water starts to boil locally and water-vapour filled cavities are formed. When these vapor-filled (not air-filled) cavities in the wake arrive in regions with a higher pressure they collapse violently, causing local shock waves in the water that can **erode** the nearby surface. This dynamic behavior of large cavities can also generate **vibrations** in the ship structure.

4.10.1 Propulsors

The most important propulsors used for shipping and offshore activities include:

- **Fixed Pitch Propellers**, see figure 4.16-a.
  The most common propulsor is the fixed pitch open screw propeller (FPP) which, as all propellers, generates a propulsive force by lift on the propeller blades. These blade sections are similar to those of airfoils, operating at some angle of attack in the flow. The geometry of the propeller blades is quite critical with respect to the occurrence of cavitation. Therefore, a specific propeller is generally designed for the specific circumstances of each ship and its engine. The thrust, and consequently the speed of the ship, is controlled by the propeller rotational speed - often called revolutions or rpm (for revolutions per minute).

- **Controllable Pitch Propellers**, see figure 4.16-b.
  In the case of a controllable pitch propeller (CPP) the thrust is controlled by changing the pitch of the blades. The shaft often has a constant rotational speed. A CCP is often used when the propeller has to operate at more than one design condition - such as free running and towing for a tug. It is also effective when rapid manoeuvering is required or when shaft generators, which require a constant rpm, are present. Reversing the thrust occurs by changing the pitch with constant revolutions in the same direction. This significantly decreases the time required to change the direction of the thrust. It is important to keep in mind that the CPP has only one design pitch; changing the pitch always reduces the efficiency.

- **Ducted Propellers**, see figure 4.16-c.
  At high propeller loadings a duct increases the propeller efficiency. A duct generates

a
Fixed Pitch Propellers

b
Controllable Pitch Propeller

c
Ducted Propeller

d
Thruster

[Source: Kuiper, 1997]

e
Dynamic Positioning with Thrusters

f
Voith-Schneider Propeller

g
Pump- or Waterjet

h
Blade Positons of Voith-Schneider Propeller
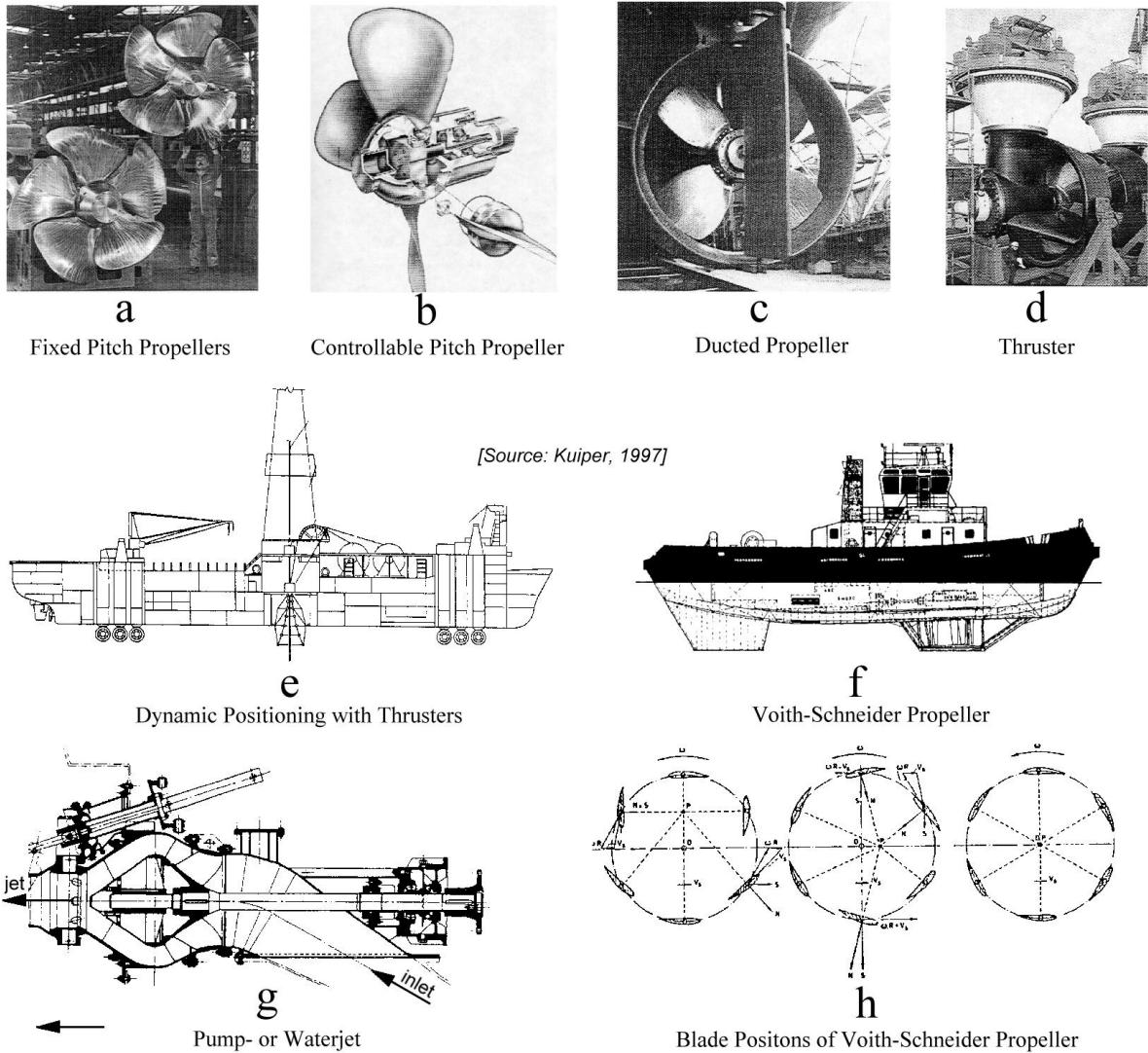
Figure 4.16: Different Propulsion Configurations

part of the total thrust due to its interaction with the propeller. This is the case with an accelerating duct, in which the flow velocity is increased due to the duct. Ducted propellers are used in a wide range of applications with heavily loaded propellers, such as for tugs. Several types of ducts, sometimes asymmetric and sometimes at some distance upstream of the propeller, have been designed to make the propeller inflow more uniform.

- **Thrusters**, see figures 4.16-d and 4.16-e.
  A propeller can be driven from above by a vertical shaft. This makes it possible to rotate the propeller along the vertical axis and to generate thrust in any chosen direction. These configurations are called thrusters. They can have an open propeller, but very often a duct is also used. The right angle drive of a thruster makes it more complicated and thus more expensive and vulnerable than a normal propeller shaft. Also the hub diameter is larger, which slightly decreases efficiency. There are some interesting advantages however. The propeller can be in front of the vertical

shaft (towing) as well as behind it (pushing). In the towing mode the inflow is more uniform; this decreases vibrations and cavitation. A steerable or azimuthing thruster may rotate around a vertical axis which makes it possible to steer with it. This makes it easier to manoeuver, especially at low speeds. They are common for dynamic positioning; the steerable direction of its thrust is fully utilized in that case.

- **Cycloidal or Voiht-Schneider Propellers**, see figures 4.16-f and 4.16-h.
  A very special propulsor is the cycloidal propeller, also called Voiht-Schneider propeller after its main developer. It consists of a number of foils on a rotating plate. These foils can rotate relative to this plate and their position is such that they are always perpendicular to the radii from a moving center point, P, as shown in figure 4.16-h. When this center point is in the center of the blade circle, there is no resulting force. When this center point is moved, a thrust is generated perpendicular to the direction in which the center point is shifted. Thus thrust can be applied in any direction just by moving the center point; rudders can be omitted. This propulsive system can be used for tugs and supply boats, for which maneuvering is important. Its efficiency, however, is lower than that of an open propeller due to the fact that the blades generate thrust over a part of their revolution only, while viscous resistance is present over the whole revolution. Voith-Schneider propellers must be mounted under a flat bottom; a bottom cover is sometimes provided for protection (see figure 4.16-f).

- **Water Jets**, see figure 4.16-g.
  This propulsor accelerates water using a pump inside the hull, instead of a propeller outside the hull. The water is drawn in from the bottom of the ship, is accelerated inside the ship by a pump and leaves the ship at the stern. This has many advantages when a propeller is too vulnerable to damage, or when a propeller is too dangerous as is the case for rescue vessels. Rudders can be omitted because of the rotating possibilities of the outlet and excellent manoeuvering qualities can be obtained, as for instance are required for pilot vessels. A pump jet can be useful in shallow water. However, the inner surface of the pump system is large and the velocities inside are high; the viscous losses are high, too. The efficiency is therefore lower than that of an open propeller.

4.10.2 Propeller Geometry

First some general geometrical definitions of the propeller are given. A sketch of a right handed propeller is given in figure 4.17-a.

- The **propeller blades** are attached to the **hub**, which is attached to the end of the propeller shaft. The propeller rotates about the shaft center line. The direction of rotation is as viewed from behind, that is towards the shaft. In normal forward operation a **right handed propeller** rotates in clockwise direction when viewed from behind.
  The propeller hub is, of course, rotational symmetric because it should not disturb the flow. The attachment of the propeller blade to the hub is a gradual transition, which is done in the **fillet area** or the **blade root**. A streamlined **cap** is generally fitted to the hub at the end of its shaft.
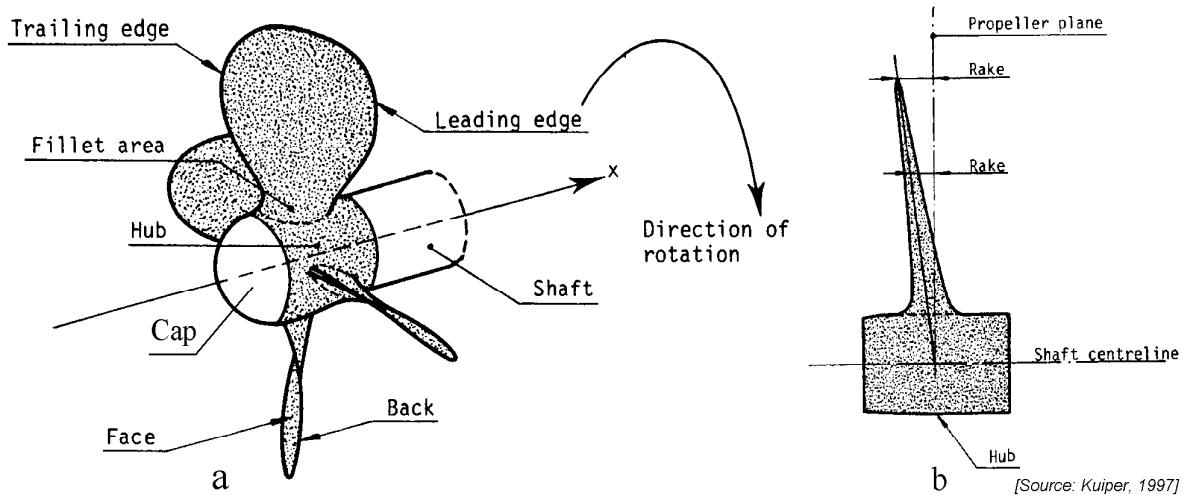
Figure 4.17: Sketch of a Propeller

- The front edge of the blade is called the **leading edge** or **nose** and the other end is the **trailing edge** or **tail**. The outermost position, where leading and trailing edges meet, is called the **blade tip**. The radius of the tip is called the **propeller radius** and the **propeller diameter** is, of course, twice its radius.

- The surface of the blade which is at the side from which the shaft comes is called the propeller **back** and the other side is the **face** of the propeller; when the ship moves forward, the propeller inflow is from its back. Because in forward speed the back side has a low average pressure and the face side has a high average pressure (this pressure difference generates the thrust), the face is also called the **pressure side** and the back the **suction side**.

Consider now an arbitrary propeller as drawn in figure 4.18-a.
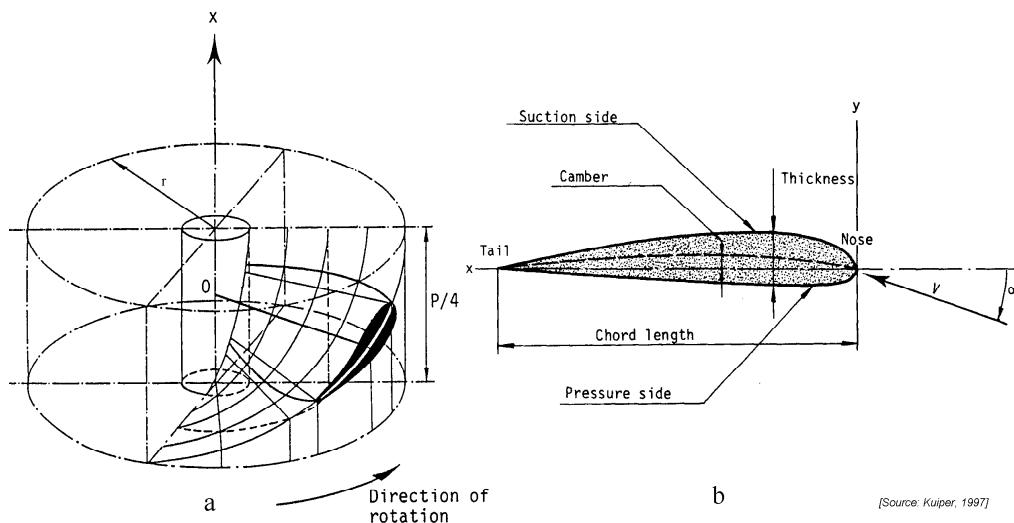
Figure 4.18: Geometry of a Propeller

- The intersection of a cylinder with radius r and a propeller blade, the **blade section**, in figure 4.18-a has the shape of an airfoil. Such a shape is also called just a **foil** or a **profile**, as given in figure 4.18-b.

- The straight line between the leading and trailing edge of the profile is called the **chord line** of the profile and the distance between nose and tail is the **chord length**, c, of the foil.

- Generally, the origin of the local coordinate system of a profile is taken at the leading edge. The x-direction is towards the tail, the y-direction upwards, perpendicular to the chord. The angle between the nose-tail line and the undisturbed flow (relative to the blade) is the **angle of attack**, α.

- The distance between the suction side and the pressure side, measured perpendicular to the chord is the **thickness**, $t(x)$, of the profile. The line of mid-thickness over the chord is the **camber line**.

- The blade sections of the propeller have a certain pitch. The chord line or nose-tail line of the blade section - a helix on the cylinder - becomes a straight pitch line, if the cylinder is developed on to a flat surface. The **propeller pitch**, P, is defined as the increase in axial direction of the pitch line over one full revolution $2\pi r$ at each radius r; see figure 4.19-a. The dimension of the pitch is a length. The ratio P/D is the **pitch ratio**. The **pitch angle**, $\theta = \arctan(P/2\pi r)$, is the angle between the pitch line and a plane perpendicular to the propeller shaft. The pitch distribution is given in a **pitch diagram**, which is simply a graph of the pitch at every radius.

- Figure 4.19-b shows the axial velocity V_e (speed of entrance) and the rotational velocity $2\pi nr$ of the water particles at a radius r from the propeller axis. As a propeller is rotating in water, it can not advance $P \cdot n$ and a certain difference occurs. The difference between $P \cdot n$ and V_e is called the **slip** of the propeller.
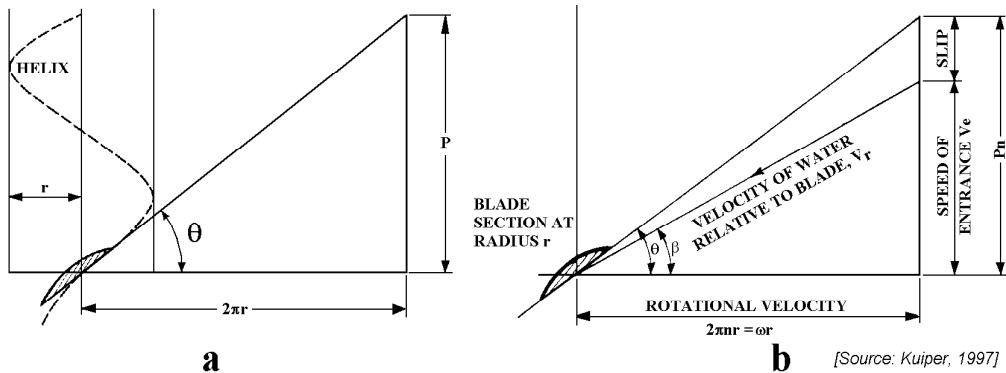
Figure 4.19: Definition of Pitch and Slip

- A significant radius, which is often used as representative for the propeller, is the radius at $r/R = 0.7$. If a pitch is given in the case of a variable pitch distribution it is usually the pitch at $0.7R$. Note that half the area of the propeller disk is within a circle with radius $0.7R$ and that, consequently, the other half is outside this region;

so the pressure at this circular line is "more or less" the average pressure over the full propeller disk.

Now, some important contours and areas will be defined:

- A plane perpendicular to the shaft and through the middle of the chord of the root section is called the **propeller plane**, see figure 4.17-b.

- The projection of the blade contour on the propeller plane gives the **projected blade contour** and its area is called the **projected blade area**. The blade sections in this projection are segments of a circle.

- The blade sections in the cylinder of figure 4.18-a are rotated into a plane parallel to the propeller plane. The angle of rotation at each radius is the pitch angle at that radius. This angle may vary over the radius; so it is a developed view. The ends of the developed blade sections form the **developed blade contour**. The blade sections in this projection remain circular.

- The circular blade sections in the developed contour can be expanded into a plane. The contour thus derived is the developed and expanded contour, generally indicated only as the **expanded contour**. The chord line of the sections in this contour is now straight. Its area is called the **expanded blade area**.

Cavitation

Cavitation inception occurs when the local pressure is equal to the vapor pressure. The local pressure is expressed in non-dimensional terms as the pressure coefficient C_p. Similarly, the **cavitation number** is expressed non-dimensionally as:

$$\boxed{\sigma = \frac{p - p_v}{\frac{1}{2}\rho V^2}} \tag{4.61}$$

where p is the undisturbed pressure in the flow at the propeller shaft $p_0 + \rho g h_s$, p_v is the vapor pressure of water, ρ is the density of water and V is the undisturbed velocity in the fluid.

The condition that cavitation occurs when the local pressure is equal to the vapor pressure, means that a profile or a propeller will start to cavitate when the lowest pressure is near the vapor pressure. This is expressed in non-dimensional terms as:

$$\sigma = -C_p(min) \tag{4.62}$$

The cavitation number or cavitation index, σ, is non-dimensional. This means that it is the parameter which has to be maintained when propeller model tests are carried out. It determines the pressure in the test section of the cavitation tunnel.

Preservation of the cavitation number in a physical "ship+propeller" model is difficult. It is largely for this reason that MARIN built a towing tank in a vacuum chamber, about two decades ago. This allowed them to reduce the atmospheric pressure and thus to keep the σ-value in their model more like that in the prototype.

Blade Area Ratio

An important parameter of the propeller is the **blade area ratio**, given as the ratio between the area of all blades and the area of the propeller plane, $A_0 = 0.25\pi D^2$:

- the projected blade area ratio, A_P/A_0 and
- the expanded blade area ratio, A_E/A_0

in which A_P is the projected blade area and A_E is the expanded blade area.

The latter, the **expanded blade area ratio**, A_E/A_0, is physically most significant; when no further indication is given, this blade area ratio is generally meant.

From the frictional resistance point of view, the blade area should be as low as possible. But a low blade area will result in low pressures (to obtain the required thrust) with high risks on cavitation. The blade area has to be chosen such that cavitation is avoided as much as possible.

Figure 4.20 shows the pressure distribution on a cavitating foil. The pressure at the nose on the back of the propeller drops down to the vapor pressure; a local cavity is the result. A lower pitch ratio (resulting in a less low pressure at the back) and a higher blade area ratio (so a larger foil area) will deliver the same thrust (with a bit lower efficiency) without cavitation.
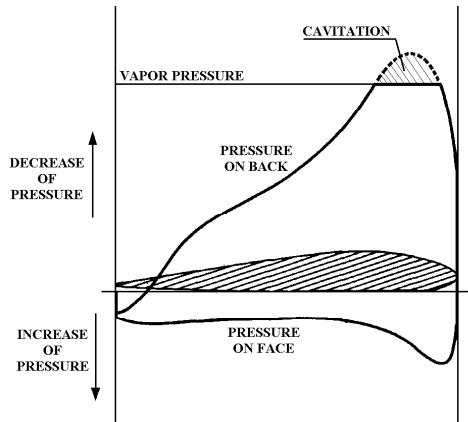
Figure 4.20: Cavitating Foil

An old and very simple formula for the minimum **projected blade area ratio** is that by Taylor:

$$\frac{A_P}{A_0} = 1.067 - 0.229 \cdot \frac{P}{D} \qquad (4.63)$$

A handsome indication for the minimum **expanded blade area ratio** gives the formula of Auf 'm Keller:

$$\frac{A_E}{A_0} = \frac{(1.3 + 0.3 \cdot Z) \cdot T}{(p - p_v) \cdot D^2} + k \qquad (4.64)$$

in which the constant k varies from 0.00 for fast naval vessels to 0.20 for highly powered full ships.

Number of Propeller Blades

The number of propeller blades, Z, is chosen in relation to possible vibrations. An 8 cylinder engine and a 4 bladed propeller may suffer from resonance frequencies because the blade passage frequency (the frequency at which a blade passes close to the rudder for example) and the engine frequencies have common harmonics. In that case vibrations can become extensive, resulting in damage.

The structure of the wake is also important for the choice of the number of blades. When the wake has strong harmonics equal to the number of blades, thrust variations may become large; these, too, can lead to vibrations.

Wageningen Propeller Series

Systematic series of propeller models have been tested by MARIN to form a basis for propeller design. The starting point of a series is its parent form. The extent and applicability of the series depends on the parameters which are varied and on the range of their variations. Several series are described in the literature.

The most extensive and widely used fixed pitch open propeller series is the **Wageningen B-series**. The basic form of the B-series is simple and it has a good performance. The extent of the series is large; some 210 propellers have been tested.

The following parameters of the B-series propellers have been varied:
  - the expanded blade area ratio, A_E/A_0, from 0.3 to 1.2
  - the number of blades, Z, from 2 to 7
  - the pitch ratio, P/D, from 0.5 to 1.4

The propellers are indicated by their number of blades and expanded blade area ratio. For instance, propeller B-4.85 has four blades and an expanded blade area ratio of 0.85. The test results are given in so-called open water diagrams per series of one blade number, one area ratio and a range of pitch ratios. The open water tests of the B-series were done at various rotation rates, n, so at various Reynolds numbers. These results were corrected to a standard Reynolds number of $Rn = 2 \cdot 10^6$ along the lines of the ITTC method, as given by equation 4.42. However, these corrections are very small.

In addition to open fixed pitch propellers, MARIN has also developed series of fixed pitch propellers in an accelerating nozzle ($\mathbf{K_a}$**-series**) and series of controllable pitch propellers in a nozzle. All available information on MARIN systematic propeller series has been summarized by [Kuiper, 1992]. The propulsive characteristics have been described by polynomials to make them usable in computer programs. Some other research institutes have also made their own propeller series, but the Wageningen Propeller Series are the most well known.

4.10.3 Propeller Mechanics

This section discusses the mechanics of a propeller in a uniform flow - the so-called **free running or open water condition**.

Open Water Characteristics

Suppose an **open water propeller** translating with a constant forward speed, V_e, and a constant number of revolutions per second, n, is immersed in a homogeneous initially stationary fluid without any currents or waves. Then, two velocity components can be

defined for this propeller: a rotational velocity, $2\pi n r$, at a certain radius, r, and an axial translation velocity, V_e; see also figure 4.19-b. The **hydrodynamic pitch angle**, β, of the flow relative to the blade sections is generally taken at $r = 0.7R$, just as was done to define the pitch:

$$\boxed{\beta_{0.7R} = \arctan\left(\frac{V_e}{0.7\pi \cdot nD}\right)} \tag{4.65}$$

An important parameter to describe the angle of attack, and therefore the lift and drag, is the **advance ratio**, J, defined by:

$$\boxed{J = \frac{V_e}{nD}} \tag{4.66}$$

The resistance of a ship was made non-dimensional in equation 4.43 by:

$$C_t = \frac{R}{\frac{1}{2}\rho V^2 S} = \frac{R}{\frac{1}{2}\rho \cdot (\text{velocity})^2 \cdot (\text{area})}$$

When using the rotational velocity at for instance $0.7R$ as a characteristic velocity and the area of the propeller disk as a characteristic area, the thrust of a propeller can be made non-dimensional in the same way by:

$$C_T = \frac{T}{\frac{1}{2}\rho \cdot (0.7\pi \cdot nD)^2 \cdot \left(\frac{\pi}{4}D^2\right)} \approx \frac{16.33}{\pi^3} \cdot \frac{T}{\rho D^4 n^2} \tag{4.67}$$

The constant $16.33/\pi^3$ can be included in the constant C_T and so the **thrust coefficient** becomes:

$$\boxed{K_T = \frac{T}{\rho D^4 n^2}} \qquad \text{and thrust becomes:} \qquad \boxed{T = K_T \cdot \rho D^4 n^2} \tag{4.68}$$

The **torque coefficient** can be written in a similar way as:

$$\boxed{K_Q = \frac{Q}{\rho D^5 n^2}} \qquad \text{and torque becomes:} \qquad \boxed{Q = K_Q \cdot \rho D^5 n^2} \tag{4.69}$$

in which:

$$
\begin{array}{lcl}
K_T & = & \text{thrust coefficient (-)} \\
K_Q & = & \text{torque coefficient (-)} \\
T & = & \text{thrust (N)} \\
Q & = & \text{torque (Nm)} \\
\rho & = & \text{density of water (kg/m}^3) \\
D & = & \text{diameter (m)} \\
n & = & \text{revolution speed (1/s)}
\end{array}
$$

These propeller performance characteristics, K_T and K_Q, in a uniform flow are given in figure 4.21.

The power delivered to the propeller is the **delivered power** P_D:

$$\boxed{P_D = Q \cdot 2\pi n} \tag{4.70}$$
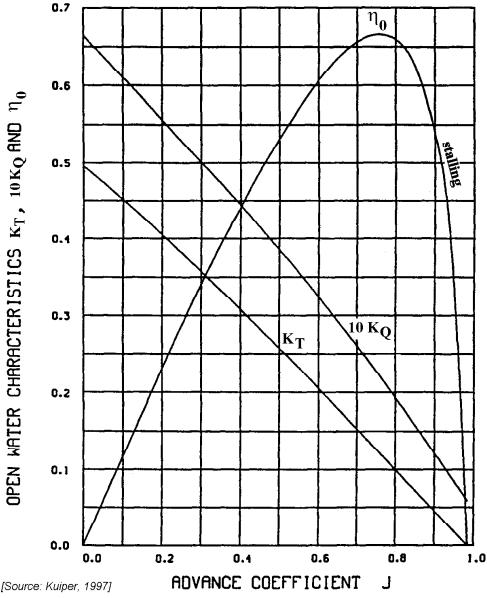
Figure 4.21: Open Water Propeller Diagram

The power delivered by the thrust is the **effective power** P_E:

$$\overline{|P_E = T \cdot V_e|} \tag{4.71}$$

The **efficiency** of the open water propeller is the ratio between effective and delivered power:

$$\eta_O = \frac{P_E}{P_D} = \frac{T \cdot V_e}{Q \cdot 2\pi n} \tag{4.72}$$

or:

$$\overline{\left| \eta_O = \frac{K_T}{K_Q} \cdot \frac{J}{2\pi} \right|} \tag{4.73}$$

In addition to the thrust and torque coefficients, K_T and K_Q, the propulsive efficiency of the open water propeller, η_O, is shown in figure 4.21 too.

Four Quadrant Measurements

The K_T-K_Q-J curves of open water propellers are restricted to the forward advance operation - that is the condition of forward speed of the ship and forward thrust of the propeller. During stopping and manoeuvering of ships and for thrusters used for dynamic positioning, it is important to know the characteristics of the propellers under other conditions. The "four quadrants" of a series of B-propellers have been measured for that purpose. An example is given in figure 4.22-a.

The thrust and torque coefficients, C_T^* and C_Q^*, in figure 4.22-b have been made non-dimensional axis using the undisturbed incoming velocity of the blade sections, V_r. Each curve is for a propeller with a different pitch ratio. The hydrodynamic pitch angle, β, is along the horizontal axis. Both the pitch ratio and β have been determined at $r = 0.7R$.
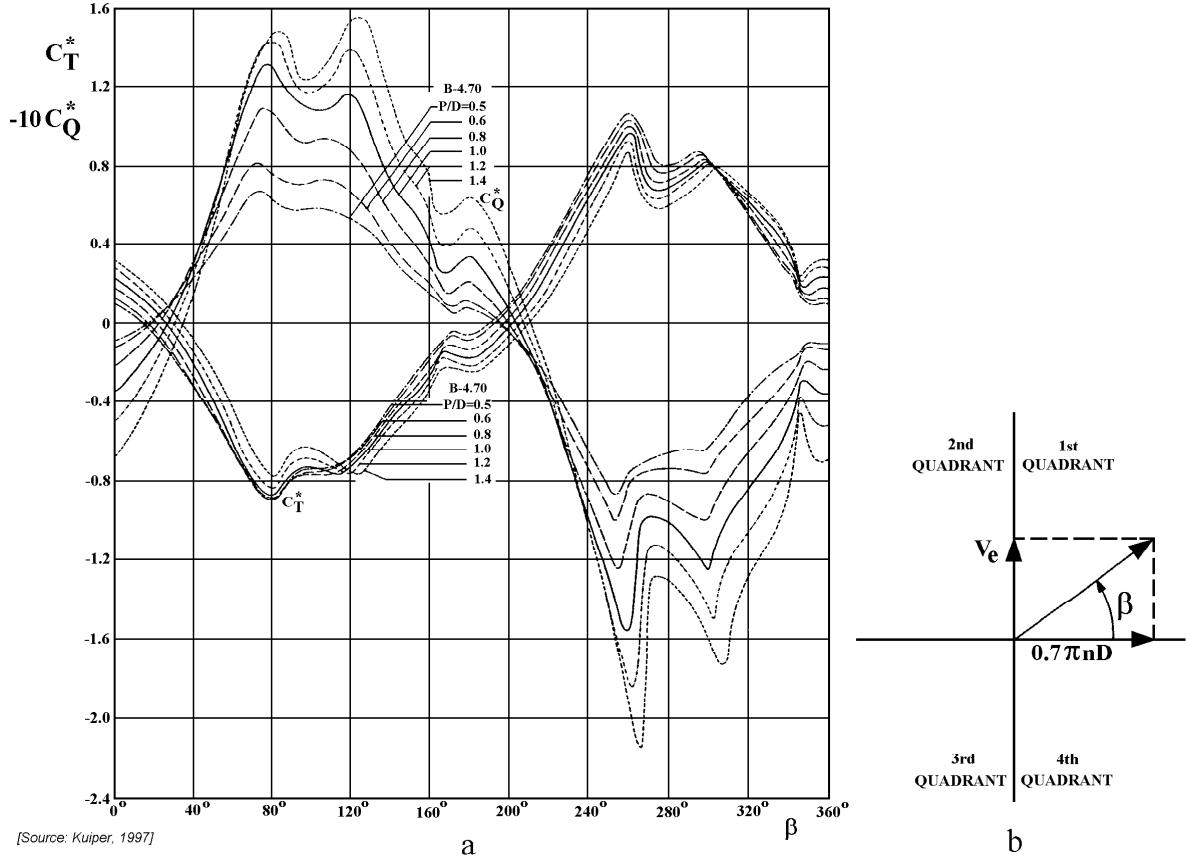
Figure 4.22: Quadrant Measurement Results of B4-70 Propellers

$$\beta = \arctan\left(\frac{V_e}{0.7\pi \cdot nD}\right)$$

$$V_r = \sqrt{V_e^2 + (0.7\pi nD)^2}$$

$$C_T^* = \frac{T}{\frac{1}{2}\rho \cdot V_r^2 \cdot \frac{\pi}{4}D^2} \qquad \text{or:} \qquad T = C_T^* \cdot \frac{1}{2}\rho \cdot V_r^2 \cdot \frac{\pi}{4}D^2$$

$$C_Q^* = \frac{Q}{\frac{1}{2}\rho \cdot V_r^2 \cdot \frac{\pi}{4}D^3} \qquad \text{or:} \qquad Q = C_Q^* \cdot \frac{1}{2}\rho \cdot V_r^2 \cdot \frac{\pi}{4}D^3 \qquad (4.74)$$

The value of β varies over 360 degrees. From 0 until approximately 40 degrees, the curves are the regular open water diagrams as treated in the previous section. The condition with $V_e = 0$, $\beta = 0$ and $n > 0$ is the so-called bollard condition. The different combinations of directions of V_e and n, so the four quadrants of β, are listed below:

β	V_e	n
0°-90°	$V_e > 0$	$n > 0$
90°-180°	$V_e > 0$	$n < 0$
180°-270°	$V_e < 0$	$n < 0$
270°-360°	$V_e < 0$	$n > 0$

4.10.4   Ship Propulsion

This section treats the behavior of the **propeller behind the ship** and its interaction with the ship.

Wake Fraction

The **velocity deficit** behind the ship is a measure of its still water resistance. The velocity deficit in the propeller plane (without the propeller present) can be integrated and averaged over the propeller plane. This velocity is the average entrance velocity, V_e, in the propeller plane when the propeller is absent. It is defined in terms of the ship speed, V_s, by the **nominal wake fraction**, w_n:

$$w_n = \frac{V_s - V_e}{V_s} \qquad (4.75)$$

This definition is a non-dimensional form of the velocity deficit, $V_s - V_e$, in the propeller plane.

The wake distribution is responsible for unsteadiness in the propeller loading during one revolution, as can be seen in figure 4.23. This figure shows the lines with a constant wake fraction - thus lines with constant axial velocities of the fluid particles - at the propeller disc behind various stern types of ships.

Unsteady effects will be neglected now and the (average) nominal wake fraction will be used to obtain the (constant) open water propeller inflow, which yields the entrance velocity:

$$\overline{|V_e = V_s \cdot (1 - w)|} \qquad \text{with:} \quad w = w_n \qquad (4.76)$$

For a statistical prediction of the wake fraction of ships, reference is given to regression formulas of [Holtrop, 1984].

Thrust Deduction Fraction

The propeller has an effect on the ship's resistance, however. It increases the resistance of the ship by increasing the velocity along the hull (generally a small effect) and by decreasing the pressure around the stern. The thrust to be developed by the propeller should thus be greater than the resistance without propeller at the design speed, because the thrust has to be equal to the increased resistance.

The increase of resistance due to the propeller action is expressed as the **thrust deduction fraction**, t:
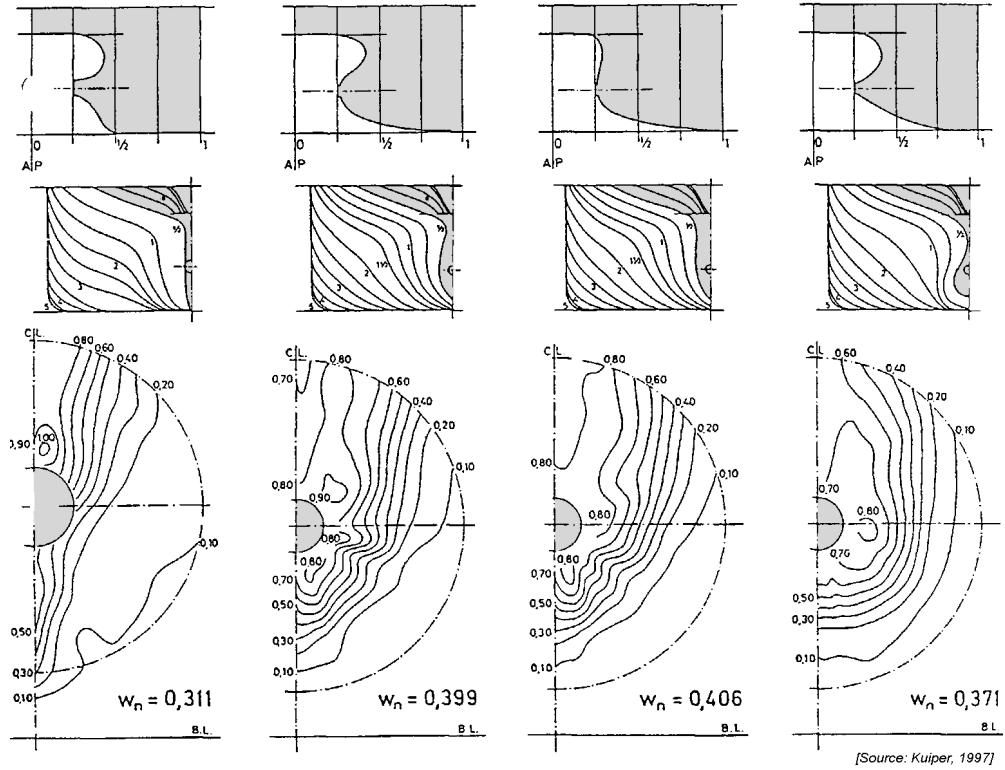
Figure 4.23: Wakes behind Various Stern Shapes

$$t = \frac{T - R}{T} \qquad (4.77)$$

where T is the thrust needed to maintain a certain design speed and R is the resistance without propeller at that speed, as found from resistance tests.

With this, the relation between resistance and thrust is:

$$\boxed{R = T \cdot (1 - t)} \qquad (4.78)$$

For a statistical prediction of the thrust deduction fraction of ships, reference is given to regression formulas of [Holtrop, 1984].

Propulsive Efficiency

The total efficiency is the ratio of the useful energy delivered by a system (output) and the energy supplied to the system (input). For the ship the output is $R \cdot V_s$ and the input is $Q \cdot \omega = Q \cdot 2\pi n$.

So the **total propulsive efficiency** is:

$$\boxed{\eta_T = \frac{R \cdot V_s}{Q \cdot 2\pi n}} \qquad (4.79)$$

This total efficiency can be divided into parts which are related to the propeller performance without the hull and to the hull without the propeller:

$$\eta_T = \frac{R \cdot V_s}{Q \cdot 2\pi n}$$

$$= \frac{T(1-t) \cdot \frac{V_e}{1-w}}{\frac{Q}{Q_O} \cdot Q_O \cdot 2\pi n}$$

$$= \left(\frac{T \cdot V_e}{Q_O \cdot 2\pi n}\right) \cdot \left(\frac{1-t}{1-w}\right) \cdot \left(\frac{Q_O}{Q}\right)$$

$$= \left(\frac{K_T}{K_Q} \cdot \frac{J}{2\pi}\right) \cdot \left(\frac{1-t}{1-w}\right) \cdot \left(\frac{Q_O}{Q}\right) \tag{4.80}$$

or:

$$\boxed{\eta_T = \eta_O \cdot \eta_H \cdot \eta_R}$$

in which, at the same thrust, Q_O is the torque of the open water propeller in a uniform flow and Q is the torque of the propeller in the wake behind the ship.

The total propulsive efficiency is thus divided into three components:

- **Open Water Efficiency:**

$$\boxed{\eta_O = \frac{T \cdot V_e}{Q_O \cdot 2\pi n} = \frac{K_T}{K_Q} \cdot \frac{J}{2\pi}} \tag{4.81}$$

This is the efficiency of the propeller alone in the mean (homogeneous) inflow, V_e. It can be derived from open water diagrams of propellers.

- **Hull Efficiency:**

$$\boxed{\eta_H = \frac{R \cdot V_s}{T \cdot V_e} = \frac{1-t}{1-w}} \tag{4.82}$$

Old but convenient rough approximations of the wake fraction and the thrust deduction fraction of full scale ships are given by:

$$w \approx 0.5 \cdot C_B - 0.05$$
$$t \approx 0.6 \cdot w \tag{4.83}$$

where C_B is the block coefficient of the ship. A fast slender container vessel with $C_B = 0.55$ will have $\eta_H \approx 1.12$ while for a crude oil carrier with $C_B = 0.85$, $\eta_H \approx 1.24$. So the effect of a hull with its wake before the propeller increases the propulsive efficiency considerably. The propeller diameter therefore has to be such that the wake is going through the propeller disk as much as possible.

When using model data, it should be noted that - contrarily to the thrust deduction fraction - the wake fraction is very sensitive for scale effect. It is left to the reader to explain this.

- **Relative Rotative Efficiency:**

$$\boxed{\eta_R = \frac{Q_O}{Q}} \tag{4.84}$$

This efficiency reflects the difference in torque in the wake and in open water at the same thrust. The relative rotative efficiency is generally close to one; $\eta_R = 0.98 - 1.00$ for single-screw ships and $\eta_R = 1.00 - 1.02$ for twin-screw ships.

See [Holtrop, 1984] for a statistical prediction of the relative rotative efficiency.

4.10.5 Propulsion versus Resistance

After completing the vessel, full scale trial tests will be carried out to verify the speed of the ship. An example of trial results is given in figure 4.24. This figure shows a comparison of predicted (from model tank test results) and measured (from full scale trial tests) data on the revolutions per minute (RPM) of the propeller and the power delivered to the propeller (SHP = Shaft Horse Power) for different ship speeds of a pilot vessel in calm water.
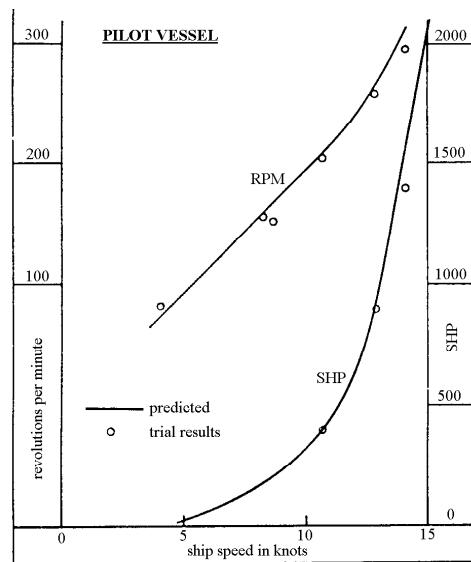
Figure 4.24: Trial Results of a Pilot Vessel.

A very practical offshore engineering application of the information from the latter sections of this chapter involves the prediction of the speed at which a barge (or other floating object) will be towed by a given tugboat. Such information can be invaluable for the logistic planning of a major offshore operation; consider the costs of keeping a larger semisubmersible crane vessel waiting (at perhaps a quarter million dollars per day) for a barge - with topsides to install - which arrives a bit later than planned.

A tugboat will of course be able to deliver more thrust than it needs to overcome its own frictional and wave making resistance. In general, the available **towing force** which a tugboat can deliver will be a function of its towing speed. This function, which decreases with increasing speed, will be known for the tug selected. In general, each tug will have a family of curves depending upon the speed of its engine. On the other hand, only one engine speed will deliver the highest overall efficiency for any given speed.

The resistance for the towed object should be known as well. This resistance force will generally be an increasing function of towing velocity. Superposition of the two curves -

one for the tugboat and one for the towed object will yield the optimum towing speed. This is the speed corresponding to the intersection point of the two curves; see figure 4.25.
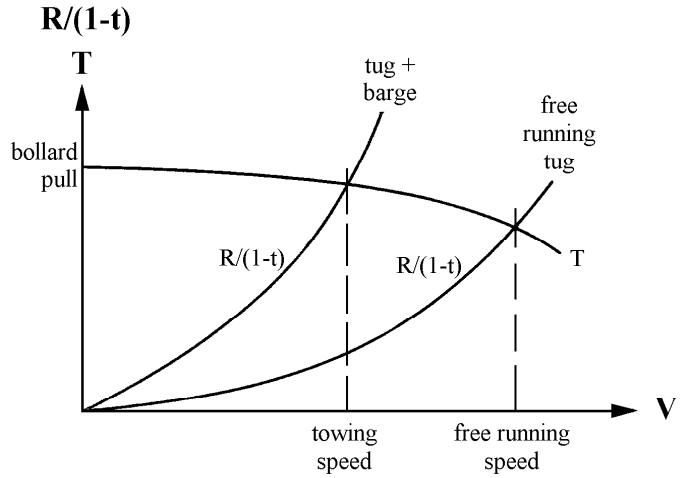
Figure 4.25: Free Running and Towing Speed of a Tug

4.10.6   Lift and Flettner Rotors

As early as the eighteenth century, artillery officers noted that spinning shells fired in a cross-wind often either overshot or undershot their targets. In 1794, the Berlin Academy offered a prize for the explanation of this. It was more than 50 years before Gustav Magnus, a Professor of Physics in Berlin conducted experiments with spinning cylinders in air to demonstrate the phenomenon.

Little was done with this information until 1922 when Anton Flettner, a German businessman, set out to apply the Magnus effect (in air) for the propulsion of a ship. Since then, Flettner rotors have been used experimentally for steering ships; they are becoming popular for steering towed remote controlled vehicles.

Flettner rotors are circular cylinders which spin in an air or water flow. Because there is friction between their surface and the surrounding fluid, they cause a circulation and thus a lift force. Their operating principle based upon the **Magnus effect** was given in chapter 3; this section concentrates on their more practical aspects.

It was shown at the end of chapter 3 that the lift force generated by a unit length of Flettner rotor with a radius R is:

$$F_L = 4\pi \ R \ \rho \ V^2 \ C \tag{4.85}$$

in which:

$$\begin{array}{rcl}
F_L & = & \text{lift force per unit length (N/m)} \\
V & = & \text{towing velocity (m/s)} \\
C & = & \text{dimensionless circulation strength (-)} \\
R & = & \text{rotor radius (m)}
\end{array}$$

C relates the circulation strength, Γ, to R and V via:
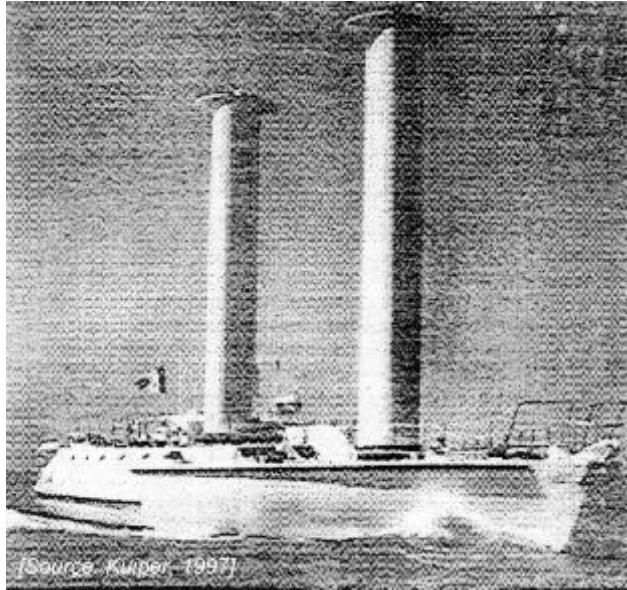
Figure 4.26: Sailboat Prototype based on Flettner Rotor Principle

$$C = -\frac{\Gamma}{4\pi \ R \ V} \tag{4.86}$$

as given in chapter 3.

It is logical to assume that Γ and thus C will be directly related to the speed of the Flettner cylinder surface, $R \ \omega$, in which ω is the angular velocity of the rotor in radians per second. When all this is substituted into the equation for F_L, one finds that the total lift force generated by a rotor will be proportional to four independent quantities which the designer or user has at his or her discretion:

$$F_L \ \alpha \ R\omega \ V \ \ell \tag{4.87}$$

in which:

$$
\begin{aligned}
\ell \ &= \ \text{length of the rotor (m)} \\
R \ &= \ \text{rotor radius (m)} \\
V \ &= \ \text{towing velocity (m/s)} \\
\omega \ &= \ \text{angular veloicity (rad/s)}
\end{aligned}
$$

The above equation is stated as a proportionality rather than an equality; it does not include the water density nor does it include coefficients to include the fact that the flow is not ideal. Indeed, no hard quantitative data has been given here. Questions such as:

- How does the spin of the rotor influence its drag?
- Can a Flettner rotor also have a cavitation problem?
- What is the relation between spin speed and torque on the one hand and the delivered circulation on the other hand?

can be asked.

The answers to these questions (among others) will depend upon experimental evidence which does not yet seem to be available in the open literature just yet. Indeed, this application of Flettner rotors is still quite new!

On a small scale, Flettner rotors are being used in the offshore industry to steer RCV's. On a larger scale, sailboats without sails have even been proposed! This design has large diameter vertical cylinders mounted vertically from the deck instead of masts. They are spun about their vertical axes by motors thus setting up a lift force in the wind much like a spinning tennis ball would. This method of propulsion has not yet proven practical at this scale, however, although prototypes have been built as shown in figure 4.26.

Chapter 5

OCEAN SURFACE WAVES

5.1 Introduction

Ocean surface waves cause periodic loads on all sorts of man-made structures in the sea. It does not matter whether these structures are fixed or floating and on the surface or deeper in the sea.

Most structures, even the so-called fixed structures, are not really rigid; they respond in some way to the wave-induced periodic loads. Examples of such response include accelerations, harmonic displacements and internal loads in ships as well as fixed structures. Waves and the resulting ship motions cause added resistance, reduced sustained speed (with associated longer travel times) and increased fuel consumption for ships. Also local erosion near pipelines and other small structures on the sea bed can be caused by waves. The ship's responses can impair safety via phenomena such as shipping water on deck or wave slamming.

In short, there is every reason to need to know about waves - the topic of this chapter - before one goes on with the discussion of all sorts of hydrodynamic problems in later chapters.

Water waves can be generated in many different ways:

- Waves generated by a ship or any other floating structure which is moving, either at a constant forward speed or by carrying out an oscillatory motion.
- Waves generated by the interaction between wind and the sea surface.
- Waves generated by astronomical forces: Tides.
- Waves generated by earthquakes or submarine landslides: Tsunamis.
- Free surface waves generated in fluids in partially filled tanks; such as fuel or cargo tanks on a ship.

A single mathematical solution for all problems related to these various types of waves does not exist; even in simple cases approximations are required. It is important to be aware of the limitations of simplifications, especially when nonlinear effects can become important. On the other hand, a simple linear approach can work quite well for many practical applications.

Wind generated waves can be classified into two basic categories: sea and swell. These are described briefly here.

- **Sea**

  A sea is a train of waves driven by the prevailing local wind field. The waves are short-crested with the lengths of the crests only a few (2-3) times the apparent wave length. Also, sea waves are very irregular; high waves are followed unpredictably by low waves and vice versa. Individual wave crests seem to propagate in different directions with tens of degrees deviation from the mean direction. The crests are fairly sharp and sometimes even small waves can be observed on these crests or there are dents in the larger wave crests or troughs. The apparent or virtual wave period, $\widetilde{T}$, varies continuously, as well as the virtual or apparent wave length, $\widetilde{\lambda}$.

- **Swell**

  A swell is waves which have propagated out of the area and local wind in which they were generated. They are no longer dependent upon the wind and can even propagate for hundreds of kilometers through areas where the winds are calm. Individual waves are more regular and the crests are more rounded than those of a sea. The lengths of the crests are longer, now several (6-7) times the virtual wave length. The wave height is more predictable, too. If the swell is high, 5 to 6 waves of approximately equal heights can pass a given point consecutively. If the waves are low, they can stay low for more than a minute even though the surface elevation remains irregular.

Wind waves, especially, are very irregular. Even so, they can be seen as a superposition of many simple, regular harmonic wave components, each with its own amplitude, length, period or frequency and direction of propagation. Such a concept can be very handy in many applications; it allows one to predict very complex irregular behavior in terms of much simpler theory of regular waves. This so-called **superposition principle**, first introduced in hydrodynamics by [St. Denis and Pierson, 1953], is illustrated in figure 5.1. To analyze complicated wave systems, it is necessary to know the properties of the simple harmonic components, such as time and location-dependent pressure in the fluid, relation between wave length and wave period, energy transport, etc.

In this respect waves are often classified into two other basic categories:

- **Deep water waves**, also sometimes referred to as **short waves**

  The water is considered to be deep if the water depth, h, is more than half the wave length, λ, so: $h/\lambda > 1/2$ or $\lambda/h < 2$. These (relatively) short waves do not 'feel' the sea floor.

- **Shallow water waves**, also sometimes referred to as **long waves**

  The water is considered to be shallow if the water depth, h, is less than $1/20$ of the wave length, λ, so: $h/\lambda < 1/20$ or $\lambda/h > 20$. The sea floor has a very large influence on the characteristics of these (relatively) long waves.

5.2   Regular Waves

Definitions used to describe the harmonic - or regular - waves and the potential theory used to solve the flow problem in waves will be treated now.

Figure 5.2 shows a harmonic wave as seen from two different perspectives. Figure 5.2-a shows what one would observe in a snapshot photo made looking at the side of a (transparent) wave flume; the wave profile is shown as a function of distance x along the flume at a fixed instant in time. Figure 5.2-b is a time record of the water level observed at one

[Source: Pierson, Neuman and James]
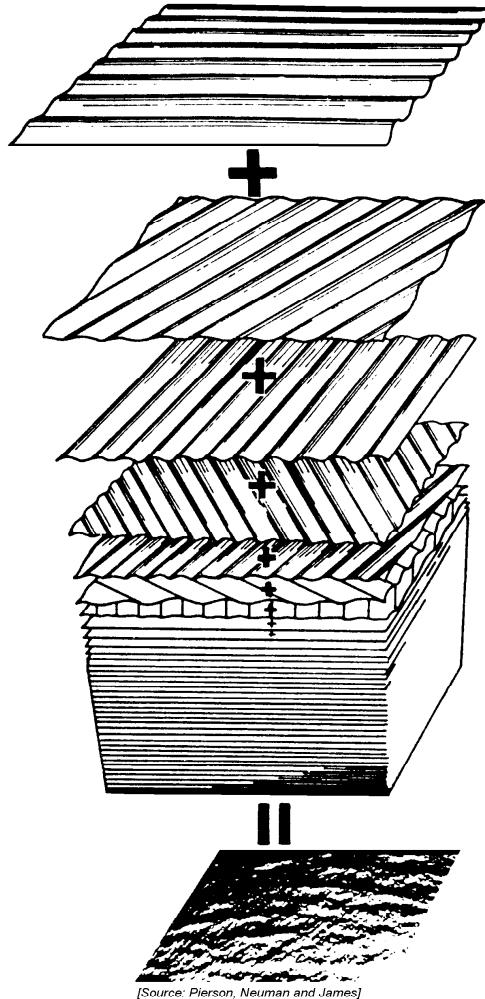
Figure 5.1: A Sum of Many Simple Sine Waves Makes an Irregular Sea

location along the flume; it looks similar in many ways to the other figure, but time t has replaced x on the horizontal axis.

Notice that the origin of the coordinate system is at the still water level with the positive z-axis directed **upward**; most relevant values of z will be negative. The **still water level** is the average water level or the level of the water if no waves were present. The x-axis is positive in the direction of wave propagation. The **water depth**, h, (a positive value) is measured between the sea bed $(z = -h)$ and the still water level.

The highest point of the wave is called its **crest** and the lowest point on its surface is the **trough**. If the wave is described by a sine wave, then its **amplitude** ζ_a is the distance from the still water level to the crest, or to the trough for that matter. The subscript $_a$ denotes amplitude, here. The wave height H is measured vertically from wave trough level to the wave crest level. Obviously:

$$\boxed{H = 2\zeta_a} \qquad \text{for a sinusoidal wave} \qquad (5.1)$$

The horizontal distance (measured in the direction of wave propagation) between any two successive wave crests is the **wave length**, λ. The distance along the time axis is the **wave period**, T. The ratio of wave height to wave length is often referred to as the dimensionless
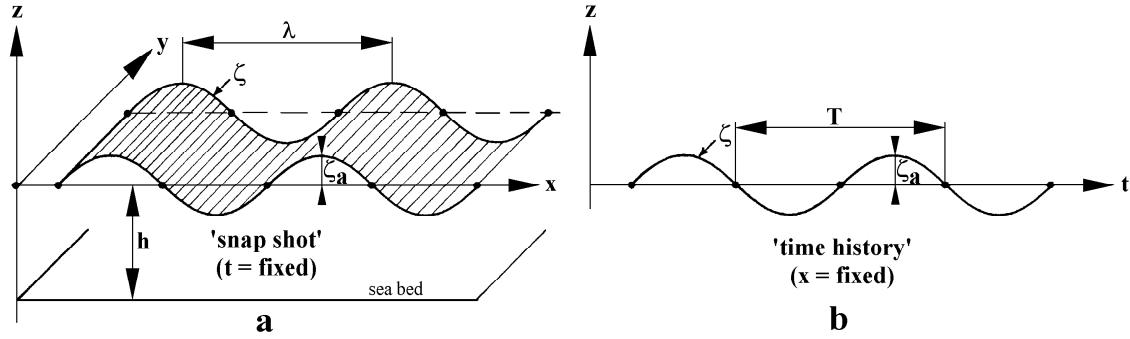
Figure 5.2: Harmonic Wave Definitions

wave steepness, H/λ.

Since the distance between any two corresponding points on successive sine waves is the same, wave lengths and periods are usually actually measured between two consecutive upward (or downward) crossings of the still water level. Such points are also called **zero-crossings**, and are easier to detect in a wave record.

Since sine or cosine waves are expressed in terms of angular arguments, the wave length and period are converted to angles using:

$$k\lambda = 2\pi \qquad \text{or:} \qquad k = \frac{2\pi}{\lambda} \qquad\qquad (5.2)$$

$$\omega T = 2\pi \qquad \text{or:} \qquad \omega = \frac{2\pi}{T} \qquad\qquad (5.3)$$

in which k is the wave number (rad/m) and ω is the circular wave frequency (rad/s).

Obviously, the wave form moves one wave length during one period so that its speed or **phase velocity**, c, is given by:

$$c = \frac{\lambda}{T} = \frac{\omega}{k} \qquad\qquad (5.4)$$

If the wave moves in the positive x-direction, the wave profile - the form of the water surface - can now be expressed as a function of both x and t as follows:

$$\zeta = \zeta_a \cos(kx - \omega t) \qquad\qquad (5.5)$$

A wave moving in the opposite (negative x-direction can be given by:

$$\zeta = \zeta_a \cos(kx + \omega t) \qquad\qquad (5.6)$$

A progressive harmonic wave is shown in figure 5.3.

5.2.1   Potential Theory

The basics of potential flow theory used here are no different from those presented in chapter 3. In order to use this linear theory with waves, it will be necessary to assume that
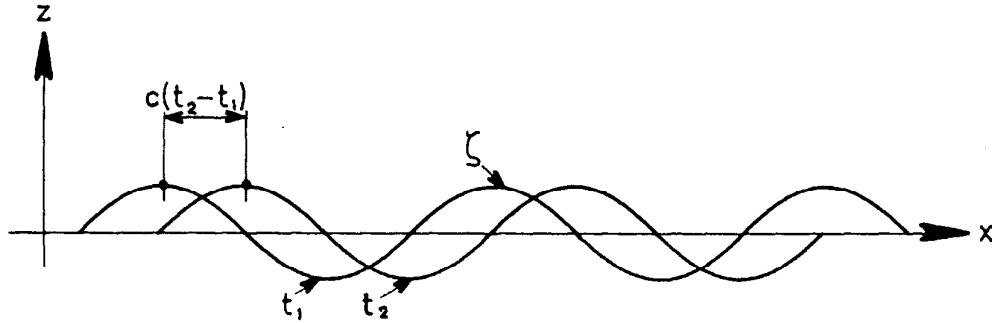
Figure 5.3: Progressive Harmonic Wave

the water surface slope is very small. This means that the wave steepness is so small that terms in the equations of the waves with a magnitude in the order of the steepness-squared can be ignored. Using the linear theory holds here that harmonic displacements, velocities and accelerations of the water particles and also the harmonic pressures will have a linear relation with the wave surface elevation.

The profile of a simple wave with a small steepness looks like a sine or a cosine and the motion of a water particle in a wave depends on the distance below the still water level. This is reason why the wave potential is written as:

$$\boxed{\Phi_w(x, z, t) = P(z) \cdot \sin{(kx - \omega t)}} \tag{5.7}$$

in which $P(z)$ is an (as yet) unknown function of z.

The velocity potential $\Phi_w(x, z, t)$ of the harmonic waves has to fulfill four requirements:
   1. Continuity condition or Laplace equation
   2. Sea bed boundary condition
   3. Free surface dynamic boundary condition
   4. Free surface kinematic boundary condition.

These requirements lead to a more complete expression for the velocity potential as will be explained in the following sections. The relationships presented in these sections are valid for all water depths, but the fact that they contain so many hyperbolic functions makes them cumbersome to use. Engineers - as opposed to (some) scientists - often look for ways to simplify the theory. The simplifications stem from the following approximations for large and very small arguments, s, as shown in figure 5.4:

$$
\begin{aligned}
\text{for large arguments, } s \quad \sinh(s) &\approx \cosh(s) \gg s \\
\tanh(s) &\approx 1
\end{aligned} \tag{5.8}
$$

$$
\begin{aligned}
\text{for small arguments, } s \quad \sinh(s) &\approx \tanh(s) \approx s \\
\cosh(s) &\approx 1
\end{aligned} \tag{5.9}
$$

In memory:

$$\sinh s = \frac{e^s - e^{-s}}{2} \qquad \cosh s = \frac{e^s + e^{-s}}{2} \qquad \tanh s = \frac{e^s - e^{-s}}{e^s + e^{-s}} \tag{5.10}$$
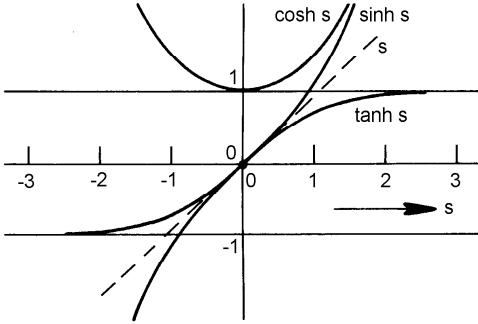
Figure 5.4: Hyperbolic Functions Limits

Continuity Condition and Laplace Equation

The velocity of the water particles (u, v, w) in the three translational directions, or alternatively (v_x, v_y, v_z), follow from the definition of the velocity potential, Φ_w:

$$u = v_x = \frac{\partial \Phi_w}{\partial x} \qquad v = v_y = \frac{\partial \Phi_w}{\partial y} \qquad w = v_z = \frac{\partial \Phi_w}{\partial z} \qquad (5.11)$$

The two-dimensional version of this can be found in chapter 3.
Since the fluid is homogeneous and incompressible, the **Continuity Condition**:

$$\frac{\partial u}{\partial x} + \frac{\partial v}{\partial y} + \frac{\partial w}{\partial z} = 0 \qquad (5.12)$$

results in the **Laplace Equation** for potential flows:

$$\nabla^2 \Phi_w = \frac{\partial^2 \Phi_w}{\partial x^2} + \frac{\partial^2 \Phi_w}{\partial y^2} + \frac{\partial^2 \Phi_w}{\partial z^2} = 0 \qquad (5.13)$$

Water particles move here in the x-z plane only, so in the equations above:

$$v = \frac{\partial \Phi_w}{\partial y} = 0 \quad \text{and} \quad \frac{\partial v}{\partial y} = \frac{\partial^2 \Phi_w}{\partial y^2} = 0 \qquad (5.14)$$

Taking this into account, a substitution of equation 5.7 in equation 5.13 yields a homogeneous solution of this equation:

$$\frac{d^2 P(z)}{dz^2} - k^2 P(z) = 0 \qquad (5.15)$$

with as solution for $P(z)$:

$$P(z) = C_1 e^{+kz} + C_2 e^{-kz} \qquad (5.16)$$

Using this result from the first boundary condition, the wave potential can be written now with two unknown coefficients as:

$$\Phi_w(x, z, t) = \left(C_1 e^{+kz} + C_2 e^{-kz} \right) \cdot \sin\left(kx - \omega t \right) \qquad (5.17)$$

in which:

$$
\begin{aligned}
\Phi_w(x, z, t) \quad &= \quad \text{wave potential (m}^2\text{/s)} \\
e \quad &= \quad \text{base of natural logarithms (-)} \\
C_1, C_2 \quad &= \quad \text{as yet undetermined constants (m}^2\text{/s)} \\
k \quad &= \quad \text{wave number (1/m)} \\
t \quad &= \quad \text{time (s)} \\
x \quad &= \quad \text{horizontal distance (m)} \\
z \quad &= \quad \text{vertical distance, positive upwards (m)} \\
\omega \quad &= \quad \text{wave frequency (1/s)}
\end{aligned}
$$

Sea Bed Boundary Condition

The vertical velocity of water particles at the sea bed is zero (no-leak condition):

$$
\frac{\partial \Phi_w}{\partial z} = 0 \qquad \text{for: } z = -h \tag{5.18}
$$

as given in figure 5.5.
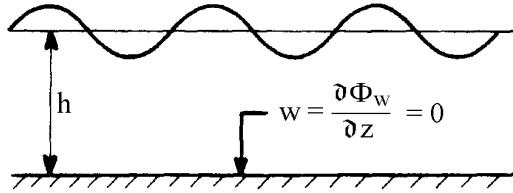
Figure 5.5: Vertical Velocity at the Sea Bed

Substituting this boundary condition in equation 5.17 provides:

$$
kC_1 e^{-kh} - kC_2 e^{+kh} = 0 \tag{5.19}
$$

or:

$$
C_1 e^{-kh} = C_2 e^{+kh} \tag{5.20}
$$

By defining:

$$
\frac{C}{2} = C_1 e^{-kh} = C_2 e^{+kh} \tag{5.21}
$$

or:

$$
C_1 = \frac{C}{2} e^{+kh} \qquad \text{and} \qquad C_2 = \frac{C}{2} e^{-kh} \tag{5.22}
$$

it follows that $P(z)$ in equation 5.16 can be worked out to:

$$
\begin{aligned}
P(z) \quad &= \quad \frac{C}{2} \left(e^{+k(h+z)} + e^{-k(h+z)} \right) \\
&= \quad C \cosh k\,(h+z)
\end{aligned} \tag{5.23}
$$

and the wave potential with only one unknown becomes:

$$
\Phi_w(x, z, t) = C \cdot \cosh k\,(h+z) \cdot \sin(kx - \omega t) \tag{5.24}
$$

in which C is an (as yet) unknown constant.

Free Surface Dynamic Boundary Condition

The pressure, p, at the free surface of the fluid, $z = \zeta$, is equal to the atmospheric pressure, p_0. This requirement for the pressure is called the **dynamic boundary condition at the free surface**, see figure 5.6.
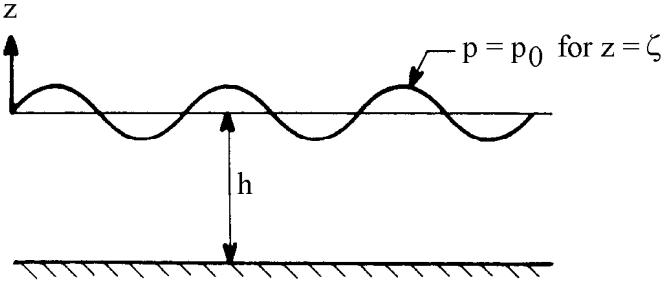
Figure 5.6: Atmospheric Pressure at the Free Surface

The Bernoulli equation for an unstationary irrotational flow (with the velocity given in terms of its three components) is in its general form:

$$\frac{\partial \Phi_w}{\partial t} + \frac{1}{2}\left(u^2 + v^2 + w^2\right) + \frac{p}{\rho} + gz = C^* \tag{5.25}$$

In two dimensions, $v = 0$ and since the waves have a small steepness (u and w are small), this equation becomes:

$$\frac{\partial \Phi_w}{\partial t} + \frac{p}{\rho} + gz = C^* \tag{5.26}$$

At the free surface this condition becomes:

$$\frac{\partial \Phi_w}{\partial t} + \frac{p_0}{\rho} + g\zeta = C^* \qquad \text{for: } z = \zeta \tag{5.27}$$

The constant value $p_0/\rho - C^*$ can be included in $\partial \Phi_w/\partial t$; this will not influence the velocities being obtained from the potential Φ_w. With this the equation becomes:

$$\frac{\partial \Phi_w}{\partial t} + g\zeta = 0 \qquad \text{for: } z = \zeta \tag{5.28}$$

The potential at the free surface can be expanded in a Taylor series, keeping in mind that the vertical displacement ζ is relatively small:

$$\left\{\Phi_w(x, z, t)\right\}_{z=\zeta} = \left\{\Phi_w(x, z, t)\right\}_{z=0} + \zeta \cdot \left\{\frac{\partial \Phi_w(x, z, t)}{\partial z}\right\}_{z=0} + \ldots\ldots$$

$$\left\{\frac{\partial \Phi_w(x, z, t)}{\partial t}\right\}_{z=\zeta} = \left\{\frac{\partial \Phi_w(x, z, t)}{\partial t}\right\}_{z=0} + O(\varepsilon^2) \tag{5.29}$$

which yields for the linearized form of the **free surface dynamic boundary condition**:

$$\boxed{\frac{\partial \Phi_w}{\partial t} + g\zeta = 0 \qquad \text{for: } z = 0} \tag{5.30}$$

With this, the wave profile becomes:

$$\zeta = -\frac{1}{g} \cdot \frac{\partial \Phi_w}{\partial t} \qquad \text{for: } z = 0 \tag{5.31}$$

A substitution of equation 5.24 in equation 5.31 yields the wave profile:

$$\zeta = \frac{\omega C}{g} \cdot \cosh kh \cdot \cos(kx - \omega t) \tag{5.32}$$

or:

$$\zeta = \zeta_a \cdot \cos(kx - \omega t) \quad \text{with:} \quad \zeta_a = \frac{\omega C}{g} \cdot \cosh kh \tag{5.33}$$

With this the corresponding wave potential, depending on the water depth h, is given by the relation:

$$\boxed{\Phi_w = \frac{\zeta_a g}{\omega} \cdot \frac{\cosh k(h+z)}{\cosh kh} \cdot \sin(kx - \omega t)} \tag{5.34}$$

In deep water with $h \to \infty$ (short waves), the wave potential becomes:

$$\Phi_w = \frac{\zeta_a g}{\omega} \cdot e^{kz} \cdot \sin(kx - \omega t) \qquad \text{(deep water)} \tag{5.35}$$

Free Surface Kinematic Boundary Condition

So far the relation between the wave period T and the wave length, λ, is still unknown. The relation between T and λ (or equivalently ω and k) follows from the boundary condition that the vertical velocity of a water particle at the free surface of the fluid is identical to the vertical velocity of that free surface itself (no-leak condition); this is a kinematic boundary condition.

Using the equation of the free surface 5.33 yields for the wave surface:

$$\begin{aligned} \frac{dz}{dt} &= \frac{\partial \zeta}{\partial t} + \frac{\partial \zeta}{\partial x} \cdot \frac{dx}{dt} \qquad \text{for: } z = \zeta \\ &= \frac{\partial \zeta}{\partial t} + u \cdot \frac{d\zeta}{dx} \end{aligned} \tag{5.36}$$

The second term in this expression is a product of two values, which are both small because of the assumed small wave steepness. This product becomes even smaller (second order) and can be ignored, see figure 5.7.

This linearization provides the vertical velocity of the wave surface:

$$\frac{dz}{dt} = \frac{\partial \zeta}{\partial t} \qquad \text{for: } z = \zeta \tag{5.37}$$

The vertical velocity of a water particle in the free surface is then:

$$\frac{\partial \Phi_w}{\partial z} = \frac{\partial \zeta}{\partial t} \qquad \text{for: } z = \zeta \tag{5.38}$$
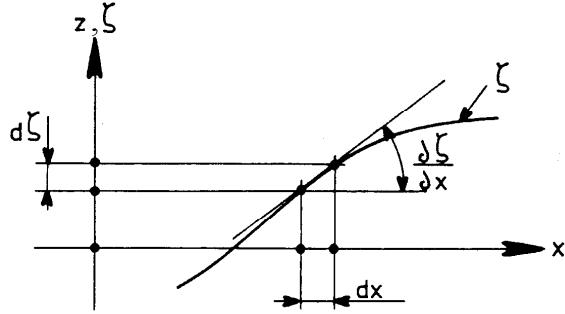
Figure 5.7: Kinematic Boundary Condition

Analogous to equation 5.30 this condition is valid for $z = 0$ too, instead of for $z = \zeta$ only. A differentiation of the free surface dynamic boundary condition (equation 5.30) with respect to t provides:

$$\frac{\partial^2 \Phi_w}{\partial t^2} + g\frac{\partial \zeta}{\partial t} = 0 \qquad \text{for } z = 0 \tag{5.39}$$

or after re-arranging terms:

$$\frac{\partial \zeta}{\partial t} + \frac{1}{g} \cdot \frac{\partial^2 \Phi_w}{\partial t^2} = 0 \qquad \text{for } z = 0 \tag{5.40}$$

Together with equation 5.37 this delivers the **free surface kinematic boundary condition** or the **Cauchy-Poisson condition**:

$$\boxed{\frac{\partial z}{\partial t} + \frac{1}{g} \cdot \frac{\partial^2 \Phi_w}{\partial t^2} = 0 \qquad \text{for: } z = 0} \tag{5.41}$$

Dispersion Relationship

The information is now available to establish the relationship between ω and k (or equivalently T and λ) referred to above. A substitution of the expression for the wave potential (equation 5.34) in equation 5.41 gives the **dispersion relation** for any arbitrary water depth h:

$$\boxed{\omega^2 = k\, g \cdot \tanh kh} \tag{5.42}$$

In many situations, ω or T will be know; one must determine k or λ. Since k appears in a nonlinear way in 5.42, that equation will generally have to be solved iteratively.
In deep water ($\tanh kh = 1$), equation 5.42 degenerates to a quite simple form which can be used without difficulty:

$$\omega^2 = k\, g \qquad \text{(deep water)} \tag{5.43}$$

and the deep water relation between T and λ becomes:

$$T = \sqrt{\frac{2\pi}{g}} \cdot \sqrt{\lambda} \qquad \text{or} \qquad \lambda = \frac{g}{2\pi} \cdot T^2 \qquad \text{(deep water)} \tag{5.44}$$

Substitution of $g = 9.81$ m/s^2 and π yields:

$$T \approx 0.80 \cdot \sqrt{\lambda} \qquad \text{or} \qquad \lambda \approx 1.56 \cdot T^2 \qquad \text{(deep water)} \qquad (5.45)$$

Note that this regular wave relation cannot be used to describe the relation between the average wave length and the average wave period of an irregular sea. However in a more regular swell, this relation can be used with an accuracy of about 10 to 15 per cent.

In shallow water, the dispersion relation is found by substituting $\tanh kh = kh$ in equation 5.42; thus:

$$\omega = k \cdot \sqrt{gh} \qquad \text{(shallow water)} \qquad (5.46)$$

and the shallow water relation between T and λ becomes:

$$T = \frac{\lambda}{\sqrt{gh}} \qquad \text{or} \qquad \lambda = T \cdot \sqrt{gh} \qquad \text{(shallow water)} \qquad (5.47)$$

Cauchy-Poisson Condition in Deep Water

In deep water (short waves), the **free surface kinematic boundary condition** or **Cauchy-Poisson condition** is often given in another form in the literature. The space and time dependent wave potential, $\Phi_w(x, z, t)$, is divided in a space-dependent part, $\phi_w(x, z)$, and a time-dependent part, $1 \cdot \sin \omega t$, by defining:

$$\Phi_w(x, z, t) = \phi_w(x, z) \cdot \sin \omega t \qquad (5.48)$$

Equation 5.41:

$$\frac{\partial z}{\partial t} + \frac{1}{g} \cdot \frac{\partial^2 \Phi_w}{\partial t^2} = 0 \qquad \text{for: } z = 0$$

can with equation 5.37 be written as:

$$\frac{\partial \zeta}{\partial t} + \frac{1}{g} \cdot \frac{\partial^2 \Phi_w}{\partial t^2} = 0 \qquad \text{for: } z = 0 \qquad (5.49)$$

and using equation 5.38 results in:

$$\frac{\partial \Phi_w}{\partial z} + \frac{1}{g} \cdot \frac{\partial^2 \Phi_w}{\partial t^2} = 0 \qquad \text{for: } z = 0 \qquad (5.50)$$

With the dispersion relation in deep water, $\omega^2 = k\, g$, the free surface kinematic boundary condition or the Cauchy-Poisson condition becomes:

$$\frac{\partial \phi_w}{\partial z} - k \cdot \phi_w = 0 \qquad \text{for } z = 0 \qquad \text{(deep water)} \qquad (5.51)$$

5.2.2 Phase Velocity

With the dispersion relation (equation 5.42) the wave celerity ($c = \lambda/T = \omega/k$) becomes:

$$\boxed{c = \sqrt{\frac{g}{k} \cdot \tanh kh}} \qquad (5.52)$$

The phase velocity increases with the wave length ($k = 2\pi/\lambda$); water waves display dispersion in that longer waves move faster than shorter ones. As a result of this phenomena, sea sailors often interpret swell (long, relatively low wind-generated waves which have moved away from the storm that generated them) as a warning of an approaching storm.

In deep water, the phase velocity is found by substituting $\tanh kh = 1$ in equation 5.52; thus:

$$c = \sqrt{\frac{g}{k}} = \frac{g}{\omega} \qquad \text{(deep water)} \tag{5.53}$$

With some further substitution, one can get:

$$c = \sqrt{\frac{g}{k}} = \sqrt{g \cdot \frac{\lambda}{2\pi}} = \sqrt{\frac{g}{2\pi} \cdot \lambda} \approx 1.25\sqrt{\lambda} \approx 1.56 \cdot T \qquad \text{(deep water)} \tag{5.54}$$

In shallow water, the phase velocity is found by substituting $\tanh kh = kh$ in equation 5.52; thus:

$$c = \sqrt{gh} \qquad \text{(shallow water)} \tag{5.55}$$

The phase velocity is now independent of the wave period; these waves are not dispersive. This celerity, $\sqrt{gh}$, is called the **critical velocity**. This velocity is of importance when sailing with a ship at shallow water. Similar effects occur with an airplane that exceeds the speed of sound. Generally, the forward ship speed will be limited to about 80% of the critical velocity, to avoid excessive still water resistance or **squat** (combined sinkage and trim). Indeed, only a ship which can plane on the water surface is able to move faster than the wave which it generates.

5.2.3   Water Particle Kinematics

The kinematics of a water particle is found from the velocity components in the x- and z-directions, obtained from the velocity potential given in equation 5.34 and the dispersion relation given in equation 5.42.

Velocities

The resulting velocity components - in their most general form - can be expressed as:

$$u = \frac{\partial \Phi_w}{\partial x} = \frac{dx}{dt} = \zeta_a \cdot \frac{kg}{\omega} \cdot \frac{\cosh k\,(h + z)}{\cosh kh} \cdot \cos\,(kx - \omega t)$$

$$w = \frac{\partial \Phi_w}{\partial z} = \frac{dz}{dt} = \zeta_a \cdot \frac{kg}{\omega} \cdot \frac{\sinh k\,(h + z)}{\cosh kh} \ \cdot \sin\,(kx - \omega t) \tag{5.56}$$

A substitution of:

$$kg = \frac{\omega^2}{\tanh kh}$$

derived from the dispersion relation in equation 5.42, provides:

$$
\boxed{u = \zeta_a \cdot \omega \cdot \frac{\cosh k\,(h+z)}{\sinh kh} \cdot \cos\,(kx - \omega t)}
$$

$$
\boxed{w = \zeta_a \cdot \omega \cdot \frac{\sinh k\,(h+z)}{\sin kh} \cdot \sin\,(kx - \omega t)} \tag{5.57}
$$

An example of a velocity field is given in figure 5.8.
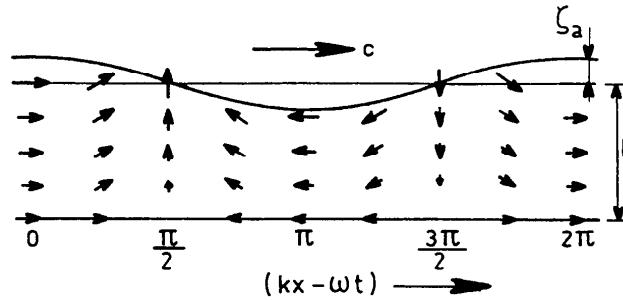
Figure 5.8: Velocity Field in a Shallow Water Wave

In deep water, the water particle velocities are given by:

$$
\begin{aligned}
u &= \zeta_a \omega \cdot e^{kz} \cdot \cos\,(kx - \omega t) \\
w &= \zeta_a \omega \cdot e^{kz} \cdot \sin\,(kx - \omega t) \qquad \text{(deep water)}
\end{aligned} \tag{5.58}
$$

An example of a velocity field is given in figure 5.9.
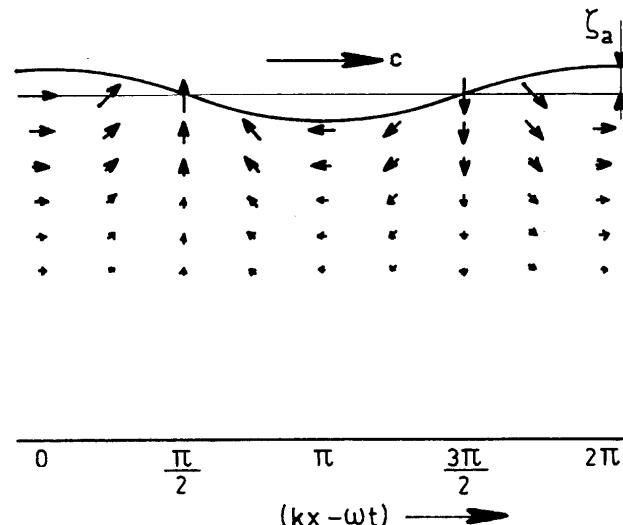
Figure 5.9: Velocity Field in a Deep Water Wave

The circular outline velocity or **orbital velocity** in deep water (short waves) is:

$$V_o = \sqrt{u^2 + w^2} = \zeta_a \omega \cdot e^{kz} \qquad \text{(deep water)} \tag{5.59}$$

In shallow water, the water velocity components are:

$$
\begin{aligned}
u &= \zeta_a \omega \cdot \frac{1}{kh} \cdot \cos(kx - \omega t) \\
w &= \zeta_a \omega \cdot \left(1 + \frac{z}{h}\right) \cdot \sin(kx - \omega t) \qquad \text{(shallow water)}
\end{aligned}
\tag{5.60}
$$

Displacements

Because of the small steepness of the wave, x and z in the right hand side of these equations can be replaced by the coordinates of the mean position of the considered water particle: x_1 and z_1. Hence the distances $x - x_1$ and $z - z_1$ are so small that differences in velocities resulting from the water motion position shifts can be neglected; they are of second order. Then, an integration of equations 5.57 over t yields the water displacements:

$$
\boxed{\;x = -\zeta_a \cdot \frac{\cosh k(h + z_1)}{\sinh kh} \cdot \sin(kx_1 - \omega t) + C_1\;}
$$
$$
\boxed{\;z = +\zeta_a \cdot \frac{\sinh k(h + z_1)}{\sinh kh} \cdot \cos(kx_1 - \omega t) + C_2\;}
\tag{5.61}
$$

Trajectories

It is obvious that the water particle carries out an oscillation in the x- and z-directions about a point (C_1, C_2). This point will hardly deviate from the situation in rest, so: $C_1 \approx x_1$ and $C_2 \approx z_1$.

The trajectory of the water particle is found by an elimination of the time, t, by using:

$$\sin^2(kx_1 - \omega t) + \cos^2(kx_1 - \omega t) = 1 \tag{5.62}$$

which provides:

$$
\boxed{\;\frac{(x - x_1)^2}{\left(\zeta_a \cdot \frac{\cosh k(h+z_1)}{\sinh kh}\right)^2} + \frac{(z - z_1)^2}{\left(\zeta_a \cdot \frac{\sinh k(h+z_1)}{\sinh kh}\right)^2} = 1\;}
\tag{5.63}
$$

This equation shows that the trajectories of water particles are ellipses in the general case, as shown in figure 5.10. The water motion obviously decreases as one moves deeper below the water surface.

Half the vertical axis of the ellipse - the vertical water displacement amplitude - is equal to ζ_a at the free surface, $z_1 = 0$. This amplitude is reduced to zero at the sea bed, $z_1 = -h$, in accordance with the sea bed boundary condition; the trajectories become horizontal line elements there.

In deep water, the trajectories of the water particles become circles:

$$(x - x_1)^2 + (z - z_1)^2 = \left(\zeta_a \cdot e^{kz_1}\right)^2 \qquad \text{(deep water)} \tag{5.64}$$
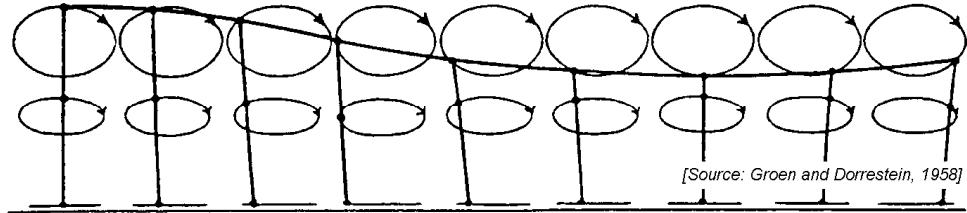
Figure 5.10: Trajectories of Water Particles in Long or Shallow Water Waves

with radii which decrease exponentially with distance below the surface. Figure 5.11 shows an example of these trajectories.
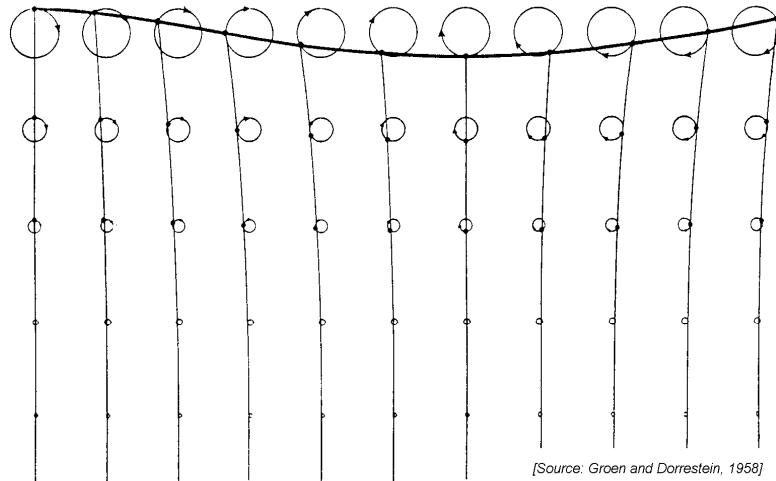
Figure 5.11: Trajectories of Water Particles in Short or Deep Water Waves

These trajectory radii, r, decrease very fast with increasing distance below the free surface as a result of the negative value for z_1 in the exponential term e^{kz_1}. This is illustrated here:

$$
\begin{aligned}
z &= 0 & \longrightarrow r = \zeta_a \cdot e^{kz} = \zeta_a \cdot e^0 &= 1.000 \cdot \zeta_a \\
z &= -0.50\lambda & \longrightarrow r = \zeta_a \cdot e^{kz} = \zeta_a \cdot e^{-\pi} &= 0.043 \cdot \zeta_a \\
z &= -\lambda & \longrightarrow r = \zeta_a \cdot e^{kz} = \zeta_a \cdot e^{-2\pi} &= 0.002 \cdot \zeta_a
\end{aligned}
$$

One should remember from kinematics that the velocity of the water particles will have a constant magnitude in this case and that it is always directed tangentially to the trajectory circle.

Accelerations

The water particle accelerations follow directly from a differentiation of the velocity components - equations 5.57. This yields:

$$
\dot{u} = +\zeta_a \cdot \omega^2 \cdot \frac{\cosh k\,(h+z)}{\sinh kh} \cdot \sin\,(kx - \omega t)
$$

$$\dot{w} = -\zeta_a \cdot \omega^2 \cdot \frac{\sinh k\,(h+z)}{\sinh kh} \cdot \cos\,(kx - \omega t)$$ (5.65)

Relative to the velocity components, the accelerations have amplitudes which have been multiplied by ω; their phases have been shifted by 90 degrees as well.
In deep water, the water particle accelerations are given by:

$$
\begin{aligned}
\dot{u} &= +\zeta_a \omega^2 \cdot e^{kz} \cdot \sin\,(kx - \omega t) \\
\dot{w} &= -\zeta_a \omega^2 \cdot e^{kz} \cdot \cos\,(kx - \omega t) \qquad \text{(deep water)}
\end{aligned}
$$ (5.66)

It is wise to note that in a circular motion, the magnitude of the acceleration is constant and that it is always directed toward the center of the circle. This acceleration vector is then also always perpendicular to the velocity vector. It can be handy to remember this when computing forces on slender horizontal members in chapter 12.

5.2.4   Pressure

The pressure, p, in first order wave theory follows from the linearized Bernoulli equation 5.26 so that:

$$\frac{\partial \Phi_w}{\partial t} + \frac{p}{\rho} + gz = 0 \qquad \text{or:} \qquad p = -\rho g z - \rho \frac{\partial \Phi_w}{\partial t}$$ (5.67)

With the wave potential from equation 5.34 the expression for the linearized pressure becomes:

$$p = -\rho g z + \rho g \zeta_a \cdot \frac{\cosh k(h+z)}{\cosh kh} \cdot \cos(kx - \omega t)$$ (5.68)

For **deep water** (short waves), the linearized pressure becomes:

$$p = -\rho g z + \rho g \zeta_a \cdot e^{kz} \cdot \cos(kx - \omega t) \qquad \text{(deep water)}$$ (5.69)

The amplitude of the dynamic part of the pressure in short waves is $\rho g \zeta_a \cdot e^{kz}$.
If the non-linear part (quadratic velocities) is retained, then the pressure in short waves becomes:

$$p = -\rho g z + \frac{1}{2} \rho g \zeta_a^2 \omega^2 \cdot e^{2kz} + \rho g \zeta_a \cdot e^{kz} \cdot \cos(kx - \omega t) \qquad \text{(deep water)}$$ (5.70)

in which use has been made of the trigonometric relation:

$$
\begin{aligned}
\frac{1}{2}\left(u^2 + w^2\right) &= \frac{1}{2}\zeta_a^2 \omega^2 \cdot e^{2kz} \cdot \left\{ \sin^2(kx - \omega t) + \cos^2(kx - \omega t) \right\} \\
&= \frac{1}{2}\zeta_a^2 \omega^2 \cdot e^{2kz}
\end{aligned}
$$

The first term in equation 5.70 is a hydrostatic part. The time-independent second term, the radiation pressure, causes the so-called second order wave drift loads on a structure; it will come up again in chapter 9. The harmonic third term causes the so-called first

order wave loads on a structure; its time-averaged contribution is zero. These loads will be treated in chapters 6 and 12.

In shallow water, the dynamic pressure behaves hydrostatically so that:

$$p = -\rho g z + \rho g \zeta_a \cos\left(kx - \omega t\right) \qquad \text{(shallow water)} \tag{5.71}$$

5.2.5 Energy

The energy in a wave and the velocity at which this energy will be transported is of importance for, among others, the propulsion resistance caused by the waves generated by ships.

Wave Energy

Two types of energy are distinguished here: kinetic energy and potential energy.
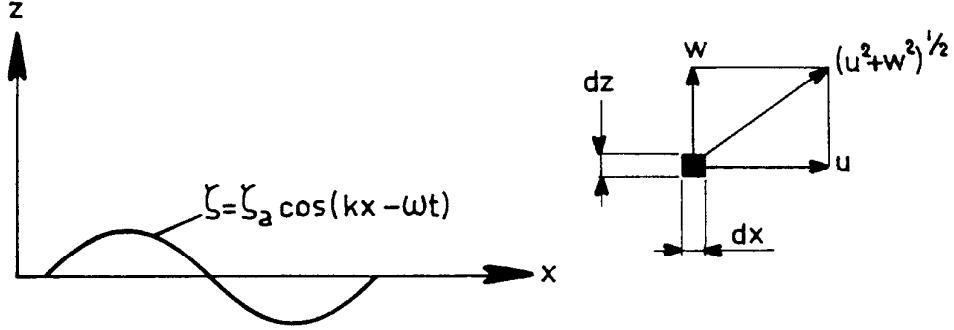
Figure 5.12: Determination of Kinetic Energy

The **kinetic energy**, K, will be calculated as follows (see figure 5.12):

$$
\begin{aligned}
K \;=\;& \int\limits_{volume} \frac{1}{2}\left(u^2 + w^2\right) \cdot dm \\[2mm]
=\;& \frac{1}{2}\rho \int\limits_{0}^{\lambda} \int\limits_{-h}^{\zeta} \left(u^2 + w^2\right) \cdot dz \cdot dx \\[2mm]
=\;& \frac{1}{2}\rho \int\limits_{0}^{\lambda} \int\limits_{-h}^{0} \left(u^2 + w^2\right) \cdot dz \cdot dx + \frac{1}{2}\rho \int\limits_{0}^{\lambda} \int\limits_{0}^{\zeta} \left(u^2 + w^2\right) \cdot dz \cdot dx
\end{aligned}
\tag{5.72}
$$

The second term is approximately equal to:

$$\frac{1}{2}\rho \int\limits_{0}^{\lambda} \int\limits_{0}^{\zeta} \left(u^2 + w^2\right) \cdot dz \cdot dx \;\approx\; \frac{1}{2}\rho \int\limits_{0}^{\lambda} \left\{ \int\limits_{0}^{\zeta} dz \right\} \left(u^2 + w^2\right) \cdot dx$$

$$= \frac{1}{2}\rho\zeta \int_0^\lambda \left(u^2 + w^2\right) \cdot dx \tag{5.73}$$

which is of second order - relative to the first term in equation 5.72 - and can be ignored. In a linearized form this equation then becomes:

$$K = \frac{1}{2}\rho \int_0^\lambda \int_{-h}^0 \left(u^2 + w^2\right) \cdot dz \cdot dx \tag{5.74}$$

A substitution of the expressions for u and w from equation 5.57 and using the dispersion relation of equation 5.42 and some algebra provides:

$$\begin{aligned} K &= \frac{1}{4}\rho g \zeta_a^2 \cdot \lambda & \text{per unit width (crest length)} \\ &= \frac{1}{4}\rho g \zeta_a^2 & \text{per unit horizontal sea surface area} \end{aligned} \tag{5.75}$$

Some trigonometric relations have been used to obtain these results:

$$\begin{aligned} \int_{-h}^0 \sinh^2 k\,(h+z) \cdot dz &= \frac{1}{4k}\sinh 2kh - \frac{1}{2}h \\ \int_{-h}^0 \cosh^2 k\,(h+z) \cdot dz &= \frac{1}{4k}\sinh 2kh + \frac{1}{2}h \\ \int_0^\lambda \sin^2(kx - \omega t) \cdot dx &= \int_0^\lambda \cos^2(kx - \omega t) \cdot dx = \frac{1}{2}\lambda \end{aligned} \tag{5.76}$$
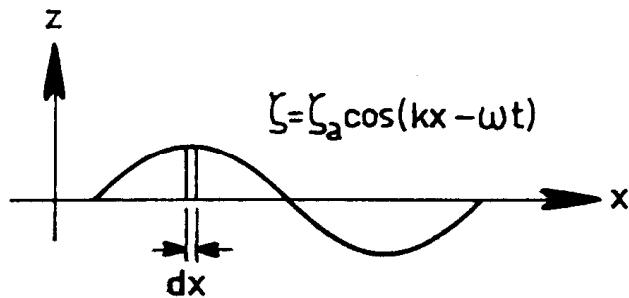
Figure 5.13: Determination of Potential Energy

The **potential energy**, P, will be calculated as follows (see figure 5.13):

$$P = \frac{1}{2}\int_0^\lambda \rho g \zeta^2 \cdot dx$$

$$= \frac{1}{2}\rho g \zeta_a^2 \int_0^\lambda \cos^2(kx - \omega t) \cdot dx \qquad (5.77)$$

Some algebra results in:

$$
\begin{aligned}
P &= \frac{1}{4}\rho g \zeta_a^2 \cdot \lambda && \text{per unit width (crest length)} \\
&= \frac{1}{4}\rho g \zeta_a^2 && \text{per unit horizontal sea surface area} && (5.78)
\end{aligned}
$$

This has the same magnitude as the kinetic energy.
The **total wave energy**, E, follows from equations 5.75 and 5.78, $E = K + P$:

$$\boxed{E = \frac{1}{2}\rho g \zeta_a^2 = \frac{1}{8}\rho g H^2 \qquad \text{per unit horizontal sea surface area}} \qquad (5.79)$$

Energy Transport or Power

The velocity at which the wave energy will be transported can be determined using figure 5.14. It shows a virtual vertical plane AA', which is perpendicular to the direction of propagation of the wave. An element in this plane (shaded in figure 5.14) is of unit width and has height dz.
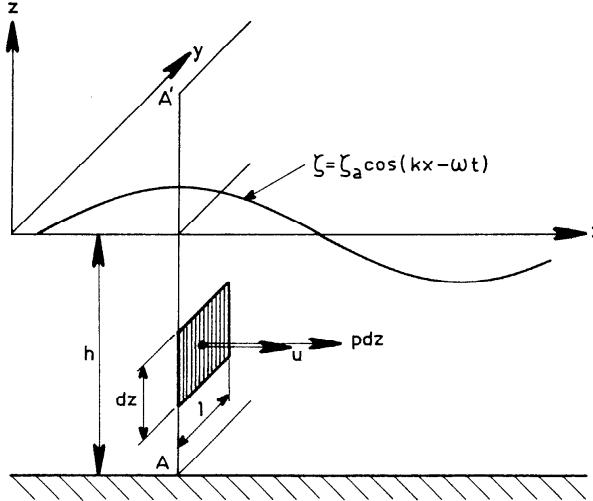
Figure 5.14: Wave Energy Transport

When the fluid passes through this plane element, a certain amount work dW will be delivered in a direction against the pressure p of the fluid.
The work done is **force times distance**:

$$dW = \{p \cdot 1 \cdot dz\} \cdot \{u \cdot dt\} \qquad (5.80)$$

The average work done over one period, T, **or power** is after linearization:

$$\overline{W} = \frac{1}{T} \int\limits_{t}^{t+T} \int\limits_{-h}^{0} p \cdot u \cdot dz \cdot dt \tag{5.81}$$

which follows if one realizes that the contribution from the uppermost segment - the **splash zone** - can be neglected:

$$\frac{1}{T} \int\limits_{t}^{t+T} \int\limits_{0}^{\zeta} p \cdot u \cdot dz \cdot dt \approx 0 \tag{5.82}$$

Substituting 5.71 for the pressure and 5.57 for u results in:

$$\overline{W} = -\frac{\rho k g^2 \zeta_a}{T \cdot \omega \cdot \sinh kh} \int\limits_{t}^{t+T} \int\limits_{-h}^{0} z \cdot \cosh k(h+z) \cdot \cos(kx - \omega t) \cdot dz \cdot dt$$

$$+ \frac{\rho k g^2 \zeta_a^2}{T \cdot \omega \cdot \sinh kh \cdot \cosh kh} \int\limits_{t}^{t+T} \int\limits_{-h}^{0} \cosh^2 k(h+z) \cdot \cos^2(kx - \omega t) \cdot dz \cdot dt \tag{5.83}$$

The first term is zero and, with the relations given in equations 5.76, the average work done or power becomes:

$$\overline{W} = \frac{\rho g \zeta_a^2 \omega}{\sinh 2kh} \cdot \left(\frac{1}{4k} \sinh 2kh + \frac{1}{2} h \right) \tag{5.84}$$

With $c = \omega/k$, this relation becomes:

$$\boxed{\overline{W} = \frac{1}{2} \rho g \zeta_a^2 \cdot \frac{c}{2} \cdot \left(1 + \frac{2kh}{\sinh 2kh} \right)} \tag{5.85}$$

or in terms of wave height:

$$\overline{W} = \frac{1}{8} \rho g H^2 \cdot \frac{c}{2} \cdot \left(1 + \frac{2kh}{\sinh 2kh} \right) \tag{5.86}$$

Group Velocity

The average work done per wave period in equation 5.85 can also be written as:

$$\overline{W} = E \cdot c_g \tag{5.87}$$

with:

$$E = \frac{1}{2} \rho g \zeta_a^2 = \frac{1}{8} \rho g H^2$$

$$\boxed{c_g = \frac{c}{2} \cdot \left(1 + \frac{2kh}{\sinh 2kh} \right)} \tag{5.88}$$

Then E is the energy of the waves per unit area and c_g is the velocity at which this energy will be transported in the waves, the **wave group velocity**.

In deep water, the wave group velocity is exactly half the phase velocity:

$$c_g = \frac{c}{2} \qquad \text{(deep water)} \tag{5.89}$$

In shallow water, the group velocity is identical to the phase velocity:

$$c_g = c \qquad \text{(shallow water)} \tag{5.90}$$

The characteristics of the wave phase velocity and the wave group velocity are shown in figure 5.15, obtained from [Newman, 1977].

[Source: Newman, 1977]
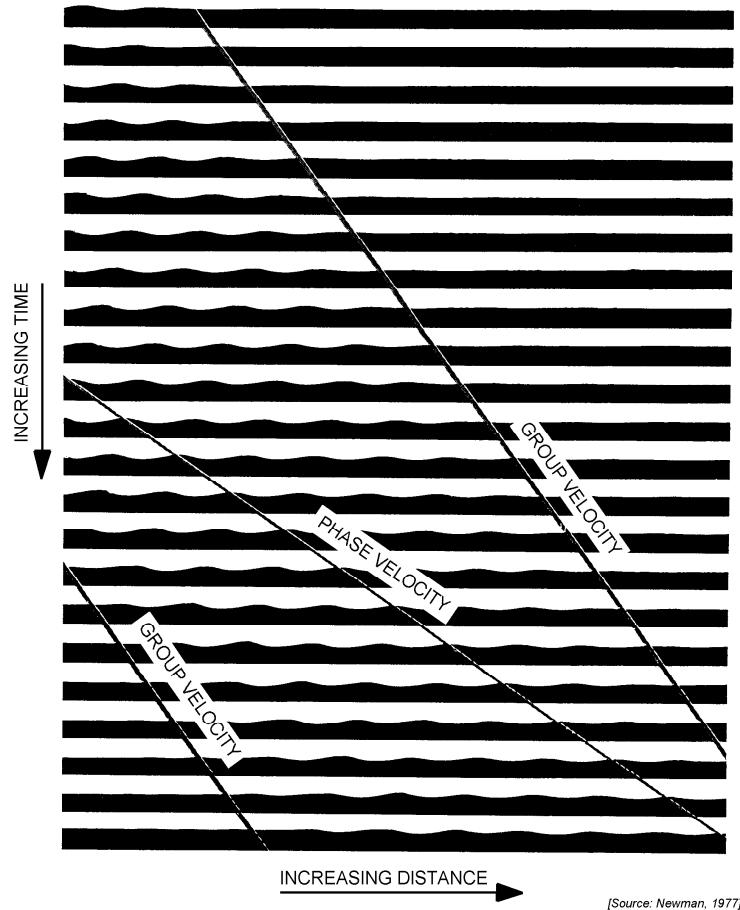
Figure 5.15: Wave Phase and Group Velocity

The sequence of images shows a plane progressive wave system advancing into calm water. The water is darkened and the lower part of the water depth is not shown. The interval between the successive images is 0.25 seconds and $\lambda/h \approx 2$. The wave energy is contained within the heavy diagonal lines and propagates with the group velocity. These wave group boundaries propagate slowly with time, due to dispersion. The position of a single wave crest is connected in successive images by the lighter line; this advances with the wave phase velocity. Each wave crest moves with the phase velocity, equal to twice the group velocity of the wave field boundaries. Thus each wave crest vanishes at the front end and, after the wave maker is turned off, arises from calm water at the back.

5.2.6   Relationships Summary

Figure 5.16 shows the relation between λ, T, c and h for a wide variety of conditions. Notice the boundaries $\lambda/h \approx 2$ and $\lambda/h \approx 20$ in this figure between short (deep water) and long (shallow water) waves.
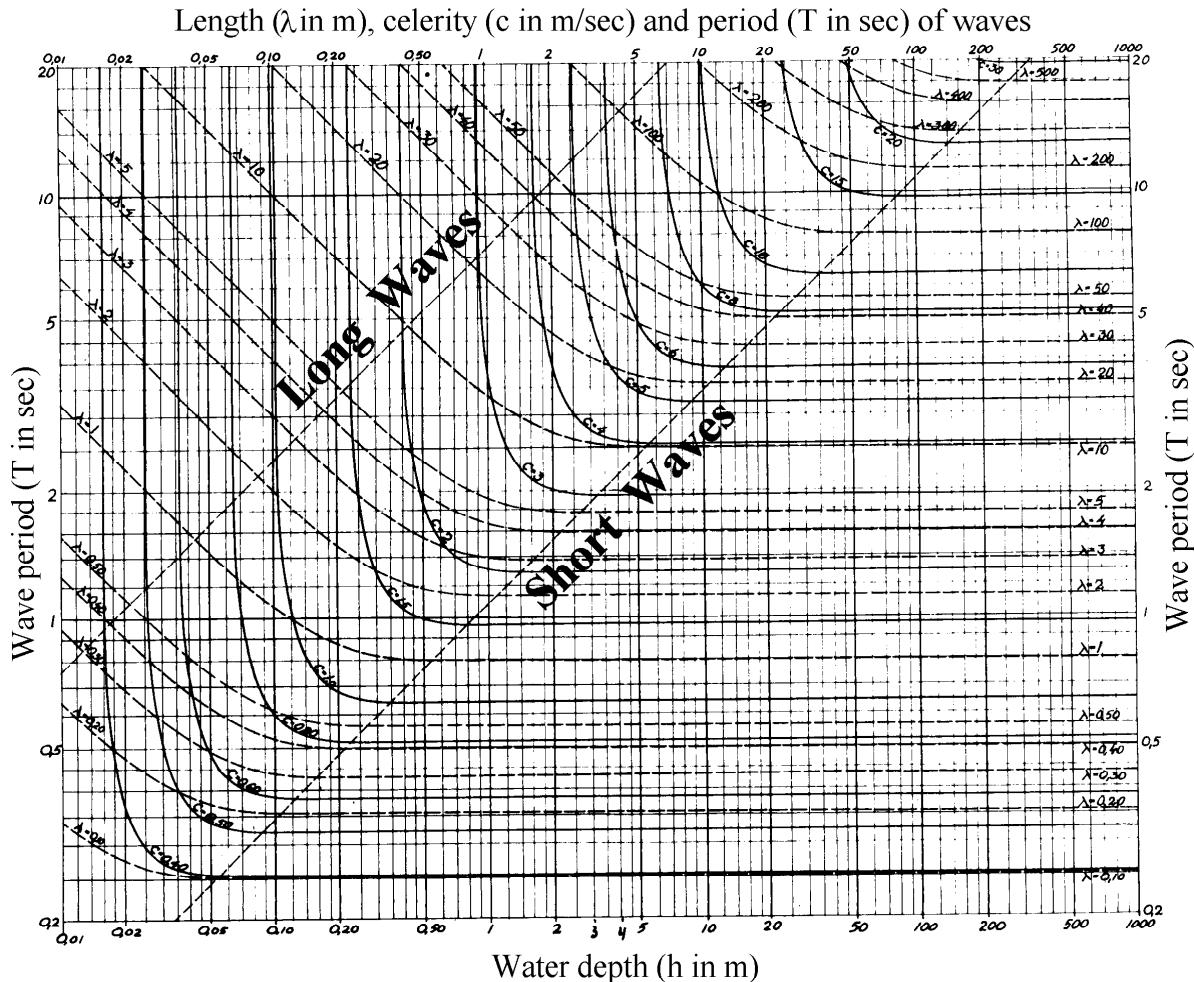
Figure 5.16: Relationships between λ, T, c and h

Some examples of the effect of the water depth on the trajectories of individual water particles under a 100 meter length wave (at $\lambda/h = 50$, 10 and 1) are presented in figure 5.17.

5.2.7   Shoaling Water

The theory in the previous sections has been worked out for water of constant depth. Attention in this section focuses on how waves change as they encounter varying water depths as they propagate. Some items - such as changes in the wave celerity and group speed - can be interfered from the theory already presented. Other wave properties including its wave height change too. Since the wave height (or amplitude) is so important for other wave-related phenomena, this section first discusses the influence of changing water depth on wave height.
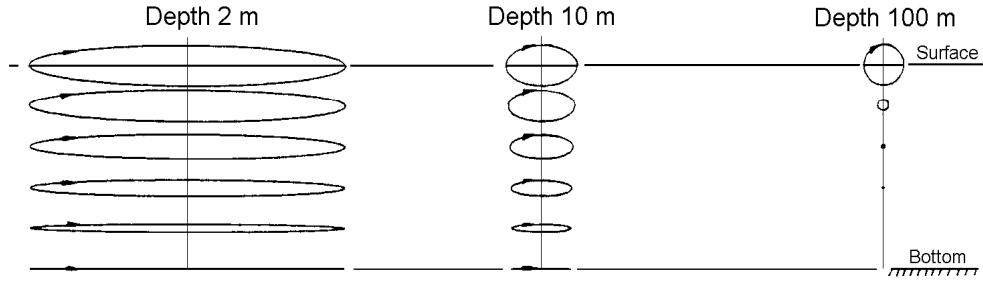
Figure 5.17: Orbit Shapes under a $\lambda = 100$ m Wave at Three Different Water Depths

Wave Height Changes

The relationship between wave height, H, and water depth, h, is embedded in the concept of conservation of energy transport through a vertical plane parallel to the wave crests. This is thus also the wave power per unit of crest length or what is sometimes called its energy flux, see equation 5.86.

By assuming that $\overline{W}$ in this equation remains constant as the water depth changes, one can compute the wave height, H_h in any water depth, h, as long as the wave height is known in some given water depth. It can be convenient for offshore and coastal engineering problems to work from (known) conditions in deep water, often denoted by a subscript "∞". When one realizes that $k = 2\pi/\lambda$ - is purely a function of h/λ or for that matter h/λ_∞, one can determine - after quite some algebra - that:

$$K_{sh} = \frac{H_h}{H_\infty} = \sqrt{\frac{1}{\tanh kh \cdot \left(1 + \frac{2kh}{\sinh 2kh}\right)}} \tag{5.91}$$

in which:

$$
\begin{aligned}
K_{sh} &= \textbf{shoaling coefficient} \\
H_\infty &= \text{wave height in deep water (m)} \\
H_h &= \text{wave height in water of depth } h \text{ (m)} \\
k &= \text{wave number at depth } h \text{ (rad/m)} \\
h &= \text{chosen water depth (m)}
\end{aligned}
$$

If wave conditions are known only at some finite water depth, then one can first use equation 5.91 to evaluate K_{sh} at that depth and then compute a new shoaling coefficient at the desired water depth. The known wave height can then be transformed to one at the new depth using the ratio of the shoaling coefficients.

Figure 5.18 shows how a wave changes height as it progresses into shallower water. The shoaling coefficient is actually plotted on the vertical axis of this figure (as wave height or velocity ratio) as a function of the dimensionless water depth h/λ_∞ on the horizontal axis. A wave progressing into shallower water would move from left to right. One sees that the wave height first decreases a bit and then recovers. It is not until a wave gets into water too shallow to be of offshore interest that its height becomes larger than in deep water.

Obviously the wave will ultimately **break** as the water depth becomes ever shallower. Only swimmers, surfboarders and coastal engineers enjoy waves breaking on the shore; sailors
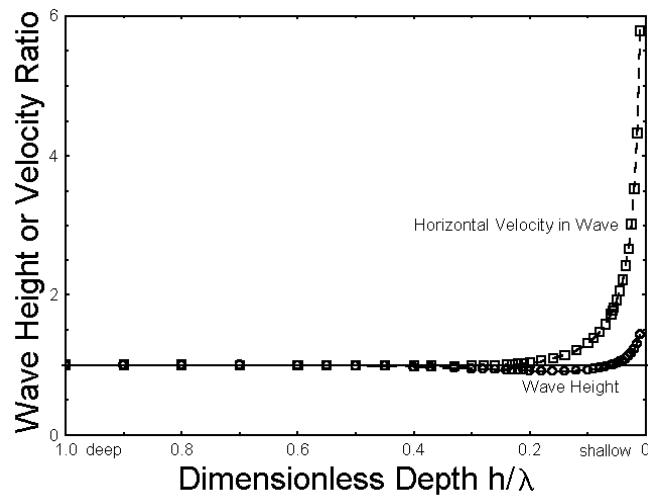
Figure 5.18: Shoaling Effects

and offshore engineers want to avoid them instead. Indeed, this oceanographic detail is left to others.

Water Motion Changes

One may conclude from the above that the effects of water shoaling - at least on the wave height - are not that spectacular. How does the amplitude of the horizontal water velocity in the wave change? Since this amplitude at the sea surface can be given by (see equation 5.57):

$$u_a(h) = K_{sh.} \cdot \frac{H_\infty}{2} \cdot \omega \cdot \frac{\cosh kh}{\sinh kh} \tag{5.92}$$

Then the velocity ratio is given by:

$$\left| \frac{u_a(h)}{u_a(\infty)} = K_{sh} \cdot \frac{\cosh kh}{\sinh kh} \right| \tag{5.93}$$

This is plotted in figure 5.18 as well; this increases more than does the wave height. Its importance will become obvious when survival loads on fixed offshore tower structures are being estimated. This is explained in chapter 13.

Wave Refraction

The wave period is the only property which does not change as a wave progresses through water of varying depth. Since the wave length does change, it is only logical, then, that the wave speed, $c = \lambda/T$, changes as well. Indeed, as the wave length becomes smaller (in shallower water) the wave must travel more slowly.

When now waves approach in such a way that their crests are not parallel to the depth contours, then one segment of each crest will be in shallower water than its neighboring segment. The segment in shallower water will move forward more slowly than that in deeper water. The wave crest - and thus its direction of propagation - will turn; this is

called **refraction** much like the similar phenomena with light in physics. The wave crests always turn in such a way that their crests become more parallel to the depth contours as they proceed into shallower water.

5.2.8 Wave Reflection and Diffraction

When a regular wave component meets a vertical wall perpendicular to its propagation direction - such as the side of a big ship - it is **reflected** and sent back where it came from with (ideally) an identical amplitude and speed. The water surface near the ship appears to move up and down - with twice the amplitude of the incoming wave - but there is no apparent wave progression. This describes a **standing wave**, which can be formulated by adding up two identical waves moving in opposite directions as given in equations 5.94.

$$
\begin{aligned}
\zeta &= \zeta_1 + \zeta_2 \\
&= \zeta_a \cos(kx - \omega t) + \zeta_a \cos(kx + \omega t) \\
&= 2\zeta_a \cos(kx) \cos(\omega t)
\end{aligned}
\tag{5.94}
$$

The amplitude of this resulting wave is twice the amplitude of the two separate progressive wave components and the phase velocity becomes zero; see figures 5.19 and 5.20.
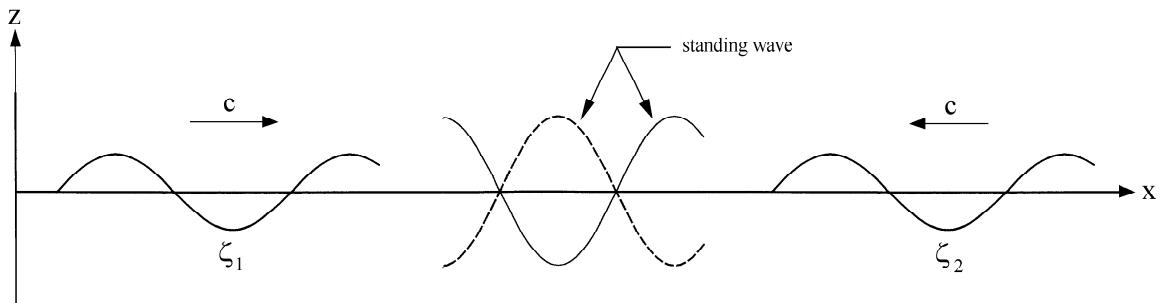
Figure 5.19: Standing Wave
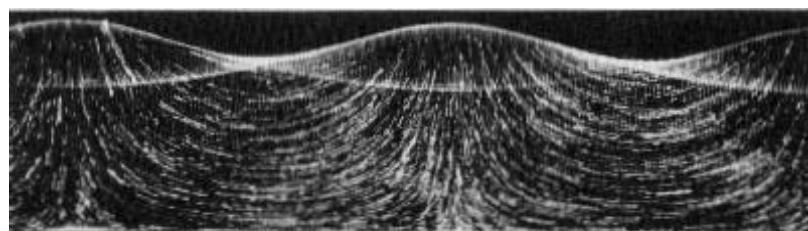
Figure 5.20: Fluid Motions under a Standing Wave

If the wave approaches the wall under an angle, then the above approach is still valid for its component perpendicular to the wall. The wave is reflected away from the wall at an angle in the same as light reflects from a flat mirror.
Wave diffraction is a process by which wave energy is propagated into a **shadow zone** - an area which is not directly in line with the approaching wave. Coastal engineers use

diffraction to predict waves in behind breakwaters in harbors. Since nearly all (fixed) breakwaters extend over the entire water depth, they work with two dimensional (in the horizontal plane) diffraction.

A large ship can also function as a floating breakwater. Indeed, persons being rescued from the sea are almost invariably picked up on the lee side of the ship - where the waves are lower.

Since the ship is floating, energy can now be transmitted to the shadow zone via the ends of the ship as well as under the ship. Wave diffraction even plays an essential role in the motion of the ship itself. Indeed, diffraction principles will be applied frequently when determining the motions of floating objects in waves. This topic is treated in chapters 6 through 9.

5.2.9   Splash Zone

Linear wave theory presented so far describes (formally) the water motion in the zone below the still water level. Indeed, as far as the theory is (strictly) concerned, the wave surface never departs from that level $z = 0$; this comes from the linearizations used. Such a limitation is especially inconvenient when splash zone hydromechanics becomes relatively more important. This can be the case when considering nonlinear phenomena in ship motions as in chapter 9 or when predicting survival loads on offshore tower structures in chapter 13. Another difficulty is that one usually finds that the wave crest elevation is generally higher than its corresponding trough is deep; the wave is actually somewhat asymmetrical, it does not have a perfect sinus-shape. Higher order wave theories were introduced to solve this latter problem.

Higher Order Wave Theories

In the past, there have been several attempts to alleviate the above limitation of linear theory in order - at least - to better describe the actual wave surface profile in mathematical terms, and - with luck - to describe the water kinematics up to the actual wave surface as well.

The theories one can find in the - primarily older - literature include the cynoidal theory and Stokes' second, third and fifth order theories. All of these theories describe only a regular wave, by the way. They are all nonlinear which means that superposition - as described in the beginning of this chapter - cannot be used with them.

Generally speaking the increasing need for statistical information on the sea and a structure's reaction to it, has led to the more widespread acceptance of linear methods in general and linear wave theory in particular. None of the above mentioned theories will be discussed here, therefore; many of them can still be found in other textbooks, however. Other ways to calculate the water motions in the splash zone have been found.

Profile Extension Methods

The first step is to realize that - especially for higher waves often used in design - the wave crest will be higher than the sinusoidal wave amplitude above the sea surface. The higher order wave theories, above, included this more or less automatically. When linear theory is used this must be done 'by hand'. It is usually assumed that the wave will extend 0.6 to

0.7 times its height above the still water level; two thirds or six tenths are commonly used fractions for this.

Once this has been taken care of, the next step is to adapt linear wave theory in some effective way. Remember that we can use the following equation to describe the horizontal water velocity component:

$$u_a(z) = \frac{H}{2} \cdot \omega \cdot \frac{\cosh k\,(h+z)}{\sinh kh} \qquad (5.95)$$

This equation is derived from equation 5.57 by substituting $\zeta_a = H/2$, for use in the range $0 \geqq z \geqq -h$; it is valid for all water depths.

There are some simple profile extension methods available:

- **Extrapolation**
  This uses unaltered linear wave theory all the way from the sea bed to the actual water surface elevation or wave crest height; z is simply allowed to be positive in the formulas. Straightforward mathematical extension of linear theory in this way leads to an 'explosion' in the exponential functions so that the velocities become exaggerated within the wave crest; such results are generally considered to be too big or over-conservative.

- **Constant Extension**
  A second relatively simple method uses conventional linear wave theory below the mean sea level. Then the water velocity found at $z = 0$ is simply used for all values of $z > 0$. This is commonly used and is quite simple in a hand calculation.
  When the wave profile is below the still water level, then one simply works with linear theory up to that level, only.

- **Wheeler Profile Stretching**
  Profile stretching is a means to make the negative z-axis extend from the actual instantaneous water surface elevation to the sea bed. Many investigators have suggested mathematical ways of doing this, but Wheeler's method presented here is the most commonly accepted, see [Wheeler, 1970]. He literally stretched the profile by replacing z (on the right hand side of equation 5.95 only!) by:

$$z' = qz + h(q-1) \qquad \text{in which:} \quad q = \frac{h}{h+\varsigma} \qquad (5.96)$$

  where:
  z' = a computational vertical coordinate (m): $-h \leqq z' \leqq 0$
  z = the actual vertical coordinate (m): $-h \leqq z \leqq \varsigma$
  q = a dimensionless ratio (-)
  ς = the elevation of the actual water surface (m), measured along the z-axis
  h = the water depth to the still water level (m)
  What one is doing, is really computing the water motion at elevation z' but using that water motion as if it were at elevation z. Wheeler stretching is a bit cumbersome for use in a purely hand calculation. It can be implemented quite easily in a spreadsheet or other computer program, however. It is popular in practice, too.

One should note the following about the formulas in this section:

- If only a maximum velocity is needed, the time function can be neglected as has been done here. The time function plays no distinctive role in any of these methods.

- All z'-values used will be negative (or zero); the exponential functions 'behave themselves'.
- Each of these approaches degenerate to linear theory if it is applied at the still water level.
- The above formulations are universal in that they can be used in any water depth, at any point under a wave profile and at any particular phase within the wave (if desired).
- Since all of these stretching methods are based upon linear wave theory, they can all be used with irregular waves.

Users should be aware that use of deep water wave theory - with its simplifications - will lead to less than conservative results as the water depth decreases; this is the reason that the full theory is used above. Indeed, water motion amplitudes within a wave are never smaller than those predicted by deep water theory.

Comparison

A check out of the behavior of all of the above computational procedures in a typical situation is done here for the following condition: $H = 15$ meters, $T = 12$ seconds and $h = 40$ meters. These values (with a crest height which is $2/3 \cdot H$) yield $q = 40/50 = 0.80$. The computed results are shown in figure 5.21.
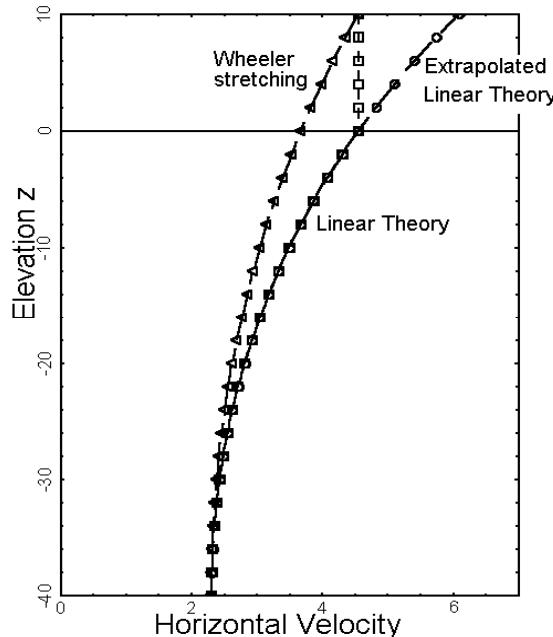
Figure 5.21: Comparison of Computed Horizontal Water Velocities

The following observations can be made:
- A consistently extrapolated Airy theory yields the largest values. This might well be expected.
- Similarly, a 'plain' Airy theory which simply neglects the wave crest entirely, yields a lower bound value.
- All methods presented give identical results at the sea bed - as they should.
- Wheeler stretching seems to yield attractive results in that they lie within the expected range and they are considerably less than the upper bound.

5.3   Irregular Waves

Now that the background of regular waves has been discussed, attention shifts to a more realistic image of the sea surface. Often the sea surface looks very confused; its image changes continuously with time without repeating itself. Both the wave length between two successive crests or troughs and the vertical distance between a crest and a trough vary continuously.

5.3.1   Wave Superposition

It was stated in the first lines of this chapter that it is possible to represent the irregular sea surface using a linear superposition of wave components. This will be demonstrated here. In fact, a superposition of only two components with identical directions but different speeds are needed to show this; see figure 5.22.
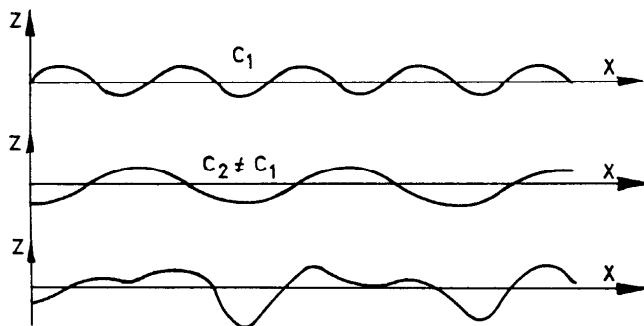
Figure 5.22: Superposition of Two Uni-Directional Harmonic Waves

A superposition of three components yields a more realistic record, even though these still come from one direction; see figure 5.23. A wave train such as this can easily be generated in a wave flume, for example. Since all of the energy travels in the same direction, the wave crests will be (theoretically) infinitely long; everything of interest can be observed in a single x-z plane.

Note that for a realistic record of uni-directional irregular waves, a superposition of at least 15 or 20 components is required in practice if one is only interested in the mean value of an output. More components are handy if additional information such as statistical distributions are needed.

If a third dimension - direction - is added to this, then the sea (as seen from above) becomes even more realistic as is shown in figures 5.24 and 5.25.

One sees from these figures that the length of the wave crests is now limited. This is a sign of the fact that wave energy is simultaneously propagating in several directions.

5.3.2   Wave Measurements

Most waves are recorded at a single fixed location. The simplest instrumentation can be used to simply record the water surface elevation as a function of time at that location. Since only a scalar, single point measurement is being made, the resulting record will yield no information about the direction of wave propagation.
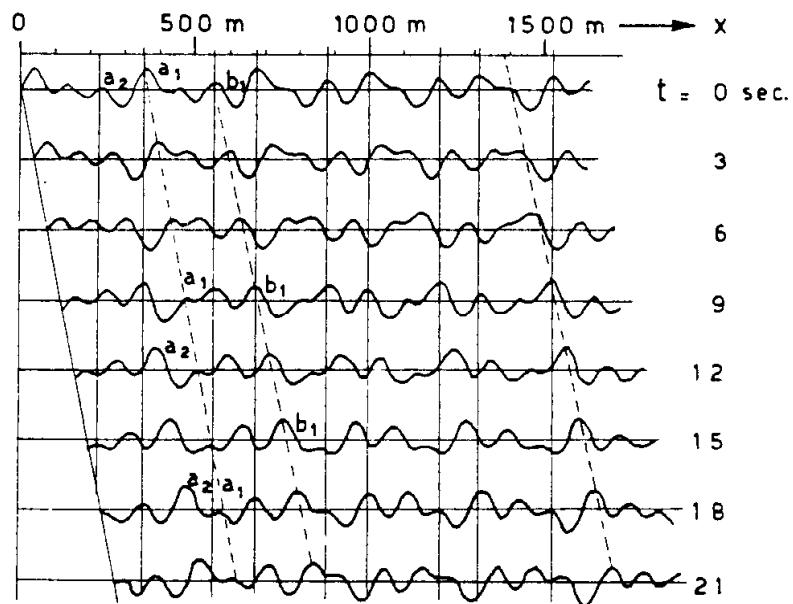
Figure 5.23: Superposition of Three Uni-Directional Harmonic Waves

[Source: Groen and Dorrestein, 1958]
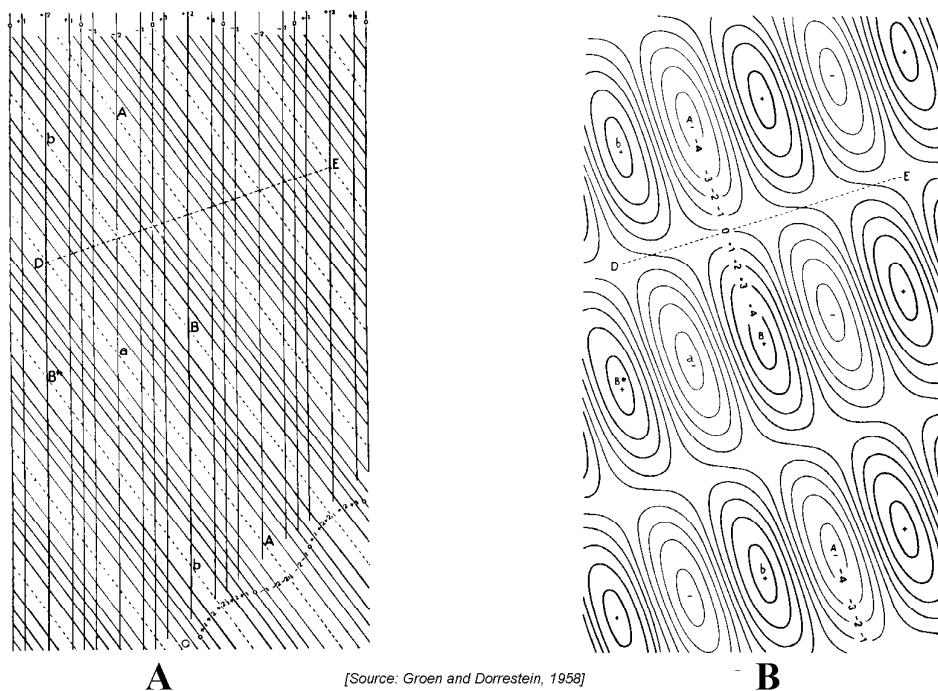
Figure 5.24: Superposition of Two Harmonic Waves with Different Directions
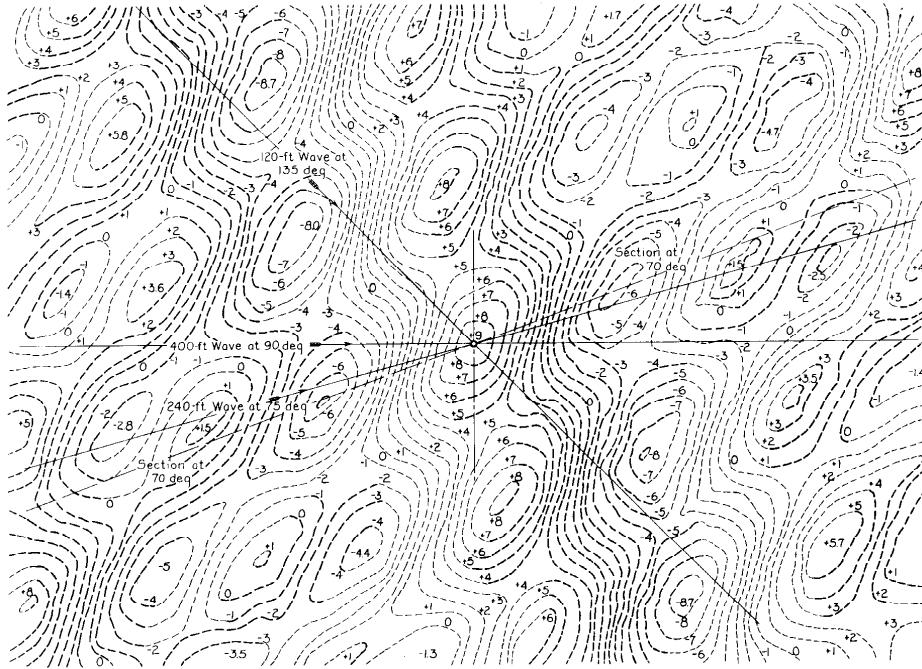
Figure 5.25: Superposition of Three Harmonic Waves with Different Directions

It is possible to measure (or to infer) wave directions at a point by using more sophisticated instruments to measure - for example - simultaneous horizontal water velocity components in two perpendicular directions and to correlate these measurements with the water surface time record.

Today it is quite common to measure wave heights from satellites using high frequency radar signals. Physically, the scatter of (or noise in) the reflected radar signal is a measure of the roughness of the surface reflecting it - in this case the sea. This noise can then be correlated with the wave height present on the sea surface.

Waves have occasionally been measured by stereo photography from above; it is pretty expensive to do. Such images have been used to study wave growth in a wind field and to determine the wave's directional spreading.

5.3.3   Simple Statistical Analysis

Figure 5.26 shows a part of a simple time history of an irregular wave. When such a time history is available, then a simple analysis can be carried out to obtain statistical data from this record. The length of this time history should be at least 100 times the longest wave period, to obtain reliable statistical information. The analysis presented in this section can be carried out by hand

Average Wave Period

The **average wave period**, $\bar{T}$, can be found easily (by hand) from the **average zero up-crossing period** or from the **average period of the wave crests or troughs**. The simplest way to do this is to divide the record duration by the number of upward (or downward) zero-crossings found minus one.
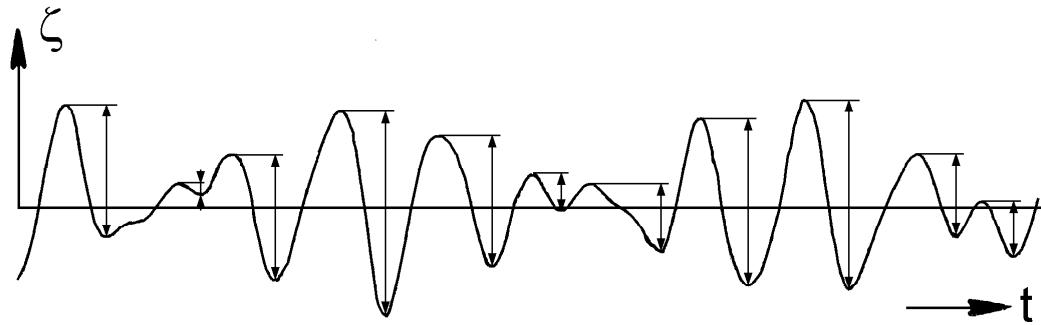
Figure 5.26: Time History of a Seaway

Wave Height Statistics

Obtaining an average wave height requires more work. Successive wave heights are measured and classified in groups with intervals of, for instance, 0.5 meter. The number of wave heights in each group is then counted. These counts for each group are divided by the total number of wave heights to obtain the frequency quotients or the **probability density function** $f(x)$. Finally these frequency quotients are added cumulatively to obtain the cumulative frequency quotients or the **distribution function** of wave heights $F(x)$. A numerical example of this approach is given in the table below.

wave height intervals (m)	wave height average (m)	number of waves n	frequency quotient $f(x)$	cumulative frequency quotient $F(x)$
0.25-0.75	0.5	15	0.100	0.100
0.75-1.25	1.0	30	0.200	0.300
1.25-1.75	1.5	55	0.367	0.667
1.75-2.25	2.0	21	0.140	0.807
2.25-2.75	2.5	14	0.093	0.900
2.75-3.25	3.0	9	0.060	0.960
3.25-3.75	3.5	5	0.033	0.993
3.75-4.25	4.0	1	0.007	1.000
total		150	1.000	

The probability density function of wave heights, $f(x)$, is given in figure 5.27-a as a histogram. The associated distribution function of wave heights, $F(x)$, is given in figure 5.27-b. As one uses even more waves to determine these functions, the functions converge to a stable form.

Statistical information can be obtained from the probability density function $f(x)$. For example, the probability that the wave height, $\widetilde{H}_w$, exceeds a certain threshold value, a, in this record is given by:

$$P\left\{\widetilde{H}_w > a\right\} = \int\limits_{a}^{\infty} f(x) \cdot dx \qquad (5.97)$$
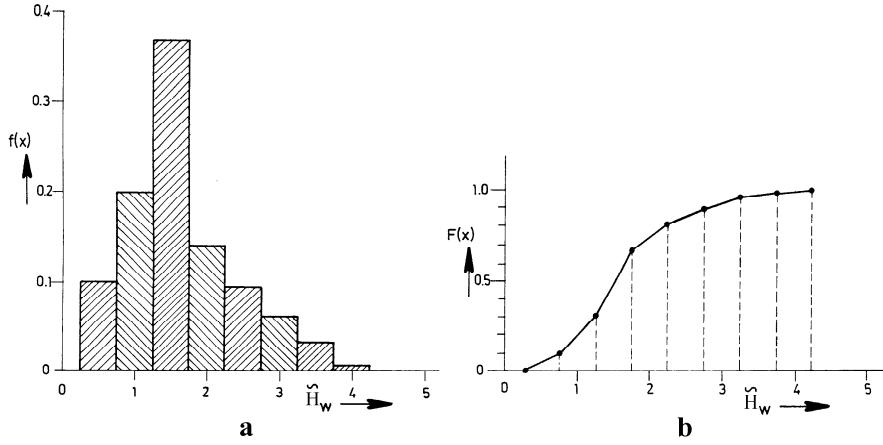
Figure 5.27: Probability Density and Distribution Functions of Wave Heights

The table shows that, if $a = 3.25$ meter, the probability of finding a wave higher than that threshold value is given by this integral (or in this case):

$$P\left\{\widetilde{H}_w > 3.25\right\} = \frac{5 + 1}{150} = 0.04 \qquad \text{or:} \qquad P\left\{\widetilde{H}_w > 3.25\right\} = 0.033 + 0.007 = 0.04 \quad (5.98)$$

Mean Wave Height

The **mean wave height** can be found very easily using either figure as follows:

$$\overline{H} = \frac{0.5 \cdot 15 + 1.0 \cdot 30 + 1.5 \cdot 55 + 2.0 \cdot 21 + 2.5 \cdot 14 + 3.0 \cdot 9 + 3.5 \cdot 5 + 4.0 \cdot 1}{150} = 1.64 \text{ m}$$

or from $f(x)$:

$$\begin{aligned} \overline{H} \quad = \quad & 0.5 \cdot 0.100 + 1.0 \cdot 0.200 + 1.5 \cdot 0.367 + 2.0 \cdot 0.140 + \\ & 2.5 \cdot 0.093 + 3.0 \cdot 0.060 + 3.5 \cdot 0.033 + 4.0 \cdot 0.07 = 1.64 \text{ m} \end{aligned}$$

Significant Wave Height

The so-called **significant wave height** $H_{1/3}$, defined as the average of the highest 1/3 of the waves in the record. Thus, in this case:

$$H_{1/3} = \frac{2.0 \cdot 21 + 2.5 \cdot 14 + 3.0 \cdot 9 + 3.5 \cdot 5 + 4.0 \cdot 1}{50} = 2.51 \text{ m}$$

or from $f(x)$:

$$H_{1/3} = \frac{2.0 \cdot 0.140 + 2.5 \cdot 0.093 + 3.0 \cdot 0.060 + 3.5 \cdot 0.033 + 4.0 \cdot 0.07}{1/3} = 2.51 \text{ m}$$

The significant wave height, $H_{1/3}$, plays an important role in many practical applications of wave statistics. Often there is a fair correlation between the significant wave height and a visually estimated wave height. This comes, perhaps, because higher waves make more of an impression on an observer than the smallest ones do.

5.3.4   More Complete Record Analysis

Now a more complete record analysis will be given; it is only possible using a computer and a digitized time record of the wave surface elevation.

Record and Sampling
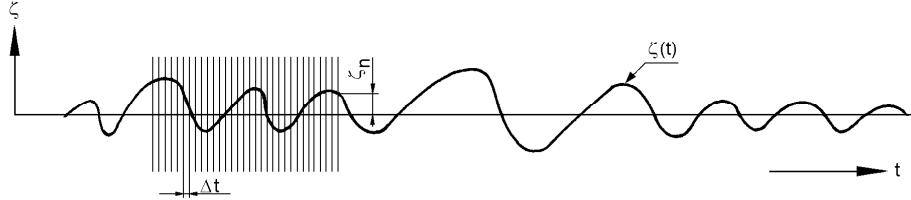
Figure 5.28: Registration and Sampling of a Wave

Consider an irregular wave record, $\zeta(t)$, as given in figure 5.28. As already has been mentioned, the length of the record should be at least 100 times the longest observed period of the waves in this record. The record will be sampled at a large number, N, equal intervals, Δt. In practice, one might make a record of about 15 to 20 minutes, spaced every half second. Unless there is a very long swell in the record, this is just long enough to capture enough waves, but still short enough to avoid extra influences such as result from tidal level changes. The average level of these N observations (relative to some arbitrary level) can be found easily and used to define the still water level. Once the elevations have been corrected to this level, one has a set of N vertical displacements, ζ_n, relative to the still water level.

Standard Deviation

The so-called **standard deviation** σ of the water level $\zeta(t)$ follows from:

$$\boxed{\sigma = \sqrt{\frac{1}{N-1} \sum_{n=1}^{N} \zeta_n^2}} \qquad \text{(standard deviation)} \qquad (5.99)$$

Notice that σ relates to the instantaneous water surface elevations, instead of crest-to-trough wave heights as was used before in the simple statistical analysis.

This standard deviation σ - also referred to as **Root Mean Square** (RMS) value - is related to the significant wave amplitude, $\zeta_{a_{1/3}}$, and the significant wave height, $H_{1/3}$, by:

$$\boxed{\zeta_{a_{1/3}} = 2 \cdot \sigma} \qquad \text{(significant wave amplitude)}$$

$$\boxed{H_{1/3} = 4 \cdot \sigma} \qquad \text{(significant wave height)} \qquad (5.100)$$
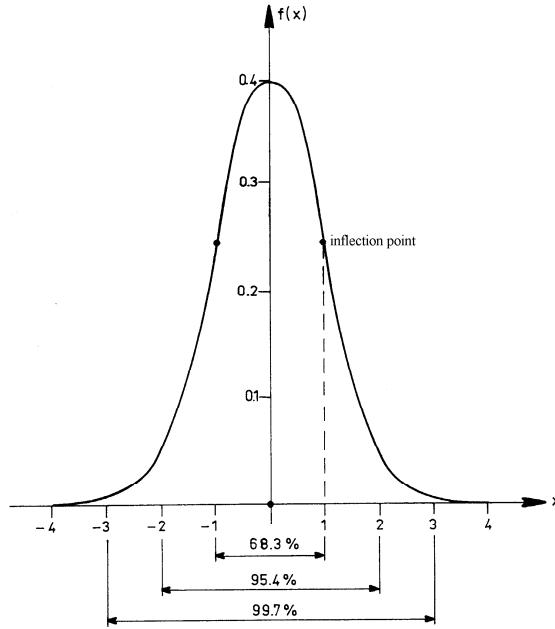
Figure 5.29: Normal or Gaussian Distribution with $\sigma = 1$

Gaussian Water Level Distribution

The above series of water levels, ζ, can be analyzed statistically. It has been found to fit a **Gaussian distribution** or **normal distribution** quite well; see figure 5.29.

This distribution - provided that the ζ-values have a mean value equal to zero - is given by:

$$
f(x) = \frac{1}{\sigma\sqrt{2\pi}} \cdot \exp\left\{-\left(\frac{x}{\sigma\sqrt{2}}\right)^2\right\} \qquad \text{(Gaussian or normal distribution)} \qquad (5.101)
$$

in which x is the variable being studied and σ is its standard deviation.

With this distribution, the probability that the water level, ζ, exceeds a chosen threshold value, a, can be calculated using:

$$
\begin{aligned}
P\{\zeta > a\} &= \int_a^\infty f(x) \cdot dx \\
&= \frac{1}{\sigma\sqrt{2\pi}} \int_a^\infty \exp\left\{-\left(\frac{x}{\sigma\sqrt{2}}\right)^2\right\} \cdot dx \qquad (5.102)
\end{aligned}
$$

This integral calculates the area under the curve to the right of the chosen value, a.

Some important values of a and corresponding probabilities, $P\{\zeta > a\}$, are given in the table below.

a	$P\{\zeta > a\}$
σ	0.320
2σ	0.046
3σ	0.003

A Gaussian or normal distribution with $\sigma = 1$ is shown in figure 5.29. This distribution has its inflection points at $x = \pm\sigma = \pm 1$ and its value at $x = 0$ is $f(0) = 1/(\sigma\sqrt{2\pi}) = 0.399$.

Rayleigh Wave Amplitude Distribution

If the range of frequencies in a wave field is not too large, one speaks of a **narrow banded frequency spectrum**. Luckily, waves - a sea or a swell - generally satisfy this condition quite well. If this is the case - and the water surface elevation is a Gaussian distribution - then the wave amplitude statistics will obey a **Rayleigh distribution**.
This Rayleigh distribution is given by:

$$f(x) = \frac{x}{\sigma^2} \cdot \exp\left\{-\left(\frac{x}{\sigma\sqrt{2}}\right)^2\right\} \qquad \text{(Rayleigh distribution)} \qquad (5.103)$$

in which x is the variable being studied and σ is its standard deviation.
With this Rayleigh distribution, the probability that the wave amplitude, ζ_a, exceeds a chosen threshold value, a, can be calculated using:

$$
\begin{aligned}
P\{\zeta_a > a\} &= \int_a^\infty f(x) \cdot dx \\
&= \frac{1}{\sigma^2}\int_a^\infty x \cdot \exp\left\{-\left(\frac{x}{\sigma\sqrt{2}}\right)^2\right\} \cdot dx \\
&= \exp\left\{-\frac{a^2}{2\sigma^2}\right\} \qquad\qquad (5.104)
\end{aligned}
$$

These probabilities for wave crest elevations can also be expressed in terms of the crest-to-trough wave heights H_w:

$$P\{H_w > H\} = \exp\left\{-2\left(\frac{H}{H_{1/3}}\right)^2\right\} \qquad (5.105)$$

in which $P\{H_w > H\}$ is the chance that any individual wave height H is exceeded in a wave field characterized by a significant wave height, $H_{1/3} = 4\sigma$.
The Rayleigh probability density function is illustrated in figure 5.30-a; figure 5.30-b shows the probability of exceeding in percentages, $P(H)$, in relation to the wave height ratio, $H/H_{1/3}$, on a logarithmic scale. Notice that all values in figures 5.30-a and 5.30-b are now positive. Indeed, if one chooses $H = 0$ in equation 5.105, then one finds that the probability that it is exceeded is exactly 1.
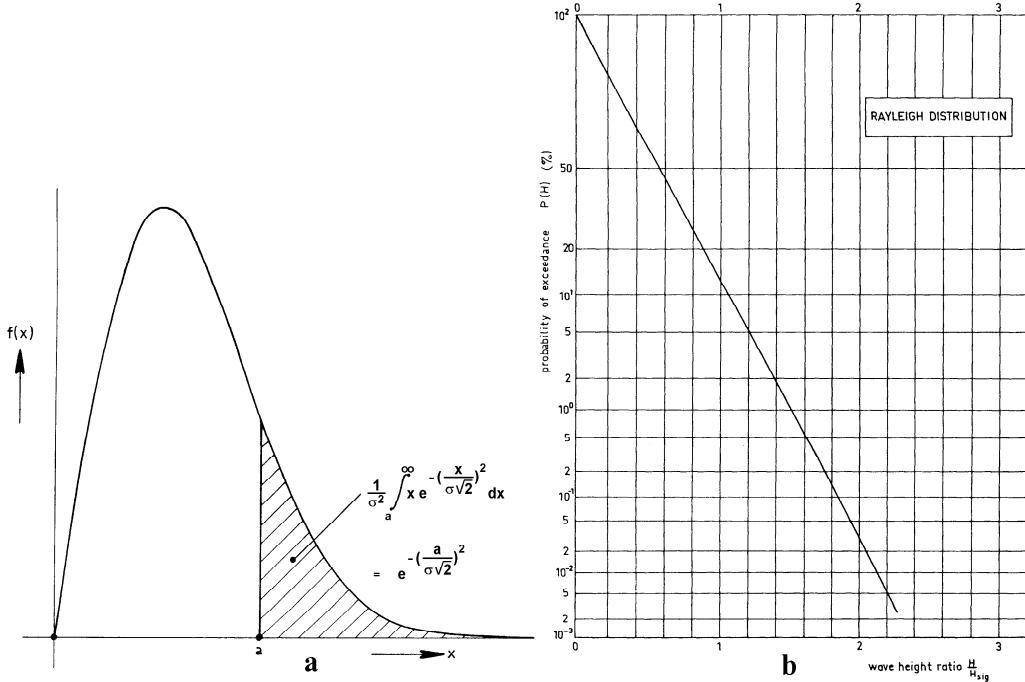
Figure 5.30: Rayleigh Probability Density Function

Maximum Wave Height

It is often desirable to make a statistically-based guess as to the highest wave that can be expected in a storm. One reasoning is to assume that the chance that this wave will be exceeded is zero and to put this value into equation 5.105 and then to solve for H. One must do this only once to find that $H = \infty$ - not too practical a result!

Instead of this, more pragmatic engineers often choose the wave height that will be exceeded (on the average) once in every 1000 (storm) waves as a maximum. This may seem arbitrary, (and it is!), but they reason that it will take at least 3 hours for 1000 waves to pass by and that by that time the worst peak of the storm will probably be past, anyway. This reasoning leads - with equation 5.105 - to a quick rule of thumb that:

$$\exp\left\{-2\left(\frac{H_{\max}}{H_{1/3}}\right)^2\right\} = \frac{1}{1000} \qquad \text{or:} \qquad \boxed{H_{\max} = 1.86 \cdot H_{1/3}} \qquad (5.106)$$

in which $H_{\max}$ is the maximum expected wave height in this 3 hours storm.

5.4 Wave Energy Spectra

Little attention has been given to wave periods so far. Periods are the reciprocal of frequency and become more apparent as a by-product of the wave frequency spectra to be discussed in this section.

5.4.1   Basic Principles

Since an irregular wave can be seen as the superposition of a series of sinusoidal waves, it is only logical to study the frequency characteristics of such an irregular signal using Fourier series analysis. To do this, one selects a time record segment containing many waves. Indeed, one assumption implicit in this analysis - see appendix C - is that the signal being studied repeats itself after each (long) interval. A wave record does not do this exactly, but that little detail is neglected in this case.

The wave elevation (in the time domain) of a long-crested irregular sea, propagating along the positive x axis, can be written as the sum of a large number of regular wave components (in the frequency domain):

$$\zeta(t) = \sum_{n=1}^{N} \zeta_{a_n} \cos(k_n x - \omega_n t + \varepsilon_n) \tag{5.107}$$

in which, for each component, n:

$$
\begin{array}{rcl}
\zeta_{a_n} & = & \text{wave amplitude component (m)} \\
\omega_n & = & \text{circular frequency component (rad/s)} \\
k_n & = & \text{wave number component (rad/m)} \\
\varepsilon_n & = & \text{random phase angle component (rad)}
\end{array}
$$

A Fourier series analysis carried out at one location would not indicate anything about k; this is location-dependent. This is not a problem in our case, since k_n and ω_n are related by the known dispersion relation already given earlier in this chapter.

The Fourier series will thus yield a set of values for ζ_{a_n} and ε_n , each associated with its own ω_n. If enough Fourier series terms are included, the entire time record at that point can be reproduced using this set of values. In practice, however, one is not really interested in the exact water level at some time t (which is already history!). It is sufficient to know only the statistical properties - now in terms of both frequency and amplitude - of the signal. This means that the ε_n can be discarded.

5.4.2   Energy Density Spectrum

Suppose a time history, as given in figure 5.28, of the wave elevation during a sufficient long but arbitrary period:

$$\tau = N \cdot \Delta t$$

The instantaneous wave elevation is supposed to has a Gaussian distribution and zero mean.

The amplitudes ζ_{a_n} can be obtained by a Fourier analysis of the signal. However, for each little time shift of the time history one will find a new series of amplitudes ζ_{a_n}. Luckily, a mean square value of ζ_{a_n} can be found: $\overline{\zeta_{a_n}^2}$.

When $\zeta(t)$ is an irregular signal without prevailing frequencies, the average values $\overline{\zeta_{a_n}^2}$ close to ω_n will not change much as a function of the frequency; $\overline{\zeta_a^2}$ is a continuous function.

The variance σ_ζ^2 of this signal equals:

$$
\begin{aligned}
\sigma_\zeta^2 &= \overline{\zeta^2} \\
&= \frac{1}{N}\sum_{n=1}^{N}\zeta_n^2 = \frac{1}{N\cdot\Delta t}\sum_{n=1}^{N}\zeta_n^2\cdot\Delta t \\
&= \frac{1}{\tau}\int_0^\tau \zeta^2(t)\cdot dt = \frac{1}{\tau}\int_0^\tau \left\{\sum_{n=1}^{N}\zeta_{a_n}\cos(\omega_n t - k_n x + \varepsilon_n)\right\}^2\cdot dt \\
&= \sum_{n=1}^{N}\frac{1}{2}\zeta_{a_n}^2
\end{aligned}
\tag{5.108}
$$

The wave amplitude ζ_{a_n} can be expressed in a wave spectrum $S_\zeta(\omega_n)$, which expression is defined by:

$$
\boxed{S_\zeta(\omega_n)\cdot\Delta\omega = \sum_{\omega_n}^{\omega_n+\Delta\omega}\frac{1}{2}\zeta_{a_n}^2(\omega)}
\tag{5.109}
$$

where $\Delta\omega$ is a constant difference between two successive frequencies. Multiplied with ρg, this expression is the energy per unit area of the waves (see equation 5.79) in the frequency interval $\Delta\omega$ see figure 5.31.
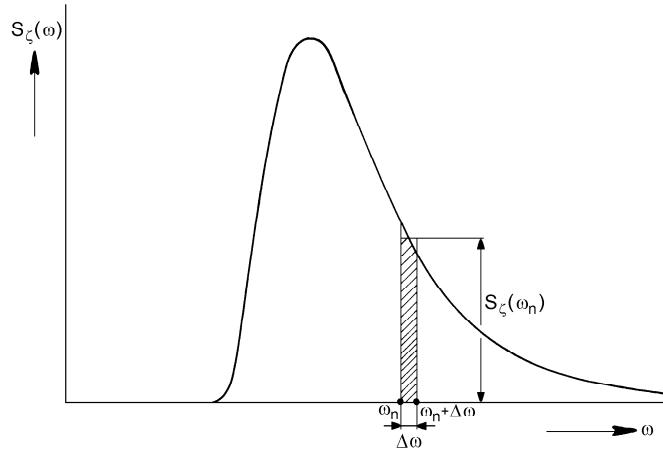
Figure 5.31: Definition of Spectral Density

Letting $\Delta\omega \to 0$, the **definition of the wave energy spectrum** $S_\zeta(\omega)$ becomes:

$$
\boxed{S_\zeta(\omega_n)\cdot d\omega = \frac{1}{2}\zeta_{a_n}^2}
\tag{5.110}
$$

and the variance σ_ζ^2 of the water surface elevation is simply equal to the area under the spectrum:

$$
\boxed{\sigma_\zeta^2 = \int_0^\infty S_\zeta(\omega)\cdot d\omega}
\tag{5.111}
$$

Figure 5.32 gives a graphical interpretation of the meaning of a wave spectrum and how it relates to the waves. The irregular wave history, $\zeta(t)$ in the time domain at the lower left hand part of the figure can be expressed via Fourier series analysis as the sum of a large number of regular wave components, each with its own frequency, amplitude and phase in the frequency domain. These phases will appear to be rather random, by the way. The value $\frac{1}{2}\zeta_a^2(\omega)/\Delta\omega$ - associated with each wave component on the ω-axis - is plotted vertically in the middle; this is the wave energy spectrum, $S_\zeta(\omega)$. This spectrum, $S_\zeta(\omega)$, can be described nicely in a formula; the phases cannot and are usually thrown away.
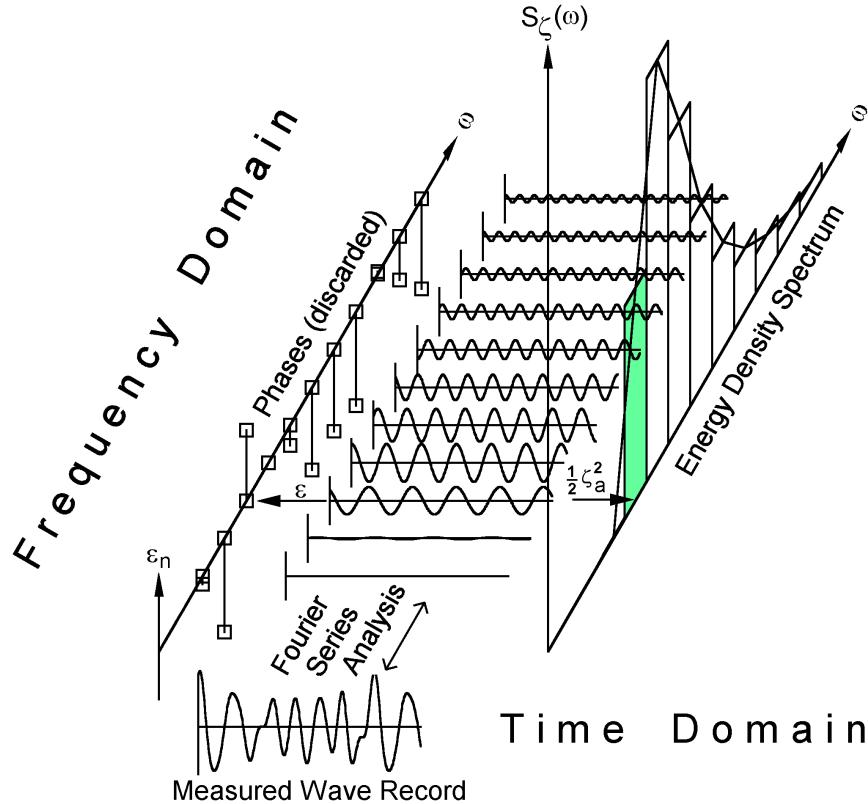
Figure 5.32: Wave Record Analysis

Spectrum Axis Transformation

When wave spectra are given as a function of frequency in Hertz ($f = 1/T$) instead of ω (in radians/second), they have to be transformed. The spectral value for the waves, $S_\zeta(\omega)$, based on ω, is not equal to the spectral value, $S_\zeta(f)$, based on f. Because of the requirement that an equal amount of energy must be contained in the corresponding frequency intervals $\Delta\omega$ and Δf, it follows that:

$$\boxed{S_\zeta(\omega) \cdot d\omega = S_\zeta(f) \cdot df} \qquad \text{or:} \qquad S_\zeta(\omega) = \frac{S_\zeta(f)}{\frac{d\omega}{df}} \qquad (5.112)$$

The relation between the frequencies is:

$$\omega = 2\pi \cdot f \qquad \text{or:} \qquad \frac{d\omega}{df} = 2\pi \qquad (5.113)$$
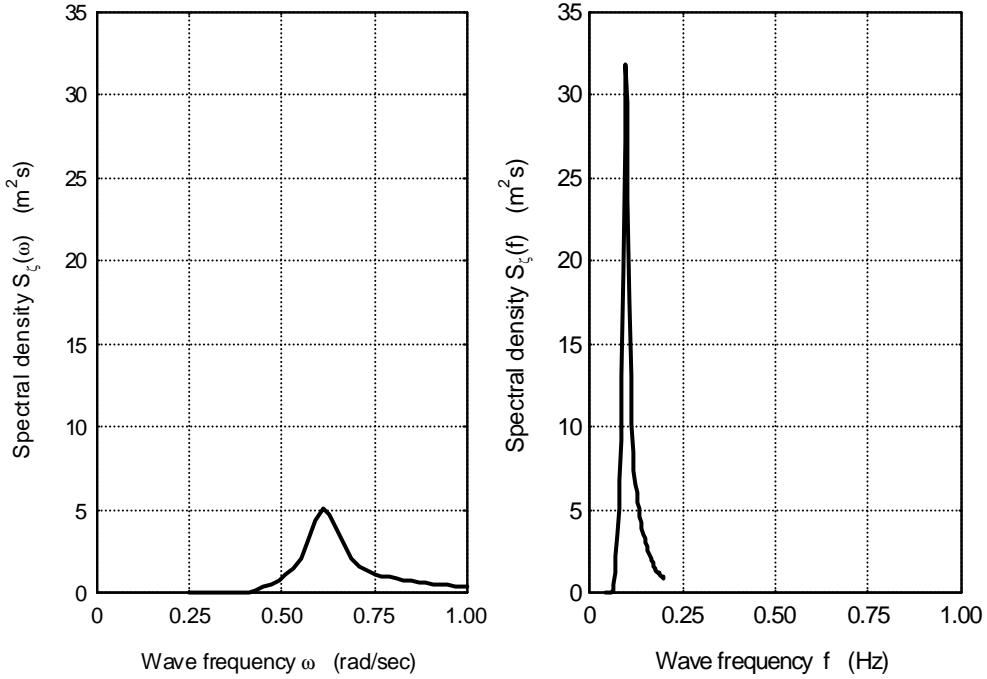
Figure 5.33: Wave Spectra on Two Different Bases

Then the wave spectrum on an ω-basis is:

$$S_\zeta(\omega) = \frac{S_\zeta(f)}{2\pi} \tag{5.114}$$

An example of a spectrum transformation is given in figure 5.33, in which it is obvious that the ratio between the corresponding frequencies is $1/(2\pi)$ while the ratio between the corresponding spectral values is 2π. The areas of both spectra (significant amplitudes) remain equal and the spectral moments provide equal average periods.

Wave Height and Period

Relationships with statistics can be found from computing the moments of the area under the spectrum with respect to the vertical axis at $\omega = 0$.

If m denotes a moment, then $m_{n\zeta}$ denotes the nth order moment given in this case by:

$$\boxed{m_{n\zeta} = \int_0^\infty \omega^n \cdot S_\zeta(\omega) \cdot d\omega} \tag{5.115}$$

This means that $m_{0\zeta}$ is the area under the spectral curve, $m_{1\zeta}$ is the first order moment (static moment) of this area and $m_{2\zeta}$ is the second order moment (moment of inertia) of this area.

As has already been indicated, $m_{0\zeta}$ is an indication of the variance squared, σ_ζ^2, of the water surface elevation. Of course this $m_{0\zeta}$ can also be related to the various wave amplitudes and heights:

$$\boxed{\sigma_\zeta = RMS = \sqrt{m_{0\zeta}}} \qquad \text{(Root Mean Square of the water surface elevation)}$$

$$\boxed{\zeta_{a_{1/3}} = 2 \cdot \sqrt{m_{0\zeta}}}$$ (significant wave amplitude)

$$\boxed{H_{1/3} = 4 \cdot \sqrt{m_{0\zeta}}}$$ (significant wave height)   (5.116)

Characteristic wave periods can be defined from the spectral moments:

$$
\begin{aligned}
m_{1\zeta} &= \omega_1 \cdot m_{0\zeta} & \text{with } \omega_1 \text{ is spectral centroid} \\
m_{2\zeta} &= \omega_2^2 \cdot m_{0\zeta} & \text{with } \omega_2 \text{ is spectral radius of inertia}
\end{aligned}
$$ (5.117)

as follows:

$$\boxed{T_1 = 2\pi \cdot \frac{m_{0\zeta}}{m_{1\zeta}}}$$ (mean centroid wave period)

$$\boxed{T_2 = 2\pi \cdot \sqrt{\frac{m_{0\zeta}}{m_{2\zeta}}}}$$ (mean zero-crossing wave period)   (5.118)

The mean zero-crossing period, T_2, is sometimes indicated by T_z. One will often find the period associated with the peak of the spectrum, T_p, in the literature as well.

Rayleigh Distribution

Expressed in terms of m_{0x}, the Rayleigh distribution of amplitudes x_a is given by:

$$\boxed{f(x) = \frac{x}{m_{0x}} \cdot \exp\left\{-\frac{x^2}{2 \cdot m_{0x}}\right\}}$$ (Rayleigh distribution)   (5.119)

in which x is the variable being studied and m_{0x} is the area under the spectral curve. With this distribution, the probability that the amplitude, x_a, exceeds a chosen threshold value, a, can be calculated using:

$$
\begin{aligned}
P\{x_a > a\} &= \int_a^\infty f(x) \cdot dx \\
&= \frac{1}{m_{0x}} \int_a^\infty x \cdot \exp\left\{-\frac{x^2}{2 \cdot m_{0x}}\right\} \cdot dx \\
&= \exp\left\{-\frac{a^2}{2 \cdot m_{0x}}\right\}
\end{aligned}
$$ (5.120)

It is obvious here that $\exp\{-u\}$ means e^{-u}.

As an example for waves, the probability that the wave height, H_w, in a certain sea state exceeds the significant wave height, $H_{1/3}$, is found by:

$$
\begin{aligned}
P\{H_w > H_{1/3}\} &= P\left\{\zeta_a > \zeta_{a_{1/3}}\right\} \\
&= \exp\left\{-\frac{\zeta_{a_{1/3}}^2}{2 \cdot m_{0\zeta}}\right\} \\
&= e^{-2} \approx 0.135 \approx \frac{1}{7}
\end{aligned}
$$ (5.121)

Wave Record Length

An important problem in the conduct of irregular wave measurements is the required total duration of the measured time histories to obtain proper spectral shapes and statistical values. This duration is presented by the total number of wave cycles, N.
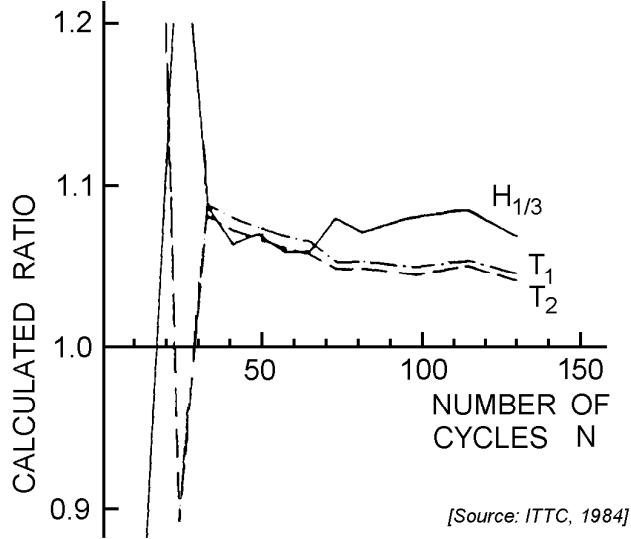
Figure 5.34: Effect of Wave Record Length

Figure 5.34 shows an example of the fluctuations in several characteristic values derived from calculated spectra based on records containing varying numbers of wave cycles. Using a wave record of a sea with a period $T_1 \approx 6$ s, calculations were carried out for various record lengths, expressed in a varied number of N cycles. The ratios of the calculated characteristics $H_{1/3}$, T_1 and T_2 for N cycles and those for a very large number of cycles are presented in the figure. It can be seen that these ratios become more or less constant for $N > 50$. This value can be considered as a rough standard for the absolute minimum required number of cycles. It can be seen from the figure that a much larger number is required to produce results approaching the base line, where this ratio becomes 1.0.

According to the 17$^{\text{th}}$ International Towing Tank Conference in 1984, $N = 50$ should be taken as a lower limit. Larger values are to be preferred and it is more usual to take $N = 100$ as the usual standard. A number $N = 200$ or above is considered excellent practice by the I.T.T.C. In practice, a record length equal to 100 times the largest expected single wave period in the irregular waves is often used as a safe standard. This means a wave record length of about 15 to 20 minutes.

As well as influencing the outcome of spectral analyses in the frequency domain, the number of wave cycles, N, also affects the validity of statistical quantities calculated in the time domain such as mean values, probability densities and distributions of extreme values.

5.4.3 Standard Wave Spectra

Just as for wave height statistics, investigators have attempted to describe a wave frequency spectrum in a standard form. Two important ones often found in the literature are described here. The mathematical formulations of these normalized uni-directional wave

energy spectra are based on two parameters: the significant wave height, $H_{1/3}$, and average wave periods $\overline{T}$, defined by T_1, T_2 or T_p:

$$\boxed{S_\zeta(\omega) = H_{1/3}^2 \cdot f\left(\omega, \overline{T}\right)} \tag{5.122}$$

Note that this definition means that the spectral values are proportional to the significant wave height squared; in other words $S_\zeta(\omega)/H_{1/3}^2$ is a function of ω and $\overline{T}$ only.

Bretschneider Wave Spectra

One of the oldest and most popular wave spectra was given by **Bretschneider.** It is especially suited for open sea areas. It is given mathematically by:

$$S_\zeta(\omega) = \frac{173 \cdot H_{1/3}^2}{T_1^4} \cdot \omega^{-5} \cdot \exp\left\{\frac{-692}{T_1^4} \cdot \omega^{-4}\right\} \tag{5.123}$$

For non-truncated mathematically defined spectra of this type, the theoretical relations between the characteristic periods are listed below:

$$T_1 \;=\; 1.086 \cdot T_2 \;=\; 0.772 \cdot T_p$$

$$0.921 \cdot T_1 \;=\; T_2 \;=\; 0.711 \cdot T_p$$

$$1.296 \cdot T_1 \;=\; 1.407 \cdot T_2 \;=\; T_p \tag{5.124}$$

Another name of this wave spectrum is **Modified Two-Parameter Pierson-Moskowitz Wave Spectrum**. This formulation was accepted by the 2nd International Ship Structures Congress in 1967 and the 12th International Towing Tank Conference in 1969 as a standard for seakeeping calculations and model experiments. This is reason why this spectrum is also called the **ISSC Wave Spectrum** or the **ITTC Wave Spectrum**.

The original **One-Parameter Pierson-Moskowitz Wave Spectrum** for fully developed seas can be obtained by using a fixed relation between the significant wave height and the average wave period in the Bretschneider definition:

$$T_1 = 3.86 \cdot \sqrt{H_{1/3}} \quad \text{and} \quad T_2 = 3.56 \cdot \sqrt{H_{1/3}} \tag{5.125}$$

In reality a measured spectral form differs from theoretical formulations which give only a mean distribution. Figure 5.35 shows a comparison between a measured wave spectrum and the corresponding Bretschneider (Pierson-Moskowitz) wave spectrum during a storm in the Atlantic Ocean on 4 February 1979.

JONSWAP Wave Spectra

In 1968 and 1969 an extensive wave measurement program, known as the Joint North Sea Wave Project (JONSWAP) was carried out along a line extending over 100 miles into the North Sea from Sylt Island. Analysis of the data - in which the TU Delft participated - yielded a spectral formulation for fetch-limited (or coastal) wind generated seas.

The following definition of a **Mean JONSWAP** wave spectrum is advised by the 17th ITTC in 1984 for fetch limited situations:

$$S_\zeta(\omega) = \frac{320 \cdot H_{1/3}^2}{T_p^4} \cdot \omega^{-5} \cdot \exp\left\{\frac{-1950}{T_p^4} \cdot \omega^{-4}\right\} \cdot \gamma^A \tag{5.126}$$
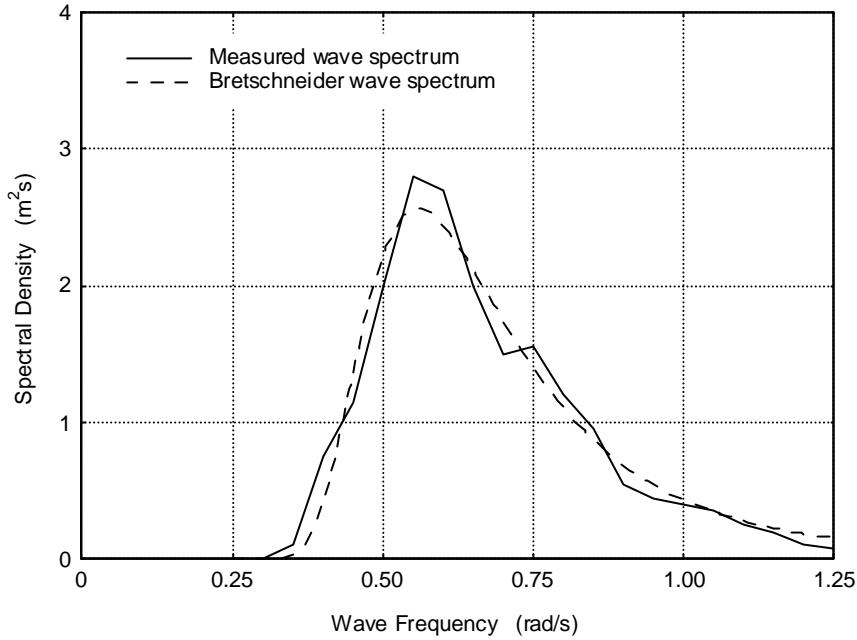
Figure 5.35: Comparison of a Measured and a Normalised Wave Spectrum

with:

$$\gamma = 3.3 \quad \text{(peakedness factor)}$$

$$A = \exp\left\{-\left(\frac{\frac{\omega}{\omega_p}-1}{\sigma\sqrt{2}}\right)^2\right\}$$

$$\omega_p = \frac{2\pi}{T_p} \quad \text{(circular frequency at spectral peak)}$$

$$\sigma = \text{a step function of } \omega: \text{ if } \omega < \omega_p \text{ then: } \sigma = 0.07$$
$$\text{if } \omega > \omega_p \text{ then: } \sigma = 0.09$$

Taking $\gamma^A = 1.522$ results in the formulation of the Bretschneider wave spectrum with the peak period T_p.

For non-truncated mathematically defined JONSWAP spectra, the theoretical relations between the characteristic periods are listed below:

$$T_1 = 1.073 \cdot T_2 = 0.834 \cdot T_p$$

$$0.932 \cdot T_1 = T_2 = 0.777 \cdot T_p$$

$$1.199 \cdot T_1 = 1.287 \cdot T_2 = T_p \tag{5.127}$$

Sometimes, a third free parameter is introduced in the JONSWAP wave spectrum by varying the peakedness factor γ.

Wave Spectra Comparison

Figure 5.36 compares the Bretschneider and mean JONSWAP wave spectra for three sea states with a significant wave height, $H_{1/3}$, of 4 meters and peak periods, T_p, of 6, 8 and

10 seconds, respectively.
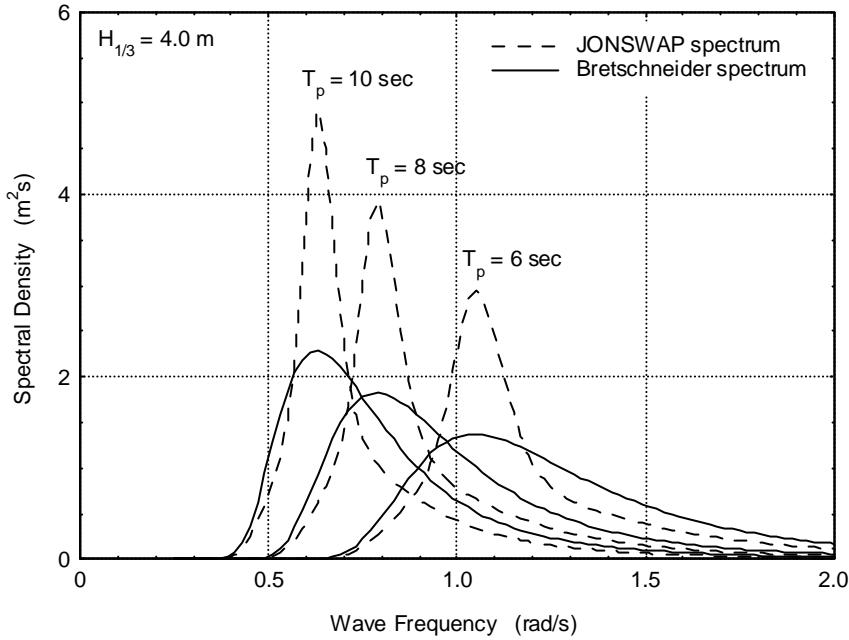
Figure 5.36: Comparison of Two Spectral Formulations

The figure shows the more pronounced peak of the JONSWAP spectrum.

Directional Spreading

A cosine-squared rule is often used to introduce directional spreading to the wave energy. When this is done, the unidirectional wave energy found in the previous sections is scaled as in the following formula:

$$S_\zeta(\omega, \mu) = \left\{ \frac{2}{\pi} \cdot \cos^2\left(\mu - \overline{\mu}\right) \right\} \cdot S_\zeta(\omega) \tag{5.128}$$

with:

$$-\frac{\pi}{2} \leq \left(\mu - \overline{\mu}\right) \leq +\frac{\pi}{2}$$

in which $\overline{\mu}$ is the dominant wave direction. A comparison of a measured wave directionality with this directional spreading is given in figure 5.37.

Because the directionality function in this theory is a scalar, the form of the spectrum along each direction is the same; only its intensity varies as a function of direction. At sea, this distribution depends on the local weather situation at that moment (for the wind waves or sea) as well as on the weather in the whole ocean in the recent past (for any swell component). Deviations from the theoretical distribution will certainly appear when, for instance, when sea and swell travel in quite different directions.

5.4.4   Transformation to Time Series

Especially when solving non-linear problems - such as in chapters 9 or 12, for example - one often needs a deterministic time record of water levels which has the statistical properties
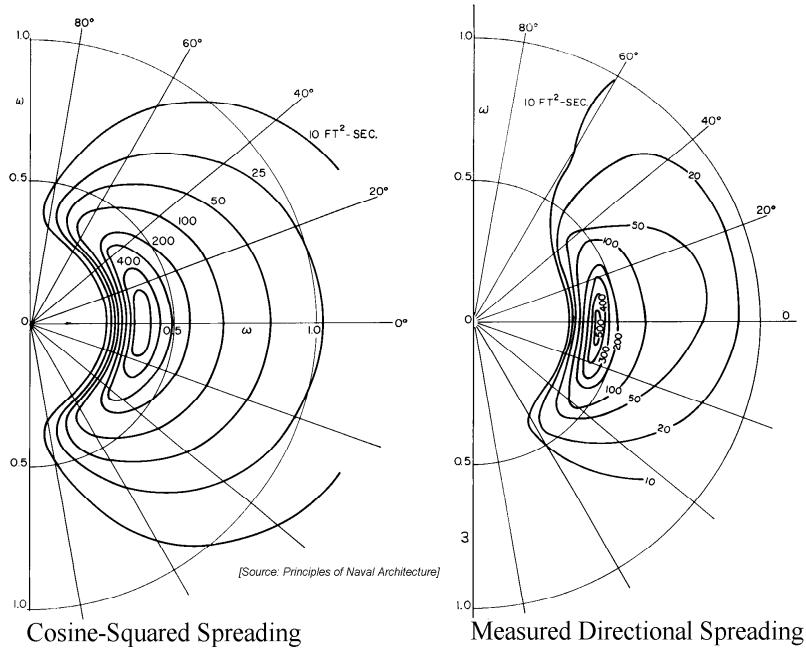
Figure 5.37: Wave Spectra with Directional Spreading

one would associate with a known spectrum. This is often referred to as the **inverse problem** in wave statistics. (It is at moments such as this that one is sorry that the phase information from the Fourier series analysis - which yielded the spectrum in the first place - has been thrown away.)

Luckily, there is no real need to reproduce the input time record exactly; what is needed is a record which is only **statistically indistinguishable** from the original signal. This means that it must have the same energy density spectrum as the original. This is done by filling in all the necessary constants in equation 5.107 which is repeated here for convenience.

$$\zeta(t) = \sum_{n=1}^{N} \zeta_{a_n} \cos(k_n x - \omega_n t + \varepsilon_n)$$

The desired output - whether it is the water surface elevation as in this equation or anything else such as the horizontal component of the water particle velocity 17 meters below the sea surface - depends upon three variables for each chosen frequency component, ω_n: k_n, ε_n and an amplitude such as ζ_{a_n}.

Successive ω_n values are generally chosen at equally spaced intervals $\Delta\omega$ along the frequency axis of the given spectrum. Note that with a constant frequency interval, $\Delta\omega$, this time history repeats itself after $2\pi/\Delta\omega$ seconds.

The amplitudes, ζ_{a_n}, can be determined knowing that the area under the associated segment of the spectrum, $S_\zeta(\omega) \cdot \Delta\omega$ is equal to the variance of the wave component. Equation 5.109 is adapted a bit for this so that:

$$\boxed{\zeta_{a_n} = 2\sqrt{S_\zeta(\omega) \cdot \Delta\omega}} \tag{5.129}$$

The wave numbers, k_n, can be computed from the chosen frequency ω_n using a dispersion relationship.

When obtaining the wave spectrum $S_\zeta(\omega)$ from the irregular wave history, the phase angles ε_n have been thrown away. New ε_n-values must be selected from a set of uniformly distributed random numbers in the range $0 \leq \varepsilon_n < 2\pi$. While ε_n is needed to generate the time record - and they may not all be set equal to zero!- the exact (randomly selected) ε_n do not influence the record's statistics. Looked at another way: By choosing a new random set of ε_n values, one can generate a new, statistically identical but in detail different time record.

This procedure is illustrated by extending figure 5.32 as shown below in figure 5.38. Note that the original (on the left in the figure) and the newly obtained wave history (on the right hand part of the figure) differ because different phase angles have been used. However, they contain an equal amount of energy and are statistically identical.
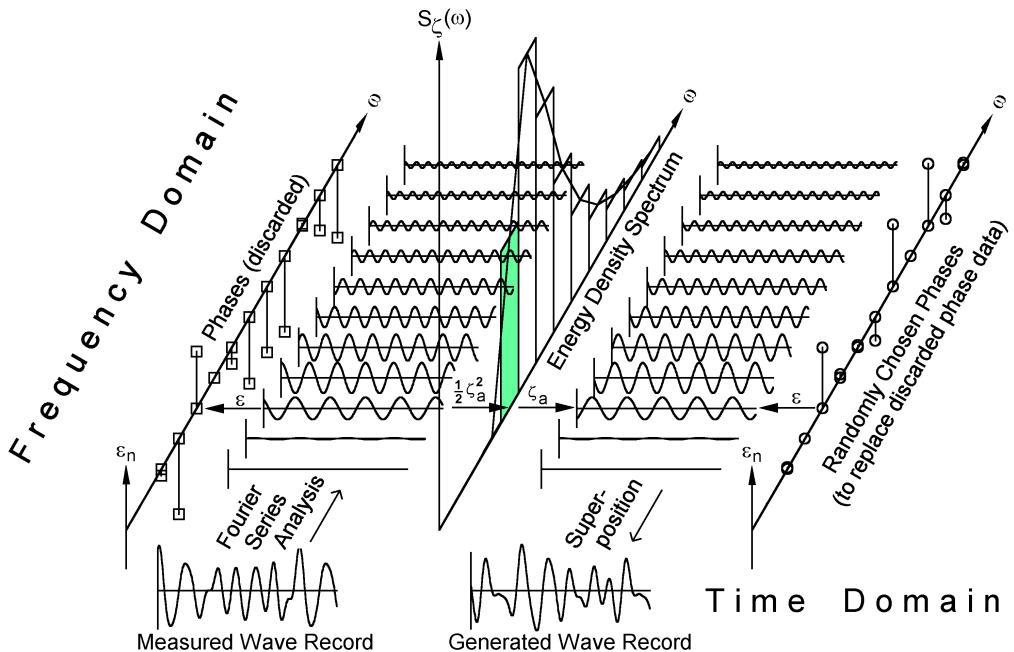
Figure 5.38: Wave Record Analysis and Regeneration

Directional spreading can be introduced as well by breaking each frequency component up into a number of directional components. One should not underestimate the (extra) computational effort however.

5.5   Wave Prediction and Climatology

In 1805, the British Admiral Sir Francis Beaufort devised an observation scale for measuring winds at sea. His scale measures winds by observing their effects on sailing ships and waves. Beaufort's scale was later adapted for use on land and is still used today by many weather stations. A definition of this Beaufort wind force scale is given in figure 5.39.

The pictures in figure 5.40 give a visual impression of the sea states in relation to Beaufort's scale. Storm warnings are usually issued for winds stronger than Beaufort force 6.

BEAUFORT WIND FORCE SCALE

Beaufort Number	Dutch KNMI description	U.S. Weather Service description	Racing Sailor's description (C.A. Marchay, 1964)	Beaufort description for square rigged ships 1806	Wind Press. N/m²		km per hr.	meters per sec.	miles per hr. (U.S. Statute)	Knots
0	Windstil	Calm					0	0	0	0
										1
1	zwakke	Light air	Boredom	Just Steerage Way	0.14	1.4	2	0.5	1	1
								1.5	3	3
2		Light breeze	Mild pleasure	1-3 knots close hauled	2.4	5.7	7	2.1	4	4
								3.1	7	6
3	matige	Gentle breeze	Pleasure	4-5 knots close hauled	7.7	16	13	3.6	8	7
								5.1	12	10
4		Moderate breeze	Great Pleasure	6-7 knots close hauled	19	41	20	5.7	13	11
								8	18	16
5	vrij krach- tige	Fresh breeze	Delight	Hull Speed Full Sail	46	67	32	9	19	17
								11	24	21
6	krachtige	Strong breeze	Delight tinged with anxiety		77	115	41	11	25	22
								14	31	27
7	harde	Moderate Gale	Anxiety tinged with fear		125	172	52	14	32	28
								17	38	33
8	stormach- tige	Gale	Fear tinged with terror		182	250	63	18	39	34
								21	46	40
9	storm	Strong Gale	Great terror		270	350	76	21	47	41
								24	54	47
10	zware storm	Whole Gale	Panic		360	480	89	25	55	48
								28	63	55
11	zeer zware storm	Storm	I want my mummy!!		500	630	104	29	64	56
								33	75	63
12	orkaan	Hurricane	Yes, Mr. Jones	above 630 bare poles	above 630		above 120	above 33	above 75	above 63

WIND SPEEDS

Beau- fort Number
0
1
2
3
4
5
6
7
8
9
10
11
12

Figure 5.39: Beaufort's Wind Force Scale
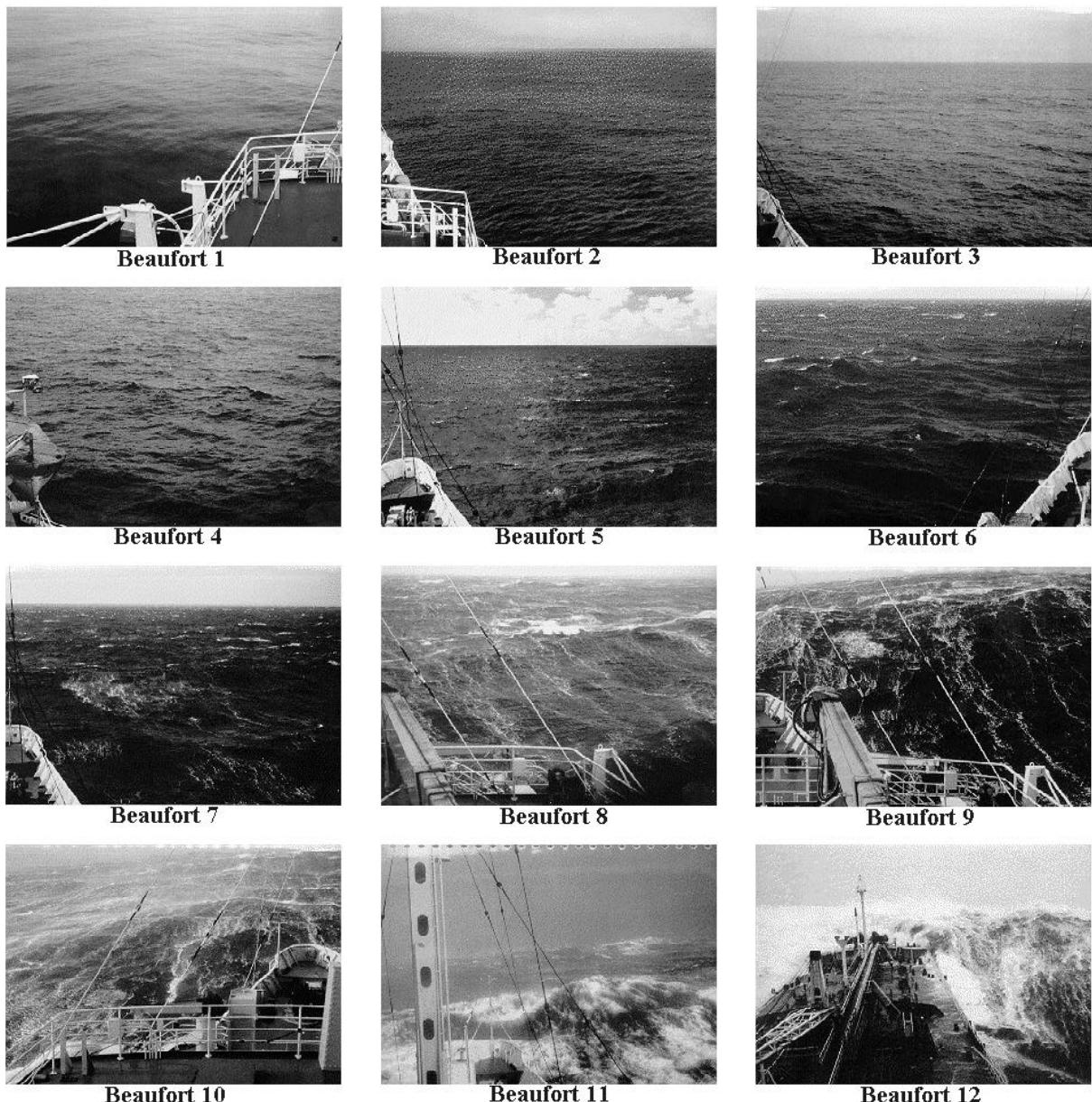
Figure 5.40: Sea State in Relation to Beaufort Wind Force Scale

5.5.1   Single Storm

The previous sections have shown that an entire storm can be characterized by just two numbers: one related to the wave period and one to the wave height. It now becomes important to predict these values from other data - such as geographical and meteorological information.

Wave Prediction

In general, prediction models are based upon the following parameters:

- **wind speed**,
- distance over which the waves have travelled under that wind field, called **fetch** and
- **duration** of the wind speed.

Coastal engineers often add fourth parameter: the water depth. This is less important for offshore engineering applications and will not be included here. Figure 5.41 shows the relevant parameter relations for deep water.
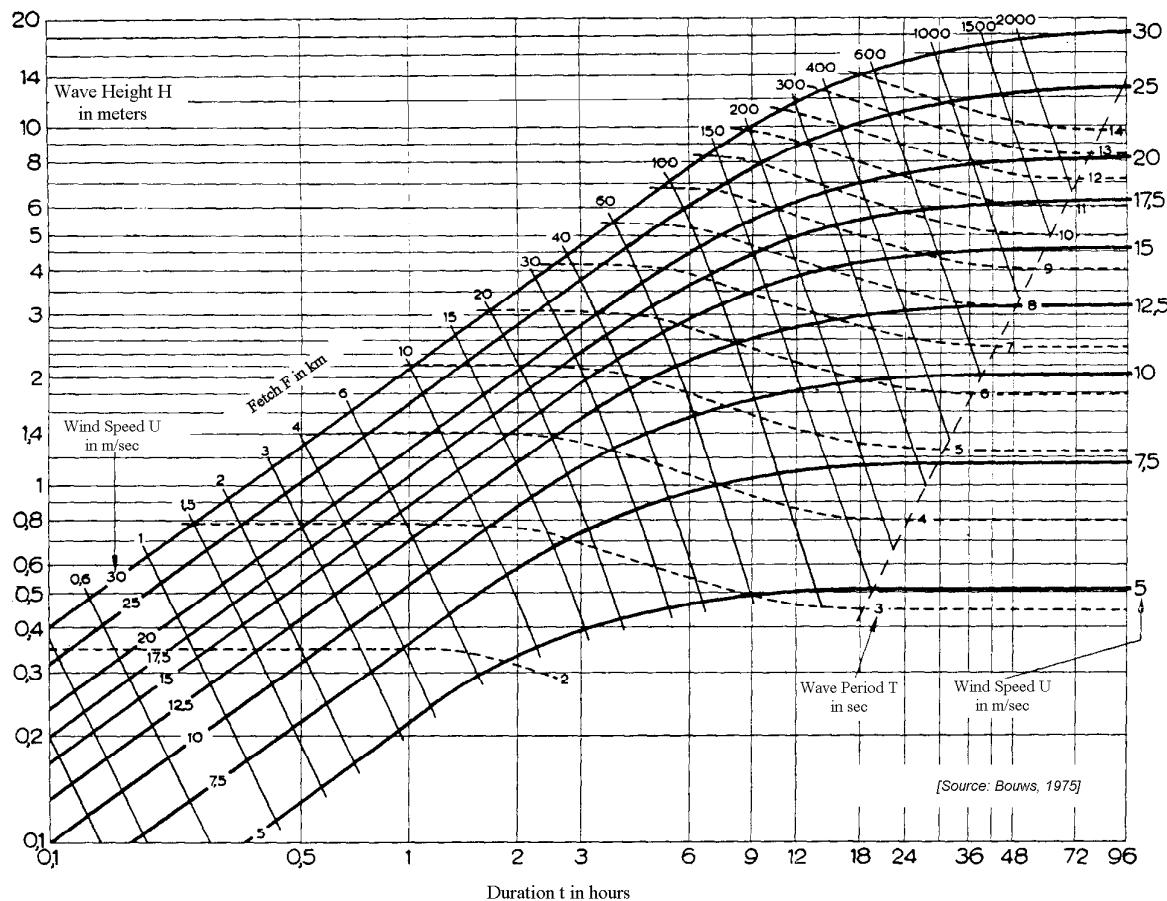
Figure 5.41: Parameter Relations of a Fetch-Limited Fully Developed Sea

Significant wave heights (m) are to be read off along the logarithmic scale on the left. One can enter the diagram with a wind speed (m/s) along the vertical axis on the right and the fetch (km) chosen from the values written along the upper curve.
One then reads off three remaining items:

- **Wave Height** H in meters, on the left of the figure,

- **Duration** t **in** hours, needed to generate the wave under the chosen conditions on the bottom of the figure and

- **Wave Period** T in seconds, by interpolating between the dashed lines.

Most oceanographers consider a fully developed sea to be one in which - for a given wind speed - the remaining wave conditions (height and period) are no longer influenced by either the storm duration or fetch length and thus one's location. Even if one were to travel around the globe with the constant wind field, one would find that the wave height no longer increased. Fully developed sea conditions are represented in this figure by the triangular area on the right in which the wave height (for a given wind speed) is indeed independent of the duration or the fetch.

Suppose, as an exercise with figure 5.41, a wind speed of 10 m/sec (Beaufort force 5).
With a fetch of 60 km, the sea no longer increases after 6 hours. This sea is defined by a significant wave height of 1.5 meters with an average wave period of 4.8 seconds.
With a fetch of 600 km, the sea no longer increases after 40 hours. This sea is defined by a significant wave height of 2.0 meters with an average wave period of 6.4 seconds.
Notice that, if one were to wait longer at a given location than the time duration found in this figure, the wave height would not increase further even though the waves are not oceanographically fully developed; they are limited in this case by the fetch.

Storm Wave Data

The table below, for "Open Ocean Areas" and "North Sea Areas" gives **an indication** of an average relationship between the Beaufort wind scale (or the associated average wind velocity) at 19.5 meters above the sea and the significant wave height $H_{1/3}$ and the average wave periods T_1 and T_2, defined before. These data have been plotted in figure 5.42.

Wave Spectrum Parameter Estimates								
Scale of Beaufort	Wind Speed at 19.5 m above sea	Open Ocean Areas (Bretschneider)			North Sea Areas (JONSWAP)			
	(kn)	$H_{1/3}$ (m)	T_1 (s)	T_2 (s)	$H_{1/3}$ (m)	T_1 (s)	T_2 (s)	γ $(-)$
1	2.0	1.10	5.80	5.35	0.50	3.50	3.25	3.3
2	5.0	1.20	5.90	5.45	0.65	3.80	3.55	3.3
3	8.5	1.40	6.00	5.55	0.80	4.20	3.90	3.3
4	13.5	1.70	6.10	5.60	1.10	4.60	4.30	3.3
5	19.0	2.15	6.50	6.00	1.65	5.10	4.75	3.3
6	24.5	2.90	7.20	6.65	2.50	5.70	5.30	3.3
7	30.5	3.75	7.80	7.20	3.60	6.70	6.25	3.3
8	37.0	4.90	8.40	7.75	4.85	7.90	7.35	3.3
9	44.0	6.10	9.00	8.30	6.10	8.80	8.20	3.3
10	51.5	7.45	9.60	8.80	7.45	9.50	8.85	3.3
11	59.5	8.70	10.10	9.30	8.70	10.00	9.30	3.3
12	>64.0	10.25	10.50	9.65	10.25	10.50	9.80	3.3
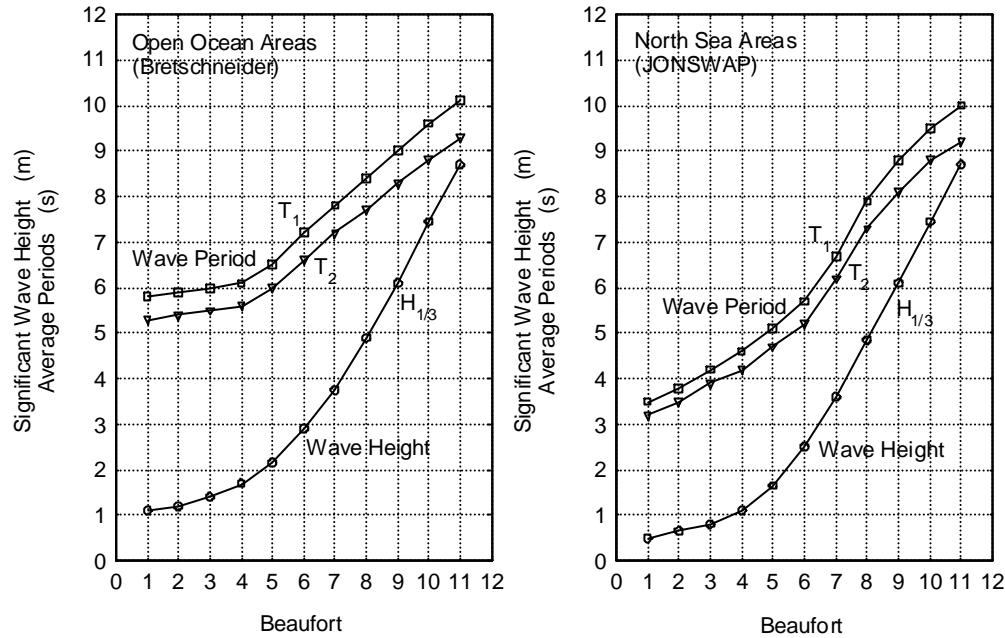
Figure 5.42: Wave Spectrum Parameter Estimates

This table and figure 5.42 show lower and shorter waves in North Sea Areas, when compared at the same wind strength (Beaufort number) with those in Open Ocean Areas.

Other open ocean definitions for the North Atlantic and the North Pacific, obtained from [Bales, 1983] and adopted by the 17th ITTC (1984) as a reliable relationship for these areas, are given in the table below. The modal or central periods in this table correspond with the peak period, T_p, as defined before.

Open Ocean Annual Sea State Occurrences from Bales (1983) for the North Atlantic and the North Pacific							
Sea State Number ($-$)	Significant Wave Height $H_{1/3}$ (m)		Sustained Wind Speed 1) (kn)		Probability of Sea State (%)	Modal Wave Period T_p (s)	
	Range	Mean	Range	Mean		Range 2)	Most 3) Probable
North Atlantic							
0 - 1	0.0 - 0.1	0.05	0 - 6	3	0	-	-
2	0.1 - 0.5	0.3	7 - 10	8.5	7.2	3.3 - 12.8	7.5
3	0.50 - 1.25	0.88	11 - 16	13.5	22.4	5.0 - 14.8	7.5
4	1.25 - 2.50	1.88	17 - 21	19	28.7	6.1 - 15.2	8.8
5	2.5 - 4.0	3.25	22 - 27	24.5	15.5	8.3 - 15.5	9.7
6	4 - 6	5.0	28 - 47	37.5	18.7	9.8 - 16.2	12.4
7	6 - 9	7.5	48 - 55	51.5	6.1	11.8 - 18.5	15.0
8	9 - 14	11.5	56 - 63	59.5	1.2	14.2 - 18.6	16.4
>8	>14	>14	>63	>63	<0.05	18.0 - 23.7	20.0
North Pacific							
0 - 1	0.0 - 0.1	0.05	0 - 6	3	0	-	-
2	0.1 - 0.5	0.3	7 - 10	8.5	4.1	3.0 - 15.0	7.5
3	0.50 - 1.25	0.88	11 - 16	13.5	16.9	5.2 - 15.5	7.5
4	1.25 - 2.50	1.88	17 - 21	19	27.8	5.9 - 15.5	8.8
5	2.5 - 4.0	3.25	22 - 27	24.5	23.5	7.2 - 16.5	9.7
6	4 - 6	5.0	28 - 47	37.5	16.3	9.3 - 16.5	13.8
7	6 - 9	7.5	48 - 55	51.5	9.1	10.0 - 17.2	15.8
8	9 - 14	11.5	56 - 63	59.5	2.2	13.0 - 18.4	18.0
>8	>14	>14	>63	>63	0.1	20.0	20.0

Note:

1) Ambient wind sustained at 19.5 m above surface to generate fully-developed seas. To convert to another altitude h_2, apply $V_2 = V_1 \cdot (h_2/19.5)^{1/7}$.

2) Minimum is 5 percentile and maximum is 95 percentile for periods given wave height range.

3) Based on periods associated with central frequencies included in Hindcast Climatology.

The above tables for the North Atlantic and North Pacific Oceans also include information on the long term climatology of the waves. This will be discussed in the next section.

Notice that all the methods in this section actually link wave data to wind data. This is quite common since wind data is often much more available than wave data or can be predicted rather easily from other available meteorological data.

5.5.2 Long Term

Longer term wave climatology is used to predict the statistical chance that a given wave-sensitive offshore operation - such as lifting a major top-side element into place - will be delayed by sea conditions which are too rough. Chapter 11 will be devoted entirely to various applications of this general topic in a broad sense. The current section treats the necessary input data on wave climate.

In general, wave climatology often centers on answering one question: What is the chance that some chosen threshold wave condition will be exceeded during some interval - usually days, weeks or even a year? To determine this, one must collect - or obtain in some other way such as outlined in the previous section - and analyze the pairs of data ($H_{1/3}$ and $\overline{T}$) and possibly even including the wave direction, μ, as well) representing each 'storm' period.

Wave Scatter Diagram

Sets of characteristic wave data values can be grouped and arranged in a table such as that given below based upon data from the northern North Sea. A 'storm' here is an arbitrary time period - often of 3 or 6 hours - for which a single pair of values has been collected.

The number in each cell of this table indicates the chance (on the basis of 1000 observations in this case) that a significant wave height (in meters) is between the values in the left column and in the range of wave periods listed at the top and bottom of the table. Figure 5.43 shows a graph of this table.

↓ H_{sig} (m)	4-5	5-6	6-7	7-8	8-9	9-10	10-11	11-12	12-13	13-14	$\sum_{row}$
>12								0+			
11,5-12,0					0+						1
11,0-11,5											
10,5-11,0											
10,0-10,5											
9,5-10,0					0+		1		0+		2
9,0-9,5						0+		0+			1
8,5-9,0					1	1	1	1			4
8,0-8,5						1	1	0+			2
7,5-8,0				0+	1	3	1	1			6
7,0-7,5				1	2	3		1			7
6,5-7,0				1	5	3	1	0+			10
6,0-6,5				4	7	4	1	1	0+		17
5,5-6,0			2	5	7	3	2				19
5,0-5,5			4	10	9	3	1	1	0+		28
4,5-5,0		1	11	18	3	1	1	0+	0+		36
4,0-4,5		3	24	15	12	3	2	1			60
3,5-4,0		8	29	20	9	4	1	1			72
3,0-3,5	1	21	36	21	12	6	1				98
2,5-3,0	2	37	37	22	7	2	1	1			109
2,0-2,5		14	52	53	21	8	4	1			153
1,5-2,0	1	28	49	36	21	13	6	1	1		156
1,0-1,5	6	34	42	38	19	13	5	1	0+		158
0,5-1,0	1	8	15	16	11	5	1	1	0+		58
0,0-0,5		1	0+		0+						2
Periods→	4-5	5-6	6-7	7-8	8-9	9-10	10-11	11-12	12-13	calm:	1
										Total:	1000

Wave Climate Scatter Diagram for Northern North Sea

Note: 0+ in this table indicates that less than 0.5 observation in 1000 was recorded for the given cell.

This scatter diagram includes a good distinction between **sea** and **swell**. As has already been explained early in this chapter, swell tends to be low and to have a relatively long period. The cluster of values for wave heights below 2 meters with periods greater than 10 seconds is typically swell in this case.

A second example of a wave scatter diagram is the table below for all wave directions in the winter season in areas 8, 9, 15 and 16 of the North Atlantic Ocean, as obtained from Global Wave Statistics.

Winter Data of Areas 8, 9, 15 and 16 of the North Atlantic (Global Wave Statistics)											
	T_2 (s)										
H_s (m)	3.5	4.5	5.5	6.5	7.5	8.5	9.5	10.5	11.5	12.5	13.5	Total
14.5	0	0	0	0	2	30	154	362	466	370	202	1586
13.5	0	0	0	0	3	33	145	293	322	219	101	1116
12.5	0	0	0	0	7	72	289	539	548	345	149	1949
11.5	0	0	0	0	17	160	585	996	931	543	217	3449
10.5	0	0	0	1	41	363	1200	1852	1579	843	310	6189
9.5	0	0	0	4	109	845	2485	3443	2648	1283	432	11249
8.5	0	0	0	12	295	1996	5157	6323	4333	1882	572	20570
7.5	0	0	0	41	818	4723	10537	11242	6755	2594	703	37413
6.5	0	0	1	138	2273	10967	20620	18718	9665	3222	767	66371
5.5	0	0	7	471	6187	24075	36940	27702	11969	3387	694	111432
4.5	0	0	31	1586	15757	47072	56347	33539	11710	2731	471	169244
3.5	0	0	148	5017	34720	74007	64809	28964	7804	1444	202	217115
2.5	0	4	681	13441	56847	77259	45013	13962	2725	381	41	210354
1.5	0	40	2699	23284	47839	34532	11554	2208	282	27	2	122467
0.5	5	350	3314	8131	5858	1598	216	18	1	0	0	19491
Total	5	394	6881	52126	170773	277732	256051	150161	61738	19271	4863	999995

These wave scatter diagrams can be used to determine the long term probability for storms exceeding certain sea states. Each cell in this table presents the probability of occurrence of its significant wave height and zero-crossing wave period range. This probability is equal to the number in this cell divided by the sum of the numbers of all cells in the table, for instance:

$$\Pr\left\{4 < H_{1/3} < 5 \text{ and } 8 < T_2 < 9\right\} = \frac{47072}{999996} = 0.047 = 4.7\%$$

For instance, the probabilty on a storm with a significant wave height between 4 and 6 meters with a zero-crossing period between 8 and 10 seconds is:

$$\Pr\left\{3 < H_{1/3} < 5 \text{ and } 8 < T_2 < 10\right\} = \frac{47072 + 56347 + 74007 + 64809}{999996} = 0.242 = 24.2\%$$

The probabilty for storms exceeding a certain significant wave height is found by adding the numbers of all cells with a significant wave height larger than this certain significant wave height and dividing this number by the sum of the numbers in all cells, for instance:

$$\Pr\left\{H_{1/3} > 10\right\} = \frac{6189 + 3449 + 1949 + 1116 + 1586}{999996} = 0.014 = 1.4\%$$

Note that the above scatter diagram is based exclusively on winter data. Such diagrams are often available on a monthly, seasonal or year basis. The data in these can be quite different; think of an area in which there is a very pronounced hurricane season, for example. Statistically, the North Sea is roughest in the winter and smoothest in summer.

5.5.3 Statistics

Just as with waves in an individual storm, one often wants to estimate the storm intensity (wave characteristics in this case) that one should associate with some chosen and very low chance of exceedance. To do this one will usually have to extrapolate the wave data collected as in the scatter diagrams above. Two statistical distribution can be used to do this; they are described individually here.

Semi-Logarithmic Distribution

It has been found empirically that storm data - such as that presented in the wave scatter diagram for the North Sea, above, behave quite nicely if the wave height is plotted versus the logarithm of the chance of exceedance. The processing of the data in that scatter diagram is very analogous to that for waves in a single storm given much earlier in this chapter.

The plot resulting from the North Sea is given in figure 5.43. The graph is pretty much a straight line for lower probabilities, that would be needed to predict extreme events by linear extrapolation. Obviously this segment of the graph can be extrapolated to whatever lower probability one wishes to choose. This can be done using the formula:

$$\log\left\{(P(H)\right\} = \frac{1}{a}H$$

in which a is related to the slope of the curve; see figure 5.43.

Figure 5.43: Logarthmic Distribution of Data from Northern North Sea

Weibull Distribution

A generalization of the exponential distribution given above - the Weibull distribution - is often used, too. In equation form:
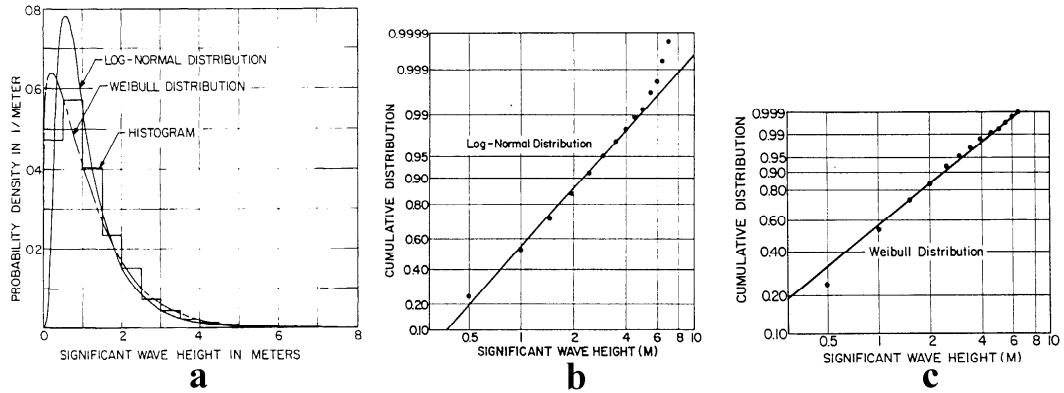
Figure 5.44: Histogram and Log-Normal and Weibull Distributions

$$P(H) = \exp\left\{ -\left(\frac{H-c}{a}\right)^{b} \right\} \qquad (5.130)$$

in which a is a scaling parameter (m), b is a fitting parameter (-) and c is a lower bound for H (m).

Figure 5.44-a shows a histogram of wave heights. A log-normal and a Weibull fit to these data are shown in figures 5.44-b and 5.44-c.

In many cases the value of b in the Weibull equation above is close to 1. If - as is usually the case with waves - $c = 0$ and b is exactly 1, then the Weibull distribution reduces to the log-normal distribution given earlier.

Chapter 6

RIGID BODY DYNAMICS

6.1 Introduction

The dynamics of rigid bodies and fluid motions are governed by the combined actions of different external forces and moments as well as by the inertia of the bodies themselves. In fluid dynamics these forces and moments can no longer be considered as acting at a single point or at discrete points of the system. Instead, they must be regarded as distributed in a relatively smooth or a continuous manner throughout the mass of the fluid particles. The force and moment distributions and the kinematic description of the fluid motions are in fact continuous, assuming that the collection of discrete fluid molecules can be analyzed as a continuum.

Typically, one can anticipate force mechanisms associated with the fluid inertia, its weight, viscous stresses and secondary effects such as surface tension. In general three principal force mechanisms (inertia, gravity and viscous) exist, which can be of comparable importance. With very few exceptions, it is not possible to analyze such complicated situations exactly - either theoretically or experimentally. It is often impossible to include all force mechanisms simultaneously in a (mathematical) model. They can be treated in pairs as has been done when defining dimensionless numbers - see chapter 4 and appendix B. In order to determine which pair of forces dominate, it is useful first to estimate the orders of magnitude of the inertia, the gravity and the viscous forces and moments, separately. Depending on the problem, viscous effects can often be ignored; this simplifies the problem considerably.

This chapter discusses the hydromechanics of a simple rigid body; mainly the attention focuses on the motions of a simple floating vertical cylinder. The purpose of this chapter is to present much of the theory of ship motions while avoiding many of the purely hydrodynamic complications; these are left for later chapters.

6.2 Ship Definitions

When on board a ship looking toward the **bow** (front end) one is looking **forward**. The **stern** is **aft** at the other end of the ship. As one looks forward, the **starboard** side is one's right and the **port** side is to one's left.

6.2.1   Axis Conventions

The motions of a ship, just as for any other rigid body, can be split into three mutually perpendicular translations of the center of gravity, G, and three rotations around G. In many cases these motion components will have small amplitudes.

Three right-handed orthogonal coordinate systems are used to define the ship motions:

- An **earth-bound** coordinate system $S(x_0, y_0, z_0)$.
  The (x_0, y_0)-plane lies in the still water surface, the positive x_0-axis is in the direction of the wave propagation; it can be rotated at a horizontal angle μ relative to the translating axis system $O(x, y, z)$ as shown in figure 6.1. The positive z_0-axis is directed upwards.

- A **body–bound** coordinate system $G(x_b, y_b, z_b)$.
  This system is connected to the ship with its origin at the ship's center of gravity, G. The directions of the positive axes are: x_b in the longitudinal forward direction, y_b in the lateral port side direction and z_b upwards. If the ship is floating upright in still water, the (x_b, y_b)-plane is parallel to the still water surface.

- A **steadily translating** coordinate system $O(x, y, z)$.
  This system is moving forward with a constant ship speed V. If the ship is stationary, the directions of the $O(x, y, z)$ axes are the same as those of the $G(x_b, y_b, z_b)$ axes. The (x, y)-plane lies in the still water surface with the origin O at, above or under the time-averaged position of the center of gravity G. The ship is supposed to carry out oscillations around this steadily translating $O(x, y, z)$ coordinate system.
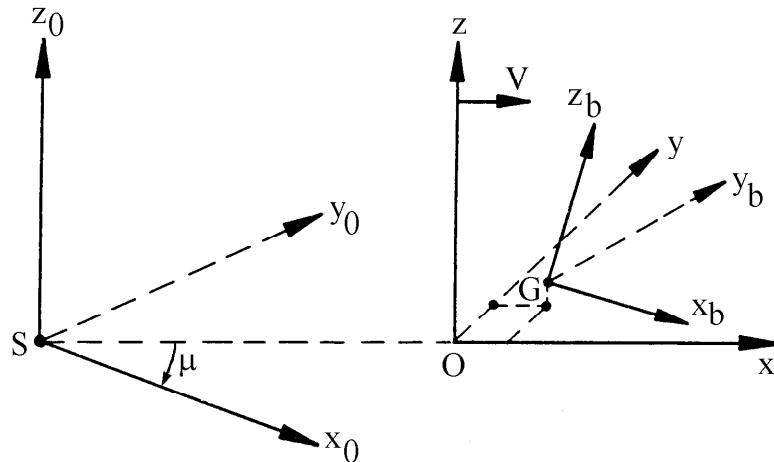
Figure 6.1: Coordinate Systems

The harmonic elevation of the wave surface ζ is defined in the earth-bound coordinate system by:

$$\zeta = \zeta_a \cos(\omega t - k x_0) \tag{6.1}$$

in which:

$$\zeta_a \quad = \quad \text{wave amplitude (m)}$$
$$k = 2\pi/\lambda \quad = \quad \text{wave number (rad/m)}$$
$$\lambda \quad = \quad \text{wave length (m)}$$
$$\omega \quad = \quad \text{circular wave frequency (rad/s)}$$
$$t \quad = \quad \text{time (s)}$$

6.2.2 Frequency of Encounter

The wave speed c, defined in a direction with an angle μ (wave direction) relative to the ship's speed vector V, follows from:

$$\boxed{c = \frac{\omega}{k} = \frac{\lambda}{T}} \qquad \text{(see chapter 5)} \tag{6.2}$$

The steadily translating coordinate system $O(x, y, z)$ is moving forward at the ship's speed V, which yields:

$$\boxed{x_0 = Vt \cos\mu + x \cos\mu + y \sin\mu} \tag{6.3}$$
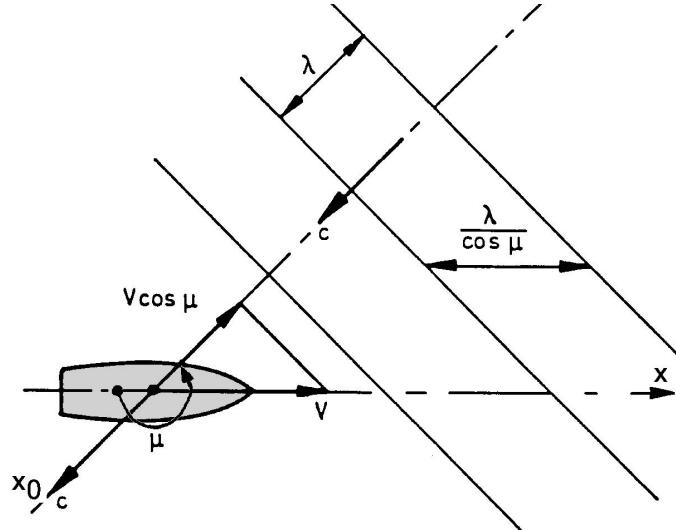
Figure 6.2: Frequency of Encounter

When a ship moves with a forward speed, the frequency at which it encounters the waves, ω_e, becomes important. Then the period of encounter, T_e, see figure 6.2, is:

$$T_e = \frac{\lambda}{c + V\cos(\mu - \pi)} = \frac{\lambda}{c - V\cos\mu} \tag{6.4}$$

and the circular frequency of encounter, ω_e, becomes:

$$\omega_e = \frac{2\pi}{T_e} = \frac{2\pi\,(c - V\cos\mu)}{\lambda} = k\,(c - V\cos\mu) \tag{6.5}$$

Note that $\mu = 0$ for following waves.

Using $k \cdot c = \omega$ from equation 6.2, the relation between the frequency of encounter and the wave frequency becomes:

$$\boxed{\omega_e = \omega - kV\cos\mu} \tag{6.6}$$

Note that at zero forward speed ($V = 0$) or in beam waves ($\mu = 90°$ or $\mu = 270°$) the frequencies ω_e and ω are identical.

In deep water, with the dispersion relation $k = \omega^2/g$, this frequency relation becomes:

$$\omega_e = \omega - \frac{\omega^2}{g}V\cos\mu \qquad \text{(deep water)} \tag{6.7}$$

Using the frequency relation in equation 6.6 and equations 6.1 and 6.3, it follows that the wave elevation can be given by:

$$\underline{|\zeta = \zeta_a\cos(\omega_e t - kx\cos\mu - ky\sin\mu)|} \tag{6.8}$$

6.2.3   Motions of and about CoG

The resulting six ship motions in the steadily translating $O(x, y, z)$ system are defined by three translations of the ship's center of gravity (**CoG**) in the direction of the x-, y- and z-axes and three rotations about them as given in the introduction:

$$
\begin{array}{rll}
\text{Surge} &:& x = x_a\cos(\omega_e t + \varepsilon_{x\zeta}) \\
\text{Sway} &:& y = y_a\cos(\omega_e t + \varepsilon_{y\zeta}) \\
\text{Heave} &:& z = z_a\cos(\omega_e t + \varepsilon_{z\zeta}) \\
\text{Roll} &:& \phi = \phi_a\cos(\omega_e t + \varepsilon_{\phi\zeta}) \\
\text{Pitch} &:& \theta = \theta_a\cos(\omega_e t + \varepsilon_{\theta\zeta}) \\
\text{Yaw} &:& \psi = \psi_a\cos(\omega_e t + \varepsilon_{\psi\zeta})
\end{array}
\tag{6.9}
$$

in which each of the ε values is a different phase angle.

The phase shifts of these motions are related to the harmonic wave elevation at the origin of the steadily translating $O(x, y, z)$ system. This origin is located at the average position of the ship's center of gravity - even though no wave can be measured there:

$$\text{Wave elevation at } O \text{ or } G: \qquad \underline{|\zeta = \zeta_a\cos(\omega_e t)|} \tag{6.10}$$

6.2.4   Displacement, Velocity and Acceleration

The harmonic velocities and accelerations in the steadily translating $O(x, y, z)$ coordinate system are found by taking the derivatives of the displacements. This will be illustrated here for roll:

$$
\begin{array}{rll}
\text{Displacement} &:& \underline{|\phi = \phi_a\cos(\omega_e t + \varepsilon_{\phi\zeta})|} \qquad \text{(see figure 6.3)} \\[2mm]
\text{Velocity} &:& \underline{\left|\dot{\phi} = -\omega_e\phi_a\sin(\omega_e t + \varepsilon_{\phi\zeta})\right|} = \omega_e\phi_a\cos(\omega_e t + \varepsilon_{\phi\zeta} + \pi/2) \\[2mm]
\text{Acceleration} &:& \underline{\left|\ddot{\phi} = -\omega_e^2\phi_a\cos(\omega_e t + \varepsilon_{\phi\zeta})\right|} = \omega_e^2\phi_a\cos(\omega_e t + \varepsilon_{\phi\zeta} + \pi)
\end{array}
\tag{6.11}
$$

The phase shift of the roll motion with respect to the wave elevation in figure 6.3, $\varepsilon_{\phi\zeta}$, is positive because when the wave elevation passes zero at a certain instant, the roll motion already has passed zero. Thus, if the roll motion, ϕ, comes before the wave elevation, ζ, then the phase shift, $\varepsilon_{\phi\zeta}$, is defined as positive. This convention will hold for all other responses as well of course.

Figure 6.4 shows a sketch of the time histories of the harmonic angular displacements, velocities and accelerations of roll. Note the mutual phase shifts of $\pi/2$ and π.
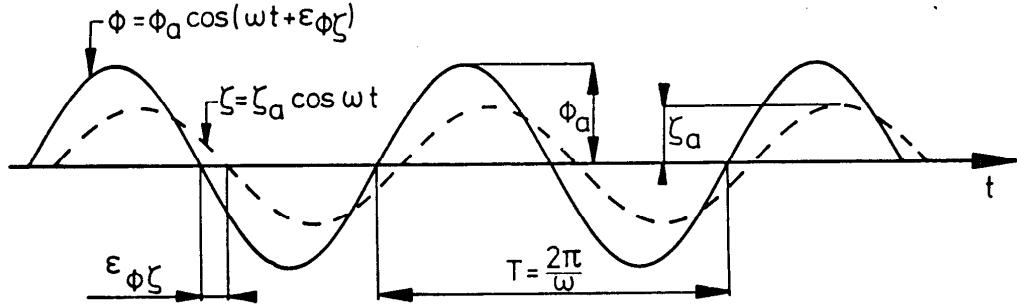
Figure 6.3: Harmonic Wave and Roll Signal
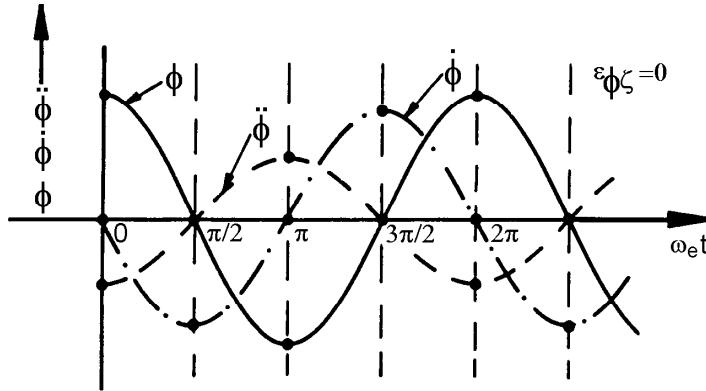
Figure 6.4: Displacement, Acceleration and Velocity

6.2.5 Motions Superposition

Knowing the motions of and about the center of gravity, G, one can calculate the motions in any point on the structure using superposition.

Absolute Motions

Absolute motions are the motions of the ship in the steadily translating coordinate system $O(x, y, z)$. The angles of rotation ϕ, θ and ψ are assumed to be small (for instance < 0.1 rad.), which is a necessity for linearizations. They must be expressed in radians, because in the linearization it is assumed that:

$$\boxed{\sin \phi \approx \phi} \qquad \text{and} \qquad \boxed{\cos \phi \approx 1.0} \tag{6.12}$$

For small angles, the transformation matrix from the body-bound coordinate system to the steadily translating coordinate system is very simple:

$$\begin{pmatrix} x \\ y \\ z \end{pmatrix} = \begin{pmatrix} 1 & -\psi & \theta \\ \psi & 1 & -\phi \\ -\theta & \phi & 1 \end{pmatrix} \cdot \begin{pmatrix} x_b \\ y_b \\ z_b \end{pmatrix} \tag{6.13}$$

Using this matrix, the components of the **absolute harmonic motions** of a certain point

$P(x_b, y_b, z_b)$ on the structure are given by:

$$\boxed{x_P = x - y_b\psi + z_b\theta}$$

$$\boxed{y_P = y + x_b\psi - z_b\phi}$$

$$\boxed{z_P = z - x_b\theta + y_b\phi} \tag{6.14}$$

in which x, y, z, ϕ, θ and ψ are the motions of and about the center of gravity, G, of the structure.

As can be seen in equation 6.14, the vertical motion, z_P, in a point $P(x_b, y_b, z_b)$ on the floating structure is made up of heave, roll and pitch contributions. When looking more detailed to this motion, it is called here now h, for convenient writing:

$$
\begin{aligned}
h\left(\omega_e, t\right) &= z - x_b\theta + y_b\phi \\
&= z_a \cos(\omega_e t + \varepsilon_{z\zeta}) - x_b\theta_a \cos(\omega_e t + \varepsilon_{\theta\zeta}) + y_b\phi_a \cos(\omega_e t + \varepsilon_{\phi\zeta}) \\
&= \quad \{+z_a \cos\varepsilon_{z\zeta} - x_b\theta_a \cos\varepsilon_{\theta\zeta} + y_b\phi_a \cos\varepsilon_{\phi\zeta}\} \cdot cos(\omega_e t) \\
&\quad - \{+z_a \sin\varepsilon_{z\zeta} - x_b\theta_a \sin\varepsilon_{\theta\zeta} + y_b\phi_a \sin\varepsilon_{\phi\zeta}\} \cdot sin(\omega_e t)
\end{aligned}
\tag{6.15}
$$

As this motion h has been obtained by a linear superposition of three harmonic motions, this (resultant) motion must be harmonic as well:

$$
\begin{aligned}
h\left(\omega_e, t\right) &= h_a \cos(\omega_e t + \varepsilon_{h\zeta}) \\
&= \{h_a \cos\varepsilon_{h\zeta}\} \cdot \cos(\omega_e t) - \{h_a \sin\varepsilon_{h\zeta}\} \cdot \sin(\omega_e t)
\end{aligned}
\tag{6.16}
$$

in which h_a is the motion amplitude and $\varepsilon_{h\zeta}$ is the phase lag of the motion with respect to the wave elevation at G.

By equating the terms with $\cos(\omega_e t)$ in equations 6.15 and 6.16 ($\omega_e t = 0$, so the $\sin(\omega_e t)$-terms are zero) one finds the in-phase term $h_a \cos\varepsilon_{h\zeta}$; equating the terms with $\sin(\omega_e t)$ in equations 6.15 and 6.16 ($\omega_e t = \pi/2$, so the $\cos(\omega_e t)$-terms are zero) provides the out-of-phase term $h_a \sin\varepsilon_{h\zeta}$ of the vertical displacement in P:

$$
\begin{aligned}
h_a \cos\varepsilon_{h\zeta} &= +z_a \cos\varepsilon_{z\zeta} - x_b\theta_a \cos\varepsilon_{\theta\zeta} + y_b\phi_a \cos\varepsilon_{\phi\zeta} \\
h_a \sin\varepsilon_{h\zeta} &= +z_a \sin\varepsilon_{z\zeta} - x_b\theta_a \sin\varepsilon_{\theta\zeta} + y_b\phi_a \sin\varepsilon_{\phi\zeta}
\end{aligned}
\tag{6.17}
$$

Since the right hand sides of equations 6.17 are known, the amplitude h_a and phase shift $\varepsilon_{h\zeta}$ become:

$$\boxed{h_a = \sqrt{\left(h_a \sin\varepsilon_{h\zeta}\right)^2 + \left(h_a \cos\varepsilon_{h\zeta}\right)^2}}$$

$$\boxed{\varepsilon_{h\zeta} = \arctan\left\{\frac{h_a \sin\varepsilon_{h\zeta}}{h_a \cos\varepsilon_{h\zeta}}\right\} \quad \text{with: } 0 \le \varepsilon_{h\zeta} \le 2\pi} \tag{6.18}$$

The phase angle $\varepsilon_{h\zeta}$ has to be determined in the correct quadrant between 0 and 2π. This depends on the signs of both the numerator and the denominator in the expression for the arctangent. If the phase shift $\varepsilon_{h\zeta}$ has been determined between $-\pi/2$ and $+\pi/2$ and $h_a \cos\varepsilon_{h\zeta}$ is negative, then π should be added or subtracted from this $\varepsilon_{h\zeta}$ to obtain the correct phase shift.

For ship motions, the relations between displacement or rotation, velocity and acceleration are very important. The vertical velocity and acceleration of point P on the structure follow simply from the first and second derivative with respect to the time of the displacement in equation 6.15:

$$
\begin{aligned}
\dot{h} &= -\omega_e h_a \, \sin\left(\omega_e t + \varepsilon_{h\zeta}\right) = \left\{\omega_e h_a\right\} \cdot \cos\left(\omega_e t + \left\{\varepsilon_{h\zeta} + \pi/2\right\}\right) \\
\ddot{h} &= -\omega_e^2 h_a \cos\left(\omega_e t + \varepsilon_{h\zeta}\right) = \left\{\omega_e^2 h_a\right\} \cdot \cos\left(\omega_e t + \left\{\varepsilon_{h\zeta} + \pi\right\}\right)
\end{aligned}
\tag{6.19}
$$

The amplitudes of the motions and the phase shifts with respect to the wave elevation at G are given between braces $\{...\}$ here.

Vertical Relative Motions

The vertical relative motion of the structure with respect to the undisturbed wave surface is the motion that one sees when looking overboard from a moving ship, downwards toward the waves. This relative motion is of importance for shipping water on deck and slamming (see chapter 11). The **vertical relative motion** s at $P(x_b, y_b)$ is defined by:

$$
\boxed{s = \zeta_P - h} = \zeta_P - z + x_b\theta - y_b\phi
\tag{6.20}
$$

with for the local wave elevation:

$$
\zeta_P = \zeta_a \cos(\omega_e t - kx_b \cos\mu - ky_b \sin\mu)
\tag{6.21}
$$

where $-kx_b \cos\mu - ky_b \sin\mu$ is the phase shift of the local wave elevation relative to the wave elevation in the center of gravity.

The amplitude and phase shift of this relative motion of the structure can be determined in a way analogous to that used for the absolute motion.

6.3 Single Linear Mass-Spring System

Consider a seaway with irregular waves of which the energy distribution over the wave frequencies (the wave spectrum) is known. These waves are input to a system that possesses linear characteristics. These frequency characteristics are known, for instance via model experiments or computations. The output of the system is the motion of the floating structure. This motion has an irregular behavior, just as the seaway that causes the motion. The block diagram of this principle is given in figure 6.5.

The first harmonics of the motion components of a floating structure are often of interest, because in many cases a very realistic mathematical model of the motions in a seaway can be obtained by making use of a superposition of these components at a range of frequencies; motions in the so-called **frequency domain** will be considered here.

In many cases the ship motions mainly have a linear behavior. This means that, at each frequency, the different ratios between the motion amplitudes and the wave amplitudes and also the phase shifts between the motions and the waves are constant. Doubling the input (wave) amplitude results in a doubled output amplitude, while the phase shifts between output and input does not change.

As a consequence of linear theory, the resulting motions in irregular waves can be obtained by adding together results from regular waves of different amplitudes, frequencies and possibly propagation directions. With known wave energy spectra and the calculated frequency characteristics of the responses of the ship, the response spectra and the statistics of these responses can be found.
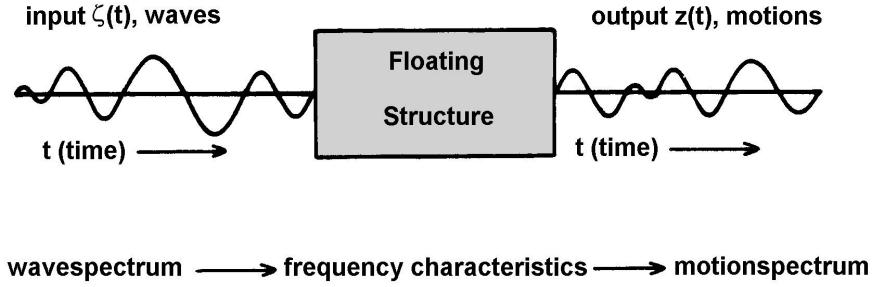
Figure 6.5: Relation between Motions and Waves

6.3.1   Kinetics

A rigid body's equation of motions with respect to an earth-bound coordinate system follow from Newton's second law. The vector equations for the translations of and the rotations about the center of gravity are respectively given by:

$$\boxed{\vec{F} = \frac{d}{dt}\left(m\vec{U}\right)} \quad \text{and} \quad \boxed{\vec{M} = \frac{d}{dt}\left(\vec{H}\right)} \tag{6.22}$$

in which:

$\vec{F}$ = resulting external force acting in the center of gravity (N)
m = mass of the rigid body (kg)
$\vec{U}$ = instantaneous velocity of the center of gravity (m/s)
$\vec{M}$ = resulting external moment acting about the center of gravity (Nm)
$\vec{H}$ = instantaneous angular momentum about the center of gravity (Nms)
t = time (s)

The total mass as well as its distribution over the body is considered to be constant during a time which is long relative to the oscillation period of the motions.

Loads Superposition

Since the system is linear, the resulting motion in waves can be seen as a superposition of the motion of the body in still water and the forces on the restrained body in waves. Thus, two important assumptions are made here for the loads on the right hand side of the picture equation in figure 6.6:

a. The so-called **hydromechanical forces and moments** are induced by the harmonic oscillations of the rigid body, moving in the undisturbed surface of the fluid.

b. The so-called **wave exciting forces and moments** are produced by waves coming in on the restrained body.

The vertical motion of the body (a buoy in this case) follows from Newton's second law:

$$\boxed{\frac{d}{dt}\left(\rho\nabla \cdot \dot{z}\right) = \rho\nabla \cdot \ddot{z} = F_h + F_w} \tag{6.23}$$

in which:
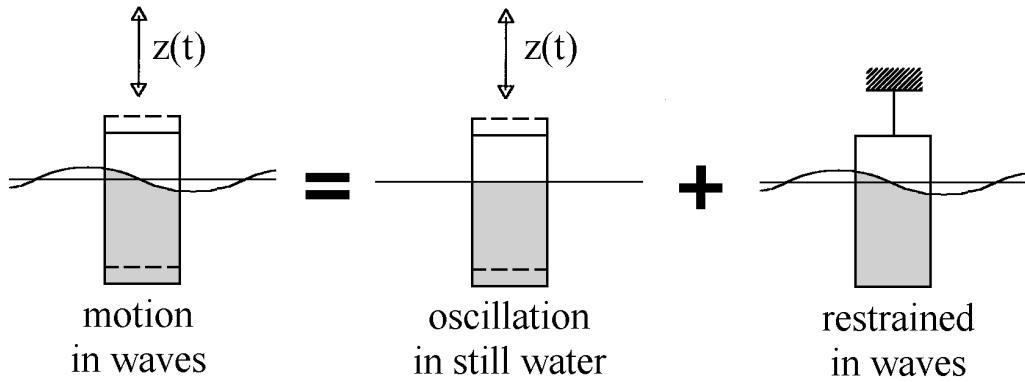
Figure 6.6: Superposition of Hydromechanical and Wave Loads

ρ = density of water (kg/m^3)
∇ = volume of displacement of the body (m^3)
F_h = hydromechanical force in the z-direction (N)
F_w = exciting wave force in the z-direction (N)

This superposition will be explained in more detail for a circular cylinder, floating in still water with its center line in the vertical direction, as shown in figure 6.7.
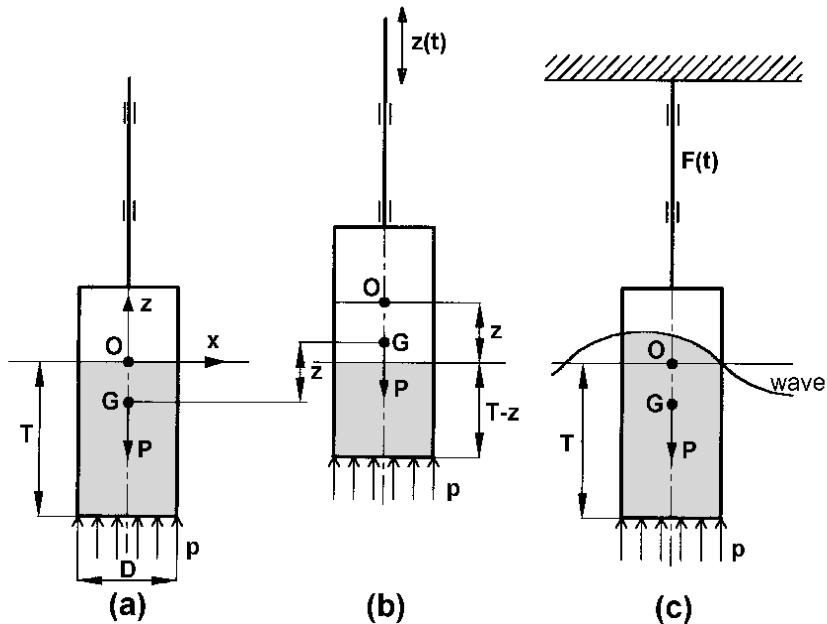
Figure 6.7: Heaving Circular Cylinder

6.3.2 Hydromechanical Loads

First, a **free decay test** in still water will be considered. After a vertical displacement upwards (see 6.7-b), the cylinder will be released and the motions can die out freely. The

vertical motions of the cylinder are determined by the solid mass m of the cylinder and the hydromechanical loads on the cylinder.

Applying Newton's second law for the heaving cylinder:

$$
\begin{aligned}
m\ddot{z} &= \text{sum of all forces on the cylinder} \\
&= -P + pA_w - b\dot{z} - a\ddot{z} \\
&= -P + \rho g\left(T - z\right)A_w - b\dot{z} - a\ddot{z}
\end{aligned}
\tag{6.24}
$$

With Archimedes' law $P = \rho g T A_w$, the linear equation of the heave motion becomes:

$$
\boxed{\left(m + a\right)\ddot{z} + b\dot{z} + cz = 0}
\tag{6.25}
$$

in which:

$$
\begin{aligned}
z &= \text{vertical displacement (m)} \\
P = mg &= \text{mass force downwards (N)} \\
m = \rho A_w T &= \text{solid mass of cylinder (kg)} \\
a &= \text{hydrodynamic mass coefficient (Ns}^2\text{/m = kg)} \\
b &= \text{hydrodynamic damping coefficient (Ns/m = kg/s)} \\
c = \rho g A_w &= \text{restoring spring coefficient (N/m = kg/s}^2\text{)} \\
A_w = \tfrac{\pi}{4}D^2 &= \text{water plane area (m}^2\text{)} \\
D &= \text{diameter of cylinder (m)} \\
T &= \text{draft of cylinder at rest (s)}
\end{aligned}
$$

The terms $a\ddot{z}$ and $b\dot{z}$ are caused by the hydrodynamic reaction as a result of the movement of the cylinder with respect to the water. The water is assumed to be ideal and thus to behave as in a potential flow.
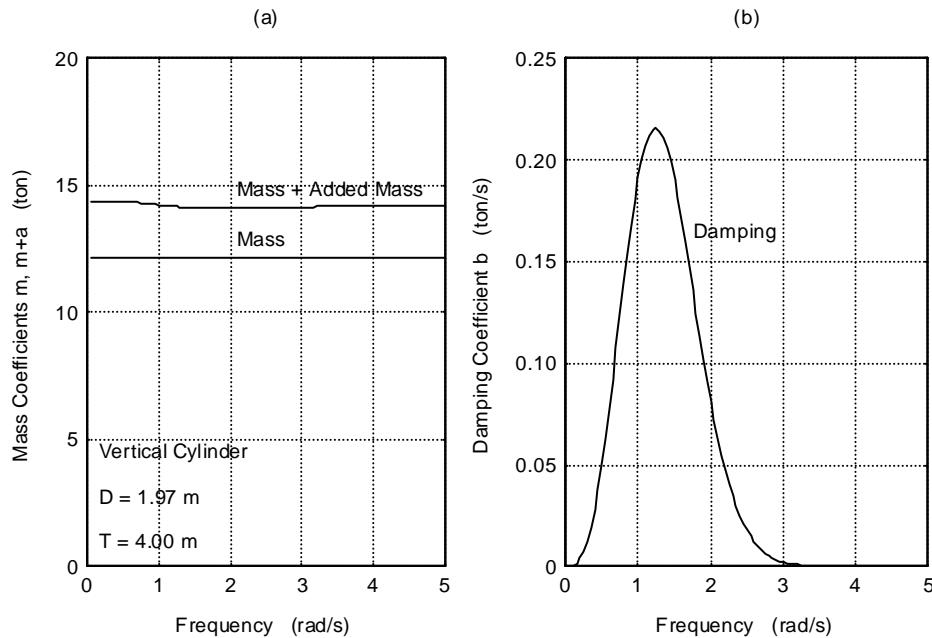
Figure 6.8: Mass and Damping of a Heaving Vertical Cylinder

The vertical oscillations of the cylinder will generate waves which propagate radially from it. Since these waves transport energy, they withdraw energy from the (free) buoy's oscillations; its motion will die out. This so-called wave damping is proportional to the velocity of the cylinder $\dot{z}$ in a linear system. The coefficient b has the dimension of a mass per unit of time and is called the **(wave or potential) damping** coefficient. Figure 6.8-b shows the hydrodynamic damping coefficient b of a vertical cylinder as a function of the frequency of oscillation.

In an actual viscous fluid, friction also causes damping, vortices and separation phenomena quite similar to that discussed in chapter 4. Generally, these viscous contributions to the damping are non-linear, but they are usually small for most large floating structures; they are neglected here for now.

The other part of the hydromechanical reaction force $a\ddot{z}$ is proportional to the vertical acceleration of the cylinder in a linear system. This force is caused by accelerations that are given to the water particles near to the cylinder. This part of the force does not dissipate energy and manifests itself as a standing wave system near the cylinder. The coefficient a has the dimension of a mass and is called the **hydrodynamic mass** or **added mass**. Figure 6.8-a shows the hydrodynamic mass a of a vertical cylinder as a function of the frequency of oscillation.

In his book, [Newman, 1977] provides added mass coefficients for deeply submerged 2-D and 3-D bodies.

Graphs of the three added mass coefficients for 2-D bodies are shown in figure 6.9. The added mass m_{11} corresponds to longitudinal acceleration, m_{22} to lateral acceleration in equatorial plane and m_{66} denotes the rotational added moment of inertia. These potential coefficients have been calculated by using conformal mapping techniques as will be explained in chapter 7.
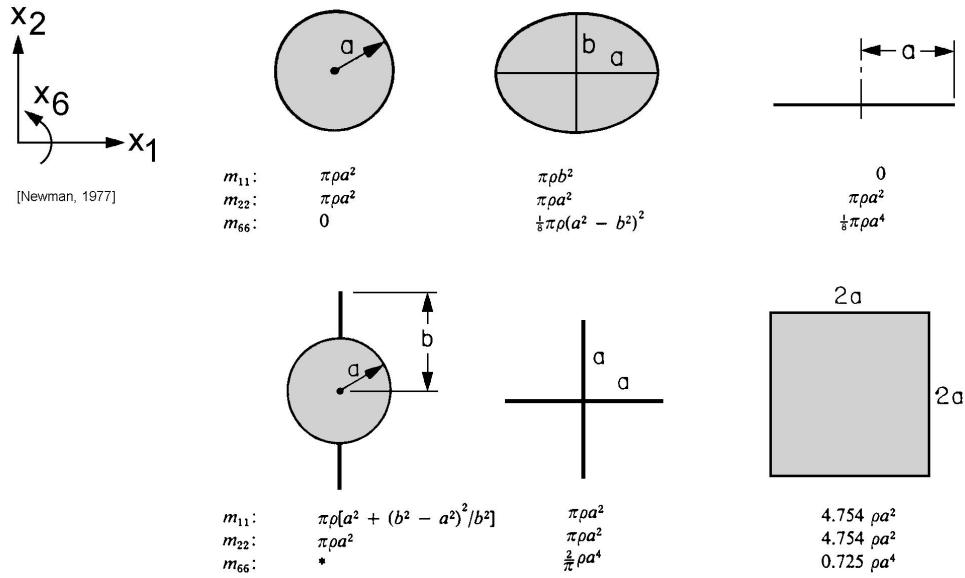
Figure 6.9: Added Mass Coefficients of 2-D Bodies

Graphs of the three added mass coefficients of 3-D spheroids, with a length $2a$ and a maximum diameter $2b$, are shown in figure 6.10. In this figure, the coefficients have been

made dimensionless using the mass and moment of inertia of the displaced volume of the fluid by the body. The added mass m_{11} corresponds to longitudinal acceleration, m_{22} to lateral acceleration in equatorial plane and m_{55} denotes the added moment of inertia for rotation about an axis in the equatorial plane.
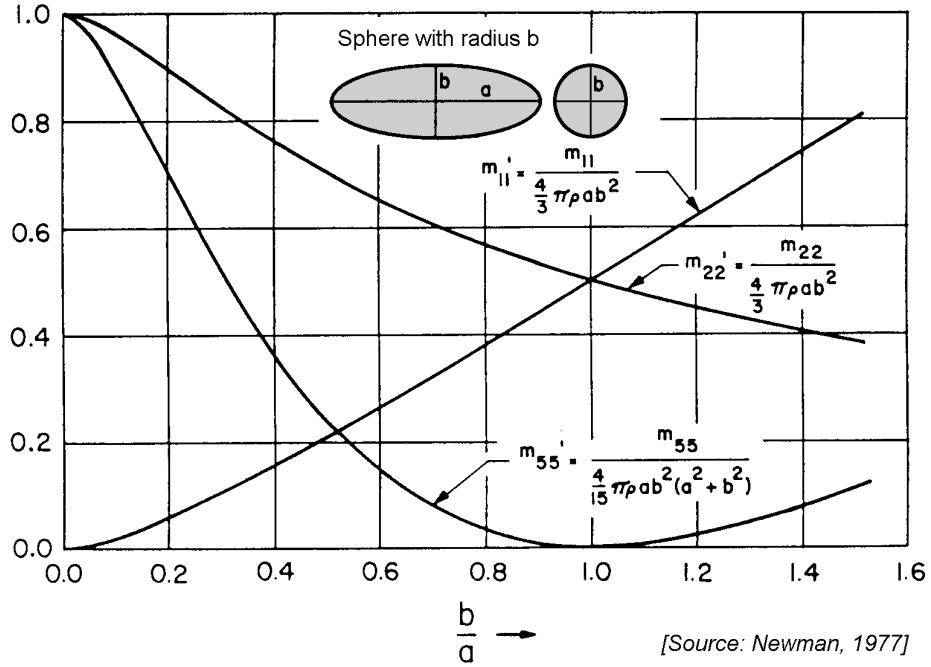
Figure 6.10: Added Mass Coefficients of Ellipsoids

Note that the potential damping of all these deeply submerged bodies is zero since they no longer generate waves on the water surface.

Since the bottom of the cylinder used in figure 6.8 is deep enough under the water surface, it follows from figure 6.10 that the added mass a can be approximated by the mass of a hemisphere of fluid with a diameter D. The damping coefficient, b, will approach to zero, because a vertical oscillation of this cylinder will hardly produce waves. The actual ratio between the added mass and the mass of the hemisphere, as obtained from 3-D calculations, varies for a cylinder as given in figure 6.8-a between 0.95 and 1.05.

It appears from experiments that in many cases both the acceleration and the velocity terms have a sufficiently linear behavior at small amplitudes; they are linear for practical purposes. The **hydromechanical forces** are the total reaction forces of the fluid on the oscillating cylinder, caused by this motion in initially still water:

$$m\ddot{z} = F_h \qquad \text{with:} \quad F_h = -a\ddot{z} - b\dot{z} - cz \tag{6.26}$$

and the equation of motion for the cylinder with a decaying motion in still water becomes:

$$(m + a) \cdot \ddot{z} + b \cdot \dot{z} + c \cdot z = 0 \tag{6.27}$$

A similar approach can be followed for the other motions. In case of angular motions, for instance roll motions, the uncoupled equation of motion (now with moment terms) of the cylinder in still water becomes:

$$(m + a) \cdot \ddot{\phi} + b \cdot \dot{\phi} + c \cdot \phi = 0 \qquad (6.28)$$

and the coefficients in the acceleration term, a and m, are (added) mass moment of inertia terms. Coupling between motions will be discussed in chapter 8.

Energy Relations

Suppose the cylinder is carrying out a vertical harmonic oscillation:

$$z = z_a \sin \omega t$$

in initially still water of which the linear equation of motion is given by equation 6.27. The separate work done by the mass, damping and spring force components in this equation (force component times distance) per unit of time during one period of oscillation, T, are:

$$\frac{1}{T} \int_0^T \{(m + a) \cdot \ddot{z}\} \cdot \{\dot{z} \cdot dt\} \;=\; \frac{-z_a{}^2 (m + a)\, \omega^3}{T} \int_0^T \sin \omega t \cdot \cos \omega t \cdot dt = 0$$

$$\frac{1}{T} \int_0^T \{b \cdot \dot{z}\} \cdot \{\dot{z} \cdot dt\} \;=\; \frac{z_a{}^2 b\, \omega^2}{T} \int_0^T \cos^2 \omega t \cdot dt = \frac{1}{2} b\, \omega^2 z_a{}^2$$

$$\frac{1}{T} \int_0^T \{c \cdot z\} \cdot \{\dot{z} \cdot dt\} \;=\; \frac{z_a{}^2 c\, \omega}{T} \int_0^T \sin \omega t \cdot \cos \omega t \cdot dt = 0 \qquad (6.29)$$

with:

$$T = 2\pi/\omega \quad = \text{oscillation period (s)}$$
$$\dot{z} \cdot dt = dz \quad = \text{distance covered in } dt \text{ seconds (m)}$$

It is obvious from these equations that only the damping force $\{b \cdot \dot{z}\}$ dissipates energy; damping is the reason why the heave motion, z, dies out.

Observe now a floating horizontal cylinder as given in figure 6.11, carrying out a vertical harmonic oscillation in initially still water: $z = z_a \sin \omega t$, which causes radiated waves defined by: $\zeta = \zeta_a \sin(\omega t + \varepsilon)$. A frequency-dependent relation between the damping coefficient, b, and the amplitude ratio of radiated waves and the vertical oscillation, ζ_a/z_a, can be found; see also [Newman, 1962].

The energy E (the work done per unit of time) provided by the hydrodynamic damping force is the over one period (T) integrated damping force ($b \cdot \dot{z}$) times covered distance ($\dot{z} \cdot dt$) divided by the time (T):

$$E \;=\; \frac{1}{T} \int_0^T \{b \cdot \dot{z}\} \cdot \{\dot{z} \cdot dt\}$$

$$\;=\; \frac{1}{2} b\, \omega^2 z_a{}^2 \qquad (6.30)$$

This energy provided by the above mentioned hydrodynamic damping force is equal to the energy dissipated by the radiated waves. This is 2 (radiation of waves to two sides) times
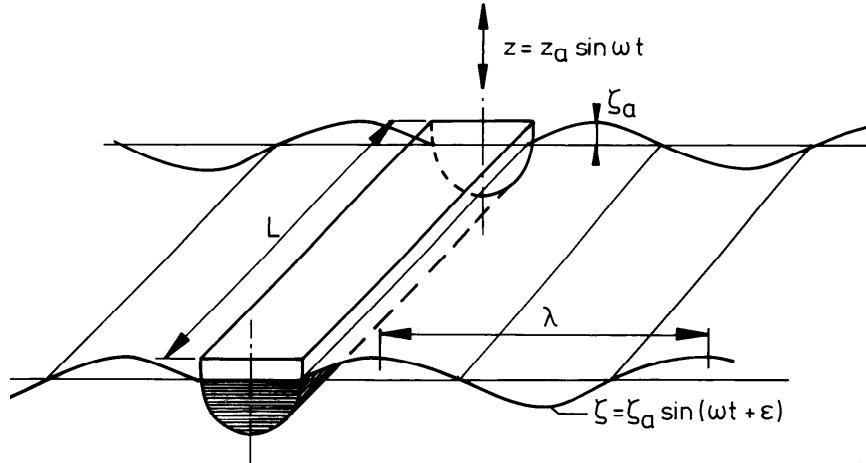
Figure 6.11: Oscillating Horizontal Cylinder

the energy of the waves per unit area ($\frac{1}{2}\rho g\zeta_a{}^2$) times the covered distance by the radiated wave energy ($c_g{\cdot}T$) in one period (T) times the length of the cylinder (L), divided by the time (T):

$$
\begin{aligned}
E &= \frac{1}{T}\cdot 2\cdot\left\{\frac{1}{2}\rho g\zeta_a{}^2\right\}\cdot\{c_g{\cdot}T\cdot L\} \\
&= \frac{\rho g^2\zeta_a{}^2 L}{2\,\omega}
\end{aligned}
\tag{6.31}
$$

To obtain the right hand side of this equation, use has been made of the definition of the group velocity of the waves in deep water: $c_g = c/2 = g/(2\,\omega)$; see chapter 5.

Thus, the potential damping coefficient per unit of length is defined by:

$$
\frac{1}{2}b\,\omega^2 z_a{}^2 = \frac{\rho g^2\zeta_a{}^2 L}{2\,\omega}
\tag{6.32}
$$

or:

$$
\boxed{b' = \frac{b}{L} = \frac{\rho g^2}{\omega^3}\left(\frac{\zeta_a}{z_a}\right)^2}
\tag{6.33}
$$

Similar approaches can be applied for sway and roll oscillations.

The motions are defined here by $z = z_a\sin\omega t$. It is obvious that a definition of the body oscillation by $z = z_a\cos\omega t$ will provide the same results, because this means only an introduction of a constant phase shift of $-\pi/2$ in the body motion as well as in the generated waves.

Linearisation of Nonlinear damping

In some cases (especially roll motions) viscous effects do influence the damping and can result in nonlinear damping coefficients. Suppose a strongly non-linear roll damping moment, M, which can be described by:

$$
M = b^{(1)}\cdot\dot\phi + b^{(2)}\cdot\left|\dot\phi\right|\cdot\dot\phi + b^{(3)}\cdot\dot\phi^3
\tag{6.34}
$$

The modulus of the roll velocity in the second term is required to give the proper sign to its contribution. This damping moment can be linearised by stipulating that an identical amount of energy be dissipated by a linear term with an **equivalent linear damping coefficient** $b^{(eq)}$:

$$\frac{1}{T}\int_0^T \left\{b^{(eq)} \cdot \dot{\phi}\right\} \cdot \left\{\dot{\phi} \cdot dt\right\} = \frac{1}{T}\int_0^T \left\{b^{(1)} \cdot \dot{\phi} + b^{(2)} \cdot \left|\dot{\phi}\right| \cdot \dot{\phi} + b^{(3)} \cdot \dot{\phi}^3\right\} \cdot \left\{\dot{\phi} \cdot dt\right\} \quad (6.35)$$

Define the roll motion by $\phi = \phi_a \cos(\omega t + \varepsilon_{\phi\zeta})$, as given in equation 6.9. Then a substitution of $\dot{\phi} = -\phi_a \omega \sin(\omega t + \varepsilon_{\phi\zeta})$ in equation 6.35 and the use of some mathematics yields:

$$\boxed{M = b^{(eq)} \cdot \dot{\phi}} \qquad \text{with:} \qquad \boxed{b^{(eq)} = b^{(1)} + \frac{8}{3\pi} \cdot \omega \cdot \phi_a \cdot b^{(2)} + \frac{3}{4} \cdot \omega^2 \cdot \phi_a^2 \cdot b^{(3)}} \quad (6.36)$$

Note that this equivalent linear damping coefficient depends on both the frequency and the amplitude of oscillation.

Restoring Spring Terms

For free floating bodies, restoring 'spring' terms are present for the heave, roll and pitch motions only. The restoring spring term for heave has been given already; for the angular motions they follow from the linearized static stability phenomena as given in chapter 2:

$$\begin{aligned} \text{heave} \quad &: \quad c_{zz} = \rho g A_{WL} \\ \text{roll} \quad &: \quad c_{\phi\phi} = \rho g \nabla \cdot \overline{GM} \\ \text{pitch} \quad &: \quad c_{\theta\theta} = \rho g \nabla \cdot \overline{GM}_L \end{aligned}$$

in which $\overline{GM}$ and $\overline{GM}_L$ are the transverse and longitudinal initial metacentric heights.

Free Decay Tests

In case of a pure free heaving cylinder in still water, the linear equation of the heave motion of the center of gravity, G, of the cylinder is given by equation 6.27:

$$\boxed{(m + a) \cdot \ddot{z} + b \cdot \dot{z} + c \cdot z = 0}$$

This equation can be rewritten as:

$$\boxed{\ddot{z} + 2\nu \cdot \dot{z} + \omega_0{}^2 \cdot z = 0} \quad (6.37)$$

in which the damping coefficient and the undamped natural frequency are defined by:

$$\boxed{2\nu = \frac{b}{m+a}} \text{ (a)} \qquad \text{and} \qquad \boxed{\omega_0{}^2 = \frac{c}{m+a}} \text{ (b)} \quad (6.38)$$

A non-dimensional damping coefficient, κ, is written as:

$$\kappa = \frac{\nu}{\omega_0} = \frac{b}{2\sqrt{(m+a) \cdot c}} \quad (6.39)$$

This damping coefficient is written as a fraction between the actual damping coefficient, b, and the **critical damping** coefficient, $b_{cr} = 2\sqrt{(m+a) \cdot c}$; so for critical damping: $\kappa_{cr} = 1$. Herewith, the equation of motion 6.37 can be re-written as:

$$\boxed{\ddot{z} + 2\kappa\omega_0 \cdot \dot{z} + \omega_0{}^2 \cdot z = 0}$$ (6.40)

The buoy is deflected to an initial vertical displacement, z_a, in still water and then released. The solution of the equation 6.37 of this decay motion becomes after some mathematics:

$$z = z_a e^{-\nu t}\left(\cos\omega_z t + \frac{\nu}{\omega_z}\sin\omega_z t\right)$$ (6.41)

where $z_a e^{-\nu t}$ is the decrease of the "crest" after one period.
Then the **logarithmic decrement** of the motion is:

$$\nu T_z = \kappa\omega_0 T_z = \ln\left\{\frac{z(t)}{z(t+T_z)}\right\}$$ (6.42)

Because $\omega_z{}^2 = \omega_0{}^2 - \nu^2$ for the natural frequency oscillation and the damping is small ($\nu < 0.20$) so that $\nu^2 \ll \omega_0{}^2$, one can neglect ν^2 here and use $\omega_z \approx \omega_0$; this leads to:

$$\omega_0 T_z \approx \omega_z T_z = 2\pi$$ (6.43)

The non-dimensional damping is given now by:

$$\boxed{\kappa = \frac{1}{2\pi}\ln\left\{\frac{z(t)}{z(t+T_z)}\right\}} = b \cdot \frac{\omega_0}{2c}$$ (6.44)

These κ-values can easily be found when results of decay tests with a model in still water are available. These are usually in a form such as is shown in figure 6.12.
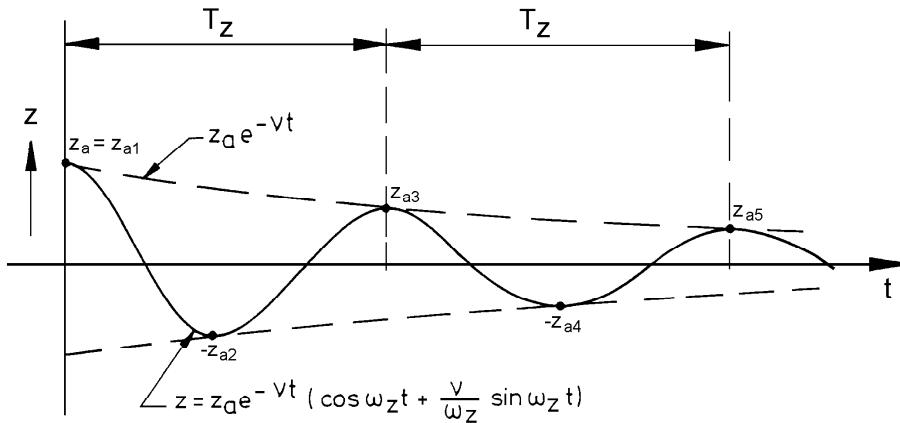
Figure 6.12: Determination of Logarithmic Decrement

Be aware that this damping coefficient is determined by assuming an uncoupled heave motion (no other motions involved). Strictly, this damping coefficient is not valid for the actual coupled motions of a free floating cylinder which will be moving in all directions simultaneously.

The results of free decay tests are presented by plotting the non-dimensional damping coefficient (obtained from two successive positive or negative maximum displacements z_{a_i} and $z_{a_{i+2}}$ by:

$$\kappa = \frac{1}{2\pi} \cdot \ln\left\{\frac{z_{a_i}}{z_{a_{i+2}}}\right\} \quad \text{versus} \quad \overline{z_a} = \left|\frac{z_{a_i} + z_{a_{i+2}}}{2}\right| \tag{6.45}$$

To avoid spreading in the successively determined κ-values, caused by a possible zero-shift of the measuring signal, double amplitudes can be used instead:

$$\kappa = \frac{1}{2\pi} \cdot \ln\left\{\frac{z_{a_i} - z_{a_{i+1}}}{z_{a_{i+2}} - z_{a_{i+3}}}\right\} \quad \text{versus} \quad \overline{z_a} = \left|\frac{z_{a_i} - z_{a_{i+1}} + z_{a_{i+2}} - z_{a_{i+3}}}{4}\right| \tag{6.46}$$

It is obvious that this latter method has preference in case of a record with small amplitudes. The decay coefficient κ can therefore be estimated from the decaying oscillation by determining the ratio between any pair of successive (double) amplitudes. When the damping is very small and the oscillation decays very slowly, several estimates of the decay can be obtained from a single record. The method is not really practical when ν is much greater than about 0.2 and is in any case strictly valid for small values of ν only. Luckily, this is generally the case.

The potential mass and damping at the natural frequency can be obtained from all of this. From equation 6.38-b follows:

$$a = \frac{c}{\omega_0^2} - m \tag{6.47}$$

in which the natural frequency, ω_0, follows from the measured oscillation period and the solid mass, m, and the spring coefficient, c, are known from the geometry of the body.

From equation 6.38-a, 6.38-b and equation 6.39 follows:

$$b = \frac{2\kappa c}{\omega_0} \tag{6.48}$$

in which κ follows from the measured record by using equation 6.45 or 6.46 while c and ω_0 have to be determined as done for the added mass a.

It is obvious that for a linear system a constant κ-value should be found in relation to $\overline{z_a}$. Note also that these decay tests provide no information about the relation between the potential coefficients and the frequency of oscillation. Indeed, this is impossible since decay tests are carried out at one frequency only; the natural frequency.

Forced Oscillation Tests

The relation between the potential coefficients and the frequency of oscillation can be found using forced oscillation tests. A schematic of the experimental set-up for the forced heave oscillation of a vertical cylinder is given in figure 6.13. The crank at the top of the figure rotates with a constant and chosen frequency, ω, causing a vertical motion with amplitude given by the radial distance from the crank axis to the pin in the slot. Vertical forces are measured in the rod connecting the exciter to the buoy.

During the forced heave oscillation, the vertical motion of the model is defined by:

$$z(t) = z_a \sin \omega t \tag{6.49}$$
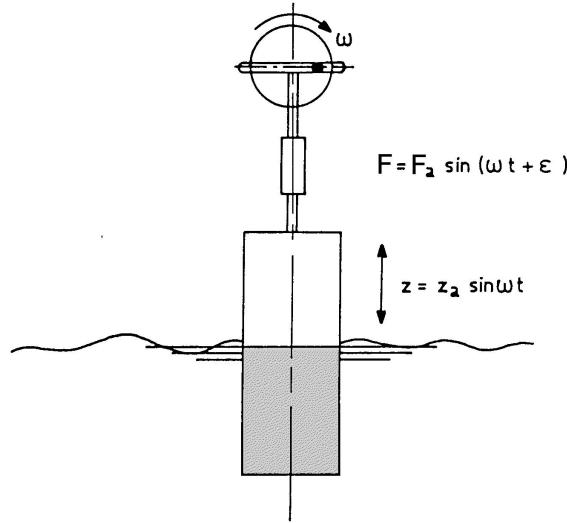
Figure 6.13: Forced Oscillation Test

and the heave forces, measured by the transducer, are:

$$F_z(t) = F_a \sin(\omega t + \varepsilon_{Fz}) \tag{6.50}$$

The (linear) equation of motion is given by:

$$\boxed{(m+a)\,\ddot{z} + b\dot{z} + cz = F_a \sin(\omega t + \varepsilon_{Fz})} \tag{6.51}$$

The component of the exciting force in phase with the heave motion is associated with inertia and stiffness, while the out-of-phase component is associated with damping. With:

$$
\begin{aligned}
z &= z_a \sin \omega t \\
\dot{z} &= z_a \omega \cos \omega t \\
\ddot{z} &= -z_a \omega^2 \sin \omega t
\end{aligned}
\tag{6.52}
$$

one obtains:

$$z_a\left\{-(m+a)\,\omega^2 + c\right\}\sin\omega t + z_a b\omega \cos\omega t = F_a \cos\varepsilon_{Fz}\sin\omega t + F_a \sin\varepsilon_{Fz}\cos\omega t \tag{6.53}$$

which provides:

$$\text{from } \omega t = \frac{\pi}{2}: \qquad \boxed{a = \frac{c - \frac{F_a}{z_a}\cos\varepsilon_{Fz}}{\omega^2} - m}$$

$$\text{from } \omega t = 0: \qquad \boxed{b = \frac{\frac{F_a}{z_a}\sin\varepsilon_{Fz}}{\omega}}$$

$$\text{from geometry:} \qquad \boxed{c = \rho g A_w} \tag{6.54}$$

To obtain the 'spring' stiffness, c, use has to be made of A_w (area of the waterline), which can be obtained from the geometry of the model. It is possible to obtain the stiffness coefficient from static experiments as well. In such a case equation 6.51 degenerates:

$$\ddot{z} = 0 \quad \text{and} \quad \dot{z} = 0 \qquad \text{yielding:} \qquad c = \frac{F_z}{z}$$

in which z is a constant vertical displacement of the body and F_z is a constant force (Archimedes' law).

The in-phase and out-of-phase parts of the exciting force during an oscillation can be found easily from an integration over a whole number (N) periods (T) of the measured signal $F(t)$ multiplied with $\cos \omega t$ and $\sin \omega t$, respectively:

$$F_a \sin \varepsilon_{Fz} = \frac{2}{NT} \int_0^{NT} F(t) \cdot \cos \omega t \cdot dt$$

$$F_a \cos \varepsilon_{Fz} = \frac{2}{NT} \int_0^{NnT} F(t) \cdot \sin \omega t \cdot dt \qquad (6.55)$$

These are nothing more than the first order (and averaged) Fourier series components of $F(t)$; see appendix C.

6.3.3 Wave Loads

Waves are now generated in the test basin for a new series of tests. The object is restrained so that one now measures (in this vertical cylinder example) the vertical wave load on the fixed cylinder. This is shown schematically in figure 6.7-c.

The classic theory of deep water waves (see chapter 5) yields:

$$\text{wave potential} \quad : \qquad \Phi = \frac{-\zeta_a g}{\omega} e^{kz} \sin(\omega t - kx) \qquad (6.56)$$

$$\text{wave elevation} \quad : \qquad \zeta = \zeta_a \cos(\omega t - kx) \qquad (6.57)$$

so that the pressure, p, on the **bottom** of the cylinder $(z = -T)$ follows from the linearized Bernoulli equation:

$$\begin{aligned} p &= -\rho \frac{\partial \Phi}{\partial t} - \rho g z \\ &= \rho g \zeta_a e^{kz} \cos(\omega t - kx) - \rho g z \\ &= \rho g \zeta_a e^{-kT} \cos(\omega t - kx) + \rho g T \end{aligned} \qquad (6.58)$$

Assuming that the diameter of the cylinder is small relative to the wave length $(kD \approx 0)$, so that the pressure distribution on the bottom of the cylinder is essentially uniform, then the pressure becomes:

$$p = \rho g \zeta_a e^{-kT} \cos(\omega t) + \rho g T \qquad (6.59)$$

Then the vertical force on the bottom of the cylinder is:

$$F = \left\{ \rho g \zeta_a e^{-kT} \cos(\omega t) + \rho g T \right\} \cdot \frac{\pi}{4} D^2 \qquad (6.60)$$

where D is the cylinder diameter and T is the draft.

The harmonic part of this force is the regular harmonic **wave force**, which will be considered here. More or less in the same way as with the hydromechanical loads (on the oscillating body in still water), this wave force can also be expressed as a spring coefficient c times a **reduced or effective** wave elevation ζ^*:

$$\boxed{F_{FK} = c \cdot \zeta^*} \quad \text{with:} \quad c = \rho g \frac{\pi}{4} D^2 \qquad \text{(spring coeff.)}$$

$$\zeta^* = e^{-kT} \cdot \zeta_a \cos(\omega t) \qquad \text{(deep water)} \qquad (6.61)$$

This wave force is called the **Froude-Krilov force**, which follows from an integration of the pressures on the body in the **undisturbed** wave.

Actually however, a part of the waves will be diffracted, requiring a correction of this Froude-Krilov force. Using the relative motion principle described earlier in this chapter, one finds additional force components: one proportional to the vertical acceleration of the water particles and one proportional to the vertical velocity of the water particles.

The total **wave force** can be written as:

$$\boxed{F_w = a\ddot{\zeta}^* + b\dot{\zeta}^* + c\zeta^*} \qquad (6.62)$$

in which the terms $a\ddot{\zeta}^*$ and $b\dot{\zeta}^*$ are considered to be corrections on the Froude-Krilov force due to diffraction of the waves by the presence of the cylinder in the fluid.

The "reduced" wave elevation is given by:

$$\zeta^* = \zeta_a e^{-kT} \cos(\omega t)$$
$$\dot{\zeta}^* = -\zeta_a e^{-kT} \omega \sin(\omega t)$$
$$\ddot{\zeta}^* = -\zeta_a e^{-kT} \omega^2 \cos(\omega t) \qquad (6.63)$$

A substitution of equations 6.63 in equation 6.62 yields:

$$F_w = \zeta_a e^{-kT} \left\{ c - a\omega^2 \right\} \cos(\omega t) - \zeta_a e^{-kT} \left\{ b\omega \right\} \sin(\omega t) \qquad (6.64)$$

Also, this wave force can be written independently in terms of in-phase and out-of-phase terms:

$$F_w = F_a \cos(\omega t + \varepsilon_{F\zeta})$$
$$= F_a \cos(\varepsilon_{F\zeta}) \cos(\omega t) - F_a \sin(\varepsilon_{F\zeta}) \sin(\omega t) \qquad (6.65)$$

Equating the two in-phase terms and the two out-of-phase terms in equations 6.64 and 6.65 result in two equations with two unknowns:

$$F_a \cos(\varepsilon_{F\zeta}) = \zeta_a e^{-kT} \left\{ c - a\omega^2 \right\}$$
$$F_a \sin(\varepsilon_{F\zeta}) = \zeta_a e^{-kT} \left\{ b\omega \right\} \qquad (6.66)$$

Adding the squares of these two equations results in the wave force amplitude:

$$\boxed{\frac{F_a}{\zeta_a} = e^{-kT} \sqrt{\left\{ c - a\omega^2 \right\}^2 + \left\{ b\omega \right\}^2}} \qquad (6.67)$$

and a division of the in-phase and the out-of-phase term in equation 6.66, results in the phase shift:

$$\varepsilon_{F\zeta} = \arctan\left\{\frac{b\omega}{c - a\omega^2}\right\} \quad \text{with: } 0 \leq \varepsilon_{z\zeta} \leq 2\pi \tag{6.68}$$

The phase angle, $\varepsilon_{F\zeta}$, has to be determined in the correct quadrant between 0 and 2π. This depends on the signs of both the numerator and the denominator in the expression for the arctangent.

The wave force amplitude, F_a, is proportional to the wave amplitude, ζ_a, and the phase shift $\varepsilon_{F\zeta}$ is independent of the wave amplitude, ζ_a; the system is linear.
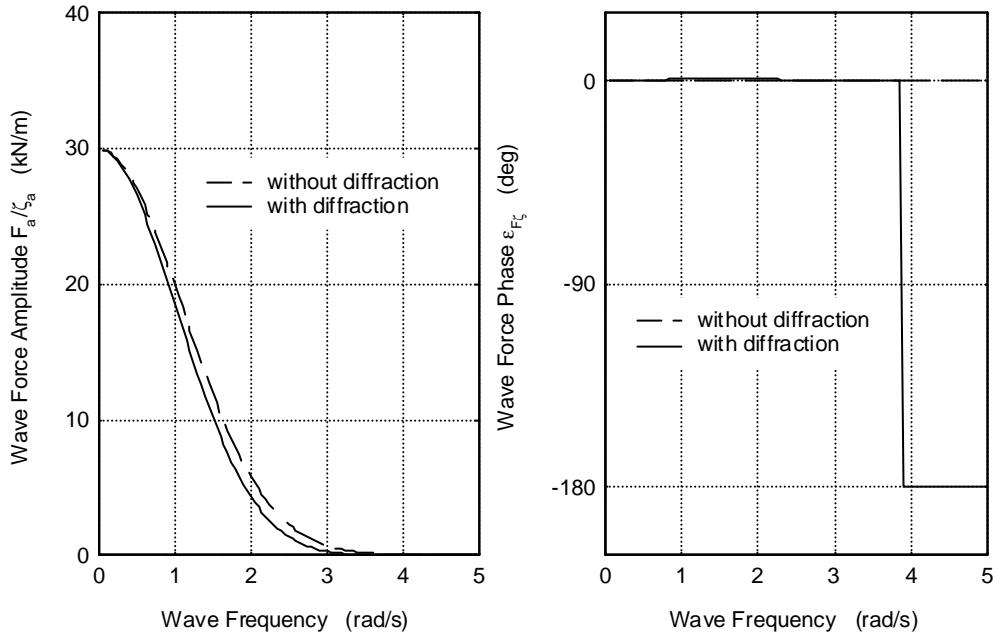
Figure 6.14: Vertical Wave Force on a Vertical Cylinder

Figure 6.14 shows the wave force amplitude and phase shift as a function of the wave frequency. For low frequencies (long waves), the diffraction part is very small and the wave force tends to the Froude-Krilov force, $c\zeta^*$. At higher frequencies there is an influence of diffraction on the wave force on this vertical cylinder. There, the wave force amplitude remains almost equal to the Froude-Krilov force.

Diffraction becomes relatively important for this particular cylinder as the Froude-Krylov force has become small; a phase shift of $-\pi$ occurs then quite suddenly. Generally, this happens the first time as the in-phase term, $F_a\cos(\varepsilon_{F\zeta})$, changes sign (goes through zero); a with ω decreasing positive Froude-Krylov contribution and a with ω increasing negative diffraction contribution (hydrodynamic mass times fluid acceleration), while the out-of-phase diffraction term (hydrodynamic damping times fluid velocity), $F_a\sin(\varepsilon_{F\zeta})$, maintains its sign.

6.3.4   Equation of Motion

Equation 6.23: $m\ddot{z} = F_h + F_w$ can be written as: $m\ddot{z} - F_h = F_w$. Then, the solid mass term and the hydromechanic loads in the left hand side (given in equation 6.25) and the

exciting wave loads in the right hand side (given in equation 6.62) provides the equation of motion for this heaving cylinder in waves:

$$\boxed{(m+a)\,\ddot{z} + b\dot{z} + cz = a\ddot{\zeta}^* + b\dot{\zeta}^* + c\zeta^*} \tag{6.69}$$

Using the relative motion principle, this equation can also be found directly from Newton's second law and the total relative motions of the water particles ($\ddot{\zeta}^*$, $\dot{\zeta}^*$ and ζ^*) of the heaving cylinder in waves:

$$m\ddot{z} = a\left(\ddot{\zeta}^* - \ddot{z}\right) + b\left(\dot{\zeta}^* - \dot{z}\right) + c\left(\zeta^* - z\right) \tag{6.70}$$

In fact, this is also a combination of the equations 6.25 and 6.62.

6.3.5   Response in Regular Waves

The heave response to the regular wave excitation is given by:

$$\begin{aligned}
z &= z_a \cos(\omega t + \varepsilon_{z\zeta}) \\
\dot{z} &= -z_a \omega \sin(\omega t + \varepsilon_{z\zeta}) \\
\ddot{z} &= -z_a \omega^2 \cos(\omega t + \varepsilon_{z\zeta})
\end{aligned} \tag{6.71}$$

A substitution of 6.71 and 6.63 in the equation of motion 6.69 yields:

$$\begin{aligned}
z_a \left\{c - (m+a)\,\omega^2\right\} \cos(\omega t + \varepsilon_{z\zeta}) - z_a \left\{b\omega\right\} \sin(\omega t + \varepsilon_{z\zeta}) = \\
= \zeta_a e^{-kT} \left\{c - a\omega^2\right\} \cos(\omega t) - \zeta_a e^{-kT} \left\{b\omega\right\} \sin(\omega t)
\end{aligned} \tag{6.72}$$

or after splitting the angle $(\omega t + \varepsilon_{z\zeta})$ and writing the out-of-phase term and the in-phase term separately:

$$\begin{aligned}
z_a \left\{\left\{c - (m+a)\,\omega^2\right\} \cos(\varepsilon_{z\zeta}) - \left\{b\omega\right\} \sin(\varepsilon_{z\zeta})\right\} & \quad \cos(\omega t) \\
-z_a \left\{\left\{c - (m+a)\,\omega^2\right\} \sin(\varepsilon_{z\zeta}) + \left\{b\omega\right\} \cos(\varepsilon_{z\zeta})\right\} & \quad \sin(\omega t) = \\
= \zeta_a e^{-kT} \left\{c - a\omega^2\right\} & \quad \cos(\omega t) \\
-\zeta_a e^{-kT} \left\{b\omega\right\} & \quad \sin(\omega t)
\end{aligned} \tag{6.73}$$

By equating the two out-of-phase terms and the two in-phase terms, one obtains two equations with two unknowns:

$$\begin{aligned}
z_a \left\{\left\{c - (m+a)\,\omega^2\right\} \cos(\varepsilon_{z\zeta}) - \left\{b\omega\right\} \sin(\varepsilon_{z\zeta})\right\} &= \zeta_a e^{-kT} \left\{c - a\omega^2\right\} \\
z_a \left\{\left\{c - (m+a)\,\omega^2\right\} \sin(\varepsilon_{z\zeta}) + \left\{b\omega\right\} \cos(\varepsilon_{z\zeta})\right\} &= \zeta_a e^{-kT} \left\{b\omega\right\}
\end{aligned} \tag{6.74}$$

Adding the squares of these two equations results in the heave amplitude:

$$\boxed{\frac{z_a}{\zeta_a} = e^{-kT} \sqrt{\frac{\left\{c - a\omega^2\right\}^2 + \left\{b\omega\right\}^2}{\left\{c - (m+a)\,\omega^2\right\}^2 + \left\{b\omega\right\}^2}}} \tag{6.75}$$

and elimination of $z_a/\zeta_a e^{-kT}$ in the two equations in 6.74 results in the phase shift:

$$\boxed{\varepsilon_{z\zeta} = \arctan\left\{\frac{-mb\omega^3}{\left(c - a\omega^2\right)\left\{c - (m+a)\,\omega^2\right\} + \left\{b\omega\right\}^2}\right\} \quad with : 0 \le \varepsilon_{z\zeta} \le 2\pi} \tag{6.76}$$

The phase angle $\varepsilon_{z\zeta}$ has to be determined in the correct quadrant between 0 and 2π. This depends on the signs of both the numerator and the denominator in the expression for the arctangent.

The requirements of linearity is fulfilled: the heave amplitude z_a is proportional to the wave amplitude ζ_a and the phase shift $\varepsilon_{z\zeta}$ is not dependent on the wave amplitude ζ_a.

Generally, these amplitudes and phase shifts are called:

$$\left. \begin{array}{rcl} \frac{F_a}{\zeta_a}(\omega) \text{ and } \frac{z_a}{\zeta_a}(\omega) & = & \text{amplitude characteristics} \\ \varepsilon_{F\zeta}(\omega) \text{ and } \varepsilon_{z\zeta}(\omega) & = & \text{phase characteristics} \end{array} \right\} \textbf{ frequency characteristics}$$

The response amplitude characteristics $\frac{z_a}{\zeta_a}(\omega)$ are also referred to as **Response Amplitude Operator** (RAO).
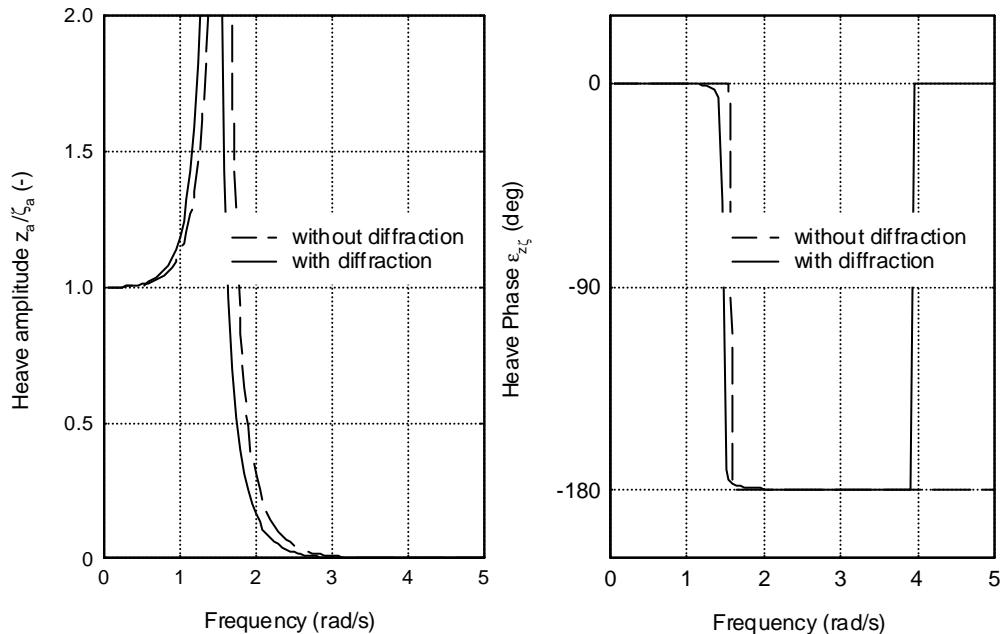
Figure 6.15: Heave Motions of a Vertical Cylinder

Figure 6.15 shows the frequency characteristics for heave together with the influence of diffraction of the waves. The annotation "without diffraction" in these figures means that the wave load consists of the Froude-Krilov force, $c\zeta^*$, only.

Equation 6.75 and figure 6.16 show that with respect to the motional behavior of this cylinder three frequency areas can be distinguished:

1. The low frequency area, $\omega^2 \ll c/(m+a)$, with vertical motions dominated by the restoring spring term.
   This yields that the cylinder tends to "follow" the waves as the frequency decreases; the RAO tends to 1.0 and the phase lag tends to zero. At very low frequencies, the wave length is large when compared with the horizontal length (diameter) of the cylinder and it will "follow" the waves; the cylinder behaves like a ping-pong ball in waves.

2. The natural frequency area, $\omega^2 \approx c/(m+a)$, with vertical motions dominated by the damping term.

   This yields that a high resonance can be expected in case of a small damping. A phase shift of $-\pi$ occurs at about the natural frequency, $\omega^2 \approx c/(m+a)$; see the denominator in equation 6.76. This phase shift is very abrupt here, because of the small damping b of this cylinder.

3. The high frequency area, $\omega^2 \gg c/(m+a)$, with vertical motions dominated by the mass term.

   This yields that the waves are "losing" their influence on the behavior of the cylinder; there are several crests and troughs within the horizontal length (diameter) of the cylinder. A second phase shift appears at a higher frequency, $\omega^2 \approx c/a$; see the denominator in equation 6.76. This is caused by a phase shift in the wave load.
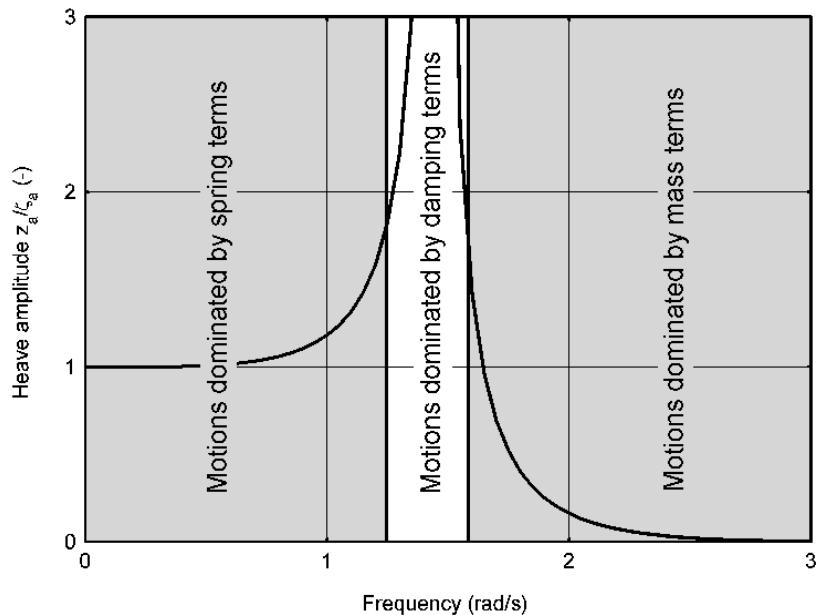
Figure 6.16: Frequency Areas with Respect to Motional Behavior

Note: From equations 6.67 and 6.75 follow also the heave motion - wave force amplitude ratio and the phase shift between the heave motion and the wave force:

$$\frac{z_a}{F_a} = \frac{1}{\sqrt{\{c - (m+a)\,\omega^2\}^2 + \{b\omega\}^2}}$$

$$\varepsilon_{zF} = \varepsilon_{z\zeta} + \varepsilon_{\zeta F} = \varepsilon_{z\zeta} - \varepsilon_{F\zeta} \qquad (6.77)$$

6.3.6   Response in Irregular Waves

The wave energy spectrum was defined in chapter 5 by:

$$S_\zeta(\omega) \cdot d\omega = \frac{1}{2}\,\zeta_a^2(\omega) \qquad (6.78)$$

Analogous to this, the energy spectrum of the heave response $z(\omega, t)$ can be defined by:

$$
\begin{aligned}
S_z(\omega) \cdot d\omega &= \frac{1}{2} z_a^2(\omega) \\
&= \left| \frac{z_a}{\zeta_a}(\omega) \right|^2 \cdot \frac{1}{2} \zeta_a^2(\omega) \\
&= \left| \frac{z_a}{\zeta_a}(\omega) \right|^2 \cdot S_\zeta(\omega) \cdot d\omega
\end{aligned}
\tag{6.79}
$$

Thus, the heave response spectrum of a motion can be found by using the **transfer function** of the motion and the wave spectrum by:

$$
\boxed{ S_z(\omega) = \left| \frac{z_a}{\zeta_a}(\omega) \right|^2 \cdot S_\zeta(\omega) }
\tag{6.80}
$$

The principle of this transformation of wave energy to response energy is shown in figure 6.17 for the heave motions being considered here.

The irregular wave history, $\zeta(t)$ - below in the left hand side of the figure - is the sum of a large number of regular wave components, each with its own frequency, amplitude and a random phase shift. The value $\frac{1}{2}\zeta_a^2(\omega)/\Delta\omega$ - associated with each wave component on the ω-axis - is plotted vertically on the left; this is the wave energy spectrum, $S_\zeta(\omega)$. This part of the figure can be found in chapter 5 as well, by the way.

Each regular wave component can be transferred to a regular heave component by a multiplication with the transfer function $z_a/\zeta_a(\omega)$. The result is given in the right hand side of this figure. The irregular heave history, $z(t)$, is obtained by adding up the regular heave components, just as was done for the waves on the left. Plotting the value $\frac{1}{2}z_a^2(\omega)/\Delta\omega$ of each heave component on the ω-axis on the right yields the heave response spectrum, $S_z(\omega)$.

The **moments** of the heave response spectrum are given by:

$$
\boxed{ m_{nz} = \int_0^\infty S_z(\omega) \cdot \omega^n \cdot d\omega } \qquad \text{with: } n = 0, 1, 2, ...
\tag{6.81}
$$

where $n = 0$ provides the area, $n = 1$ the first moment and $n = 2$ the moment of inertia of the spectral curve.

The significant heave amplitude can be calculated from the spectral density function of the heave motions, just as was done for waves. This **significant heave amplitude**, defined as the mean value of the highest one-third part of the amplitudes, is:

$$
\boxed{ \bar{z}_{a_{1/3}} = 2 \cdot RMS = 2\sqrt{m_{0z}} }
\tag{6.82}
$$

in which $RMS \; (= \sqrt{m_{0z}})$ is the **Root Mean Square** value.

A **mean period** can be found from the centroid of the spectrum:

$$
\boxed{ T_{1z} = 2\pi \cdot \frac{m_{0z}}{m_{1z}} }
\tag{6.83}
$$
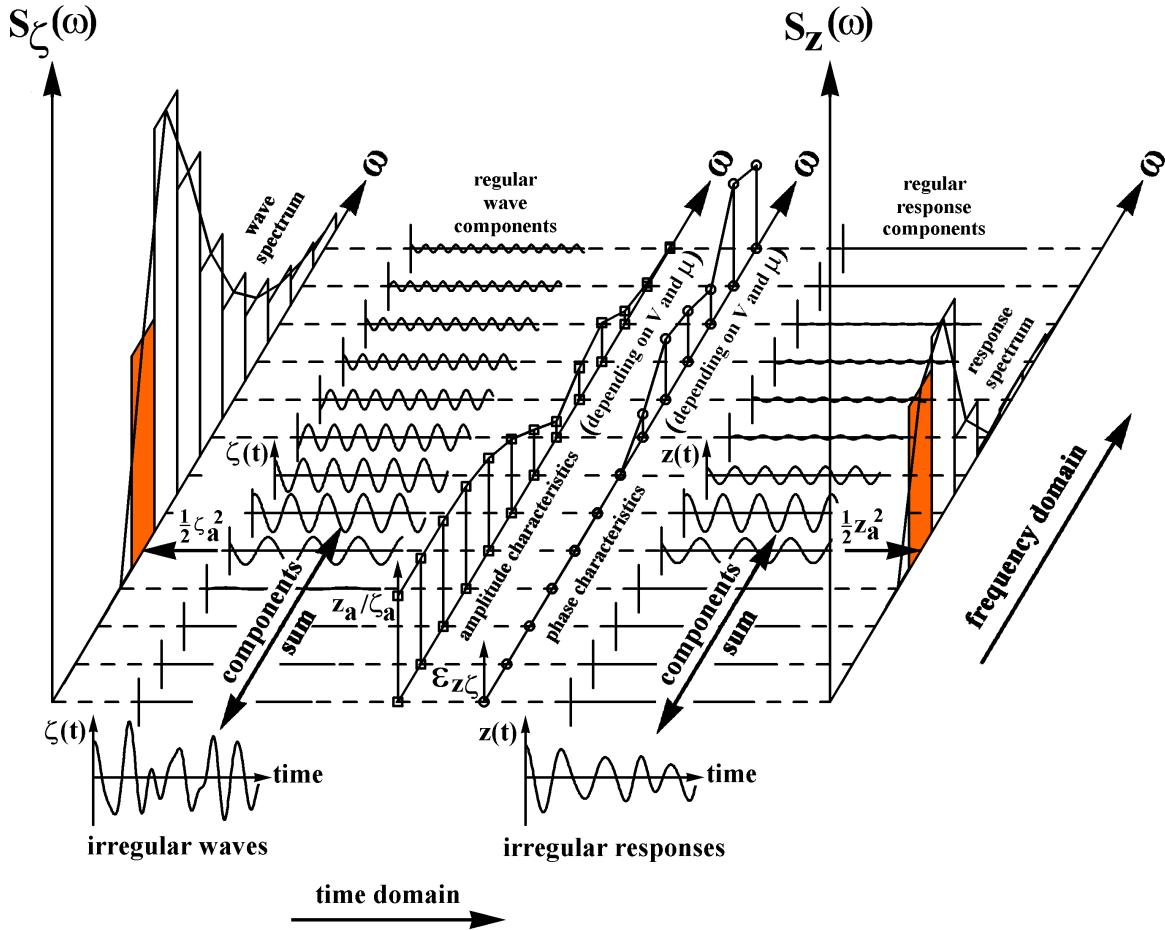
Figure 6.17: Principle of Transfer of Waves into Responses

Another definition, which is equivalent to the **average zero-crossing period**, is found from the spectral radius of gyration:

$$\boxed{T_{2z} = 2\pi \cdot \sqrt{\frac{m_{0z}}{m_{2z}}}} \tag{6.84}$$

6.3.7   Spectrum Axis Transformation

When wave spectra are given as a function of frequencies in Herz ($f = 1/T$) and one needs this on an ω-basis (in radians/sec), they have to be transformed just as was done for waves in chapter 5. The heave spectrum on this ω-basis becomes:

$$
\begin{aligned}
S_z(\omega) &= \frac{S_z(f)}{2\pi} \\
&= \left| \frac{z_a}{\zeta_a}(f \text{ or } \omega) \right|^2 \cdot \frac{S_\zeta(f)}{2\pi}
\end{aligned}
\tag{6.85}
$$

6.4   Second Order Wave Drift Forces

Now that the first order behavior of linear (both mechanical as well as hydromechanical) systems has been handled, attention in the rest of this chapter shifts to nonlinear systems. Obviously hydrodynamics will get the most emphasis in this section, too.

The effects of second order wave forces are most apparent in the behavior of anchored or moored floating structures. In contrast to what has been handled above, these are horizontally restrained by some form of mooring system. Analyses of the horizontal motions of moored or anchored floating structures in a seaway show that the responses of the structure on the irregular waves include three important components:

1. A mean displacement of the structure, resulting from a constant load component. Obvious sources of these loads are current and wind. In addition to these, there is also a so-called **mean wave drift force**. This drift force is caused by non-linear (second order) wave potential effects. Together with the mooring system, these loads determine the new equilibrium position - possibly both a translation and (influenced by the mooring system) a yaw angle - of the structure in the earth-bound coordinate system. This yaw is of importance for the determination of the wave attack angle.

2. An oscillating displacement of the structure at frequencies corresponding to those of the waves; the wave-frequency region.
   These are linear motions with a harmonic character, caused by the **first order wave loads**. The principle of this has been presented above for the vertically oscillating cylinder. The time-averaged value of this wave load and the resulting motion component are zero.

3. An oscillating displacement of the structure at frequencies which are much lower than those of the irregular waves; the low-frequency region.
   These motions are caused by non-linear elements in the wave loads, the **low-frequency wave drift forces**, in combination with spring characteristics of the mooring system. Generally, a moored ship has a low natural frequency in its horizontal modes of motion as well as very little damping at such frequencies. Very large motion amplitudes can then result at resonance so that a major part of the ship's dynamic displacement (and resulting loads in the mooring system) can be caused by these low-frequency excitations.

Item 2 of this list has been discussed in earlier parts of this chapter; the discussion of item 1 starts below; item 3 is picked up later in this chapter and along with item 1 again in chapter 9.

6.4.1   Mean Wave Loads on a Wall

Mean wave loads in regular waves on a wall can be calculated simply from the pressure in the fluid, now using the more complete (not-linearized!) Bernoulli equation. The superposition principle can still be used to determine these loads in irregular waves. When the waves are not too long, this procedure can be used, too, to estimate the mean wave drift forces on a ship in beam waves (waves approaching from the side of the ship).

Regular Waves

A regular wave (in deep water) hits a vertical wall with an infinite depth as shown in figure 6.18. This wave will be reflected fully, so that a standing wave (as described in chapter 5) results at the wall.
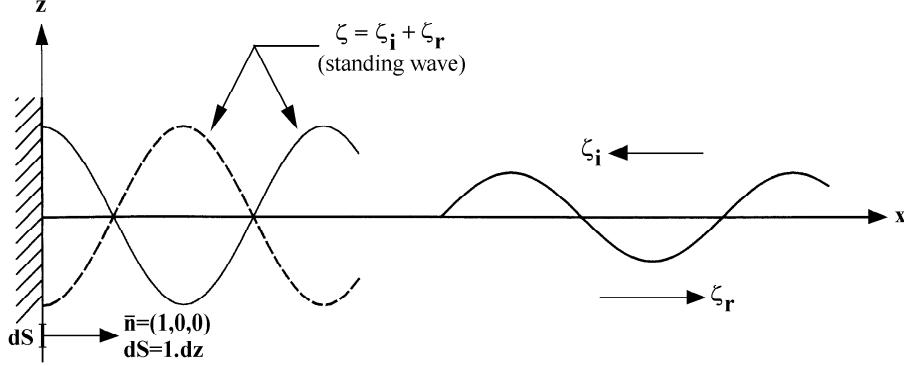
Figure 6.18: Regular Wave at a Wall

The incident undisturbed wave is defined by:

$$\boxed{\Phi_i = -\frac{\zeta_a g}{\omega} \cdot e^{kz} \cdot \sin(+kx + \omega t)} \quad \text{and} \quad \overline{\underline{|\zeta_i = \zeta_a \cdot \cos(+kx + \omega t)|}} \tag{6.86}$$

and the reflected wave by:

$$\boxed{\Phi_r = -\frac{\zeta_a g}{\omega} \cdot e^{kz} \cdot \sin(-kx + \omega t)} \quad \text{and} \quad \overline{\underline{|\zeta_r = \zeta_a \cdot \cos(-kx + \omega t)|}} \tag{6.87}$$

Then the total wave system can be determined by a superposition of these two waves; this results in a standing wave system:

$$\begin{aligned}
\Phi &= \Phi_i + \Phi_r = -2 \cdot \frac{\zeta_a g}{\omega} \cdot e^{kz} \cdot \cos(kx) \cdot \sin(\omega t) \\
\zeta &= \zeta_i + \zeta_r = 2 \cdot \zeta_a \cdot \cos(kx) \cdot \cos(\omega t)
\end{aligned} \tag{6.88}$$

The pressure in the fluid follows from the complete Bernoulli equation:

$$\begin{aligned}
p &= -\rho g \cdot z - \rho \cdot \frac{\partial \Phi}{\partial t} - \frac{1}{2}\rho \cdot (\nabla\Phi)^2 \\
&= -\rho g \cdot z - \rho \cdot \frac{\partial \Phi}{\partial t} - \frac{1}{2}\rho \cdot \left\{ \left(\frac{\partial \Phi}{\partial x}\right)^2 + \left(\frac{\partial \Phi}{\partial z}\right)^2 \right\}
\end{aligned} \tag{6.89}$$

The derivatives of the potential $\Phi(x, z, t)$ with respect to t, x and z are given by:

$$\begin{aligned}
\frac{\partial \Phi}{\partial t} &= -2 \cdot \zeta_a \cdot g \cdot e^{kz} \cdot \cos(kx) \cdot \cos(\omega t) \\
u = \frac{\partial \Phi}{\partial x} &= +2 \cdot \zeta_a \cdot \omega \cdot e^{kz} \cdot \sin(kx) \cdot \sin(\omega t) \\
w = \frac{\partial \Phi}{\partial z} &= -2 \cdot \zeta_a \cdot \omega \cdot e^{kz} \cdot \cos(kx) \cdot \sin(\omega t)
\end{aligned} \tag{6.90}$$

At the wall $(x = 0)$, the wave elevation and the derivatives of the potential are:

$$
\begin{aligned}
\zeta &= 2 \cdot \zeta_a \cdot \cos(\omega t) \\
\frac{\partial \Phi}{\partial t} &= -2 \cdot \zeta_a \cdot g \cdot e^{kz} \cdot \cos(\omega t) \\
u = \frac{\partial \Phi}{\partial x} &= 0 \\
w = \frac{\partial \Phi}{\partial z} &= -2 \cdot \zeta_a \cdot \omega \cdot e^{kz} \cdot \sin(\omega t)
\end{aligned}
\tag{6.91}
$$

and the pressure on the wall is:

$$
\begin{aligned}
p &= -\rho g \cdot z - \rho \cdot \frac{\partial \Phi}{\partial t} - \frac{1}{2}\rho \cdot \left\{ \left(\frac{\partial \Phi}{\partial x}\right)^2 + \left(\frac{\partial \Phi}{\partial z}\right)^2 \right\} \\
&= -\rho g \cdot z + 2\rho g \cdot \zeta_a \cdot e^{kz} \cdot \cos(\omega t) - \frac{1}{2}\rho \cdot \left(4\zeta_a{}^2 \cdot \omega^2 \cdot e^{2kz} \sin^2(\omega t)\right) \\
&= -\rho g \cdot z + 2\rho g \cdot \zeta_a \cdot e^{kz} \cdot \cos(\omega t) - \rho \cdot \zeta_a{}^2 \cdot \omega^2 \cdot e^{2kz} \cdot (1 - \cos(2\omega t)) \tag{6.92}
\end{aligned}
$$

This time-varying pressure on the wall can also be written as:

$$
p = \bar{p}^{(0)} + \tilde{p}^{(1)} + \bar{p}^{(2)} + \tilde{p}^{(2)} \tag{6.93}
$$

where:

$$
\begin{aligned}
\bar{p}^{(0)} &= -\rho g \cdot z \\
\tilde{p}^{(1)} &= +2\rho g \cdot \zeta_a \cdot e^{kz} \cdot \cos(\omega t) \\
\bar{p}^{(2)} &= -\rho \cdot \zeta_a{}^2 \cdot \omega^2 \cdot e^{2kz} \\
\tilde{p}^{(2)} &= +\rho \cdot \zeta_a{}^2 \cdot \omega^2 \cdot e^{2kz} \cdot \cos(2\omega t) \tag{6.94}
\end{aligned}
$$

The general expression for the mean force on the wall follows from:

$$
\overline{F} = -\overline{\int_{-\infty}^{\zeta} (\bar{p} \cdot \bar{n}) \cdot dS} \tag{6.95}
$$

where the superscript bar over the entire integral indicates a (long) time average. Because $\bar{n} = (1, 0, 0)$ and $dS = 1 \cdot dz$, this mean force becomes:

$$
\bar{F} = -\overline{\int_{-\infty}^{\zeta(t)} p(z, t) \cdot dz} \tag{6.96}
$$

which is split into two parts over the vertical axis; one above and one below the still water level:

$$
\bar{F} = -\overline{\int_{-\infty}^{0} p(z, t) \cdot dz} - \overline{\int_{0}^{\zeta(t)} p(z, t) \cdot dz} \tag{6.97}
$$

$$
= \overline{F_1} + \overline{F_2} \tag{6.98}
$$

where:
$$p(z,t) = \bar{p}^{(0)} + \tilde{p}^{(1)} + \bar{p}^{(2)} + \tilde{p}^{(2)} \qquad \text{and} \qquad \zeta(t) = \tilde{\zeta}^{(1)}(t) \tag{6.99}$$

The first part $\overline{F_1}$ comes from the integration from $-\infty$ to 0; it contributes to the integration of $\bar{p}^{(0)}$ and $\bar{p}^{(2)}$ only:

$$
\begin{aligned}
\overline{F_1} &= -\overline{\int_{-\infty}^{0} p(z,t) \cdot dz} \\
&= -\int_{-\infty}^{0} \left(-\rho g z - \rho \cdot \zeta_a{}^2 \cdot \omega^2 \cdot e^{2kz} \right) \cdot dz \\
&= \rho \cdot \omega^2 \cdot \zeta_a{}^2 \int_{-\infty}^{0} e^{2kz} \cdot dz \\
&= +\frac{1}{2}\rho g \cdot \zeta_a{}^2 \tag{6.100}
\end{aligned}
$$

This force is directed away from the wall. The static first term $(-\rho g z)$ has been left out of consideration, while the dispersion relation for deep water $(\omega^2 = kg)$ has been utilized in the second term.

The second part, $\overline{F_2}$, comes from the integration from 0 to $\zeta(t)$; it contributes to the integration of $\bar{p}^{(0)}$ and $\tilde{p}^{(1)}$ only, so that the time-dependent force $F_2(t)$ becomes:

$$
\begin{aligned}
F_2(t) &= -\int_{0}^{\zeta(t)} p(z,t) \cdot dz \\
&= -\int_{0}^{\zeta(t)} \left(-\rho g \cdot z + \rho g \cdot \zeta(t) \right) \cdot dz \\
&= +\rho g \int_{0}^{\zeta(t)} z \cdot dz \;-\; \rho g \int_{0}^{\zeta(t)} \zeta(t) \cdot dz \\
&= +\frac{1}{2}\rho g \cdot \{\zeta(t)\}^2 - \rho g \cdot \{\zeta(t)\}^2 \\
&= -\frac{1}{2}\rho g \cdot \{\zeta(t)\}^2 \tag{6.101}
\end{aligned}
$$

Because
$$\zeta(t) = 2 \cdot \zeta_a \cdot \cos(\omega t) \qquad \text{and} \qquad \cos^2(\omega t) = \frac{1}{2} \cdot (1 + \cos(2\omega t)) \tag{6.102}$$

this part of the force becomes:

$$
\begin{aligned}
F_2(t) &= -\frac{1}{2}\rho g \cdot 4 \cdot \zeta_a{}^2 \cdot \cos^2(\omega t) \\
&= -\rho g \cdot \zeta_a{}^2 \cdot (1 + \cos(2\omega t)) \tag{6.103}
\end{aligned}
$$
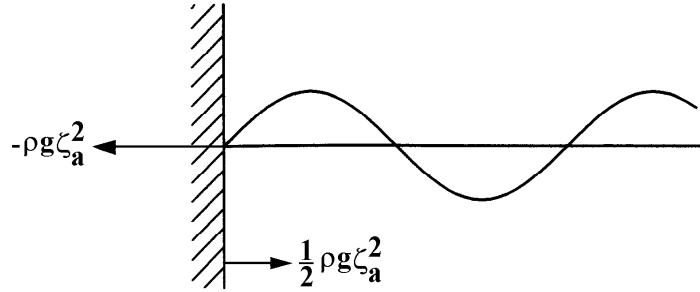
Figure 6.19: Mean Wave Loads on a Wall

The desired time-averaged value becomes:

$$\overline{F_2} = -\rho g \cdot \zeta_a{}^2 \tag{6.104}$$

where ζ_a is the amplitude of the incoming wave. This force is directed toward the wall. Finally, see figure 6.19, the total time-averaged force $\bar{F}$ per meter length of the wall becomes:

$$\begin{aligned} \bar{F} &= \overline{F_1} + \overline{F_2} \\ &= +\frac{1}{2}\rho g \cdot \zeta_a{}^2 - \rho g \cdot \zeta_a{}^2 \end{aligned} \tag{6.105}$$

Thus:

$$\boxed{\bar{F} = -\frac{1}{2}\rho g \cdot \zeta_a{}^2} \tag{6.106}$$

in which it is assumed that the incident wave is fully reflected. This total force has a magnitude proportional to the square of the incoming wave amplitude and it is directed toward the wall.

Note that this force is also directly related to the energy per unit area of the incoming waves as found in chapter 5:

$$E = \frac{1}{2}\rho g \cdot \zeta_a^2 \tag{6.107}$$

Comparison of equations 6.106 and 6.107 reveals that the mean wave drift force is numerically equal to the energy per unit area of the incoming waves.

Irregular Waves

The discovery just made above will be utilized to determine the mean wave drift force from irregular waves as well. This is done via the wave spectrum, defined by:

$$S_\zeta(\omega) \cdot d\omega = \frac{1}{2}\zeta_a{}^2(\omega) \quad \text{with a zero order moment: } m_0 = \int\limits_0^\infty S_\zeta(\omega) \cdot d\omega \tag{6.108}$$

Then the total force on the wall can be written as:

$$\bar{F} = -\sum \frac{1}{2}\rho g \cdot \zeta_a{}^2(\omega)$$

$$= -\rho g \int\limits_0^\infty S_\zeta(\omega) \cdot d\omega$$

$$= -\rho g \cdot m_{0\zeta} \tag{6.109}$$

Because:

$$H_{1/3} = 4\sqrt{m_{0\zeta}} \quad \text{or} \quad m_{0\zeta} = \frac{1}{16} \cdot H_{1/3}{}^2 \tag{6.110}$$

it follows that the mean wave drift force can be expressed as:

$$\boxed{\bar{F} = \frac{-1}{16} \cdot \rho g \cdot H_{1/3}{}^2} \quad \text{per metre length of the wall} \tag{6.111}$$

Approximation for Ships

It has been assumed so far that the incident wave is fully reflected. When the waves are not too long, so that the water motion is more or less concentrated near the sea surface (over the draft of the ship), full reflection can be assumed for large ships too. Then, equation 6.111 can be used for a first estimation of the mean wave drift forces on a ship in beam waves.

The mean wave drift force on an example ship with a length L of 300 meters in beam waves with a significant wave height $H_{1/3}$ of 4.0 meters can be approximated easily. **Assuming that all waves will be reflected**, the mean wave drift force is:

$$\begin{aligned} \bar{F} &= \frac{1}{16} \cdot \rho g \cdot H_{1/3}{}^2 \cdot L \\ &= \frac{1}{16} \cdot 1.025 \cdot 9.806 \cdot 4.0^2 \cdot 300 \approx 3000 \text{ kN} \end{aligned} \tag{6.112}$$

6.4.2   Mean Wave Drift Forces

[Maruo, 1960] showed for the two-dimensional case of an infinitely long cylinder floating in regular waves with its axis perpendicular to the wave direction that the mean wave drift force per unit length satisfies:

$$\boxed{\bar{F}' = \frac{1}{2}\rho g \cdot \zeta_{ar}{}^2} \tag{6.113}$$

in which ζ_{ar} is the amplitude of the wave reflected and scattered by the body in a direction opposite to the incident wave.

Generally only a part of the incident regular wave will be reflected; the rest will be transmitted underneath the floating body. Besides the reflected wave, additional waves are generated by the heave, pitch and roll motions of the vessel. The reflected and scattered waves have the same frequency as the incoming wave, so that the sum of these components still has the same frequency as the incoming wave. Their amplitudes will depend on the amplitudes and relative phases of the reflected and scattered wave components. The amplitudes of these components and their phase differences depend on the frequency of the incident wave, while the amplitudes can be assumed to be linearly proportional to the amplitude of the incident wave. This is because it is the incident wave amplitude which causes the body to move in the first place. In equation form:

$$\zeta_{ar} = R(\omega) \cdot \zeta_a \tag{6.114}$$

in which $R(\omega)$ is a reflection coefficient.

This means that the mean wave drift force in regular waves per meter length of the cylinder can be written as:

$$F_d' = \frac{1}{2}\rho g \cdot \{R(\omega) \cdot \zeta_a\}^2 \qquad (6.115)$$

This expression indicates that the mean wave drift force is proportional to the incident wave amplitude squared. Note that in case of the previously discussed wall: $R(\omega) = 1.0$.

6.4.3 Low-Frequency Wave Drift Forces

[Hsu and Blenkarn, 1970] and [Remery and Hermans, 1971] studied the phenomenon of the mean and slowly varying wave drift forces in a random sea from the results of model tests with a rectangular barge with breadth B. It was moored in irregular head waves to a fixed point by means of a bow hawser. The wave amplitudes provide information about the slowly varying **wave envelope** of an irregular wave train. The wave envelope is an imaginary curve joining successive wave crests (or troughs); the entire water surface motion takes place with the area enclosed by these two curves.

It seems logical in the light of the earlier results to expect that the square of the envelope amplitude will provide information about the drift forces in irregular waves. To do this, one would (in principle) make a spectral analysis of the square of this wave envelope. In other words, the spectral density of the square of the wave amplitude provides information about the mean period and the magnitude of the slowly varying wave drift force.

In practice it is very difficult to obtain an accurate wave envelope spectrum due to the long wave record required. Assuming that about 200-250 oscillations are required for an accurate spectral analysis and that the mean period of the wave envelope record is about 100 seconds, the total time that the wave elevation has to be recorded can be up to 7 hours.

Another very simple method is based on individual waves in an irregular wave train. Assume that the irregular wave train is made up of a sequence of single waves of which the wave amplitude is characterized by the height of a wave crest or the depth of a wave trough, ζ_{ai}, while the period, T_i, (or really half its value) is determined by the two adjacent zero crossings (see figure 6.20).
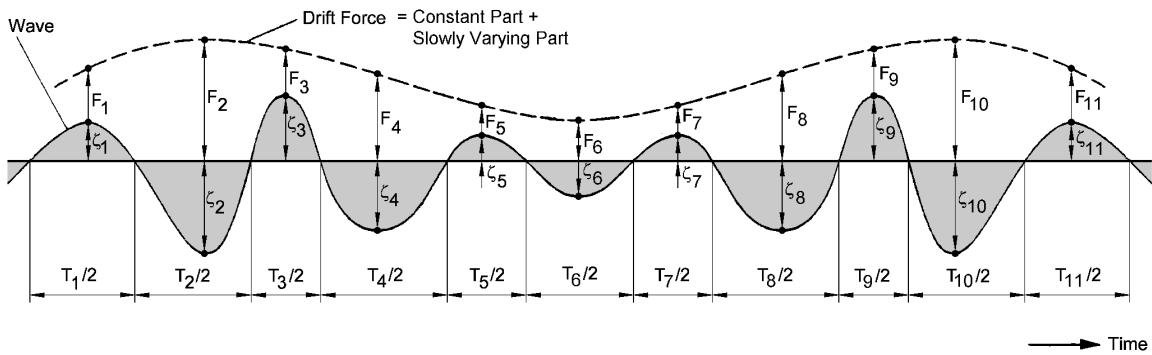
Figure 6.20: Wave Drift Forces Obtained from a Wave Record

Each of the so obtained single waves (one for every crest or trough) is considered to be one out of a regular wave train, which exerts (in this case) a surge drift force on the barge:

$$F_i = \frac{1}{2}\rho g \cdot \{R(\omega_i) \cdot \zeta_{ai}\}^2 \cdot B \qquad \text{with:} \quad \omega_i = \frac{2\pi}{T_i} \tag{6.116}$$

When this is done for all wave crests and troughs in a wave train, points on a curve representing a slowly varying wave drift force, $F(t)$, will be obtained. This drift force consists of a slowly varying force (the low-frequency wave drift force) around a mean value (the mean wave drift force); see figure 6.20.
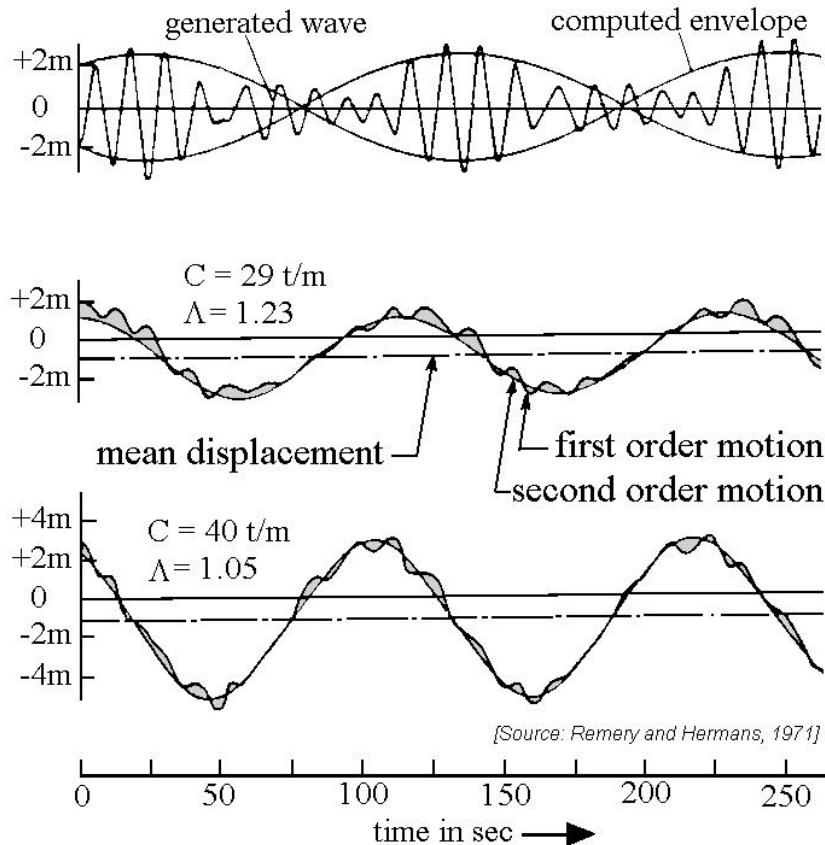
Figure 6.21: Low-Frequency Surge Motions of a Barge

These low-frequency wave drift forces on the barge will induce low-frequency surge motions with periods of for instance over 100 seconds. An example is given in figure 6.21 for two different spring constants, C. The period ratio, Λ, in this figure is the ratio between the natural surge period of the system (ship plus mooring) and the wave envelope period. (Another term for the wave envelope period is **wave group period**.) As can be seen in this figure the first order (wave-frequency) surge motions are relatively small, when compared with the second order (low-frequency) motions. This becomes especially true near resonance (when $\Lambda \to 1.0$).

Resonance may occur when wave groups are present with a period in the vicinity of the natural period of the mooring system. Due to the low natural frequency for surge of the bow hawser - barge system and the low damping at this frequency, large surge motions can

result. According to [Remery and Hermans, 1971], severe horizontal motions can be built up within a time duration of only a few consecutive wave groups. Obviously, information about the occurrence of wave groups will be needed to predict this response. This is a matter for oceanographers.

6.4.4   Additional Responses

The table below summarizes possible responses of a system (such as a moored vessel) to regular and irregular waves. Both linear and nonlinear mooring systems are included here; mooring systems can be designed to have nearly linear characteristics, but most are at least a bit nonlinear.

The right hand side of the table below gives the motions which are possible via each of the 'paths' from left to right. There will always be first order response to first order excitations; these have been discussed already as has the response of a linear or non-linear system to higher order excitations.

Wave	Excitation	System	Response
Regular	First order	Linear	First order (single frequency)
Regular	First order	Nonlinear	Subharmonic (single low frequency)
Regular	Higher order	Linear	Time-independent drift
Regular	Higher order	Nonlinear	Time-independent drift
Irregular	First order	Linear	First order (wave frequencies)
Irregular	First order	Nonlinear	Subharmonic (uncertain)
Irregular	Higher order	Linear	Time-dependent drift
Irregular	Higher order	Nonlinear	Time-dependent drift

Subharmonic Response

One path in the table above has not been discussed yet. This involves a subharmonic response of a nonlinear system to a first order excitation from either regular or irregular waves. The response, itself, looks much like the response to slow drift forces; these two are difficult indeed to distinguish. Luckily perhaps, a significant time is needed to build up

subharmonic resonant motions of high amplitude. This implies that the excitation must remain very nicely behaved over quite some time in order for this to happen. Waves at sea are very often too irregular; this subharmonic motion breaks down before large amplitudes are generated.

6.5   Time Domain Approach

If (as has been assumed so far in most of this chapter) the system is linear, such that its behavior is linearly related to its displacement, velocity and acceleration, then the behavior of the system can be studied in the frequency domain.

However, in a lot of cases there are several complications which violate this linear assumption, for instance nonlinear viscous damping, forces and moments due to currents, wind, anchoring and not to mention second order wave loads. If the system is nonlinear, then superposition principle - the foundation of the frequency domain approach - is no longer valid. Instead, one is forced to revert to the direct solution of the equations of motion as functions of time. These equations of motion result directly from Newton's second law. Approaches to their solution are presented in this section.

6.5.1   Impulse Response Functions

The hydromechanical reaction forces and moments, due to time varying ship motions, can be described using the classic formulation given by [Cummins, 1962]. Complex potential problems, can be handled via frequency-dependent potential coefficients as done by [Ogilvie, 1964]. The principle of this approach will be demonstrated here for a motion with one degree of freedom. Insight about the possibilities of this method is more important in this section than the details of the derivations involved; the result is more important than the exact route leading to it.

Cummins Equation

The floating object is assumed to be a linear system with a translational (or rotational) velocity as input and the reaction force (or moment) of the surrounding water as output. The object is assumed to be at rest at time $t = t_0$.

During a short time interval, Δt, the body experiences an impulsive displacement, Δx, with a constant velocity, V, so that:

$$\Delta x = V \cdot \Delta t \tag{6.117}$$

During this impulsive displacement, the water particles will start to move. Since potential flow is assumed, a velocity potential, Φ, proportional to the velocity, V, can be defined:

$$\Phi(x, y, z, t) = \Psi(x, y, z) \cdot V(t) \qquad \text{for: } t_0 < t < t_0 + \Delta t \tag{6.118}$$

in which Ψ is the normalized velocity potential.
Note: This Ψ is not a stream function as used in chapter 3; this notation is used here to remain consistent with other literature.

The water particles are still moving after this impulsive displacement, Δx. Because the system is assumed to be linear, the motions of the fluid, described by the velocity potential, Φ, are proportional to the impulsive displacement, Δx. So:

$$\Phi(x, y, z, t) = \chi(x, y, z, t) \cdot \Delta x \qquad \text{for: } t > t_0 + \Delta t \qquad (6.119)$$

in which χ is another normalized velocity potential.

A general conclusion can be that the impulsive displacement, Δx, during the time interval $(t_0, t_0 + \Delta t)$ influences the motions of the fluid during this interval as well as during all later time intervals. Similarly, the motions during the interval $(t_0, t_0 + \Delta t)$ are influenced by the motions before this interval; the system has a form of **"memory"**.

When the object performs an arbitrarily time-dependent varying motion, this motion can be considered to be a succession of small impulsive displacements, so that then the resulting total velocity potential, $\Phi(t)$, during the interval $(t_m, t_m + \Delta t)$ becomes:

$$\Phi(t) = V_m \cdot \Psi + \sum_{k=1}^{m} \{\chi(t_{m-k}, t_{m-k} + \Delta t) \cdot V_k \cdot \Delta t\} \qquad (6.120)$$

with:

$$
\begin{aligned}
m &= \text{number of time steps (-)} \\
t_m &= t_0 + m \cdot \Delta t \text{ (s)} \\
t_{m-k} &= t_0 + (m - k) \cdot \Delta t \text{ (s)} \\
V_m &= \text{velocity component during time interval } (t_m, t_m + \Delta t) \text{ (m/s)} \\
V_k &= \text{velocity component during time interval } (t_{m-k}, t_{m-k} + \Delta t) \text{ (m/s)} \\
\Psi &= \text{normalized velocity potential caused by a displacement} \\
&\quad \text{during time interval } (t_m, t_m + \Delta t) \\
\chi &= \text{normalized velocity potential caused by a displacement} \\
&\quad \text{during time interval } (t_{m-k}, t_{m-k} + \Delta t)
\end{aligned}
$$

Letting Δt go to zero, yields:

$$\Phi(t) = \dot{x}(t) \cdot \Psi + \int_{-\infty}^{t} \chi(t - \tau) \cdot \dot{x}(\tau) \cdot d\tau \qquad (6.121)$$

in which $\dot{x}(\tau)$ is the velocity component of the body at time τ.

The pressure in the fluid follows from the linearized Bernoulli equation:

$$p = -\rho \cdot \frac{\partial \Phi}{\partial t} \qquad (6.122)$$

An integration of these pressures over the wetted surface, S, of the floating object yields the expression for the hydrodynamic reaction force (or moment), F.

With n is the generalized directional cosine in a vector notation, F becomes:

$$
\begin{aligned}
F &= -\int\int_{S} p \cdot n \cdot dS \\
&= \left\{\rho \int\int_{S} \Psi \cdot n \cdot dS\right\} \cdot \ddot{x}(t) \\
&\quad + \int_{-\infty}^{t} \left\{\rho \int\int_{S} \frac{\partial \chi(t - \tau)}{\partial t} \cdot n \cdot dS\right\} \cdot \dot{x}(\tau) \cdot d\tau \qquad (6.123)
\end{aligned}
$$

By defining:

$$A = \rho \iint\limits_{S} \Psi \cdot n \cdot dS$$

$$B(t) = \rho \iint\limits_{S} \frac{\partial \chi(t - \tau)}{\partial t} \cdot n \cdot dS \qquad (6.124)$$

the hydrodynamic force (or moment) becomes:

$$F = A \cdot \ddot{x}(t) + \int\limits_{-\infty}^{t} B(t - \tau) \cdot \dot{x}(\tau) \cdot d\tau \qquad (6.125)$$

Together with a linear restoring spring term $C \cdot x$ and a linear external load, $X(t)$, Newton's second law yields the linear equation of motion in the time domain:

$$(M + A) \cdot \ddot{x}(t) + \int\limits_{-\infty}^{t} B(t - \tau) \cdot \dot{x}(\tau) \cdot d\tau + C \cdot x(t) = X(t) \qquad (6.126)$$

in which:

$\ddot{x}(t)$	$=$	translational (or rotational) acceleration at time t (m/s^2)
$\dot{x}(t)$	$=$	translational (or rotational) velocity in at time t (m/s)
$x(t)$	$=$	translational (or rotational) displacement at time t (m)
M	$=$	solid mass or mass moment of inertia (kg)
A	$=$	hydrodynamic (or added) mass coefficient (kg)
$B(t), B(\tau)$	$=$	retardation functions (Ns/m)
C	$=$	spring coefficient from ship geometry (N/m)
$X(t)$	$=$	external load in at time t (N)
t, τ	$=$	time (s)

By replacing "τ" by "$t - \tau$" in the damping part and changing the integration boundaries, this part can be written in a more convenient form:

$$\boxed{(M + A) \cdot \ddot{x}(t) + \int\limits_{0}^{\infty} B(\tau) \cdot \dot{x}(t - \tau) \cdot d\tau + C \cdot x(t) = X(t)} \qquad (6.127)$$

This type of equation is often referred to as a "Cummins Equation" in honor of his work; see [Cummins, 1962].

Coefficient Determination

If present, the linear restoring (hydrostatic) spring coefficient, C, can be determined easily from the underwater geometry and - when rotations are involved - the center of gravity of the floating object.
The velocity potentials, Ψ and χ, have to be found to determine the coefficients, A and B. A direct approach is rather complex. An easier method to determine A and B has

been found by [Ogilvie, 1964]. He made use of the hydrodynamic mass and damping data determined using existing frequency domain computer programs based on potential theory. This allowed him to express the needed coefficients A and B relatively simply in terms of the calculated hydrodynamic mass and damping data. His approach is developed here.
The floating object is assumed to carry out an harmonic oscillation with a unit amplitude:

$$x = 1.0 \cdot \cos(\omega t) \tag{6.128}$$

Substitution of this in the Cummins equation 6.127 yields:

$$-\omega^2 \cdot (M + A) \cdot \cos(\omega t) - \omega \cdot \int_0^\infty B(\tau) \cdot \sin(\omega t - \omega \tau) \cdot d\tau + C \cdot cos(\omega t) = X(t) \tag{6.129}$$

which can be worked out to yield:

$$-\omega^2 \cdot \quad \left\{ M + A - \frac{1}{\omega} \cdot \int_0^\infty B(\tau) \sin(\omega \tau) d\tau \right\} \cdot \cos(\omega t)$$

$$-\omega \cdot \quad \left\{ \int_0^\infty B(\tau) \cdot \cos(\omega \tau) \cdot d\tau \right\} \sin(\omega t) + \{C\} \cdot cos(\omega t) = X(t) \tag{6.130}$$

Alternatively, the classical frequency domain description of this motion is given by:

$$\begin{aligned} -\omega^2 \cdot \quad & \{M + a(\omega)\} \cdot \cos(\omega t) \\ -\omega \cdot \quad & \{b(\omega)\} \cdot \sin(\omega t) + \{c\} \cdot cos(\omega t) = X(t) \end{aligned} \tag{6.131}$$

with:

$a(\omega)$ = frequency-dependent hydrodynamic mass coefficient ($\text{Ns}^2/\text{m} = \text{kg}$)
$b(\omega)$ = frequency-dependent hydrodynamic damping coefficient (Ns/m)
c = restoring spring term coefficient (N/m)
$X(t)$ = external force (N)

[Ogilvie, 1964] compared the time domain and frequency domain equations 6.130 and 6.131 and found:

$$\begin{aligned} a(\omega) \quad &= \quad A - \frac{1}{\omega} \cdot \int_0^\infty B(\tau) \sin(\omega \tau) d\tau \\ b(\omega) \quad &= \quad \int_0^\infty B(\tau) \cdot \cos(\omega \tau) \cdot d\tau \\ c \quad &= \quad C \end{aligned} \tag{6.132}$$

The first two of these equations look very similar to those for determining the first order coefficients in a Fourier series; see appendix C. An inverse Fourier Transform can be used to isolate the desired function, $B(\tau)$; the coefficient, A, can be evaluated directly with a bit of algebra.

This yields the so-called **retardation function**:

$$B(\tau) = \frac{2}{\pi} \cdot \int\limits_0^\infty b(\omega) \cdot \cos(\omega\tau) \cdot d\omega \qquad (6.133)$$

The mass term is simply:

$$A = a(\omega) + \frac{1}{\omega} \cdot \int\limits_0^\infty B(\tau) \cdot \sin(\omega\tau) \cdot d\tau \qquad (6.134)$$

This expression is valid for any value of ω, and thus also for $\omega = \infty$; this provides:

$$A = a(\omega) \quad \text{evaluated at } \omega = \infty \qquad (6.135)$$

The numerical computational problems that have to be solved, because the integrations have to be carried out from 0 to ∞, are not discussed here.

Figure 6.22, is an example of the retardation function for roll of a ship.
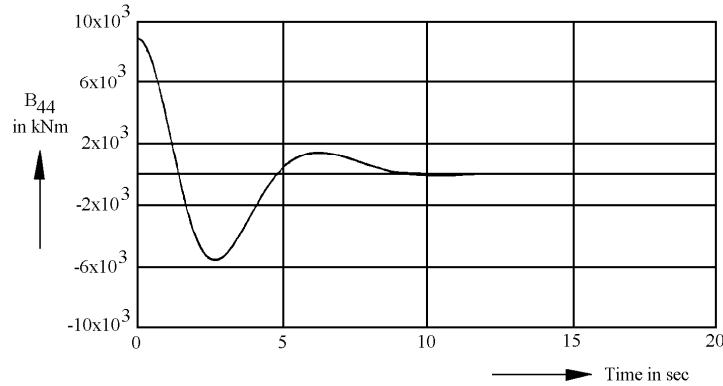
Figure 6.22: Retardation Function for Roll

Addition of (External) Loads

So far, discussion has concentrated on the left hand side of equation 6.127. Notice that this part of the equation is still linear!

Attention shifts now to the right hand side, the external force $X(t)$. Since it can be convenient to keep the left hand side of the equation of motion linear, one often moves all the nonlinear effects - even a nonlinear damping or spring force - to the opposite side, where they are all considered to be part of the external force $X(t)$.

Obviously one will have to know (or at least be able to evaluate) $X(t)$ in order to obtain a solution to the equation of motion.

Since the first order wave force is a linear phenomenon, time histories of the first order wave loads in a certain sea state can be obtained from frequency domain calculations by using the frequency characteristics of the first order wave loads and the wave spectrum by using the superposition principle:

$$\zeta(t) = \sum_{n=1}^N \zeta_{a_n} \cos(\omega_n t + \varepsilon_n)$$

with randomly chosen phase shifts, ε_n, between 0 and 2π and:

$$\zeta_{a_n} = \sqrt{2 \cdot S_\zeta(\omega_n) \cdot \Delta\omega} \quad \text{which follows from:} \quad \frac{1}{2}\zeta_{a_n}^2 = S_\zeta(\omega_n) \cdot \Delta\omega$$

see chapter 5.

With this, the time history of the first order wave load then becomes:

$$X_w(t) = \sum_{n=1}^{N} \left(\frac{X_{wa_n}}{\zeta_{a_n}}\right) \cdot \zeta_{a_n} \cos(\omega_n t + \varepsilon_n + \varepsilon_{X_w\zeta_n}) \tag{6.136}$$

in which:

$$
\begin{array}{rcl}
X_w(t) & = & \text{wave load (N)} \\
N & = & \text{number of frequencies (-)} \\
\omega_n & = & \text{wave frequency rad/s} \\
\frac{X_{wa_n}}{\zeta_{a_n}} & = & \text{transfer function of wave load (N/m)} \\
\varepsilon_{X_w\zeta_n} & = & \text{phase shift of wave load (rad)} \\
\varepsilon_n & = & \text{phase shift of wave (rad)}
\end{array}
$$

Note that with a constant frequency interval , $\Delta\omega$, this time history repeats itself after $2\pi/\Delta\omega$ seconds.

With known coefficients and the right hand side of this equation of motion, equation 6.127 can be integrated a numerically. Comparisons of calculated and transformed linear motions in the frequency domain with time domain results show a perfect agreement.

Validation Tests

A series of simple model experiments have been carried out to validate the time domain calculation routines with non-linear terms. Towing tank number 2 of the Delft Ship Hydromechanics Laboratory with a 1:40 model of the Oil Skimming Vessel m.v. Smal Agt (51.00 x 9.05 x 3.25 meter) was used for this. Horizontal impulse forces in the longitudinal and lateral direction have been introduced in a tow line between a torque-motor and the model in still water. The measured motions of the ship model have been compared with the data calculated in the time domain, using the measured time-series of the impulse forces and assumed points of application as an input. An example of the comparison is presented in figure 6.23 for the sway velocities due to a lateral impulse force amidships.

The figure shows a good agreement between the calculated and the measured sway motions. Comparable agreements have been found for the other tests.

A few years ago, the Centre for Applied Research in The Netherlands (TNO) carried out a series of full scale collision tests with two inland waterway tankers in still water, see figure 6.24. The contact forces between the two ships and the motions of the rammed ship (80.00 x 8.15 x 2.20 meter) were measured. Computer simulations of the motion behavior of the rammed ship during the collision have been carried out, using the measured contact forces on the rammed ship as an input.

Figure 6.25 shows some comparative results for a test with a collision of the rammed ship at about 0.40 L_{pp} from the bow on the port side. The ramming ship had a speed of about 15 km/hr. The measured and calculated motions of the rammed ship are presented. Sway, roll and yaw velocities are predicted here very well.
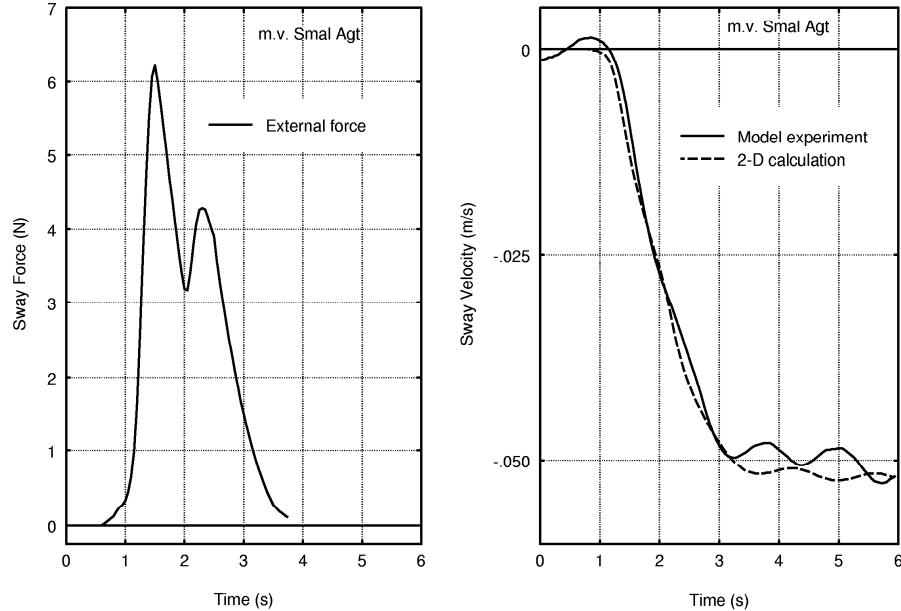
Figure 6.23: External Impulse and Resulting Motions
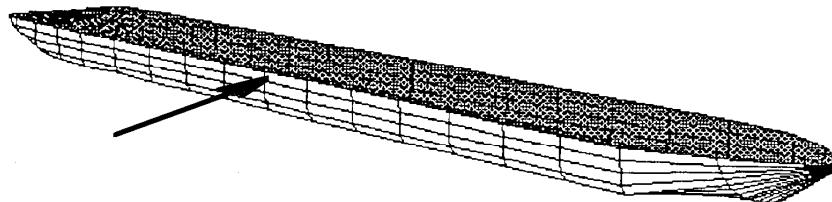
Figure 6.24: Underwater Portion of Rammed Ship

6.5.2   Direct Time Domain Simulation

Retardation functions as described above can be used to solve the equations of motion for cases in which the nonlinearities can be included in the time-dependent excitation on the right hand side of the equation. While it is possible to "move" some nonlinearities to the excitation side of the equation of motion more or less artificially, there are still many relevant physical systems which do not lend themselves to such a treatment.

One example of such a system will come up at the end of chapter 12 when the hydrodynamic drag on a moving cylinder in waves will be discussed. A perhaps more spectacular example involves the launching of an offshore tower structure from a barge. It should be obvious that the hydrodynamic mass and damping of such a structure - and of the barge from which it is launched - will change quite rapidly as the tower enters the water and load is transferred from the barge. Notice, now, that the hydromechanical coefficients - for both the tower and barge - can best be expressed as (nonlinear) *functions of the position* of the respective structures rather than of time. These functions can easily be accommodated in a time domain calculation in which all conditions can be re-evaluated at the start of each time step.
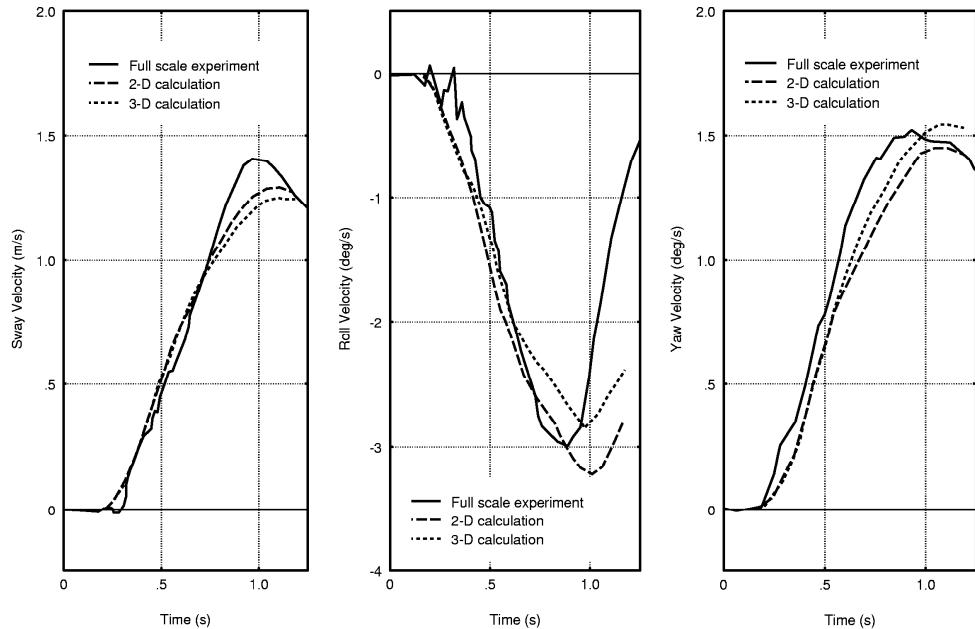
Figure 6.25: Measured and Calculated Velocities During a Ship Collision

Indeed, any system can be solved by direct integration of the equations of motion in the time domain. This approach is direct and certainly straightforward in theory, but it is often so cumbersome to carry out that it becomes impractical in practice. Admittedly, modern computers continue to shift the limits of practicality, but these limits are still very present for many offshore engineering applications.

Basic Approach

The approach is simple enough: the differential equations of motion resulting from the application of Newton's law are simply integrated - using an appropriate numerical method - in the time domain. This means that all of the input (such as a wave record) must be known as a function of time, and that a time record of the output (such as a time history of hydrodynamic force on a vibrating cable) will be generated.

Difficulties

A first and obvious difficulty with time domain simulation is that a time record of the input - such as the waves - must be provided, while generally, one only has information about the wave spectrum available. Wave records will have to be re-generated using methods as given in chapter 5.

As indicated there, by choosing different series of random phases one can generate a seemingly endless series of time records, all with identical statistical properties. There is no-one who can say which - if any - particular time record is correct. What difference does it make? The difference lies in the fact that the largest wave - very important for an extreme response, for example - may occur early in the record, or later or even not at all (during a finite record). This can have a significant influence on the interpretation of the results, of course - especially when extreme values are needed.

The interpretation of time domain simulation results forms a second difficulty in practice. A designer often needs a "design response" (an extreme dynamic internal load or displacement) with an associated (small) probability that it will be exceeded as "output" from a dynamic analysis. This interpretation difficulty is brought into focus by reviewing the process for a linear system, first.

One will generally analyze a linear system in the frequency domain; spectra of the desired response are generated directly. Since the response spectra will be of essentially the same form as the input spectra, the output can be transformed to convenient statistical data for distributions interpretation - just as is done for waves. Once this theoretical distribution has been fitted, it is a simple matter to extrapolate this to get the value associated with the chosen design probability.

When time domain simulation is used instead, one must first convert the generated time record of the output to some form of spectrum. If the system being analyzed is nonlinear, then the spectrum of the output need not look much like that of the input at all: it can contain energy at entirely different frequencies for example, so that its best representation in a mathematical form is not known. This means that one must numerically fit several theoretical forms in order to find the best one. Once this has been done, one will need to extrapolate - just as above - to a desired (low) probability of exceedance. Since the quality of this extrapolation is no better than the quality of equation fit, and the (few) computed extreme values in the generated time record disproportional influence the 'tail' of the probability distribution, one needs either very long or very many time records of the output in order to determine these extremes with sufficient accuracy. This implies that hours or even days of dynamic response will need to be simulated. Since such simulations often still run at less than real time on even fast computers, the computational effort becomes prohibitively expensive.

Constrained Time Domain Simulation

Quite some research has been invested to come to more efficient ways of carrying out a time domain simulation. Tromans has been one of the leaders in this. Since these newer methods are not yet (as of this writing) widely accepted (and the details of their mathematics would make this work significantly thicker), they will not be treated here.

Chapter 7

POTENTIAL COEFFICIENTS

7.1 Introduction

Consider a rigid body, oscillating in or below the free surface of a fluid. The fluid is assumed to be incompressible, inviscid and irrotational and without surface tension. The body is forced to carry out simple harmonic motions with a prescribed frequency of oscillation, ω. It is assumed that steady state conditions have been attained. The motion amplitudes and velocities are small enough so that all but the linear terms of the free surface condition, the kinematic boundary condition on the body and the Bernoulli equation may be neglected. The hydrodynamic pressures on the surface of the body can be obtained from the linearized Bernoulli equation, using the known velocity potentials. Integration of these pressures in the required direction provides the hydrodynamic force or moment. This force or moment can also be expressed in terms of potential mass and damping. Comparisons of the in-phase and out-of-phase parts of the two expressions provide the potential mass and damping coefficients.

This chapter details the steps needed to carry out such a computation.

7.2 Principles

Consider a rigid body floating in an ideal fluid with harmonic waves. The water depth is assumed to be finite. The time-averaged speed of the body is zero in all directions. For the sake of simple notation, it is assumed here that the $O(x, y, z)$ system is identical to the $S(x_0, y_0, z_0)$ system described in chapter 6. The x-axis is coincident with the undisturbed still water free surface and the z-axis and z_0-axis are positive upwards.

The potential theory used here will be developed (and extended) from the relations presented in chapter 5. There are a few differences, however. The velocity components (u, v, w) in chapter 5 are replaced here by (v_x, v_y, v_z) in this chapter; this is the more common notation found in the relevant literature. The wave velocity potential Φ_w in chapter 5 has been replaced here by a more general velocity potential, Φ.

The linear fluid velocity potential can be split into three parts:

$$\boxed{\Phi(x, y, z; t) = \Phi_r + \Phi_w + \Phi_d} \tag{7.1}$$

---

[0] J.M.J. Journée and W.W. Massie, *"OFFSHORE HYDROMECHANICS"*, First Edition, January 2001, Delft University of Technology. For updates see web site: http://www.shipmotions.nl.

in which:

- Φ_r = **radiation potential** from the oscillatory motion of the body in still water.

- Φ_w = incident undisturbed **wave potential.**

- Φ_d = **diffraction potential** of the waves about the restrained body.

7.2.1   Requirements

Just as in chapter 5, each of these velocity potentials has to fulfill a number of requirements and boundary conditions in the fluid. Of these, the first four are identical to those in chapter 5; only their results are presented here. Additional boundary conditions are associated with the floating body which is now present. These will be discussed in detail.

1. **Continuity Condition or Laplace Equation**

$$\boxed{\nabla^2\Phi = \frac{\partial^2\Phi}{\partial x^2} + \frac{\partial^2\Phi}{\partial y^2} + \frac{\partial^2\Phi}{\partial z^2} = 0}$$ (see chapter 5)   (7.2)

2. **Sea Bed Boundary Condition**

$$\boxed{\frac{\partial\Phi}{\partial z} = 0 \qquad \text{for: } z = -h}$$ (see chapter 5)   (7.3)

3. **Boundary Condition at the Free Surface**
   For the free surface dynamic boundary condition was found:

$$\frac{\partial\Phi}{\partial t} + g\zeta = 0 \quad \text{or} \quad \frac{\partial^2\Phi}{\partial t^2} + g\frac{\partial\zeta}{\partial t} = 0 \qquad \text{for: } z = 0 \qquad \text{(see chapter 5)} \qquad (7.4)$$

   and the vertical velocity of the water particle at $z = 0$ follows from free surface kinematic boundary condition:

$$\frac{\partial\Phi}{\partial z} = \frac{\partial\zeta}{\partial t} \qquad \text{for: } z = 0 \qquad \text{(see chapter 5)} \qquad (7.5)$$

   Combining equations 7.4 and 7.5 yields:

$$\boxed{\frac{\partial^2\Phi}{\partial t^2} + g\frac{\partial\Phi}{\partial z} = 0 \qquad for : z = 0}$$ (7.6)

   This equation is has been found already in chapter 5, when determining the Cauchy-Poisson condition in short waves (deep water). However, equation 7.6 is also valid for finite water depths.

4. **Kinematic Boundary Condition on the Oscillating Body Surface**
   The boundary condition at the surface of the rigid body, S, plays a very important role. The velocity of a water particle at a point at the surface of the body is equal to the velocity of this (watertight) body point itself. The outward normal velocity,

v_n, at a point $P(x, y, z)$ at the surface of the body (positive in the direction of the fluid) is given by:

$$\frac{\partial \Phi}{\partial n} = v_n(x, y, z; t) \tag{7.7}$$

Because the solution of the potential will be linearized, this can be written as:

$$\left| \frac{\partial \Phi}{\partial n} = v_n(x, y, z; t) = \sum_{j=1}^{6} v_j \cdot f_j(x, y, z) \right| \tag{7.8}$$

in terms of oscillatory velocities and generalized direction cosines on the surface of the body, S, given by:

$$\begin{aligned}
\text{surge}: \quad & f_1 = \cos(n, x) \\
\text{sway}: \quad & f_2 = \cos(n, y) \\
\text{heave}: \quad & f_3 = \cos(n, z) \\
\text{roll}: \quad f_4 = {} & y \cos(n, z) - z \cos(n, y) = y f_3 - z f_2 \\
\text{pitch}: \quad f_5 = {} & z \cos(n, x) - x \cos(n, z) = z f_1 - x f_3 \\
\text{yaw}: \quad f_6 = {} & x \cos(n, y) - y \cos(n, x) = x f_2 - y f_1
\end{aligned} \tag{7.9}$$

The direction cosines are called generalized, because f_1, f_2 and f_3 have been normalized (the sum of their squares is equal to 1) and used to obtain f_4, f_5 and f_6.
Note: The subscripts $1, 2, ...6$ are used here to indicate the mode of the motion. Also displacements are often indicated in literature in the same way: $x_1, x_2, ...x_6$.

5. **Radiation Condition**
   The radiation condition states that as the distance, R, from the oscillating body becomes large, the potential value tends to zero:

$$\left| \lim_{R \to \infty} \Phi = 0 \right| \tag{7.10}$$

6. **Symmetric or Anti-symmetric Condition**
   Since ships and many other floating bodies are symmetric with respect to its middle line plane, one can make use of this to simplify the potential equations:

$$\begin{array}{ll}
\left| \Phi_2(-x, y) = -\Phi_2(+x, y) \right| & \text{for sway} \\
\left| \Phi_3(-x, y) = +\Phi_3(+x, y) \right| & \text{for heave} \\
\left| \Phi_4(-x, y) = -\Phi_4(+x, y) \right| & \text{for roll}
\end{array} \tag{7.11}$$

in which Φ_i is the velocity potential for the given direction i.
This indicates that for sway and roll oscillations, the horizontal velocities of the water particles, thus the derivative $\partial \Phi / \partial x$, at any time on both sides of the body must have the same direction; these motions are anti-symmetric. For heave oscillations these velocities must be of opposite sign; this is a symmetric motion. However, for all three modes of oscillations the vertical velocities, thus the derivative $\partial \Phi / \partial y$, on both sides must have the same directions at any time.

7.2.2   Forces and Moments

The forces $\vec{F}$ and moments $\vec{M}$ follow from an integration of the pressure, p, over the submerged surface, S, of the body:

$$\vec{F} \;=\; -\iint\limits_{S} (p \cdot \vec{n}) \cdot dS$$

$$\vec{M} \;=\; -\iint\limits_{S} p \cdot (\vec{r} \times \vec{n}) \cdot dS \qquad (7.12)$$

in which $\vec{n}$ is the outward normal vector on surface dS and $\vec{r}$ is the position vector of surface dS in the $O(x, y, z)$ coordinate system.

The pressure p - via the linearized Bernoulli equation - is determined from the velocity potentials by:

$$\begin{aligned}
p \;&=\; -\rho\frac{\partial \Phi}{\partial t} - \rho g z \\
&=\; -\rho\left(\frac{\partial \Phi_r}{\partial t} + \frac{\partial \Phi_w}{\partial t} + \frac{\partial \Phi_d}{\partial t}\right) - \rho g z \qquad (7.13)
\end{aligned}$$

which can obviously be split into four separate parts, so that the hydromechanical forces $\vec{F}$ and moments $\vec{M}$ can be split into four parts too:

$$\boxed{\vec{F} = \rho\iint\limits_{S}\left(\frac{\partial \Phi_r}{\partial t} + \frac{\partial \Phi_w}{\partial t} + \frac{\partial \Phi_d}{\partial t} + g z\right)\vec{n} \cdot dS} \qquad (7.14)$$

$$\boxed{\vec{M} = \rho\iint\limits_{S}\left(\frac{\partial \Phi_r}{\partial t} + \frac{\partial \Phi_w}{\partial t} + \frac{\partial \Phi_d}{\partial t} + g z\right)(\vec{r} \times \vec{n}) \cdot dS} \qquad (7.15)$$

or:

$$\begin{aligned}
\vec{F} \;&=\; \vec{F}_r + \vec{F}_w + \vec{F}_d + \vec{F}_s \\
\vec{M} \;&=\; \vec{M}_r + \vec{M}_w + \vec{M}_d + \vec{M}_s
\end{aligned} \qquad (7.16)$$

Summarizing:

Source	Terms
Waves radiated from the oscillating body in still water	$\vec{F}_r,\ \vec{M}_r$
Approaching waves on the fixed body	$\vec{F}_w,\ \vec{M}_w$
Diffracted waves of the fixed body	$\vec{F}_d,\ \vec{M}_d$
Hydrostatic buoyancy in still water	$\vec{F}_s,\ \vec{M}_s$

These will each be discussed separately below.

7.2.3 Hydrodynamic Loads

The hydrodynamic loads are the dynamic forces and moments caused by the fluid on an oscillating body in still water; waves are radiated from the body. The **radiation potential**, Φ_r, which is associated with this oscillation in still water, can be written in terms, Φ_j, for 6 degrees of freedom as:

$$
\begin{aligned}
\Phi_r(x,y,z,t) &= \sum_{j=1}^{6} \Phi_j(x,y,z,t) \\
&= \sum_{j=1}^{6} \phi_j(x,y,z) \cdot v_j(t)
\end{aligned} \tag{7.17}
$$

in which the space and time dependent potential term, $\Phi_j(x,y,z,t)$ in direction j, is now written in terms of a separate space dependent potential, $\phi_j(x,y,z)$ in direction j, multiplied by an oscillatory velocity, $v_j(t)$ in direction j.

This allows the normal velocity on the surface of the body to be written as:

$$
\begin{aligned}
\frac{\partial \Phi_r}{\partial n} &= \frac{\partial}{\partial n} \sum_{j=1}^{6} \Phi_j \\
&= \sum_{j=1}^{6} \left\{ \frac{\partial \phi_j}{\partial n} \cdot v_j \right\}
\end{aligned} \tag{7.18}
$$

and the generalized direction cosines, as given in equation 7.9, are given by:

$$
f_j = \frac{\partial \phi_j}{\partial n} \tag{7.19}
$$

With this, the radiation term in the hydrodynamic force of equation 7.14 becomes:

$$
\begin{aligned}
\vec{F}_r &= \rho \iint_S \left(\frac{\partial \Phi_r}{\partial t} \right) \vec{n} \cdot dS \\
&= \rho \iint_S \left(\frac{\partial}{\partial t} \sum_{j=1}^{6} \phi_j v_j \right) \vec{n} \cdot dS
\end{aligned} \tag{7.20}
$$

and the moment term of equation 7.15 becomes:

$$
\begin{aligned}
\vec{M}_r &= \rho \iint_S \left(\frac{\partial \Phi_r}{\partial t} \right) (\vec{r} \times \vec{n}) \cdot dS \\
&= \rho \iint_S \left(\frac{\partial}{\partial t} \sum_{j=1}^{6} \phi_j v_j \right) (\vec{r} \times \vec{n}) \cdot dS
\end{aligned} \tag{7.21}
$$

The components of these radiation forces and moments are defined by:

$$
\vec{F}_r = (X_{r_1}, X_{r_2}, X_{r_3}) \quad \text{and} \quad \vec{M}_r = (X_{r_4}, X_{r_5}, X_{r_6}) \tag{7.22}
$$

with (see 7.19):

$$\vec{X}_{r_k} = \rho \iint\limits_S \left(\frac{\partial}{\partial t} \sum_{j=1}^{6} \phi_j v_j \right) f_k \cdot dS$$

$$= \rho \iint\limits_S \left(\frac{\partial}{\partial t} \sum_{j=1}^{6} \phi_j v_j \right) \frac{\partial \phi_k}{\partial n} \cdot dS \qquad \text{for: } k = 1, ...6 \tag{7.23}$$

Since ϕ_j and ϕ_k are not time-dependent in this expression, it reduces to:

$$\boxed{X_{r_k} = \sum_{j=1}^{6} X_{r_{kj}}} \qquad \text{for: } k = 1, ...6 \tag{7.24}$$

with:

$$\boxed{X_{r_{kj}} = \frac{dv_j}{dt} \rho \int \int\limits_S \phi_j \frac{\partial \phi_k}{\partial n} \cdot dS} \tag{7.25}$$

This radiation force or moment $X_{r_{kj}}$ in the direction k is caused by a forced harmonic oscillation of the body in the direction j. This is generally true for all j and k in the range from 1 to 6. When $j = k$, the force or moment is caused by a motion in that same direction. When $j \neq k$, the force in one direction results from the motion in another direction. This introduces what is called **coupling** between the forces and moments (or motions).

The above equation expresses the force and moment components, $X_{r_{kj}}$ in terms of still unknown potentials, ϕ_j; not everything is solved yet! A solution for this will be found later in this chapter.

Oscillatory Motion

Now an oscillatory motion is defined; suppose a motion (in a complex notation) given by:

$$\boxed{s_j = s_{a_j} e^{-i\omega t}} \tag{7.26}$$

Then the velocity and acceleration of this oscillation are:

$$\dot{s}_j = v_j = -i\omega s_{a_j} e^{-i\omega t}$$

$$\ddot{s}_j = \frac{dv_j}{dt} = -\omega^2 s_{a_j} e^{-i\omega t} \tag{7.27}$$

The hydrodynamic forces and moments can be split into a load in-phase with the acceleration and a load in-phase with the velocity:

$$X_{r_{kj}} = -M_{kj} \ddot{s}_j - N_{kj} \dot{s}_j$$

$$= \left(s_{a_j} \omega^2 M_{kj} + i s_{a_j} \omega N_{kj} \right) e^{-i\omega t}$$

$$= \left(-s_{a_j} \omega^2 \rho \iint\limits_S \phi_j \frac{\partial \phi_k}{\partial n} \cdot dS \right) e^{-i\omega t} \tag{7.28}$$

in which the last part is similar to the right hand side of equation 7.25.

So in case of an oscillation of the body in the direction j with a velocity potential ϕ_j, the hydrodynamic mass and damping (coupling)coefficients are defined by:

$$M_{kj} = -\Re e \left\{ \rho \iint_S \phi_j \frac{\partial \phi_k}{\partial n} \cdot dS \right\} \qquad \text{and} \qquad N_{kj} = -\Im m \left\{ \rho \omega \iint_S \phi_j \frac{\partial \phi_k}{\partial n} \cdot dS \right\} \quad (7.29)$$

In case of an oscillation of the body in the direction k with a velocity potential ϕ_k, the hydrodynamic mass and damping (coupling) coefficients are defined by:

$$M_{jk} = -\Re e \left\{ \rho \iint_S \phi_k \frac{\partial \phi_j}{\partial n} \cdot dS \right\} \qquad \text{and} \qquad N_{jk} = -\Im m \left\{ \rho \omega \iint_S \phi_k \frac{\partial \phi_j}{\partial n} \cdot dS \right\} \quad (7.30)$$

Green's Second Theorem

Green's second theorem transforms a large volume-integral into a much easier to handle surface-integral. Its mathematical background is beyond the scope of this text. It is valid for any potential function, regardless the fact if it fulfills the Laplace condition or not. Consider two separate velocity potentials ϕ_j and ϕ_k. Green's second theorem, applied to these potentials, is then:

$$\iiint_{V^*} \left(\phi_j \cdot \nabla^2 \phi_k - \phi_k \cdot \nabla^2 \phi_j \right) \cdot dV^* = \iint_{S^*} \left(\phi_j \frac{\partial \phi_k}{\partial n} - \phi_k \frac{\partial \phi_j}{\partial n} \right) \cdot dS^* \qquad (7.31)$$

This theorem is generally valid for all kinds of potentials; it is not necessary that they fullfil the Laplace equation.
In Green's theorem, S^* is a closed surface with a volume V^*. This volume is bounded by the wall of an imaginary vertical circular cylinder with a very large radius R, the sea bottom at $z = -h$, the water surface at $z = \zeta$ and the wetted surface of the floating body, S; see figure 7.1.
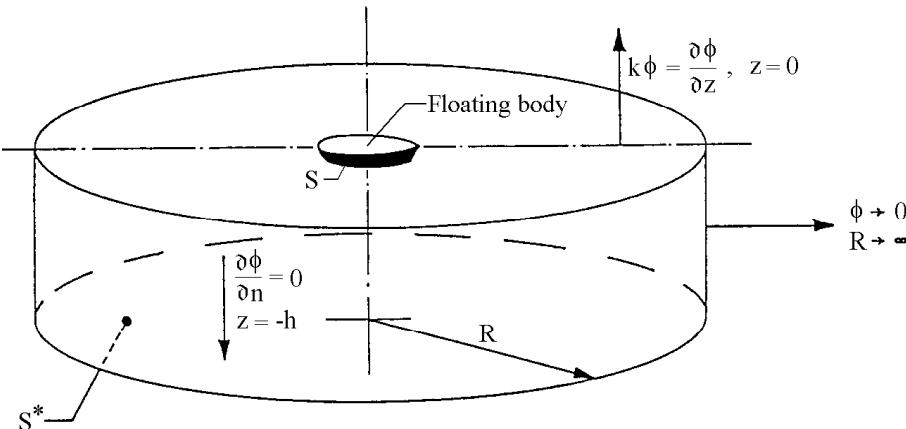
Figure 7.1: Boundary Conditions

Both of the above radiation potentials ϕ_j and ϕ_k must fulfill the Laplace equation 7.2:

$$\nabla^2 \phi_j = \nabla^2 \phi_k = 0 \tag{7.32}$$

So the left hand side of equation 7.31 becomes zero, which yields for the right hand side of equation 7.31:

$$\iint\limits_{S^*} \phi_j \frac{\partial \phi_k}{\partial n} \cdot dS^* = \iint\limits_{S^*} \phi_k \frac{\partial \phi_j}{\partial n} \cdot dS^* \tag{7.33}$$

The boundary condition at the free surface, equation 7.6, becomes for $\Phi = \phi \cdot e^{-i\omega t}$:

$$-\omega^2 \phi + g\frac{\partial \phi}{\partial z} = 0 \qquad \text{for: } z = 0 \tag{7.34}$$

or with the dispersion relation, $\omega^2/g = k \tanh kh$:

$$k \tanh kh \phi = \frac{\partial \phi}{\partial z} \qquad \text{for: } z = 0 \tag{7.35}$$

This implies that at the free surface of the fluid one can write:

$$\left. \begin{array}{l} k \tanh kh \cdot \phi_k = \frac{\partial \phi_k}{\partial z} = \frac{\partial \phi_k}{\partial n} \longrightarrow \phi_k = \frac{1}{k \tanh kh} \cdot \frac{\partial \phi_k}{\partial n} \\[2mm] k \tanh kh \cdot \phi_j = \frac{\partial \phi_j}{\partial z} = \frac{\partial \phi_j}{\partial n} \longrightarrow \phi_j = \frac{1}{k \tanh kh} \cdot \frac{\partial \phi_j}{\partial n} \end{array} \right\} \text{ at the free surface} \tag{7.36}$$

When taking also the boundary condition at the sea bed (equation 7.3) and the radiation condition on the wall of the cylinder in figure 7.1 (equation 7.10):

$$\frac{\partial \phi}{\partial n} = 0 \text{ (for: } z = -h) \quad \text{and} \quad \lim_{R \to \infty} \phi = 0$$

into account, the integral equation 7.33 over the surface S^* reduces to:

$$\boxed{\iint\limits_{S} \phi_j \frac{\partial \phi_k}{\partial n} \cdot dS = \iint\limits_{S} \phi_k \frac{\partial \phi_j}{\partial n} \cdot dS} \tag{7.37}$$

in which S is the wetted surface of the body only.
Note that in the light of the restriction introduced above, this is now (at least formally) only valid for deep water. The reader is also reminded that the ϕ_j and ϕ_k still have to be evaluated as well; this comes up again later in this chapter.

Potential Coefficients

A substitution of equation 7.37 in equations 7.29 and 7.30 provides symmetry - for the zero forward ship speed case - in the coefficients matrices with respect to their diagonals so that:

$$M_{jk} = M_{kj} \qquad \text{and} \qquad N_{jk} = N_{kj} \tag{7.38}$$

Because of the symmetry of a ship some coefficients are zero and the two matrices with hydrodynamic coefficients for ship become:

$$
\text{Hydrodynamic mass matrix:} \quad
\begin{pmatrix}
M_{11} & 0 & M_{13} & 0 & M_{15} & 0 \\
0 & M_{22} & 0 & M_{24} & 0 & M_{26} \\
M_{31} & 0 & M_{33} & 0 & M_{35} & 0 \\
0 & M_{42} & 0 & M_{44} & 0 & M_{46} \\
M_{51} & 0 & M_{53} & 0 & M_{55} & 0 \\
0 & M_{62} & 0 & M_{64} & 0 & M_{66}
\end{pmatrix}
\tag{7.39}
$$

$$
\text{Hydrodynamic damping matrix:} \quad
\begin{pmatrix}
N_{11} & 0 & N_{13} & 0 & N_{15} & 0 \\
0 & N_{22} & 0 & N_{24} & 0 & N_{26} \\
N_{31} & 0 & N_{33} & 0 & N_{35} & 0 \\
0 & N_{42} & 0 & N_{44} & 0 & N_{46} \\
N_{51} & 0 & N_{53} & 0 & N_{55} & 0 \\
0 & N_{62} & 0 & N_{64} & 0 & N_{66}
\end{pmatrix}
\tag{7.40}
$$

For clarity, the symmetry of terms about the diagonal in these matrices (for example that $M_{13} = M_{31}$ for zero forward speed) has not been included here. The terms on the diagonals (such as M_{nn} for example) are the primary coefficients relating properties such as hydrodynamic mass in one direction to the inertia forces in that same direction. Off-diagonal terms (such as M_{13}) represent hydrodynamic mass only which is associated with an inertia dependent force in one direction caused by a motion component in another.

Forward speed has an effect on the velocity potentials, but is not discussed here. This effect is quite completely explained by [Timman and Newman, 1962]. Another good reference is [Vugts, 1970].

7.2.4 Wave and Diffraction Loads

The second and third term in 7.16 can be treated together. The wave and diffraction terms in the hydrodynamic force and moment are:

$$
\vec{F}_w + \vec{F}_d = \rho \iint_S \left(\frac{\partial \Phi_w}{\partial t} + \frac{\partial \Phi_d}{\partial t} \right) \vec{n} \cdot dS
\tag{7.41}
$$

and:

$$
\vec{M}_w + \vec{M}_d = \rho \iint_S \left(\frac{\partial \Phi_w}{\partial t} + \frac{\partial \Phi_d}{\partial t} \right) (\vec{r} \times \vec{n}) \cdot dS
\tag{7.42}
$$

The principles of linear superposition allow the determination of these forces on a restrained body with zero forward speed; $\partial \Phi / \partial n = 0$. This simplifies the kinematic boundary condition on the surface of the body to:

$$
\frac{\partial \Phi}{\partial n} = \frac{\partial \Phi_w}{\partial n} + \frac{\partial \Phi_d}{\partial n} = 0
\tag{7.43}
$$

The space and time dependent potentials, $\Phi_w(x, y, z, t)$ and $\Phi_d(x, y, z, t)$, are written now in terms of isolated space dependent potentials, $\phi_w(x, y, z)$ and $\phi_d(x, y, z)$, multiplied by a normalized oscillatory velocity, $v(t) = 1 \cdot e^{-i\omega t}$:

$$
\begin{aligned}
\Phi_w(x, y, z, t) &= \phi_w(x, y, z) \cdot e^{-i\omega t} \\
\Phi_d(x, y, z, t) &= \phi_d(x, y, z) \cdot e^{-i\omega t}
\end{aligned}
\tag{7.44}
$$

Then from equation 7.43 follows:

$$\frac{\partial \phi_w}{\partial n} = -\frac{\partial \phi_d}{\partial n} \tag{7.45}$$

With this equation and equation 7.19 for the generalized direction cosines, one then finds the wave forces and moments on the restrained body in waves:

$$\begin{aligned} X_{w_k} &= -i\rho e^{-i\omega t} \iint\limits_{S} \left(\phi_w + \phi_d\right) f_k \cdot dS \\ &= -i\rho e^{-i\omega t} \iint\limits_{S} \left(\phi_w + \phi_d\right) \frac{\partial \phi_k}{\partial n} \cdot dS \qquad \text{for: } k = 1, ...6 \end{aligned} \tag{7.46}$$

in which ϕ_k is the radiation potential in direction k.

The potential of the incident waves, ϕ_w, is known (see chapter 5), but the diffraction potential, ϕ_d, has to be determined. Green's second theorem from equation 7.37 provides a relation between this diffraction potential, ϕ_d, and a radiation potential, ϕ_k:

$$\iint\limits_{S} \phi_d \frac{\partial \phi_k}{\partial n} \cdot dS = \iint\limits_{S} \phi_k \frac{\partial \phi_d}{\partial n} \cdot dS \tag{7.47}$$

and with equation 7.45 one finds:

$$\iint\limits_{S} \phi_d \frac{\partial \phi_k}{\partial n} \cdot dS = -\iint\limits_{S} \phi_k \frac{\partial \phi_w}{\partial n} \cdot dS \tag{7.48}$$

This elimination of the diffraction potential results into the so-called **Haskind relations**:

$$X_{w_k} = -i\rho e^{-i\omega t} \iint\limits_{S} \left(\phi_w \frac{\partial \phi_k}{\partial n} + \phi_k \frac{\partial \phi_w}{\partial n}\right) \cdot dS \qquad \text{for: } k = 1, ...6 \tag{7.49}$$

This limits the problem of the diffraction potential because the expression for X_{w_k} depends only on the wave potential ϕ_w and the radiation potential ϕ_k.

Note: These relations, found by [Haskind, 1957], are very important; they underlie the relative motion (displacement - velocity - acceleration) hypothesis, as used in chapter 6 and in strip theory in chapter 8. These relations are valid only for a floating body with a zero time-averaged speed in all directions. [Newman, 1962] however, has generalized the Haskind relations for a body with a constant forward speed. He derived equations which differ only slightly from those found by Haskind. According to Newman's approach the wave potential has to be defined in the moving $O(x, y, z)$ system. The radiation potential has to be determined for the constant forward speed case, taking an opposite sign into account.

The corresponding wave potential for deep water, as given in chapter 5, now becomes:

$$\begin{aligned} \Phi_w &= \frac{\zeta_a g}{\omega} \cdot e^{kz} \cdot \sin(\omega t - kx \cos \mu - ky \sin \mu) \\ &= \frac{i\zeta_a g}{\omega} \cdot e^{kz} \cdot e^{-ik(x \cos \mu + y \sin \mu)} e^{-i\omega t} \end{aligned} \tag{7.50}$$

so that the isolated space dependent term is given by:

$$\phi_w = \frac{i\zeta_a g}{\omega} \cdot e^{kz} \cdot e^{-ik(x\cos\mu + y\sin\mu)} \tag{7.51}$$

In these equations, μ is the wave direction.

The velocity of the water particles in the direction of the outward normal n on the surface of the body is:

$$
\begin{aligned}
\frac{\partial \phi_w}{\partial n} &= \frac{i\zeta_a g}{\omega} \cdot k \left\{ \frac{\partial z}{\partial n} - i \left(\frac{\partial x}{\partial n} \cos\mu + \frac{\partial y}{\partial n} \sin\mu \right) \right\} \cdot e^{kz} \cdot e^{-ik(x\cos\mu + y\sin\mu)} \\
&= \phi_w \cdot k \cdot \left\{ \frac{\partial z}{\partial n} - i \left(\frac{\partial x}{\partial n} \cos\mu + \frac{\partial y}{\partial n} \sin\mu \right) \right\} \\
&= \phi_w \cdot k \cdot \left\{ f_3 - i \left(f_1 \cos\mu + f_2 \sin\mu \right) \right\} \tag{7.52}
\end{aligned}
$$

With this, the wave loads are given by:

$$
\begin{aligned}
X_{w_k} &= -i\rho\omega e^{-i\omega t} \iint\limits_S \phi_w f_k \cdot dS \\
&\quad + i\rho\omega e^{-i\omega t} k \iint\limits_S \phi_w \phi_k \left\{ f_3 - i \left(f_1 \cos\mu + f_2 \sin\mu \right) \right\} \cdot dS \\
&\qquad\qquad\qquad\qquad\qquad\qquad\qquad \text{for: } k = 1, ...6 \tag{7.53}
\end{aligned}
$$

The first term in this expression for the wave loads is the so-called **Froude-Krilov** force or moment, which is the wave load caused by the undisturbed incident wave. The second term is caused by the wave disturbance due to the presence of the (fixed) body, the so-called **diffraction force**.

7.2.5   Hydrostatic Loads

These buoyancy forces and moments are determined using the methods explained in chapter 2. In the notation used here:

$$\vec{F}_s = \rho g \iint\limits_S z\vec{n} \cdot dS \quad \text{and} \quad \vec{M}_s = \rho g \iint\limits_S z \left(\vec{r} \times \vec{n} \right) \cdot dS$$

or more generally:

$$\boxed{X_{s_k} = \rho g \iint\limits_S z f_k \cdot dS} \qquad \text{for: } k = 1, ...6 \tag{7.54}$$

in which the X_{s_k} are the components of these hydrostatic forces and moments.

7.3   2-D Potential Theory

This section describes the 2-D potential theory as for instance has been applied in the computer code SEAWAY, developed at the Delft University of Technology, see [Journée, 1999]. This program computes the potential coefficients and the wave-frequency hydrodynamic loads on and motions of ships and other free-floating bodies with $L/B \geqslant 3$, with and without forward speed.

So far, the wave potential, $\phi_w(x, y, z)$ is known from chapter 5, but the body-shape-dependent radiation potentials, $\phi_j(x, y, z)$, have still to be determined. Several 2-D approaches for solving this problem will be shown. For this 2-D approach, each cross section of the body is considered to be part of a horizontal cylinder with constant cross section and infinite length; see figure 7.2.

[Source: Lloyd, 1989]
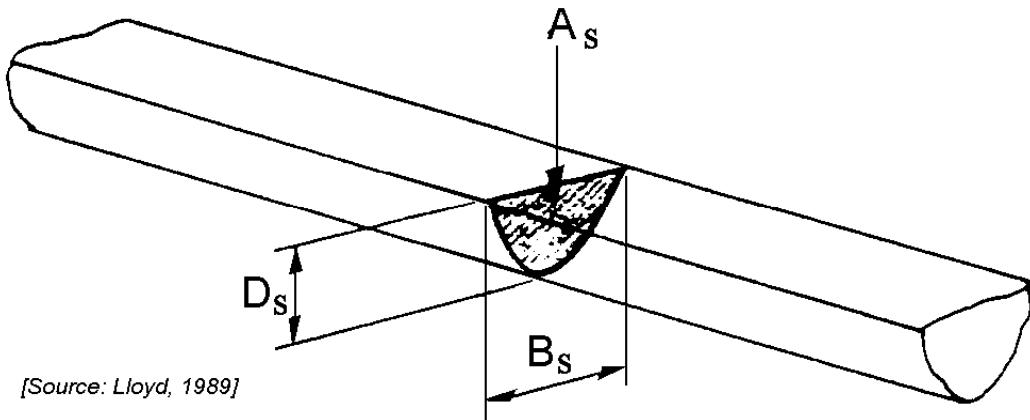
Figure 7.2: 2-D Configuration

The three-dimensional coefficients for the ship at zero mean forward speed are simply found by an integration of the 2-D values over the ship length. This so-called "strip theory method" allows also a relatively simple inclusion of the effect of ship speed.

Three basic 2-D methods are discussed here:

- **Ursell**'s analytical solution of the potential theory for a circular cross section.

- **Conformal mapping** of a ship-like cross section to the unit circle and **Tasai**'s extension of Ursell's theory to conformal mapped cross sections.

- **Frank**'s pulsating source theory, directly applied to a ship-like cross section.

These methods have been developed sequentially in time; each extends the applicability of an earlier form. Each method is discussed separately and is presented using more or less the notation of the relevant literature; this makes it easier for readers to investigate these further. Since all of the methods share the same general boundary conditions, some presentations seem very similar, but they often differ in detail.

7.3.1   Theory of Ursell

[Ursell, 1949] made the first step towards solving the general problem of calculating the two-dimensional flow around a cylinder of arbitrary shape floating in a free surface of infinitely deep water. He derived an analytical solution for an infinitely long oscillating circular cylinder, semi-immersed in a fluid, as shown for heave in figure 7.3-a. The forced oscillation of this cylinder causes a surface disturbance of the fluid. Because the cylinder is assumed to be infinitely long, the generated waves will be two-dimensional. After initial transients have died away, the oscillating cylinder generates a train of regular waves which radiate away to infinity on either side of the cylinder; these waves dissipate energy from the system.

Consider an infinitely long circular cylinder, oscillating in the surface of a fluid; its cross section is the heavy circle in figure 7.3-b. Note that a different coordinate system is used here; the x-axis is in the still water level and the y-axis is positive downwards. θ is now defined from the y-axis instead of the x-axis, too.
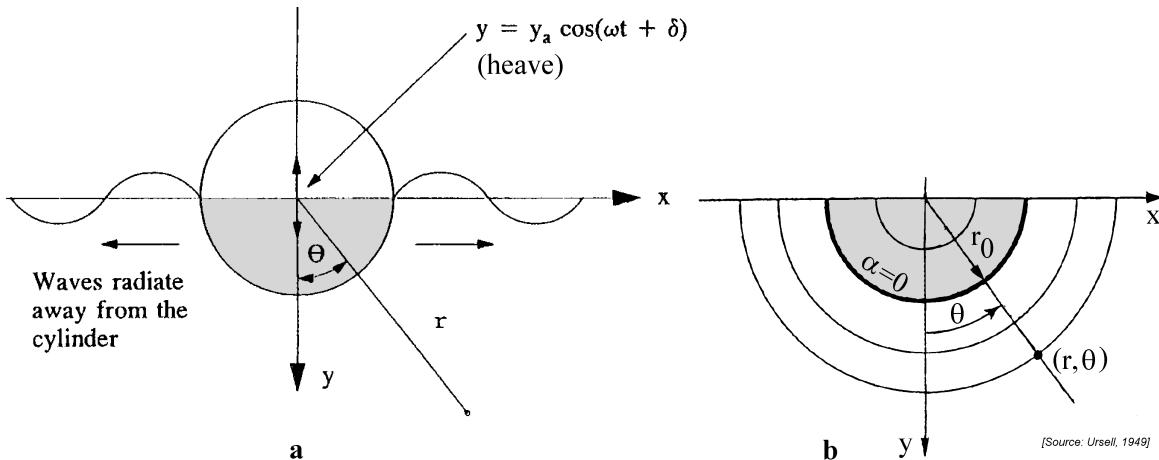
Figure 7.3: Axis System as Used by Ursell

Any point in the fluid can be described by x and y or by $r = r_0 \cdot e^{\alpha}$ and θ, in which e^{α} is the scale. The relations between the (x, y) and the (r, θ) coordinate systems are given by:

$$x = r \cdot \sin\theta = r_0 \cdot e^{\alpha} \cdot \sin\theta \qquad \text{and} \qquad y = r \cdot \cos\theta = r_0 \cdot e^{\alpha} \cdot \cos\theta \qquad (7.55)$$

The contour of the cross section of the circular cylinder follows from substituting $\alpha = 0$ in equation 7.55:

$$x_0 = r_0 \cdot \sin\theta \qquad \text{and} \qquad y_0 = r_0 \cdot \cos\theta \qquad (7.56)$$

The cylinder is forced to carry out a simple harmonic sway, heave or roll motion with a frequency of oscillation ω and a small amplitude of displacement x_a, y_a or β_a, respectively:

$$
\begin{array}{lll}
\text{for sway} & : & x = x_a \cos(\omega t + \varepsilon) \\
\text{for heave} & : & y = y_a \cos(\omega t + \delta) \\
\text{for roll} & : & \beta = \beta_a \cos(\omega t + \gamma)
\end{array}
\qquad (7.57)
$$

in which ε, δ and γ are phase angles with respect to the velocity potentials.

The sway, heave and roll velocity and acceleration components of the cylinder are now:

$$
\begin{array}{llll}
\text{for sway:} & \dot{x} = -\omega x_a \sin(\omega t + \varepsilon) & \text{and} & \ddot{x} = -\omega^2 x_a \cos(\omega t + \varepsilon) \\
\text{for heave:} & \dot{y} = -\omega y_a \sin(\omega t + \delta) & \text{and} & \ddot{y} = -\omega^2 y_a \cos(\omega t + \delta) \\
\text{for roll:} & \dot{\beta} = -\omega \beta_a \sin(\omega t + \gamma) & \text{and} & \ddot{\beta} = -\omega^2 \beta_a \cos(\omega t + \gamma) \quad (7.58)
\end{array}
$$

These forced oscillations of the cylinder cause a surface disturbance of the fluid. Because the cylinder is assumed to be infinitely long, the generated waves will be two-dimensional. These waves travel away from the cylinder and a stationary state is rapidly attained; they dissipate the energy that the forced oscillation adds.

The fluid is assumed to be incompressible, inviscid and irrotational, without any effects of surface tension. The motion amplitudes and velocities are small enough, so that all but the linear terms of the free surface condition, the kinematic boundary condition on the cylinder and the Bernoulli equation may be neglected.

Boundary Conditions

For these oscillations, the two-dimensional velocity potentials of the fluid have to fulfill the six requirements as discussed in the first section of this chapter:

1. **Laplace equation**

$$
\nabla^2 \Phi = \frac{\partial^2 \Phi}{\partial x^2} + \frac{\partial^2 \Phi}{\partial y^2} = 0 \tag{7.59}
$$

2. **Sea bed boundary condition**
   The boundary condition on the bottom in **deep water** is expressed by:

$$
\frac{\partial \Phi}{\partial y} \to 0 \qquad \text{for:} \quad y \to \infty \tag{7.60}
$$

3. **Free surface boundary condition**
   The linearized free surface condition in **deep water** is expressed as follows:

$$
\frac{\partial^2 \Phi}{\partial t^2} - g \cdot \frac{\partial \Phi}{\partial y} = 0 \quad \text{or} \quad k\Phi + \frac{\partial \Phi}{\partial y} = 0
$$

$$
\text{for:} \quad |x| \geq r_0 \quad \text{and} \quad y = 0 \qquad \text{with:} \quad k = \frac{\omega^2}{g} \tag{7.61}
$$

   In the polar coordinate system, this becomes:

$$
-\xi_r \cdot e^{\alpha} \cdot \Phi \pm \frac{\partial \Phi}{\partial \theta} = 0 \quad \text{for:} \quad \alpha \geq 0 \quad \text{and} \quad \theta = \pm\frac{\pi}{2} \tag{7.62}
$$

   in which ξ_r is the non-dimensional frequency squared:

$$
\xi_r = \frac{\omega^2}{g} \cdot r_0 \tag{7.63}
$$

4. **Kinematic boundary condition on the oscillating body surface**
   The boundary conditions for sway, heave and roll follow from the definition of the
   velocity potential on the surface S of the oscillating cylinder (thus for $\alpha = 0$):

   $$\text{sway}: \quad \frac{\partial \Phi_0(\theta)}{\partial n} = \dot{x} \cdot \frac{\partial x_0}{\partial n}$$

   $$\text{heave}: \quad \frac{\partial \Phi_0(\theta)}{\partial n} = \dot{y} \cdot \frac{\partial y_0}{\partial n}$$

   $$\text{roll}: \quad \frac{\partial \Phi_0(\theta)}{\partial n} = r_0 \dot{\beta} \cdot \frac{\partial r_0}{\partial s} \tag{7.64}$$

   in which n is the outward normal of the cylinder surface S. Using the stream functions
   Ψ, these boundary conditions are:

   $$\text{sway}: \quad \frac{\partial \Psi_0(\theta)}{\partial \theta} = -\dot{x} \cdot \frac{\partial x_0}{\partial \alpha}$$

   $$\text{heave}: \quad \frac{\partial \Psi_0(\theta)}{\partial \theta} = -\dot{y} \cdot \frac{\partial y_0}{\partial \alpha}$$

   $$\text{roll}: \quad \frac{\partial \Psi_0(\theta)}{\partial s} = -\dot{\beta} \cdot \frac{\partial}{\partial s}\left(\frac{r_0^2}{2}\right) \tag{7.65}$$

   Integration results into the following requirements for the stream functions on the
   surface of the cylinder:

   $$\text{sway}: \quad \Psi_0(\theta) = -\dot{x} r_0 \cos\theta + C(t)$$

   $$\text{heave}: \quad \Psi_0(\theta) = -\dot{y} r_0 \sin\theta + C(t)$$

   $$\text{roll}: \quad \Psi_0(\theta) = -\dot{\beta}\frac{r_0^2}{2} + C(t) \tag{7.66}$$

   in which $C(t)$ is a function of the time only.

5. **Radiation condition**
   At a large distance from the cylinder the disturbed surface of the fluid has to take
   the form of a regular progressive outgoing gravity wave. This means that all other
   (possibly present) wave systems have to tend to zero as α tends to infinity.

6. **Symmetric or anti-symmetric condition**
   If, for instance for ships, both the sway and the roll motion of the fluid are anti-
   symmetric and the heave motion is symmetrical, these velocity potentials have the
   following relation:

   $$\text{sway}: \Phi^{(2)}(-x, y) = -\Phi^{(2)}(+x, y) \quad \text{or} \quad \Phi^{(2)}(r, -\theta) = -\Phi^{(2)}(r, +\theta)$$

   $$\text{heave}: \Phi^{(3)}(-x, y) = +\Phi^{(3)}(+x, y) \quad \text{or} \quad \Phi^{(3)}(r, -\theta) = +\Phi^{(3)}(r, +\theta)$$

   $$\text{roll}: \Phi^{(4)}(-x, y) = -\Phi^{(4)}(+x, y) \quad \text{or} \quad \Phi^{(4)}(r, -\theta) = -\Phi^{(4)}(r, +\theta)$$

   $$\tag{7.67}$$

   The superscript number $^{(i)}$ denotes the mode of the motions (direction) as explained
   at the beginning of this chapter.

Velocity Potentials and Stream Functions

Ursell assumed two types of waves were produced by the oscillating cylinder in still water:

A: Standing Wave

This wave system can be described by an infinite number of **pulsating multipoles** (pulsating source-sink combinations) along the y-axis, with velocity potentials and stream functions denoted here by Φ_A and Ψ_A. The amplitudes of these waves decrease rapidly with the increasing distance from the cylinder. These waves do not dissipate energy.

B: Regular Progressive Wave

This wave system can be described by a **pulsating horizontal doublet** at the origin for the anti-symmetric sway and roll motions and a **pulsating source** at the origin for the symmetric heave motion, with velocity potentials and stream functions denoted here by Φ_B and Ψ_B. These waves dissipate energy. At a distance of a few wave lengths from the cylinder, the waves on each side can be described by a single regular wave train. The wave amplitude at infinity, η_a, is proportional to the amplitude of oscillation of the cylinder x_a, y_a or β_a, provided that these amplitudes are sufficiently small compared with the radius of the cylinder and the wave length is not much smaller than the diameter of the cylinder.

Then, the total velocity potentials and stream functions to describe the waves generated by the oscillating cylinder are:

$$\boxed{\Phi = \Phi_A + \Phi_B}$$
$$\boxed{\Psi = \Psi_A + \Psi_B} \tag{7.68}$$

[Ursell, 1949] found these potentials and worked this out further as outlined below.

The remainder of this section is intended primarily as a reference. The resulting pressure on the cross section - and the path leading to it - is more important than the derivation details.

The following **set of velocity potentials** fulfill the previous requirements for swaying, heaving and rolling circular cross sections:

$$\Phi_A = \frac{g\eta_a}{\pi\omega}\left(\sum_{m=1}^{\infty}\left\{P_{2m}\phi_{A_{2m}}(\alpha,\theta)\cos(\omega t)\right\} + \sum_{m=1}^{\infty}\left\{Q_{2m}\phi_{A_{2m}}(\alpha,\theta)\sin(\omega t)\right\}\right)$$

$$\Phi_B = \frac{g\eta_a}{\pi\omega}\left(\phi_{B_c}(\alpha,\theta)\cos(\omega t) + \phi_{B_s}(\alpha,\theta)\sin(\omega t)\right)$$

$$= \frac{g\eta_a}{\pi\omega}\left(\phi_{B_c}(x,y)\cos(\omega t) + \phi_{B_s}(x,y)\sin(\omega t)\right) \tag{7.69}$$

in which for sway and roll:

$$\phi_{A_{2m}}(\alpha,\theta) = +e^{-(2m+1)\alpha}\sin\left((2m+1)\,\theta\right) + \xi_r\frac{e^{-2m\alpha}\sin(2m\theta)}{2m}$$

$$\phi_{B_c}(x,y) = -\pi e^{-ky}\sin(kx)$$

$$\phi_{B_s}(x, y) = +\frac{|x|}{x}\pi e^{-ky}\cos(kx)$$

$$-\int_0^\infty \frac{|x|}{x}\frac{k\cos(\nu y) + \nu\sin(\nu y)}{\nu^2 + k^2}e^{-\nu|x|}d\nu + \frac{x}{k(x^2 + y^2)} \quad (7.70)$$

and for heave:

$$\phi_{A_{2m}}(\alpha, \theta) = +e^{-2m\alpha}\cos(2m\theta) + \xi_r\frac{e^{-(2m-1)\alpha}\cos\left((2m-1)\theta\right)}{2m-1}$$

$$\phi_{B_c}(x, y) = +\pi e^{-ky}\cos(kx)$$

$$\phi_{B_s}(x, y) = +\pi e^{-ky}\sin(k|x|) + \int_0^\infty \frac{k\sin(\nu y) - \nu\cos(\nu y)}{\nu^2 + k^2}e^{-\nu|x|}d\nu \quad (7.71)$$

The **set of conjugate stream functions** is expressed as:

$$\Psi_A = \frac{g\eta_a}{\pi\omega}\left(\sum_{m=1}^\infty \left\{P_{2m}\psi_{A_{2m}}(\alpha, \theta)\cos(\omega t)\right\} + \sum_{m=1}^\infty \left\{Q_{2m}\psi_{A_{2m}}(\alpha, \theta)\sin(\omega t)\right\}\right)$$

$$\Psi_B = \frac{g\eta_a}{\pi\omega}\left(\psi_{B_c}(\alpha, \theta)\cos(\omega t) + \psi_{B_s}(\alpha, \theta)\sin(\omega t)\right)$$

$$= \frac{g\eta_a}{\pi\omega}\left(\psi_{B_c}(x, y)\cos(\omega t) + \psi_{B_s}(x, y)\sin(\omega t)\right) \quad (7.72)$$

in which for sway and roll:

$$\psi_{A_{2m}}(\alpha, \theta) = -e^{-(2m+1)\alpha}\cos\left((2m+1)\theta\right) - \xi_r\frac{e^{-2m\alpha}\cos(2m\theta)}{2m}$$

$$\psi_{B_c}(x, y) = +\pi e^{-ky}\cos(kx)$$

$$\psi_{B_s}(x, y) = +\pi e^{-ky}\sin(k|x|)$$

$$+ \int_0^\infty \frac{k\sin(\nu y) - \nu\cos(\nu y)}{\nu^2 + k^2}e^{-\nu|x|}d\nu - \frac{y}{k(x^2 + y^2)} \quad (7.73)$$

and for heave:

$$\psi_{A_{2m}}(\alpha, \theta) = +e^{-2m\alpha}\sin(2m\theta) + \xi_r\frac{e^{-(2m-1)\alpha}\sin\left((2m-1)\theta\right)}{2m-1}$$

$$\psi_{B_c} = +\pi e^{-ky}\sin(kx)$$

$$\psi_{B_s} = -\pi e^{-ky}\frac{|x|}{x}\cos(kx) + \int_0^\infty \frac{k\cos(\nu y) + \nu\sin(\nu y)}{\nu^2 + k^2}e^{-\nu|x|}d\nu \quad (7.74)$$

The standing wave (A) is defined in a polar coordinate system, while the regular progressive wave (B) is defined in the (x, y) coordinate system. The wave number, k, in the latter one is related to the frequency of oscillation, ω, by the dispersion relation in deep water:

$k = \omega^2/g$. The variable ν has the dimension of the wave number k; it is not the kinematic viscosity here.

Notice the symmetric and anti-symmetric relations in the set of velocity potentials and stream functions.

The unknowns P_{2m} and Q_{2m} in these equations have to be found; they follow from the boundary conditions in the fluid.

Solution

The **stream functions for sway, heave and roll** on the surface of the cylinder ($\alpha = 0$) reduce to:

$$\Psi_0(\theta) = \frac{g\eta_a}{\pi\omega} \left\{ \left(\psi_{B0_c}(\theta) + \sum_{m=1}^{\infty} \left\{ P_{2m}\psi_{A0_{2m}}(\theta) \right\} \right) \cos(\omega t) \right.$$
$$\left. + \left(\psi_{B0_s}(\theta) + \sum_{m=1}^{\infty} \left\{ Q_{2m}\psi_{A0_{2m}}(\theta) \right\} \right) \sin(\omega t) \right\} \qquad (7.75)$$

in which:

$$\text{for sway and roll} \quad : \quad \psi_{A0_{2m}}(\theta) = \cos\left((2m+1)\theta\right) + \xi_r \frac{\cos(2m\theta)}{2m}$$

$$\text{for heave} \quad : \quad \psi_{A0_{2m}}(\theta) = \sin(2m\theta) + \xi_r \frac{\sin\left((2m-1)\theta\right)}{2m-1} \qquad (7.76)$$

where $\psi_{B0_c}(\theta)$ and $\psi_{B0_s}(\theta)$ are the values of $\psi_{B_c}(\alpha, \theta)$ and $\psi_{B_s}(\alpha, \theta)$ at the surface of the cylinder and ξ_r is the non-dimensional frequency of oscillation squared.

These expressions for the stream functions should be equal to the stream functions that satisfy the kinematic boundary conditions on the surface of the oscillating cylinder, given in equations 7.66. Doing this makes it possible to determine the values for the P_{2m} and Q_{2m} series of values as well as the amplitude ratios x_a/η_a, y_a/η_a and $\beta_a/k\eta_a$ and the phase shifts ε, δ and γ.

Once the P_{2m} and Q_{2m} series of values have been found, the **velocity potentials for sway, heave and roll** can be determined, too:

$$\Phi_0(\theta) = \frac{g\eta_a}{\pi\omega} \left\{ \left(\phi_{B0_c}(\theta) + \sum_{m=1}^{\infty} \left\{ P_{2m}\phi_{A0_{2m}}(\theta) \right\} \right) \cos(\omega t) \right.$$
$$\left. + \left(\phi_{B0_s}(\theta) + \sum_{m=1}^{\infty} \left\{ Q_{2m}\phi_{A0_{2m}}(\theta) \right\} \right) \sin(\omega t) \right\} \qquad (7.77)$$

in which:

$$\text{for sway and roll} \quad : \quad \phi_{A0_{2m}}(\theta) = \sin\left((2m+1)\theta\right) + \xi_r \frac{\sin(2m\theta)}{2m}$$

$$\text{for heave} \quad : \quad \phi_{A0_{2m}}(\theta) = \cos(2m\theta) + \xi_r \frac{\cos\left((2m-1)\theta\right)}{2m-1} \qquad (7.78)$$

Hydrodynamic Pressure

With known velocity potentials, the hydrodynamic pressure on the surface of the cylinder can be obtained from the linearized Bernoulli equation 7.13:

$$
\begin{aligned}
p(\theta) &= -\rho \frac{\partial \Phi_0(\theta)}{\partial t} \\
&= \frac{-\rho g \eta_a}{\pi} \left\{ \left(\phi_{B0_s}(\theta) + \sum_{m=1}^{\infty} \left\{ Q_{2m} \phi_{A0_{2m}}(\theta) \right\} \right) \cos(\omega t) \right. \\
&\qquad \left. - \left(\phi_{B0_c}(\theta) + \sum_{m=1}^{\infty} \left\{ P_{2m} \phi_{A0_{2m}}(\theta) \right\} \right) \sin(\omega t) \right\}
\end{aligned}
\tag{7.79}
$$

where $\phi_{B0_c}(\theta)$ and $\phi_{B0_s}(\theta)$ are the values of $\phi_{B_c}(\alpha, \theta)$ and $\phi_{B_s}(\alpha, \theta)$ at the surface of the cylinder.

It is obvious that the pressures for sway and roll are skew-symmetric in θ, thus $p(-\theta) = -p(+\theta)$, and symmetric in θ for heave, thus: $p(-\theta) = p(+\theta)$.

Hydrodynamic Loads

The two-dimensional hydrodynamic sway and heave force and roll moment can be obtained from integrations of these pressures over the contour, C_0 at $r = r_0$, of the circular cross section. When switching to polar coordinates, derivatives with respect to θ have to be used:

$$
\frac{dx_0}{d\theta} = +r_0 \cos\theta \quad \text{and} \quad \frac{dy_0}{d\theta} = -r_0 \sin\theta
\tag{7.80}
$$

With these, the loads can be expressed in terms of potential mass and damping, as equations 7.81, 7.82 and 7.83 show. A comparison of the in-phase terms $(\cos(\omega t))$ in each of these equations provides the potential mass coefficients, while a comparison of the out-of-phase terms $(\sin(\omega t))$ the potential damping coefficients provides.

$$
\begin{aligned}
F_x' &= \int_{C_0} p(\theta)\, dy_0 = 2 \int_0^{\frac{1}{2}\pi} p(\theta) \frac{dy_0}{d\theta}\, d\theta \\
&\left\{ = -2r_0 \int_0^{\frac{1}{2}\pi} p(\theta) \sin\theta\, d\theta \quad \text{(for this circular cylinder)} \right\} \\
&= -M_{22}' \cdot \ddot{x} - N_{22}' \cdot \dot{x} \qquad \text{(for a swaying cylinder)} \\
&= -M_{24}' \cdot \ddot{\beta} - N_{24}' \cdot \dot{\beta} \qquad \text{(for a rolling cylinder)}
\end{aligned}
\tag{7.81}
$$

$$
\begin{aligned}
F_y' &= -\int_{C_0} p(\theta)\, dx_0 = -2 \int_0^{\frac{1}{2}\pi} p(\theta) \frac{dx_0}{d\theta}\, d\theta \\
&\left\{ = -2r_0 \int_0^{\frac{1}{2}\pi} p(\theta) \cos\theta\, d\theta \quad \text{(for this circular cylinder)} \right\}
\end{aligned}
$$

$$= -M_{33}{}' \cdot \ddot{y} - N_{33}{}' \cdot \dot{y} \qquad \text{(for a heaving cylinder)} \tag{7.82}$$

$$M_R{}' = -\int_{C_0} p(\theta) x_0 dx_0 - \int_{C_0} p(\theta) y_0 dy_0$$

$$= -2 \int_0^{\frac{1}{2}\pi} p(\theta) \left(x_0 \frac{dx_0}{d\theta} + y_0 \frac{dy_0}{d\theta} \right) d\theta$$

$$\left\{ = -2r_0{}^2 \int_0^{\frac{1}{2}\pi} p(\theta)(\sin\theta\cos\theta - \sin\theta\cos\theta) \, d\theta \ = 0 \quad \text{(for this circular cylinder)} \right\}$$

$$= -M_{42}{}' \cdot \ddot{x} - N_{42}{}' \cdot \dot{x} \qquad \text{(for a swaying cylinder)}$$

$$= -M_{44}{}' \cdot \ddot{\beta} - N_{44}{}' \cdot \dot{\beta} \qquad \text{(for a rolling cylinder)} \tag{7.83}$$

with:

$$
\begin{aligned}
M_{22}{}' &= \text{2-D hydrodynamic mass coefficient of sway} \\
N_{22}{}' &= \text{2-D hydrodynamic damping coefficient of sway} \\
M_{42}{}' &= \text{2-D hydrodynamic mass coupling coefficient of sway into roll} \\
N_{42}{}' &= \text{2-D hydrodynamic damping coupling coefficient of sway into roll} \\
M_{33}{}' &= \text{2-D hydrodynamic mass coefficient of heave} \\
N_{33}{}' &= \text{2-D hydrodynamic damping coefficient of heave} \\
M_{24}{}' &= \text{2-D hydrodynamic mass coupling coefficient of roll into sway} \\
N_{24}{}' &= \text{2-D hydrodynamic damping coupling coefficient of roll into sway} \\
M_{44}{}' &= \text{2-D hydrodynamic mass moment of inertia coefficient of roll} \\
N_{44}{}' &= \text{2-D hydrodynamic damping coefficient of roll}
\end{aligned}
$$

7.3.2   Conformal Mapping

Ursell's derivation is valid only for a circular cross section. Since few ships have this shape, a method is needed to transform realistic shapes so that "it looks like" a circular cylinder in Ursell's method.

More or less arbitrary, but still symmetrical, cross sections can be mapped conformal to a unit circle. The general transformation formula to do this is given by:

$$\boxed{z = M_s \sum_{n=0}^{N} \left\{ a_{2n-1} \zeta^{-(2n-1)} \right\}} \tag{7.84}$$

with:

$$
\begin{aligned}
z = x + iy &= \text{specifies the ship's cross section shape (figure 7.4-b)} \\
\zeta = ie^{\alpha}e^{-i\theta} &= \text{specifies the circular cross section shape (figure 7.4-a)} \\
M_s &= \text{scale factor} \\
a_{-1} &= +1 \\
a_{2n-1} &= \text{conformal mapping coefficients } (n = 1, ..., N) \\
N &= \text{number of parameters used}
\end{aligned}
$$

Equation 7.84 is valid only for cross sections which pass through the still water level. It will not work for fully submerged cross sections, like those of a bulbous bow or a submarine. Those sections have to be treated by other methods.
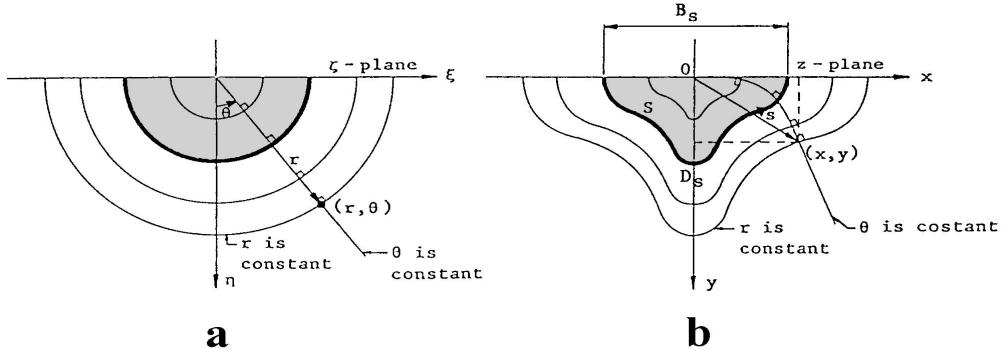
Figure 7.4: Mapping Relation between Two Planes

Equation 7.84 yields the relation between the coordinates in the z-plane (of the ship's cross section) and the variables in the ζ-plane (of the circular cross section):

$$
x = -M_s \sum_{n=0}^{N} \left\{ (-1)^n a_{2n-1} e^{-(2n-1)\alpha} \sin \left((2n-1)\theta \right) \right\}
$$

$$
y = +M_s \sum_{n=0}^{N} \left\{ (-1)^n a_{2n-1} e^{-(2n-1)\alpha} \cos \left((2n-1)\theta \right) \right\} \tag{7.85}
$$

$\alpha = 0$ in Ursell's solution corresponds to the contour of his circular cross section. Similarly, the contour of the ship's cross section follows from putting $\alpha = 0$ in the above equation, yielding:

$$
x_0 = -M_s \sum_{n=0}^{N} \left\{ (-1)^n a_{2n-1} \sin \left((2n-1)\theta \right) \right\}
$$

$$
y_0 = +M_s \sum_{n=0}^{N} \left\{ (-1)^n a_{2n-1} \cos \left((2n-1)\theta \right) \right\} \tag{7.86}
$$

The breadth on the waterline and the draft of the conformal mapped approximation of the actual cross section are given by:

$$
b_0 = 2 M_s \lambda_b = B_s \qquad \text{with:} \qquad \lambda_b = \sum_{n=0}^{N} a_{2n-1}
$$

$$
\text{so that:} \quad M_s = \frac{B_s}{2\lambda_b}
$$

$$
d_0 = M_s \lambda_d = D_s \qquad \text{with:} \qquad \lambda_d = \sum_{n=0}^{N} \left\{ (-1)^n a_{2n-1} \right\}
$$

$$
\text{so that:} \quad M_s = \frac{D_s}{\lambda_d} \tag{7.87}
$$

Lewis Conformal Mapping

A very simple and in a lot of cases also a more or less realistic transformation of the cross section can be obtained with $N = 2$ in the transformation formula (7.84). This yields the well known **Lewis transformation** (see [Lewis, 1929]).
The contour of this so-called **Lewis form** is expressed by:

$$\begin{aligned}
x_0 &= M_s \cdot ((1 + a_1) \sin \theta - a_3 \sin 3\theta) \\
y_0 &= M_s \cdot ((1 - a_1) \cos \theta + a_3 \cos 3\theta)
\end{aligned} \tag{7.88}$$

with the scale factor:

$$M_s = \frac{B_s/2}{1 + a_1 + a_3} \qquad \text{or:} \qquad M_s = \frac{D_s}{1 - a_1 + a_3} \tag{7.89}$$

and:

$$\begin{aligned}
b_0 = B_s &= \text{sectional breadth on the water line} \\
d_0 = D_s &= \text{sectional draft}
\end{aligned}$$

Now the coefficients a_1 and a_3 and the scale factor M_s can be determined in such a way that the sectional breadth, draft and area of the approximate cross section and of the actual ship cross section are identical.
The half breadth to draft ratio H_0 is given by:

$$H_0 = \frac{B_s/2}{D_s} = \frac{1 + a_1 + a_3}{1 - a_1 + a_3} \tag{7.90}$$

An integration of the Lewis form delivers the sectional area coefficient σ_s:

$$\sigma_s = \frac{A_s}{B_s D_s} = \frac{\pi}{4} \cdot \frac{1 - a_1^2 - 3a_3^2}{(1 + a_3)^2 - a_1^2} \tag{7.91}$$

in which A_s is the area of the cross section.
Putting a_1, derived from the expression for H_0, into the expression for σ_s yields a quadratic equation in a_3:

$$c_1 a_3^2 + c_2 a_3 + c_3 = 0 \tag{7.92}$$

in which:

$$\begin{aligned}
c_1 &= 3 + \frac{4\sigma_s}{\pi} + \left(1 - \frac{4\sigma_s}{\pi} \right) \cdot \left(\frac{H_0 - 1}{H_0 + 1} \right)^2 \\
c_2 &= 2c_1 - 6 \\
c_3 &= c_1 - 4
\end{aligned} \tag{7.93}$$

The (valid) solutions for a_3 and a_1 become:

$$\begin{aligned}
a_3 &= \frac{-c_1 + 3 + \sqrt{9 - 2c_1}}{c_1} \\
a_1 &= \frac{H_0 - 1}{H_0 + 1} \cdot (a_3 + 1)
\end{aligned} \tag{7.94}$$
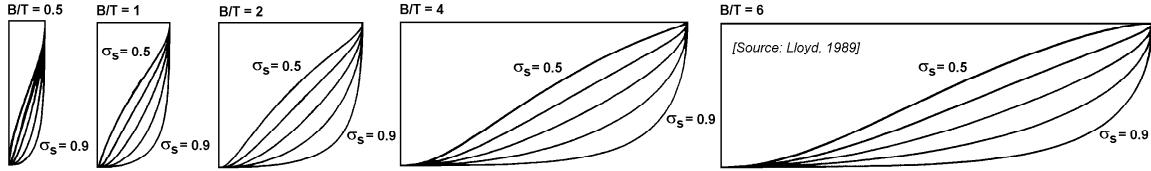
Figure 7.5: Typical Lewis Forms

Lewis forms with the solution $a_3 = \left(-c_1 + 3 - \sqrt{9 - 2c_1}\right)/c_1$ - with a minus sign before the square root - are looped; they intersect themselves somewhere in the fourth quadrant. Since ship shapes are "better behaved", these solutions are not considered here.
It is obvious that a transformation of a half immersed circle with radius R will result in $M_s = R$, $a_1 = 0$ and $a_3 = 0$.
Some typical and realistic Lewis forms are presented in figure 7.5.
In some cases the Lewis transformation can give more or less ridiculous results. The ranges of the half breadth to draft ratio H_0 and the area coefficient σ_s for the different typical Lewis forms are shown in figure 7.6.
The re-entrant and the asymmetric forms are not acceptable; conventional, bulbous and tunneled forms are considered to be valid here. Then, the area coefficient σ_s is bounded by a lower limit to omit re-entrant Lewis forms and by an upper limit to omit non-symmetric Lewis forms:

$$\text{for} \quad H_0 \leq 1.0 : \qquad \frac{3\pi}{32}\left(2 - H_0\right) < \quad \sigma_s < \frac{\pi}{32}\left(10 + H_0 + \frac{1}{H_0}\right)$$

$$\text{for} \quad H_0 \geq 1.0 : \qquad \frac{3\pi}{32}\left(2 - \frac{1}{H_0}\right) < \quad \sigma_s < \frac{\pi}{32}\left(10 + H_0 + \frac{1}{H_0}\right) \qquad (7.95)$$

If a value of σ_s is outside this range, it has to be set to the value at the nearest border of this range, in order to calculate the (best possible) Lewis coefficients.
Numerical problems with bulbous or shallow cross sections can be avoided by the requirement: $0.01 < H_0 < 100.0$.

Close-Fit Conformal Mapping

A more accurate transformation of the cross section can be obtained by using a greater number of parameters N. The scale factor M_s and the conformal mapping coefficients a_{2n-1}, with a maximum value of n varying from N=2 until N=10, can be determined successfully from the offsets of a cross section in such a manner that the mean squares of the deviations of the actual cross section from the approximate cross section is minimized. A very simple and direct iterative least squares method to determine the Close-Fit conformal mapping coefficients is given by [Journée, 1992]. The procedure starts with initial values for $[M_s \cdot a_{2n-1}]$. The initial values of M_s, a_1 and a_3 are obtained with the Lewis method, while the initial values of a_5 until a_{2N-1} are set to zero. With these $[M_s \cdot a_{2n-1}]$ values, a θ_i-value is determined for each offset in such a manner that the actual offset (x_i, y_i) lies on the normal to the approximate contour of the cross section in (x_{0i}, y_{0i}). Now θ_i has to be determined. Therefore a function $F(\theta_i)$ will be defined by the distance from the offset (x_i, y_i) to the normal of the contour to the actual cross section through (x_{0i}, y_{0i}), see figure 7.7.
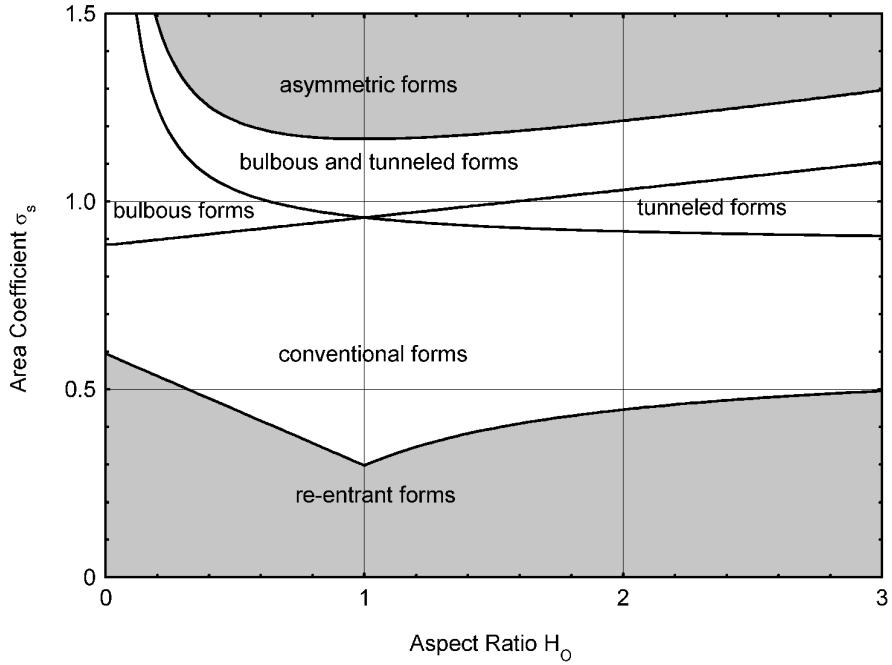
Figure 7.6: Ranges of Lewis Parameters

These offsets have to be selected at approximately equal mutual circumferential lengths, eventually with somewhat more dense offsets near sharp corners. Then α_i is defined by:

$$\cos \alpha_i = \frac{+x_{i+1} - x_{i-1}}{\sqrt{(x_{i+1} - x_{i-1})^2 + (y_{i+1} - y_{i-1})^2}}$$

$$\sin \alpha_i = \frac{-y_{i+1} + y_{i-1}}{\sqrt{(x_{i+1} - x_{i-1})^2 + (y_{i+1} - y_{i-1})^2}} \tag{7.96}$$

With this θ_i-value, the numerical value of the square of the deviation of (x_i, y_i) from (x_{0i}, y_{0i}) is calculated:

$$\left| e_i = (x_i - x_{0i})^2 + (y_i - y_{0i})^2 \right| \tag{7.97}$$

After doing this for all $I+1$ offsets, the numerical value of he sum of the squares of the deviations is known:

$$\left\| E = \sum_{i=0}^{I} \{e_i\} \right\| \tag{7.98}$$

The sum of the squares of these deviations can also be expressed as:

$$E = \sum_{i=0}^{I} \left(x_i + \sum_{n=0}^{N} (-1)^n [M_s \cdot a_{2n-1}] \sin ((2n-1)\theta_i) \right)^2$$

$$+ \sum_{i=0}^{I} \left(y_i - \sum_{n=0}^{N} (-1)^n [M_s \cdot a_{2n-1}] \cos ((2n-1)\theta_i) \right)^2 \tag{7.99}$$
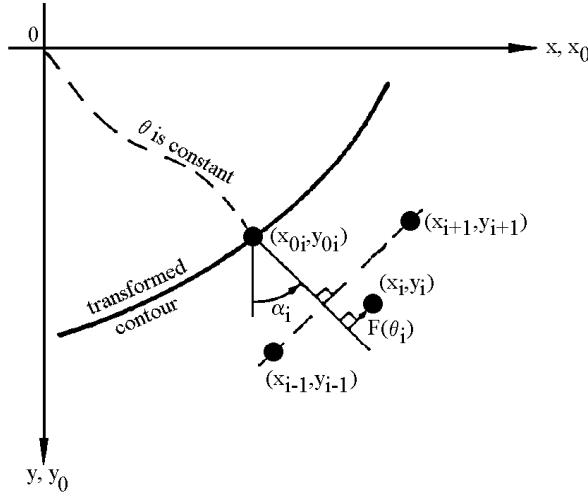
Figure 7.7: Close-Fit Conformal Mapping Definitions

Then new values of $[M_s \cdot a_{2n-1}]$ have to be obtained in such a manner that E is minimized. This means that each of the derivatives of this equation with respect to each coefficient $[M_s \cdot a_{2n-1}]$ is zero, so:

$$\boxed{\frac{\partial E}{\partial \{M_s a_{2j-1}\}} = 0} \qquad \text{for: } j = 0, ...N \tag{7.100}$$

This yields $N+1$ equations:

$$\sum_{n=0}^{N} \left\{ (-1)^n [M_s \cdot a_{2n-1}] \sum_{i=0}^{I} \cos\left((2j - 2n)\theta_i\right) \right\}$$

$$= \sum_{i=0}^{I} \left\{ -x_i \sin\left((2j - 1)\theta_i\right) + y_i \cos\left((2j - 1)\theta_i\right) \right\}$$

$$\text{for: } j = 0, ...N \tag{7.101}$$

To obtain the exact breadth and draft, the last two equations are replaced by the equations for the breadth at the waterline and the draft:

$$\sum_{n=0}^{N} \left\{ (-1)^n [M_s \cdot a_{2n-1}] \sum_{i=0}^{I} \cos\left((2j - 2n)\theta_i\right) \right\}$$

$$= \sum_{i=0}^{I} \left\{ -x_i \sin\left((2j - 1)\theta_i\right) + y_i \cos\left((2j - 1)\theta_i\right) \right\}$$

$$\text{for: } j = 0, ...N - 2$$

$$\sum_{n=0}^{N} \left\{ \quad [M_s \cdot a_{2n-1}] \right\} = B_s/2 \qquad j = N - 1$$

$$\sum_{n=0}^{N} \left\{ (-1)^n [M_s \cdot a_{2n-1}] \right\} = D_s \qquad j = N \tag{7.102}$$

These $N+1$ equations can be solved numerically so that new values for $[M_s \cdot a_{2n-1}]$ will be obtained. These new values are used instead of the initial values to obtain new θ_i-values of the $I+1$ offsets again, etc. This procedure is repeated several times and stops when the difference between the numerical E-values of two subsequent calculations becomes less than a certain threshold value, depending on the dimensions of the cross section. Because $a_{-1} = +1$ the scale factor M_s is equal to the final solution of the first coefficient $(n=0)$. The N other coefficients a_{2n-1} can be found by dividing the final solutions of $[M_s \cdot a_{2n-1}]$ by this M_s-value.

Attention has to be paid to divergence in the calculation routines and re-entrant forms. In these cases the number N will be increased until the divergence or re-entrance vanish. In the worst case a "maximum" value of N will be attained without success. One can then switch to Lewis coefficients with an area coefficient of the cross section set to the nearest border of the valid Lewis coefficient area.

Comparison

An example of conformal mapping results is given here for the amidships cross section of a container vessel, with a breadth of 25.40 meter and a draft of 9.00 meter. For the least squares method in the conformal mapping method, 33 new offsets at equidistant length intervals on the contour of this cross section can be determined by a second degree interpolation routine. The calculated data of the two-parameter Lewis and the N-parameter Close-Fit conformal mapping of this amidships cross section are given in the table below. The last line lists the RMS-values for the deviations of the 33 equidistant points on the approximate contour of this cross section.

		Lewis Conformal Mapping	N-Parameter Close Fit Conformal Mapping									
N	$(-)$	2	2	3	4	5	6	7	8	9	10
$2N$-1	$(-)$	3	3	5	7	9	11	13	15	17	19
M_s	(m)	12.2400	12.2457	12.2841	12.3193	12.3186	12.3183	12.3191	12.3190	12.3195	12.3194
a_{-1}	$(-)$	+1.0000	+1.0000	+1.0000	+1.0000	+1.0000	+1.0000	+1.0000	+1.0000	+1.0000	+1.0000
a_1	$(-)$	+0.1511	+0.1511	+0.1640	+0.1634	+0.1631	+0.1633	+0.1633	+0.1632	+0.1632	+0.1632
a_3	$(-)$	-0.1136	-0.1140	-0.1167	-0.1245	-0.1246	-0.1243	-0.1244	-0.1245	-0.1245	-0.1245
a_5	$(-)$			-0.0134	-0.0133	-0.0105	-0.0108	-0.0108	-0.0108	-0.0107	-0.0107
a_7	$(-)$				+0.0053	+0.0054	+0.0031	+0.0030	+0.0032	+0.0031	+0.0030
a_9	$(-)$					-0.0024	-0.0023	-0.0024	-0.0026	-0.0029	-0.0029
a_{11}	$(-)$						+0.0021	+0.0022	+0.0012	+0.0014	+0.0015
a_{13}	$(-)$							+0.0002	+0.0002	+0.0021	+0.0020
a_{15}	$(-)$								+0.0009	+0.0007	+0.0000
a_{17}	$(-)$									-0.0016	-0.0015
a_{19}	$(-)$										+0.0006
RMS	(m)	0.181	0.180	0.076	0.039	0.027	0.019	0.018	0.017	0.009	0.008

Figure 7.8 shows the differences between a Lewis transformation and a 10-parameter close-fit conformal mapping of a rectangular cross section with a breadth of 20.00 meters and a draft of 10.00 meters.

7.3.3   Theory of Tasai

The approach of [Ursell, 1949] is valid for circular cross sections. [Tasai, 1959] (but others too) used Ursell's approach and a conformal mapping method to obtain 2-D potential
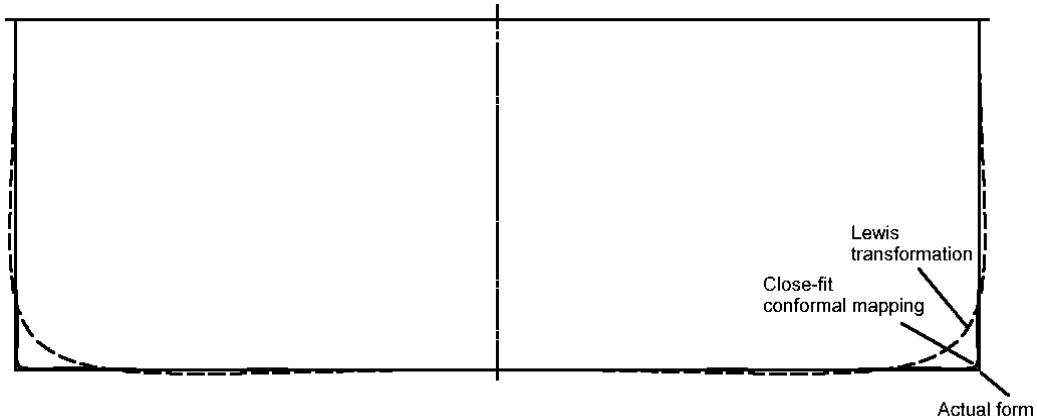
Figure 7.8: Lewis and Close-Fit Conformal Mapping of a Rectangle

coefficients for an infinitely long cylinder with ship-like cross sections, swaying, heaving and rolling in the surface of a fluid. Its cross sections are given in figure 7.9.
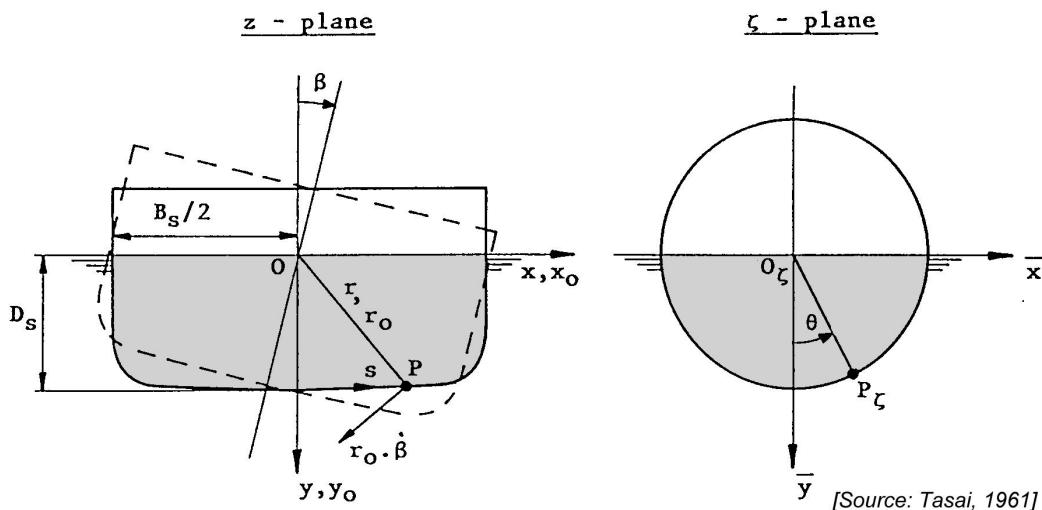
Figure 7.9: Axis System and Form used by Tasai

This represents an attempt to bring a more realistic ship form into an Ursell-like computation. The development followed here is very much like that used by Ursell.

Again, the fluid is assumed to be incompressible, inviscid and irrotational, without any effects of surface tension. The motion amplitudes and velocities are small enough, so that all but the linear terms of the free surface condition, the kinematic boundary condition on the cylinder and the Bernoulli equation may be neglected.

Boundary Conditions

Conformal mapping requires that two boundary conditions of Ursell be rewritten:

- **Free surface boundary condition**
  The free surface condition becomes:

  $$\frac{\xi_b}{\lambda_b}\Phi\sum_{n=0}^{N}\left\{(2n-1)a_{2n-1}e^{-(2n-1)\alpha}\right\} \pm \frac{\partial\Phi}{\partial\theta} = 0$$

  $$\text{for}: \quad \alpha \geq 0 \quad \text{and} \quad \theta = \pm\frac{\pi}{2} \tag{7.103}$$

  in which:

  $$\frac{\xi_b}{\lambda_b} = \frac{\omega^2}{g}M_s \quad \text{or:} \quad \xi_b = \frac{\omega^2 b_0}{2g} \text{ (non-dimensional frequency squared)} \tag{7.104}$$

- **Kinematic boundary condition on the oscillating body surface**
  Conformal mapping results in the following requirements for the stream function on the surface of the cylinder:

  $$\text{for sway}: \quad \Psi_0(\theta) = \dot{x}M_s\sum_{n=0}^{N}\left\{(-1)^n a_{2n-1}\cos\left((2n-1)\theta\right)\right\} + C(t)$$

  $$\text{for heave}: \quad \Psi_0(\theta) = \dot{y}M_s\sum_{n=0}^{N}\left\{(-1)^n a_{2n-1}\sin\left((2n-1)\theta\right)\right\} + C(t)$$

  $$\text{for roll}: \quad \Psi_0(\theta) = -\dot{\beta}\frac{b_0^2}{8\lambda_b}\left\{+\sum_{n=0}^{N}(-1)^n a_{2n-1}\sin\left((2n-1)\theta\right)\right\}^2 \tag{7.105}$$

  $$-\dot{\beta}\frac{b_0^2}{8\lambda_b}\left\{-\sum_{n=0}^{N}(-1)^n a_{2n-1}\cos\left((2n-1)\theta\right)\right\}^2 + C(t)$$

  in which $C(t)$ is a function of the time only.

Velocity Potentials and Stream Functions

The **velocity potentials and stream functions** in the fluid for sway and roll become:

$$\phi_{A_{2m}}(\alpha,\theta) = +e^{-(2m+1)\alpha}\sin\left((2m+1)\theta\right)$$

$$-\frac{\xi_b}{\lambda_b}\sum_{n=0}^{N}(-1)^n\frac{2n-1}{2m+2n}a_{2n-1}e^{-(2m+2n)\alpha}\sin\left((2m+2n)\theta\right)$$

$$\psi_{A_{2m}}(\alpha,\theta) = -e^{-(2m+1)\alpha}\cos\left((2m+1)\theta\right) \tag{7.106}$$

$$+\frac{\xi_b}{\lambda_b}\sum_{n=0}^{N}(-1)^n\frac{2n-1}{2m+2n}a_{2n-1}e^{-(2m+2n)\alpha}\cos\left((2m+2n)\theta\right)$$

and for heave:

$$\phi_{A_{2m}}(\alpha,\theta) = +e^{-2m\alpha}\cos(2m\theta)$$

$$-\frac{\xi_b}{\lambda_b}\sum_{n=0}^{N}(-1)^n\frac{2n-1}{2m+2n-1}a_{2n-1}e^{-(2m+2n-1)\alpha}\cos\left((2m+2n-1)\theta\right)$$

$$\psi_{A_{2m}}(\alpha,\theta) = +e^{-2m\alpha}\sin(2m\theta) \tag{7.107}$$

$$-\frac{\xi_b}{\lambda_b}\sum_{n=0}^{N}(-1)^n\frac{2n-1}{2m+2n-1}a_{2n-1}e^{-(2m+2n-1)\alpha}\sin\left((2m+2n-1)\theta\right)$$

Solution

The velocity potentials and stream functions for sway and roll on the surface of the cylinder, $\alpha = 0$, reduce to:

$$
\begin{aligned}
\phi_{A0_{2m}}(\theta) &= \sin\left((2m+1)\theta\right) \\
&\quad -\frac{\xi_b}{\lambda_b}\sum_{n=0}^{N}(-1)^n\frac{2n-1}{2m+2n}a_{2n-1}\sin\left((2m+2n)\theta\right) \\
\psi_{A0_{2m}}(\theta) &= \cos\left((2m+1)\theta\right) \\
&\quad -\frac{\xi_b}{\lambda_b}\sum_{n=0}^{N}(-1)^n\frac{2n-1}{2m+2n}a_{2n-1}\cos\left((2m+2n)\theta\right) \quad (7.108)
\end{aligned}
$$

and for heave to:

$$
\begin{aligned}
\phi_{A0_{2m}}(\theta) &= \cos(2m\theta) \\
&\quad -\frac{\xi_b}{\lambda_b}\sum_{n=0}^{N}(-1)^n\frac{2n-1}{2m+2n-1}a_{2n-1}\cos\left((2m+2n-1)\theta\right) \\
\psi_{A0_{2m}}(\theta) &= \sin(2m\theta) \\
&\quad -\frac{\xi_b}{\lambda_b}\sum_{n=0}^{N}(-1)^n\frac{2n-1}{2m+2n-1}a_{2n-1}\sin\left((2m+2n-1)\theta\right) \quad (7.109)
\end{aligned}
$$

Again, the resulting pressure on the cross section - and the path leading to it - is more important than the derivation details.

Hydrodynamic Pressure

With known velocity potentials, the hydrodynamic pressure on the surface of the cylinder can be obtained from the linearized Bernoulli equation:

$$
\begin{aligned}
p(\theta) &= -\rho\frac{\partial\Phi_0(\theta)}{\partial t} \\
&= \frac{-\rho g\eta_a}{\pi}\left(\phi_{B0_s}(\theta) + \sum_{m=1}^{\infty}Q_{2m}\phi_{A0_{2m}}(\theta)\right)\cos(\omega t) \\
&\quad \frac{-\rho g\eta_a}{\pi}\left(\phi_{B0_c}(\theta) + \sum_{m=1}^{\infty}P_{2m}\phi_{A0_{2m}}(\theta)\right)\sin(\omega t) \quad (7.110)
\end{aligned}
$$

The pressures for sway and roll are still skew-symmetric in θ and for heave still symmetric in θ.

Hydrodynamic Loads

The two-dimensional hydrodynamic sway and heave force and roll moment can be obtained from integrations of these pressures over the contour, $r = r_0$, of the circular cross section. When switching to polar coordinates, derivatives with respect to θ has to be used:

$$
\frac{dx_0}{d\theta} = -M_s\sum_{n=0}^{N}(-1)^n(2n-1)a_{2n-1}\cos\left((2n-1)\theta\right)
$$

$$\frac{dy_0}{d\theta} \;=\; -M_s \sum_{n=0}^{N}(-1)^n(2n-1)a_{2n-1}\sin\left((2n-1)\theta\right) \tag{7.111}$$

With these, the loads can be expressed in terms of potential mass and damping terms and a comparison of the in-phase and out-of-phase terms delivers the potential coefficients.

$$
\begin{aligned}
F_x{}' \;&=\; \int_{C_0} p(\theta)dy_0 \;=\; 2\int_0^{\frac{1}{2}\pi} p(\theta)\frac{dy_0}{d\theta}d\theta \\
&=\; -M_{22}{}'\cdot\ddot{x} \;-\; N_{22}{}'\cdot\dot{x} \qquad \text{(for a swaying cylinder)} \\
&=\; -M_{24}{}'\cdot\ddot{\beta} \;-\; N_{24}{}'\cdot\dot{\beta} \qquad \text{(for a rolling cylinder)}
\end{aligned}
$$

$$
\begin{aligned}
F_y{}' \;&=\; -\int_{C_0} p(\theta)dx_0 \;=\; -2\int_0^{\frac{1}{2}\pi} p(\theta)\frac{dx_0}{d\theta}d\theta \\
&=\; -M_{33}{}'\cdot\ddot{y} \;-\; N_{33}{}'\cdot\dot{y} \qquad \text{(for a heaving cylinder)}
\end{aligned}
$$

$$
\begin{aligned}
M_R{}' \;&=\; -\int_{C_0} p(\theta)x_0 dx_0 \;-\; \int_{C_0} p(\theta)y_0 dy_0 \;=\; -2\int_0^{\frac{1}{2}\pi} p(\theta)\left(x_0\frac{dx_0}{d\theta}+y_0\frac{dy_0}{d\theta}\right)d\theta \\
&=\; -M_{42}{}'\cdot\ddot{x} \;-\; N_{42}{}'\cdot\dot{x} \qquad \text{(for a swaying cylinder)} \\
&=\; -M_{44}{}'\cdot\ddot{\beta} \;-\; N_{44}{}'\cdot\dot{\beta} \qquad \text{(for a rolling cylinder)} \tag{7.112}
\end{aligned}
$$

Thus, comparisons of the in-phase and out-of-phase parts of these expressions for sway, heave and roll deliver the 2-D potential coefficients of this approximate cross section. Notice that, in contradiction with the case of Ursell's rolling circular cross section, the roll moment $M_R{}'$ is not zero here.

7.3.4   Theory of Frank

As a consequence of conformal mapping to the unit circle, the cross sections need to have a certain breadth at the water surface; $x = r_0 \cdot e^{\alpha}$. Fully submersed cross sections, such as at the bulbous bow, cannot be mapped. Mapping problems can also appear for cross sections outside the area coefficients range $0.5 < \sigma_s < 1.0$. These cases require another approach, which is discussed here.

[Frank, 1967] considered an actual cross section of a ship. He used a non-circular cylinder, whose cross section is a simply connected region, which is fully or partly immersed horizontally in a previously undisturbed fluid of infinite depth; see figure 7.10.

The x-axis coincides with the undisturbed free surface and the y-axis is positive upwards. The cross sectional contour C_0 of the submerged portion of the cylinder lies in the lower half plane and the y-axis is the axis of symmetry of C_0.

The cylinder is forced to carry out a simple harmonic motion $A^{(m)}\cdot\cos(\omega t)$ with a prescribed frequency of oscillation ω. The superscript $^{(m)}$ (as used by Frank and maintained here) may take on the values 2, 3 and 4, denoting swaying, heaving and rolling motions, respectively, as explained earlier. It is assumed that steady state conditions have been attained.
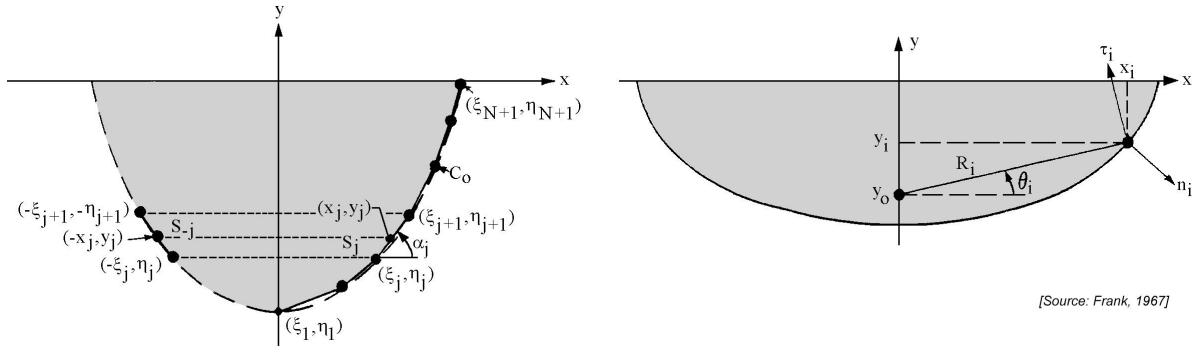
Figure 7.10: Axes System and Notation, as Used by Frank

Again, the fluid is assumed to be incompressible, inviscid and irrotational, without any effects of surface tension. The motion amplitudes and velocities are small enough, so that all but the linear terms of the free surface condition, the kinematic boundary condition on the cylinder and the Bernoulli equation may be neglected.

Boundary Conditions

A velocity potential has to be found:

$$\Phi^{(m)}(x, y, t) = \Re e \left\{ \phi^{(m)}(x, y) \cdot e^{-i\omega t} \right\}$$ (7.113)

satisfying the six conditions as discussed in the first section of this chapter:

1. **Laplace equation**
   The equation of Laplace is now:

$$\nabla^2 \Phi^{(m)} = \frac{\partial^2 \Phi^{(m)}}{\partial x^2} + \frac{\partial^2 \Phi^{(m)}}{\partial y^2} = 0$$ (7.114)

2. **Sea bed boundary condition**
   For deep water, the boundary condition on the bottom is expressed by:

$$\frac{\partial \Phi^{(m)}}{\partial y} \rightarrow 0 \qquad \text{for:} \quad y \rightarrow -\infty$$ (7.115)

3. **Free surface boundary condition**
   The linearized free surface condition outside the cylinder in deep water is expressed as follows:

$$\frac{\partial^2 \Phi^{(m)}}{\partial t^2} + g \frac{\partial \Phi^{(m)}}{\partial y} = 0 \qquad \text{for:} \quad y = 0$$ (7.116)

   in which g is the acceleration of gravity.

4. **Kinematic boundary condition on the oscillating body surface**
   The normal velocity component of the fluid at the surface of the oscillating cylinder is equal to the normal component of the forced velocity of the cylinder. If v_n is the

component of the forced velocity of the cylinder in the direction of the outgoing unit normal vector **n**, then the kinematic boundary condition has to be satisfied at the mean position of the cylindrical surface:

$$\vec{n} \cdot \vec{\nabla} \Phi^{(m)} = v_n \tag{7.117}$$

5. **Radiation condition**
   At a large distance from the cylinder the disturbed surface of the fluid has to take the form of a regular progressive outgoing gravity wave.

6. **Symmetric or anti-symmetric condition**
   Because both the sway and the roll motion are anti-symmetric and the heave motion is symmetrical, these velocity potentials have the following relation:

$$
\begin{aligned}
\text{sway}: & \quad \Phi^{(2)}(-x, y) = -\Phi^{(2)}(+x, y) \\
\text{heave}: & \quad \Phi^{(3)}(-x, y) = +\Phi^{(3)}(+x, y) \\
\text{roll}: & \quad \Phi^{(4)}(-x, y) = -\Phi^{(4)}(+x, y)
\end{aligned}
\tag{7.118}
$$

Velocity Potentials

A potential function, based on pulsating point-sources and satisfying these six conditions, has been given by [Frank, 1967]. Based on earlier work of [Wehausen and Laitone, 1960], the complex potential at z of a pulsating point-source of unit strength at the point ζ in the lower half plane, as shown in figure 7.10, was given by Frank as:

$$
G^*(z, \zeta; t) = \frac{1}{2\pi} \left\{ \ln(z - \zeta) - \ln(z - \widehat{\zeta}) + 2PV \int\limits_0^\infty \frac{e^{-ik(z-\widehat{\zeta})}}{\nu - k} dk \right\} \cdot \quad \cos \omega t
$$
$$
- \left\{ e^{-i\nu(z-\widehat{\zeta})} \right\} \cdot \quad \sin \omega t \tag{7.119}
$$

where:

$$z = x + iy \qquad \zeta = \xi + i\eta \qquad \widehat{\zeta} = \xi - i\eta \tag{7.120}$$

In here, ζ is defined in the lower half plane and $\widehat{\zeta}$ in the upper half plane (mirrored), while $\nu = \omega^2/g$ is the wave number in deep water and $PV \int\limits_0^\infty \frac{e^{-ik(z-\widehat{\zeta})}}{\nu-k} dk$ is a principle value integral with a variable k. These somewhat unconventional notations come from Frank's report and are maintained here.

With this, the real part of the point-source potential is defined by:

$$H(x, y, \xi, \eta; t) = \Re e \left\{ G^*(z, \zeta; t) \right\} \tag{7.121}$$

The space and time dependent source potential term, $G^*(z, \zeta; t)$, is now written in terms of a separate space dependent potential, $G(z, \zeta)$, multiplied by an oscillatory motion, $e^{-i\omega t}$:

$$G^*(z, \zeta; t) = G(z, \zeta) \cdot e^{-i\omega t} \tag{7.122}$$

With this space dependent potential:

$$
\begin{aligned}
G(z,\zeta) = \frac{1}{2\pi} \cdot \quad & \Re e \left\{ \ln(z-\zeta) - \ln(z-\widehat{\zeta}) + 2 \int\limits_{0}^{\infty} \frac{e^{-ik(z-\widehat{\zeta})}}{\nu - k} dk \right\} \\
- i \cdot \quad & \Re e \left\{ e^{-i\nu(z-\widehat{\zeta})} \right\}
\end{aligned}
\tag{7.123}
$$

two expressions for the point-source potential, satisfying all six boundary conditions, are found:

$$
\begin{aligned}
H(x,y,\xi,\eta;t \quad\quad) &= \Re e \left\{ \quad G(z,\zeta) \cdot e^{-i\omega t} \right\} \\
H(x,y,\xi,\eta;t - \frac{\pi}{2\omega}) &= \Re e \left\{ i \cdot G(z,\zeta) \cdot e^{-i\omega t} \right\}
\end{aligned}
\tag{7.124}
$$

Since the problem is linear, a superposition of these two valid expressions for the point-source potential H results in the velocity potential:

$$
\Phi^{(m)}(x,y;t) = \Re e \left\{ \int\limits_{C_0} Q(s) \cdot G(z,\zeta) \cdot e^{-i\omega t} \cdot ds \right\}
\tag{7.125}
$$

where C_0 is the submerged contour of the cylindrical cross section at its mean or rest position and $Q(s)$ represents the complex source density as a function of the position along C_0.

Application of the kinematic boundary condition on the oscillating cylinder at z yields:

$$
\begin{aligned}
\Re e \left\{ (\vec{n} \cdot \vec{\nabla}) \int\limits_{C_0} Q(s) \cdot G(z,\zeta) \cdot ds \right\} &= 0 \\
\Im m \left\{ (\vec{n} \cdot \vec{\nabla}) \int\limits_{C_0} Q(s) \cdot G(z,\zeta) \cdot ds \right\} &= A^{(m)} \cdot \omega \cdot n^{(m)}
\end{aligned}
\tag{7.126}
$$

where $A^{(m)}$ denotes the amplitude of oscillation and $n^{(m)}$ the direction cosine of the normal velocity at z on the cylinder. Both $A^{(m)}$ and $n^{(m)}$ depend on the mode of motion of the cylinder, as will be shown below.

The fact that $Q(s)$ is complex implies that the last two equations represent a set of coupled integral equations for the real functions $\Re e\{Q(s)\}$ and $\Im m\{Q(s)\}$. Frank describes the evaluation of the integrals in his report; special attention is focussed there on the singularity for $z = \zeta$ and $k = \nu$.

Solution

Select $N + 1$ points (ξ_i, η_i) which lie on C_0 in the fourth quadrant. Connect these $N + 1$ points by successive straight lines. N straight line segments are obtained which, together with their reflected images in the third quadrant, yield an approximation to the given contour as shown in figure 7.10. The coordinates, length and angle associated with the j-th segment are identified by the subscript j, whereas the corresponding quantities for the

reflected image in the third quadrant are denoted by the subscript $-j$, so that by symmetry $\xi_{-j} = -\xi_j$ and $\eta_{-j} = -\eta_j$ for $1 \leq j \leq N + 1$.

Potentials and pressures are to be evaluated at the midpoint of each segment and for $1 \leq i \leq N$ the coordinates of the midpoint of the i-th segment are:

$$x_i = \frac{\xi_i + \xi_{i+1}}{2} \qquad \text{and} \qquad y_i = \frac{\eta_i + \eta_{i+1}}{2} \tag{7.127}$$

The length of the i-th segment and the angle between by this segment and the positive x axis are:

$$|s_i| = \sqrt{\left(\xi_{i+1} - \xi_i\right)^2 + \left(\eta_{i+1} - \eta_i\right)^2} \qquad \alpha_i = \arctan\left\{\frac{\eta_{i+1} - \eta_i}{\xi_{i+1} - \xi_i}\right\} \tag{7.128}$$

The outgoing unit vector normal to the cross section at the i-th midpoint (x_i, y_i) is:

$$\vec{n}_i = \vec{i}\sin\alpha_i - \vec{j}\cos\alpha_i \tag{7.129}$$

where $\vec{i}$ and $\vec{j}$ are unit vectors in the x- and y-directions, respectively.

The cylinder is forced into a simple harmonic motion with radian frequency ω, according to the displacement equation:

$$S^{(m)} = A^{(m)} \cdot \cos\omega t \tag{7.130}$$

for $m = 2$, 3 or 4, corresponding to sway, heave or roll, respectively. The rolling motions are about an axis through a point $(0, y_0)$ in the symmetry plane of the cylinder.

In the translational modes, any point on the cylinder moves with the velocity:

$$\begin{aligned} \text{sway:} \quad \vec{v}^{(2)} &= -\vec{i}\,A^{(2)}\omega\sin\omega t \\ \text{heave:} \quad \vec{v}^{(3)} &= -\vec{j}\,A^{(3)}\omega\sin\omega t \end{aligned} \tag{7.131}$$

The rolling motion is illustrated in figure 7.10. Considering a point (x_i, y_i) on C_0, an inspection of this figure yields:

$$\begin{aligned} R_i = \sqrt{x_i{}^2 + (y_i - y_0)^2} \qquad \text{and} \qquad \theta_i &= \arctan\left\{\frac{y_i - y_0}{x_i}\right\} \\ &= \arcsin\left\{\frac{y_i - y_0}{R_i}\right\} \\ &= \arccos\left\{\frac{x_i}{R_i}\right\} \end{aligned} \tag{7.132}$$

Therefore, by elementary two-dimensional kinematics, the unit vector in the direction θ is:

$$\begin{aligned} \vec{\tau}_i &= -\vec{i}\sin\theta_i + \vec{j}\cos\theta_i \\ &= -\frac{y_i - y_0}{R_i}\vec{i} + \frac{x_i}{R_i}\vec{j} \end{aligned} \tag{7.133}$$

so that:

$$\begin{aligned} \text{roll:} \quad \vec{v}^{(4)} &= R_i S^{(4)}\vec{\tau}_i \\ &= \omega A^{(4)}\left\{(y_i - y_0)\,\vec{i} - x_i\vec{j}\right\}\sin\omega t \end{aligned} \tag{7.134}$$

The normal components of the velocity $v_i{}^{(m)} = \vec{n}_i \cdot \vec{v}^{(m)}$ at the midpoint of the i-th segment (x_i, y_i) are:

$$
\begin{aligned}
\text{sway:} \quad v_i{}^{(2)} &= -\omega A^{(2)} \sin \alpha_i \sin \omega t \\
\text{heave:} \quad v_i{}^{(3)} &= +\omega A^{(3)} \cos \alpha_i \sin \omega t \\
\text{roll:} \quad v_i{}^{(4)} &= +\omega A^{(4)} \left\{ (y_i - y_0) \sin \alpha_i + x_i \cos \alpha_i \right\} \sin \omega t
\end{aligned} \tag{7.135}
$$

Defining:

$$
n_i{}^{(m)} = \frac{v_i{}^{(m)}}{A^{(m)} \omega \sin \omega t} \tag{7.136}
$$

then, consistent with the previously mentioned notation, the direction cosines for the three modes of motion are:

$$
\begin{aligned}
\text{sway:} \quad n_i{}^{(2)} &= +\sin \alpha_i \\
\text{heave:} \quad n_i{}^{(3)} &= -\cos \alpha_i \\
\text{roll:} \quad n_i{}^{(4)} &= +(y_i - y_0) \sin \alpha_i + x_i \cos \alpha_i
\end{aligned} \tag{7.137}
$$

These equations illustrate that heaving is symmetrical: $n_{-i}{}^{(3)} = n_i{}^{(3)}$. Swaying and rolling, however are antisymmetric modes: $n_{-i}{}^{(2)} = -n_i{}^{(2)}$ and $n_{-i}{}^{(4)} = -n_i{}^{(4)}$.

The set of two coupled integral equations for the real functions $\Re e\{Q(s)\}$ and $\Im m\{Q(s)\}$, given before, are applied at the midpoints of each of the N segments. It is assumed that over an individual segment the complex source strength $Q(s)$ remains constant, although it varies from segment to segment. With these stipulations, the set of coupled integral equations becomes a set of $2N$ linear algebraic equations in the unknowns:

$$
\begin{aligned}
\Re e \left\{ Q^{(m)} \cdot (s_j) \right\} &= Q_j{}^{(m)} \\
\Im m \left\{ Q^{(m)} \cdot (s_j) \right\} &= Q_{N+j}{}^{(m)}
\end{aligned} \tag{7.138}
$$

Thus, for $i = 1, 2, \ldots, N$:

$$
\begin{aligned}
+\sum_{j=1}^{N} \left\{ Q_j{}^{(m)} \cdot I_{ij}{}^{(m)} \right\} + \sum_{j=1}^{N} \left\{ Q_{N+j}{}^{(m)} \cdot J_{ij}{}^{(m)} \right\} &= 0 \\
-\sum_{j=1}^{N} \left\{ Q_j{}^{(m)} \cdot J_{ij}{}^{(m)} \right\} + \sum_{j=1}^{N} \left\{ Q_{N+j}{}^{(m)} \cdot I_{ij}{}^{(m)} \right\} &= \omega \cdot A^{(m)} \cdot n_i{}^{(m)}
\end{aligned} \tag{7.139}
$$

where the superscript $^{(m)}$ in these $2N^2$ equations denotes the mode of motion.

The influence coefficients $I_{ij}{}^{(m)}$ and $J_{ij}{}^{(m)}$ and the potential $\Phi^{(m)}(x_i, y_i; t)$ have been evaluated by [Frank, 1967]. The resulting velocity potential consists of a term in-phase with the displacement and a term in-phase with the velocity.

The hydrodynamic pressure at (x_i, y_i) along the cylinder is obtained from the velocity potential by means of the linearized Bernoulli equation:

$$
p^{(m)}(x_i, y_i, \omega; t) = -\rho \cdot \frac{\partial \Phi^{(m)}}{\partial t}(x_i, y_i, \omega; t) \tag{7.140}
$$

Since:

$$
\begin{aligned}
p^{(m)}(x_i, y_i, \omega; t) = \quad & p_a{}^{(m)}(x_i, y_i; \omega) \cdot \cos \omega t \\
& + p_v{}^{(m)}(x_i, y_i; \omega) \cdot \sin \omega t
\end{aligned} \tag{7.141}
$$

where $p_a{}^{(m)}$ and $p_v{}^{(m)}$ are the hydrodynamic pressures in-phase with the displacement and in-phase with the velocity, respectively.

As indicated by the previous expressions, the potential as well as the pressure is a function of the oscillation frequency ω. The hydrodynamic force or moment per unit length of the cylinder, necessary to sustain the oscillations, is the integral of $p^{(m)} \cdot n^{(m)}$ over the submerged contour of the cross section C_0. It is assumed that the pressure at the i-th midpoint is the mean pressure for the i-th segment, so that the integration reduces to a summation, so that:

$$\left| M^{(m)}(\omega) = 2 \sum_{i=1}^{N} p_a{}^{(m)}(x_i, y_i; \omega) \cdot n_i{}^{(m)} \cdot |s_i| \right|$$

$$\left| N^{(m)}(\omega) = 2 \sum_{i=1}^{N} p_v{}^{(m)}(x_i, y_i; \omega) \cdot n_i{}^{(m)} \cdot |s_i| \right| \tag{7.142}$$

for the potential inertia and damping forces or moments, respectively.

7.3.5   Comparative Results

Figure 7.11 compares the calculated coefficients for an amidships cross section of a container vessel with the three previous methods:

- Ursell-Tasai's method with 2-parameter Lewis conformal mapping.

- Ursell-Tasai's method with 10-parameter close-fit conformal mapping.

- Frank's pulsating source method.

With the exception of the roll motions, the three results are very close. The roll motion deviation, predicted with the Lewis conformal mapping method, is caused by the description of the "bilge" by the simple Lewis transformation, as can be seen in figure 7.8.

A disadvantage of Frank's method can be the large computing time, when compared with Ursell-Tasai's method. Generally, it is advised to use Ursell-Tasai's method with 10 parameter close-fit conformal mapping. For submerged sections, bulbous sections and sections with an area coefficient, σ_s, less than 0.5, Frank's pulsating source method should be used.

7.4   3-D Potential Theory

The previous main section of this chapter has discussed the potential theory for two-dimensional (plane) shapes. Floating bodies are obviously three-dimensional and it can be appropriate therefore to attempt to determine their potential theory coefficients directly in three dimensions, similar to what Frank did in the two-dimensional case. Just as earlier in this chapter, the presentation here is intended to provide only a bit of insight into the derivation path being followed. The path and the result is more important than the derivation details.

Three-dimensional methods to evaluate the hydrodynamic loads and motions of fixed or (with zero mean forward speed) floating structures in waves have been developed based
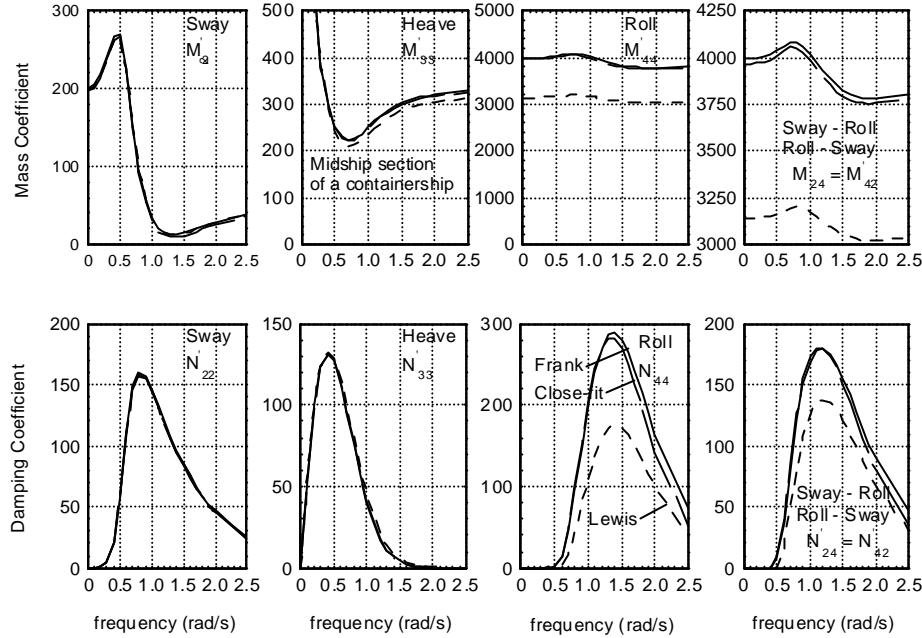
Figure 7.11: Comparison of Calculated Coefficients

on linear three-dimensional potential theory, see for instance [Oortmerssen, 1976a]. Experimental verification of results of computations has been carried out for bodies with a large variety of shapes, see [Oortmerssen, 1976a] and [Pinkster, 1980]. Such comparisons show that 3-D diffraction methods generally can be applied to most body shapes and are therefore a good tool to investigate such effects at zero mean forward speed.

This section gives a brief description of the 3-D diffraction theory as used in the computer program DELFRAC developed at the Delft University of Technology. It computes the wave-frequency hydrodynamic loads on free-floating or fixed bodies as well as the wave-frequency motions of floating bodies. Second order wave drift forces can be computed as well; these are discussed in chapter 9.

The method is restricted to arbitrarily shaped bodies with **zero mean forward speed**. This is an acceptable simplification for the majority of the fixed or floating structures in use today in the offshore industry. It should be mentioned however, that attention is shifting to the development of methods taking into account low forward speed or (alternatively) current effects; see [Huijsmans, 1996]. The treatment of such methods is beyond the scope of this text, however.

7.4.1 Diffraction Theory

The diffraction theory used in this approach is given here for an arbitrarily shaped, fixed or free-floating body. Use is made of a right-handed, earth-bound $S(x_0, y_0, z_0)$ system of axes with origin at the mean water level and the z_0-axis vertically upwards. The body axis $G(x_b, y_b, z_b)$ has its origin in the center of gravity G of the body; the x_b-axis is towards the bow and y_b to port. The positive z_b-axis is upwards. This coordinate system coincides with another earth-bound system of fixed axes $O(x, y, z)$ in the mean position of the structure. This is the same system as was used in chapter 6.

The wave elevation and all potentials are referenced to the fixed $O(x, y, z)$ system of axes. Phase shifts of body motions are referenced to the undisturbed wave elevation at the center of gravity ($G = O$) of the body; even though no wave can be measured there.

According to linear potential theory, the potential of a floating body is a superposition of the potentials due to the undisturbed incoming wave Φ_w, the potential due to the diffraction of the undisturbed incoming wave on the fixed body Φ_d and the radiation potentials due to the six body motions Φ_j:

$$\boxed{\Phi = \sum_{j=1}^{6} \Phi_j + \Phi_w + \Phi_d} \tag{7.143}$$

Again, the fluid is assumed to be incompressible, inviscid and irrotational, without any effects of surface tension. The motion amplitudes and velocities are small enough, so that all but the linear terms of the free surface condition, the kinematic boundary condition on the body and the Bernoulli equation may be neglected.

The potentials have to satisfy the same boundary conditions, as discussed before:

1. **Laplace equation**
   The continuity condition or Laplace equation:

   $$\frac{\partial^2 \Phi}{\partial x^2} + \frac{\partial^2 \Phi}{\partial y^2} + \frac{\partial^2 \Phi}{\partial z^2} = 0 \tag{7.144}$$

   holds in the fluid domain.

2. **Sea bed boundary condition**
   At the sea bed:

   $$\frac{\partial \Phi}{\partial z} = 0 \quad \text{with:} \quad z = -h_o \tag{7.145}$$

   in which h_o is the distance from the origin of the earth-bound coordinate system, $O(x, y, z)$, to the sea bed. Note that, in contrast to the earlier theory, this treatment is for water with a finite depth.

3. **Free surface boundary condition**
   At the mean free surface:

   $$g\frac{\partial \Phi}{\partial z} + \frac{\partial^2 \Phi}{\partial t^2} = 0 \tag{7.146}$$

4. **Kinematic boundary condition on the oscillating body surface**
   On the wetted part of the oscillating hull of the structure (in its mean position):

   $$\frac{\partial \Phi}{\partial n} = \vec{v}.\vec{n} \tag{7.147}$$

   in which $\vec{v}$ is the velocity of a point on the hull of the body and $\vec{n}$ is the normal vector of the hull, positive into the fluid.

5. **Radiation condition**
   The body motion and diffraction potentials have to satisfy a radiation condition which states that at great distance from the body these potentials disappear. This condition imposes a uniqueness which would not otherwise be present, see [Oortmerssen, 1976a].

6. **Symmetric or anti-symmetric condition**

   If, for instance for ships, both the sway and the roll motion of the fluid are anti-symmetric and the heave motion is symmetrical, the velocity potentials have the following relation:

$$\begin{aligned}
\Phi^{(2)}(-x,y) &= -\Phi^{(2)}(+x,y) && \text{for sway} \\
\Phi^{(3)}(-x,y) &= +\Phi^{(3)}(+x,y) && \text{for heave} \\
\Phi^{(4)}(-x,y) &= -\Phi^{(4)}(+x,y) && \text{for roll}
\end{aligned} \tag{7.148}$$

   However, this symmetry condition has not to be used in DELFRAC necessarily, because this program is suitable for any hull form..

The free-surface condition follows from the assumptions that the pressure at the surface is constant and that water particles do not pass through the free surface. The condition on the wetted surface of the body assures the no-leak condition of the (oscillating) hull. The condition at the sea bed is also a no-leak condition.

Up to now no specific wave conditions have been applied. The boundary conditions are general and apply to all possible realizations of wave conditions. The theory is developed here for a unidirectional regular wave. Just as in chapter 5, superposition can then be used to study all sorts of irregular wave conditions - even those with directional spreading.

In regular waves a linear potential Φ, which is a function of the earth-fixed coordinates and of time t, can be written as a product of a space-dependent term and a harmonic time-dependent term as follows:

$$\boxed{\Phi(x,y,z;t) = \phi(x,y,z) \cdot e^{-i\omega t}} \tag{7.149}$$

The boundary conditions for the potential, Φ, result in similar conditions for the space dependent term, ϕ.

Note: Following [Tuck, 1970] a convenient formulation can be obtained by writing:

$$\phi = -i\omega \sum_{j=0}^{7} \phi_j \zeta_j \tag{7.150}$$

in which $j = 0$ represents the undisturbed incoming wave, $j = 1, ...6$ are associated with each of the motion modes of the body and $j = 7$ represents the diffracted wave.

The **space-dependent part** of the velocity potential ϕ_0 - associated with an undisturbed long-crested regular wave in water of constant depth h - is given by:

$$\phi_0 = \frac{\zeta_0 g}{\omega} \cdot \frac{\cosh k(h_o + z)}{\cosh kh} \cdot e^{ik(x\cos\mu + y\sin\mu)} \tag{7.151}$$

in which:

ζ_0 = amplitude of undisturbed wave (m)
$k = 2\pi/\lambda$ = wave number at shallow water (rad/m)
λ = wave length (m)
μ = wave direction (rad); zero for a wave travelling in the positive x-direction
ω = wave frequency (rad/s)
h_o = distance from the origin, O, of the earth-fixed axes to the sea bed (m)
h = water depth (m)

The following dispersion relation links the water depth h, the wave frequency ω, and the wave number k:

$$
\begin{aligned}
\nu \cdot g &= \omega^2 \\
&= kg \cdot \tanh kh
\end{aligned}
\tag{7.152}
$$

in which $\nu = \omega^2/g$ is the wave number in deep water.

In regular long-crested waves the undisturbed wave elevation follows from the free surface dynamic boundary condition:

$$
\zeta = -\frac{1}{g} \cdot \frac{\partial \Phi}{\partial t} \qquad \text{(see chapter 5)}
\tag{7.153}
$$

which results in:

$$
\zeta(x, y; t) = \zeta_0 \cdot e^{ik(x \cos \mu + y \sin \mu) - i\omega t}
\tag{7.154}
$$

The motions of the body in the j-mode relative to its body axes are given by:

$$
\zeta_j(t) = \overline{\zeta}_j \cdot e^{-i\omega t}
\tag{7.155}
$$

in which the overline indicates the complex amplitude of the motion.

Note that this overline (which applies to the complex potentials etc.) is neglected in the remainder of this section.

The complex potential ϕ follows from the superposition of the undisturbed wave potential ϕ_0, the wave diffraction potential ϕ_7 and the potentials ϕ_j associated with the j-modes of motion of the body ($j = 1, ...6$):

$$
\phi = -i\omega \left\{ (\phi_0 + \phi_7) \zeta_0 + \sum_{j=1}^{6} \phi_j \zeta_j \right\}
\tag{7.156}
$$

The fluid pressure follows from the Bernoulli equation:

$$
\begin{aligned}
p(x, y, z; t) &= -\rho \frac{\partial \Phi}{\partial t} \\
&= \rho \omega^2 \left\{ (\phi_0 + \phi_7) \zeta_0 + \sum_{j=1}^{6} \phi_j \zeta_j \right\} \cdot e^{-i\omega t}
\end{aligned}
\tag{7.157}
$$

The first order wave exciting forces ($k = 1, 2, 3$) and moments ($k = 4, 5, 6$) in the kth direction are:

$$
\begin{aligned}
X_k &= -\iint\limits_{S_0} p \, n_k \cdot dS_0 \\
&= -\rho \omega^2 \zeta_0 e^{-i\omega t} \iint\limits_{S_0} (\phi_0 + \phi_7) \, n_k \cdot dS_0
\end{aligned}
\tag{7.158}
$$

and the oscillating hydrodynamic forces and moments in the kth direction are:

$$
\begin{aligned}
F_k &= -\iint\limits_{S_0} p \, n_k \cdot dS_0 \\
&= -\rho \omega^2 \sum_{j=1}^{6} \zeta_j e^{-i\omega t} \iint\limits_{S_0} \phi_j \, n_k \cdot dS_0
\end{aligned}
\tag{7.159}
$$

in which:

$$
\begin{aligned}
S_0 &= \text{mean wetted surface of the body} \\
n_k &= \text{direction cosine of surface element } dS_0 \text{ for the } k\text{-mode}
\end{aligned}
$$

The generalized direction cosines on S_0 are defined as follows:

$$
\begin{aligned}
n_1 &= \cos(n, x) \\
n_2 &= \cos(n, y) \\
n_3 &= \cos(n, z) \\
n_4 &= y n_3 - z n_2 \\
n_5 &= z n_1 - x n_3 \\
n_6 &= x n_2 - y n_1
\end{aligned}
\tag{7.160}
$$

The added mass and damping (coupling) coefficients are defined as follows:

$$
a_{kj} = -\Re e\left[\rho \iint_{S_0} \phi_j\, n_k \cdot dS_0 \right]
$$

$$
b_{kj} = -\Im m\left[\rho\omega \iint_{S_0} \phi_j\, n_k \cdot dS_0 \right]
\tag{7.161}
$$

The following symmetry relationships apply to these coefficients :

$$
\begin{aligned}
a_{kj} &= a_{jk} \\
b_{kj} &= b_{jk}
\end{aligned}
\tag{7.162}
$$

so that both matrices are symmetric.

7.4.2   Solving Potentials

The incident wave potential, ϕ_0, is given in equation 7.151

According to [Lamb, 1932], the potential ϕ_j at a point (x, y, z) on the mean wetted body surface S_0 due to a motion in the mode j $(j = 1, ...6)$ and the diffraction potential ϕ_7 can be represented by a continuous distribution of single sources on the body surface:

$$
\boxed{\phi_j(x, y, z) = \frac{1}{4\pi} \iint_{S_0} \sigma_j(\widehat{x}, \widehat{y}, \widehat{z}) \cdot G(x, y, z, \widehat{x}, \widehat{y}, \widehat{z}) \cdot dS_0} \qquad \text{for } j = 1, ...7 \tag{7.163}
$$

in which:

- $\phi_j(x, y, z)$ is the **potential function** in a point (x, y, z) on the mean wetted body surface, S_0. The cases with $j = 1, ...6$ correspond to the potentials due to a motion of the body in the jth mode, while ϕ_7 is the potential of the diffracted waves. The individual potentials satisfy all boundary conditions.

- $\sigma_j(\widehat{x}, \widehat{y}, \widehat{z})$ is the complex **source strength** in a point $(\widehat{x}, \widehat{y}, \widehat{z})$ on the mean wetted body surface, S_0, due to a motion of the body in the j-mode.

- $G(x, y, z, \widehat{x}, \widehat{y}, \widehat{z})$ is the **Green's function** or **influence function** of the pulsating source $\sigma_j(\widehat{x}, \widehat{y}, \widehat{z})$ in a point located at $(\widehat{x}, \widehat{y}, \widehat{z})$ on the potential $\phi_j(x, y, z)$ in a point located at (x, y, z), singular for $(\widehat{x}, \widehat{y}, \widehat{z}) = (x, y, z)$. This Green's function satisfies the Laplace equation, the linearized boundary conditions on the sea bed and on the free surface and the radiation condition at infinity.

Equivalent Green's functions are given by [Wehausen and Laitone, 1960] and [John, 1949]:

$$\overline{|G(x, y, z, \widehat{x}, \widehat{y}, \widehat{z})|} \text{ according to [Wehausen and Laitone, 1960]} = \qquad (7.164)$$

$$\frac{1}{r} + \frac{1}{r_1}$$

$$+ PV \int\limits_0^\infty \frac{2(\xi + \nu)e^{-\xi h} \cdot \cosh \xi(h_o + \widehat{z}) \cdot \cosh \xi(h_o + z)}{\xi \sinh \xi h - \nu \cosh \xi h} \cdot J_0(\xi R) \cdot d\xi$$

$$+ i \cdot \frac{2\pi(k^2 - \nu^2) \cdot \cosh k(h_o + \widehat{z}) \cdot \cosh k(h_o + z)}{(k^2 - \nu^2)h - \nu} \cdot J_0(kR)$$

$$\overline{|G(x, y, z, \widehat{x}, \widehat{y}, \widehat{z})|} \text{ according to [John, 1949]} = \qquad (7.165)$$

$$2\pi \cdot \frac{\nu^2 - k^2}{(k^2 - \nu^2)\, h + \nu} \cdot \cosh k(h_o + z) \cdot \cosh k(h_o + \widehat{z}) \cdot \{Y_0(kr) - iJ_0(kR)\}$$

$$+ \sum_{i=1}^\infty \frac{4\left(k_i^2 + \nu^2\right)}{\left(k_i^2 + \nu^2\right) h - \nu} \cdot \cos k_i(h_o + z) \cdot \cos k_i(h_o + \widehat{z}) \cdot K_0(k_iR)$$

in which:

$$
\begin{aligned}
r &= \sqrt{(x - \widehat{x})^2 + (y - \widehat{y})^2 + (z - \widehat{z})^2} \\
r_1 &= \sqrt{(x - \widehat{x})^2 + (y - \widehat{y})^2 + (z + 2h_o + \widehat{z})^2} \quad (= \text{mirrored}) \\
R &= \sqrt{(x - \widehat{x})^2 + (y - \widehat{y})^2} \\
\xi &= \text{a variable} \\
J_0,\ K_0 \text{ and } Y_0 &= \text{Bessel functions} \\
k_i &= \text{positive solutions of } \tanh(k_i h) + \nu = 0
\end{aligned}
$$

Although these two representations are equivalent, one of the two may be preferred for numerical computations depending on the values of the variables. In general, equation 7.165 is the most convenient representation for calculations, but when $R = 0$ the value of K_0 becomes infinite, so that equation 7.164 must be used when R is small or zero.

In DELFRAC and many other similar diffraction computer codes, use is made of the FINGREEN subroutine supplied by MIT for the purpose of computing the Green's function and its derivatives. Computation involving both formulations has been speeded up through the use of polynomial expressions, see [Newman, 1985].

The unknown source strengths $\sigma_j(\widehat{x}, \widehat{y}, \widehat{z})$ are determined based on the normal velocity boundary condition on the body, see equation 7.157 combined with equation 7.163:

$$
\begin{aligned}
\frac{\partial \phi_j}{\partial n} &= n_j \\
&= -\frac{1}{2}\sigma_j(x, y, z) + \frac{1}{4\pi} \iint\limits_{S_0} \sigma_j(\widehat{x}, \widehat{y}, \widehat{z}) \cdot \frac{\partial G(x, y, z, \widehat{x}, \widehat{y}, \widehat{z})}{\partial n} \cdot dS_0 \qquad (7.166)
\end{aligned}
$$

In the above equations, the operator $\partial/\partial n$ signifies the gradient in the direction of the normal to the surface of the body. For the solution of the motion potentials ϕ_j, the right-hand side of the above equation 7.166 is given by the direction cosines defined by equation 7.160.

For the solution of the diffraction potential ϕ_7 (restrained body), the right-hand side is given by:

$$n_7 = \frac{\partial \phi_7}{\partial n} = -\frac{\partial \phi_0}{\partial n} \tag{7.167}$$

Solving the integral equation 7.166 results in the unknown source strengths. Substitution of these in equation 7.162 and in equation 7.159 yields the added mass and damping coefficients and the wave forces respectively.

Finally the motions ζ_j are determined from the solution of the following coupled equations of motion for six degrees of freedom:

$$\boxed{\sum_{j=1}^{6} \left\{ -\omega^2 (m_{kj} + a_{kj}) - i\omega b_{kj} + c_{kj} \right\} \cdot \zeta_j = X_k} \qquad \text{for } k = 1, ...6 \tag{7.168}$$

with:

$$
\begin{aligned}
m_{kj} \quad &= \quad \text{inertia matrix of the body for inertia coupling in the } k\text{-mode} \\
&\qquad \text{for acceleration in the } j\text{-mode} \\
a_{kj} \quad &= \quad \text{added mass matrix for the force on the body in the } k\text{-mode} \\
&\qquad \text{due to acceleration of the body in the } j\text{-mode} \\
b_{kj} \quad &= \quad \text{damping matrix for the force on the body in the } k\text{-mode} \\
&\qquad \text{due to velocity of the body in the } j\text{-mode} \\
c_{kj} \quad &= \quad \text{spring matrix for the force on the body in the } k\text{-mode} \\
&\qquad \text{due to motion of the body in the } j\text{-mode} \\
X_k \quad &= \quad \text{wave force on the body in the } k\text{-mode}
\end{aligned}
$$

The b_{kj} and c_{kj} matrices may contain contributions arising from mechanical damping devices and springs or even a mooring system.

7.4.3 Numerical Aspects

By discretizing the mean wetted surface of a body into N panels, on which the source strengths are homogeneously distributed, the following discretized form of equation 7.166 is obtained:

$$-\frac{1}{2}\sigma_{mj} + \frac{1}{4\pi}\sum_{n=1}^{N}\sigma_{nj}\frac{\partial G_{mn}}{\partial n}\triangle S_n = n_{mj} \qquad \text{for } m = 1, ...N \quad n \neq m \tag{7.169}$$

The normal velocity requirement can only be met at one point for each panel into which the mean wetted surface of the hull is divided. It is customary to chose the centroid of the panel. Such points are known as **collocation points**; see appendix D.

Equation 7.169 is transformed into a set of simultaneous linear equations in N unknown complex source strengths:

$$
\begin{pmatrix}
A_{11} & \dots & \dots & \dots & A_{1N} \\
\dots & A_{22} & \dots & \dots & \dots \\
\dots & \dots & A_{33} & \dots & \dots \\
\dots & \dots & \dots & \dots & \dots \\
A_{N1} & \dots & \dots & \dots & A_{NN}
\end{pmatrix}
\cdot
\begin{pmatrix}
\sigma_{1,j} \\
\dots \\
\dots \\
\dots \\
\sigma_{N,j}
\end{pmatrix}
=
\begin{pmatrix}
n_{1,j} \\
\dots \\
\dots \\
\dots \\
n_{N,j}
\end{pmatrix}
\tag{7.170}
$$

in which:

$$
\begin{aligned}
A_{nn} &= -\frac{1}{2} \\
A_{nm} &= \frac{1}{4\pi}\frac{\partial G_{mn}}{\partial n}\,\triangle S_n \\
\sigma_{n,j} &= \text{unknown source strength} \\
n_{nj} &= \text{normal velocity component on the oscillating body}
\end{aligned}
$$

This set of equations can be solved by direct solution techniques or by iterative solvers. The computational effort involved with iterative solvers is quadratic in the number of unknowns while for direct solvers the effort is a cubic function of the number of unknowns.

It should be noted that in the evaluation of the coefficients A_{nm} due care has to be taken when the field point (center of a target panel) is close to the source point. Inaccuracies will occur due to the $1/r$-behavior of the influence function G_{mn} as seen in equation 7.164. In this case, the $1/r$-contribution is subtracted from the influence function and is analytically integrated over the finite sized source panel under the assumption that the source strength is homogeneously distributed. Use can be made of an algorithm provided by [Fang, 1985]. Similar cases of inaccurate evaluations of the influence functions based directly upon equation 7.164 and equation 7.165 are found when a source panel is very close to the sea bed and when close to the free surface. The solution in both cases is to remove the relevant terms from the above-mentioned equations and to insert equivalent analytical integrations over the source panel.

The above modifications concern simple contributions to the influence function, such as the $1/r$, $1/r_1$ or logarithmic contributions. Where more complicated contributions are concerned such as expressed in the Principle Value integral part of equation 7.164, $(PV \int ...... d\xi)$, a more accurate evaluation of the contribution to the influence function can be made for smaller values of r by the application of Gauss quadrature methods. These simply imply that for smaller values of r the source panel is split into 4 or more parts and the total influence function is the sum of the influences from the parts of the total panel under the assumption that the source strength per unit surface is the same for all parts of the panel. In this way the influence function can be determined more accurately without increasing the number of unknowns to be solved.

A numerical problem associated with the solution of equation 7.170 is the occurrence of so-called **irregular frequencies**. For certain, discrete wave frequencies the determinant of the coefficients A_{mn} will become zero, yielding unrealistic results. "Leakage" of the effects of these irregular frequencies to a band around these frequencies occurs due to the discretization of the body. Irregular frequencies are associated with eigenfrequencies of the internal (non-physical) flow of the body. An effective method to reduce the effects of

irregular frequencies is, among others, to "close" the body by means of discretization of the free surface inside the body (putting a "lid" on the free surface inside the body); see the added mass and damping of a hemisphere in figure 7.12. The solid line in this figure results from including the "lid". Increasing the number of panels does not remove the irregular frequency but tends to restrict the effects to a narrower band around it; see for instance [Huijsmans, 1996]. It should be mentioned that irregular frequencies only occur for free surface piercing bodies; fully submerged bodies do not display these characteristics.
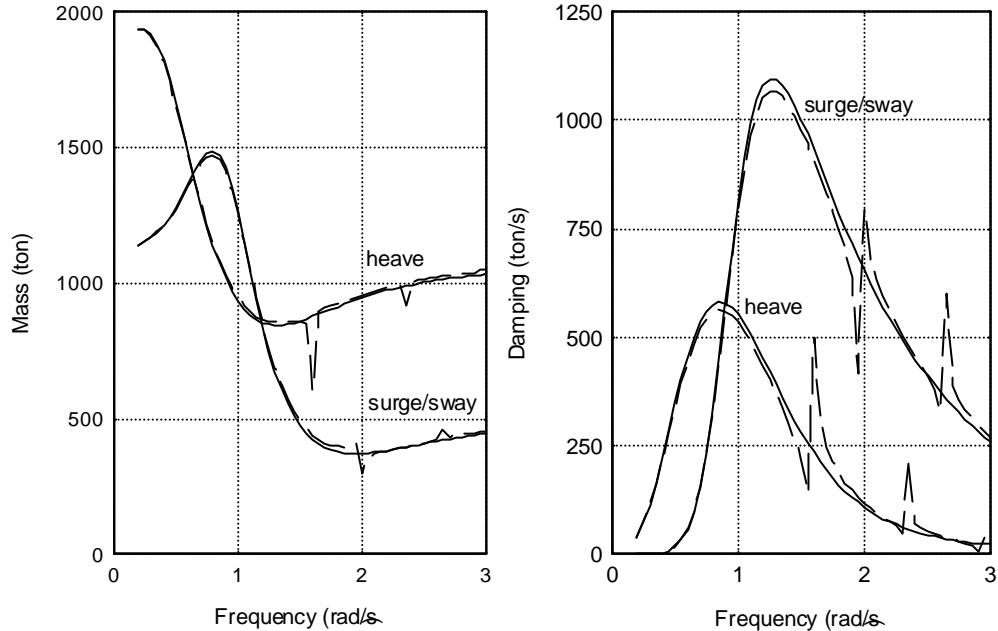
Figure 7.12: Effect of "Lid-Method" on Irregular Frequencies

Solving equation 7.170 using direct solution methods (LU-decomposition) is time consuming if the number of unknowns (N complex quantities σ) is large. The time taken to solve the equations by a direct method is proportional to N^3. Iterative solvers are proportional to N^2. However, due to other program overhead, such as the evaluation of the coefficients A_{mn} for each wave frequency, iterative solvers only become faster if there are more than about 500 panels on a body. Normally a tanker-shaped vessel can be described adequately by 300-600 panels. In day-to-day practice one tends to use the direct method based on LU-decomposition.

A useful method to reduce computation times lies in exploiting any geometrical symmetry a body may have. A ship-shaped vessel will generally have port side - starboard side symmetry while, for instance a simple barge or a semi-submersible will often have both port side - starboard side as well as fore - aft symmetry. In the latter case we need only describe one quadrant of the hull shape. The three remaining quadrants can be obtained by simply copying, but taking into account sign changes in the coordinates.

The reduction in computation time lies in the fact that, for instance for a vessel with port side - starboard side symmetry, the matrix of influence coefficients A_{mn} also shows

symmetry. In such cases the matrix of influence coefficients has the following structure:

$$
\begin{pmatrix}
A_{11} & ... & ... & A_{1N} \\
... & A_{22} & ... & ... \\
... & ... & ... & ... \\
A_{N1} & ... & ... & A_{NN}
\end{pmatrix}
=
\begin{pmatrix}
A & B \\
B & A
\end{pmatrix}
\tag{7.171}
$$

The right-hand-side of equation 7.171 expresses the fact that the self-influence of the port side half of the vessel (upper left A) is the same as the self-influence of the starboard half of the vessel (lower right A). The cross-influence of sources on the port side half of the vessel on panels on the starboard half of the vessel is contained in the lower left matrix B. The corresponding cross-influence of sources on the starboard half of the vessel on panels on the port side half are contained in the upper right matrix B.

For vessels which have double symmetry i.e. port side - starboard and fore - aft symmetry, the matrix of influence coefficients has the following structure:

$$
\begin{pmatrix}
A_{11} & ... & ... & A_{1N} \\
... & A_{22} & ... & ... \\
... & ... & ... & ... \\
A_{N1} & ... & ... & A_{NN}
\end{pmatrix}
=
\begin{pmatrix}
A & B & C & D \\
B & A & D & C \\
C & D & A & B \\
D & C & B & A
\end{pmatrix}
\tag{7.172}
$$

It is left as an exercise for the reader to deduce the effect that exploitation of such symmetries can have on the computational effort involved in solving equation 7.170.

7.5   Experimental Determination

The hydrodynamic coefficients in the equations of motion can be obtained experimentally by decay tests or by forced oscillation tests with ship models. The principle and limitations of these tests have been explained in chapter 6.

Free decay tests with a ship model in still water can be carried out only for those motions which have a hydromechanical restoring force or moment; heave, pitch and roll motions. External springs can be used for the other ship motions: surge, sway and yaw. The hydrodynamic coefficients can be found for a restricted range of (natural) frequencies, by varying the stiffness of these springs (if possible) in these decay tests.

Forced oscillation tests in still water yield the hydrodynamic mass and damping coefficients at any frequency of oscillation from the measured exciting loads. The coupling coefficients between the motions can be obtained as well. By means of forced oscillation tests with ship models, the relation between the potential coefficients and the frequency of oscillation can be found.

7.5.1   Free Decay Tests

Free decay test methodology has been discussed in chapter 6; only an example of some results for roll of ships is given here.

The successively found values for the dimensionless roll damping coefficient, κ, plotted as a function of the mean roll amplitude, ϕ_a, will often have a non-linear behavior as illustrated in figure 7.13.
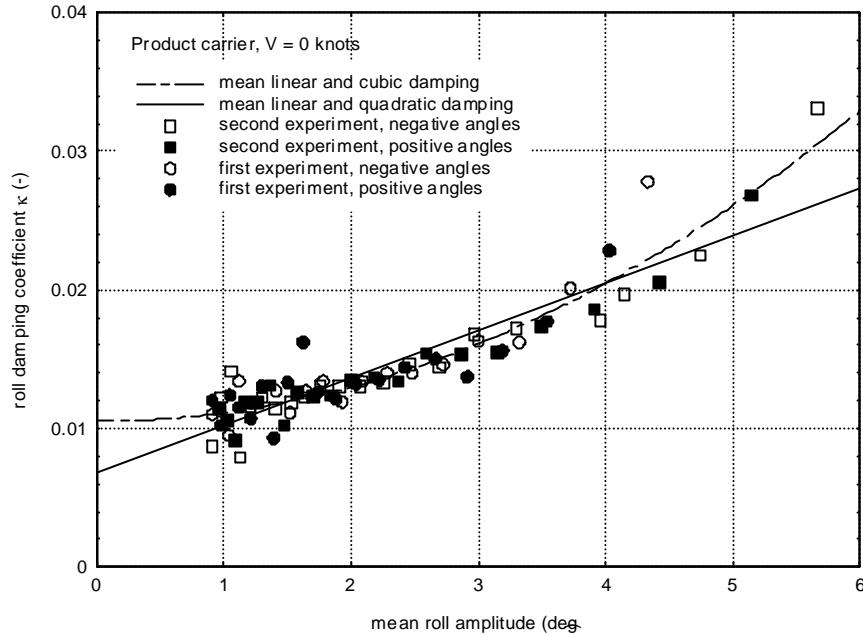
Figure 7.13: Nonlinear Roll Damping

This behavior can be described by:

$$\boxed{\kappa = \kappa_1 + \kappa_2\phi_a \quad \left(+\kappa_3\phi_a^2\right)} \tag{7.173}$$

This implies that during frequency domain calculations the damping term depends on the solution for the roll amplitude. With a certain wave amplitude, this problem can be solved in an iterative manner. A less accurate method is to use a fixed ϕ_a. Generally, a linearization will be carried out as described in chapter 6.

Note that a linear damping results in a 'horizontal' line in figure 7.13, $\kappa = \kappa_1$.

[Journée, 1991] published results of a series of free decay experiments with rectangular barge models at an even keel condition and with the center of gravity at the waterline. During these experiments, the models (with B/T values up to 10) were free to carry out heave and roll motions only. He found that the roll damping coefficients of these barges can be approximated by:

$$
\begin{aligned}
\kappa_1 &= 0.00130 \cdot \left(\frac{B}{T}\right)^2 \qquad \text{(barge with } G \text{ at waterline)} \\
\kappa_2 &= 0.500 \\
\kappa_3 &= 0.000
\end{aligned}
\tag{7.174}
$$

in which B is the breadth and T is the draft of the barge.

For large breadth-draft ratios of these barges $(B/T > 10)$, generally the potential part of the roll damping becomes so important that, at least from a practical point of view, the viscous part of the damping can be ignored.

7.5.2   Forced Oscillation Tests

The model is mounted on two vertical struts along its longitudinal center line, spaced symmetrically with respect to the center of gravity. If the struts are oscillated in unison, so that the strut motions aft and forward are the same, the model executes a sinusoidal heave motion. If the strut motions are opposite (a phase shift of 180 degrees) the model executes a sinusoidal pitch motion. All other motions are restrained and the forces necessary to impose the heave or pitch oscillation are measured by transducers at the ends of the struts and suitably recorded. To avoid internal stresses, the aft transducer is fitted with a swinging link or mounted on a horizontal sled.

A schematic of the experimental set-up for forced heave and pitch oscillations is given in figure 7.14.

[Source: Lloyd, 1989]
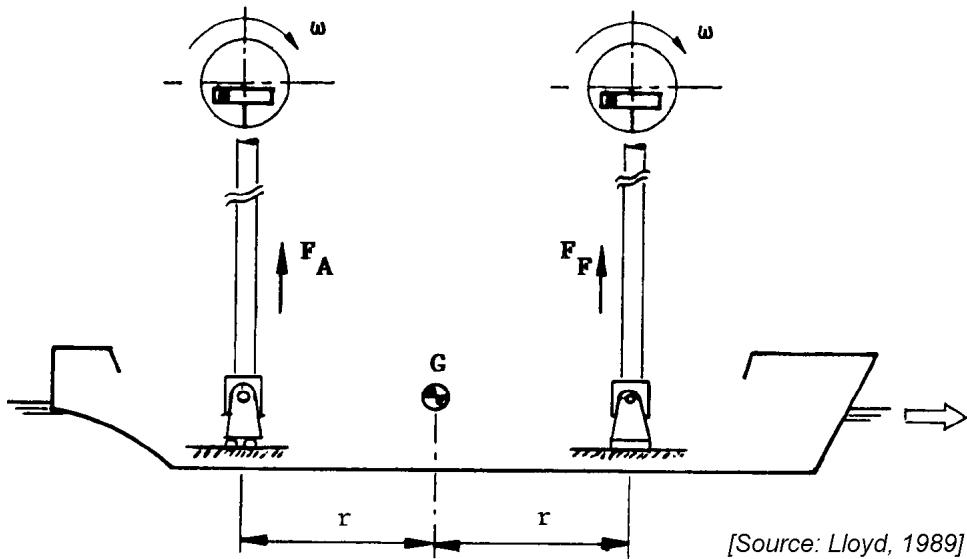
Figure 7.14: Forced Heave Oscillation Experiment

During the forced heave or pitch oscillations the vertical motions of the transducer aft and forward are $z_A(t)$ and $z_F(t)$ respectively, with equal amplitudes z_a.
Then the motions of the model are defined by:

$$\text{heave oscillations} \quad : \quad z(t) = z_A(t) = z_F(t) = z_a \sin \omega t \qquad (7.175)$$

$$\text{pitch oscillations} \quad : \quad \theta(t) = \arctan \left\{ \frac{z_A(t) - z_F(t)}{2r} \right\} \approx \frac{z_a}{r} \sin \omega t = \theta_a \sin \omega t$$

During both type of oscillations, the heave forces and pitch moments can be obtained from the measured forces in the transducer aft $F_A(t)$ and the transducer forward $F_F(t)$:

$$\text{heave force} \quad : \quad F_z(t) = F_A(t) + F_F(t) \quad = F_a \sin(\omega t + \varepsilon_{Fz})$$

$$\text{pitch moment} \quad : \quad M_\theta(t) = r \left\{ F_A(t) - F_F(t) \right\} = M_a \sin(\omega t + \varepsilon_{Mz}) \qquad (7.176)$$

Heave Oscillations

The linear equations of motion during the heave oscillations are given by:

$$a\ddot{z} + b\dot{z} + cz \quad = \quad F_a \sin\left(\omega t + \varepsilon_{Fz}\right)$$

$$d\ddot{z} + e\dot{z} + fz \quad = \quad M_a \sin\left(\omega t + \varepsilon_{Mz}\right) \tag{7.177}$$

The components of the force and moment which are in-phase with the heave motion are associated with the inertia and stiffness coefficients, while the out-of-phase components (also called in literature: quadrature components) are associated with damping.
With:

$$z = z_a \sin\omega t \qquad \dot{z} = z_a\omega\cos\omega t \qquad \ddot{z} = -z_a\omega^2 \sin\omega t \tag{7.178}$$

we obtain:

$$z_a\left(-a\omega^2 + c\right)\sin\omega t + z_a b\omega \cos\omega t \quad = \quad F_a \cos\varepsilon_{Fz}\sin\omega t + F_a \sin\varepsilon_{Fz}\cos\omega t$$
$$z_a\left(-d\omega^2 + f\right)\sin\omega t + z_a e\omega \cos\omega t \quad = \quad M_a \cos\varepsilon_{Mz}\sin\omega t + M_a \sin\varepsilon_{Mz}\cos\omega t \tag{7.179}$$

which provides:

$$
\begin{aligned}
a = \ \rho\nabla + a_{zz} \ &= \ \frac{c - \frac{F_a}{z_a}\cos\varepsilon_{Fz}}{\omega^2} \quad \text{with:} \quad c = c_{zz} = \rho g A_w \\[2mm]
b = \qquad b_{zz} \ &= \ \frac{\frac{F_a}{z_a}\sin\varepsilon_{Fz}}{\omega} \\[2mm]
d = \qquad a_{\theta z} \ &= \ \frac{f - \frac{M_a}{z_a}\cos\varepsilon_{Mz}}{\omega^2} \quad \text{with:} \quad f = c_{\theta z} = \rho g S_w \\[2mm]
e = \qquad b_{\theta z} \ &= \ \frac{\frac{M_a}{z_a}\sin\varepsilon_{Mz}}{\omega}
\end{aligned} \tag{7.180}
$$

To obtain the stiffness coefficients c and f, use has to be made of A_w (area of the waterline) and S_w (first order moment of the waterline), which can be obtained from the geometry of the ship model.
It is also possible to obtain the stiffness coefficients from static experiments:

$$\ddot{z} = 0 \quad \text{and} \quad \dot{z} = 0 \qquad \text{provides:} \qquad c = \frac{F}{z} \quad \text{and} \quad f = \frac{M}{z}$$

Pitch Oscillations

The linear equations during the pitch oscillations are given by:

$$
\begin{aligned}
a\ddot{\theta} + b\dot{\theta} + c\theta \ &= \ F_a \sin\left(\omega t + \varepsilon_{F\theta}\right) \\
d\ddot{\theta} + e\dot{\theta} + f\theta \ &= \ M_a \sin\left(\omega t + \varepsilon_{M\theta}\right)
\end{aligned} \tag{7.181}
$$

The components of the force and moment which are in-phase with the pitch motion are associated with the inertia and stiffness coefficients, while the out-of-phase components are associated with damping.
With:

$$\theta = \theta_a \sin\omega t \qquad \dot{\theta} = \theta_a\omega\cos\omega t \qquad \ddot{\theta} = -\theta_a\omega^2 \sin\omega t \tag{7.182}$$

we obtain:

$$\theta_a\left(-a\omega^2 + c\right)\sin\omega t + \theta_a b\omega\cos\omega t \quad = \quad F_a \cos\varepsilon_{F\theta}\sin\omega t + F_a \sin\varepsilon_{F\theta}\cos\omega t$$
$$\theta_a\left(-d\omega^2 + f\right)\sin\omega t + \theta_a e\omega\cos\omega t \quad = \quad M_a \cos\varepsilon_{M\theta}\sin\omega t + M_a \sin\varepsilon_{M\theta}\cos\omega t \tag{7.183}$$

which provides:

$$a = \quad a_{z\theta} = \frac{c - \frac{F_a}{\theta_a}\cos\varepsilon_{F\theta}}{\omega^2} \quad \text{with:} \quad c = c_{z\theta} = \rho g S_w$$

$$b = \quad b_{z\theta} = \frac{\frac{F_a}{\theta_a}\sin\varepsilon_{F\theta}}{\omega}$$

$$d = I_{yy} + a_{\theta\theta} = \frac{f - \frac{M_a}{\theta_a}\cos\varepsilon_{M\theta}}{\omega^2} \quad \text{with:} \quad f = c_{\theta\theta} = \rho g \nabla \overline{GM_L}$$

$$e = \quad b_{\theta\theta} = \frac{\frac{M_a}{\theta_a}\sin\varepsilon_{M\theta}}{\omega} \tag{7.184}$$

To obtain the stiffness coefficients c and f, use has been made of S_w (first order moment of the waterline) and $\overline{GM_L}$ (longitudinal metacentric height), which can be obtained from the geometry of the ship model.

It is also possible to obtain the stiffness coefficients from static experiments:

$$\ddot{\theta} = 0 \quad \text{and} \quad \dot{\theta} = 0 \qquad \text{provides:} \qquad c = \frac{F}{\theta} \quad \text{and} \quad f = \frac{M}{\theta} \tag{7.185}$$

Signal Processing

The in-phase and out-of-phase parts of the measured signal can be found easily from an integration over an integer number n of periods T of the measure signals multiplied by $\cos\omega t$ and $\sin\omega t$, respectively. This is in fact a first order Fourier analysis; see appendix C.

For the heave oscillations, this results in:

$$F_a \sin\varepsilon_{Fz} = \frac{2}{nT}\int_0^{nT}(F_A(t) + F_F(t))\cdot\cos\omega t \cdot dt$$

$$F_a \cos\varepsilon_{Fz} = \frac{2}{nT}\int_0^{nT}(F_A(t) + F_F(t))\cdot\sin\omega t \cdot dt$$

$$M_a \sin\varepsilon_{Mz} = \frac{2r}{nT}\int_0^{nT}(F_A(t) - F_F(t))\cdot\cos\omega t \cdot dt$$

$$M_a \cos\varepsilon_{Mz} = \frac{2r}{nT}\int_0^{nT}(F_A(t) - F_F(t))\cdot\sin\omega t \cdot dt \tag{7.186}$$

Similar expressions can be found for the pitch oscillations.

Equations of Motion

With the measured hydromechanical coefficients, the coupled linear equations of heave and pitch motions in still water are given by:

$$(\rho\nabla + a_{zz})\ddot{z} + b_{zz}\dot{z} + c_{zz}z + a_{z\theta}\ddot{\theta} + b_{z\theta}\dot{\theta} + c_{z\theta}\theta = 0$$

$$(I_{xx} + a_{\theta\theta})\ddot{\theta} + b_{\theta\theta}\dot{\theta} + c_{\theta\theta}\theta + a_{\theta z}\ddot{z} + b_{\theta z}\dot{z} + c_{\theta z}z = 0 \tag{7.187}$$

7.6 Viscous Damping

Motion damping is caused by the generated waves which dissipate energy from the moving structure as well as by viscous effects such as skin friction, vortices, etc. In most cases viscous effects are neglected in motion calculations of offshore structures as well as for the sway, heave, pitch and yaw motions of ships. The major part of the damping is caused by the wave (or potential) damping and the viscous damping contribution to these are of minor importance.

7.6.1 Viscous Surge Damping

Generally, the hydromechanical coefficients for surge are small. The hydrodynamic mass is 5-8 % of the ship's mass and the damping is small. In fact, the total damping components for surge of sailing ships have been treated already in chapter 4, because this damping coefficient can be written as:

$$b_{xx} = \frac{dR_t}{dV} = \frac{dR_f}{dV} + \frac{dR_r}{dV}$$

where R_t is the total resistance, R_f is the frictional (viscous) resistance and R_r is the residual (potential) resistance and V is the forward ship speed; the viscous part of the surge damping is dR_f/dV.

7.6.2 Viscous Roll Damping
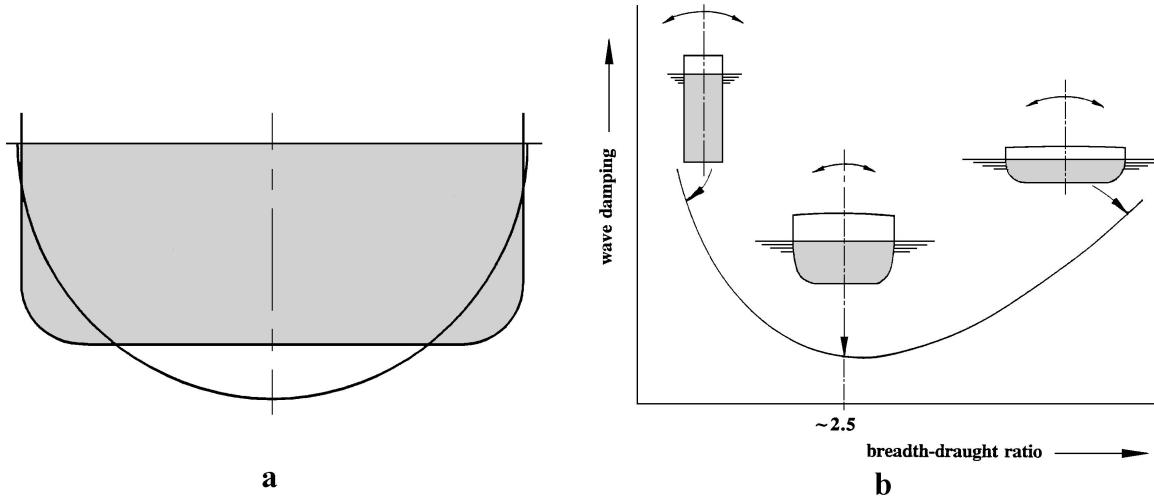
Figure 7.15: Roll Damping as Function of Shape and B/T Ratio

Viscous damping can be significant for rolling ships. This is because the wave potential damping for roll is generally relatively small itself. A circular cylinder, rotating about its center, does not produce waves; its potential roll damping is zero. For a breadth-draft ratio of about 2.5, the major part of the ship has a "more or less" circular cross section, see figure 7.15-a.

Thus, for many ships a small potential roll damping can be expected too. A relatively significant viscous contribution, for instance due to bilge keels, can be expected.

The relation between the roll damping and the breadth-draft ratio of a cross section of a ship is given in figure 7.15-b.

As indicated above, the roll damping is minimum at a breadth-draft ratio of about 2.5. For very low breadth-draft ratios (paddle-type wave maker) and for high breadth-draft ratios (wave damper of a towing carriage in a towing tank) the wave damping component is very high.

For the estimation of the non-potential parts of the roll damping, in many cases use can be made of work published by [Ikeda et al., 1978]. This empirical method is often called the "Ikeda method" and it estimates viscous roll damping contributions due to forward ship speed, skin friction, eddy making, lift and bilge keels, see figure 7.16.
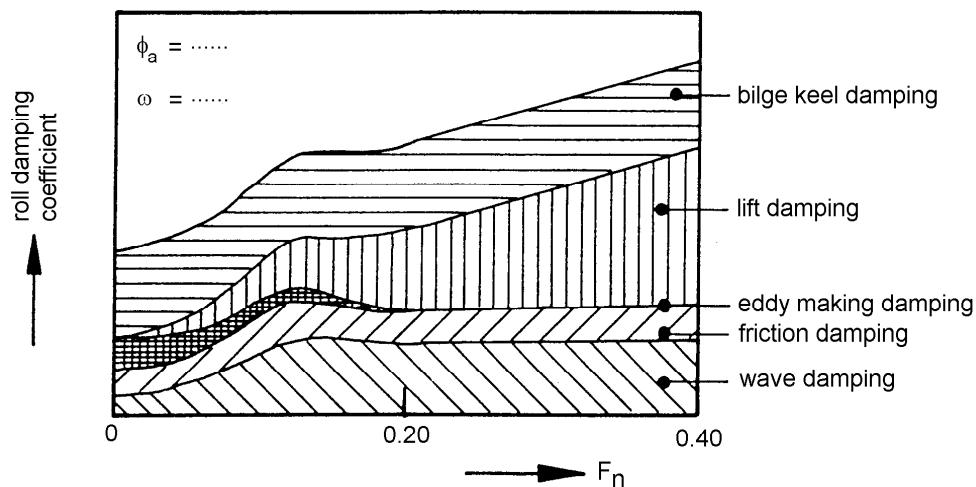
Figure 7.16: Roll Damping Components

Ikeda, Himeno and Tanaka claim fairly good agreements between their prediction method and experimental results. They conclude that the method can be used safely for ordinary ship forms, which conclusion has been confirmed by numerous experiments carried out by other researchers. But for unusual ship forms, very full ship forms and ships with a very large breadth to draft ratio the method is not always accurate sufficiently.

Chapter 8

FLOATING STRUCTURES IN WAVES

8.1 Introduction

The (uncoupled) motions of a simple rigid body at zero forward speed have been discussed in chapter 6. Potential coefficients and their determination for more complex hull forms, such as those of ships and offshore structures, have been described in chapter 7.

This chapter deals with the kinetics, the equations of motion for six degrees of freedom and some motion related phenomena for ships and offshore structures, partly including the forward speed effect.

8.2 Kinetics

The total mass as well as its distribution over the body is considered to be constant with time. For ships and other floating structures, this assumption is normally valid during a time which is large relative to the period of the motions. This holds that small effects, such as for instance a decreasing mass due to fuel consumption, can be ignored.

The solid mass matrix of a floating structure is given below.

$$
\text{Solid mass matrix: } m = \begin{pmatrix}
\rho\nabla & 0 & 0 & 0 & 0 & 0 \\
0 & \rho\nabla & 0 & 0 & 0 & 0 \\
0 & 0 & \rho\nabla & 0 & 0 & 0 \\
0 & 0 & 0 & I_{xx} & 0 & -I_{xz} \\
0 & 0 & 0 & 0 & I_{yy} & 0 \\
0 & 0 & 0 & -I_{zx} & 0 & I_{zz}
\end{pmatrix} \tag{8.1}
$$

The moments of inertia here are often expressed in terms of the radii of inertia and the solid mass of the structure. Since Archimedes law is valid for a floating structure:

$$
\begin{aligned}
I_{xx} &= k_{xx}{}^2 \cdot \rho\nabla \\
I_{yy} &= k_{yy}{}^2 \cdot \rho\nabla \\
I_{zz} &= k_{zz}{}^2 \cdot \rho\nabla
\end{aligned} \tag{8.2}
$$

When the distribution of the solid mass of a ship is unknown, the radii of inertia can be approximated by:

$$\text{for ships:} \quad \begin{cases} k_{xx} & \approx & 0.30 \cdot B \text{ to } 0.40 \cdot B \\ k_{yy} & \approx & 0.22 \cdot L \text{ to } 0.28 \cdot L \\ k_{zz} & \approx & 0.22 \cdot L \text{ to } 0.28 \cdot L \end{cases}$$

in which L is the length and B is the breadth of the ship; the (generally small) coupling terms, $I_{xz} = I_{zx}$, are simply neglected.

Bureau Veritas proposes for the gyradius in roll:

$$k_{xx} = 0.289 \cdot B \cdot \left(1.0 + \left(\frac{2 \cdot \overline{KG}}{B} \right)^2 \right) \tag{8.3}$$

in which $\overline{KG}$ is the height of the center of gravity, G, above the keel.

For many ships without cargo on board (ballast condition), the mass is concentrated at the ends (engine room aft and ballast water forward to avoid a large trim), while for ships with cargo on board (full load condition) the - more or less amidships laden - cargo plays an important role. Thus, the radii of inertia, k_{yy} and k_{zz}, are usually smaller in the full load condition than in the ballast condition for normal ships. Note that the longitudinal radius of gyration of a long homogeneous rectangular beam with a length L is equal to about $0.29 \cdot L \left(= \sqrt{1/12} \cdot L \right)$.

As already mentioned in chapter 6, the equations of motions of a rigid body in a space fixed coordinate system follow from Newton's second law. The vector equations for the translations of and the rotations about the center of gravity are given respectively by:

$$\boxed{\vec{F} = \frac{d}{dt}\left(m\vec{U} \right)} \quad \text{and} \quad \boxed{\vec{M} = \frac{d}{dt}\left(\vec{H} \right)} \tag{8.4}$$

in which:

$$
\begin{array}{rcl}
\vec{F} & = & \text{resulting external force acting in the center of gravity} \\
m & = & \text{mass of the rigid body} \\
\vec{U} & = & \text{instantaneous velocity of the center of gravity} \\
\vec{M} & = & \text{resulting external moment acting about the center of gravity} \\
\vec{H} & = & \text{instantaneous angular momentum about the center of gravity} \\
t & = & \text{time}
\end{array}
$$

As mentioned in chapter 6 as well, two important assumptions are made for the loads in the right hand side of these equations:

a. The so-called **hydromechanical forces and moments** are induced by the harmonic oscillations of the rigid body, moving in the undisturbed surface of the fluid.

b. The so-called **wave exciting forces and moments** are produced by waves coming in on the restrained body.

Since the system is linear, these loads are added to obtain the total loads. Thus, after assuming small motions, symmetry of the body and that the x-, y- and z-axes are principal

axes, one can write the following six motion equations for the ship:

$$\text{Surge:} \quad \frac{d}{dt}\left(\rho\nabla\cdot\dot{x}\right) \quad = \rho\nabla\cdot\ddot{x} \quad = X_{h_1} + X_{w_1}$$

$$\text{Sway:} \quad \frac{d}{dt}\left(\rho\nabla\cdot\dot{y}\right) \quad = \rho\nabla\cdot\ddot{y} \quad = X_{h_2} + X_{w_2}$$

$$\text{Heave:} \quad \frac{d}{dt}\left(\rho\nabla\cdot\dot{z}\right) \quad = \rho\nabla\cdot\ddot{z} \quad = X_{h_3} + X_{w_3}$$

$$\text{Roll:} \quad \frac{d}{dt}\left(I_{xx}\cdot\dot{\phi} - I_{xz}\cdot\dot{\psi}\right) = I_{xx}\cdot\ddot{\phi} - I_{xz}\cdot\ddot{\psi} = X_{h_4} + X_{w_4}$$

$$\text{Pitch:} \quad \frac{d}{dt}\left(I_{yy}\cdot\dot{\theta}\right) \quad = I_{xx}\cdot\ddot{\theta} \quad = X_{h_5} + X_{w_5}$$

$$\text{Yaw:} \quad \frac{d}{dt}\left(I_{zz}\cdot\dot{\psi} - I_{zx}\cdot\dot{\phi}\right) = I_{zz}\cdot\ddot{\psi} - I_{zx}\cdot\ddot{\phi} = X_{h_6} + X_{w_6} \quad (8.5)$$

in which:

$$
\begin{array}{lll}
\rho & = & \text{density of water} \\
\nabla & = & \text{volume of displacement of the ship} \\
I_{ij} & = & \text{solid mass moment of inertia of the ship} \\
X_{h_1}, X_{h_2}, X_{h_3} & = & \text{hydromechanical forces in the } x\text{-}, y\text{- and } z\text{-directions respectively} \\
X_{h_4}, X_{h_5}, X_{h_6} & = & \text{hydromechanical moments about the } x\text{-}, y\text{- and } z\text{-axes respectively} \\
X_{w_1}, X_{w_2}, X_{w_3} & = & \text{exciting wave forces in the } x\text{-}, y\text{- and } z\text{-directions respectively} \\
X_{w_4}, X_{w_5}, X_{w_6} & = & \text{exciting wave moments about the } x\text{-}, y\text{- and } z\text{-axes respectively}
\end{array}
$$

Note: in many applications, $I_{xz} = I_{zx}$ is not known or small; hence their terms are often omitted.

8.3 Coupled Equations of Motion

Once the mass of the floating object and its distribution within that object are known, the coupled equations of motion in 6 degrees of freedom in waves can be written.

8.3.1 General Definition

Based on Newton's second law, the general equations of motion are given by:

$$\boxed{\sum_{j=1}^{6} m_{i,j}\cdot\ddot{x}_j = F_i} \qquad \text{for: } i = 1,...6 \qquad (8.6)$$

in which:

$$
\begin{array}{lll}
m_{i,j} & = & \text{6x6 matrix of solid mass and inertia of the body} \\
\ddot{x}_j & = & \text{acceleration of the body in direction } j \\
F_i & = & \text{sum of forces or moments acting in direction } i
\end{array}
$$

When defining a linear system, with simple harmonic wave exciting forces and moments given by:

$$\overline{\left| F_{w_i}(\omega_e, t) = F_{wa_i}(\omega_e) \cdot \cos\left(\omega_e t + \varepsilon_{F_i}(\omega_e)\right) \right|} \tag{8.7}$$

the resulting simple harmonic motions are:

$$
\begin{aligned}
x_j(\omega_e, t) &= x_{a_j}(\omega_e) \cdot \cos(\omega_e t) \\
\dot{x}_j(\omega_e, t) &= -\omega_e \cdot x_{a_j}(\omega_e) \cdot \sin(\omega_e t) \\
\ddot{x}_j(\omega_e, t) &= -\omega_e^2 \cdot x_{a_j}(\omega_e) \cdot \cos(\omega_e t)
\end{aligned}
\tag{8.8}
$$

The hydromechanical forces and moments $F_{h_{i,j}}$, acting on an oscillating object in still water, consist of:

- linear hydrodynamic reaction forces and moments expressed in terms with the hydrodynamic mass and damping coefficients:

$$-a_{i,j}(\omega_e) \cdot \ddot{x}_j(\omega_e, t) - b_{i,j}(\omega_e) \cdot \dot{x}_j(\omega_e, t) \tag{8.9}$$

- linear hydrostatic restoring forces and moments expressed in a term with a spring coefficient:

$$-c_{i,j} \cdot x_j(\omega_e, t) \tag{8.10}$$

With these expressions, the 6 equations of motion become:

$$
\sum_{j=1}^{6} m_{i,j} \cdot \ddot{x}_j = \sum_{j=1}^{6} \left\{ -a_{i,j}(\omega_e) \cdot \ddot{x}_j(\omega_e, t) - b_{i,j}(\omega_e) \cdot \dot{x}_j(\omega_e, t) - c_{i,j} \cdot x_j(\omega_e, t) \right.
$$
$$
\left. + F_{wa_i}(\omega_e) \cdot \cos\left(\omega_e t + \varepsilon_i(\omega_e)\right) \right\}
$$
$$
\text{for: } i = 1, ...6 \tag{8.11}
$$

After ordering the terms, the general linear equations of motion for 6 degrees of freedom in the frequency domain are:

$$
\sum_{j=1}^{6} \left\{ (m_{i,j} + a_{i,j}(\omega_e)) \cdot \ddot{x}_j(\omega_e, t) + b_{i,j}(\omega_e) \cdot \dot{x}_j(\omega_e, t) + c_{i,j} \cdot x_j(\omega_e, t) \right\}
$$
$$
= F_{wa_i}(\omega_e) \cdot \cos(\omega_e t + \varepsilon_i(\omega_e))
$$
$$
\text{for: } i = 1, ...6 \tag{8.12}
$$

The hydrodynamic coefficients, $a_{i,j}(\omega_e)$ and $b_{i,j}(\omega_e)$, and the exciting wave load components, $F_{wa_i}(\omega_e)$ and $\varepsilon_i(\omega_e)$, can be calculated with two- or three-dimensional techniques given in chapter 7.

8.3.2   Motion Symmetry of Ships

Generally, a ship has a vertical-longitudinal plane of symmetry, so that its motions can be split into symmetric and anti-symmetric components. Surge, heave and pitch motions are symmetric motions, that is to say that a point to starboard has the same motion as the mirrored point to port side. It is obvious that the remaining motions sway, roll and yaw are anti-symmetric motions. Symmetric and anti-symmetric motions are not coupled; they

don't have any effect on each other. For instance, a vertical force acting at the center of gravity can cause surge, heave and pitch motions, but will not result in sway, roll or yaw motions.

Because of this symmetry and anti-symmetry, two sets of three coupled equations of motion can be distinguished for ships:

$$
\left.
\begin{array}{lll}
\text{Surge}: & \rho\nabla \cdot \ddot{x} & -X_{h_1} = X_{w_1} \\
\text{Heave}: & \rho\nabla \cdot \ddot{z} & -X_{h_3} = X_{w_3} \\
\text{Pitch}: & I_{xx} \cdot \ddot{\theta} & -X_{h_5} = X_{w_5}
\end{array}
\right\} \quad \text{symmetric motions}
$$

$$
\left.
\begin{array}{llll}
\text{Sway}: & \rho\nabla \cdot \ddot{y} & & -X_{h_2} = X_{w_2} \\
\text{Roll}: & I_{xx} \cdot \ddot{\phi} & -I_{xz} \cdot \ddot{\psi} & -X_{h_4} = X_{w_4} \\
\text{Yaw}: & I_{zz} \cdot \ddot{\psi} & -I_{zx} \cdot \ddot{\phi} & -X_{h_6} = X_{w_6}
\end{array}
\right\} \quad \text{anti-symmetric motions}
$$

The coupled surge, heave and pitch equations of motion are:

$$
\left.
\begin{array}{l}
\begin{array}{llll}
(\rho\nabla + a_{11}) \cdot \ddot{x} & +b_{11} \cdot \dot{x} & +c_{11} \cdot x & \\
\quad +a_{13} \cdot \ddot{z} & +b_{13} \cdot \dot{z} & +c_{13} \cdot z & \\
\quad +a_{15} \cdot \ddot{\theta} & +b_{15} \cdot \dot{\theta} & +c_{15} \cdot \theta & = X_{w_1} \quad \text{(surge)}
\end{array} \\[3em]
\begin{array}{llll}
a_{31} \cdot \ddot{x} & +b_{31} \cdot \dot{x} & +c_{31} \cdot x & \\
+(\rho\nabla + a_{33}) \cdot \ddot{z} & +b_{33} \cdot \dot{z} & +c_{33} \cdot z & \\
\quad +a_{35} \cdot \ddot{\theta} & +b_{35} \cdot \dot{\theta} & +c_{35} \cdot \theta & = X_{w_3} \quad \text{(heave)}
\end{array} \\[3em]
\begin{array}{llll}
a_{51} \cdot \ddot{x} & +b_{51} \cdot \dot{x} & +c_{51} \cdot x & \\
\quad +a_{53} \cdot \ddot{z} & +b_{53} \cdot \dot{z} & +c_{53} \cdot z & \\
+(+I_{yy} + a_{55}) \cdot \ddot{\theta} & +b_{55} \cdot \dot{\theta} & +c_{55} \cdot \theta & = X_{w_5} \quad \text{(pitch)}
\end{array}
\end{array}
\right\} \quad \begin{array}{c} \text{symmetric} \\ \text{motions} \end{array}
$$

The coupled sway, roll and yaw equations of motion are:

$$
\left.
\begin{array}{l}
\begin{array}{llll}
(\rho\nabla + a_{22}) \cdot \ddot{y} & +b_{22} \cdot \dot{y} & +c_{22} \cdot y & \\
\quad +a_{24} \cdot \ddot{\phi} & +b_{24} \cdot \dot{\phi} & +c_{24} \cdot \phi & \\
\quad +a_{26} \cdot \ddot{\psi} & +b_{26} \cdot \dot{\psi} & +c_{26} \cdot \psi & = X_{w_2} \quad \text{(sway)}
\end{array} \\[3em]
\begin{array}{llll}
a_{42} \cdot \ddot{y} & +b_{42} \cdot \dot{y} & +c_{42} \cdot y & \\
+(+I_{xx} + a_{44}) \cdot \ddot{\phi} & +b_{44} \cdot \dot{\phi} & +c_{44} \cdot \phi & \\
+(-I_{xz} + a_{46}) \cdot \ddot{\psi} & +b_{46} \cdot \dot{\psi} & +c_{46} \cdot \psi & = X_{w_4} \quad \text{(roll)}
\end{array} \\[3em]
\begin{array}{llll}
a_{62} \cdot \ddot{y} & +b_{62} \cdot \dot{y} & +c_{62} \cdot y & \\
+(-I_{zx} + a_{64}) \cdot \ddot{\phi} & +b_{64} \cdot \dot{\phi} & +c_{64} \cdot \phi & \\
+(+I_{zz} + a_{66}) \cdot \ddot{\psi} & +b_{66} \cdot \dot{\psi} & +c_{66} \cdot \psi & = X_{w_6} \quad \text{(yaw)}
\end{array}
\end{array}
\right\} \quad \begin{array}{c} \text{anti-symmetric} \\ \text{motions} \end{array}
$$

Note that this distinction between symmetric and anti-symmetric motions disappears when the ship is anchored. Then, for instance, the pitch motions can generate roll motions via the anchor lines.

8.3.3 2-D Strip Theory

Strip theory is a computational method by which the forces on and motions of a three-dimensional floating body can be determined using results from two-dimensional potential

theory. This method has been described in the literature by several of authors; for a clear description reference is given to a doctor's thesis by [Vugts, 1970]. The two-dimensional potential theory has been discussed in chapter 7; its utilization will be discussed in the present chapter. Just as in chapter 7, the result of the theoretical work and the path leading to it, is more important than the derivation details.

Strip theory considers a ship to be made up of a finite number of transverse two-dimensional slices which are rigidly connected to each other. Each of these slices will have a form which closely resembles the segment of the ship which it represents. Each slice is treated hydrodynamically as if it is a segment of an infinitely long floating cylinder; see figure 8.1.
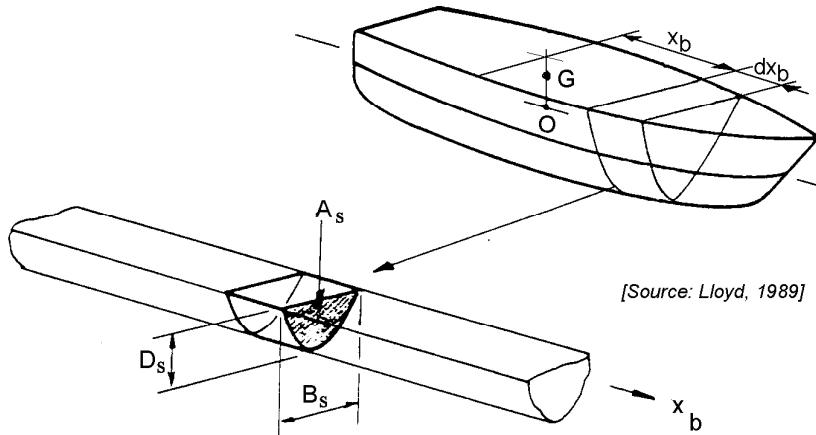
Figure 8.1: Strip Theory Representation by Cross Sections

This means that all waves which are produced by the oscillating ship (hydromechanical loads) and the diffracted waves (wave loads) are assumed to travel perpendicular to the middle line plane (thus parallel to the y-z plane) of the ship. This holds too that the strip theory supposes that the fore and aft side of the body (such as a pontoon) does not produce waves in the x direction. For the zero forward speed case, interactions between the cross sections are ignored as well.

Fundamentally, strip theory is valid for long and slender bodies only. In spite of this restriction, experiments have shown that strip theory can be applied successfully for floating bodies with a length to breadth ratio larger than three, ($L/B \geqq 3$), at least from a practical point of view.

When applying the strip theory, the loads on the body are found by an integration of the 2-D loads:

$$\text{surge:} \qquad X_{h_1} = \int_L X'_{h_1} \cdot dx_b \qquad\qquad X_{w_1} = \int_L X'_{w_1} \cdot dx_b$$

$$\text{sway:} \qquad X_{h_2} = \int_L X'_{h_2} \cdot dx_b \qquad\qquad X_{w_2} = \int_L X'_{w_2} \cdot dx_b$$

$$\text{heave:} \qquad X_{h_3} = \int_L X'_{h_3} \cdot dx_b \qquad\qquad X_{w_3} = \int_L X'_{w_3} \cdot dx_b$$

roll:
$$X_{h_4} = \int_L X'_{h_4} \cdot dx_b \qquad\qquad X_{w_4} = \int_L X'_{w_4} \cdot dx_b$$

pitch:
$$X_{h_5} = -\int_L X'_{h_3} \cdot x_b \cdot dx_b \qquad\qquad X_{w_5} = -\int_L X'_{w_3} \cdot x_b \cdot dx_b$$

yaw:
$$X_{h_6} = \int_L X'_{h_2} \cdot x_b \cdot dx_b \qquad\qquad X_{w_6} = \int_L X'_{w_2} \cdot x_b \cdot dx_b \qquad (8.13)$$

in which:

$$X'_{h_j} = \text{sectional hydromechanical force or moment}$$
$$\text{in direction } j \text{ per unit ship length}$$
$$X'_{w_j} = \text{sectional exciting wave force or moment}$$
$$\text{in direction } j \text{ per unit ship length}$$

The appearance of two-dimensional surge forces seems strange here. It is strange! A more or less empirical method is used in program SEAWAY of [Journée, 1999] for the surge motion, by defining an equivalent longitudinal cross section which is swaying. Then, the 2-D hydrodynamic sway coefficients of this equivalent cross section are translated to 2-D hydrodynamic surge coefficients by an empirical method based on theoretical results from three-dimensional calculations and these coefficients are used to determine 2-D loads. In this way, all sets of six surge loads can be treated in the same numerical way in program SEAWAY for the determination of the 3-D loads. Inaccuracies of the hydromechanical coefficients of (slender) ships are of minor importance, because these coefficients are relatively small.

Note how in the strip theory the pitch and yaw moments are derived from the 2-D heave and sway forces, respectively, while the roll moments are obtained directly.

The equations of motions are defined in the moving axis system with the origin at the average position of the center of gravity, G. All two-dimensional potential coefficients have been defined so far in an axis system with the origin, O, in the water plane; the hydromechanical and exciting wave moments have to be corrected for the distance $\overline{OG}$.

Potential Coefficients

As mentioned before, in strip theory calculations the two-dimensional sway, heave and roll coefficients can be calculated by three methods which are summarized here; full details are given in chapter 7:

1. Ursell-Tasai's Method with Lewis Conformal Mapping
   Ursell derived an analytical solution for solving the problem of calculating the hydrodynamic coefficients of an oscillating circular cylinder in the surface of a fluid. Tasai added the so-called Lewis transformation - which is a very simple and in a lot of cases also more or less realistic method to transform ship-like cross sections to this unit circle - to Ursell's solution . This transformation is carried out by using a scale factor and two mapping coefficients. Only the breadth, the draft and the area of the mapped cross section will be equal to that of the actual cross section.

2. Ursell-Tasai's Method with N-Parameter Conformal Mapping

   A more accurate mapping has been added by Tasai too, by using more than only two mapping coefficients. The accuracy obtained depends on the number of mapping coefficients. Generally, a maximum of 10 coefficients are used for defining the cross section. These coefficients are determined in such a way that the Root Mean Square of the differences between the offsets of the mapped and the actual cross section is minimal.

3. Frank's Pulsating Source Method

   Mapping methods require an intersection of the cross section with the water plane and, as a consequence of this, they are not suitable for submerged cross sections, like at a bulbous bow. Also, conformal mapping can fail for cross sections with very low sectional area coefficients, such as are sometimes present in the aft body of a ship. Frank considered a cylinder of constant cross sections with an arbitrarily symmetrical shape, of which the cross sections are simply a region of connected line elements. This vertical cross section can be fully or partly immersed in a previously undisturbed fluid of infinite depth. He developed an integral equation method utilizing the Green's function which represents a complex potential of a pulsating point source of unit strength at the midpoint of each line element. Wave systems were defined in such a way that all required boundary conditions were fulfilled. The linearized Bernoulli equation provides the pressures after which the potential coefficients were obtained from the in-phase and out-of-phase components of the resultant hydrodynamic loads.

Forward Ship Speed

In case of a forward ship speed V, potential functions defined in the earth bounded coordinate system (x_0, y_0, z_0) have to be transformed to potential functions in the ship's steadily translating coordinate system (x, y, z). This requires an operator which transforms the derivative of a function $F(x_0, y_0, z_0, t)$, in the earth bounded (fixed) coordinate system, to the derivative of a function $F(x, y, z, t)$, in the ship's steadily translating coordinate system:

$$x \;=\; x_0 - Vt \qquad y = y_0 \qquad z = z_0$$

$$\frac{\partial}{\partial t} F(x_0, y_0, z_0, t) \;=\; \frac{\partial}{\partial t} F(x, y, z, t) + \frac{\partial}{\partial x} F(x, y, z, t) \cdot \frac{dx}{dt}$$

$$=\; \frac{\partial}{\partial t} F(x, y, z, t) - V \cdot \frac{\partial}{\partial x} F(x, y, z, t)$$

$$=\; \left(\frac{\partial}{\partial t} - V \cdot \frac{\partial}{\partial x} \right) F(x, y, z, t)$$

$$=\; \frac{D}{Dt} F(x, y, z, t) \tag{8.14}$$

Thus, the operator is given by:

$$\boxed{\frac{D}{Dt} = \left(\frac{\partial}{\partial t} - V \cdot \frac{\partial}{\partial x} \right)} \tag{8.15}$$

When assuming small surge motions ($x \approx x_b$), this operator can also be written as:

$$\boxed{\frac{D}{Dt} \approx \left(\frac{\partial}{\partial t} - V \cdot \frac{\partial}{\partial x_b}\right)} \tag{8.16}$$

The effect of this operator can be understood easily when one realizes that in that earth-bound coordinate system the sailing ship penetrates through a "virtual vertical disk". When a ship sails with speed V and a trim angle, θ, through still water, the relative vertical velocity of a water particle with respect to the bottom of the sailing ship becomes $V \cdot \theta$.

Relative to an oscillating ship moving forward with speed V in the undisturbed surface of the fluid, the equivalent displacements, $\zeta^*_{h_j}$, velocities, $\dot{\zeta}^*_{h_j}$, and accelerations, $\ddot{\zeta}^*_{h_j}$, in the arbitrary direction j of a water particle in a cross section are defined by:

$$\zeta^*_{h_j}, \qquad \dot{\zeta}^*_{h_j} = \frac{D}{Dt}\left\{\zeta^*_{h_j}\right\} \qquad \text{and} \qquad \ddot{\zeta}^*_{h_j} = \frac{D}{Dt}\left\{\dot{\zeta}^*_{h_j}\right\} \tag{8.17}$$

Relative to a restrained ship, moving forward with speed V in waves, the equivalent j components of water particle displacements, $\zeta^*_{w_j}$, velocities, $\dot{\zeta}^*_{w_j}$, and accelerations, $\ddot{\zeta}^*_{w_j}$, in a cross section are defined in a similar way by:

$$\zeta^*_{w_j}, \qquad \dot{\zeta}^*_{w_j} = \frac{D}{Dt}\left\{\zeta^*_{w_j}\right\} \qquad \text{and} \qquad \ddot{\zeta}^*_{w_j} = \frac{D}{Dt}\left\{\dot{\zeta}^*_{w_j}\right\} \tag{8.18}$$

Two different types of strip theory methods are discussed here:

1. **Ordinary Strip Theory Method**
   According to this classic method, the uncoupled two-dimensional potential hydrome-chanical loads and wave loads in an arbitrary direction j are defined by:

$$\boxed{X^*_{h_j} = \frac{D}{Dt}\left\{M'_{jj} \cdot \dot{\zeta}^*_{h_j}\right\} + N'_{jj} \cdot \dot{\zeta}^*_{h_j} + X'_{rs_j}}$$
$$\boxed{X^*_{w_j} = \frac{D}{Dt}\left\{M'_{jj} \cdot \dot{\zeta}^*_{w_j}\right\} + N'_{jj} \cdot \dot{\zeta}^*_{w_j} + X'_{fk_j}} \tag{8.19}$$

   This is the first formulation of the strip theory that can be found in the literature. It contains a more or less intuitive approach to the forward speed problem, as published in detail by [Korvin-Kroukovsky and Jacobs, 1957] and others.

2. **Modified Strip Theory Method**
   According to this modified method, these loads become:

$$\boxed{X^*_{h_j} = \frac{D}{Dt}\left\{\left(M'_{jj} - \frac{i}{\omega_e}N'_{jj}\right) \cdot \dot{\zeta}^*_{h_j}\right\} + X'_{rs_j}}$$
$$\boxed{X^*_{w_j} = \frac{D}{Dt}\left\{\left(M'_{jj} - \frac{i}{\omega_e}N'_{jj}\right) \cdot \dot{\zeta}^*_{w_j}\right\} + X'_{fk_j}} \tag{8.20}$$

   This formulation is a more fundamental approach of the forward speed problem, as published in detail by [Tasai, 1969] and others.

In equations 8.19 and 8.20 M'_{jj} and N'_{jj} are the 2-D potential mass and damping coefficients. X'_{rs_j} is the two-dimensional quasi-static restoring spring term, generally present for heave, roll and pitch only. X'_{fk_j} is the two-dimensional Froude-Krilov force or moment which is calculated by an integration of the directional pressure gradient in the undisturbed wave over the cross sectional area of the hull.

Equivalent directional components of the orbital acceleration and velocity, derived from these Froude-Krilov loads, are used to calculate the diffraction parts of the total wave forces and moments.

From a theoretical point of view, one should prefer the use of the modified method, but it appeared from user's experience that for ships with moderate forward speed ($Fn \leqq 0.30$), the ordinary method provides sometimes a better fit with experimental data.

The hydromechanical and wave loads are explained in the following sections as an example for coupled heave and pitch motions only. A similar approach can be used for the other motions.

Note however, that the potential coefficients will be determined in an axes system with the origin, O, in the waterline and that ship motions will be defined with the origin at the center of gravity, G. This requires, for instance, for roll moments corrections with sway forces times the lever arm $\overline{OG}$. Detailed information about these corrections are given by [Vugts, 1970] or [Journée, 2000].

Hydromechanical Loads

The hydromechanical forces for heave and moments for pitch are found by integrating the two-dimensional heave values over the ship length:

$$
\begin{aligned}
X_{h_3} &= \int_L X'_{h_3} \cdot dx_b \\
X_{h_5} &= -\int_L X'_{h_3} \cdot x_b \cdot dx_b
\end{aligned}
\tag{8.21}
$$

The vertical motions of the water particles, relative to each cross section of an oscillating ship in still water, are defined by using equations 8.17 and 8.15:

$$
\begin{aligned}
\zeta^*_{h_3} &= -z + x_b \cdot \theta \\
\dot{\zeta}^*_{h_3} &= -\dot{z} + x_b \cdot \dot{\theta} - V \cdot \theta \\
\ddot{\zeta}^*_{h_3} &= -\ddot{z} + x_b \cdot \ddot{\theta} - 2V \cdot \dot{\theta}
\end{aligned}
\tag{8.22}
$$

The two-dimensional potential hydromechanical force on a heaving cross section in still water, as defined in equations 8.19 and 8.20, becomes:

$$
\boxed{X'_{h_3} = \left(M'_{33} \boxed{+ \frac{V}{\omega_e^2} \cdot \frac{dN'_{33}}{dx_b}} \right) \cdot \ddot{\zeta}^*_{h_3} + \left(N'_{33} - V \cdot \frac{dM'_{33}}{dx_b} \right) \cdot \dot{\zeta}^*_{h_3} + 2\rho g \cdot y_w \cdot \zeta^*_{h_3}}
\tag{8.23}
$$

In this and following equations, the additional terms associated with the Modified Strip Theory are enclosed in rectangles. Ignore these terms to get the Ordinary Strip Theory.

This results in the following hydromechanical expressions and coefficients for the coupled heave and pitch equations:

$$
\begin{aligned}
-X_{h_3} &= a_{33} \cdot \ddot{z} + b_{33} \cdot \dot{z} + c_{33} \cdot z + a_{35} \cdot \ddot{\theta} + b_{35} \cdot \dot{\theta} + c_{35} \cdot \theta \\
-X_{h_5} &= a_{53} \cdot \ddot{z} + b_{53} \cdot \dot{z} + c_{53} \cdot z + a_{55} \cdot \ddot{\theta} + b_{55} \cdot \dot{\theta} + c_{55} \cdot \theta
\end{aligned}
\tag{8.24}
$$

with:

$$
a_{33} = + \int_L M'_{33} \cdot dx_b \;\; \boxed{+ \frac{V}{\omega_e^2} \int_L \frac{dN'_{33}}{dx_b} \cdot dx_b}
$$

$$
b_{33} = + \int_L \left(N'_{33} - V \cdot \frac{dM'_{33}}{dx_b} \right) \cdot dx_b
$$

$$
c_{33} = + 2\rho g \int_L y_w \cdot dx_b
$$

$$
a_{35} = - \int_L M'_{33} \cdot x_b \cdot dx_b \; - \frac{V}{\omega_e^2} \int_L \left(N'_{33} - V \cdot \frac{dM'_{33}}{dx_b} \right) \cdot dx_b
$$

$$
\boxed{- \frac{V}{\omega_e^2} \int_L N'_{33} \cdot dx_b \; - \frac{V}{\omega_e^2} \int_L \frac{dN'_{33}}{dx_b} \cdot x_b \cdot dx_b}
$$

$$
b_{35} = - \int_L \left(N'_{33} - V \cdot \frac{dM'_{33}}{dx_b} \right) \cdot x_b \cdot dx_b \; + 2V \int_L M'_{33} \cdot dx_b \;\; \boxed{+ \frac{V^2}{\omega_e^2} \int_L \frac{dN'_{33}}{dx_b} \cdot dx_b}
$$

$$
c_{35} = - 2\rho g \int_L y_w \cdot x_b \cdot dx_b
\tag{8.25}
$$

$$
a_{53} = - \int_L M'_{33} \cdot x_b \cdot dx_b \;\; \boxed{- \frac{V}{\omega_e^2} \int_L \frac{dN'_{33}}{dx_b} \cdot x_b \cdot dx_b}
$$

$$
b_{53} = - \int_L \left(N'_{33} - V \cdot \frac{dM'_{33}}{dx_b} \right) \cdot x_b \cdot dx_b
$$

$$
c_{53} = - 2\rho g \int_L y_w \cdot x_b \cdot dx_b
$$

$$
a_{55} = + \int_L M'_{33} \cdot x_b^2 \cdot dx_b \; + \frac{V}{\omega_e^2} \int_L \left(N'_{33} - V \cdot \frac{dM'_{33}}{dx_b} \right) \cdot x_b \cdot dx_b
$$

$$
\boxed{+ \frac{V}{\omega_e^2} \int_L N'_{33} \cdot x_b \cdot dx_b \; + \frac{V}{\omega_e^2} \int_L \frac{dN'_{33}}{dx_b} \cdot x_b^2 \cdot dx_b}
$$

$$
b_{55} = + \int_L \left(N'_{33} - V \cdot \frac{dM'_{33}}{dx_b} \right) \cdot x_b^2 \cdot dx_b \; - 2V \int_L M'_{33} \cdot x_b \cdot dx_b \;\; \boxed{- \frac{V^2}{\omega_e^2} \int_L \frac{dN'_{33}}{dx_b} \cdot x_b \cdot dx_b}
$$

$$
c_{55} = + 2\rho g \int_L y_w \cdot x_b^2 \cdot dx_b
\tag{8.26}
$$

The derivatives of M'_{33} and N'_{33} have to be determined numerically over the whole ship length in such a way that the following relation is fulfilled:

$$
\int_{x_b(0)-\varepsilon}^{x_b(L)+\varepsilon} \frac{df(x_b)}{dx_b} dx_b = \int_{x_b(0)-\varepsilon}^{x_b(0)} \frac{df(x_b)}{dx_b} dx_b + \int_{x_b(0)}^{x_b(L)} \frac{df(x_b)}{dx_b} dx_b + \int_{x_b(L)}^{x_b(L)+\varepsilon} \frac{df(x_b)}{dx_b} dx_b
$$

$$
= f(0) + \int_{x_b(0)}^{x_b(L)} \frac{df(x_b)}{dx_b} dx_b - f(L)
$$

$$
= 0 \tag{8.27}
$$

with $\varepsilon \ll L$, while $f(x_b)$ is equal to the local values of $M'_{33}(x_b)$ or $N'_{33}(x_b)$; see figure 8.2.
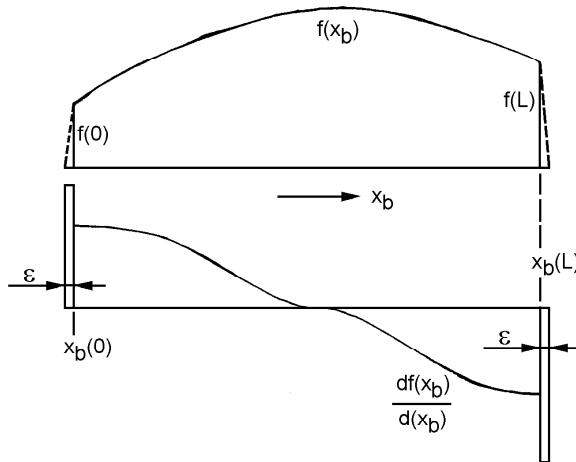
Figure 8.2: Integration of Longitudinal Derivatives

The numerical integrations of the derivatives are carried out in the region $x_b(0) \le x_b \le x_b(L)$ only. So, the additional **so-called "end terms"** $f(0)$ and $f(L)$ are defined by:

$$
f(0) = \int_{x_b(0)-\varepsilon}^{x_b(0)} \frac{df(x_b)}{dx_b} \cdot dx_b \quad \text{and} \quad f(L) = \int_{x_b(L)}^{x_b(L)+\varepsilon} \frac{df(x_b)}{dx_b} \cdot dx_b \tag{8.28}
$$

Because the integration of the derivatives has to be carried out in the region $x_b(0) - \varepsilon \le x_b \le x_b(L) + \varepsilon$, some algebra provides the integral and the first and second order moments (with respect to G) over the whole ship length:

$$
\int_{x_b(0)-\varepsilon}^{x_b(L)+\varepsilon} \frac{df(x_b)}{dx_b} \cdot dx_b = 0
$$

$$\int\limits_{x_b(0)-\varepsilon}^{x_b(L)+\varepsilon} \frac{df(x_b)}{dx_b} \cdot x_b \cdot dx_b = - \int\limits_{x_b(0)}^{x_b(L)} f(x_b) \cdot dx_b$$

$$\int\limits_{x_b(0)-\varepsilon}^{x_b(L)+\varepsilon} \frac{df(x_b)}{dx_b} \cdot x_b^2 \cdot dx_b = -2 \int\limits_{x_b(0)}^{x_b(L)} f(x_b) \cdot x_b \cdot dx_b \tag{8.29}$$

Using this, more simple expressions for the total hydromechanical coefficients in the coupled heave and pitch equations can be obtained:

$$a_{33} = + \int_L M'_{33} \cdot dx_b$$

$$b_{33} = + \int_L N'_{33} \cdot dx_b$$

$$c_{33} = +2\rho g \int_L y_w \cdot dx_b$$

$$a_{35} = - \int_L M'_{33} \cdot x_b \cdot dx_b - \frac{V}{\omega_e^2} \int_L N'_{33} \cdot dx_b$$

$$b_{35} = - \int_L N'_{33} \cdot x_b \cdot dx_b + V \int_L M'_{33} \cdot dx_b$$

$$c_{35} = -2\rho g \int_L y_w \cdot x_b \cdot dx_b \tag{8.30}$$

$$a_{53} = - \int_L M'_{33} \cdot x_b \cdot dx_b \boxed{+\frac{V}{\omega_e^2} \int_L N'_{33} \cdot dx_b}$$

$$b_{53} = - \int_L N'_{33} \cdot x_b \cdot dx_b - V \int_L M'_{33} \cdot dx_b$$

$$c_{53} = -2\rho g \int_L y_w \cdot x_b \cdot dx_b$$

$$a_{55} = + \int_L M'_{33} \cdot x_b^2 \cdot dx_b + \frac{V}{\omega_e^2} \int_L N'_{33} \cdot x_b \cdot dx_b + \frac{V^2}{\omega_e^2} \int_L M'_{33} \cdot dx_b$$

$$\boxed{- \frac{V}{\omega_e^2} \int_L N'_{33} \cdot x_b \cdot dx_b}$$

$$b_{55} = + \int_L N'_{33} \cdot x_b^2 \cdot dx_b \boxed{+\frac{V^2}{\omega_e^2} \int_L N'_{33} \cdot dx_b}$$

$$c_{55} = +2\rho g \int_L y_w \cdot x_b^2 \cdot dx_b \approx \rho g \nabla \cdot \overline{GM}_L \tag{8.31}$$

Note that both strip theory methods are identical for the zero forward speed case.

Wave Loads

By assuming that:
$$x \approx x_b \qquad y \approx y_b \qquad z \approx z_b \tag{8.32}$$
which is exactly true for the restrained ship, the expressions for the wave surface and the first order wave potential can be written in the body-bound coordinate system as:

$$\zeta = \zeta_a \cos(\omega_e t - kx_b \cos \mu - ky_b \sin \mu)$$

$$\Phi_w = \frac{-\zeta_a g}{\omega} \cdot \frac{\cosh k(h + z_b)}{\cosh(kh)} \cdot \sin(\omega_e t - kx_b \cos \mu - ky_b \sin \mu) \tag{8.33}$$

in which μ is the wave direction.

The local vertical relative orbital velocity of the water particles follows from the derivative of the wave potential as given in chapter 5. Equations 8.18 and 8.15 provide the vertical relative orbital acceleration:

$$\dot{\zeta}'_{w3} = \frac{\partial \Phi_w}{\partial z_b}$$

$$= \frac{-kg}{\omega} \cdot \frac{\sinh k(h + z_b)}{\cosh(kh)} \cdot \zeta_a \sin(\omega_e t - kx_b \cos \mu - ky_b \sin \mu)$$

$$\ddot{\zeta}'_{w3} = -kg \cdot \frac{\sinh k(h + z_b)}{\cosh(kh)} \cdot \zeta_a \cos(\omega_e t - kx_b \cos \mu - ky_b \sin \mu) \tag{8.34}$$

The pressure in the fluid follows from the linearized Bernoulli equation:

$$p = -\rho g z_b + \rho g \cdot \frac{\cosh k(h + z_b)}{\cosh(kh)} \cdot \zeta_a \cos(\omega_e t - kx_b \cos \mu - ky_b \sin \mu)$$

$$= p_0 + \frac{\partial p}{\partial x_b} \cdot dx_b + \frac{\partial p}{\partial y_b} \cdot dy_b + \frac{\partial p}{\partial z_b} \cdot dz_b \tag{8.35}$$

Only the vertical pressure gradient is of importance for the vertical loads on of a cross section:

$$\frac{\partial p}{\partial z_b} = -\rho g + \rho kg \cdot \frac{\sinh k(h + z_b)}{\cosh(kh)} \cdot \zeta_a \cos(\omega_e t - kx_b \cos \mu - ky_b \sin \mu) \tag{8.36}$$

which can be expressed in terms of the vertical orbital acceleration - instead - as:

$$\frac{\partial p}{\partial z_b} = -\rho \cdot (g + \ddot{\zeta}'_{w3}) \tag{8.37}$$

Figure 8.3 shows that the vertical Froude-Krilov force can be written as:

$$X'_{fk_3} = -\int_{-T}^{\zeta} \int_{-y_b}^{+y_b} \frac{\partial p}{\partial z_b} \cdot dy_b \cdot dz_b$$

$$= \rho \int_{-T}^{\zeta} \int_{-y_b}^{+y_b} (g + \ddot{\zeta}'_{w3}) \cdot dy_b \cdot dz_b \tag{8.38}$$
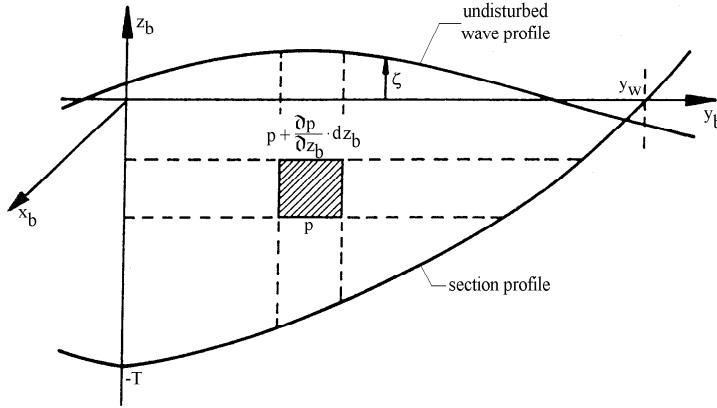
Figure 8.3: Wave Pressure Distribution for Heave

After neglecting the second order terms and some algebra, this Froude-Krilov force can be written as a spring term:

$$X'_{fk_3} = 2\rho g y_w \cdot C_3 \cdot \zeta_a \cos(\omega_e t - k x_b \cos \mu) \tag{8.39}$$

with:

$$C_3 = \frac{\sin(-ky_w \sin \mu)}{-ky_w \sin \mu} - \frac{k}{y_w} \cdot \int\limits_{-T}^{0} \frac{\sin(-ky_b \sin \mu)}{-ky_b \sin \mu} \cdot \frac{\sinh k(h + z_b)}{\cosh(kh)} \cdot y_b \cdot dz_b \tag{8.40}$$

or in deep water with long waves relative to the breadth of the cross section $(ky_w \ll 1)$:

$$C_3 = 1 - \frac{k}{y_w} \cdot \int\limits_{-T}^{0} e^{kz_b} \cdot y_b \cdot dz_b \tag{8.41}$$

By expanding the exponent in C_3 from equation 8.41 in a series, one finds:

$$C_3 = 1 - k \cdot \frac{A}{2y_w} - k^2 \cdot \frac{S_y}{2y_w} - k^3 \cdot \frac{I_y}{4y_w} - ...... \tag{8.42}$$

with:

$$A = 2 \int\limits_{-T}^{0} y_b \cdot dz_b \qquad S_y = 2 \int\limits_{-T}^{0} y_b \cdot z_b \cdot dz_b \qquad I_y = 2 \int\limits_{-T}^{0} y_b \cdot z_b^2 \cdot dz_b \tag{8.43}$$

For deep water with long waves relative to the breadth and draft of the cross section $(ky_w \ll 1$ and $kT \ll 1)$ one can write:

$$C_3 \approx e^{-kT_3^*} \qquad \text{or} \qquad T_3^* \approx \frac{-\ln C_3}{k} \tag{8.44}$$

Now, T_3^* can be considered as the draft at which the pressure is equal to the average pressure on the cross section in the fluid. By defining $\zeta_{a_3}^* = C_3 \cdot \zeta_{a_3}$, the term $\rho g \cdot \zeta_{a_3}^*$ becomes the amplitude of this mean pressure.

The effective vertical components of the orbital accelerations and velocities in undisturbed waves are defined at this draft T_3^* too:

$$\ddot{\zeta}_{w_3}^* \quad = \quad -kg \cdot \zeta_{a_3}^* \cos(\omega_e t - kx_b \cos\mu)$$

$$\dot{\zeta}_{w_3}^* \quad = \quad \frac{-kg}{\omega} \cdot \zeta_{a_3}^* \sin(\omega_e t - kx_b \cos\mu) \tag{8.45}$$

With this, the two-dimensional wave exciting force on a restrained cross section of a ship in waves, as defined in equations 8.19 and 8.20, becomes:

$$X'_{w_3} = \left(M'_{33} \boxed{+\frac{V}{\omega_e^2} \cdot \frac{dN'_{33}}{dx_b}} \right) \cdot \ddot{\zeta}_{w_3}^* + \left(N'_{33} - V \cdot \frac{dM'_{33}}{dx_b} \right) \cdot \dot{\zeta}_{w_3}^* + X'_{fk_3} \tag{8.46}$$

in which only the modified strip theory includes the outlined term.

These **equivalent accelerations and velocities** in the undisturbed wave are used to determine the additional wave loads due to diffraction of the waves. They are considered as potential mass and damping terms, just as applied for the hydromechanical loads. This is the reason why this approach called the **relative motion principle** in strip theory. The total wave loads for heave and pitch follows from all this:

$$X_{w_3} \quad = \quad +\int\limits_L M'_{33} \cdot \ddot{\zeta}_{w_3}^* \cdot dx_b \boxed{+\frac{V}{\omega \cdot \omega_e} \int\limits_L \frac{dN'_{33}}{dx_b} \cdot \ddot{\zeta}_{w_3}^* \cdot dx_b}$$

$$+ \int\limits_L \left(\boxed{\frac{\omega}{\omega_e} \cdot} N'_{33} - V \cdot \frac{dM'_{33}}{dx_b} \right) \cdot \dot{\zeta}_{w_3}^* \cdot dx_b$$

$$+ \int\limits_L X'_{fk_3} \cdot dx_b \tag{8.47}$$

$$X_{w_5} \quad = \quad -\int\limits_L M'_{33} \cdot x_b \cdot \ddot{\zeta}_{w_3}^* \cdot dx_b \boxed{-\frac{V}{\omega \cdot \omega_e} \int\limits_L \frac{dN'_{33}}{dx_b} \cdot x_b \cdot \ddot{\zeta}_{w_3}^* \cdot dx_b}$$

$$- \int\limits_L \left(\boxed{\frac{\omega}{\omega_e} \cdot} N'_{33} - V \cdot \frac{dM'_{33}}{dx_b} \right) \cdot x_b \cdot \dot{\zeta}_{w_3}^* \cdot dx_b$$

$$- \int\limits_L X'_{fk_3} \cdot x_b \cdot dx_b \tag{8.48}$$

Note that both strip theory methods are identical here for the zero forward speed case and that the (generally small) influence of the surge wave loads on the pitch wave moment has been ignored here, too.

Heave and Pitch Equations

Putting all this together yields the coupled equations of motion of heave and pitch:

$$\begin{aligned}
(\rho\nabla + a_{33}) \cdot \ddot{z} + b_{33} \cdot \dot{z} + c_{33} \cdot z + a_{35} \cdot \ddot{\theta} + b_{35} \cdot \dot{\theta} + c_{35} \cdot \theta &= X_{w_3} \\
a_{53} \cdot \ddot{z} + b_{53} \cdot \dot{z} + c_{53} \cdot z + (I_{xx} + a_{55}) \cdot \ddot{\theta} + b_{55} \cdot \dot{\theta} + c_{55} \cdot \theta &= X_{w_5}
\end{aligned} \tag{8.49}$$

which can be solved as described in chapter 6.

8.3.4 3-D Panel Method

This method is restricted to arbitrarily shaped bodies with zero mean forward speed. This is an acceptable simplification for the majority of the fixed or floating structures in use today in the offshore industry.

The panel method is a numerical method to calculate the (potential) flow around a body, based on the principle of Green's integral theorem. According to this theorem it is possible to transform a three-dimensional linear homogeneous differential equation into a two-dimensional integral equation. In that way the three-dimensional Laplace (potential) equation can be transformed to a surface integral equation, known as Green's identity. The integral equation represents a distribution of sources (or sinks) and dipoles on the surface. To solve the integral equation numerically, the surface of the body is divided in a number of panels, as shown for a crude oil carrier in figure 8.4.
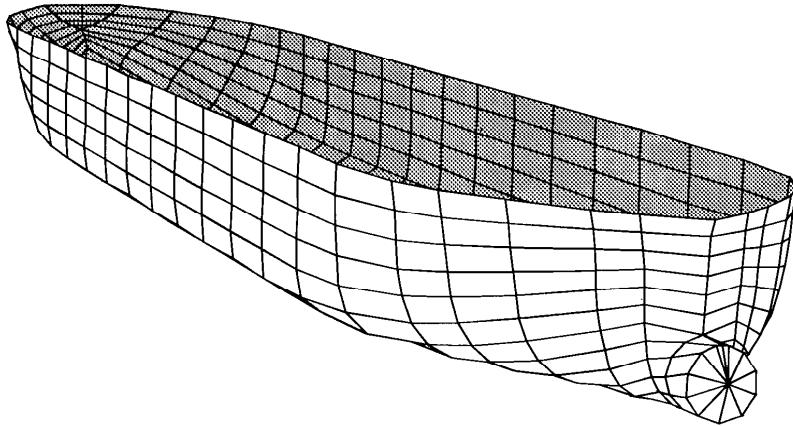
Figure 8.4: 3-D Representation of the Hull Form of a Crude Oil Carrier

The body surface is divided in N panels small enough to assume that the sources and doublets strength and the fluid pressure is constant over each element. Now a set of integral equations is made, from which the velocity potentials can be found. The integral equation can be discretized for each panel by substituting an unknown strength of the source and dipole distribution. By using the boundary condition of tangential flow, the unknown strength of the sources and dipoles can be solved. If the strength of each dipole or source is known the velocities can be determined on the surface.

Note that there are now no restrictions on the form and shape of the body. This method works equally well for a ship, the base of a concrete GBS structure or a semi-submersible. The method will work - in principle - with any size of structure as well.

The advantage of panel methods is that the problem is reduced to a two-dimensional (surface) problem instead of a three-dimensional (volume) problem. The grid generation is also reduced to a two dimensional problem. So the grid has to be generated on the surface of the body only. This is in contrast to the three dimensional grid generation, where a lot of points have to be generated in the space around the body. Another advantage is that N^2 equations, instead of N^3 equations, have to be solved to determine the velocity field.

Panel methods are the most common technique used to analyze the linear steady state response of large-volume structures in regular waves. A wave spectrum is used to describe

a sea state and irregular sea results can be obtained by linear superposition of results from regular incident waves.

It is assumed that oscillation amplitudes of the fluid and the body are small relative to cross-sectional dimensions of the body.

Since the panel is based on potential theory, the effect of flow separation is neglected. As a consequence, the method should not be applied to slender structures, risers or tethers. Methods for such structures are discussed in chapter 12.

The quality of the results depends on the size and the number of panels used to schematic the body. There is no unique way to approximate the body surface by elements. Since it assumed that the source and dipole densities - and consequently the fluid pressure - are constant over each element, one should use smaller elements in areas where the flow changes more rapidly. It should be realized that the numerical solution for velocities never is satisfactory on an element closest to a sharp corner. The reason is that the potential flow solution has a singularity there, and that this is inconsistent with the assumption that the source density and velocity potential are constant over an element. In reality the flow will separate at a sharp corner. This effect is not included in the method.

In the wave zone the element size should be small compared to the wave length. A characteristic length of an element ought to be less than 1/8 of the wave length.

In the case of semi-submersibles and at least a vertical column with circular cross-section there ought to be at least 16 circumferential elements at any height. As a consequence panelling of a semi-submersible platform requires a relatively fine grid mesh. The result of that is that numerical models of diffraction radiation should not be used in the pre-design process of for instance semi-submersibles.

Typical values for the total number of elements for an offshore structure may vary from 500 to 1500. However, figure 8.5 shows an example where 12608 panels where used for the total structure.

[Source: Korsmeyer et.al., 1988]
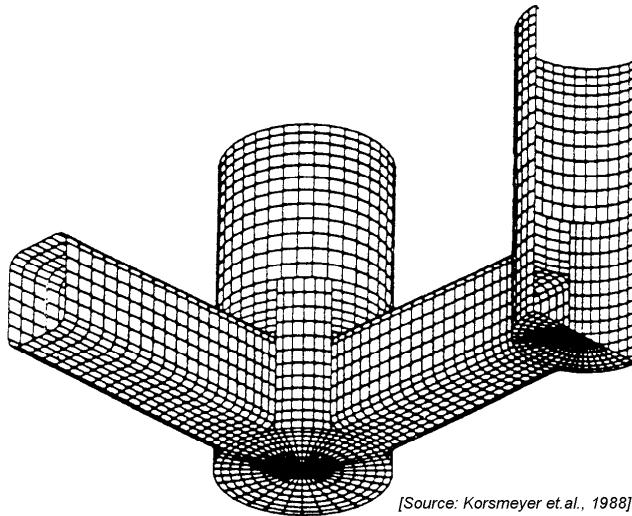
Figure 8.5: Submerged Portion of One Quadrant of a Six Column TLP

Iterative solutions of the system of linear equations for the source densities are required in order to be within practical limits of CPU time on available computer hardware. The best way to find a sufficient number of elements, is to do calculations with increasing numbers

of elements and check the convergence of the results.

Methods to evaluate the hydrodynamic loads and motions of floating or fixed structures in waves have been developed based on linear three-dimensional potential theory, see for instance [Oortmerssen, 1976a]. Both, the wave-frequency hydrodynamic loads on free-floating or fixed bodies and the wave-frequency motions of floating bodies as well as the second order wave drift forces can be computed. Experimental verification of results of computations has been carried out for bodies with a large variety of shapes. Such comparisons have shown that 3-D diffraction methods generally can be applied to most body shapes and are therefore a good tool to investigate such effects.

It may be noted that the 3-D method as described here is suitable for the zero forward speed case only. Generally the potential coefficients are determined in a coordinate system with $G = O$ in the water line, so that a correction for the actual $\overline{OG}$-value is required.

8.4 Motions in Regular Waves

Each equation of motion can be split into an equation with in-phase parts and an equation with out-of-phase components. After dividing the left and right hand terms of these equations by the wave amplitude ζ_a, two sets of six coupled equations of motion are available. The unknown variables in the 6 coupled equations of motions in the **vertical plane** are:

$$\left.\begin{array}{lll} \text{surge:} & \frac{x_a}{\zeta_a} \cdot \cos \varepsilon_{x\zeta} & \text{and} \quad \frac{x_a}{\zeta_a} \cdot \sin \varepsilon_{x\zeta} \\[2ex] \text{heave:} & \frac{z_a}{\zeta_a} \cdot \cos \varepsilon_{z\zeta} & \text{and} \quad \frac{z_a}{\zeta_a} \cdot \sin \varepsilon_{z\zeta} \\[2ex] \text{pitch:} & \frac{\theta_a}{\zeta_a} \cdot \cos \varepsilon_{\theta\zeta} & \text{and} \quad \frac{\theta_a}{\zeta_a} \cdot \sin \varepsilon_{\theta\zeta} \end{array}\right\} \tag{8.50}$$

The unknown variables in the 6 coupled equations of motions in the **horizontal plane** are:

$$\left.\begin{array}{lll} \text{sway:} & \frac{y_a}{\zeta_a} \cdot \cos \varepsilon_{y\zeta} & \text{and} \quad \frac{y_a}{\zeta_a} \cdot \sin \varepsilon_{y\zeta} \\[2ex] \text{roll:} & \frac{\phi_a}{\zeta_a} \cdot \cos \varepsilon_{\phi\zeta} & \text{and} \quad \frac{\phi_a}{\zeta_a} \cdot \sin \varepsilon_{\phi\zeta} \\[2ex] \text{yaw:} & \frac{\psi_a}{\zeta_a} \cdot \cos \varepsilon_{\psi\zeta} & \text{and} \quad \frac{\psi_a}{\zeta_a} \cdot \sin \varepsilon_{\psi\zeta} \end{array}\right\} \tag{8.51}$$

These 2 sets of equations of motion have to be solved numerically. Their terms are explained below.

8.4.1 Frequency Characteristics

The **transfer functions** (also called **response amplitude operators**) of the motions are the motion amplitude component to wave amplitude ratios. They and the phase shifts of these motions relative to the (virtual) wave elevation at the ship's center of gravity follow from the solution to 8.50 and 8.51:

$$\frac{x_a}{\zeta_a} \qquad \frac{y_a}{\zeta_a} \qquad \frac{z_a}{\zeta_a} \qquad \frac{\theta_a}{\zeta_a} \qquad \frac{\phi_a}{\zeta_a} \qquad \frac{\psi_a}{\zeta_a}$$

and

$$\varepsilon_{x\zeta} \qquad \varepsilon_{y\zeta} \qquad \varepsilon_{z\zeta} \qquad \varepsilon_{\theta\zeta} \qquad \varepsilon_{\phi\zeta} \qquad \varepsilon_{\psi\zeta}$$

The transfer functions of the translations are dimensionless. The transfer functions of the rotations can be made non-dimensional by dividing the amplitude of the rotations by the amplitude of the wave slope, $k\zeta_a$, instead of the wave amplitude, ζ_a, yielding:

$$\frac{x_a}{\zeta_a} \qquad \frac{y_a}{\zeta_a} \qquad \frac{z_a}{\zeta_a} \qquad \frac{\theta_a}{k\zeta_a} \qquad \frac{\psi_a}{k\zeta_a} \qquad \frac{\phi_a}{k\zeta_a}$$

The remainder of this section gives some general properties of these frequency characteristics.

Figures 8.6 and 8.7 show the frequency characteristics of the coupled heave and pitch motions of a crude oil carrier, as computed, using the SEAWAY strip theory program, see [Journée, 1999], for 0 and 16 knots forward ship speed in head and beam deep water waves.
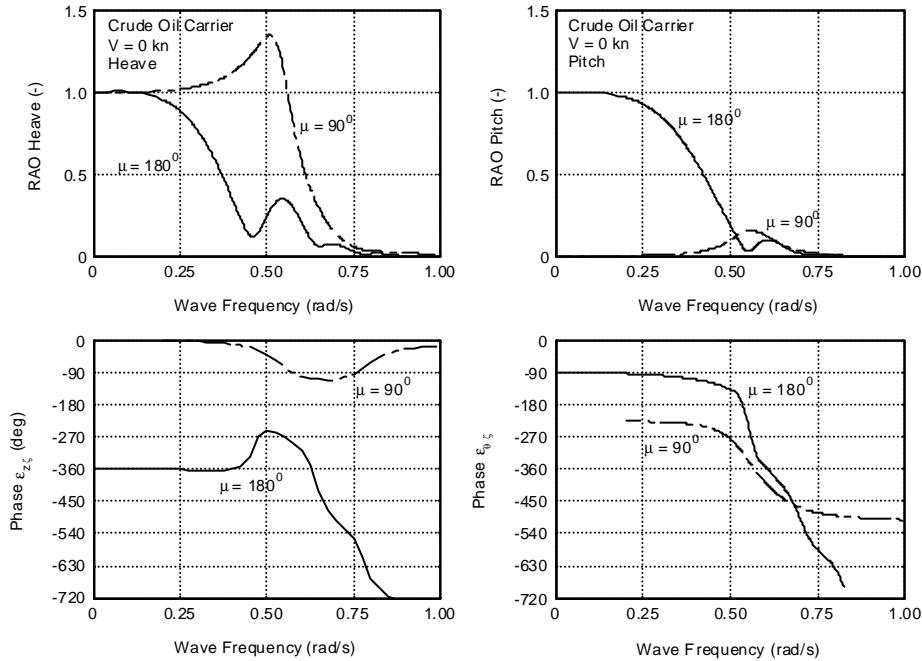
Figure 8.6: Heave and Pitch of a Crude Oil Carrier, V = 0 Knots

Examine first the heave and pitch motions at zero forward speed in head waves at deep water. These are the solid line curves in figure 8.6. In very long waves ($\omega \rightarrow 0$), the ship behaves like a sea gull in waves; she follows the wave surface. The heave amplitude, z_a, tends to the wave amplitude, ζ_a, and the pitch amplitude, θ_a, tends to the wave slope amplitude, $k\zeta_a$. Both dimensionless transfer functions tend to 1.0. The ship follows the wave surface, so the phase shift for heave, $\varepsilon_{z\zeta}$, tends to zero or -360°and the phase of the pitch angle relative to the wave elevation, $\varepsilon_{\theta\zeta}$, tends to -90°. Resonance can appear, depending on the magnitude of the damping, somewhere in the neighborhood of the natural frequencies.

Notice that resonance does not always appear at the natural frequency. When determining the natural frequency, the right hand side of the (uncoupled) equation of motion is zero, while when determining the resonant frequency, the right hand side of the (coupled) equation of motion contains the frequency-dependent wave load(s). Both, the natural frequencies and the frequency-dependent wave loads determine the resonant frequencies. Also, coupling effects play a role.

Resonances are usually marked in these diagrams by a local maximum in the response amplitude operator (**RAO**) and a rather abrupt change in response phase. At frequencies somewhat higher than the natural frequencies of heave and pitch, the transfer functions decrease and at still higher frequencies - as wave lengths becomes shorter than the ship length - the transfer functions tend to zero. No general conclusion can be drawn about the behavior of the phase shifts at higher frequencies.

Examining these motions in beam waves ($\mu = 90°$, the dashed lined in figure 8.6), in very long waves ($\omega \to 0$), the ship behaves like a sea-gull in waves again; it follows the wave surface. The heave amplitude, z_a, tends to the wave amplitude, ζ_a; the non-dimensional transfer function tends to 1.0. The phase shift, $\varepsilon_{z\zeta}$, tends to zero. In beam waves, it is not the wave length to ship length ratio but the wave length to ship breadth ratio that is of importance. When taking this into account, the heave motion behavior in beam waves is more or less similar to this motion in head waves, but the resonance peak can be higher. However, the pitch moments and motions become very small in the whole frequency range. Pitch motions in beam waves can be caused only by the anti-symmetry of the aft and fore body of the vessel with respect to its amidships section.

Comparable considerations can be given for the motions at forward speed, as given in figure 8.7. Notice the start of an "overshoot" in the heave and pitch motions in head waves. RAO's larger than 1.0 at wave lengths of about the ship length are common for high speed vessels.
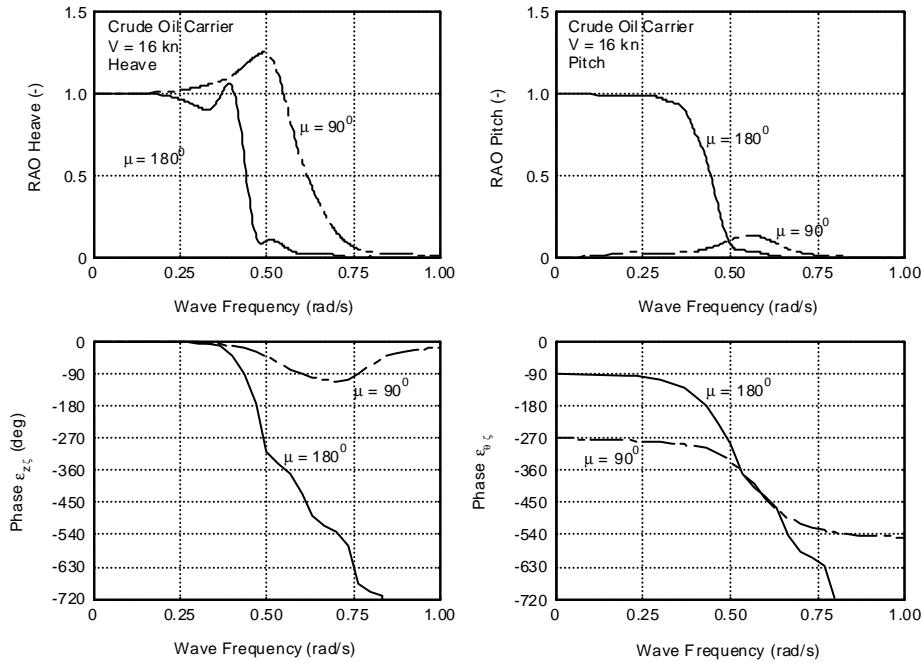
Figure 8.7: Heave and Pitch of a Crude Oil Carrier, V = 16 Knots

An example of predicted and measured transfer functions of the motions in all six degrees of freedom of an aircraft carrier sailing at 25 knots (obtained from Principles of Naval Architecture,1989) is given in figure 8.8. Each column in the figure is for a different wave direction. Notice that the frequency scale has been changed to an equivalent wave length over ship length scale.
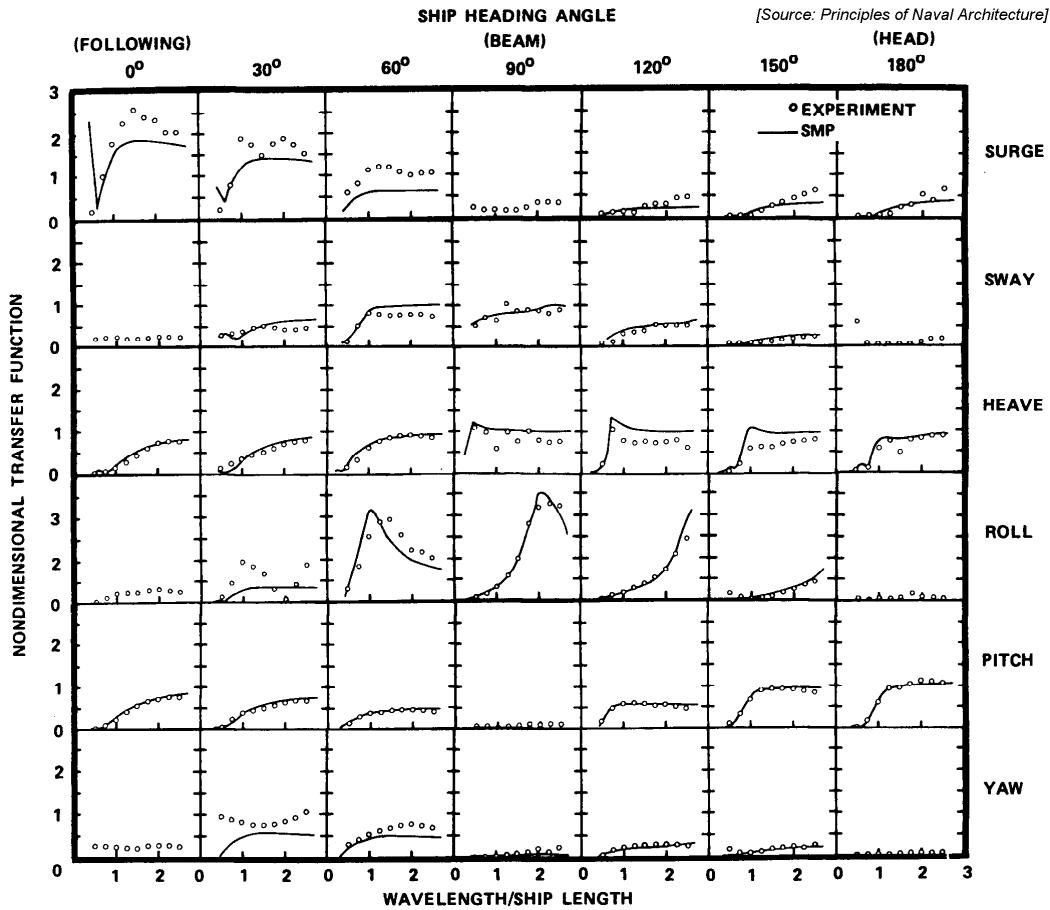
Figure 8.8: Measured and Calculated RAO's of an Aircraft Carrier

Figure 8.9 shows the speed dependent transfer functions of the roll motions in beam waves and the pitch motions in head waves of a container ship. Notice the opposite effect of forward speed on these two angular motions, caused by a with forward speed strongly increasing lift-damping of the roll motions. The flow around the sailing and rolling ship is asymmetric and the ship behaves like an airfoil.

8.4.2   Harmonic Motions

When the translations of, and the rotations about, the center of gravity are known, the motions of any point, $P(x_b, y_b, z_b)$, on the ship can be determined - again by superposition.

Displacements

The harmonic **longitudinal displacement** is given by:

$$
\begin{aligned}
x_p &= x \; - y_b \cdot \psi \; + z_b \cdot \theta \\
&= x_{p_a} \cdot \cos(\omega_e t + \varepsilon_{x_p \zeta})
\end{aligned}
\tag{8.52}
$$

The harmonic **lateral displacement** is given by:

$$
y_p \;=\; y \; + x_b \cdot \psi \; - z_b \cdot \phi
$$
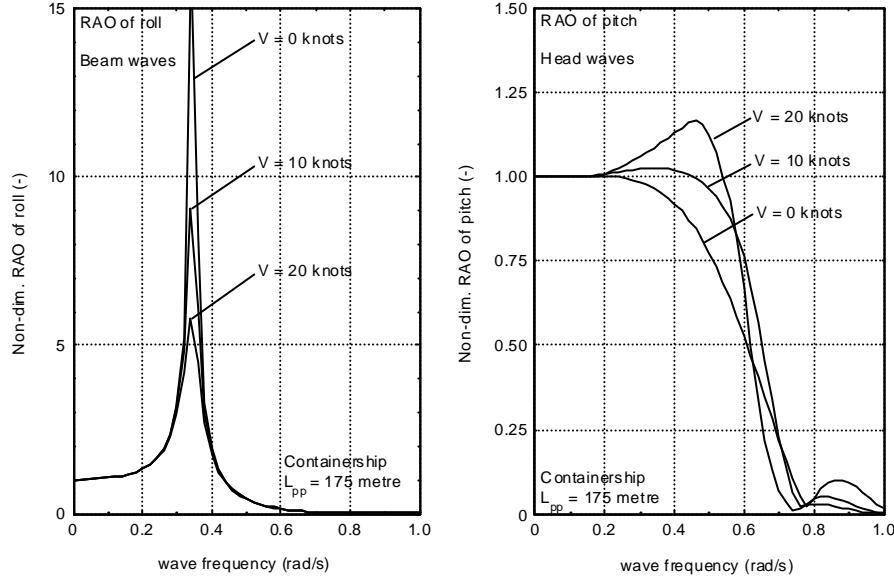
Figure 8.9: RAO's of Roll and Pitch of a Containership

$$= y_{p_a} \cdot \cos(\omega_e t + \varepsilon_{y_p \zeta}) \tag{8.53}$$

The harmonic **vertical displacement** is given by:

$$\begin{aligned} z_p &= z - x_b \cdot \theta - y_b \cdot \phi \\ &= z_{p_a} \cdot \cos(\omega_e t + \varepsilon_{z_p \zeta}) \end{aligned} \tag{8.54}$$

Velocities

The harmonic velocities in the x_b-, y_b- and z_b-direction of point $P(x_b, y_b, z_b)$ on the ship are obtained by taking the derivative of the three harmonic displacements.
The harmonic **longitudinal velocity** is given by:

$$\begin{aligned} \dot{x}_p &= \dot{x} - y_b \cdot \dot{\psi} + z_b \cdot \dot{\theta} \\ &= -\omega_e \cdot x_{p_a} \cdot \sin(\omega_e t + \varepsilon_{x_p \zeta}) \\ &= \dot{x}_{p_a} \cdot \cos(\omega_e t + \varepsilon_{\dot{x}_p \zeta}) \end{aligned} \tag{8.55}$$

The harmonic **lateral velocity** is given by:

$$\begin{aligned} \dot{y}_p &= \dot{y} + x_b \cdot \dot{\psi} - z_b \cdot \dot{\phi} \\ &= -\omega_e \cdot y_{p_a} \cdot \sin(\omega_e t + \varepsilon_{y_p \zeta}) \\ &= \dot{y}_{p_a} \cdot \cos(\omega_e t + \varepsilon_{\dot{y}_p \zeta}) \end{aligned} \tag{8.56}$$

The harmonic **vertical velocity** is given by:

$$\begin{aligned} \dot{z}_p &= \dot{z} - x_b \cdot \dot{\theta} + y_b \cdot \dot{\phi} \\ &= -\omega_e \cdot z_{p_a} \cdot \sin(\omega_e t + \varepsilon_{z_p \zeta}) \\ &= \dot{z}_{p_a} \cdot \cos(\omega_e t + \varepsilon_{\dot{z}_p \zeta}) \end{aligned} \tag{8.57}$$

Accelerations

The harmonic accelerations in the x_b-, y_b- and z_b-direction of point $P(x_b, y_b, z_b)$ on the ship are obtained by taking the second derivative of the three harmonic displacements. However, in a ship-bound axes system, a longitudinal and transverse component of the acceleration of gravity, g, has to be added to the longitudinal and lateral accelerations respectively; this yields the total accelerations that the ship and its structural parts and cargo "feel".

The harmonic **longitudinal acceleration** is given by:

$$
\begin{aligned}
\ddot{x}_p &= \ddot{x} - y_b \cdot \ddot{\psi} + z_b \cdot \ddot{\theta} - g \cdot \theta \\
&= -\omega_e^2 \cdot x_{p_a} \cdot \cos(\omega_e t + \varepsilon_{x_p \zeta}) - g \cdot \theta_a \cdot \cos(\omega_e t + \varepsilon_{\theta \zeta}) \\
&= \ddot{x}_{p_a} \cdot \cos(\omega_e t + \varepsilon_{\ddot{x}_p \zeta})
\end{aligned}
\tag{8.58}
$$

The harmonic **lateral acceleration** is given by:

$$
\begin{aligned}
\ddot{y}_p &= \ddot{y} + x_b \cdot \ddot{\psi} - z_b \cdot \ddot{\phi} + g \cdot \phi \\
&= -\omega_e^2 \cdot y_{p_a} \cdot \cos(\omega_e t + \varepsilon_{y_p \zeta}) + g \cdot \phi_a \cdot \cos(\omega_e t + \varepsilon_{\phi \zeta}) \\
&= \ddot{y}_{p_a} \cdot \cos(\omega_e t + \varepsilon_{\ddot{y}_p \zeta})
\end{aligned}
\tag{8.59}
$$

The harmonic **vertical acceleration** is given by:

$$
\begin{aligned}
\ddot{z}_p &= \ddot{z} - x_b \cdot \ddot{\theta} + y_b \cdot \ddot{\phi} \\
&= -\omega_e^2 \cdot z_{p_a} \cdot \cos(\omega_e t + \varepsilon_{z_p \zeta}) \\
&= \ddot{z}_{p_a} \cdot \cos(\omega_e t + \varepsilon_{\ddot{z}_p \zeta})
\end{aligned}
\tag{8.60}
$$

Vertical Relative Displacements

The harmonic vertical relative displacement with respect to the undisturbed wave surface of point $P(x_b, y_b, z_b)$ connected to the ship can be obtained too:

$$
\begin{aligned}
s_p &= \zeta_p - z + x_b \cdot \theta - y_b \cdot \phi \\
&= s_{p_a} \cdot \cos(\omega_e t + \varepsilon_{s_p \zeta})
\end{aligned}
\tag{8.61}
$$

with:

$$
\zeta_p = \zeta_a \cos(\omega_e t - k x_b \cos \mu - k y_b \sin \mu)
\tag{8.62}
$$

This relative motion plays a role in shipping water phenomena, which will be discussed in chapter 11. It may be noted that the sign of the relative motion is chosen here in such a way that a positive relative displacement implies a decrease of the freeboard.

Figure 8.10 shows the speed dependent transfer functions of the absolute and the relative vertical bow motions of a container ship in head waves. Note the opposite characteristics of these two motions in shorter and longer waves.
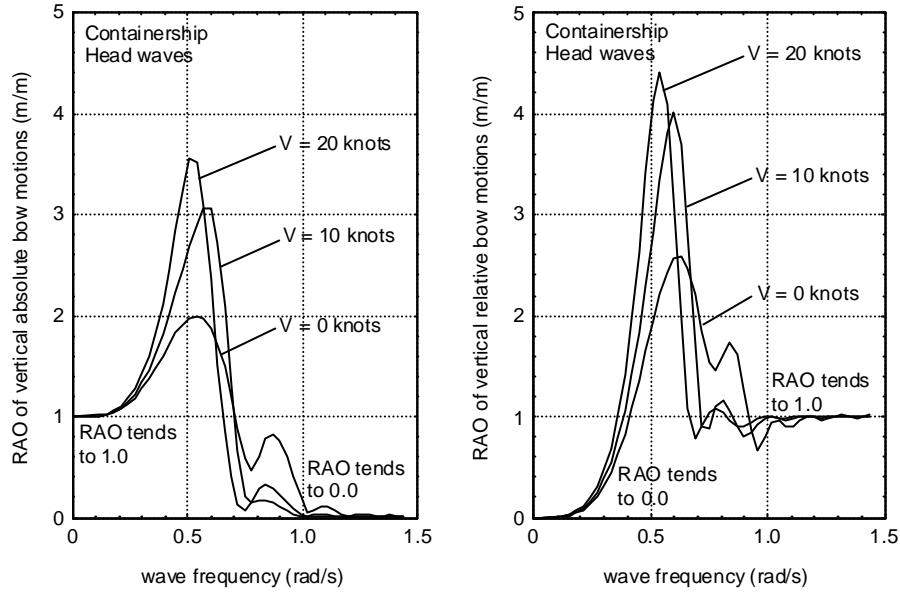
Figure 8.10: Absolute and Relative Vertical Motions at the Bow

Vertical Relative Velocities

The harmonic vertical relative velocity with respect to the undisturbed wave surface of a certain point, $P(x_b, y_b, z_b)$, connected to the ship, can be obtained by:

$$\dot{s} = \frac{D}{Dt}\left\{\zeta_p - z + x_b \cdot \theta - y_b \cdot \phi\right\}$$

$$= \dot{\zeta}_p - \dot{z} + x_b \cdot \dot{\theta} - V \cdot \theta - y_b \cdot \dot{\phi} \tag{8.63}$$

with:

$$\dot{\zeta}_p = -\omega \cdot \zeta_a \sin(\omega_e t - kx_b \cos \mu - ky_b \sin \mu) \tag{8.64}$$

This velocity can play an important role in slamming of the bow of the ship; this will be discussed in chapter 11.

8.4.3 Dynamic Swell-Up

An oscillating ship will produce waves which in turn will influence the vertical relative motion of the ship. A so-called **dynamic swell-up** (which is a typical ship hydromechanical phrase for this phenomenon) should be taken into account.

[Tasaki, 1963] carried out forced oscillation tests with several ship models in still water and obtained an empirical formula for the dynamic swell-up at the forward perpendicular in head waves:

$$\frac{\Delta s_a}{s_a} = \frac{C_B - 0.45}{3} \cdot \sqrt{\frac{\omega_e^2 L}{g}} \tag{8.65}$$

with the restrictions:

block coefficient:	$0.60 < C_B < 0.80$
Froude number:	$0.16 < F_n < 0.29$
frequency of encounter:	$1.60 < \omega_e^2 L_{pp}/g < 2.60$

In this formula, s_a is the amplitude of the relative motion at the forward perpendicular as obtained in head waves, calculated from the heave, the pitch and the wave motions.
Then the actual amplitude of the relative motions becomes:

$$s_a^* = s_a + \Delta s_a \tag{8.66}$$

A simple but much more fundamental method to determine the dynamic swell up forward is given by [Journée and van 't Veer, 1995]; it is explained here.
Let an oscillating body produce damping waves, $\Delta\zeta$, with amplitude $\Delta\zeta_a$. When the vertical relative motions of a point fixed to the vessel with respect to the wave elevation are calculated, the influence of the radiated damping waves must be added to the undisturbed incoming wave. Then the vertical relative motions, s, at a point, $P(x_b, y_b)$, can be calculated using:

$$s(x_b, y_b) = \zeta(x_b, y_b) + \Delta\zeta - z(x_b, y_b) \tag{8.67}$$

where ζ is the incoming wave elevation and $z(x_b, y_b)$ is the vertical motion of the vessel in $P(x_b, y_b)$ and where the radiated wave elevation is given by:

$$\Delta\zeta = \Delta\zeta_a \cdot \cos(\omega t - k|y_b| + \pi) \tag{8.68}$$

For zero forward speed, the amplitude ratio of the local heave motion, $z_a(x_b)$, at a cross section, x_b, of the body and the produced transverse radiated waves, $\Delta\zeta_a(x_b)$, follows from the damping coefficient, $b'_{33}(x_b)$, and the wave speed, $c = g/\omega$:

$$\frac{z_a(x_b)}{\Delta\zeta_a(x_b)} = \frac{1}{\omega} \cdot \sqrt{\frac{\rho g c}{b'_{33}(x_b)}} \tag{8.69}$$

This has already been discussed for an oscillating cylinder in chapter 6.
Using this equation, the ratio of the amplitudes from the radiated waves due to the heaving cross section and the incoming wave becomes:

$$\frac{\Delta\zeta_a(x_b)}{\zeta_a} = \frac{z_a(x_b)}{\zeta_a} \cdot \omega \cdot \sqrt{\frac{b'_{33}(x_b)}{\rho g c}} \tag{8.70}$$

In case of a forward ship speed, V, the cross section is oscillating with the encounter frequency, ω_e, and therefore the wave velocity, c_e, of the radiated waves depends on this frequency:

$$c_e = \frac{g}{\omega_e} \tag{8.71}$$

Due to the forward speed the radiated waves are swept back in the wake. The wave elevation at a certain point, $P(x_p, y_p)$, in the ship-bounded axes system is now a result of the radiated waves from a cross section further ahead. The x_b-position of this cross section can be calculated simply, using:

$$x_b = x_p + |y_p| \cdot \frac{V}{c_e} \tag{8.72}$$

The amplitude of the radiated waves with a non-zero forward speed can now be calculated using the damping coefficient based on the encounter frequency and the previous expression for x_b:

$$\frac{\Delta\zeta_a(x_p, y_p)}{\zeta_a} = \frac{z_a(x_b)}{\zeta_a} \cdot \omega_e \cdot \sqrt{\frac{b'_{33}(x_b)}{\rho g c_e}} \tag{8.73}$$

This calculation method has been verified by using available results of experiments of [Journée, 1976a], carried out with a self propelled 1:50 model of a fast cargo ship in regular head waves; see figure 8.11. In the ballast condition of the model, the vertical relative motions have been measured at four ship speeds at 10 % of the length aft of the forward perpendicular. The curves in these figures marked by "undisturbed wave" refer to not accounting for a dynamic swell-up; the curves marked by "disturbed wave" refer to accounting for a dynamic swell-up as described above. The figures show a strongly improved agreement between the measured and the predicted relative motions taking a dynamic swell-up in to account, especially at frequencies near resonance.
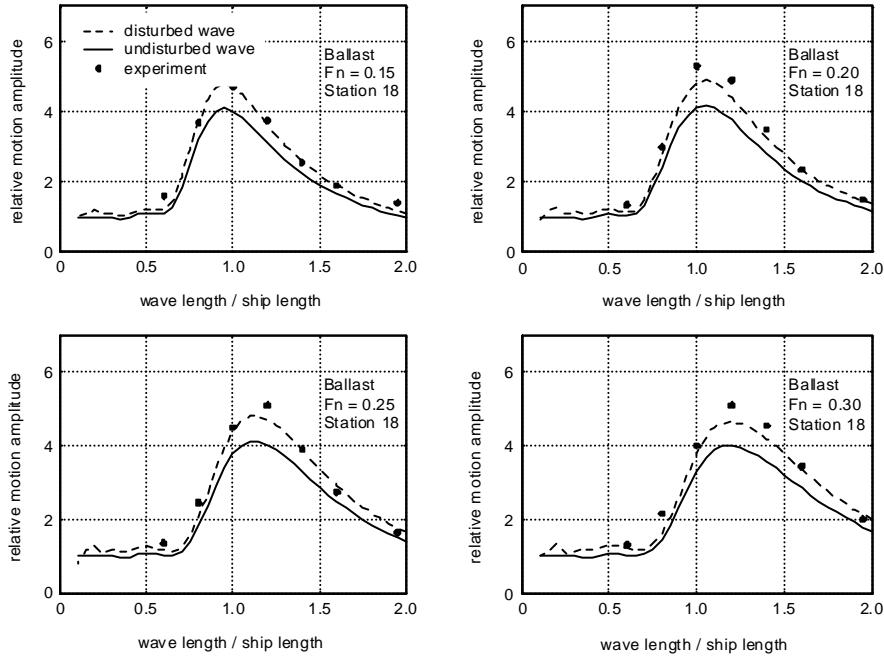
Figure 8.11: Vertical Relative Motions in Head Waves of a Fast Cargo Ship

8.5 Motions in Irregular Waves

Once the transfer functions between wave energy and motion (component) energy are known, one can transform any wave energy spectrum to a corresponding motion energy spectrum. This was explained in chapter 6 for a ship which is not sailing; the average speed was zero.

When a ship is sailing, it will generally encounter or "meet" the waves with a different apparent frequency, the frequency of encounter ω_e, than one would observe from a fixed location; see chapter 6. The first part of this section describes additional necessary wave spectrum axis transformations.

8.5.1 Spectrum Transformations

The spectral value of the waves, $S_\zeta(\omega_e)$, based on ω_e is not equal to the spectral value, $S_\zeta(\omega)$, based on ω. Because there must be an equal amount of energy in the frequency

bands $\Delta\omega$ and $\Delta\omega_e$, it follows that:

$$\overline{|S_\zeta(\omega_e) \cdot d\omega_e = S_\zeta(\omega) \cdot d\omega|} \tag{8.74}$$

This transformation rule is demonstrated in figure 8.12.
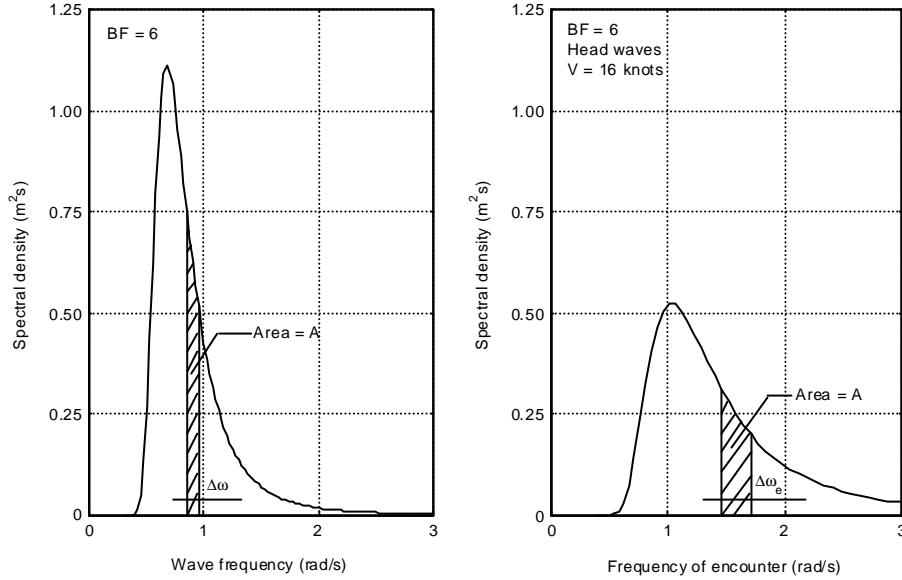
Figure 8.12: Transformation of Wave Spectra

The following relation is found from equation 8.74:

$$\boxed{S_\zeta(\omega_e) = \frac{S_\zeta(\omega)}{\frac{d\omega_e}{d\omega}}} \tag{8.75}$$

The relation between the frequency of encounter and the wave frequency in deep water has been found in chapter 6:

$$
\begin{aligned}
\omega_e &= \omega - \frac{\omega^2}{g} V \cdot \cos\mu \\
&= \omega \cdot \left(1 - \frac{V}{c} \cdot \cos\mu\right) \qquad \text{(by using: } c = g/\omega)
\end{aligned} \tag{8.76}
$$

in which:

$$
\begin{aligned}
\omega &= \text{wave frequency in a fixed reference (rad/s)} \\
\omega_e &= \text{frequency of encounter in a moving reference (rad/s)} \\
V &= \text{forward ship speed (m/s)} \\
c &= \text{wave speed (m/s)} \\
\mu &= \text{ship heading relative to wave direction (rad)}
\end{aligned}
$$

Thus, for deep water:

$$\frac{d\omega_e}{d\omega} = 1 - \frac{2\omega V \cdot \cos\mu}{g} \tag{8.77}$$
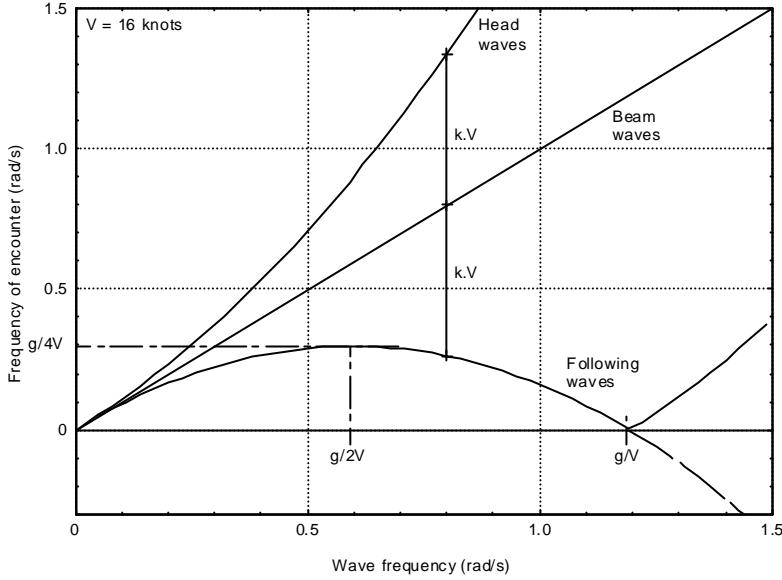
Figure 8.13: Relation between ω_e and ω

Equation 8.76 is plotted in figure 8.13 for a forward speed of 16 knots. The upper curve is for head waves - approaching from the bow; the frequency of encounter becomes higher than the wave frequency ($\omega_e > \omega$).

There is no frequency shift for waves which approach from abeam ($\mu = \pm\pi/2$) so that $\omega_e = \omega$ as is shown in the figure, too.

The situation with following seas requires the most thought:

- When $\omega_e \to 0$, the speed of the waves becomes high and ω_e is only slightly influenced by V (which is smaller than c).

- As ω increases - from small values - the wave speed decreases slowly so that V becomes more and more important. From equation 8.77 follows that ω_e has a maximum value (with waves coming from behind) when $\omega = g/(2V)$. The corresponding ω_e value is $\omega_e = g/(4V)$; this is the highest apparent frequency that will be observed with waves coming from behind. Since $d\omega_e/d\omega$ is here zero, one can expect problems with $S_\zeta(\omega_e)$ at this frequency - see equation 8.75.

- As ω increases beyond $\omega = g/(2V)$, the wave speeds continue to decrease so that ω_e deceases as well.

- At some even higher frequency $\omega = g/V$, the wave speed, c, matches the ship speed, V. The ship can "surf" on this wave!

- Waves with frequencies higher than $\omega = g/V$ are moving more slowly than the ship. The ship intercepts these waves from behind so that these behave as head waves! Because negative frequencies are not "normal" - these values are shown by the dashed line - their absolute value is plotted instead.

Note as well that for any wave frequency, ω, the difference between the encounter frequency in head waves and the absolute wave frequency (equal to the encounter frequency in beam

seas) is the same as the difference between this absolute wave frequency and its encounter frequency in a following sea. This follows from the symmetry in equation 8.76. These two values are labeled "$k \cdot V$" in figure 8.13.
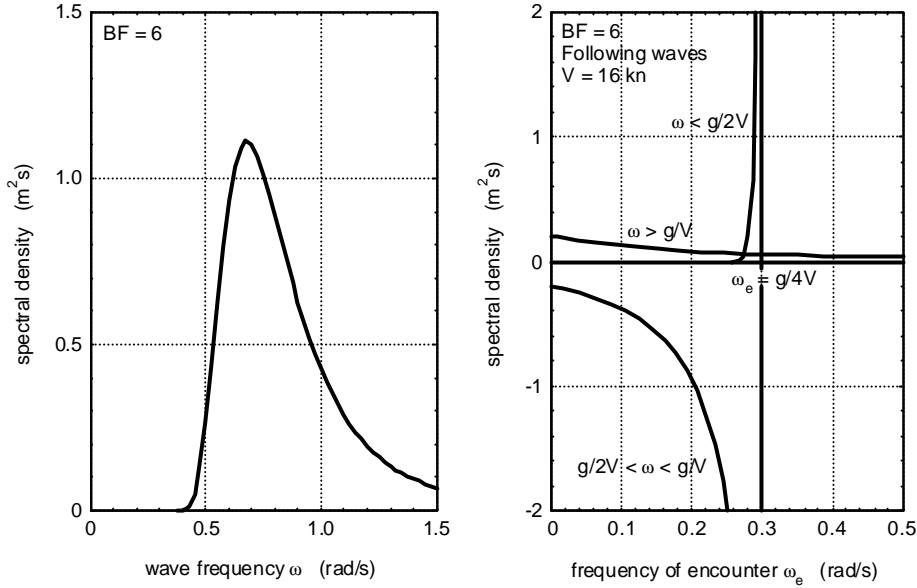
Figure 8.14: Transformed Wave Spectrum in Following Waves

Figure 8.14 shows how a wave spectrum is distorted when it is transformed in terms of encounter frequency in following waves. This type of distortion takes place whenever the waves have a velocity component in the same sense as the ship speed - whenever the waves approach from any direction aft of "beam seas". This spectrum will be hard to work with! When waves are approaching from any direction forward of "beam seas" encounter frequencies only become higher than the absolute frequencies; no special problems are encountered - see figure 8.15.

This is all used as is described below.

8.5.2   Response Spectra

The response spectrum of a motion (or response, r) on the basis of encounter frequency, ω_e, can be found from the transfer function of the motion and the wave spectrum by:

$$S_r(\omega_e) = \left| \frac{r_a}{\zeta_a}(\omega_e) \right|^2 \cdot S_\zeta(\omega_e) \tag{8.78}$$

The moments of the response spectrum are given by:

$$m_{nr} = \int_0^\infty \omega_e^n \cdot S_r(\omega_e) \cdot d\omega_e \qquad \text{with: } n = 0, 1, 2, ... \tag{8.79}$$

This computation causes no difficulty when $S_{\zeta\zeta}(\omega_e)$ is not well behaved - as in following seas. This problem can be avoided if the necessary moments are computed as follows, instead of using equation 8.79:
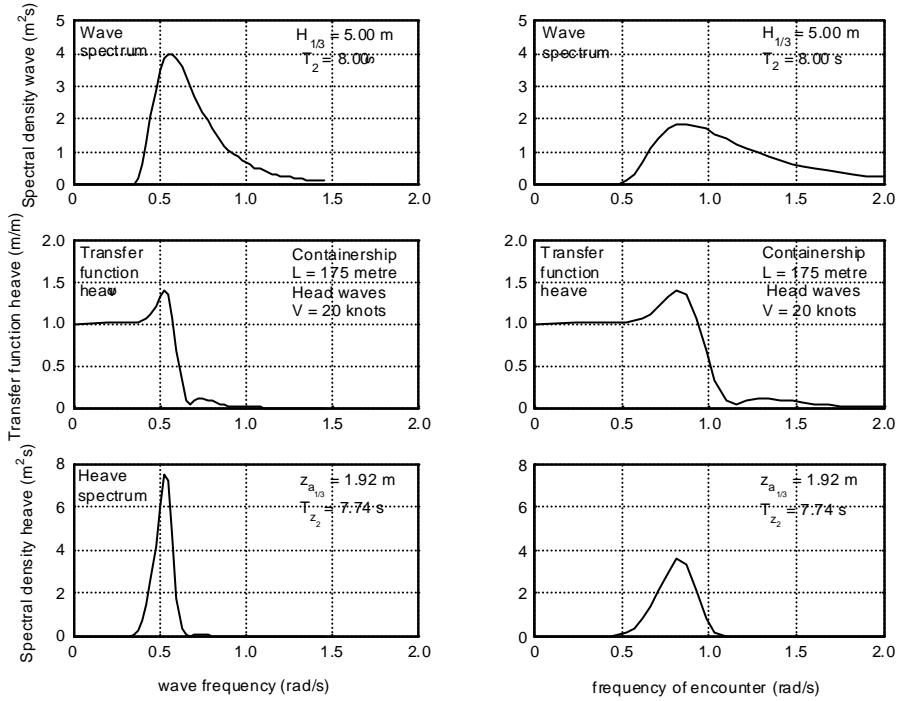
Figure 8.15: Heave Spectra in the Wave and Encounter Frequency Domains

$$
\begin{aligned}
m_{0r} &= \int\limits_0^\infty S_r(\omega_e) \cdot d\omega_e & = \int\limits_0^\infty S_r(\omega) \cdot d\omega \\[2mm]
m_{1r} &= \int\limits_0^\infty \omega_e \cdot S_r(\omega_e) \cdot d\omega_e & = \int\limits_0^\infty \omega_e \cdot S_r(\omega) \cdot d\omega \\[2mm]
m_{2r} &= \int\limits_0^\infty \omega_e^2 \cdot S_r(\omega_e) \cdot d\omega_e & = \int\limits_0^\infty \omega_e^2 \cdot S_r(\omega) \cdot d\omega
\end{aligned}
\tag{8.80}
$$

This avoids integrations of $S_r(\omega_e)$ or $S_\zeta(\omega_e)$ over ω_e.

Note that a negative spectral value in figure 8.14 does not imply a negative energy; both $S_\zeta(\omega_e)$ and $d\omega_e$ are negative and the energy is their product: the area $S_\zeta(\omega_e) \cdot d\omega_e$ (which is positive).

The significant amplitude can be calculated from the spectral density function of a response. The significant amplitude is defined to be the mean value of the highest one-third part of the highest response amplitudes, or equivalently:

$$
\boxed{r_{a_{1/3}} = 2\sqrt{m_{0r}} = 2 \cdot RMS}
\tag{8.81}
$$

A mean period can be found from the centroid of the spectrum (T_{1r}) or from the radius of gyration of the spectrum (zero-upcrossing period, T_{2r}):

$$
\boxed{T_{1r} = 2\pi \cdot \frac{m_{0r}}{m_{1r}}} \qquad \text{and} \qquad \boxed{T_{2r} = 2\pi \cdot \sqrt{\frac{m_{0r}}{m_{2r}}}}
\tag{8.82}
$$

Because of the linearity, which results in a linear relationship between the motion amplitude and the regular wave amplitude, and the (ideal) wave spectrum defined by $S_{\zeta\zeta}(\omega) = H_{1/3}^2 \cdot f(\omega, T)$, the calculated significant response amplitude values in irregular waves are often presented as:

$$\frac{r_{a_{1/3}}}{H_{1/3}} \quad \text{versus:} \quad T \ (\ = T_1,\ T_2 \text{ or } T_p)$$

in which $H_{1/3}$ is the significant wave height, $T \ (= T_1,\ T_2 \text{ or } T_p)$ are mean wave periods and $f(\omega, T)$ is a function of ω and T only.

Spectra of response velocities and accelerations are found by a multiplication of the RAO of the displacement with ω_e and ω_e^2, respectively. Because the squares of the RAO are used to define the response spectra, the spectral moments can be written as:

$$
\begin{aligned}
m_{0\dot{r}} &= m_{2r} &&\text{and} & m_{0\ddot{r}} &= m_{2\dot{r}} = m_{4r} \\
m_{1\dot{r}} &= m_{3r} &&\text{and} & m_{1\ddot{r}} &= m_{3\dot{r}} = m_{5r} \\
m_{2\dot{r}} &= m_{4r} &&\text{and} & m_{2\ddot{r}} &= m_{4\dot{r}} = m_{6r}
\end{aligned}
\tag{8.83}
$$

8.5.3   First Order Motions

Figure 8.16 shows an example of the striking influence of the average wave period on a response spectrum. This response is the heave motion of a 175 meter container ship, sailing with a speed of 20 knots in head waves with a significant wave height of 5.0 meters.
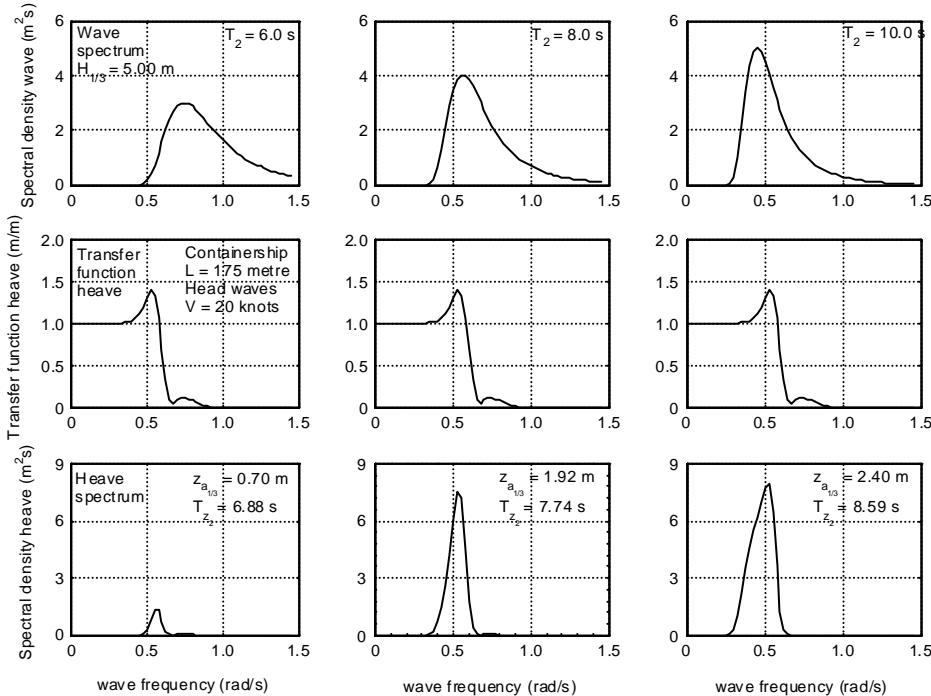
Figure 8.16: Effect of Wave Period on Heave

For the wave spectrum with an average period of 6.0 seconds, the transfer function has very low values in the wave frequency range. The response spectrum becomes small; only

small motions result. As the average wave period gets larger (to the right in figure 8.16), the response increases dramatically.

A similar effect will be obtained for a larger range of average wave periods if the transfer function of the motion shifts to the low frequency region. A low natural frequency is required to obtain this. This principle has been used when designing semi-submersibles, which have a large volume under water and a very small spring term for heave (small water plane area). However, such a shape does not make much of a wave when it oscillates; it has little potential damping. This results in large (sometimes very large) RAO's at the natural frequency. As long as there is (almost) no wave energy at this frequency, the response spectrum will remain small.
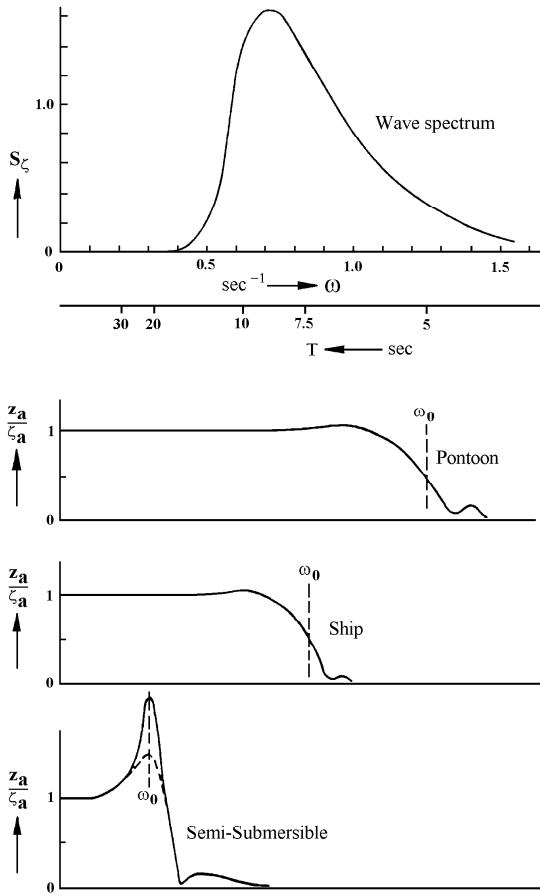
Figure 8.17: Effect of Natural Period on Heave Motions

Figure 8.17 shows a wave spectrum with sketches of RAO's for heave of three different types of floating structures at zero forward speed:

- The **pontoon** has a relatively high natural frequency and as a result of this significant RAO values over a large part of the normal wave frequency range. Almost all wave energy will be transferred into heave motions, which results in a large motion spectrum.
  An extreme example is the **wave buoy**, which has (ideally) an RAO of 1.0 over the whole frequency range. Then the response spectrum becomes identical to the wave

spectrum, which is of course the aim of this measuring tool. It should follow the water surface like a sea gull!

- The **ship**, with a lower natural frequency, transfers a smaller but still considerable part of the wave energy into heave motions.

- The **semi-submersible** however, with a very low natural frequency (large mass and small intersection with the water line), transfers only a very small part of the wave energy; very low first order heave motions will appear; it remains essentially stable in the waves.

One can conclude that the natural frequency is a very important phenomenon which dictates (to a significant extent) the behavior of the structure in waves. Whenever possible, the natural frequency should be shifted out of the wave frequency region.

The fact that the resonant frequency of a motion does not necessarily coincide with the natural frequency has been explained earlier in this chapter. A clear example of this is given by [Hooft, 1970], as shown in figure 8.18, for a semi-submersible platform with different dimensions of the under water geometry. This geometry has been configured in such a way that the responses are minimal at the natural frequency.

Platform	Dimensions (m)			
	D_1	l_1	D_2	l_2
1	11.11	16.52	10.06	111.10
2	11.11	20.71	8.91	133.50
3	11.11	25.82	8.02	155.80
4	25.00	31.61	17.33	150.00
5	25.00	38.12	15.30	175.00
6	25.00	55.06	11.62	225.00

[Source: Hooft, 1970]
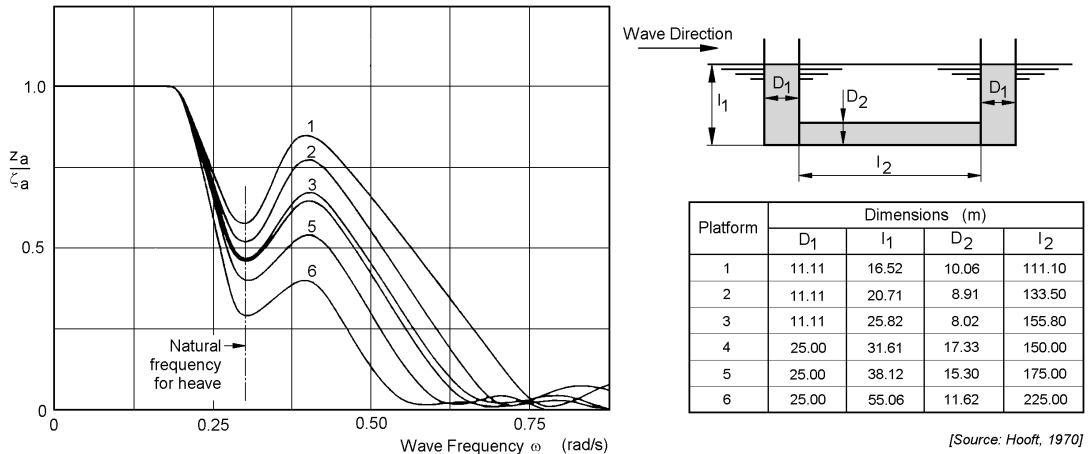
Figure 8.18: Heave Responses of Semi-Submersible Platforms in Waves

8.5.4   Probability of Exceeding

The probability density function of the maximum and minimum values, in case of a spectrum with a frequency range which is not too wide, is given by the Rayleigh distribution - see chapter 5:

$$f(r_a) = \frac{r_a}{m_{0r}} \cdot \exp\left\{\frac{-r_a^2}{2m_{0r}}\right\} \tag{8.84}$$

This implies that the probability of exceeding a threshold value a by the response amplitude r_a becomes:

$$P\{r_a > a\} = \int_a^\infty \frac{r_a}{m_{0r}} \cdot \exp\left\{\frac{-r_a^2}{2m_{0r}}\right\} \cdot dr_a \tag{8.85}$$

Thus:

$$P\{r_a > a\} = \exp\left\{\frac{-a^2}{2m_{0r}}\right\}$$

The average number of times per hour that this happens follows from:

$$N_{hour} = \frac{3600}{T_{2r}} \cdot P\{r_a > a\} \tag{8.86}$$

Note that the zero-crossing period, T_{2r}, is used here, because this period determines the number of cycles per hour.

8.6 Liquids in Tanks

When a double bottom tank, a cargo tank or any other space in a rolling vessel contains a fluid with a free surface, gravity waves will appear at this surface. These gravity waves will cause additional roll exciting moments from within the vessel. In theory this is true for pitch as well, but the generally relatively large longitudinal metacentric height makes the ship less sensitive to this.

Consider a rectangular tank with a length l and a breadth b, which has been filled until a level h with a (non-viscous) fluid. The bottom of the tank is s meters above the center of rotation (center of gravity, G) of the vessel. Figure 8.19 shows a 2-D sketch of this tank with the axis system and notations.
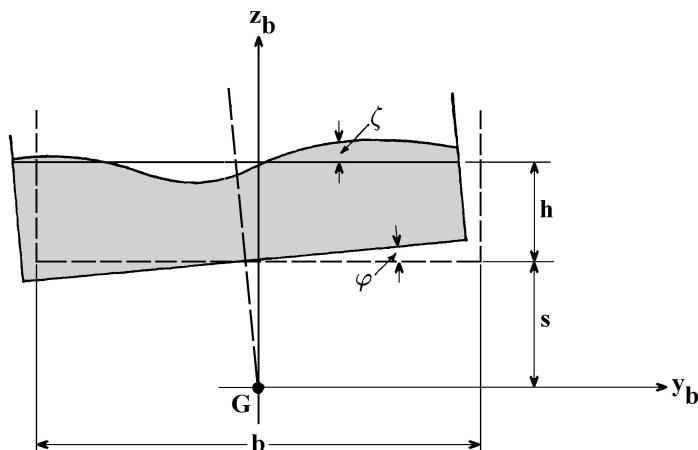
Figure 8.19: Definitions of a Rolling Tank

The natural frequency of the surface waves in a rolling tank appears when the wave length, λ, equals twice the breadth, b, so: $\lambda = 2b$.

With the wave number and the dispersion relation:

$$k = \frac{2\pi}{\lambda} \quad \text{and} \quad \omega = \sqrt{kg \tanh(kh)} \tag{8.87}$$

it follows for the natural frequency of surface waves in the tank:

$$\omega_0 = \sqrt{\frac{\pi g}{b} \tanh\left(\frac{\pi h}{b}\right)} \tag{8.88}$$

At small liquid depths ($h/b <\approx 0.1$), these resonant frequencies can be associated with high wave amplitudes. Under these circumstances a hydraulic jump or bore is formed, which travels periodically back and forth between the walls of the tank. This hydraulic jump can be a strongly non-linear phenomenon. Extensive 2-D model experiments on the behavior of the fluid in these so-called **free surface tanks** was carried out in the sixties by [Bosch and Vugts, 1966]. The experimental results of their study are nowadays still used to design a very simple anti-rolling device which works also at zero forward speed: the free-surface anti-roll tank. Apart from this experimental research, a fundamental theory, based on gas-dynamics for the shock wave in a gas flow under similar resonance circumstances, was developed in the sixties by [Verhagen and van Wijngaarden, 1965]. They used two different approaches: one for low and high frequencies and another one for frequencies near to the natural frequency of the tank. Recently, their approaches to describe the linear(ized) motions of the fluid have been implemented in a ship motions computer code. A very good agreement between theory and experiments was found, see [Journée, 1997].

At larger water depths ($h/b >\approx 0.1$), the behavior of the fluid tends to be more linear. Linear potential theory with the pulsating source method of [Frank, 1967], as described before for strip theory, can be used as well to describe the motions and resulting counteracting moments of fluids in a tank.
First, the study of [Bosch and Vugts, 1966] on the effect of a free-surface tanks with a low water depth on roll motions will be summarized. Then, an application of the potential theory of [Frank, 1967] for the estimation of counteracting roll moments of fluids in a liquid cargo tank and its effect on roll motions is given and the results are discussed.

8.6.1   Anti-Roll Tanks
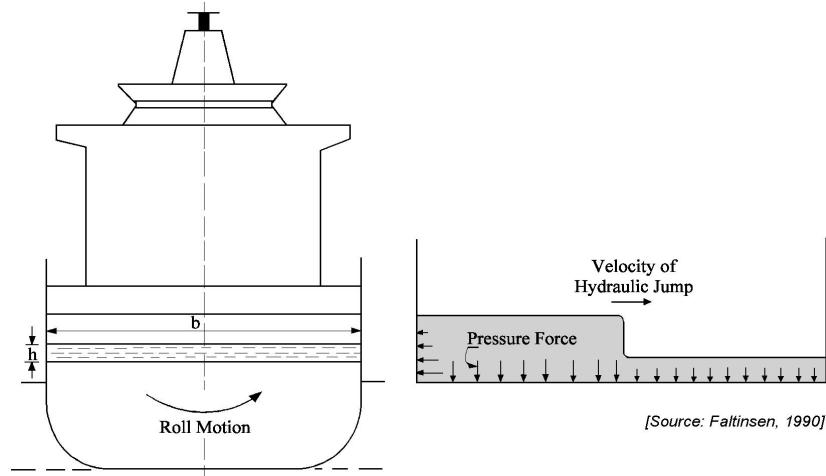
Figure 8.20: Passive Anti-Roll Stabilizer and Hydraulic Jump

A passive free-surface tank can be a very good tool to reduce roll motions, especially at low speeds where anti-roll fins are not effective. This tank has a breadth equal to the ship's breadth and its length is about 1.5 to 2.5 meter, depending on the size of the ship. The roll damping, caused by a passive free-surface tank, is essentially based on the existence of a hydraulic jump or bore in the tank, as shown in figure 8.20. [Bosch and Vugts, 1966] have described the physical behavior of passive free-surface tanks, used as an anti-roll device. They assembled extensive quantitative information on the counteracting moments caused by the water transfer in the tank. Using their notation, the roll motions and the exciting moments of an oscillating rectangular free-surface tank, are defined by:

$$
\begin{aligned}
\varphi &= \varphi_a \cos(\omega t) \\
K_t &= K_{t_a} \cos(\omega t + \varepsilon_{t\varphi})
\end{aligned}
\tag{8.89}
$$

In a practical frequency range, [Bosch and Vugts, 1966] have presented experimental data on the roll moment amplitudes, K_{t_a}, and the phase shifts of these moments with respect to roll, ε_t, for three roll amplitudes ($\varphi_a = 0.033, 0.067, 0.100$ rad), four centers of rotations ($-0.40 \leqq s/b \leqq +0.20$) and five water depths ($0.02 \leqq h/b \leqq 0.10$). An example of the experimental data is given figure 8.21.

The external roll moment due to a free surface tank, oscillating with a frequency ω, can be written as:

$$
K_t = a_{4\varphi} \cdot \ddot{\varphi} + b_{4\varphi} \cdot \dot{\varphi} + c_{4\varphi} \cdot \varphi
\tag{8.90}
$$

with:

$$
\begin{aligned}
a_{4\varphi} &= 0 \\
b_{4\varphi} &= \frac{K_{t_a}}{\omega \varphi_a} \cdot \sin \varepsilon_{t\varphi} \\
c_{4\varphi} &= \frac{K_{t_a}}{\varphi_a} \cdot \cos \varepsilon_{t\varphi}
\end{aligned}
\tag{8.91}
$$

It is obvious that for an anti-roll free-surface tank, build in the ship, the motions of ship and tank are similar:

$$
\phi_a = \varphi_a \qquad \text{and} \qquad \omega_e = \omega
$$

One can express the roll motion of the ship as well as the tank moment on the ship as:

$$
\begin{aligned}
\phi &= \phi_a \cos(\omega_e t + \varepsilon_{\phi\zeta}) \\
\\
K_t &= K_{t_a} \cos(\omega_e t + \varepsilon_{\phi\zeta} + \varepsilon_{t\varphi})
\end{aligned}
\tag{8.92}
$$

Then, an additional exciting moment has to be added to the right hand side of the equations of motion for roll:

$$
\boxed{X_{tank_4} = a_{44_{tank}} \cdot \ddot{\phi} + b_{44_{tank}} \cdot \dot{\phi} + c_{44_{tank}} \cdot \phi}
\tag{8.93}
$$

with:

$$
\begin{aligned}
a_{44_{tank}} &= 0 \\
b_{44_{tank}} &= \frac{K_{t_a}}{\omega_e \phi_a} \cdot \sin \varepsilon_{t\varphi} \\
c_{44_{tank}} &= \frac{K_{t_a}}{\phi_a} \cdot \cos \varepsilon_{t\varphi}
\end{aligned}
\tag{8.94, 8.95}
$$
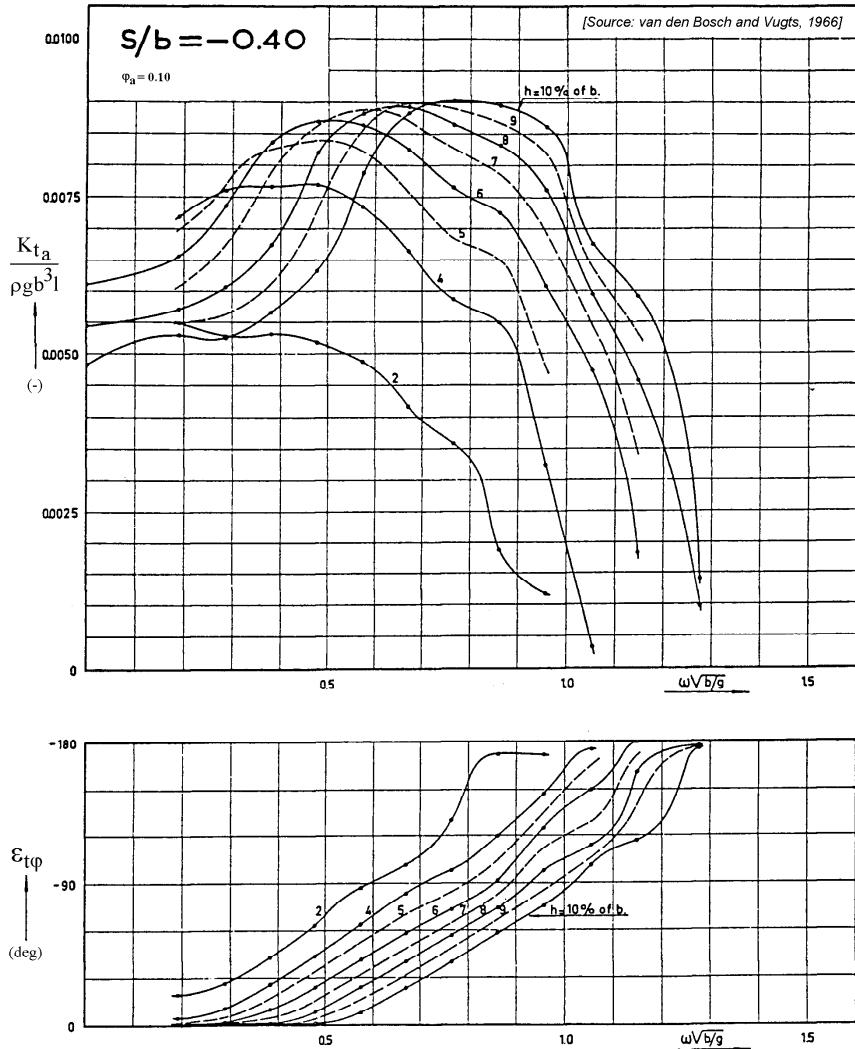
Figure 8.21: Experimental Data on Anti-Roll Free Surface Tanks

This holds that the anti-roll coefficients $a_{44_{tank}}$, $b_{44_{tank}}$ and $c_{44_{tank}}$ have to be subtracted from the coefficients a_{44}, b_{44} and c_{44} in the left hand side of the equations of motion for roll.

Figure 8.22 shows the significant reduction of the roll transfer functions for a trawler with a free surface tank.

8.6.2   Tank Loads

[Frank, 1967] used a cylinder, whose cross section is a simply connected region, which is fully or partly immersed horizontally in a previously undisturbed fluid of infinite depth for the calculation of the 2-D potential mass and damping of ship-like cross sections, see chapter 7.

Frank's method is suitable for the computation of the potential mass and damping of symmetric 2-D shapes, in or below the surface of a fluid. This method has been incorporated in a lot of 2-D ship motions computer programs, all over the world. Starting from the
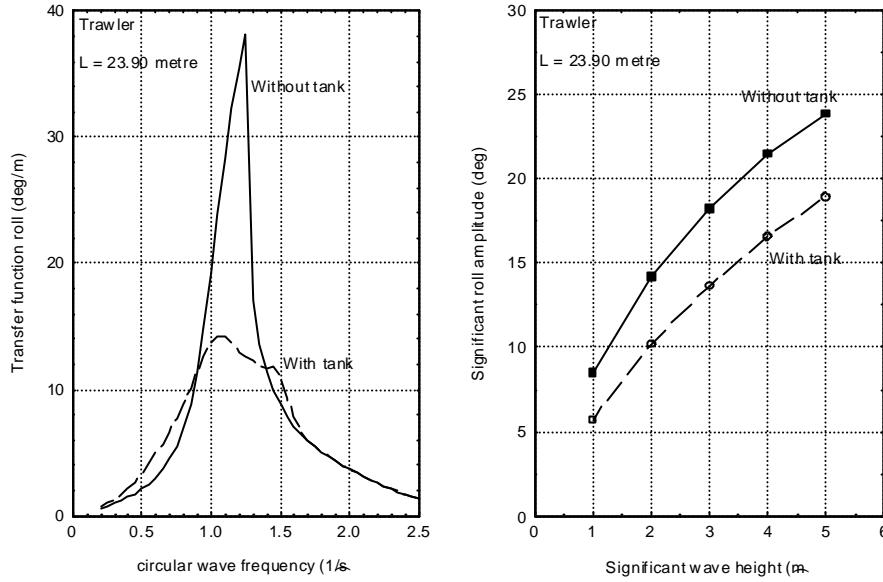
Figure 8.22: Effect of Free Surface Tanks on Roll

keel point of the cross section, the input data (the off-sets) have to be read in an upwards order. Then, the (outward) normal on the elements of the cross section will be defined to be positive in the direction of the fluid outside the cross section.

This method can be adapted easily to calculate the linear loads due to a potential flow fluid in an oscillating symmetrical tank, too. Starting from the intersection of the free surface with the tank wall, the offsets of the tank have to be read in a downwards order - in an opposite sequence as has been done for the cross section of a ship. By doing this, the (inward) normal on the elements of the cross section of the tank will be defined to be positive in the direction of the fluid in the tank. Then, the calculated potential mass and damping delivers the in-phase and out-of-phase parts of the loads due to the moving liquid in the tank. With this, the in-phase and out-of-phase parts of the additional 2-D excitation forces and moments on the ship in and about an origin at the still water fluid surface in a rectangular tank are:

$$\text{Sway tank force, in-phase:} \quad X_{2c} = \omega^2 M^{(2)} x_{2a}$$

$$\text{Sway tank force, out-of-phase:} \quad X_{2s} = -\omega N^{(2)} x_{2a}$$

$$\text{Heave tank force, in-phase:} \quad X_{3c} = \omega^2 M^{(3)} x_{3a}$$

$$\text{Heave tank force, out-of-phase:} \quad X_{3s} = -\omega N^{(3)} x_{3a}$$

$$\text{Roll tank moment, in-phase:} \quad X_{4c} = \omega^2 M^{(4)} x_{4a} + \rho g \left\{ bh \left(s + \frac{h}{2} \right) + \frac{b^3}{12} \right\} x_{4a}$$

$$\text{Roll tank moment, out-of-phase:} \quad X_{4s} = -\omega N^{(4)} x_{4a} \qquad (8.96)$$

in which $M^{(i)}$ and $N^{(i)}$ are the potential mass and damping terms obtained by Frank's method.

The roll moments above must be "translated" to moments about the ship's center of gravity. The second and third term in the in-phase roll moment expression, X_{4c}, are additional "static" terms caused by the "solid or frozen" liquid and by the emerged and immersed wedges of the "fluid or thawed" liquid; see chapter 2 on static floating stability.

This approach can be carried out easily with many existing 2-D, but also 3-D, ship motions computer programs.

Roll Moments

Forced roll oscillation experiments have been carried out with a 2-D model of a cargo tank of an LNG carrier to verify this theoretical approach. A sketch of this 1:25 model of the tank is given in figure 8.23.
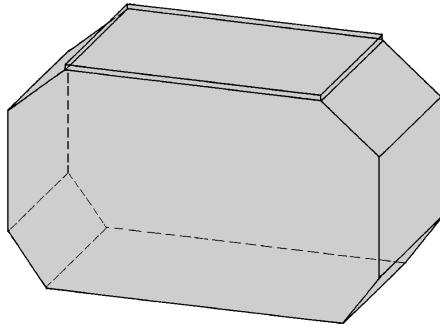
Figure 8.23: LNG Cargo Tank

The exciting roll moments have been measured for a range of oscillation frequencies and a fixed roll amplitude of 0.10 radians for several tank filling levels. Figure 8.24 shows measured and predicted in-phase and out-of-phase parts of the first harmonic of the roll moments of a 45 per cent filled LNG tank as a function of the frequency of oscillation, see [Journée, 1997]. Except at the natural frequency of the fluid in the tank, a fairly good prediction has been found with Frank's 2-D pulsating source method as incorporated in the 2-D computer program SEAWAY. Use of the 3-D computer code DELFRAC provides a similar agreement.

Roll Motions

To investigate the effect of free surface (liquid cargo) tanks on the roll motions of a ship, three tanks as given in figure 8.23 were build in a 1:60 model of an LNG carrier and equally filled with water up to 45 % of the tank height. All other cargo tanks were assumed to be filled up to 97.5 per cent, which was simulated in the experiments by solid ballast weights and an adaptation of the ship's roll radius of gyration.

First, the three cargo tanks are supposed to be equally filled up to 45 % of the tank height with a homogeneous frozen liquid cargo with a stowage factor of 1.00 ton/m^3, simulated during the experiments by solid ballast weights. The unknown radius of gyration for roll of the model has been obtained from free decay tests and the roll motions have been calculated with strip theory program SEAWAY, using the semi-empirical method of [Ikeda et al., 1978] to obtain the linearized viscous roll damping coefficients.

Then, the cargo is "allowed to melt". The ship's roll radius of gyration caused by its own mass has been obtained from the radius of gyration of the ship with the frozen liquid cargo and a theoretical correction for thawing this cargo. The exciting roll moments due to the liquid cargo have been obtained with Frank's method. Now, the roll motions have been calculated, including the effect of the fluid motions in the three tanks.
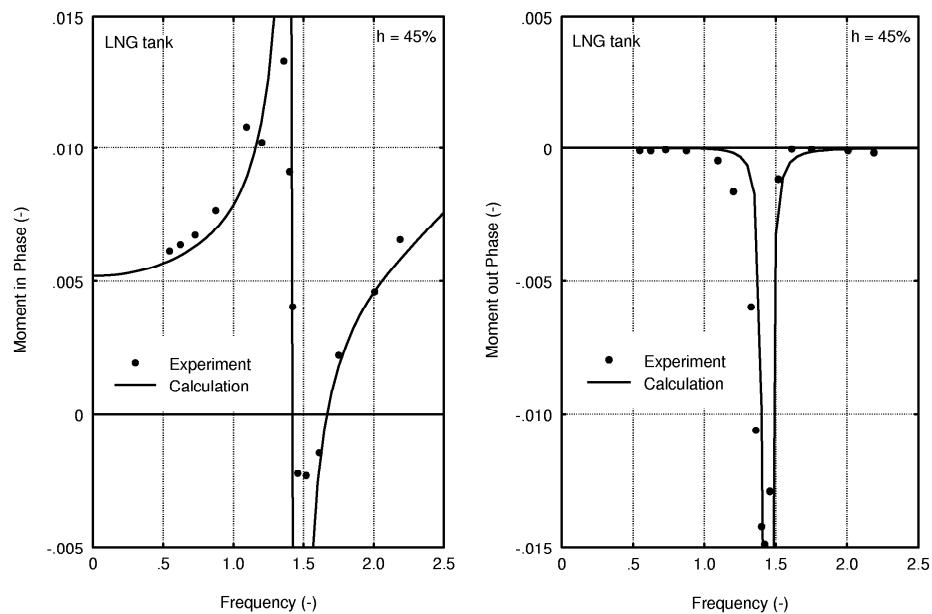
Figure 8.24: Loads Caused by an LNG Cargo Tank
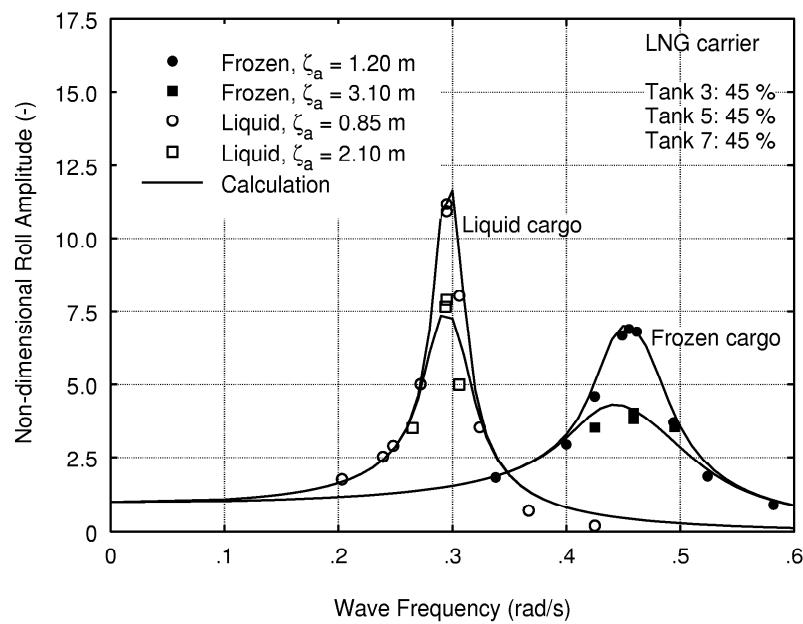
Figure 8.25: Roll an LNG Carrier

Except for some overestimation at higher frequencies, figure 8.25 shows a very good agreement between the predicted and the measured response amplitude operators for roll. However, it must be noted that the natural roll frequency of the ship is about half the lowest natural frequency of the fluid in the three cargo tanks. When these frequencies are closer to each other, non-linear effects caused by the bore or the hydraulic jump at the surface of the fluid in the tanks will play a much more important role.

8.7   Internal Loads

Attention so far has focussed on the external loads on and response of a floating structure caused by the surrounding sea and even liquids stored in tanks on board. This section goes a step further to study the resulting internal reaction forces and moments within the ship structure which is treated here as a single member for which the shear forces as well as bending moments on transverse planes are to be determined.
Obviously additional data on the ship will be needed in order to carry out these computations; the required information includes:
  - $m'(x_b)$:   mass or weight distribution along the ship's length
  - $z'_m(x_b)$:   distribution along the ship's length of the vertical location of the
                center of gravity
  - $k'_{xx}(x_b)$:   distribution along the ship's length of the mass radius of gyration
Figure 8.26 shows the mass distribution, $m'(x_b)$, as well as the mass of the displacement distribution, $\rho A_x(x_b)$, of a cruise ship. Indeed, one often finds that the ship's weight exceeds its buoyancy toward the bow and the stern; this is compensated by an excess of buoyancy amidships.
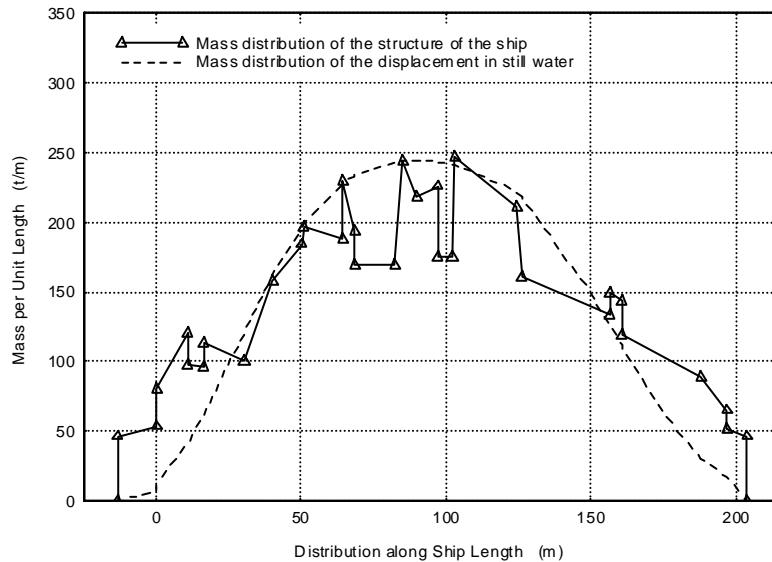
Figure 8.26: Mass Distributions of a Cruise Ship

The total mass of the ship, m, is found by an integration of the masses per unit length,

$m'(x_b)$:

$$m = \int\limits_{stern}^{bow} m'(x_b) \cdot dx_b \tag{8.97}$$

It is obvious that this integrated mass should be equal to the mass of displacement, calculated from the underwater hull form:

$$m = \rho \int\limits_{stern}^{bow} A_x(x_b) \cdot dx_b = \rho \nabla \tag{8.98}$$

The longitudinal position of the center of gravity, x_G, is found from the mass and the distribution of the masses over the length:

$$x_G = \frac{1}{m} \int\limits_{stern}^{bow} m'(x_b) \cdot x_b \cdot dx_b \tag{8.99}$$

The ship's center of buoyancy, x_B, must be at the same longitudinal position (no external trimming moment), so that :

$$x_G = x_B \tag{8.100}$$

The transverse radius of inertia, k_{xx}, is found from the mass and the distribution of the radii of gyration of the masses, $k'_{xx}(x_b)$, over the length:

$$k_{xx}^2 = \frac{1}{m} \int\limits_{stern}^{bow} m'(x_b) \cdot k'^2_{xx}(x_b) \cdot dx_b \tag{8.101}$$

For a relatively slender body, the longitudinal radius of gyration of the mass, k_{yy} and k_{zz}, are found from the mass and the distribution of the masses over the length:

$$k_{yy}^2 = k_{zz}^2 = \frac{1}{m} \int\limits_{stern}^{bow} m'(x_b) \cdot x_b^2 \cdot dx_b \tag{8.102}$$

The position in height of the center of gravity, z_G, is found from the mass and the distribution of the heights of the centers of gravity, $z'_m(x_b)$, over the length:

$$z_G = \frac{1}{m} \int\limits_{stern}^{bow} m'(x_b) \cdot z'_m(x_b) \cdot dx_b \tag{8.103}$$

It is obvious that this value should be zero for an axes system with the origin in the center of gravity, G.

8.7.1   Basic Approach

The ship will be made schematic as a single beam along its longitudinal axis in order to determine its the internal loads on each of its transverse cross sections. These internal loads can come from:

- axial normal force parallel to the x_b axis,
- vertical or horizontal shear in a plane parallel to the (y_b, z_b) plane,
- torsion about an axis parallel to the x_b axis,
- bending about axes parallel to the y_b or z_b axes.

Unlike most more conventional beams, generally all of this beam's properties will be functions of position along its length. The moment of inertia of its area for example will be smaller near the bow and stern of most ships.

The axes system (of which the hydrodynamic sign convention differs from that commonly used in structural engineering) and the internal load definitions are given in figure 8.27.
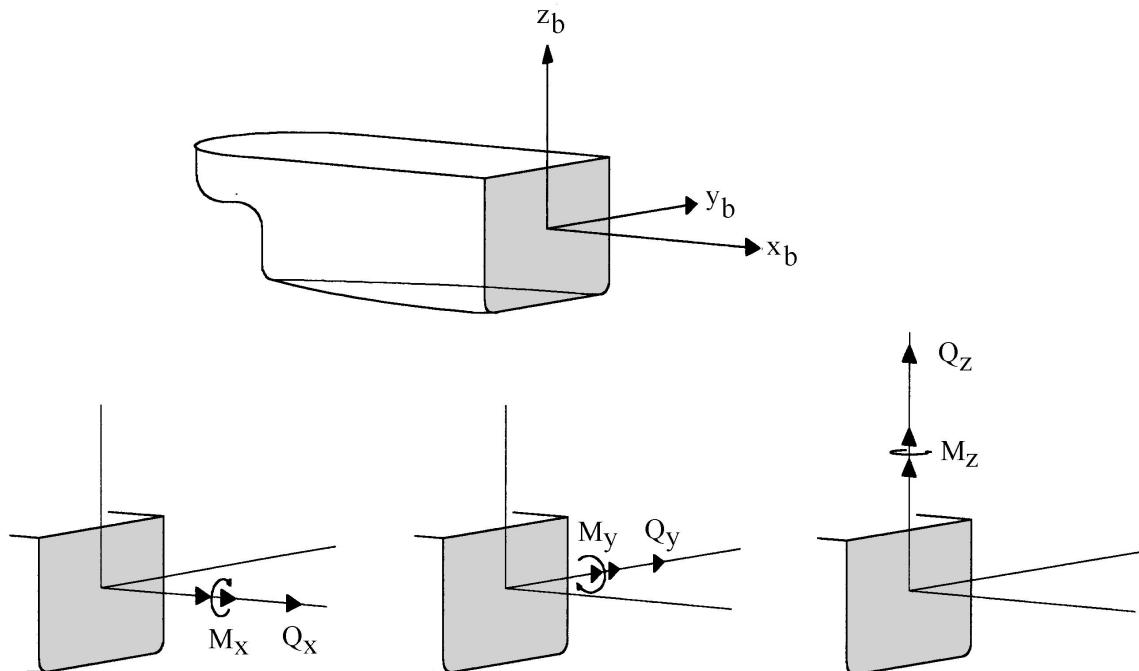
Figure 8.27: Axis System and Internal Load Definitions

Consider a section of the ship with a length dx_b, as illustrated in figure 8.28, to calculate the shear forces and the bending and torsional moments.

When the ship slice is subjected by a load distribution $q(x_b)$, this implies for the slice:

$$q(x_b) \cdot dx_b = -dQ(x_b) \qquad \text{so:} \qquad \boxed{\frac{dQ(x_b)}{dx_b} = -q(x_b)}$$

$$Q(x_b) \cdot dx_b = +dM(x_b) \qquad \text{so:} \qquad \boxed{\frac{dM(x_b)}{dx_b} = +Q(x_b)} \qquad (8.104)$$

in which $Q(x_b)$ is the shear force and $M(x_b)$ is the bending moment.
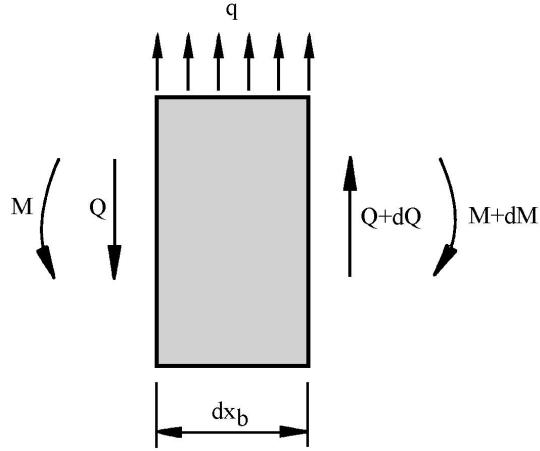
Figure 8.28: Loads on a Cross Section

The shear force and the bending moment in a cross section at $x_b = x_1$ follow from an integration of these sectional loads from the stern of the ship to this cross section. Indeed, both Q and M must be zero at the ends of the ship.

The shear force, $Q(x_1)$, and the bending moment, $M(x_1)$, in a cross section at $x_b = x_1$ can be expressed in the load distribution, $q(x_b)$, by the following integrals:

$$Q(x_1) = - \int_{stern}^{x_1} q(x_b) \cdot dx_b \qquad (8.105)$$

$$
\begin{aligned}
M(x_1) &= - \int_{stern}^{x_1} q(x_b) \cdot (x_1 - x_b) \cdot dx_b \\
&= + \int_{stern}^{x_1} q(x_b) \cdot x_b \cdot dx_b - x_1 \cdot \int_{stern}^{x_1} q(x_b) \cdot dx_b \\
&= + \int_{stern}^{x_1} q(x_b) \cdot x_b \cdot dx_b + Q(x_1) \cdot x_1 \qquad (8.106)
\end{aligned}
$$

For the torsional moment, an approach similar to that given for the shear force can be used.

8.7.2 Static Equilibrium

Static conditions are used first to make a number of concepts more clear. The "ship as a beam" is subjected to two distributed vertical loads: one from the weight of the ship and one from its buoyancy. While overall equilibrium of the ship requires that the total (integrated) buoyant force be equal to the total (integrated) weight of the floating body, their distributions need not be exactly the same so that a net load on any transverse section can be defined.

Consider the forces acting on a section of the ship with a length dx_b. The vertical forces on a transverse 'slice' of a ship in still water are given by:

$$(m' \cdot dx_b) \cdot (-g) = q_z(x_b) \cdot dx_b \tag{8.107}$$

in which:

$$\boxed{q_z(x_b) = \{\rho \cdot A_x(x_b) - m'(x_b)\} \cdot g} \tag{8.108}$$

where A_x is the cross sectional area.

With equations 8.105 and 8.106, the vertical shear force, $Q_z(x_1)$, and the bending moment, $M_y(x_1)$, in still water in a cross section can be obtained from the vertical load, $q_x(x_b)$, by the following integrals:

$$\boxed{Q_z(x_1) = - \int_{stern}^{x_1} q_z(x_b) \cdot dx_b}$$

$$\boxed{M_y(x_1) = + \int_{stern}^{x_1} q_z(x_b) \cdot x_b \cdot dx_b + Q_z(x_1) \cdot x_1} \tag{8.109}$$

Figure 8.29 shows an example of a calculated still water bending moment, M_y, curve of a cruise ship with a weight and buoyancy distribution as given in figure 8.26.
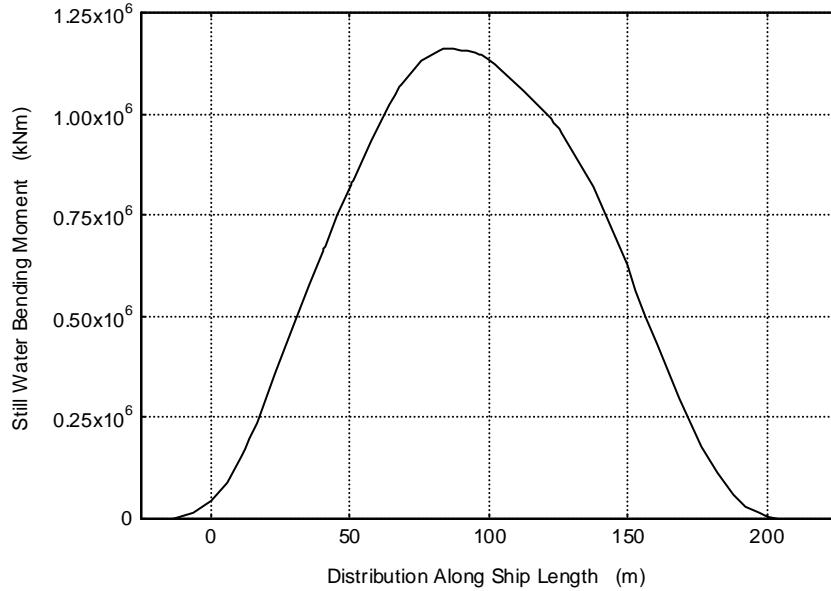
Figure 8.29: Distribution of Still Water Bending Moments of a Cruise Ship

The generally positive moment here is common in ships. As used here, a positive moment implies that the bow and stern of the ship tend to bend down. This if often called **hogging**; the opposite tendency is called **sagging**.

Still water bending moments can become significant. A well-known example of some years ago is the supertanker Energy Concentration moored in Europoort. It suffered the consequences of completely emptying the amidships cargo tanks while the fore and aft tanks

remained completely filled. In this case the ship hogged so much that the lower part of the hull failed in compression and 'folded'; luckily the tanks affected were empty so that a major oil spill was averted.

[Source: Boon, 1997]

Figure 8.30: Damaged Supertanker Energy Concentration

Static shear forces as well as bending moments must also be kept in mind when moving a heavy offshore structure on to a transport barge - or when launching a heavy tower offshore, too, for that matter. Nothing in the offshore industry as spectacular as the fate of the above tanker is known to the authors, however. The important lesson from these examples is that even when the ship (as a whole) is in static equilibrium, it may at the same time be experiencing some very significant internal loads.

As long as the center of gravity of each transverse 'slice' of the ship lies on its midline plane of symmetry, there will be no torsional moment (about the x-axis) generated in the ship. On the other hand, a barge carrying two heavy loads - one forward and to port with the other on the starboard side aft - would have a significant internal torsional moment about its longitudinal axis. Such a loading would disrupt the dynamic behavior of the ship as well, reason enough to leave this topic for others.

The bending moment about the z-axis will always be zero for a free-floating ship in still water.

8.7.3 Quasi-Static Equilibrium

A quasi-static situation exists when none of the dynamic excitations involve accelerations. This means that they change so slowly that the object can be considered to respond statically to the external loads. Quasi-static horizontal loads can be exerted on a moored floating structure by currents and wind, especially when the heading of the ship is not optimal.

The ship is now a beam (when seen from above) which has a location-dependent distributed load and concentrated reaction forces (similar to the supports of a conventional beam) at the mooring line attachment points. Otherwise, the analysis is much like that for the static vertical load case handled above. In general the ends of the ship are still 'free' so that both the horizontal crosswise shear, Q_y, and moment, M_z, will be zero at each end of the ship.

There is more to this that has not yet been considered, however! In general the horizontal forces from the anchor lines, the transverse wind loads and the transverse current loads will not all act at the same elevation; the various forces will act at different elevations in the (x, z) plane. This has two consequences.

As a whole, the floating body will generally come to a static roll angle so that any imbalance of the externally caused external moments will be held in equilibrium by a static roll moment. A good example of this is how a sailboat with the wind on the beam will heel as a result of the wind load in one direction on the sails and the lateral hydrodynamic resistance of the hull working in the other direction; see figure 8.31.
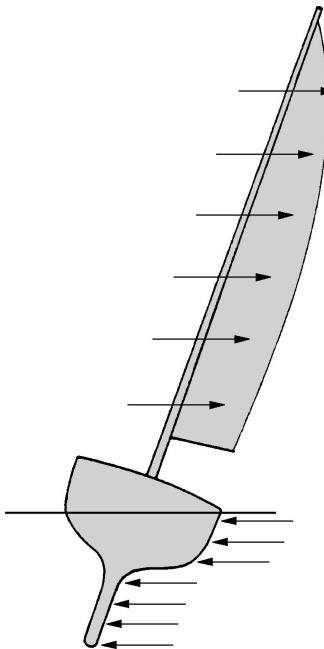
Figure 8.31: Lateral Forces on a Sailboat

Even though this static roll moment will bring the sailboat (in this example) into over-all equilibrium, internal torsional moments will generally still exist. Indeed, with most sailboats, the entire moment from the sail is transferred to the hull at the cross-section where the mast is located. This moment can be distributed to the rest of the hull only via torsional moments about the ship's x-axis.

Quasi-static axial forces can be present in a ship which is sailing (not necessarily a sailboat now), too. The force driving the ship forward (from the propeller) is transferred via its shaft to a thrust bearing where this load is transferred to the hull. The hull forward of this location is obviously 'pushed' through the water; there will obviously be a compressive normal stress in the ship sections forward of the thrust bearing. By the same reasoning, all ship sections aft of the thrust bearing will be under a slight tension as the after body of the ship is pulled through the water.

A more striking example of this would be a tugboat (see figure 8.32) pulling a barge or even a gravity platform being moved to its offshore location. In this case both the towing force transferred to the ship via its towing bollard and the propulsion force at its thrust bearing are point loads in the axial force diagram. Since the towing bollard is generally forward of the thrust bearing, the ship sections between these locations will be under compression.
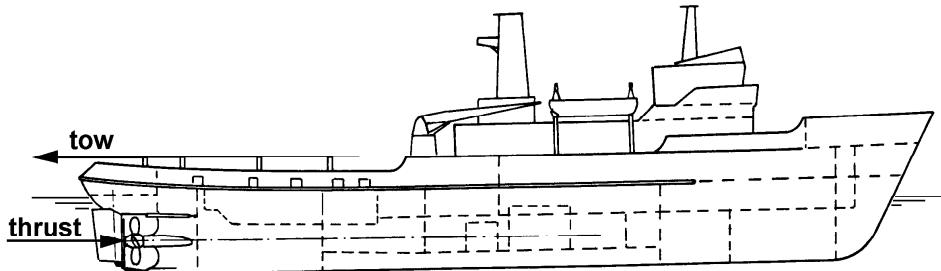
Figure 8.32: Concentration of Axial Forces on a Tug

When viewed from the side, these two forces are not colinear; indeed they deliver a couple about the y-axis; this will be compensated by a small positive (bow up) trim of the tug.

Large square-rigged sailing ships suffered at times from the opposite problem. The driving force from their sails was sometimes centered high in the masts, the ship's hydrodynamic resistance was below the water line. The generated couple now forced the bow down so that it was deeper than normal in the water (this is often referred to as rooting). This increases wave resistance which only reinforces the problem. Admiral Beaufort obviously was practicing good seamanship when he recommended that the highest sails be taken in first as the wind increased; see chapter 5.

8.7.4 Dynamic Equilibrium

The dynamics will be investigated using the principle of **dynamic equilibrium**, using Newton's second law. The dynamic forces and moments should of course be combined with its static component - equation 8.109 - in order to calculate the maximum shear force and bending moment components at each section.

A lot of load components contribute to dynamic forces and moments in a hull; the motion components as well as the direct hydromechanical and wave exciting forces and moments contribute directly and sometimes in more than one way. Shear forces and bending moments are local loads and non-linearities can play a significant role. This is one of the reasons why the strip theory does not predict them always very accurate; deviations up to about 25 percent are possible.

Anchor line forces become dynamic as well, now, making the computation even more complex in terms of bookkeeping. Indeed, since mooring line tensions will generally depend upon the instantaneous position of their attachment point, they can even introduce a coupling between vertical motions on the one hand, and roll motions and dynamic torsional moments on the other. These aspects have not been taken into account here.

Lateral Dynamic Loads

Consider the horizontal forces acting on a section of the ship with a length dx_b. According to Newton's second law, the harmonic lateral dynamic load per unit length on a transverse 'slice' of the ship is given by:

$$
\begin{aligned}
q_y(x_b) \;=\; & +X'_{hy}(x_b) + X'_{wy}(x_b) \\
& + \rho g A_x(x_b) \cdot \phi \\
& - m'(x_b) \cdot \left\{ \ddot{y} + x_b \cdot \ddot{\psi} - z'_m \cdot \ddot{\phi} + g \cdot \phi \right\}
\end{aligned}
\tag{8.110}
$$

where $A_x(x_b)$ is the sectional area, $X'_{hy}(x_b)$ and $X'_{wy}(x_b)$ are the sectional hydromechanical and wave forces for sway and $m'g\phi$ is the lateral mass-force component due to the definition of the lateral loads in the ship-bound axes system, respectively.

With equations 8.105 and 8.106, the harmonic lateral shear force, $Q_y(x_1)$, and the bending moment, $M_z(x_1)$, in waves in cross section x_1 can be obtained from the horizontal load, $q_y(x_b)$, by the following integrals:

$$
\boxed{\;Q_y(x_1) = Q_{y_a}\cos(\omega_e t + \varepsilon_{Q_z\zeta}) = -\int\limits_{stern}^{x_1} q_y(x_b) \cdot dx_b\;}
$$

$$
\boxed{\;M_z(x_1) = M_{z_a}\cos(\omega_e t + \varepsilon_{M_z\zeta}) = -\int\limits_{stern}^{x_1} q_y(x_b) \cdot x_b \cdot dx_b - Q_y(x_1) \cdot x_1\;} \tag{8.111}
$$

Vertical Dynamic Loads

Consider the vertical forces acting on a section of the ship with a length dx_b. According to Newton's second law, the harmonic longitudinal and vertical dynamic forces per unit length on a transverse 'slice' of the ship are given by:

$$
\begin{aligned}
q_x(x_b) \;=\;& +X'_{hx}(x_b) + X'_{wx}(x_b) - m'(x_b) \cdot \left\{ \ddot{x} - \overline{bG}(x_b) \cdot \ddot{\theta} \right\} \\[6pt]
q_z(x_b) \;=\;& +X'_{hz}(x_b) + X'_{wz}(x_b) - m'(x_b) \cdot \left\{ \ddot{z} - x_b \cdot \ddot{\theta} \right\}
\end{aligned}
\tag{8.112}
$$

where $\overline{bG}(x_b)$ is the distance of the centroid of the cross section to the x_b axis and $X'_{hx}(x_b)$, $X'_{hz}(x_b)$ and $X'_{wx}(x_b)$, $X'_{wz}(x_b)$ are the sectional hydromechanical and wave forces for surge and heave, respectively.

With equations 8.105 and 8.106, the harmonic vertical shear force, $Q_z(x_1)$, and the bending moment, $M_y(x_1)$, in waves in cross section x_1 can be obtained from the longitudinal and vertical loads, $q_x(x_b)$ and $q_z(x_b)$, by the following integrals:

$$
\boxed{\;Q_z(x_1) = Q_{z_a}\cos(\omega_e t + \varepsilon_{Q_z\zeta}) = -\int\limits_{stern}^{x_1} q_z(x_b) \cdot dx_b\;}
$$

$$
\boxed{\;M_y(x_1) = M_{y_a}\cos(\omega_e t + \varepsilon_{M_y\zeta}) = +\int\limits_{stern}^{x_1} q_x(x_b) \cdot \overline{bG}(x_b) \cdot dx_b\;}
$$

$$\left| \quad + \int_{stern}^{x_1} q_z(x_b) \cdot x_b \cdot dx_b \ + Q_z(x_1) \cdot x_1 \right| \qquad (8.113)$$

Figure 8.33 shows a comparison between measured and calculated distribution of the vertical wave bending moment amplitudes over the length of the ship
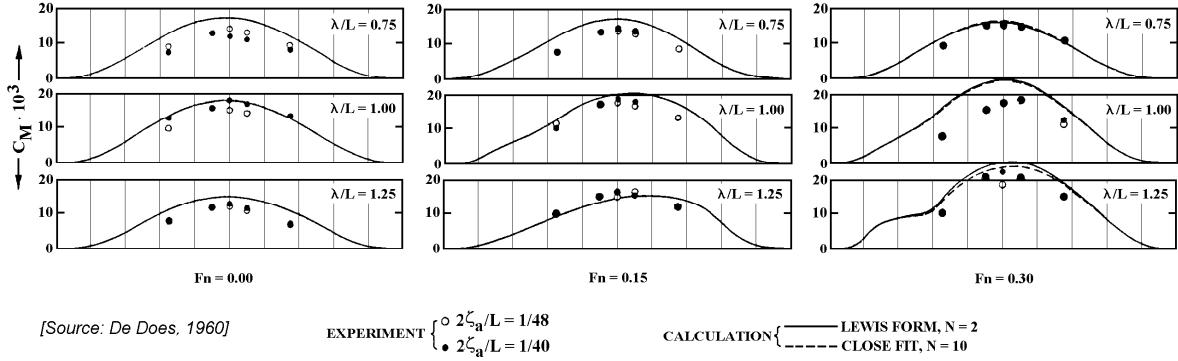
Figure 8.33: Distribution of Vertical Bending Moment Amplitudes

Torsional Dynamic Loads

Consider the moments acting on a section of the ship with a length dx_b. According to Newton's second law, the harmonic torsional dynamic moment per unit length on a transverse 'slice' of the ship about a longitudinal axis at a distance z_1 above the ship's center of gravity is given by:

$$\begin{aligned} q_\phi(x_b, z_1) \ = \ & +X'_{h\phi}(x_b) + X'_{w\phi}(x_b) \qquad\qquad (8.114) \\ & +z_1 \cdot q_y(x_b) - m'(x_b) \cdot \left\{ k'^2_{xx} \cdot \ddot{\phi} - z'_m \cdot (\ddot{y} + x_b \cdot \ddot{\psi} + g \cdot \phi) \right\} \end{aligned}$$

where $X'_{h\phi}(x_b)$ and $X'_{w\phi}(x_b)$ are the sectional hydromechanical and wave moments for roll, respectively.

With equation 8.105, the harmonic torsional moment, $M_x(x_1, z_1)$, in waves in cross section x_1 at a distance z_1 above the ship's center of gravity can be obtained from the torsional loads, $q_\phi(x_b, z_1)$, by the following integral:

$$\left| M_x(x_1, z_1) = M_{x_a} \cos(\omega_e t + \varepsilon_{M_x \zeta}) = - \int_{stern}^{x_1} q_\phi(x_b, z_1) \cdot dx_b \right| \qquad (8.115)$$

It is important to realize, for example, that a ship sailing in quartering waves -approaching from about 45 degrees off the stern - can experience very significant dynamic torsional moments - even if it is not rolling very much. Both the wave direction (and associated relative phases along the ship's axis) and the low frequency of encounter contribute to a large transfer function value in this case.

8.7.5 Internal Loads Spectra

The internal loads spectra can be calculated in a way similar to that described earlier for other harmonic responses.

8.7.6 Fatigue Assessments

It has already been pointed out that the transfer functions for any of the above forces can be computed by carefully (and properly!) superposing the components for the already known functions for forces and ship motions. One can go even deeper into the structural engineering aspects, however as long as the system remains linear in its behavior.

Knowing all six of the load components on a ship cross-section, a marine structural engineer can - knowing a lot more details of the internal structure of the ship - convert each of these forces to associated stress components. Stress concentration factors and other details must now be taken into account along the way, of course.

These stress components can in turn be combined to determine principal stresses and even to carry out a fatigue analysis. Structural engineering and offshore hydromechanics are often very closely linked - if not married - within offshore engineering! This will show up again when sea fastening of offshore structures to transport barges is discussed in chapter 11.

Fatigue analyses depend upon two independent input data items:

- Magnitude of the (local) stress change - stress range.
- Associated number of cycles with this stress range.

This information can then be combined using the Miner-Palmgren rule to obtain an overall fatigue damage estimate. The structural analysis details of this are left to others more expert in this field, but a bit more about each of the above two items is discussed here.

The magnitude of the stress change within a ship or other large structure will be linearly related to the ambient waves. If the object has a fixed location, then wave climate data is relatively easy to obtain and work with. Even if the object is only seasonally, one can approach the wave data in a quite straight forward way - see chapter 5.

More "portable" objects - such as a major pipe laying vessel that may spend some time near Australia before going to the west coast of Africa before coming to the North sea for a while - present a formidable bookkeeping problem. If the problem to be solved involves the determination of the "remaining fatigue life" of an existing vessel, then obtaining the cumulative - location and time dependent - wave climate presents a significant problem. The pragmatic solution in a design situation, on the other hand, would be to determine fatigue life based upon continuous exposure to some defined wave climate such as that for the northern North Sea.

Global and Local Loads

Fatigue sensitive locations in a vessel are the deck, bottom and possibly the sides-shell. The loads important for fatigue can be split in global and local loads. Global loads are loads in a cross section of the hull girder and make equilibrium with the "acceleration forces" due to the motions and the pressure integration over the specific hull section; these have been determined above. Local internal loads result from pressures at specific spots on the hull inducing additional locally fluctuating stresses. The simple effect of external

pressure variations (from waves) causing local (bending) stresses in the hull plating is an example of this.

Global loads - important for fatigue - are the vertical and horizontal bending moments. An important local load is the external pressure causing cyclic bending of longitudinals between their supporting frames (webs or web/bulkhead). The local external pressure loading is mainly of interest for tankers and bulk carriers. Especially FPSO tankers operated on the North Sea are to be examined thoroughly on the fatigue strength since they are built according to the rules for trading vessels but are used differently. These vessels more often encounter head waves and are permanently on site in a harsh environment.

Fatigue in the deck structure is induced by vertical and horizontal bending of the hull girder. The bottom structure is loaded both by the vertical and horizontal bending moments and the external wave pressure. The side shell is mainly loaded by the external wave pressure and horizontal bending moment and slightly by the vertical bending moment depending on the position of the neutral axis; see figure 8.34, illustrating the global and local loads acting on a vessel.
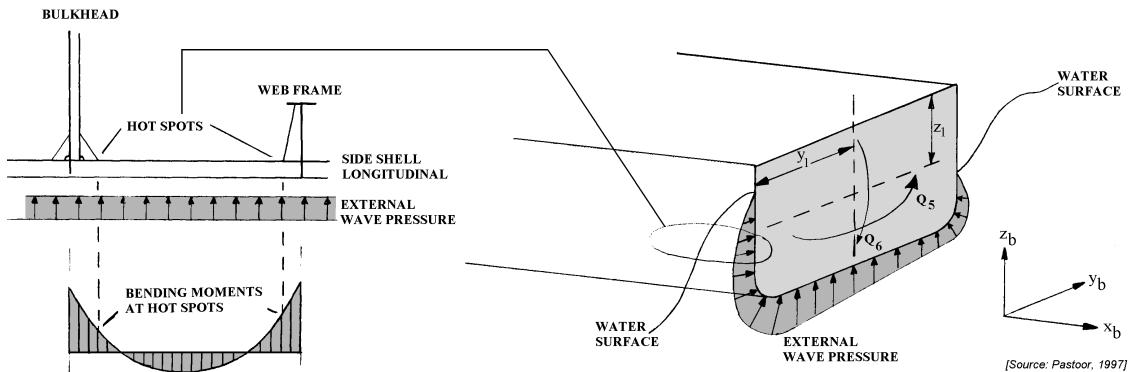
Figure 8.34: Global and Local Loads Acting on a Cross Section

Combining the horizontal and vertical wave bending moments is done by calculating one stress transfer function at the spot of interest.

$$H_{\sigma\zeta}(y_b, z_b, \omega) \cos(\omega t + \varepsilon_{\sigma\zeta}) = \frac{z_1}{I_{yy}} \quad H_{Q_5\zeta}(y_b, z_b, \omega) \cos(\omega t + \varepsilon_{Q_5\zeta})$$

$$+ \frac{y_1}{I_{zz}} \quad H_{Q_6\zeta}(y_b, z_b, \omega) \cos(\omega t + \varepsilon_{Q_6\zeta}) \qquad (8.116)$$

Expand the cosines into cosine products and sine products. One can determine $H_{\sigma\zeta}$ and $\varepsilon_{\sigma\zeta}$ by stating that the equation must be valid for $\omega t = 0$ and $\omega t = \pi/2$. This gives:

$$
\begin{aligned}
H_{\sigma\zeta}(y_b, z_b, \omega) \cos\varepsilon_{\sigma\zeta} &= \frac{z_1}{I_{yy}} H_{Q_5\zeta}(y_b, z_b, \omega) \cos\varepsilon_{Q_5\zeta} + \frac{y_1}{I_{zz}} H_{Q_6\zeta}(y_b, z_b, \omega) \cos\varepsilon_{Q_6\zeta} \\
H_{\sigma\zeta}(y_b, z_b, \omega) \sin\varepsilon_{\sigma\zeta} &= \frac{z_1}{I_{yy}} H_{Q_5\zeta}(y_b, z_b, \omega) \sin\varepsilon_{Q_5\zeta} + \frac{y_1}{I_{zz}} H_{Q_6\zeta}(y_b, z_b, \omega) \sin\varepsilon_{Q_6\zeta}
\end{aligned}
$$

$$(8.117)$$

Squaring and summing these equations results in an expressions for $H_{\sigma\zeta}$ and dividing these two equations gives an expression for $\tan\varepsilon_{\sigma\zeta}$.

The external pressure can be incorporated as well for those position which are always wet - the bottom and bilges. In this case a pressure transfer function is required along with a structural model to determine the local stress contribution - just as is needed for the global internal loads as well. Side shell loading is more complicated. Since the water surface is fluctuating the side shell is sometimes wet and sometimes dry. Hence this loading is strongly nonlinear which is difficult to account for properly. For calculation routines and ways to combine this nonlinear load with the global loads one is referred to [Cramer and et.al., 1993], [Pastoor, 1997b] and [Pastoor, 1997a].

Once the proper overall transfer functions and some form of cumulative wave scatter diagram has been determined, each of its "cells" - with its own characteristic wave height and period - can be transformed to:

- A characteristic stress variation dependent upon the waves and a whole "chain" of transfer functions.

- A number of stress variation cycles dependent upon the wave period and the number of observations associated with that wave scatter diagram cell.

Often several adjacent cells in the wave scatter diagram are combined when carrying out this transformation.
Once this procedure has been followed for all wave scatter diagram cells, one can sum up the results in order to obtain the input data for a Miner-Palmgren sum.

8.8   Added Resistance in Waves

A ship moving forward in a wave field will generate "two sets of waves": waves associated with forward speed through still water and waves associated with its vertical relative motion response to waves. Since both wave patterns dissipate energy, it is logical to conclude that a ship moving through still water will dissipate less energy than one moving through waves. The extra wave-induced loss of energy can be treated as an added propulsion resistance - see chapter 4.
Figure 8.35 shows the resistance in regular waves as a function of the time: a constant part due the calm water resistance and an oscillating part due to the motions of the ship, relative to the incoming regular waves. The time-averaged part of the increase of resistance is called: the added resistance due to waves, R_{aw}.
Two theoretical methods for the estimation of the time-averaged added resistance of a ship due to its vertical motions relative to the waves are described here:

- a **radiated wave energy method**
  introduced by [Gerritsma and Beukelman, 1972] and suitable for head to beam waves

- an **integrated pressure method**
  introduced by [Boese, 1970] and suitable for all wave directions.
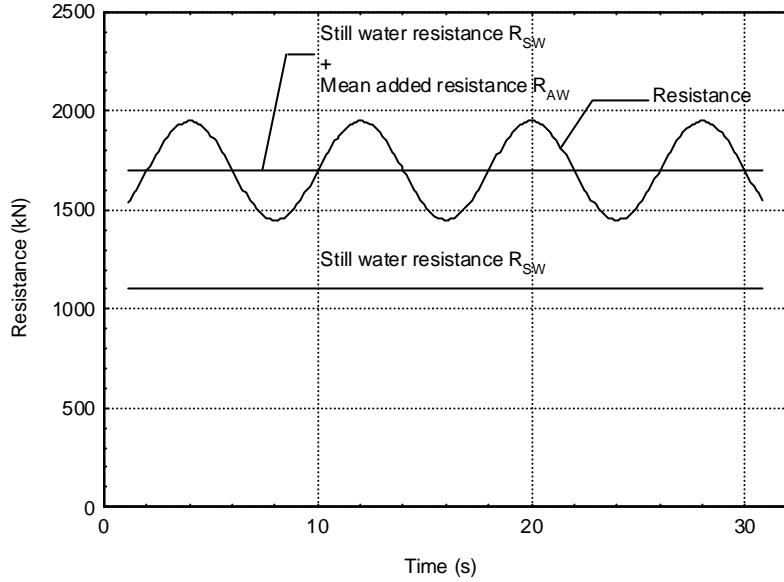
Figure 8.35: Increase of Resistance in Regular Waves

8.8.1 Radiated Energy Method

The energy relation of an oscillating body has been determined in chapter 6. Based on this relation and strip theory, the radiated wave energy during one period of oscillation of a ship in regular waves is defined by [Gerritsma and Beukelman, 1972] as:

$$
\begin{aligned}
P &= \int\limits_{L} \left\{ \int\limits_{0}^{T_e} (b'_{33} \cdot V_z^*) \cdot (V_z^* \cdot dt) \right\} \cdot dx_b \\
&= \int\limits_{0}^{T_e} \int\limits_{L} b'_{33} \cdot V_z^{*\,2} \cdot dx_b \cdot dt
\end{aligned}
\tag{8.118}
$$

in which:

b'_{33} = hydrodynamic damping coefficient of the vertical motion of the cross section,
V_z^* = vertical average velocity of the water particles, relative to the cross sections,
T_e = period of vertical oscillation of the cross section.

The speed dependent hydrodynamic damping coefficient for the vertical motion of a cross section is defined here as shown before in equation 8.25:

$$
b'_{33} = N'_{33} - V \cdot \frac{dM'_{33}}{dx_b}
\tag{8.119}
$$

The harmonic vertical relative velocity of a point on the ship with respect to the water particles is defined by:

$$
\begin{aligned}
V_z &= \dot{\zeta}'_{w_3} - \frac{D}{Dt}\{z - x_b \cdot \theta + y_b \cdot \phi\} \\
&= \dot{\zeta}'_{w_3} - \left(\dot{z} - x_b \cdot \dot{\theta} + V \cdot \theta + y_b \cdot \dot{\phi} \right)
\end{aligned}
\tag{8.120}
$$

For a cross section of the ship, an equivalent harmonic vertical relative velocity has to be found. This equivalent relative velocity is defined by:

$$
\begin{aligned}
V_z^* &= \dot{\zeta}_{w_3}^* - \left(\dot{z} - x_b \cdot \dot{\theta} + V \cdot \theta\right) \\
&= V_{z_a}^* \cdot \cos(\omega_e t + \varepsilon_{V_z^*\zeta})
\end{aligned}
\tag{8.121}
$$

With this the radiated energy during one period of oscillation is given by:

$$
P = \frac{\pi}{\omega_e} \int_L \left(N_{33}' - V \cdot \frac{dM_{33}'}{dx_b}\right) \cdot V_{z_a}^{*\,2} \cdot dx_b
\tag{8.122}
$$

To maintain a constant forward ship speed, this energy should be provided by the ship's propulsion plant. A mean added resistance, R_{aw}, has to be gained. The energy provided to the surrounding water is given by:

$$
\begin{aligned}
P &= R_{aw} \cdot \left(V - \frac{c}{\cos\mu}\right) \cdot T_e \\
&= R_{aw} \cdot \frac{2\pi}{-k\cos\mu}
\end{aligned}
\tag{8.123}
$$

From this the transfer function of the mean added resistance according to Gerritsma and Beukelman can be found:

$$
\boxed{\frac{R_{aw}}{\zeta_a^2} = \frac{-k\cos\mu}{2\omega_e} \cdot \int_L \left(N_{33}' - V \cdot \frac{dM_{33}'}{dx_b}\right) \cdot \left(\frac{V_{z_a}^*}{\zeta_a}\right)^2 \cdot dx_b}
\tag{8.124}
$$

This method gives good results in head to beam waves. However, this method fails in following waves. When the wave speed in following waves approaches the ship speed the frequency of encounter in the denominator tends to zero. At these low frequencies, the potential sectional mass is very high and the potential sectional damping is almost zero. The damping multiplied with the relative velocity squared in the numerator does not tend to zero, as fast as the frequency of encounter. This is caused by the presence of a natural frequency for heave and pitch at this low ω_e, so a high motion peak can be expected. This results in extreme (positive and negative) added resistances.

8.8.2   Integrated Pressure Method

[Boese, 1970] calculates the added resistance by integrating the longitudinal components of the oscillating pressures on the wetted surface of the hull. A second small contribution of the longitudinal component of the vertical hydrodynamic and wave forces has been added. The wave elevation is given by:

$$
\zeta = \zeta_a \cos(\omega_e t - kx_b \cos\mu - ky_b \sin\mu)
\tag{8.125}
$$

The pressure in the undisturbed waves in deep water is given by:

$$
p = -\rho g z + \rho g \cdot e^{kz}\zeta
\tag{8.126}
$$

The horizontal force on an oscillating cross section is given by:

$$f(x_b, t) = \int_{-D_s+z_x}^{\zeta} p \, dz_b \qquad \text{with: } z_x = z - x_b \theta \qquad (8.127)$$

As the mean added resistance during one period will be calculated, the constant term and the first harmonic term can be ignored, so:

$$
\begin{aligned}
f^*(x_b, t) &= -\frac{1}{2}\rho g \left\{ \zeta^2 - (-D_s + z_x)^2 \right\} \\
&= -\frac{1}{2}\rho g \left(\zeta - z_x \right)^2
\end{aligned}
\qquad (8.128)
$$

The vertical relative motion is defined by $s = \zeta - z_x$, so:

$$f^*(x_b, t) = -\frac{1}{2}\rho g \, s^2 \qquad (8.129)$$

The average horizontal force on a cross section follows from:

$$\overline{f^*}(x_b) = \int_0^{T_e} f^*(x_b, t) \, dt = \frac{1}{4}\rho g \, s_a^2 \qquad (8.130)$$

The added resistance due to this force is:

$$R_{aw_1} = 2 \int_L \overline{f^*}(x_b) \left(-\frac{dy_w}{dx_b} \right) dx_b \qquad (8.131)$$

so that this part of the mean added resistance reduces to:

$$R_{aw_1} = -\frac{1}{2}\rho g \int_L s_a^2 \frac{dy_w}{dx_b} \, dx_b \qquad (8.132)$$

The integrated vertical hydromechanical and wave forces in the ship bounded axis system varies not only in time but also in direction with the pitch angle. From this follows a second contribution to the mean added resistance:

$$
\begin{aligned}
R_{aw_2} &= \frac{-1}{T_e} \int_0^{T_e} \left\{ X_{h_3}(t) + X_{w_3}(t) \right\} \theta(t) \, dt \\
&= \frac{-1}{T_e} \int_0^{T_e} \rho \nabla \ddot{z}(t) \, \theta(t) \, dt
\end{aligned}
\qquad (8.133)
$$

This second contribution can be written as:

$$R_{aw_2} = \frac{1}{2}\rho \nabla \, \omega_e^2 \, z_a \, \theta_a \, \cos(\varepsilon_{z\zeta} - \varepsilon_{\theta\zeta}) \qquad (8.134)$$

so that the transfer function of the total mean added resistance according to Boese is given by:

$$\boxed{\frac{R_{aw}}{\zeta_a^2} = \frac{1}{2}\rho g \int_L \left(\frac{s_a}{\zeta_a} \right)^2 \frac{dy_w}{dx_b} \, dx_b \; + \frac{1}{2}\rho \nabla \, \omega_e^2 \, \frac{z_a}{\zeta_a} \frac{\theta_a}{\zeta_a} \, \cos(\varepsilon_{z\zeta} - \varepsilon_{\theta\zeta})} \qquad (8.135)$$

8.8.3   Non-dimensional Presentation

The transfer function of the mean added resistance R_{aw}/ζ_a^2 is often presented in a non-dimensional way as:

$$\boxed{R'_{aw} = \frac{R_{aw}}{\rho g \zeta_a^2 B^2/L}} \tag{8.136}$$

in which:

$$
\begin{aligned}
L &= \text{length between perpendiculars} \\
B &= \text{(maximum) breadth of the waterline}
\end{aligned}
$$

Figure 8.36 shows a comparison of calculated and measured added resistance data of a container vessel. Because of the added resistance of a ship due to the waves is proportional to the relative motions squared, inaccuracies in the predicted motions will be amplified in resistance errors.
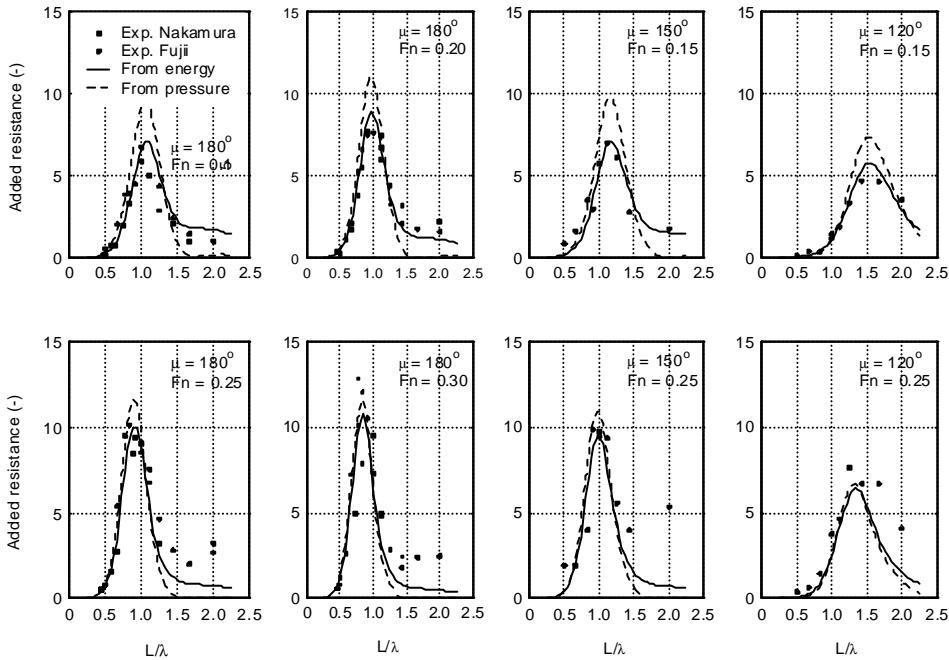
Figure 8.36: Computed and Measured Added Resistance

The deviations in the figure at low wave lengths (high frequencies) are caused by diffraction of the waves against the ship; this effect has not been taken into account. But the amount energy in irregular waves at these high frequencies is small; so generally, these deviations will not have a large influence on the added resistance in irregular waves.

8.8.4   Added Resistance in Irregular Waves

The mean added resistance in a frequency range $\Delta\omega$ can be written as:

$$
\begin{aligned}
R_{aw}(\omega) &= 2 \cdot \left| \frac{R_{aw}}{\zeta_a^2}(\omega) \right| \cdot \frac{1}{2}\zeta_a^2 \tag{8.137} \\
&= 2 \cdot \left| \frac{R_{aw}}{\zeta_a^2}(\omega) \right| \cdot S_\zeta(\omega) \cdot \Delta\omega \tag{8.138}
\end{aligned}
$$

Then, the total mean added resistance in a seaway follows from a summation or an integration of the contributions over the whole frequency range:

$$\overline{R}_{AW} = 2 \sum_{\omega=0}^{\infty} \left| \frac{R_{aw}}{\zeta_a^2}(\omega) \right| \cdot S_\zeta(\omega) \cdot \Delta\omega \tag{8.139}$$

Thus:

$$\boxed{\overline{R}_{AW} = 2 \int_0^\infty \left| \frac{R_{aw}}{\zeta_a^2}(\omega) \right| \cdot S_\zeta(\omega) \cdot d\omega} \tag{8.140}$$

Because of the linear motions, which results in a linear relation between the mean added resistance and the regular wave amplitude squared, and the (ideal) wave spectrum defined by $S_\zeta(\omega) = H_{1/3}^2 \cdot f(\omega, T)$, the calculated mean added resistance values in irregular waves are often presented as:

$$\frac{\overline{R}_{AW}}{H_{1/3}^2} = 2 \int_0^\infty \left| \frac{R_{aw}}{\zeta_a^2}(\omega) \right| \cdot f(\omega, T) \cdot d\omega \quad \text{versus} \quad T = T_1,\, T_2 \text{ or } T_p$$

in which $H_{1/3}$ is the significant wave height, $T \ (= T_1,\, T_2 \text{ or } T_p)$ are mean wave periods and $f(\omega, T)$ is a function of ω and T only.

.

Chapter 9

NON-LINEAR BEHAVIOR

9.1 Introduction

A physical description of nonlinear wave excitation forces as well as the response of floating structures has been given in chapter 6, where the so-called **second order wave drift forces** are described. They consist of **mean wave drift forces** and **low-frequency wave drift forces**. Both are the result of a non-linear behavior of the structure in the waves.

The present chapter - in which the theory is part based for a major part on the doctor's thesis of [Pinkster, 1980] on low-frequency second order wave exciting forces on floating structures - starts by describing situations in which higher order wave forces are important. These motivate the more detailed treatment of the associated computations later in this chapter.

9.2 Some Typical Phenomena

Investigations into the fundamental aspects of the behavior of offshore structures have often been guided by the behavior as observed at sea and as determined from model testing of such structures in realistically simulated wind, wave and current environments.

This section describes examples of the behavior of these structures which have been shown to be of significant influence on the design of the structures or on operational aspects of offshore work. All of these examples have motivated extensive fundamental research to explain the observed behavior.

9.2.1 Bow-Hawser Moored Vessel in Wind and Current

Shuttle tankers, either loading or discharging crude oil offshore, are often moored to a single point mooring (SPM) with a bow hawser.

It has been observed that such vessels can have **large amplitude horizontal motions** (surge, sway and yaw) **in steady winds and currents**. These motions lead in turn to large peak loads in the bow hawser. An example, showing the time record of the bow

---

hawser force of a 200 thousand ton deadweight (kTDW) tanker, is given in figure 9.1. The lower part of the figure shows the bow hawser tension force as a function of time.
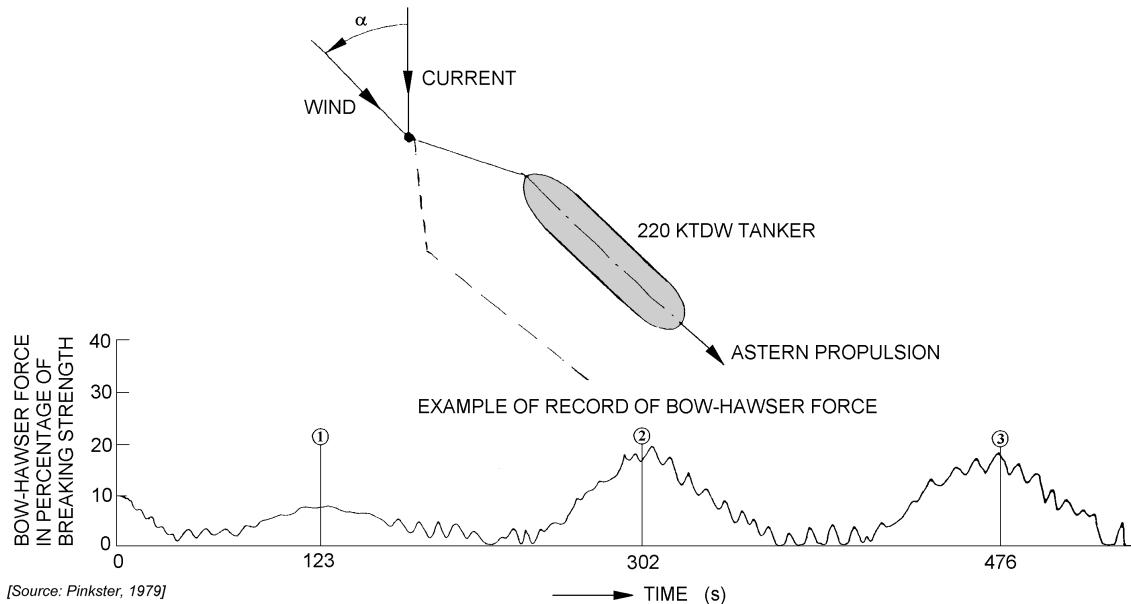
Figure 9.1: Unstable Horizontal Motions of a Bow Hawser Moored Tanker

This example shows that significant dynamic effects can occur, even in the absence of time variations in the environmental forces. In this particular case, these effects are due to inherent instabilities in the horizontal motions of the tanker, which are related to the length of the bow-hawser.

Figure 9.2 shows the regions of unstable horizontal motions as a function of the angle between the wind and current on the one hand and the length of the bow-hawser on the other hand. See [Wichers, 1979] for further details.

9.2.2   Large Concrete Structure under Tow

After completion of a large concrete Gravity Base Structure in sheltered deep water, it is towed out to the field by 6 to 8 large ocean going tugs. Narrow and shallow fjord passages have to be negotiated on the way out to the open sea. These passages put restrictions on the swept path and the draft of the platform.

Figure 9.3 shows that while under tow, this type of platform performs oscillatory motions in all six degrees of freedom in addition to its constant forward motion. These oscillatory motions are related - to a considerable extent - to the oscillatory components in the flow about the platform, as well as the inherent "towing stability" of the platform.

Important aspects of the flow about the platform are the vortex-shedding phenomenon about the large diameter vertical columns and flow separation about the large base structure. The towing force needed for the transportation of the platform is important; this determines the number and size of the tugs. The force necessary to hold the platform on location prior to being ballasted down to rest on the sea bed is determined by, among other factors, the current force that may be exerted by a tidal current. Figure figure 9.4 shows an example of the quadratic increase of the current force with the current velocity.
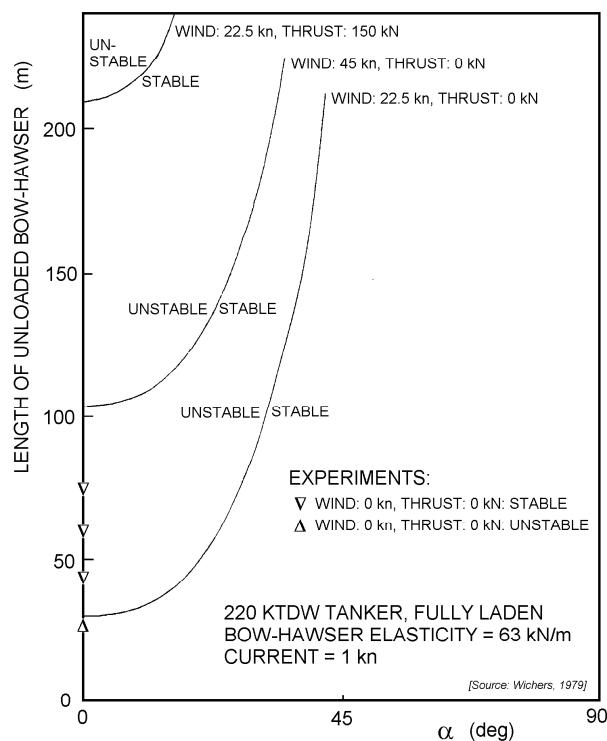
Figure 9.2: Stability Criterion for a Tanker as a Function of Bow Hawser Length
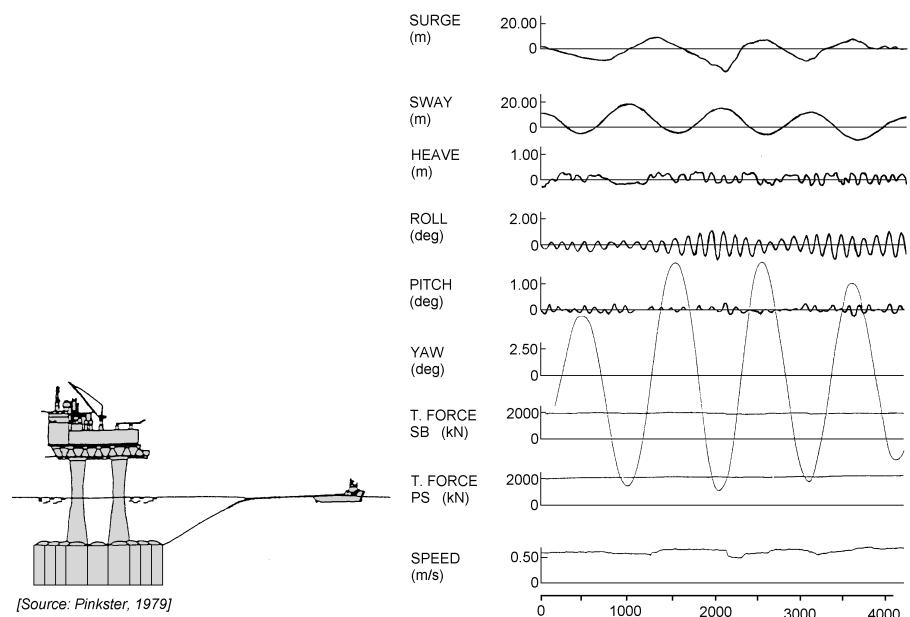
Figure 9.3: Motions of a Large Concrete Platform
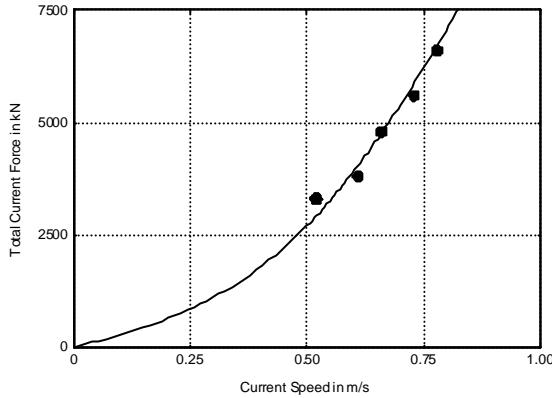
Figure 9.4: Current Force on Gravity Base Structure

Currents are usually assumed to be constant in time, but in some cases, such as during the positioning of this type of platforms, current speed variations may also give rise to undesirable horizontal platform motions. Figure 9.5 shows an example of current velocity variations - expressed in terms of the measured mean, maximum and minimum current velocities - and the spectral density of the current velocity.
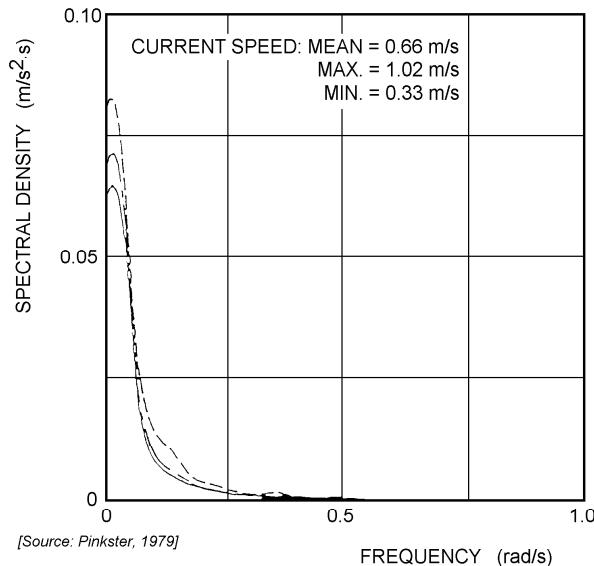
Figure 9.5: Current Speed Fluctuations

As is seen in figure 9.5, velocity variations are of low-frequency nature. Often the natural frequency of the horizontal motions of a moored structure (or a structure being positioned) is low due to the large mass on the one hand and the relatively soft restraining system on the other hand. There is little damping at such low frequencies as well; relatively large dynamic motions can result.

9.2.3   Horizontal Motions of Moored Tankers in Waves

Figure 9.6 shows the wave elevation record and the motions of a permanently moored tanker in high head sea conditions. It is seen that the heave and pitch motions contain the same frequencies; their amplitudes are in the order of the wave amplitudes and wave slopes respectively. This behavior is predicted using methods as given in chapters 6 and 8.
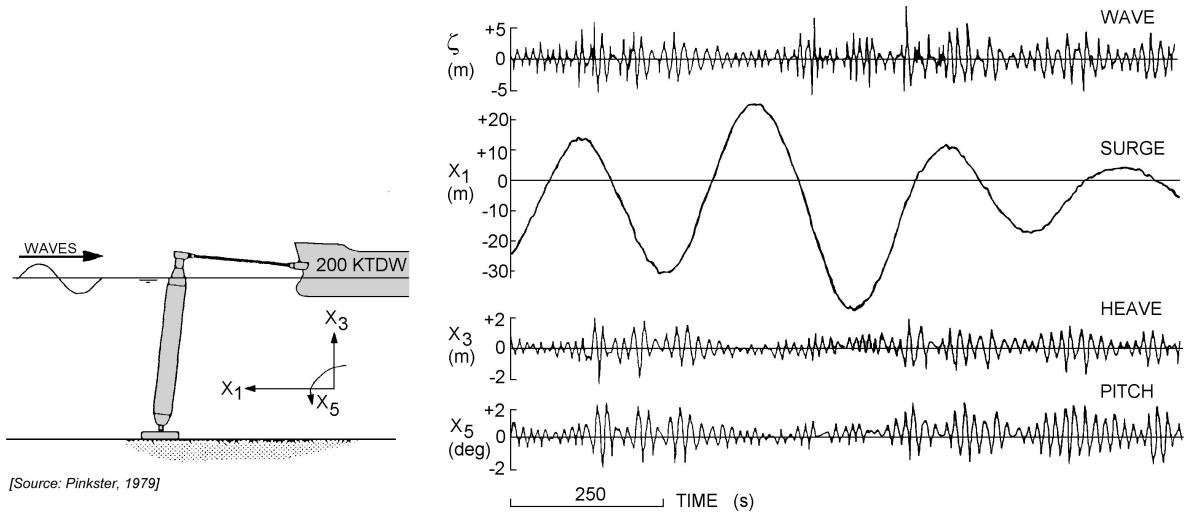
Figure 9.6: Record of the Motions of a Moored Tanker Model in Head Waves

The surge motion, besides containing a (small) wave frequency motion component, is dominated by a low frequency component with a significant larger amplitude.
Upon closer examination it appears that the large amplitude surge motion contains frequencies near the natural surge period of the moored vessel as dictated by the combination of the vessel mass and the mooring stiffness. The vessel is in fact carrying out resonant low frequency surge motions in response to small wave forces containing frequencies corresponding to the low natural surge frequency of the moored vessel. The response is further aggravated by the fact that surge motion damping is especially small at this low frequency. It will be clear that the mooring system forces will be dominated by this effect; its design must account for this. This requires a careful analysis of the phenomena involved. A brief introduction is given here.

Wave loads on structures as well as their responses to those loads can be split into several components. A table of these is given in chapter 6. These are summarized here too.
Firstly there are wave loads which have the same frequencies as the waves and are linearly proportional in amplitude to the wave amplitudes. These are known as **first order wave forces**. Secondly, there are wave load components which have frequencies both higher and lower than the frequencies of the waves. These forces are proportional to the square of the wave amplitudes and known as **second order wave forces**.
Low frequency second order wave forces have frequencies which correspond to the frequencies of wave groups present in irregular waves. These forces, which, beside containing time-varying components, also contain a non-zero mean component, are known as **wave drift forces**. This name is a consequence of the fact that a vessel, floating freely in waves,

will tend to drift in the direction of propagation of the waves under influence of the mean second order forces.

High frequency second order forces contain frequencies corresponding to double the frequency of the waves (also known as **sum frequencies**). The horizontal motions response of moored structures to these forces is generally small.

The fact that low frequency drift forces can cause large amplitude horizontal motion responses in moored vessels and that these motions are related to the wave group phenomenon was demonstrated by [Remery and Hermans, 1971] in chapter 6. One of the results of their investigations is shown in figure 9.7. In this figure the low frequency surge motion amplitude of a barge moored in head seas consisting of regular wave groups (superposition of two regular waves with small frequency difference corresponding to the wave group frequency) is shown. It is seen that when the period of the wave groups equals the natural surge period of the moored vessel, large motion amplitudes are the result.

[Source: Remery and Hermans, 1971]

$$\Lambda = \frac{\text{NATURAL PERIOD OF SURGE MOTION}}{\text{PERIOD OF WAVE GROUPS}}$$
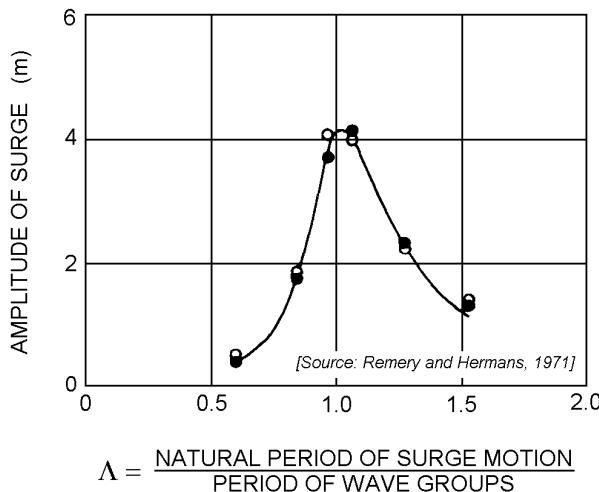
Figure 9.7: Surge Motions of a Moored Barge in Regular Head Wave Groups

Figure 9.8, taken from reference [Pinkster, 1976], shows that the low frequency surge motions of a barge moored in head seas increase more or less as a linear function of the square of the significant wave height. This implies that the wave force is a **quadratic function** of the wave amplitude.

9.2.4   Motions and Mooring Forces of Semi-Submersibles

Figure 9.9 shows that not only tankers and other mono-hull vessels are subject to the effects of first and second order wave forces. This figure shows the surge motion of a large semi-submersible crane vessel (SSCV) and the forces in the mooring lines. A large low frequency component is superimposed on wave frequency components.

Figure 9.10 shows a time record of the low frequency second order wave drift force on a semi-submersible. The relationship between the occurrence of groups of waves in the incident wave train and peaks in the wave drift force are very clear.

A tension leg platform (TLP) is a semi-submersible structure with vertical mooring tethers which restrain the vertical motions of the platform. It is also subject to these wave loads.
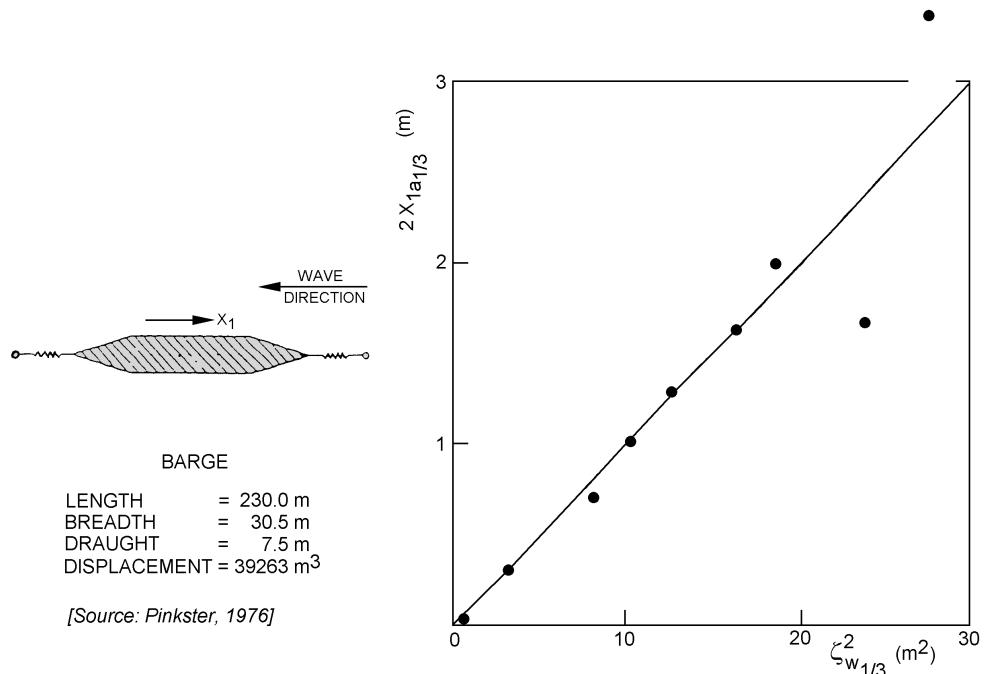
Figure 9.8: Low Frequency Surge Motions of a Barge in Irregular Head Waves
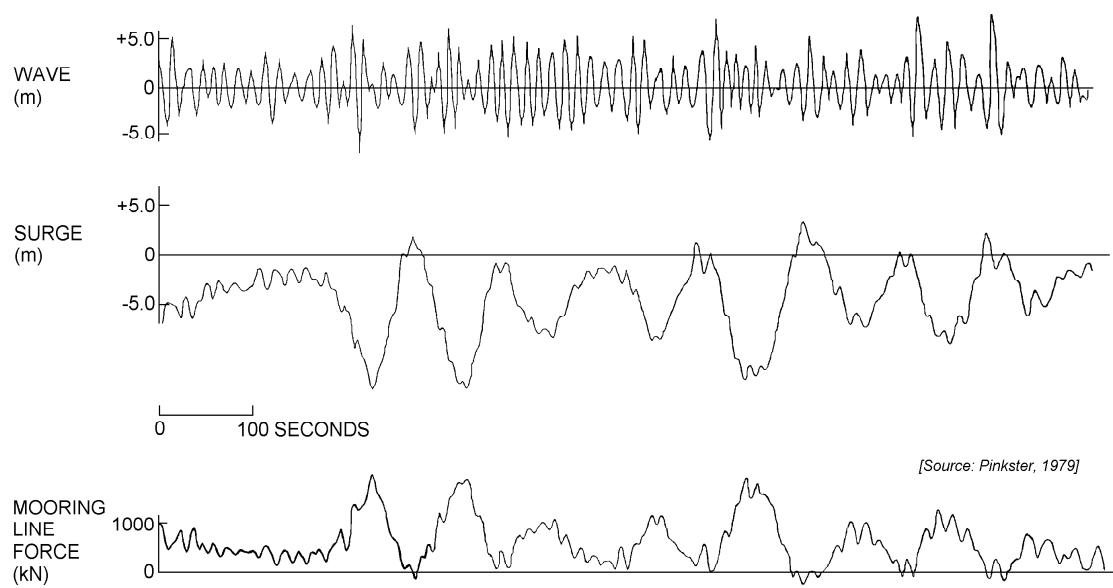
Figure 9.9: Surge Motions and Mooring Line Forces of a SSCV
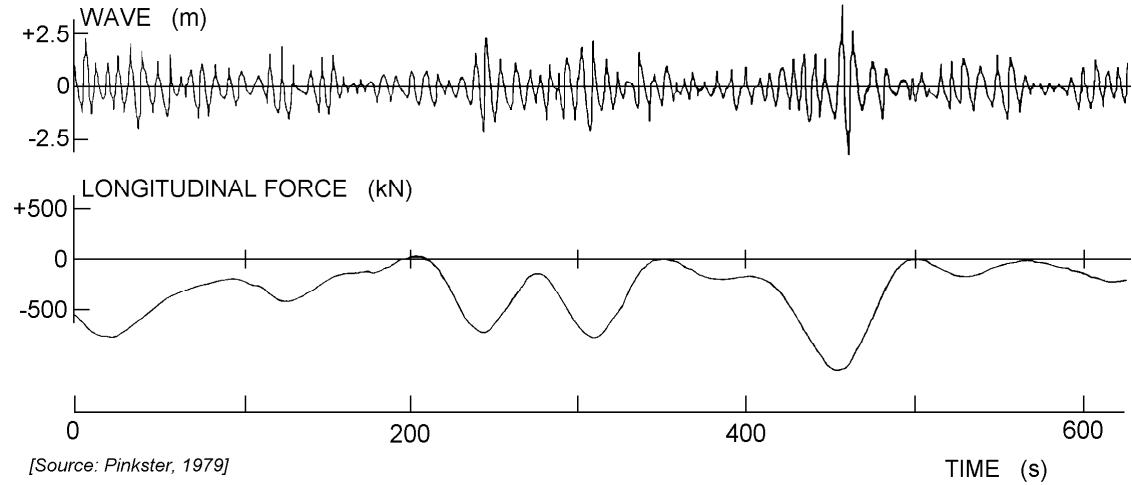
Figure 9.10: Second Order Wave Forces of a Semi-Submersible

Figure 9.11 shows the surge sway and yaw motions of a TLP in irregular waves coming at an angle to the longitudinal axis of the platform. The low frequency components in all three motion components is clear. The corresponding forces in the mooring tethers of the TLP - given in figure 9.12 - are dominated by wave frequency components, however. Although not apparent from this figure, tether forces sometimes contain contributions from sum-frequency second order wave forces which can have frequencies coinciding with the natural frequency of the vertical motion of a TLP. These frequencies can be high due to the high axial stiffness of the tethers.
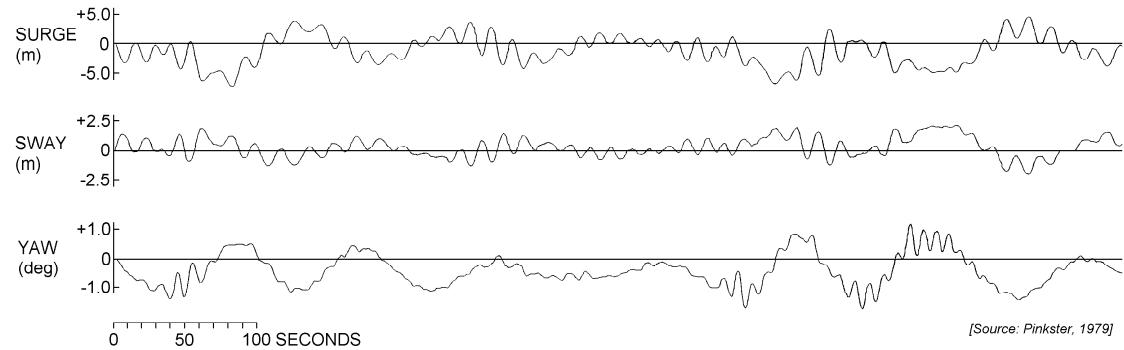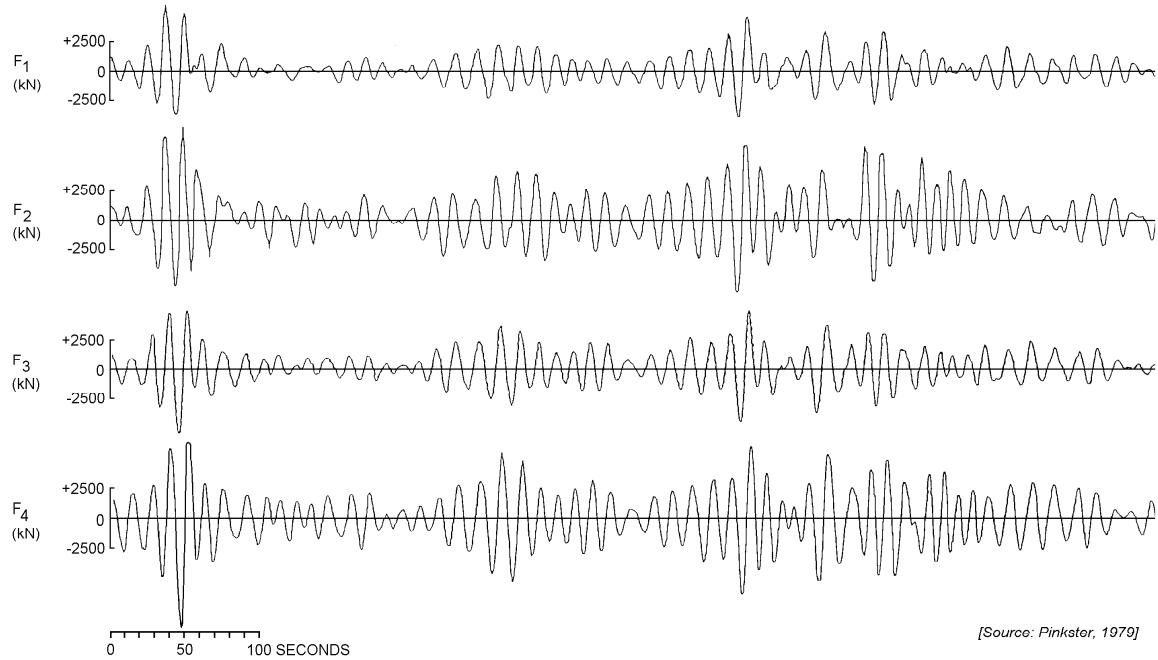
Figure 9.11: Horizontal TLP Motions in Irregular Seas

9.2.5   Vertical Motions of Ships in Long Waves
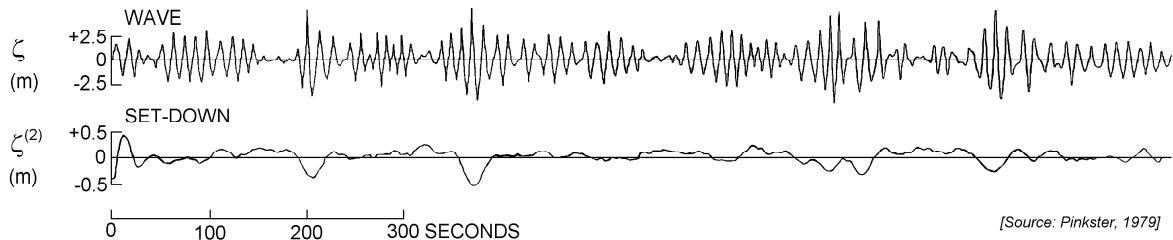
A different non-linear effect in irregular waves is the occurrence of wave set-down. This is the phenomenon whereby the "mean" water level is lower under groups of higher waves and higher under groups of smaller waves. The phenomenon has been extensively analyzed using potential theory. Set-down appears as low-frequency second order term in the power series expansion of the potential and the corresponding wave elevation.

Figure 9.12: TLP Tether Forces in Irregular Seas

An example of the set-down measured in an irregular wave train is shown in figure 9.13. In this case the set-down record has been obtained by low-pass filtering of the measured wave elevation record. Bearing in mind the time scale shown in the figure, it is clear that the set-down wave components can be considered to be equivalent to long waves.

Figure 9.13: Wave and Set-Down Records

When the horizontal dimensions of a floating object are small compared to this wave length the vertical motions of the object follows the wave elevation and slope closely. A sea gull swimming in waves is an extreme example of this. One can conclude from figure 9.14 that this must be true for even relatively large vessels such as a 125,000 m^3 LNG carrier. If the water depth is about 15 meters, then with an "average" long wave period of about 80 seconds, the wave length will be in the order of a kilometer; this is long enough to let the LNG tanker behave like a sea gull.

Figure 9.15 finally, shows the three components contributing to the total vertical motions of the LNG carrier sailing in shallow water. The total vertical displacement consist of a sinkage contribution (a static contribution related to square of the forward speed), a wave
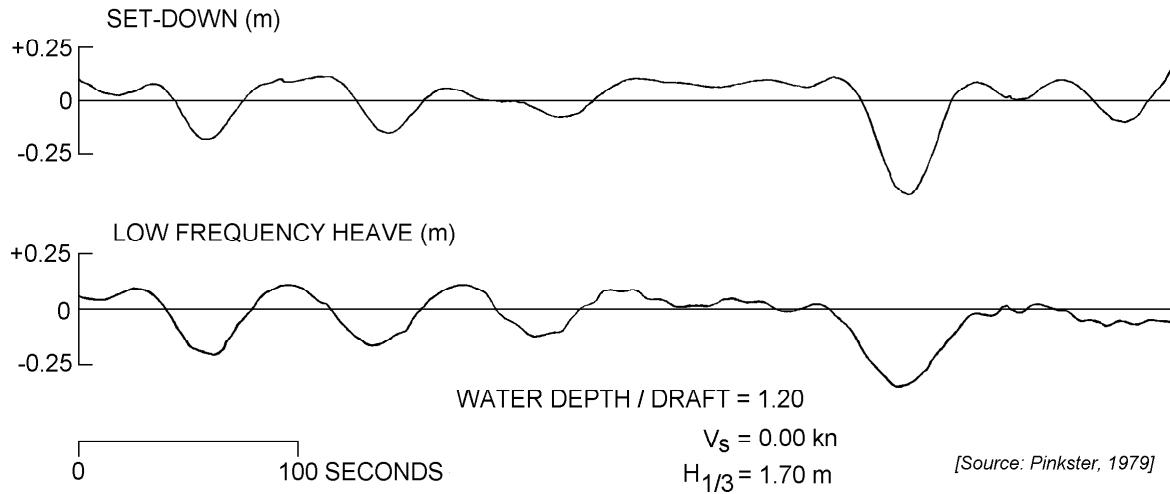
Figure 9.14: Second Order Vertical Motions of an LNG Carrier in Head Seas

frequency contribution (linearly related to the wave elevation) and a **group frequency** contribution (due to the second order wave set-down effect in the incident waves).
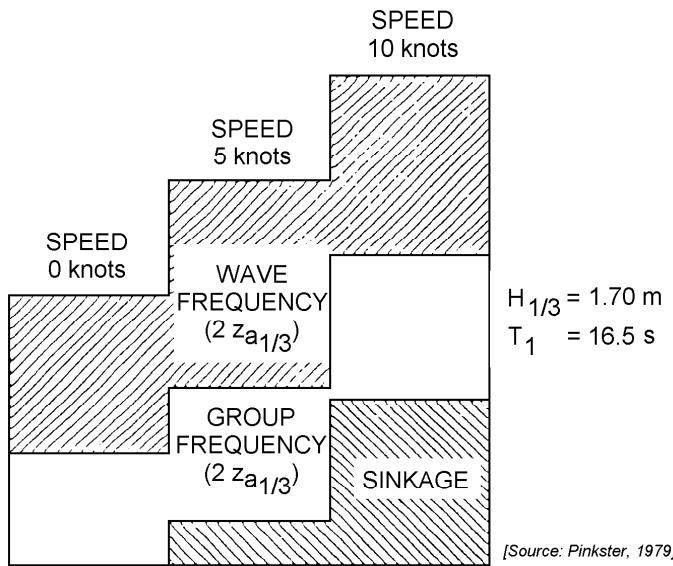
Figure 9.15: Heave Motion Components of an LNG Carrier in Head Waves

9.2.6   Behavior of a Jetty-Moored Tanker

In most harbors, tankers are moored to jetties by means of mooring lines and fenders. A number of these jetties are situated at open locations so that the vessels moored to them are subject to the effects of wind, waves and current. Vessel motions and mooring system forces are the result. Sometimes passing ships induce significant transient mooring loads as well.

Figures 9.16 through 9.20 - with data taken from [Oortmerssen et al., 1984] - give some results of model tests and simulations with a 200 kTDW tanker moored to a jetty in wind and waves.

Figure 9.16 shows the spectral density of the three irregular waves in which the model tests were carried out.

Figure 9.17 shows a record of the horizontal motions and the mooring line and fender forces in beam waves with a relatively short period (spectrum 3) and a steady beam wind of 20 m/s.

Figure 9.18 shows the spectra of the sway motion in beam waves with a long period (spectrum 1) and a steady beam wind of 20 m/s.

Figure 9.19 shows a record of the horizontal motions and the mooring line and fender forces in bow-quartering waves and a steady beam wind of 20 m/s.

Figure 9.20 shows the spectra of the sway motion and the fender forces in beam waves with a relatively short period (spectrum 3) without wind effects.

These results clearly show that the motions and mooring forces show two distinct frequency ranges: components with wave frequencies and components with very low frequencies.

From foregoing discussions it will be clear that low frequency components in the motions and forces are related to the drift force phenomenon. However, in the case of jetty moorings, which have highly nonlinear restoring characteristics (fenders are much stiffer than mooring lines), even monochromatic wave frequency excitation of the vessel can induce motions and mooring forces which contain significant sub- and super-harmonics of the wave frequency. An example is shown in figure 9.21, which has been taken from [Oortmerssen, 1976b]. Note that in this case the excitation side of the equations of motion will be reasonably linear while it is now the left hand side which has a distinctly nonlinear spring term. This is an example of a sub-harmonic excitation. The period of the excitation is now an integer multiple of the excitation frequency as was pointed out in chapter 6.

9.3   Wave Drift Forces and Moments

It is generally acknowledged that the existence of wave drift forces was first reported by [Suyehiro, 1924]. While experimenting with a model rolling in beam seas, he found that the waves exerted a steady horizontal force which he attributed to the reflection of the incoming waves by the model. The importance of the mean and low frequency wave drift forces from the point of view of motion behavior and mooring loads is generally recognized nowadays. It has been mentioned in chapter 6 that work by [Hsu and Blenkarn, 1970] and [Remery and Hermans, 1972] indicated that large amplitude low frequency horizontal motions of moored vessels could be induced by slowly varying wave drift forces in irregular waves. These authors also stressed the importance of knowledge of the mean second order forces in regular waves in this problem. A considerable number of papers have been published since, reflecting increased insight in the phenomena involved.

Initially, the solution to the problem of predicting motions and mooring forces was sought in better quantitative data on the low frequency wave drift forces. Accurate knowledge of these forces, it was felt, would allow accurate estimates to be made of low frequency horizontal motions and mooring forces. Due to the resonant motion response of the moored vessels to the wave drift forces, it is nowadays known that for accurate prediction of low frequency motions in irregular seas attention must also be paid to the hydrodynamic reac-

WAVE SPECTRUM	$H_{1/3}$ (m)	T_1 (s)
1	1.64	16.5
2	1.58	7.5
3	1.98	7.6

[Source: Oortmerssen et.al, 1984]
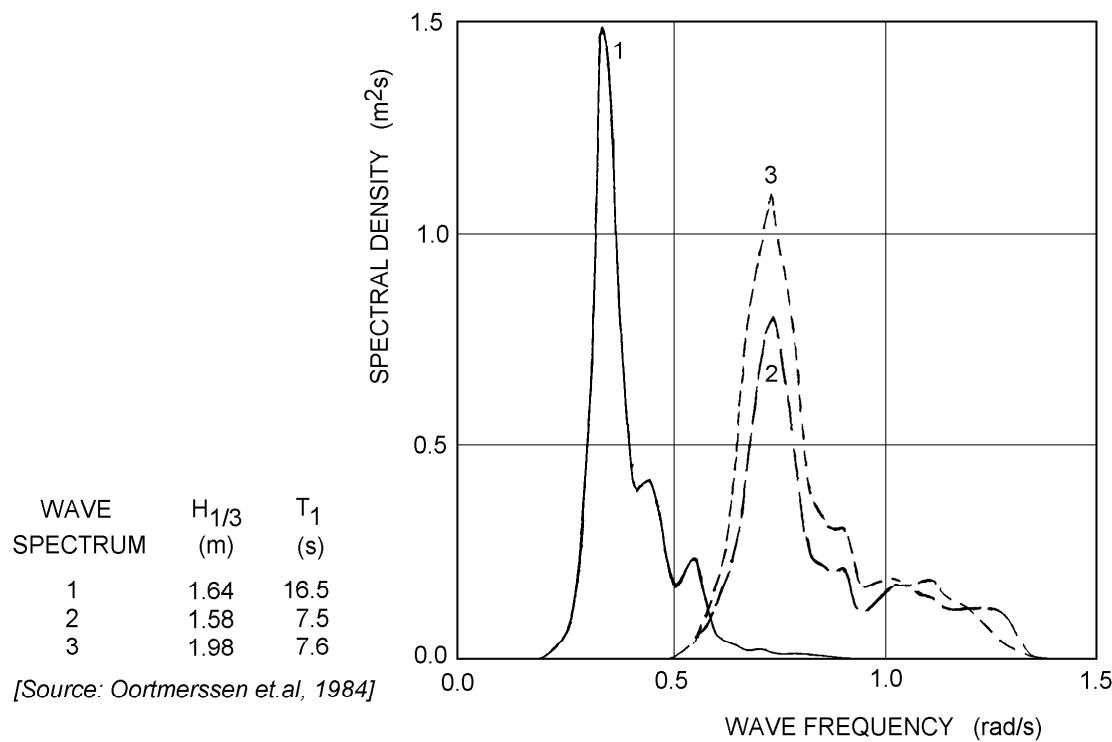
Figure 9.16: Wave Spectra Used for a Jetty Moored Tanker

MODEL TEST
MOORSIM

[Source: Oortmerssen et.al, 1984]
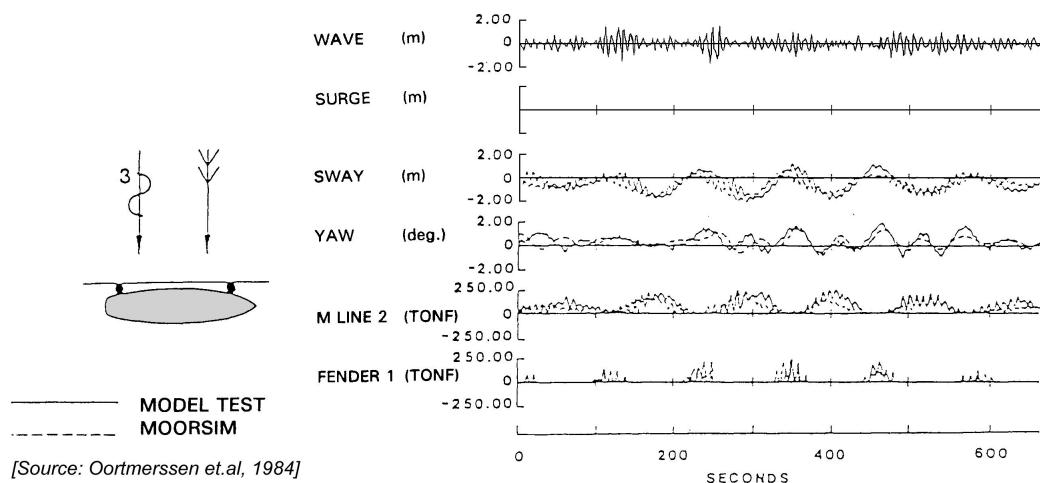
Figure 9.17: Behavior in Beam Waves and Beam Wind
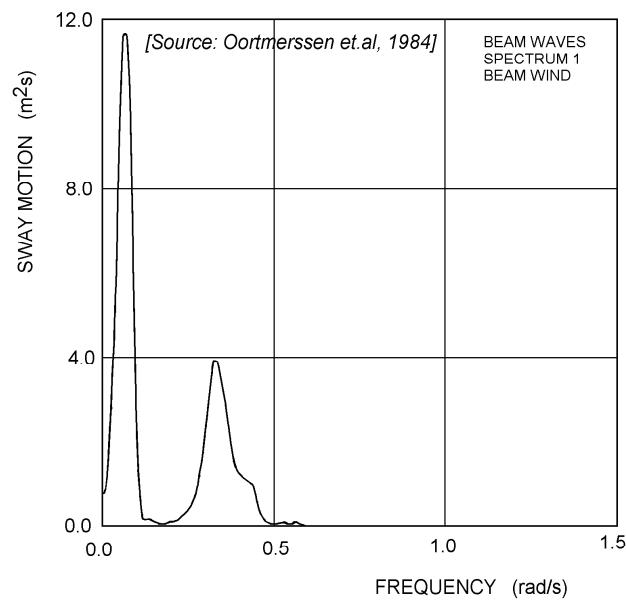
Figure 9.18: Spectra of Sway Motions in Beam Waves and Beam Wind
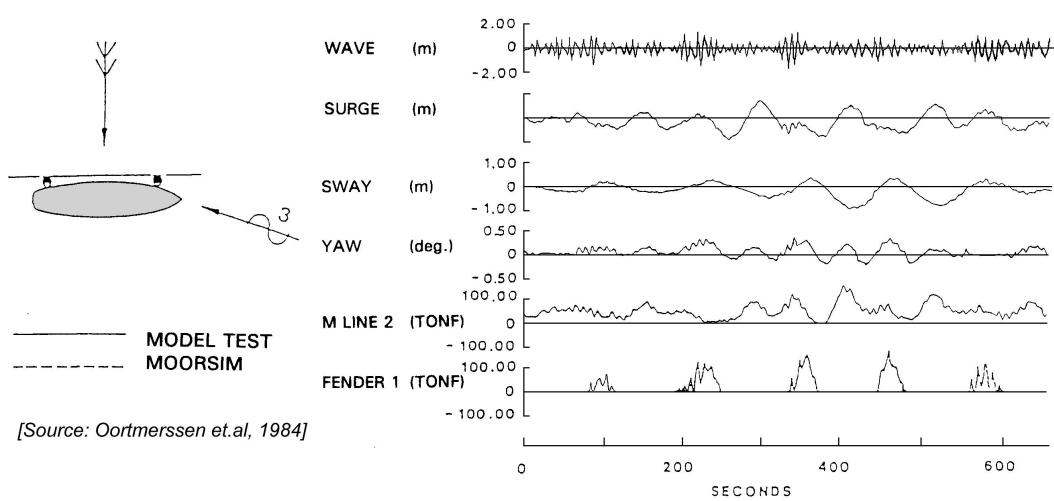
Figure 9.19: Behavior in Bow-Quartering Waves and Beam Wind
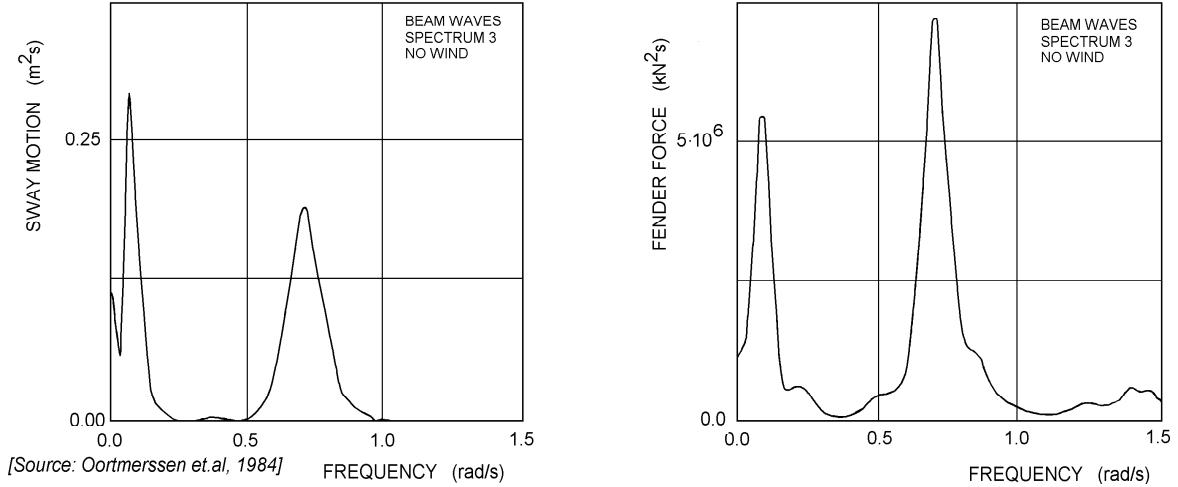
Figure 9.20: Spectra of Sway Motions and Fender Forces in Beam Waves without Wind

tion forces. On the basis of experimental and theoretical results it is generally agreed that, for engineering purposes, the wave drift forces are second order wave forces. This means that the forces are quadratic functions of the height of the incident waves.

[Pinkster, 1976] and [Pinkster, 1977] introduced a computation method based on direct integration of all pressure contributions on the wetted hull of the body. This method is also exact within potential theory.

[Faltinsen and Loken, 1978b] and [Faltinsen and Loken, 1978a] applied a similar method to the two dimensional case of cylinders in beam waves. They succeeded in giving a complete solution which includes the mean wave drift force in regular waves and the low frequency oscillating wave drift force in regular wave groups.

[Pinkster and Hooft, 1978] and [Pinkster, 1979] use a method of direct integration - for three-dimensional cases - the mean and low frequency part of the wave drift forces using an approximation for the force contribution due to the second order non-linear potential.

In general it has been found that for voluminous bodies, such as ships, methods based on potential theory give good results when compared with model test results. Discrepancies occur at wave frequencies near, for instance, roll resonance. In such cases viscous effects - not accounted for by potential theory - become important. For relatively slender objects such as some semi-submersibles, viscous effects may become important at all frequencies; see for instance [Dev, 1996] for the relevant work in this field.

This section deals, almost entirely, with the wave drift exciting forces and moments as determined by [Pinkster, 1980].

9.3.1 Second Order Wave Forces

Expressions for the second order wave force and moment will be deduced in this section based on the **direct integration method** of pressures on the hull. This method is straightforward and gives insight in the mechanism by which waves and the body interact to produce the force. First, the boundary conditions for the various potentials are treated; special attention is given to the boundary conditions at the body.
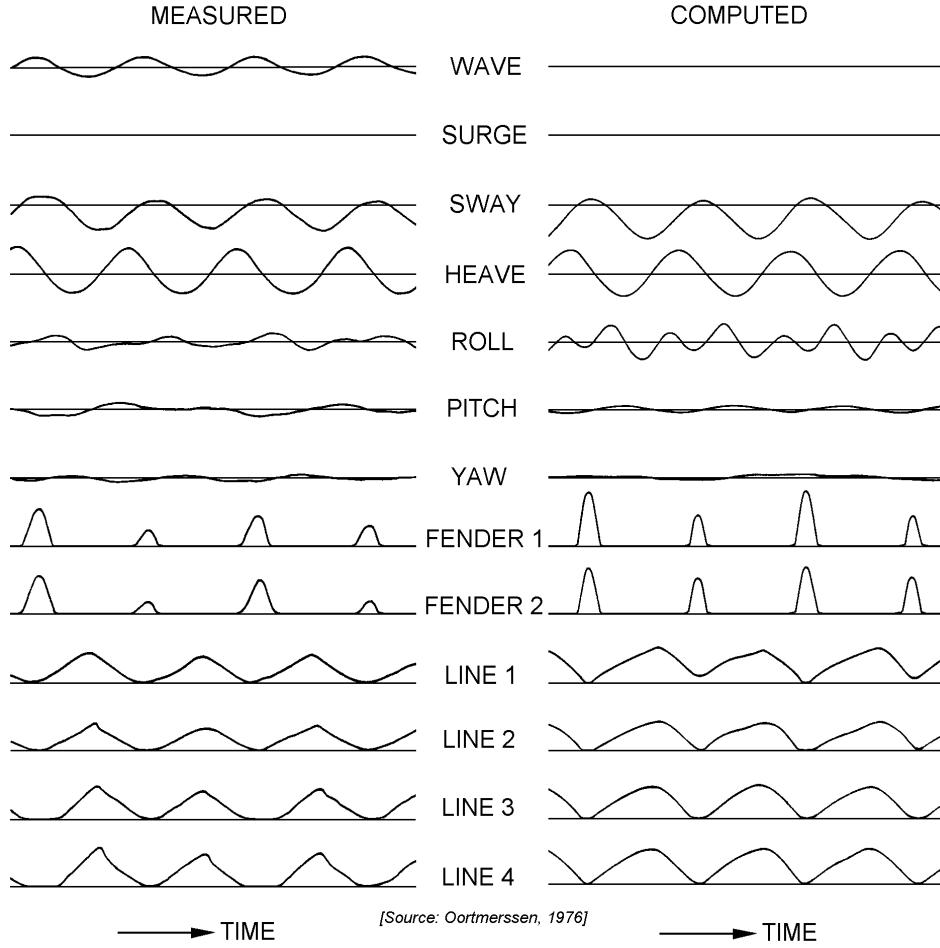
Figure 9.21: Measured and Computed Ship Motions and Mooring Forces

The theory is developed using perturbation methods. This means that all quantities such as wave height, motions, potentials, pressures etc., are assumed to vary only very slightly relative to some initial static value and may all be written in the following form:

$$X = X^{(0)} + \varepsilon X^{(1)} + \varepsilon^2 X^{(2)} \tag{9.1}$$

where $X^{(0)}$ denotes the static value, $X^{(1)}$ indicates the first order oscillatory variation, $X^{(2)}$ the second order variation. The parameter ε is some small number, with $\varepsilon \ll 1$, which denotes the order of oscillation. First order in this case means linearly related to the wave height and second order means that the quantity depends on the square of the wave height. In the following, quantities are of second order if preceded by ε^2. If, as in many cases, the ε^2 is discarded, this is due to the fact that the expression contains only second order quantities. In such instances second order quantities are recognized by the superscript $^{(2)}$ or by the fact that a component is the product of two first order quantities with superscript $^{(1)}$. For instance, the pressure component $-\frac{1}{2}\left(\nabla\Phi^{(1)}\right)^2$ should be recognized as a second order quantity.

The derivation of the second order wave forces and moments is based at first on the assumption that the body is floating in small amplitude waves. It is furthermore assumed that the body is only allowed to move in response to the first order hydrodynamic forces

at frequencies within the wave frequency region. Frequencies outside this region or higher orders of motion are not permitted. This means that expressions obtained for the second order wave forces contain only the wave exciting forces.

Coordinate Systems
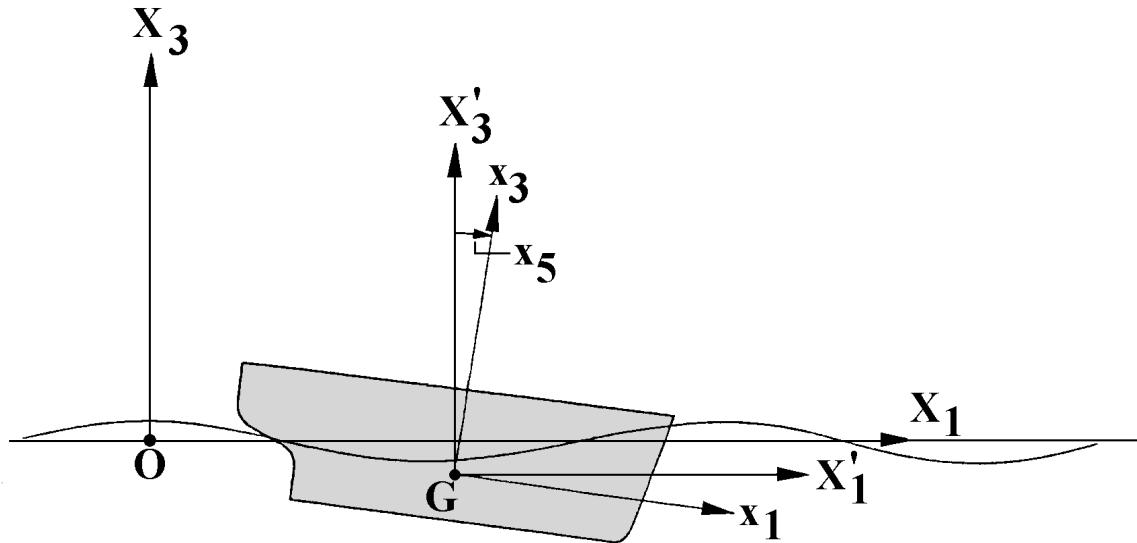
Figure 9.22: System of Coordinate Axes

Use is made here of three systems of coordinate axes (see figure 9.22):

- The first system of coordinate axes O-(X_1, X_2, X_3) is a right-handed **earth-bound axes system** with origin O, the X_1- and X_2-axes in the mean free surface of the sea and the X_3-axis positive upwards.
  A point in space has position or displacement vector $\vec{X} = (X_1, X_2, X_3)$.

- The second system is a right-handed system of G-(x_1, x_2, x_3) **body-bound axes system** with as origin the centre of gravity, G, of the body, the positive x_1- axis in the longitudinal direction (bow) and the positive x_3-axis upwards. In the mean position of the oscillating vessel this axes system is parallel to the earth-bound O-(X_1, X_2, X_3) system.
  The hull surface is uniquely defined in this system of axes. A point on the body surface has position vector $\vec{x} = (x_1, x_2, x_3)$ in the body-bound axes system. The orientation of a surface element in this system of coordinates is defined by the outward pointing normal vector $\vec{n} = (n_1, n_2, n_3)$.

- The third system of coordinates G-(X'_1, X'_2, X'_3) is a **moving axes system** with its origin in the mean position of the center of gravity, G, of the body. Its axes are always **parallel** to the axes of the earth-bound O-(X_1, X_2, X_3) system. So this axes system does not translate or rotate with the ship's motions; it translates only with the forward ship speed which is **not** present here..

The roll, pitch and yaw motions about the body-bound axes of the structure are given by the Eulerian angles x_4, x_5 and x_6, respectively.

First and Second Order Wave Loads

The **first order** wave loads have been defined in the chapter 7. There, the "body-in-waves" has no motions (zero order) in the earth-bound axis system. The waves are approaching a restrained body. Thus, first order fluid motions and resulting first order fluid forces have been considered there.

For the determination of the **second order** wave loads, the "body-in-waves" is carrying out a first order harmonic motion, **forced** by first order wave loads. The waves are approaching a harmonic oscillating body. Then, second order fluid motions and resulting second order fluid forces have to be considered too.

Body Motions

If the body has small amplitude motions resulting from the first order oscillatory wave forces, the resultant displacement vector $\vec{X} = (X_1, X_2, X_3)$ of a point on the body - relative to the earth-bound system of axes - is also a small first order quantity:

$$\vec{X} = \varepsilon \vec{X}^{(1)} \tag{9.2}$$

with:

$$\vec{X}^{(1)} = \vec{X_G}^{(1)} + R^{(1)} \cdot \vec{x} \tag{9.3}$$

where $\vec{X_G}^{(1)}$ is the oscillatory first order motion vector of the center of gravity of the body, $\vec{x} = (x_1, x_2, x_3)$ is the position vector of the point on the body in the body-bound axes system and $R^{(1)}$ is the linearized rotation transformation matrix, defined as:

$$R^{(1)} = \begin{bmatrix} 0 & -x_6^{(1)} & +x_5^{(1)} \\ +x_6^{(1)} & 0 & -x_4^{(1)} \\ -x_5^{(1)} & +x_4^{(1)} & 0 \end{bmatrix} \tag{9.4}$$

in which $x_4^{(1)}$, $x_5^{(1)}$ and $x_6^{(1)}$ are the first order roll, pitch and yaw motions of the structure. Similarly, the velocity $\vec{V}$ of a point on the body relative to the earth-bound system of axes, $O\text{-}(X_1, X_2, X_3)$, is also a first order quantity and follows from:

$$\vec{V} = \varepsilon \vec{V}^{(1)} = \dot{\vec{X}} = \varepsilon \, \dot{\vec{X}}^{(1)} \tag{9.5}$$

with:

$$\dot{\vec{X}}^{(1)} = \vec{V}^{(1)} = \dot{\vec{X}}_G^{(1)} + \dot{R}^{(1)} \cdot \vec{x} \tag{9.6}$$

where:

$$\dot{R}^{(1)} = \begin{bmatrix} 0 & -\dot{x}_6^{(1)} & +\dot{x}_5^{(1)} \\ +\dot{x}_6^{(1)} & 0 & -\dot{x}_4^{(1)} \\ -\dot{x}_5^{(1)} & +\dot{x}_4^{(1)} & 0 \end{bmatrix} \tag{9.7}$$

in which $\dot{x}_4^{(1)}$, $\dot{x}_5^{(1)}$ and $\dot{x}_6^{(1)}$ are the first order roll, pitch and yaw angular velocities of the structure.

Note that $\vec{X}$ and $\vec{V}$ and their derivatives are the (oscillatory) motions of the body; so far they are not the motions of the fluid.

The orientation of surface elements of the body relative to the G-(x_1, x_2, x_3) body-bound axes are denoted by the outward pointing normal vector $\vec{n}$. When the body is carrying out small first order motions, the orientation of a surface element relative to the fixed O-(X_1, X_2, X_3) or G-(X_1', X_2', X_3') system of axes becomes:

$$\vec{N} = \vec{n} + \varepsilon \vec{N}^{(1)} \tag{9.8}$$

with:

$$\vec{N}^{(1)} = R^{(1)} \cdot \vec{n} \tag{9.9}$$

where the linearized rotation transformation matrices, $R^{(1)}$, follows from equation 9.4.

Fluid Motions

The fluid domain is - just as when determining the hydromechanical coefficients in chapter 7 - bounded by: 1) the surface of the body, 2) the free sea surface, 3) the sea bed and 4) a vertical cylinder with an infinite radius. Assuming that the fluid is inviscid, irrotational, homogeneous and incompressible, the fluid motion may be described by means of the velocity potential Φ:

$$\Phi = \varepsilon \Phi^{(1)} + \varepsilon^2 \Phi^{(2)} + ... \tag{9.10}$$

The potentials are defined relative to the earth-bound system of axes, O-(X_1, X_2, X_3).

As has been pointed out in chapter 7, the (linearized) first order potential $\Phi^{(1)}$ consists of the sum of potentials associated with the undisturbed incoming waves, $\Phi_w^{(1)}$, the diffracted waves, $\Phi_d^{(1)}$, and waves due to the first order body motions, $\Phi_b^{(1)}$, respectively; thus:

$$\Phi^{(1)} = \Phi_w^{(1)} + \Phi_d^{(1)} + \Phi_b^{(1)} \tag{9.11}$$

Continuity Condition

Both the first and the second order potentials must satisfy the equation of continuity within the fluid domain; the Laplace equation (see chapter 7) has to be fulfilled by both potentials as well:

$$\nabla^2 \Phi^{(1)} = 0 \qquad \text{and} \qquad \nabla^2 \Phi^{(2)} = 0 \tag{9.12}$$

Sea Bed Boundary Condition

Both potentials must satisfy the boundary condition at the horizontal sea bed, too:

$$\frac{\partial \Phi^{(1)}}{\partial X_3} = 0 \qquad \text{and} \qquad \frac{\partial \Phi^{(2)}}{\partial X_3} = 0 \qquad \text{for: } X_3 = -h \tag{9.13}$$

where h is the water depth in the O-(X_1, X_2, X_3) axis system.

Free Surface Boundary Condition

In order to derive the boundary condition at the mean free surface use has to be made of the Bernoulli equation and the assumption that fluid elements in the free surface remain there at all times (no-leak condition); see chapter 7. A Taylor expansion can be used to transform the boundary conditions at the actual moving free surface ($X_3 = \zeta$) into boundary conditions at the mean free surface ($X_3 = 0$); see also chapter 5.
Then the **homogeneous** boundary condition becomes:

$$g \cdot \frac{\partial \Phi^{(1)}}{\partial X_3} + \frac{\partial^2 \Phi^{(1)}}{\partial t^2} = 0 \qquad (9.14)$$

For the **particular solution** of the boundary condition of $\Phi^{(2)}$, only the final result - which is very complex to solve as will be explained later - is given here:

$$g \cdot \frac{\partial \Phi^{(2)}}{\partial X_3} + \frac{\partial^2 \Phi^{(2)}}{\partial t^2} = -2 \left(\vec{\nabla} \Phi^{(1)} \cdot \vec{\nabla} \frac{\partial \Phi^{(1)}}{\partial t} \right) + \frac{\partial \Phi^{(1)}}{\partial t} \cdot \left(\frac{\partial^2 \Phi^{(1)}}{\partial X_3^2} + \frac{1}{g} \cdot \frac{\partial^2}{\partial t^2} \left(\frac{\partial \Phi^{(1)}}{\partial X_3} \right) \right) \qquad (9.15)$$

This equation will be used further on in this chapter.

Body Boundary Condition

In general the boundary condition on the body is that no fluid passes through the hull (no-leak condition); the relative velocity between the fluid and the hull in the direction of the normal to the hull must be zero; see chapter 7.
This boundary condition has to be satisfied **at the instantaneous position of the hull surface**; thus the fluid motions in the direction of the normal on the body, $\vec{\nabla} \Phi \cdot \vec{N}$, have to be equal to the body motion in this normal direction, $\vec{V} \cdot \vec{N}$:

$$\vec{\nabla} \Phi \cdot \vec{N} = \vec{V} \cdot \vec{N} \qquad (9.16)$$

or taking into account equations 9.5, 9.8 and 9.10:

$$\left(\varepsilon \vec{\nabla} \Phi^{(1)} + \varepsilon^2 \vec{\nabla} \Phi^{(2)} \right) \cdot \left(\vec{n} + \varepsilon \vec{N}^{(1)} \right) = \left(\varepsilon \vec{V}^{(1)} \right) \cdot \left(\vec{n} + \varepsilon \vec{N}^{(1)} \right) \qquad (9.17)$$

Grouping similar powers of ε results in the first and second order body boundary conditions. The boundary conditions for the first order potential, $\varepsilon \Phi^{(1)}$, on the body is as follows:

$$\vec{\nabla} \Phi^{(1)} \cdot \vec{n} = \vec{V}^{(1)} \cdot \vec{n} \qquad (9.18)$$

The boundary condition for the second order potential on the body, $\varepsilon^2 \Phi^{(2)}$, states that:

$$\vec{\nabla} \Phi^{(2)} \cdot \vec{n} = \left(\vec{V}^{(1)} - \vec{\nabla} \Phi^{(1)} \right) \cdot \vec{N}^{(1)} \qquad (9.19)$$

in which the first part, $\vec{V}^{(1)} \cdot \vec{N}^{(1)}$, represents the body motions and the second part, $\vec{\nabla} \Phi^{(1)} \cdot \vec{N}^{(1)}$, the fluid motions.
Equations 9.18 and 9.19 have to be satisfied at the instantaneous position of the surface of the body. Assuming that the motions are small, and applying a Taylor expansion,

similar conditions may be stipulated for the potentials **at the mean position of the hull surface**.

The first order boundary condition then becomes:

$$\vec{\nabla}\Phi^{(1)} \cdot \vec{n} = \vec{V}^{(1)} \cdot \vec{n} \tag{9.20}$$

and the second order boundary condition becomes:

$$\vec{\nabla}\Phi^{(2)} \cdot \vec{n} = -\left(\vec{X}^{(1)} \cdot \vec{\nabla}\right) \cdot \left(\vec{\nabla}\Phi^{(1)} \cdot \vec{n}\right) + \left(\vec{V}^{(1)} - \vec{\nabla}\Phi^{(1)}\right) \cdot \vec{N}^{(1)} \tag{9.21}$$

in which the last term is the difference of the two velocity vectors along the hull surface caused by the first order change of the direction normal.

The potentials and their derivatives in equations 9.20 and 9.21 have to be evaluated at the mean position of the body.

Substitution of equation 9.11 in boundary condition 9.20 - so splitting the potential in three parts - yields the following:

$$\left(\vec{\nabla}\Phi_w^{(1)} + \vec{\nabla}\Phi_d^{(1)} + \vec{\nabla}\Phi_b^{(1)}\right) \cdot \vec{n} = \vec{V}^{(1)} \cdot \vec{n} \tag{9.22}$$

It is customary to decompose this equation into two components:

- Diffraction component:

$$\left(\vec{\nabla}\Phi_w^{(1)} + \vec{\nabla}\Phi_d^{(1)}\right) \cdot \vec{n} \;=\; 0 \qquad \text{(see chapter 7)} \tag{9.23}$$
$$\text{or} \tag{9.24}$$
$$\vec{\nabla}\Phi_d^{(1)} \cdot \vec{n} \;=\; -\vec{\nabla}\Phi_w^{(1)} \cdot \vec{n} \tag{9.25}$$

- Motion component:

$$\vec{\nabla}\Phi_b^{(1)} \cdot \vec{n} = \vec{V}^{(1)} \cdot \vec{n} \tag{9.26}$$

The methods in use to solve for the unknown first order potentials $\Phi_w^{(1)}$, $\Phi_d^{(1)}$ and $\Phi_b^{(1)}$ have already been discussed in chapters 5 and 7.

Substitution of the first order potential $\Phi^{(1)}$ from 9.11 in the non-homogeneous second order free surface boundary condition of equation 9.15 shows that the second order potential includes in the most general form the following components:

$$
\begin{aligned}
\Phi^{(2)} = \quad & \Phi_d^{(2)} \\
& +\Phi_{ww}^{(2)} + \Phi_{dd}^{(2)} + \Phi_{bb}^{(2)} + \Phi_{wd}^{(2)} + \Phi_{wb}^{(2)} + \Phi_{db}^{(2)} + \Phi_{dw}^{(2)} + \Phi_{bw}^{(2)} + \Phi_{bd}^{(2)}
\end{aligned}
\tag{9.27}
$$

The first potential on the right-hand side of equation 9.27, $\Phi_d^{(2)}$, is a potential which satisfies the homogeneous boundary condition:

$$g \cdot \frac{\partial \Phi_d^{(2)}}{\partial X_3} + \frac{\partial^2 \Phi_d^{(2)}}{\partial t^2} = 0 \tag{9.28}$$

and $\Phi_d^{(2)}$ is therefore an "ordinary" potential which satisfies the linearized free surface condition.

The last nine components on the right-hand side of equation 9.27 are potentials which are particular solutions to the type of boundary condition as given in equation 9.18.
For instance for $\Phi_{ww}^{(2)}$:

$$ g \cdot \frac{\partial \Phi_{ww}^{(2)}}{\partial X_3} + \frac{\partial^2 \Phi_{ww}^{(2)}}{\partial t^2} = -2 \left(\vec{\nabla} \Phi_w^{(1)} \cdot \vec{\nabla} \frac{\partial \Phi_w^{(1)}}{\partial t} \right) + \frac{\partial \Phi_w^{(1)}}{\partial t} \left(\frac{\partial^2 \Phi_w^{(1)}}{\partial X_3^2} + \frac{1}{g} \cdot \frac{\partial^2}{\partial t^2} \left(\frac{\partial \Phi_w^{(1)}}{\partial X_3} \right) \right) \quad (9.29) $$

Equation 9.27 can be written simplified by letting $\Phi_w^{(2)}$ represent the sum of the last nine components on the right-hand side of the equation, so that:

$$ \Phi^{(2)} = \Phi_d^{(2)} + \Phi_w^{(2)} \tag{9.30} $$

This $\Phi_w^{(2)}$ may be regarded as the second order equivalent of the first order undisturbed incoming wave potential $\Phi_w^{(1)}$.
Substitution of equation 9.30 in the second order boundary condition 9.21 yields:

$$ \left(\vec{\nabla} \Phi_w^{(2)} + \vec{\nabla} \Phi_d^{(2)} \right) \cdot \vec{n} = \quad - \left(\vec{X}^{(1)} \cdot \vec{\nabla} \right) \cdot \vec{\nabla} \Phi^{(1)} \cdot \vec{n} \quad + \left(\vec{V}^{(1)} - \vec{\nabla} \Phi^{(1)} \right) \cdot \vec{N}^{(1)} \tag{9.31} $$

or for the diffraction potential:

$$ \vec{\nabla} \Phi_d^{(2)} \cdot \vec{n} = \quad -\vec{\nabla} \Phi_w^{(2)} \cdot \vec{n} \quad - \left(\vec{X}^{(1)} \cdot \vec{\nabla} \right) \cdot \vec{\nabla} \Phi^{(1)} \cdot \vec{n} \quad + \left(\vec{V}^{(1)} - \vec{\nabla} \Phi^{(1)} \right) \cdot \vec{N}^{(1)} \tag{9.32} $$

If the right-hand side of this equation is known, $\Phi_d^{(2)}$ can be solved for the entire structure using numerical methods.

In general, however, $\Phi_w^{(2)}$ in equation 9.32 presents **a problem due to the complexity** of the surface boundary condition expressed by equation 9.15.
[Faltinsen and Loken, 1978a] have found exact solutions of this problem for two-dimensional cases, applicable to vessels in beam seas. [Newman, 1993] has developed numerical methods to solve for the second order potential for the three-dimensional case. [Pinkster, 1980] suggest an approximation for $\Phi_d^{(2)}$ which is applicable to three-dimensional problems.
In a later section of this chapter it will be shown that the second order potential $\Phi_d^{(2)}$ accounts only for a part of the second order wave forces.

Boundary Conditions at Infinity

A radiation condition for the potentials $\Phi_w^{(1)}$, $\Phi_b^{(1)}$ and $\Phi_d^{(2)}$ - which states that at a great distance from the body the waves associated with these potentials move outwards - must be satisfied. This restriction imposes a uniqueness which would not otherwise be present. Since the components of $\Phi_w^{(2)}$ are particular solutions to the free surface boundary condition 9.15 - which is defined over the complete free surface - a radiation condition need not be imposed on this term.

Symmetry Condition

The symmetry conditions, as discussed in chapter 5 and 7, are not taken into account here. The structure can have any arbitrary under water form.

Pressure at a Point within the Fluid

If the velocity potential Φ is known, the fluid pressure at a point is determined using the (non-linear) Bernoulli equation (see chapter 5):

$$p = -\rho g X_3 - \rho \frac{\partial \Phi}{\partial t} - \frac{1}{2}\rho \left(\vec{\nabla}\Phi\right)^2 \tag{9.33}$$

Assuming that this point is carrying out small - first order - wave frequency motions, $\vec{X}^{(1)}$, about a mean position, $\vec{X}^{(0)}$, and applying a Taylor expansion to the pressure in its mean position, yields:

$$p = p^{(0)} + \varepsilon p^{(1)} + \varepsilon^2 p^{(2)} \tag{9.34}$$

where:

- Hydrostatic pressure:
$$p^{(0)} = -\rho g X_3^{(0)} \tag{9.35}$$

- First order pressure:
$$p^{(1)} = -\rho g X_3^{(1)} - \rho \frac{\partial \Phi^{(1)}}{\partial t} \tag{9.36}$$

- Second order pressure:
$$p^{(2)} = -\frac{1}{2}\rho \left(\vec{\nabla}\Phi^{(1)}\right)^2 - \rho \frac{\partial^2 \Phi^{(2)}}{\partial t^2} - \rho \left(\vec{X}^{(1)} \cdot \vec{\nabla}\frac{\partial \Phi^{(1)}}{\partial t}\right) \tag{9.37}$$

The derivatives of the potentials in the above equations have to be evaluated at the mean position of the point.
It has been assumed that the point is moving within the fluid domain. The same expression can be used to determine the pressure on a point on the hull of the body. This means that derivatives of the potentials are taken at the mean position of the hull. This position is actually alternately within and outside the actual fluid domain. This appears to be permissible if the potential functions are sufficiently "smooth" at the boundaries; see [Joseph, 1973]. This is assumed to be satisfied in this case.

Direct Pressure Integration

Since in general one is concerned with the slow wave drift force induced motions of bodies in the horizontal plane, the wave drift force should be determined in the $G\text{-}(x, y, z)$ coordinate system.
The fluid force exerted on the body, relative to the $G\text{-}(x, y, z)$ system of axes - which is the system with axes parallel to the axes of the earth-bound system, $O\text{-}(X_1, X_2, X_3)$ - follows from:

$$\vec{F} = - \iint\limits_{S} p \cdot \vec{N} \cdot dS \qquad (9.38)$$

where S is the instantaneous wetted surface and $\vec{N}$ is the instantaneous normal vector to the surface element dS relative to the $G(x, y, z)$ system of axes. The normal vector, $\vec{N}$, is given by equation 9.8 and the pressure, p, by equation 9.34.

The **instantaneous wetted surface**, S, is split into two parts: **a constant part**, S_0, up to the static hull waterline and **an oscillating part**, s, the splash zone between the static hull waterline and the wave profile along the body; see figure 9.23.
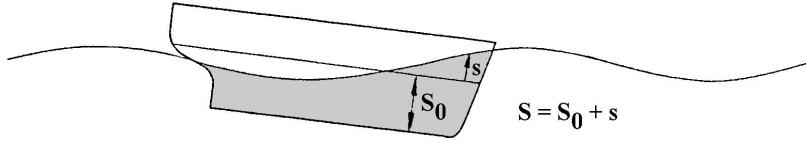
Figure 9.23: Wetted Surface

Substitution of all this in 9.38 yields for the fluid force exerted on the body:

$$
\begin{aligned}
\vec{F} = \ & - \iint\limits_{S_0} \left(p^{(0)} + \varepsilon p^{(1)} + \varepsilon^2 p^{(2)} \right) \cdot \left(\vec{n} + \varepsilon \vec{N}^{(1)} \right) \cdot dS \\
& - \iint\limits_{s} \left(p^{(0)} + \varepsilon p^{(1)} + \varepsilon^2 p^{(2)} \right) \cdot \left(\vec{n} + \varepsilon \vec{N}^{(1)} \right) \cdot dS \qquad (9.39)
\end{aligned}
$$

which can be written as follows:

$$\vec{F} = \vec{F}^{(0)} + \varepsilon \vec{F}^{(1)} + \varepsilon^2 \vec{F}^{(2)} + O(\varepsilon^3) \qquad (9.40)$$

with:

$$
\begin{aligned}
\vec{F}^{(0)} = \ & - \iint\limits_{S_0} \left(p^{(0)} \cdot \vec{n} \right) \cdot dS \qquad (9.41) \\
\varepsilon \vec{F}^{(1)} = \ & - \iint\limits_{S_0} \left(p^{(0)} \cdot \varepsilon \vec{N}^{(1)} \right) \cdot dS - \iint\limits_{S_0} \left(\varepsilon p^{(1)} \cdot \vec{n} \right) \cdot dS \\
& - \iint\limits_{s} \left(p^{(0)} \cdot \vec{n} \right) \cdot dS \qquad (9.42) \\
\varepsilon^2 \vec{F}^{(2)} = \ & - \iint\limits_{S_0} \left(\varepsilon p^{(1)} \cdot \varepsilon \vec{N}^{(1)} \right) \cdot dS - \iint\limits_{S_0} \left(\varepsilon^2 p^{(2)} \cdot \vec{n} \right) \cdot dS \\
& - \iint\limits_{s} \left(p^{(0)} \cdot \varepsilon \vec{N}^{(1)} \right) \cdot dS - \iint\limits_{s} \left(\varepsilon p^{(1)} \cdot \vec{n} \right) \cdot dS \qquad (9.43)
\end{aligned}
$$

Thus the fluid force is split here into three parts:
  - a hydrostatic fluid force, $\vec{F}^{(0)}$,
  - a first order oscillatory fluid force, $\vec{F}^{(1)}$,

- a second order fluid force, $\vec{F}^{(2)}$.

The **hydrostatic fluid force**, $\vec{F}^{(0)}$, follows from integration of the hydrostatic pressure, $p^{(0)}$, over the mean wetted surface, S_0, as given in equation 9.41:

$$
\begin{aligned}
\vec{F}^{(0)} &= -\iint_{S_0} \left(p^{(0)} \cdot \vec{n}\right) \cdot dS \\
&= \rho g \iint_{S_0} \left(X_3^{(0)} \cdot \vec{n}\right) \cdot dS \\
&= (0, 0, \rho g \nabla)
\end{aligned}
\tag{9.44}
$$

which yields only a vertical force contribution, $F_3^{(0)}$, (no horizontal components):

$$
\begin{aligned}
F_3^{(0)} &= \rho g \iint_{S_0} (X_3 \cdot n_3) \cdot dS \\
&= \rho g \nabla
\end{aligned}
\tag{9.45}
$$

in which ∇ is here the volume of displacement.

The **first order oscillatory fluid force**, $\vec{F}^{(1)}$, follows from equation 9.42:

$$
\begin{aligned}
\vec{F}^{(1)} &= -\iint_{S_0} \left(p^{(0)} \cdot \vec{N}^{(1)}\right) \cdot dS - \iint_{S_0} \left(p^{(1)} \cdot \vec{n}\right) \cdot dS \\
&\quad - \iint_{s} \left(p^{(0)} \cdot \vec{n}\right) \cdot dS
\end{aligned}
\tag{9.46}
$$

which includes three integral terms:

1. Products of the hydrostatic pressures, $p^{(0)}$, and the first order oscillatory components of the normal vector, $\vec{N}^{(1)}$, which give first order force contributions over the constant part, S_0, of the wetted surface:

$$
\begin{aligned}
\vec{F}_A^{(1)} &= -\iint_{S_0} \left(p^{(0)} \cdot \vec{N}^{(1)}\right) \cdot dS \\
&= \rho g \iint_{S_0} \left(X_3^{(0)} \cdot \vec{N}^{(1)}\right) \cdot dS
\end{aligned}
\tag{9.47}
$$

which is - after using equation 9.9 (linear rotation-transformation) - equal to:

$$
\begin{aligned}
\vec{F}_A^{(1)} &= \rho g \iint_{S_0} \left(X_3^{(0)} \cdot \{R^{(1)} \cdot \vec{n}\}\right) \cdot dS \\
&= R^{(1)} \cdot (0, 0, \rho g \nabla)
\end{aligned}
\tag{9.48}
$$

This force component is caused by the rotating body axes; roll and pitch motions result in horizontal forces.

2. Products of the first order pressures, $p^{(1)}$, and the normal vector, $\vec{n}$, which give also first order force contributions over the constant part, S_0, of the wetted surface:

$$
\vec{F}_B^{(1)} = -\iint_{S_0} \left(p^{(1)} \cdot \vec{n}\right) \cdot dS
\tag{9.49}
$$

3. Products of the hydrostatic pressures, $p^{(0)}$, and the normal vector, $\vec{n}$, which give (in principle) first order force contributions because of its integration over the oscillatory part, s, of the wetted surface.

$$\vec{F}_C^{(1)} = -\iint_s \left(p^{(0)} \cdot \vec{n} \right) \cdot dS = 0 \tag{9.50}$$

This term is zero because the hydrostatic pressure at the oscillating surface, $p^{(0)}$, is zero because it has to be determined at $X_3 = 0$.

Thus, the total first order fluid force follows from adding equations 9.48, 9.49 and 9.50:

$$\vec{F}^{(1)} = R^{(1)} \cdot (0, 0, \rho g \nabla) - \iint_{S_0} \left(p^{(1)} \cdot \vec{n} \right) \cdot dS \tag{9.51}$$

The **second order fluid force**, $\vec{F}^{(2)}$, follows from equation 9.43:

$$
\begin{aligned}
\vec{F}^{(2)} &= -\iint_{S_0} \left(p^{(1)} \cdot \vec{N}^{(1)} \right) \cdot dS - \iint_{S_0} \left(p^{(2)} \cdot \vec{n} \right) \cdot dS \\
&\quad - \iint_s \left(p^{(0)} \cdot \vec{N}^{(1)} \right) \cdot dS - \iint_s \left(p^{(1)} \cdot \vec{n} \right) \cdot dS
\end{aligned} \tag{9.52}
$$

which includes four integral terms:

1. Products of the first order pressures, $p^{(1)}$, and the first order oscillatory components of the normal vector, $\vec{N}^{(1)}$, give second order force contributions over the constant part, S_0, of the wetted surface:

$$\vec{F}_A^{(2)} = -\iint_{S_0} \left(p^{(1)} \cdot \vec{N}^{(1)} \right) \cdot dS \tag{9.53}$$

When using equation 9.9 for $\vec{N}^{(1)}$ and equation 9.51 for the first order fluid force, one can write:

$$
\begin{aligned}
\vec{F}_A^{(2)} &= -R^{(1)} \cdot \iint_{S_0} \left(p^{(1)} \cdot \vec{n} \right) \cdot dS \\
&= R^{(1)} \cdot \left\{ \vec{F}^{(1)} - R^{(1)} \cdot (0, 0, \rho g \nabla) \right\} \\
&= R^{(1)} \cdot \left\{ \vec{F}^{(1)} - R^{(1)} \cdot (0, 0, mg) \right\}
\end{aligned} \tag{9.54}
$$

Equation 9.54 shows that a second order force along the earth-bound axes follows from the rotation of the first order fluid force and the gravitational force acting on the body; both relative to the body axes system. The last term deliver horizontal forces caused by the roll and pitch motions.

According to Newton's law, one may state that:

$$\vec{F}^{(1)} - R^{(1)} \cdot (0, 0, \rho g \nabla) = m \cdot \ddot{\vec{X}}_G^{(1)} \tag{9.55}$$

from which it follows that:

$$\vec{F}_A^{(2)} = R^{(1)} \cdot \left\{ \vec{F}^{(1)} + R^{(1)} \cdot (0, 0, \rho g \nabla) \right\}$$
$$= m \cdot R^{(1)} \cdot \overset{\rightarrow (1)}{\ddot{X}_G} \tag{9.56}$$

2. Products of the second order pressures, $p^{(2)}$, and the normal vector, $\vec{n}$, also give second order force contributions over the constant part, S_0, of the wetted surface:

$$\vec{F}_B^{(2)} = -\iint_{S_0} \left(p^{(2)} \cdot \vec{n} \right) \cdot dS \tag{9.57}$$

This part, $\vec{F}_B^{(2)}$, involves a straightforward integration of the second order pressure $p^{(2)}$ as given in equation 9.37 over the constant part, S_0, of the wetted surface of the body:

$$\vec{F}_B^{(2)} = \iint_{S_0} \left\{ \frac{1}{2} \rho \left(\vec{\nabla} \Phi^{(1)} \right)^2 + \rho \frac{\partial \Phi^{(2)}}{\partial t} + \rho \vec{X}^{(1)} \cdot \vec{\nabla} \frac{\partial \Phi^{(1)}}{\partial t} \right\} \cdot \vec{n} \cdot dS \tag{9.58}$$

3. Products of the hydrostatic pressures, $p^{(0)}$, and the first order oscillatory components of the normal vector, $\vec{N}^{(1)}$, give (in principle) second order force contributions because of its integration over the oscillatory part, s, of the wetted surface.

$$\vec{F}_C^{(2)} = -\iint_s \left(p^{(0)} \cdot \vec{N}^{(1)} \right) \cdot dS \tag{9.59}$$

Using equation 9.9 yields:

$$\vec{F}_C^{(2)} = -R^{(1)} \cdot \iint_s \left(p^{(0)} \cdot \vec{n} \right) \cdot dS = 0 \tag{9.60}$$

This term is zero because the hydrostatic pressure at the oscillating surface, $p^{(0)}$, is zero because it has to be determined at $X_3 = 0$.

4. Products of the first order pressures, $p^{(1)}$, and the normal vector, $\vec{n}$, give second order force contributions because of its integration over the oscillatory part, s, of the wetted surface.

$$\vec{F}_D^{(2)} = -\iint_s \left(p^{(1)} \cdot \vec{n} \right) \cdot dS \tag{9.61}$$

This part, $\vec{F}_D^{(2)}$, with an integration over the oscillating part, s, of the wetted surface, is found by substituting the expression for the first order pressure $p^{(1)}$ as given in equation 9.36 in here and writing the surface element dS as:

$$dS = dX_3 \cdot dl \tag{9.62}$$

in which dl is a differential length along the water line.
Also taking into account that the dynamic part of the pressure in the fluid at the waterline is:

$$-\rho \frac{\partial \Phi^{(1)}}{\partial t} = \rho g \zeta^{(1)} \tag{9.63}$$

this integral for $\vec{F}_D^{(2)}$ becomes:

$$\vec{F}_D^{(2)} = -\int\limits_{wl} \int\limits_{X_{3wl}^{(1)}}^{\zeta^{(1)}} \rho g \left(-X_3 + \zeta^{(1)}\right) \vec{n} \cdot dX_3 \cdot dl \tag{9.64}$$

The relative wave height, $\zeta_r^{(1)}$, is defined by a superposition of the first order wave elevation, $\zeta^{(1)}$, and the first order vertical motion of the hull at the water line, $X_{3wl}^{(1)}$:

$$\zeta_r^{(1)} = \zeta^{(1)} - X_{3wl}^{(1)} \tag{9.65}$$

This results in:

$$\vec{F}_D^{(2)} = -\oint\limits_{wl} \frac{1}{2} \rho g \left(\zeta_r^{(1)}\right)^2 \cdot \vec{n} \cdot dl \tag{9.66}$$

Finally, the **total second order fluid force** is found from the separate contributions in equations 9.56, 9.58, 9.60 and 9.66:

$$
\begin{aligned}
\vec{F}^{(2)} &= \vec{F}_A^{(2)} + \vec{F}_B^{(2)} + \vec{F}_D^{(2)} \qquad \left(\text{Remember: } \vec{F}_C^{(2)} = 0\right) \\[1ex]
&= m \cdot R^{(1)} \cdot \ddot{\vec{X}}_G^{(1)} \\
&\quad + \iint\limits_{S_0} \left\{ \frac{1}{2}\rho \left(\vec{\nabla}\Phi^{(1)}\right)^2 + \rho \frac{\partial\Phi^{(2)}}{\partial t} + \rho \vec{X}^{(1)} \cdot \vec{\nabla}\frac{\partial\Phi^{(1)}}{\partial t} \right\} \cdot \vec{n} \cdot dS \\
&\quad - \oint\limits_{wl} \frac{1}{2}\rho g \left(\zeta_r^{(1)}\right)^2 \cdot \vec{n} \cdot dl
\end{aligned}
\tag{9.67}
$$

Notice that the added resistance of a ship in waves (also a second order phenomenon), as obtained by [Boese, 1970] in chapter 8, consists of two of these second order contributions:

$$R_{aw} = \vec{F}_A^{(2)} + \vec{F}_D^{(2)} \qquad \text{according to [Boese, 1970]} \tag{9.68}$$

Both of these contributions are related to products of two first order terms, as used in the linear theory in chapter 8. Of course, the contribution of $\vec{F}_B^{(2)}$ is missing in the linear theory there; this term includes the second order pressures.

9.3.2 Second Order Wave Moments

The moment of the fluid forces about the axes of the $G(X_1', X_2', X_3')$ system of coordinates follows from:

$$\vec{M} = -\iint\limits_{S} p \cdot \left(\vec{X}' \times \vec{N}\right) \cdot dS \tag{9.69}$$

The derivation is analogous to that followed for the force and the final expression for the second order wave moment is:

$$
\begin{aligned}
\vec{M}^{(2)} \;=\;& I \cdot R^{(1)} \cdot \ddot{\vec{X}}_G^{(1)} \\[2mm]
& + \iint_{S_0} \left\{ \frac{1}{2}\rho \left(\vec{\nabla}\Phi^{(1)} \right)^2 + \rho\frac{\partial \Phi^{(2)}}{\partial t} + \rho \cdot \vec{X}^{(1)} \cdot \vec{\nabla}\frac{\partial \Phi^{(1)}}{\partial t} \right\} \cdot (\vec{x} \times \vec{n}) \cdot dS \\[2mm]
& - \oint_{wl} \frac{1}{2}\rho g \left(\zeta_r^{(1)} \right)^2 \cdot (\vec{x} \times \vec{n}) \cdot dl
\end{aligned}
\tag{9.70}
$$

in which I is the mass moment of inertia about the considered body axis of the structure.

9.3.3   Quadratic Transfer Functions

In this section it will be shown that equations 9.67 and 9.70 which are, in waves, functions of time, may be used to compute quadratic transfer functions for the mean and low frequency force and moment components. These in turn will allow determination of the wave drift forces and moments in the frequency domain, and after taking double Fourier transforms, allow prediction of the forces in the time domain, see [Dalzell, 1976] and [Kim and Breslin, 1976].

The procedure to obtain the quadratic transfer functions of the forces will first be **illustrated** by taking the low frequency part of the longitudinal component of the last part of equation 9.67 which refers to the force contribution due to the relative wave height:

$$
F_1^{(2)} = F_1^{(2)}(t) = - \oint_{wl} \frac{1}{2}\rho g \left(\zeta_r^{(1)}(t,l) \right)^2 \cdot n_1 \cdot dl
\tag{9.71}
$$

In irregular long-crested waves, the elevation - to first order of the incoming, undisturbed waves - referred to the mean position of the centre of gravity of the floating body may be written as:

$$
\zeta^{(1)}(t) = \sum_{i=1}^{N} \zeta_i^{(1)} \cdot \cos\left(\omega_i t + \tilde{\varepsilon}_i \right)
\tag{9.72}
$$

The first order relative wave height at a point l on the waterline of the body may be written as follows:

$$
\zeta_r^{(1)}(t,l) = \sum_{i=1}^{N} \zeta_i^{(1)} \cdot \zeta_{r_i}^{(1)\prime}(l) \cdot \cos(\omega_i t + \tilde{\varepsilon}_i + \varepsilon_{r_i}(l))
\tag{9.73}
$$

Substitution of 9.73 in equation 9.71 leads to:

$$
\begin{aligned}
F_1^{(2)}(t) \;=\;& \sum_{i=1}^{N}\sum_{j=1}^{N} \zeta_i^{(1)}\zeta_j^{(1)} P_{ij} \cdot \cos\left\{ (\omega_i - \omega_j)t + (\tilde{\varepsilon}_i - \tilde{\varepsilon}_j) \right\} \\[2mm]
& + \sum_{i=1}^{N}\sum_{j=1}^{N} \zeta_i^{(1)}\zeta_j^{(1)} Q_{ij} \cdot \sin\left\{ (\omega_i - \omega_j)t + (\tilde{\varepsilon}_i - \tilde{\varepsilon}_j) \right\}
\end{aligned}
\tag{9.74}
$$

The high frequency terms (sum frequency terms) have been disregarded in this equation. In equation 9.74 P_{ij} and Q_{ij} are the components of the time independent quadratic transfer function with:

$$P_{ij} = \oint_{wl} \frac{1}{4} \rho g \zeta_{r_i}^{(1)'}(l) \cdot \zeta_{r_j}^{(1)'}(l) \cdot \cos\left\{\varepsilon_{r_i}(l) - \varepsilon_{r_j}(l)\right\} \cdot n_1 \cdot dl \tag{9.75}$$

$$Q_{ij} = \oint_{wl} \frac{1}{4} \rho g \zeta_{r_i}^{(1)'}(l) \cdot \zeta_{r_j}^{(1)'}(l) \cdot \sin\left\{\varepsilon_{r_i}(l) - \varepsilon_{r_j}(l)\right\} \cdot n_1 \cdot dl \tag{9.76}$$

Taking now the low frequency part of the square of the wave elevation given by equation 9.72 results in:

$$\left(\zeta_{LF}^{(1)}(t)\right)^2 = \sum_{i=1}^{N} \sum_{j=1}^{N} \frac{1}{2} \zeta_i^{(1)} \zeta_j^{(1)} \cdot \cos\left\{(\omega_i - \omega_j)t + (\tilde{\varepsilon}_i - \tilde{\varepsilon}_j)\right\} \tag{9.77}$$

Comparison with equation 9.74 shows that P_{ij} and Q_{ij} are transfer functions which give that part of the wave drift force which is in-phase and out-of-phase respectively with the low frequency part of the square of the incident waves.

It will be clear that similar developments can be made for other contributions to the wave drift forces which are dependent on products of first order quantities.

Approximation for Second Order Potential Contribution

As mentioned in a previous section, the contribution to the drift forces due to the second order potential presents special problems due to the non-linear nature of the free-surface condition and the complexity of the body boundary conditions. This section discusses a method to approximate the effect of the second order potential.

The approximation is based on the assumption that the major part of the low frequency second order force due to the second order potential is the wave exciting force component due to the contribution $\Phi_{ww}^{(2)}$ of the undisturbed incoming waves to the second order potential. This assumes that the first order diffraction and body motion potentials $\Phi_d^{(1)}$ and $\Phi_b^{(1)}$ are small relative to the undisturbed wave potential $\Phi_w^{(1)}$. This means that the right-hand side of the free surface boundary condition of equation 9.15 only involves terms associated with the first order velocity potential $\Phi_w^{(1)}$ of the undisturbed incoming waves. The second order potential which satisfies this boundary condition and the boundary condition at the sea bed as well as the equation of continuity has been given by [Bowers, 1975].

We now consider a regular wave group travelling in the positive X_1-direction consisting of two regular waves with frequencies ω_i and ω_j with $\omega_i > \omega_j$.

The first order velocity potential associated with these waves is:

$$\Phi_w^{(1)} = -\sum_{i=1}^{N} \frac{\zeta_i^{(1)} g \cosh k_i (X_3 - h)}{\omega_i \cosh k_i h} \cdot \sin(k_i X_1 - \omega_i t + \tilde{\varepsilon}_i) \tag{9.78}$$

The low frequency component of the second order potential associated with these waves is as follows:

$$\Phi_{ww}^{(2)} = -\sum_{i=1}^{N} \sum_{j=1}^{N} \zeta_i^{(1)} \zeta_j^{(1)} \cdot A_{ij} \cdot \frac{\cosh\{(k_i - k_j)(X_3 - h)\}}{\cosh(k_i - k_j) h} \cdot$$

$$\cdot \sin\{(k_i - k_j)X_1 - (\omega_i - \omega_j)t + (\tilde{\varepsilon}_i - \tilde{\varepsilon}_j)\} \tag{9.79}$$

in which A_{ij} is a coefficient depending on ω_i and ω_j and on the water depth h:

$$A_{ij} = \frac{g}{2} \cdot \frac{B_{ij} + C_{ij}}{(\omega_i - \omega_j)^2 - (k_i - k_j)g \cdot \tanh(k_i - k_j)\,h} \tag{9.80}$$

in which:

$$B_{ij} = \frac{k_i^2}{\omega_i \,\cosh^2 k_i\,h} - \frac{k_j^2}{\omega_j \,\cosh^2 k_j\,h} \tag{9.81}$$

$$C_{ij} = \frac{2k_i k_j \cdot (\omega_i - \omega_j) \cdot (1 + \tanh\,k\,h\,\tanh\,k_j\,h)}{\omega_i \,\omega_j} \tag{9.82}$$

The low frequency component of this second order potential represents a long wave which is induced by the presence of the regular wave group. The phase of this long wave - relative to the wave group - is such that it has a trough where the wave group attains its maximum wave elevation and a crest where it attains its minimum elevation. This is shown in figure 9.24.
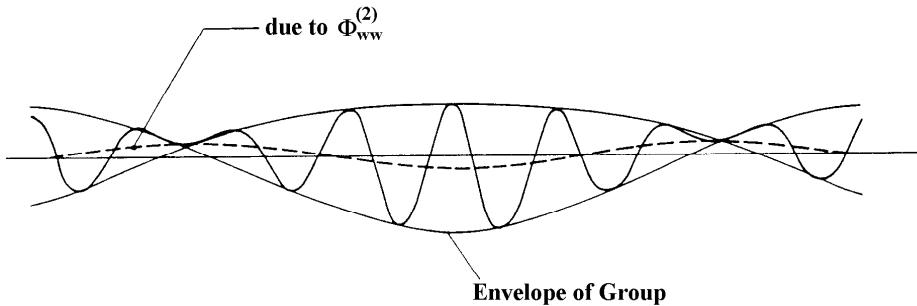
Figure 9.24: Wave due to Second Order Potential in a Regular Wave Group

The potential associated with such a wave does not satisfy the boundary condition on the body which for the simplified case is assumed to be equivalent to the normal first order boundary condition. This means that contributions due to products of first order quantities are neglected in the right-hand-side of equation 9.32.
The second order diffraction potential $\Phi_d^{(2)}$ in equation 9.36 satisfies the equation of continuity, the boundary condition at the sea floor, the radiation condition and the homogeneous free surface condition:

$$g \cdot \frac{\partial \Phi}{\partial X_3} + \frac{\partial^2 \Phi}{\partial t^2} = 0 \tag{9.83}$$

This last relationship gives rise to the well known dispersion relationship:

$$\omega^2 = kg \cdot \tanh kh \tag{9.84}$$

The incoming waves due to the low frequency second order potential have a wave number equal to $k_i - k_j$ and a wave frequency equal to $\omega_i - \omega_j$. These waves do not satisfy the dispersion equation 9.84.

If the incoming waves have a frequency of $\omega_i - \omega_j$ then the diffracted waves have the same frequency; the wave number will follow from the relationship:

$$(\omega_i - \omega_j)^2 = k\,g \cdot \tanh k\,h \tag{9.85}$$

In order to simplify the situation we allow the diffracted waves to have the same wave number $k_i - k_j$ as the incoming waves. This means that differences will occur in the diffracted waves further away from the body. Close to the body the situation will be similar since the boundary condition at the body still has to be satisfied. The reason for this assumption regarding the wave number of the diffracted waves will be apparent from the following.

The problem has been reduced to a situation where one has to determine the wave exciting force on the body due to a wave which has a velocity potential given by equation 9.79. The diffracted waves have the same wave number as the incoming waves. This is solved by considering the ordinary first order wave exciting force $F^{(1)}$ on the body in a regular wave with wave number equal to $k_i - k_j$ in an ordinary gravity field. For such a case the associated wave frequency ω will be in accordance with the dispersion relationship equation 9.84. The frequency of this wave can be made equal to the frequency $\omega_i - \omega_j$ of the second order waves by selecting a different value for the acceleration of gravity:

$$g_{ij} = \frac{(\omega_i - \omega_j)^2}{(k_i - k_j) \cdot \tanh(k_i - k_j)h} \tag{9.86}$$

Since the wave exciting force is proportional to the acceleration of gravity, the initial force $F^{(1)}$ in a wave with frequency ω, which follow from equation 9.84, becomes a second order wave force with frequency $\omega_i - \omega_j$ by simply applying the factor:

$$n_{ij} = \frac{g_{ij}}{g} \tag{9.87}$$

to the initial force.

This does not complete the transformation however, since besides satisfying the requirement that wave number and wave frequency be equal, the amplitude of the potentials must also be equal. After alteration of the acceleration of gravity, the transformed potential of the first order wave is:

$$\Phi = -\frac{\zeta_a^{(1)}\,g_{ij}}{(\omega_i - \omega_j)} \cdot \frac{\cosh\{(k_i - k_j)(X_3 - h)\}}{\cosh(k_i - k_j)\,h} \cdot \sin\left\{(k_i - k_j)X_1 - (\omega_i - \omega_j)t + (\tilde{\varepsilon}_i - \tilde{\varepsilon}_j)\right\} \tag{9.88}$$

The amplitude of the second order potential is given in equation 9.79. Equality of the amplitudes means that:

$$\frac{\zeta_a^{(1)}\,g_{ij}}{(\omega_i - \omega_j)} = \zeta_i^{(1)}\,\zeta_j^{(1)} \cdot A_{ij} \tag{9.89}$$

This means that the first order wave amplitude must be selected so that:

$$\zeta_a^{(1)} = \zeta_i^{(1)}\,\zeta_j^{(1)} \cdot \frac{A_{ij}(\omega_i - \omega_j)}{g_{ij}} \tag{9.90}$$

The first order force $F^{(1)}$ is determined for a value of unity for the wave amplitude ζ_a. Since forces are proportional to the wave amplitude, equation 9.90 gives a second correction factor

which has to be applied to the force $F^{(1)}$ in order to give the required second order force $F^{(2)}$:

$$F_{ij}^{(2)} = n_{ij} \cdot \frac{\zeta_i^{(1)} \zeta_j^{(1)} \cdot A_{ij} (\omega_i - \omega_j)}{g_{ij}} \cdot F^{(1)} \tag{9.91}$$

which, taking into account equation 9.87, gives:

$$F_{ij}^{(2)} = f_{ij} \cdot F^{(1)} \tag{9.92}$$

where:

$$f_{ij} = \frac{\zeta_i^{(1)} \zeta_j^{(1)} \cdot A_{ij} (\omega_i - \omega_j)}{g} \tag{9.93}$$

Equation 9.92 transforms a first order wave force into a second order wave force. As can be seen from this equation, the second order force becomes a function of two frequencies ω_i and ω_j. This approximation for the second order force can also be expressed in terms of contributions to the coefficients P_{ij} and Q_{ij}.

Wave Drift Forces in Regular Wave Groups

From the previous sections it was seen that the total wave drift forces may thus be expressed in terms of transfer functions which are a function of two frequencies.
The most elementary sea state which gives low frequency wave drift forces is one which consists of two regular waves with amplitude, frequency and random phase of $\zeta_1, \omega_1, \varepsilon_1$ and $\zeta_2, \omega_2, \varepsilon_2$ respectively, with $\omega_1 > \omega_2$.

$$\zeta(t) = \zeta_1 \cdot \cos(\omega_1 t + \varepsilon_1) + \zeta_2 \cdot \cos(\omega_2 t + \varepsilon_2) \tag{9.94}$$

The wave drift force in such a case is:

$$
\begin{aligned}
F^{(2)}(t) = \quad & \zeta_1^2 . P_{11} + \zeta_2^2 . P_{22} \\
& + \zeta_1 \zeta_2 (P_{12} + P_{21}) \cdot \cos\{(\omega_1 - \omega_2)t + (\varepsilon_1 - \varepsilon_2)\} \\
& + \zeta_1 \zeta_2 (Q_{12} - Q_{21}) \cdot \sin\{(\omega_1 - \omega_2)t + (\varepsilon_1 - \varepsilon_2)\}
\end{aligned}
\tag{9.95}
$$

The frequency of the low frequency part of the wave drift force is equal to the difference between the frequencies of the regular wave components. This is the frequency of the regular wave group which is the result of superposition of two regular waves (see figure 9.25). It is noted that the constant part of the wave drift force is the sum of the constant parts due to each of the wave components. The amplitude of the quadratic transfer function is:

$$|T_{ij}| = \sqrt{P_{ij}^2 + Q_{ij}^2} \tag{9.96}$$

Since P_{ij} and Q_{ij}, etc. never occur in isolation, it can be so arranged that certain symmetry relations are valid:

$$
\begin{aligned}
P_{ij} &= P_{ji} \tag{9.97} \\
Q_{ij} &= -Q_{ji} \tag{9.98} \\
|T_{ij}| &= |T_{ji}| \tag{9.99}
\end{aligned}
$$
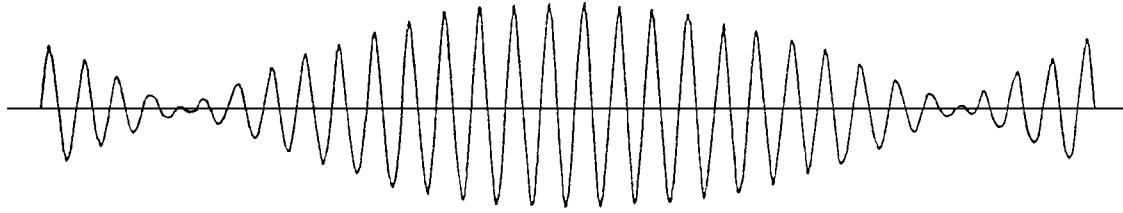
Figure 9.25: Regular Wave Group

Frequency Domain Calculation of Mean and Low Frequency Drift Force

The mean drift force in irregular waves with spectral density $S_{\zeta\zeta}(\omega)$ is found by putting $\omega_1 = \omega_2$ in equation 9.74:

$$F_{1_{mean}}^{(2)} = \sum_{i=1}^{N} \zeta_i^{(1)^2} \cdot P_{ii} \tag{9.100}$$

which, taking into account that:

$$\zeta_i^{(1)^2} = 2 \cdot S_\zeta(\omega_i) \cdot d\omega_i \qquad \text{(see chapter 5)} \tag{9.101}$$

results in:

$$F_{1_{mean}}^{(2)} = 2 \int_0^\infty S_\zeta(\omega) \cdot P(\omega, \omega) \cdot d\omega \tag{9.102}$$

where $P(\omega, \omega)$ is known as the mean drift force coefficient in regular waves.
By using equation 9.74 with $i = j$, $P(\omega, \omega)$ is also written as:

$$P(\omega, \omega) = \frac{F_1}{\zeta_a^2}(\omega) \tag{9.103}$$

Similarly it can be shown that the spectral density of the low frequency part of the wave drift force is:

$$S_F(\mu) = 8 \int_0^\infty S_\zeta(\omega_1) \cdot S_\zeta(\omega_2) \cdot |T(\omega_1, \omega_2)|^2 \cdot d\omega \tag{9.104}$$

where $\omega_1 - \omega_2 = \mu$ is the low frequency and $| T(\omega_1, \omega_2) |$ is the amplitude of the quadratic transfer function.
Equation 9.104 can also be written as:

$$S_F(\mu) = 8 \int_0^\infty S_\zeta(\omega + \mu) \cdot S_\zeta(\omega) \cdot |T(\omega + \mu, \omega)|^2 \cdot d\omega \tag{9.105}$$

9.3.4 Computed Results of Wave Drift Forces

The expression for the wave drift forces and moments given by equations 9.67 and 9.70 have been evaluated at MARIN, using a three-dimensional singularity distribution computer program, see [Pinkster, 1977] and [Pinkster, 1980]. The computations have been performed for a number of the cases and the results have been compared with some analytical solutions and results of model tests. All results are for zero forward speed.

Mean Drift Forces in Regular Waves

Figure 9.26 compares the computed horizontal drift force on a free floating hemisphere to an analytical result given by [Kudou, 1977].

Figure 9.27 compares the computed mean vertical drift force on a long free floating submerged cylinder in beam seas to two-dimensional analytical results given by [Ogilvie, 1963].

Figure 9.28 compares the computed mean horizontal drift force on a long free floating cylinder in beam seas to two-dimensional results given by [Faltinsen and Loken, 1979] based on Maruo's theory.

Figure 9.30 (see also [Pinkster, 1979] and [Pinkster, 1980]) compares the computed mean drift force on a rectangular barge and a semi-submersible in head seas to results of measurements carried out at MARIN. The vessels are shown in figure 9.29. In general it can be said that the computations compare favorably with analytical solutions and results of model tests.
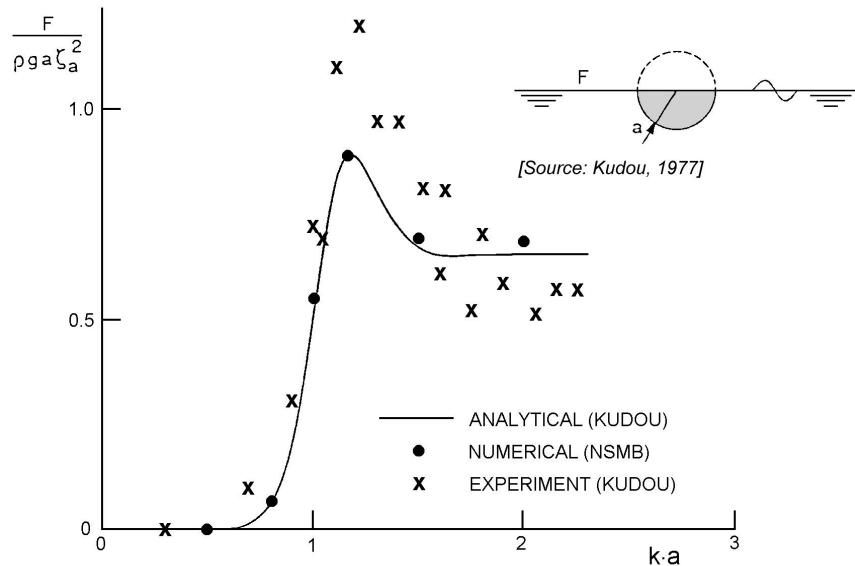
Figure 9.26: Mean Horizontal Wave Drift Forces on a Floating Sphere

Components of Mean Wave Drift Forces

This section gives results of calculations which reveals the importance of various contributions to the mean drift forces as given by equation 9.67; this yields after re-arranging the terms in this equation in a sequence as given by [Pinkster, 1980]:
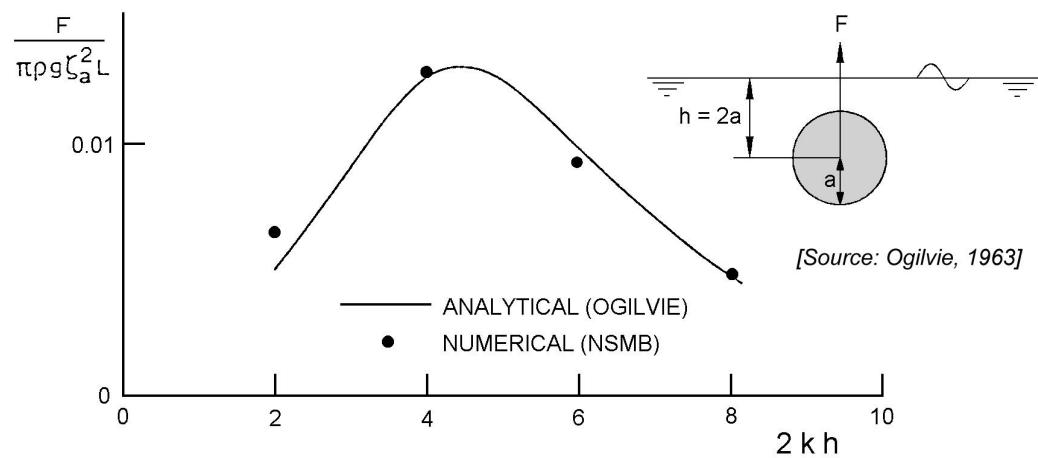
Figure 9.27: Mean Vertical Wave Drift Forces on a Submerged Cylinder
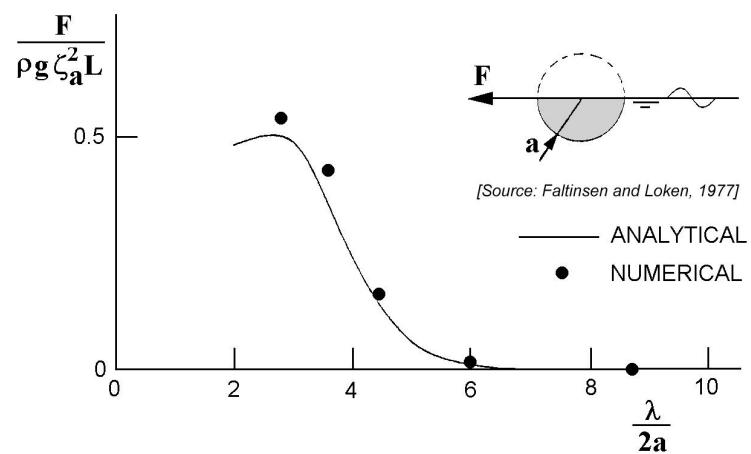
Figure 9.28: Mean Horizontal Wave Drift Forces on a Cylinder
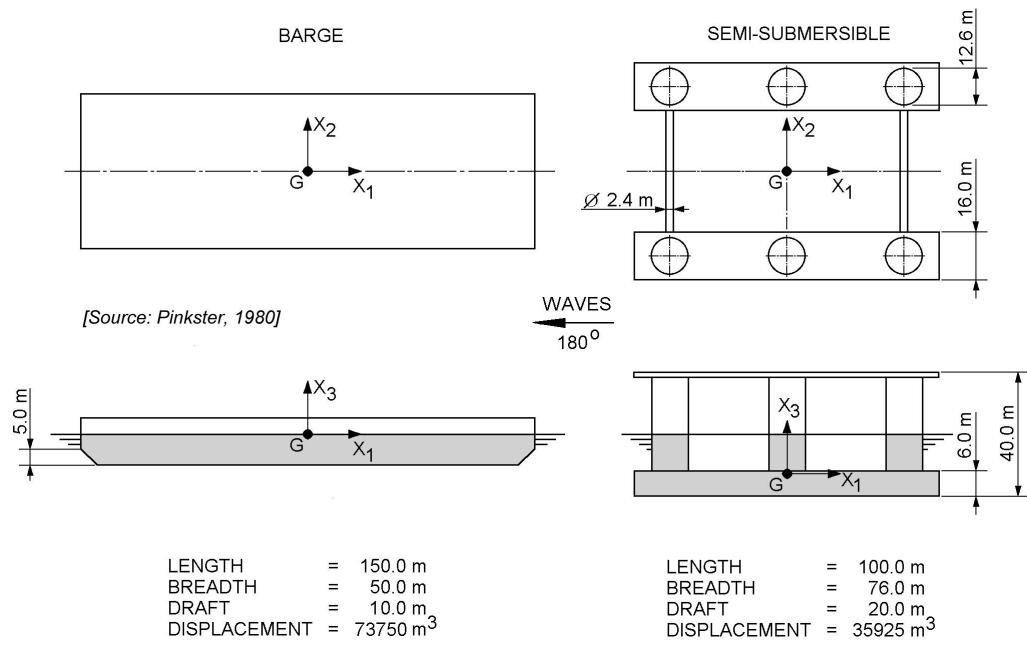
Figure 9.29: Vessels used for Experiments
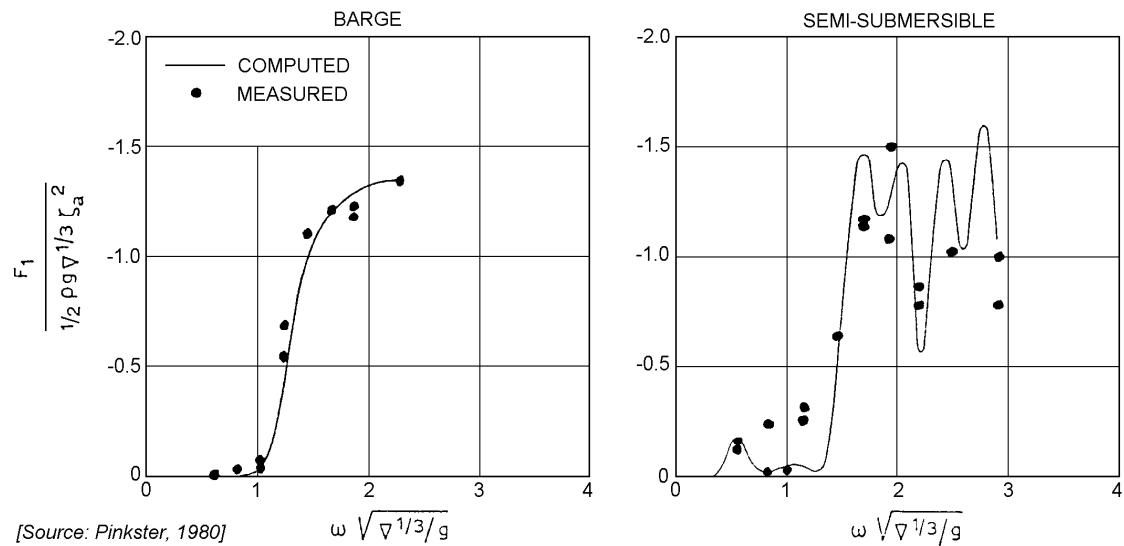
Figure 9.30: Mean Surge Drift Forces in Regular Head Waves

$$\vec{F}^{(2)} = -\frac{1}{2}\rho g \oint_{wl} \left(\zeta_r^{(1)}\right)^2 \cdot \vec{n} \cdot dl$$

$$+\frac{1}{2}\rho \iint_{S_0} \left(\vec{\nabla}\Phi^{(1)}\right)^2 \cdot \vec{n} \cdot dS$$

$$+\rho \iint_{S_0} \vec{X}^{(1)} \cdot \vec{\nabla}\frac{\partial \Phi^{(1)}}{\partial t} \cdot \vec{n} \cdot dS$$

$$+m \cdot R^{(1)} \cdot \ddot{\vec{X}}_G^{(1)}$$

$$+\rho \iint_{S_0} \frac{\partial \Phi^{(2)}}{\partial t} \cdot \vec{n} \cdot dS \qquad (9.106)$$

Figure 9.31 gives the five components of the computed mean surge drift force on a rectangular barge and a semi-submersible in head waves.
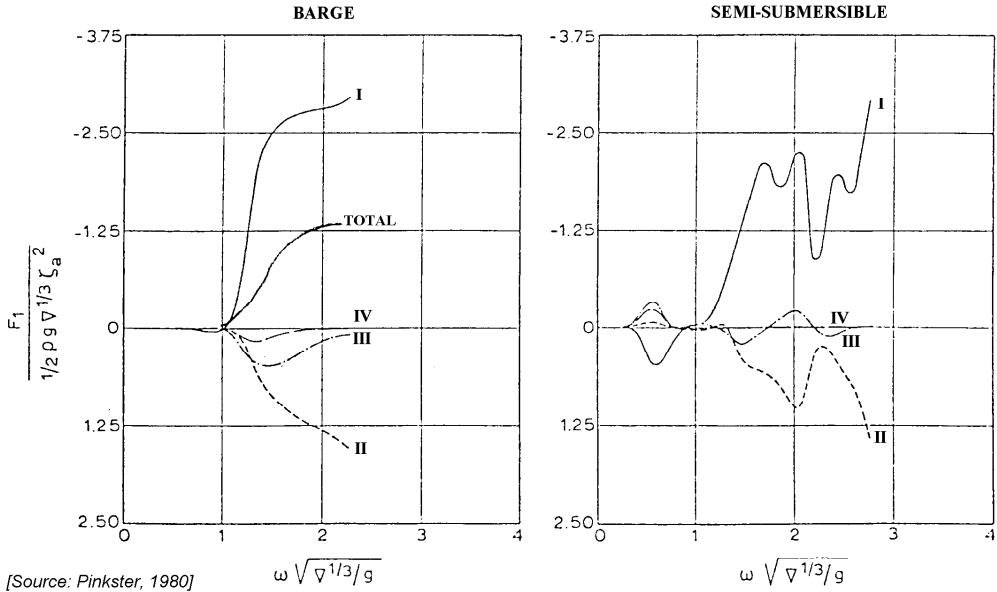
Figure 9.31: Components of Computed Mean Surge Drift Forces

The numerals in these figures refer to the following components of the mean force:

I: Relative wave height contribution:

$$-\frac{1}{2}\rho g \oint_{wl} \left(\zeta_r^{(1)}\right)^2 \cdot n_1 \cdot dl$$

II: Pressure drop due to velocity squared:

$$\frac{1}{2}\rho \iint_{S_0} \left(\vec{\nabla}\Phi^{(1)}\right)^2 \cdot n_1 \cdot dS \qquad (9.107)$$

III: Pressure due to product of gradient of first order pressure and first order motion:

$$\rho \iint\limits_{S_0} \left(\vec{X}^{(1)} \cdot \vec{\nabla}\Phi^{(1)} \right) \cdot n_1 \cdot dS \tag{9.108}$$

IV: Contribution due to product of pitch motion and heave inertia force:

$$m \cdot x_5^{(1)} \cdot \ddot{X}_{3_G}^{(1)} \tag{9.109}$$

V: Contribution due to the second order potential $\Phi^{(2)}$, which is zero in regular waves:

$$\rho \iint\limits_{S_0} \frac{\partial \Phi^{(2)}}{\partial t} \cdot \vec{n} \cdot dS \tag{9.110}$$

The results in figure 9.31 show that in general contribution I due to the relative wave height is dominant, while the three remaining terms II, III and IV tend only to reduce somewhat the effect of contribution I. For high frequencies (to the right in the figures) terms III and IV vanish since the body motions - on which these terms are dependent - reduce to zero in short waves. This leaves only the terms I and II.

For the semi-submersible in figure 9.31 it is apparent that it is the wave drift forces acting on the columns which form the greater part of the total horizontal wave drift forces.

Figure 9.32 shows the computed contributions to the mean horizontal drift force on the floating sphere. In this case only contributions I, II and III play a part. As the frequency increases again only contributions I and II remain.

Figure 9.33 shows the computed contributions to the vertical force on the submerged cylinder in beam seas. Since there is no waterline, only contributions II and III play a role. For high frequencies only II remains.

9.3.5 Low Frequency Motions

In view of the analogy which exists between the low frequency waves, the drift forces and the low frequency part of the square of the elevations of the incident waves as indicated by equations 9.74 and 9.77, we will look at some aspects of the waves. This will give some indications regarding the properties of the low frequency wave drift forces.

The irregular waves are assumed to behave as a random Gaussian process. Thus, the wave elevation in a fixed point in irregular waves, may be written as follows:

$$\zeta(t) = \sum_{i=1}^{N} \zeta_i \cdot \sin\left(\omega_i t + \tilde{\varepsilon}_i\right) \tag{9.111}$$

where $\tilde{\varepsilon}_i$ is a random phase angle.

In amplitude modulated form this becomes:

$$\zeta(t) = A(t) \cdot \sin\left(\omega_0 t + \varepsilon(t)\right) \tag{9.112}$$

where:
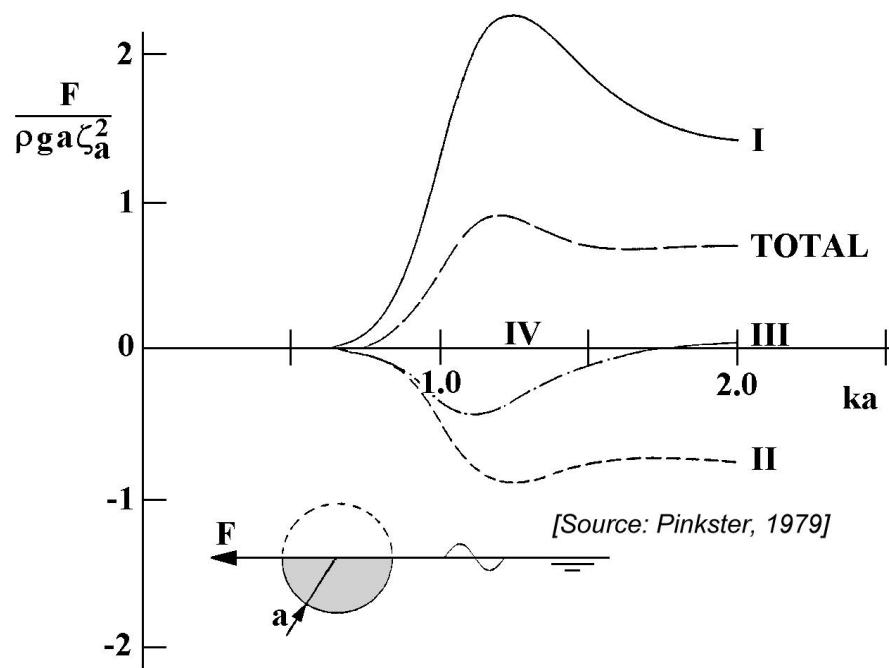
Figure 9.32: Components of Computed Mean Horizontal Drift Forces on a Sphere
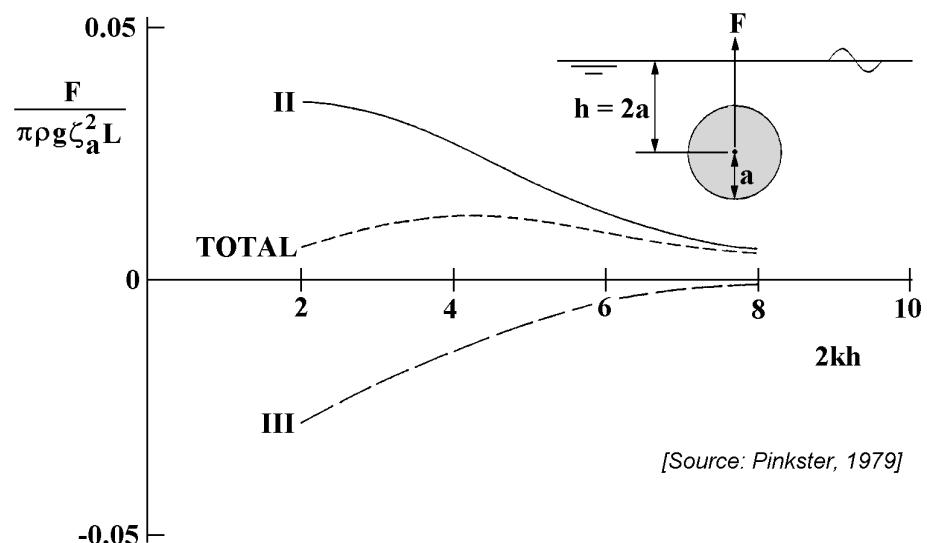
Figure 9.33: Components of Computed Mean Vertical Drift Forces on a Submerged Cylinder

$$A(t) = \quad = \quad \text{wave envelope} = \sqrt{\sum_{i=1}^{N}\sum_{i=1}^{N} \zeta_i\zeta_j \cdot \cos\left\{(\omega_i - \omega_j)t + (\tilde{\varepsilon}_i - \tilde{\varepsilon}_j)\right\}}$$

$$\varepsilon(t) \quad = \quad \text{slowly varying phase angle}$$

$$\omega_0 \quad = \quad \text{some centrally chosen fixed wave frequency}$$

The behavior of the wave envelope, $A(t)$, contains information with respect to the grouping of waves. Squaring the wave elevation, $\zeta(t)$, and taking only the low frequency part gives:

$$\zeta_{lf}^2(t) \quad = \quad \frac{1}{2}\sum_{i=1}^{N}\sum_{j=1}^{N} \zeta_i\zeta_j \cdot \cos\left\{(\omega_i - \omega_j)t + (\tilde{\varepsilon}_i - \tilde{\varepsilon}_j)\right\}$$

$$= \quad \frac{1}{2}A^2(t) \tag{9.113}$$

This shows that the low frequency part of the square of the wave elevation also contains information on wave grouping.

From equation 9.113 it follows that:

$$A^2(t) = 2\zeta_{lf}^2(t) \tag{9.114}$$

Based on the assumption that the wave elevations are normally distributed, it can be shown that the spectral density, $S_g(\mu)$ of $A^2(t)$, is related to the normal wave spectrum, $S_\zeta(\omega)$, in the following way:

$$S_g(\mu) = 8\int_{0}^{\infty} S_\zeta(\omega) \cdot S_\zeta(\omega + \mu) \cdot d\omega \tag{9.115}$$

The distribution function of $A^2(t)$ is, for a narrow-banded spectrum:

$$f(A^2) = \frac{1}{2m_0} \cdot e^{-\frac{A^2}{2m_0}} \tag{9.116}$$

where:

$$m_0 = \int_{0}^{\infty} S_\zeta(\omega) \cdot d\omega \tag{9.117}$$

This is the Rayleigh distribution for wave heights used in chapter 5.

From the above, it follows that knowledge of $S_\zeta(\omega)$ and the assumption that the wave elevation is normally distributed is sufficient to calculate the spectral density and distribution function of $A^2(t)$. From this relationship it follows that the spectral density and distribution may also be calculated from the low frequency part of the square of the record of the wave elevation measured in the basin. If the waves are completely random then the spectral density and distribution obtained from and based on the normal (first) spectrum of the waves should correspond with the spectral density and distribution of $2\zeta_{lf}^2$ calculated directly from the wave record.

The distribution function $p(A^2)$ and $p(2\zeta_{lf}^2)$ and the spectral density of the waves and of A^2 and $2\zeta_{lf}^2$ are shown in figure 9.34 and figure 9.35 respectively for an irregular wave train generated in a basin of MARIN.

From equation 9.114 it follows that the wave envelope is related to the low-pass filtered square of the wave elevation:

$$A(t) = \sqrt{2} \cdot \zeta_{lf}(t) \tag{9.118}$$
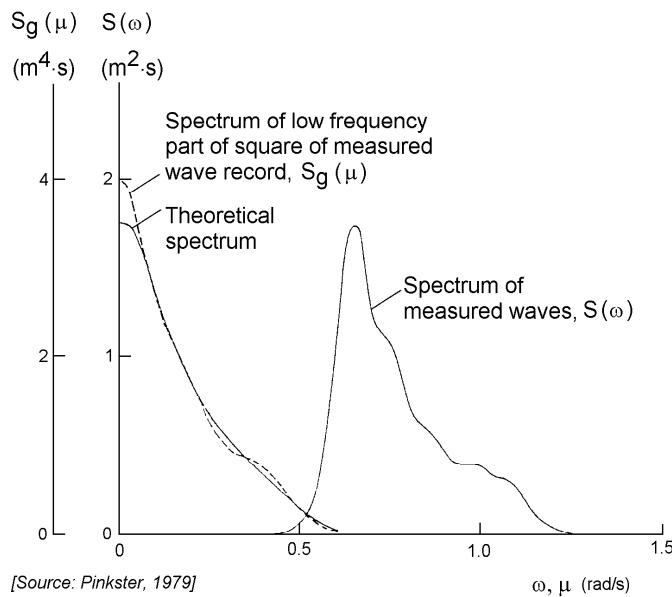
Figure 9.34: Wave Spectra and Low-Frequency Part of the Square of a Wave Record
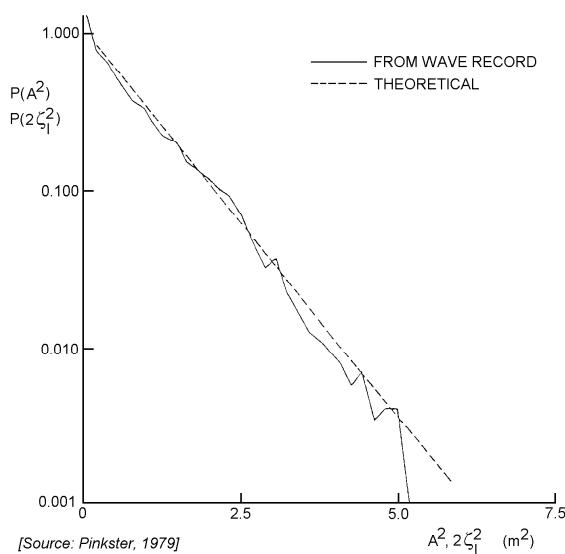
Figure 9.35: Distribution Function of Low-Frequency Part of the Square of a Wave Record

In order to show that this operation does indeed represents the wave envelope, results are plotted in figure 9.36 showing the wave elevation $\zeta(t)$ and the corresponding wave envelope $A(t)$ calculated in accordance with equation 9.118. Also shown in the same figure is the record of the wave elevation $\zeta(t)$ divided by the envelope $A(t)$.

According to equation 9.112:

$$\sin\left(\omega_0 t + \varepsilon(t)\right) = \frac{\zeta(t)}{A(t)} \tag{9.119}$$

From this it is seen that the signal oscillates between $+1$ and -1 with varying frequency. From figure 9.36 it is seen that generally this agrees quite well with theory. The slowly varying nature of the frequency can be seen quite clearly.

In the foregoing, both the behavior of the envelope $A(t)$ and the square of the envelope have been treated. More attention should, however, be given to the behavior of the square of the envelope in view of the analogy between this quantity and the low frequency second order wave drifting forces.
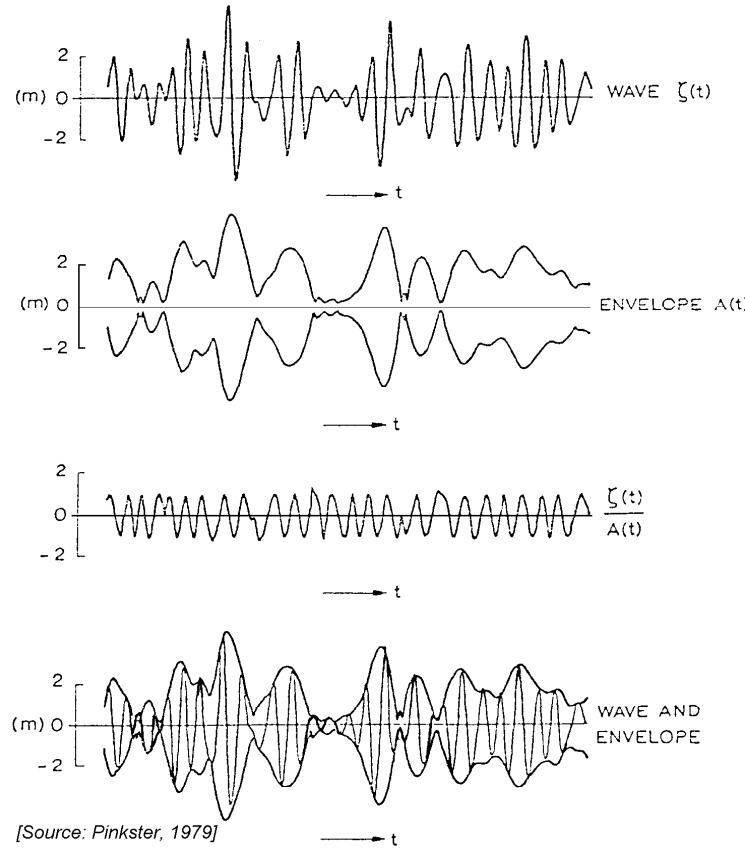
Figure 9.36: Irregular Waves and Wave Enveloppe

The similarity between the low frequency surge and sway drift forces on a tanker in bow quartering waves and the low frequency part of the square of the incident waves is apparent in figure 9.37. These results were measured during model tests.

The distribution function of the low frequency surge drift force in irregular waves measured on a tanker in head seas is given in figure 9.38.

[Source: Pinkster, 1979]
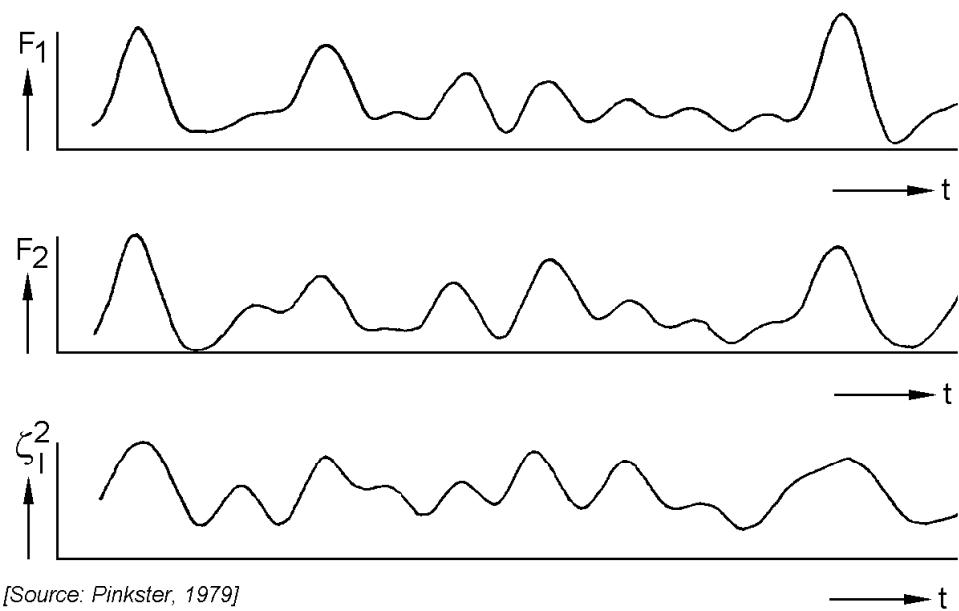
Figure 9.37: Low-Frequency Surge and Sway Drift Forces on a Tanker and Low-Frequency Part of Wave Height Squared

[Source: Pinkster, 1979]
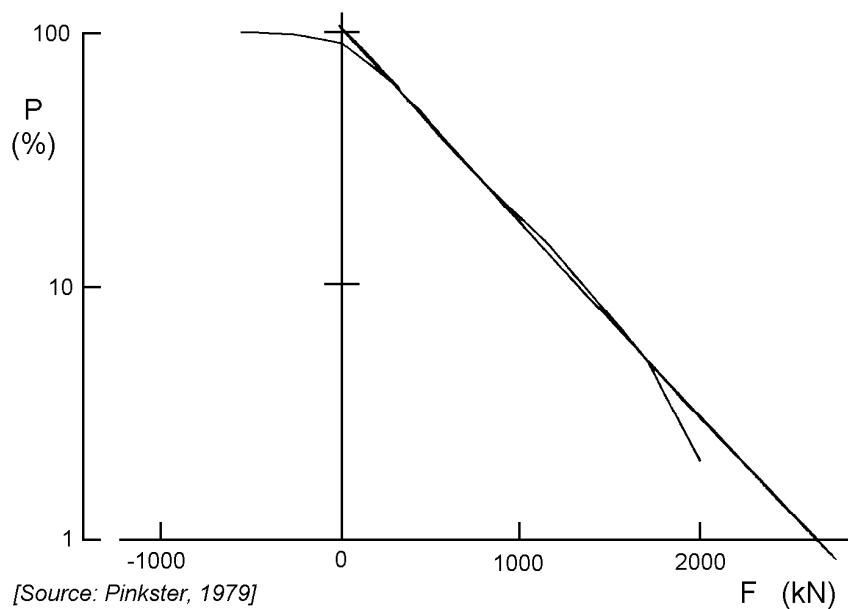
Figure 9.38: Distribution Function of the Low-Frequency surge Drift Forces on a Tanker in Irregular Head Waves

It is seen that this resembles an exponential distribution valid for the low frequency part of the square of the wave height.

In the beginning of this chapter, results were given on the wave drift forces on a tanker moored in shallow water. In such cases, the influence of the second order potential $\Phi^{(2)}$ on the wave drift forces become more pronounced. Results were also given on the low frequency "set-down" waves associated with the second order potential of the undisturbed incoming waves.

9.3.6   Simple Frequency Domain Method

A simple qualitative model is introduced in this section. It yields insight about the influence of mean and low frequency wave drift forces in irregular waves on the motions of a moored vessel. This model, simple though it may seem, has proved to be a very useful tool to explain and to predict low frequency motions of such vessels.

If a vessel is moored by means of a mooring system with linear restoring characteristics, the low frequency surge or sway motions may be approximated by the following equation of motion:

$$(m + a)\ddot{x} + b\dot{x} + cx = F^{(2)}(t) \tag{9.120}$$

where:

$$
\begin{aligned}
m + a &= \text{virtual mass} \\
b &= \text{damping coefficient} \\
c &= \text{restoring coefficient} \\
F^{(2)}(t) &= \text{time dependent low frequency wave drift force}
\end{aligned}
$$

The mean displacement from the zero position due to the mean wave drift force is found from:

$$X_{mean} = \frac{F^{(2)}_{mean}}{c} \tag{9.121}$$

where $F^{(2)}_{mean}$ is given by equation 9.102 and equation 9.103.

The root-mean-square of the low frequency part of the motion is found from:

$$m_{0x} = \sigma_x^2 = \int_0^\infty \left| \frac{x_a}{F_a}(\mu) \right|^2 \cdot S_f(\mu) \cdot d\mu \tag{9.122}$$

where:

$$
\begin{aligned}
S_f(\mu) &= \text{spectral density of the wave drift force given by equation 9.105} \\
\left| \frac{x_a}{F_a}(\mu) \right| &= \text{frequency dependent motion amplitude response function}
\end{aligned}
$$

The motion amplitude response function follows from:

$$\left| \frac{x_a}{F_a}(\mu) \right| = \frac{1}{\sqrt{\{c - (m + a)\mu^2\}^2 + b^2\mu^2}} \tag{9.123}$$

see chapter 6.

For slightly damped systems, which applies to many cases of moored vessels, the following assumption may be made with respect to the spectral density of the low frequency drift force:

$$S_f(\mu) \approx S_f(\mu_e) \tag{9.124}$$

where μ_e is the natural frequency of the moored vessel defined by:

$$\mu_e = \sqrt{\frac{c}{m+a}} \tag{9.125}$$

This result implies that the major part of the motion response will be due to excitation near the natural frequency. In that case, equation 9.122 may be approximated by:

$$\sigma_x^2 = S_f(\mu_e) \cdot \int\limits_0^\infty \left| \frac{x_a}{F_a}(\mu) \right|^2 \cdot d\mu \tag{9.126}$$

If the natural frequency of the system is close to zero, the following approximation can also be applied:

$$S_f(\mu_e) \approx S_f(0) \tag{9.127}$$

From equation 9.105 it follows that:

$$S_f(0) = 8 \int\limits_0^\infty S_\zeta^2(\omega) \cdot |T(\omega, \omega)|^2 \cdot d\omega \tag{9.128}$$

Since $Q(\omega, \omega) = 0$ (from equation 9.98) and taking into account equation 9.103 this becomes:

$$S_f(0) = 8 \int\limits_0^\infty S_\zeta^2(\omega) \cdot \left| \frac{F}{\zeta_a^2}(\omega) \right|^2 \cdot d\omega \tag{9.129}$$

In this case the mean-square of the low frequency part of the motions can be written as follows:

$$\sigma_x^2 = S_f(0) \int\limits_0^\infty \left| \frac{x_a}{F_a}(\mu) \right|^2 \cdot d\mu \tag{9.130}$$

Taking into account equation 9.123 this becomes:

$$\sigma_x^2 = \frac{\pi}{2bc} \cdot S_f(0) \tag{9.131}$$

which reveals the remarkable fact that the virtual mass $(m+a)$ of the vessels has no direct bearing on the mean or the low frequency motion.

From equation 9.131, it is seen that besides the exciting force, the most important factors determining the motions appear to be the damping b and the stiffness c of the mooring system. The trend suggested by equation 9.131 is also seen in results given by [Remery and Hermans, 1972] on the influence of the parameter c on the RMS value of the low frequency surge motion of a barge moored in head seas.

The general characteristic of the mooring force as expressed by the mean-square of the mooring force cx is found by multiplying equation 9.131 by c^2:

$$\sigma_{mf}^2 = \frac{\pi c}{2b} \cdot S_f(0) \tag{9.132}$$

This reveals that as the stiffness c of a mooring system increases, so does the RMS value of the low frequency mooring force.

It must be remembered that equations 9.131 and 9.132 can only be used in an indicative way. In many cases the mooring system will not be linear, or the number of degrees of freedom of the moored vessel will be too great to allow such simplifications as made here. We refer to [Oortmerssen, 1976b] and [Wichers, 1988] for more details concerning simulation techniques for moored vessels.

9.4   Remarks

The theory relating to second order wave drift forces has been treated in this chapter. Some results of computations have been compared with results derived analytically and by means of model tests. These results apply to the mean drift forces in regular waves, which can be used to estimate the mean and low frequency drift forces in irregular waves.

The low frequency part of the wave drift forces should theoretically, be determined by considering the drift forces in regular wave groups. In such cases the second order potential also contributes to the force, see [Pinkster, 1980]. [Faltinsen and Loken, 1979] have indicated that, for vessels floating in beam seas, the sway drift forces calculated using only information on the mean drift forces in regular waves gives results which are sufficiently accurate for engineering purposes. Results given by [Pinkster and Hooft, 1978] and [Pinkster, 1979] on the low frequency drift forces on a barge and a semi-submersible in head waves generally confirms the conclusion provided the frequency of interest is low. Frequencies of interest for moored vessels are the natural frequencies of the horizontal motions induced by the presence of the mooring system. In some cases the natural frequencies of vertical motions can also be of interest from the point of view of vertical motions induced by the low frequency wave drift forces.

It can be shown that, in at least one case, the mean wave drift forces in regular waves cannot be used to estimate the low frequency drift forces in irregular waves. This case concerns the low frequency sway drift force on a free floating, submerged cylinder in beam seas. According to [Ogilvie, 1963], the mean wave drift force in regular waves is zero for all wave frequencies. This means that the low frequency wave drift force in irregular waves estimated using only the mean wave drift force will be zero as well. Computations carried out using the method given by [Pinkster, 1979] which determines the low frequency force in regular wave groups show that this will not be true. The table below presents amplitudes of low-frequency sway drift forces in regular wave groups on a submerged cylinder in beam waves, with its center one diameter below the mean free surface:

$\dfrac{F_{2_{ij}}}{\pi \rho g L \zeta_1 \zeta_2}$			
	$2k_i h$		
$2k_j h$	2	4	6	8
2	0.00	0.08	0.09	0.08
4		0.00	0.06	0.07
6			0.00	0.05
8				0.00

Chapter 10

STATION KEEPING

10.1 Introduction

Precise positioning and long term motion control of ships and other floating structures are important in offshore operations. Mooring systems and thrusters are major tools for maintaining a structure in position in current, wind and waves. The increasing application of large offshore structures has put high demands upon the design of these positioning arrangements. Important parameters in this respect are the large displacement of the structure, deep and hostile waters and the required round-the-year workability.

The external loads on the structure have been discussed in earlier chapters. This chapter treats some other important phenomena of station keeping problems of a floating structure, such as mooring systems, thruster performance and motion control.

10.2 Mooring Systems

Any mooring system is made of a number of lines (chain, wire or synthetic rope) with their upper ends attached to different points of the floating structure and their lower ends anchored at the sea bed.

The cables are constructed from steel chain, rope or a combination of both. The ropes are available in constructions from steel and natural or synthetic fibres. Multi-component cable lines - cables composed of two or more lengths of different material - are used to get a heavy chain at the sea bed and a lighter rope close to the water surface. This results in an optimal combination of stiffness and total weight. The tension forces in the cables are dependent on the cable weight, its elastic properties and the mooring system.

Typical and important types of mooring systems are:

- Catenary Line Mooring
  This are the oldest and still most common mooring systems. It derives its restoring force primarily by lifting and lowering the weight of the mooring line, at least in the static sense. Generally, this yields a hard spring system with a force increasing more than directly proportional to the displacement. In a spread mooring system as given in figure 10.1, several pre-tension anchor lines are arrayed around the structure to

---

hold it in the desired location. The normal case is that the anchors can be easily moved, which implies that these anchors can not be loaded by too large vertical forces. To ensure that the anchors are kept in position, it is necessary that a significant part of the anchor line lie on the sea bed.

- Taut Line Mooring
  The mooring system has a pattern of taut, light-weight lines radiating outward. The lines have a low net submerged weight, which means that the catenary action has been eliminated. The system gets its restoring force as a function of horizontal displacement primarily from elastic stretch of the line itself. Synthetic fibers are most common for this type of mooring.

- Tension Leg Mooring
  This special mooring system is used for tension leg platforms (TLP), as has been shown in chapter 9. The buoyancy of this platform exceeds its weight and a net downward force is supplied by the vertically tensioned mooring, secured by dead-weight or anchor piles. These mooring lines provide essentially total restraint against vertical movements of the platform in water depths of about 1 km or less. When the floating object is horizontally displaced from its equilibrium position, the restoring force on the object results from the horizontal component of the mooring leg tension.

The pre-tension in the cable is often established by the use of winches on the floating structure. The winches pull on the cables to establish the desired cable configuration. As the structure moves in response to unsteady environmental loads, the tension in the cable changes due to varying cable geometry. Thus, the mooring cables have an effective stiffness which - combined with the motions of the structure - introduce forces depending on the mooring cable characteristics.

Offshore mooring systems are discussed in detail by [Massie, 1997]. The mooring forces on the floating structure are an input in the equations of motion of the structure in the time domain. Two methods to obtain these forces on the structure - a static approach and a simple dynamic approach - are given here. The positions of the anchor point and the suspension point as well as the length of the cable line and its strain characteristics are supposed to be known in these methods.

The hydromechanical interaction between waves and currents and the moving mooring or towing line can lead to significant forces. Sometimes they even exceed the net gravity force on the line. This is discussed in detail in chapter 12. The axial resistance of a line in the water is much lower than its transverse (cylinder drag) resistance. See chapter 4 for an indication of this. Hydrodynamic interaction introduces hysteresis damping in a mooring system.

10.2.1   Definitions

Consider a cable with an un-stretched length L, at the lower end attached to an anchor point, A, and at the upper end attached to a suspension point, B, on a floating structure. In an earth-bound right-handed coordinate system, S-(X_1, X_2, X_3), with the origin somewhere in the fluid (S is often taken in the still water plane) and the vertical axis positive upwards, the anchor point, A, is given by (X_{1A}, X_{2A}, X_{3A}) and the suspension point, B, of the cable on the floating structure is given by (x_{bB}, y_{bB}, z_{bB}); see figure 10.1.
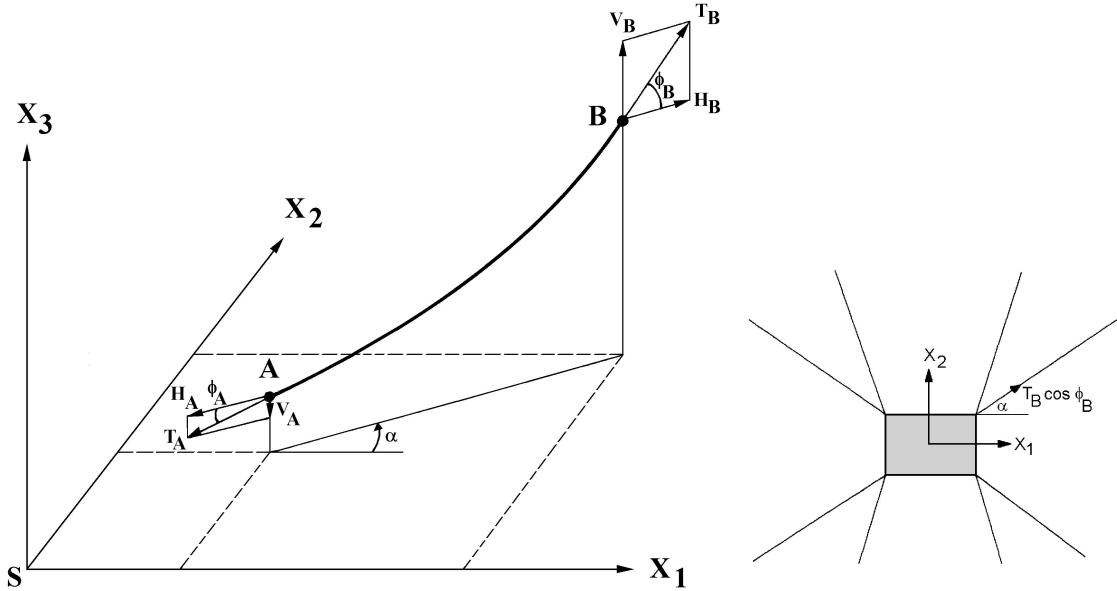
Figure 10.1: Cable Line in an Earth-Bound Axes System

The center of gravity, G, of the structure is given by (X_{1G}, X_{2G}, X_{3G}). A steadily translating coordinate system is given by G-(x_1, x_2, x_3), with roll, pitch and yaw angles x_4, x_5 and x_6 about these axes.

In the body-bound system of axes, G-(x_b, y_b, z_b), the suspension point, B, of the cable on the floating structure is defined by (x_{bB}, y_{bB}, z_{bB}).

In the earth-bound system of axes, the components of this suspension point, (X_{1B}, X_{2B}, X_{3B}), on the moving structure are found by:

$$
\begin{aligned}
X_{1B} = X_{1G} \quad & +x_{bB} \cdot (+\cos x_5 \cdot \cos x_6) \\
& +y_{bB} \cdot (-\cos x_4 \cdot \sin x_6 + \sin x_4 \cdot \sin x_5 \cdot \cos x_6) \\
& +z_{bB} \cdot (+\sin x_4 \cdot \sin x_6 + \cos x_4 \cdot \sin x_5 \cdot \cos x_6)
\end{aligned}
$$

$$
\begin{aligned}
X_{2B} = X_{2G} \quad & +x_{bB} \cdot (+\cos x_5 \cdot \sin x_6) \\
& +y_{bB} \cdot (+\cos x_4 \cdot \cos x_6 + \sin x_4 \cdot \sin x_5 \cdot \sin x_6) \\
& +z_{bB} \cdot (-\sin x_4 \cdot \cos x_6 + \cos x_4 \cdot \sin x_5 \cdot \sin x_6)
\end{aligned}
$$

$$
\begin{aligned}
X_{3B} = X_{3G} \quad & +x_{bB} \cdot (-\sin x_5) \\
& +y_{bB} \cdot (+\sin x_4 \cdot \cos x_5) \\
& +z_{bB} \cdot (+\cos x_4 \cdot \cos x_5) \quad (10.1)
\end{aligned}
$$

or in a linearized form as used in previous chapters:

$$
\begin{aligned}
X_{1B} &= X_{1G} + x_{bB} - y_{bB} \cdot x_6 + z_{bB} \cdot x_5 \\
X_{2B} &= X_{2G} + x_{bB} \cdot x_6 + y_{bB} + z_{bB} \cdot x_4 \\
X_{3B} &= X_{3G} - x_{bB} \cdot x_5 + y_{bB} \cdot x_4 + z_{bB} \quad (10.2)
\end{aligned}
$$

10.2.2   Static Catenary Line

Consider now this cable with an un-stretched length L, at the lower end attached to an anchor point, A, and at the upper end attached to a suspension point, B, in a vertical plane through this cable line. A two-dimensional sketch of this catenary anchor line is shown in figure 10.2.
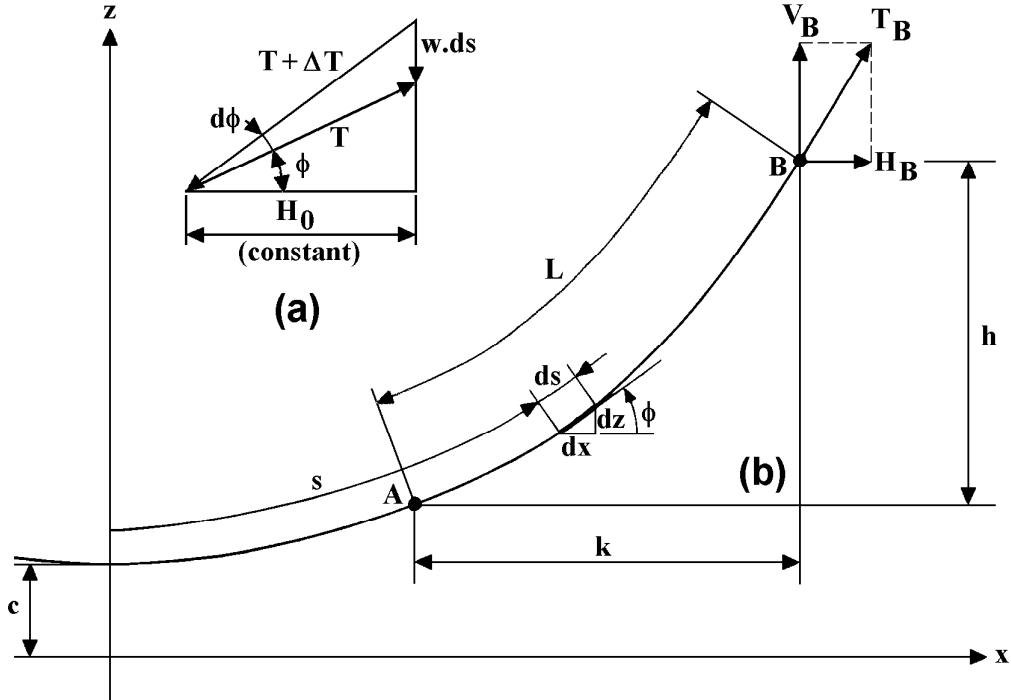
Figure 10.2: Cable Curve Symbols

For obtaining the equations of a static cable line, reference can be given to a number of papers in this field; for instance [Massie, 1997] and [Korkut and Hebert, 1970].

Inelastic Cable Line

Suppose: the length of the cable, L, is known and the relative positions of two - in principle arbitrary - points A and B on the cable are defined by the distances k and h. The anchor point is defined in a new 2-D coordinate system (see figure 10.2) by (x_A, z_A) and the suspension point on the structure is defined by (x_B, z_B) with:

$$x_B = x_A + k \qquad \text{and} \qquad z_B = z_A + h \tag{10.3}$$

The position of the origin of the axis system (x, z) relative to the cable line follows from two unknown coefficients, C_1 and C_2, as will be explained in the following.
When defining:

$$u = \frac{dz}{dx} \quad \text{and} \quad c = \frac{H_0}{w} \tag{10.4}$$

in which w is the weight per unit length of the cable in water (see also figure 10.2-a), it can be found that:

$$ds \;=\; \sqrt{1 + u^2} \cdot dx$$

$$du \quad = \quad d\left(\frac{dz}{dx}\right) = d\left(\tan\phi\right) = \frac{w \cdot ds}{H_0} = \frac{ds}{c}$$

$$du \quad = \quad \frac{\sqrt{1+u^2}}{c} \cdot dx \qquad \text{or:} \qquad dx = c \cdot \frac{du}{\sqrt{1+u^2}} \tag{10.5}$$

With this, an integral equation will be obtained:

$$\int dx = c \cdot \int \frac{du}{\sqrt{1+u^2}} \tag{10.6}$$

Integration of this equation provides:

$$x = c \cdot \ln\left(u + \sqrt{1+u^2}\right) + C_1 = \frac{c}{\sinh u} + C_1 \tag{10.7}$$

or:

$$u = \sinh\left(\frac{x}{c} - C_1\right) \tag{10.8}$$

Herein, the constant C_1 will be zero because the origin in figure 10.2 is chosen in such a way that the derivative $u = dz/dx$ is zero for x is zero, so:

$$u = \sinh\left(\frac{x}{c}\right) \tag{10.9}$$

Then the equation of the cable curve can be written as:

$$z = \int_0^x u \cdot dx = c \cdot \cosh\left(\frac{x}{c}\right) + C_2 \tag{10.10}$$

The origin in figure 10.2 is chosen in such a way that $C_2 = 0$, thus:

$$z = c \cdot \cosh\left(\frac{x}{c}\right) \tag{10.11}$$

This means that $z = c$ for $x = 0$.
Also, the distance s can be obtained:

$$s = \int_0^x \sqrt{1+u^2} \cdot dx = \int_0^x \sqrt{1 + \sinh^2\left(\frac{x}{c}\right)} \cdot dx \tag{10.12}$$

or:

$$s = c \cdot \sinh\left(\frac{x}{c}\right) \tag{10.13}$$

Combining equations 10.11 and 10.13 provides a simple relation between z and s:

$$z^2 - s^2 = c^2 \tag{10.14}$$

from which after some algebra for the points A and B on the cable line follows:

$$\sqrt{L^2 - h^2} = c\sqrt{2} \cdot \sinh\left(\frac{k}{2c}\right) \tag{10.15}$$

The values k, h and L are known, so the value of c has to be found from this equation in an iterative manner.

But, after expanding the sinh-expression in series:

$$\sinh\left(\frac{k}{2c}\right) = \frac{k}{2c} + \frac{k^3}{48c^3} + \ldots\ldots \qquad (10.16)$$

and neglecting the higher order terms in here, the value of c can be found directly:

$$c = \sqrt{\frac{k^3}{24 \cdot \left(\sqrt{2\left(L^2 - h^2\right)} - k\right)}} \qquad (10.17)$$

The relative position of the anchor point, x_A, can be found after some algebra by writing down $L + h$ with equations 10.13 and 10.11. A substitution of $x_M = x_A + k/2$ and $\sinh\{k/(2c)\}$ from equation 10.15 in here provides x_A. Then, z_A follows from x_A and equation 10.11. The coordinates of the suspension point, x_B and z_B, follow from those of the anchor point and equation 10.3.

$$\begin{aligned} x_A &= c \cdot \ln\left(\sqrt{\frac{L+h}{2\left(L-h\right)}}\right) - \frac{k}{2} & x_B &= x_A + k \\ z_A &= c \cdot \cosh\left(\frac{x_A}{c}\right) & z_B &= z_A + h \end{aligned} \qquad (10.18)$$

On a flat horizontal sea bed, the magnitude of x_A should always be positive. If from calculations follows that x_A is negative, the cable is lying on the sea bed. In this case the length of the free hanging part of the cable has to be determined by an iterative method until $x_A = 0$ has been reached. This point will become the new anchor point of the cable line. Then, the distance between the old and the new anchor point plus the length of the free hanging part of the cable is equal to the total length of the cable.

Finally, in any cross section of the cable, the forces are given by:

$$H = w \cdot c \qquad V = w \cdot s \qquad T = w \cdot z \qquad (10.19)$$

Then, the cable force components in the anchor point and the suspension point are:

$$\begin{aligned} H_A &= w \cdot c & H_B &= H_A \\ V_A &= w \cdot c \cdot \sinh\left(\frac{x_A}{c}\right) & V_B &= w \cdot c \cdot \sinh\left(\frac{x_B}{c}\right) \\ T_A &= \sqrt{H_A^2 + V_A^2} & T_B &= \sqrt{H_B^2 + V_B^2} \\ \phi_A &= \arctan\left\{\sinh\left(\frac{x_A}{c}\right)\right\} & \phi_B &= \arctan\left\{\sinh\left(\frac{x_B}{c}\right)\right\} \end{aligned} \qquad (10.20)$$

Elastic Cable Line

In the previous, the elongation of the cable due to the tension force in the cable has not been taken into account. For this, the cable characteristics have to be defined. These characteristics are given here by the following relation between the tension force, T, in the cable and the specific strain of the cable, ε:

$$\begin{aligned} T &< T_{lin}: & T &= \frac{(EA)^2}{4 \cdot T_{lin}} \cdot \varepsilon^2 \\ T &> T_{lin}: & T &= -T_{lin} + EA \cdot \varepsilon \end{aligned} \qquad (10.21)$$

with:

$$
\begin{array}{lll}
E & = & \text{elasticity modulus of the cable} \\
A & = & \text{cross sectional area of the cable} \\
\varepsilon = \Delta L / L & = & \text{specific strain of the cable} \\
T_{lin} & = & \text{tension force in the cable at the boundary between} \\
& & \text{the linear and the non-linear elasticity}
\end{array}
$$

These force-strain characteristics are shown in figure 10.3.
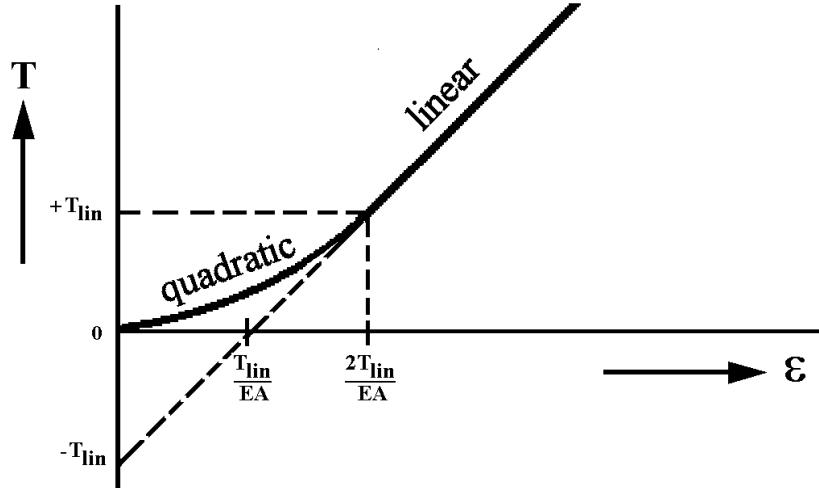
Figure 10.3: Cable Line Characteristics

Thus, $T_{lin} = 0$ provides the characteristics of a linear spring and a very large value of T_{lin} results in a quadratic force-strain relation. With these cable characteristics, the effect of an elongation of the cable can be taken into account.

The actual length of the cable is given by:

$$
L = L_0 + \Delta L_0 \tag{10.22}
$$

in which L_0 is the length of the not-loaded cable and ΔL_0 is the elongation due to the tension force in the cable.

First, the cable curve algorithms have to be solved for a cable length equal to the length of the not-loaded cable, so: $\Delta L_0 = 0$. This results in a known distribution of the tension forces $T(s)$ in the cable. With the cable characteristics, the distribution of the strain of the cable $\varepsilon(s)$ can be determined.

Then, the new total elongation follows from:

$$
\Delta L_0 = \int_0^L \varepsilon(s) \cdot ds \tag{10.23}
$$

This integration can be carried out numerically by dividing the cable length into n (for instance $n = 20$) line elements. The integration provides a new length L of the cable and the calculation procedure has to be repeated with this new length. A numerical procedure, such as a 'Regula Falsi' method, can be used to obtain a balance.

If a significant part of the cable is lying on the horizontal sea bed, then a certain friction of the cable over the sea bed can be taken into account.

Figure 10.4 shows an example of results of static catenary line calculations for an anchored platform. Figure 10.4-a shows the platform anchored by two anchor lines of chain at 100 m water depth. Figure 10.4-b shows the horizontal forces at the suspension points of both anchor lines as a function of the horizontal displacement of the platform. Finally, figure 10.4-c shows the relation between the total horizontal force on the platform and its horizontal displacement. This figure shows clearly the non-linear relation between the horizontal force on the platform and its horizontal displacement.
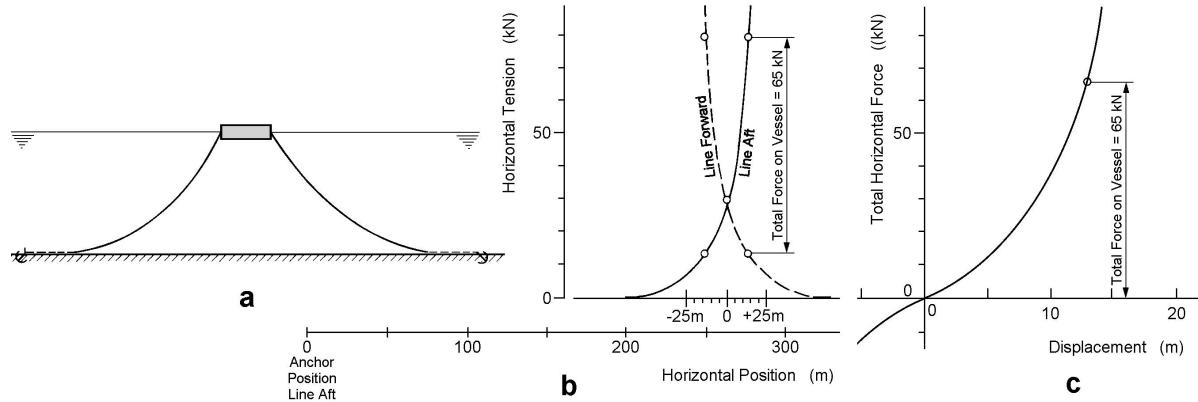
Figure 10.4: Horizontal Forces on a Platform as Function of its Horizontal Displacement

10.2.3   Dynamic Effects

In practical situations, the dynamic behavior of cable lines may contribute to the maximum tension significantly. Important parameters in this respect are the non-linear static load excursion, the low-frequency (pre-)tension and the amplitude and frequency of the exciting upper end oscillation. So far, the non-linear static load excursion has been accounted for but the dynamic behavior of the cable line has been ignored.

The prime dynamic tension increase, originated from the normal drag forces related to large global cable line motions at the middle sections. Long periods of slackness - even at low frequencies of oscillation - can occur due to 'flying' of the line under the influence of gravity and drag only. With increasing frequencies, the drag and the inertia equals the gravity forces resulting in an 'elevated equilibrium' of the line and the normal motions of the upper section of the line yields lower tension values. Inertia effects becomes of importance at higher frequencies, especially for steel wires and multi-component lines. Also, currents and waves will influence the hydrodynamic drag on the mooring lines.

Lumped Mass Method

[Van den Boom, 1985] describes a technique which implies that the behavior of a continuous line is modelled as a set of concentrated masses connected by massless springs. This involves the lumping of all effects of mass, external forces and internal reactions at a finite number of points along the line. By applying the equations of dynamic equilibrium (stress/strain) to each mass, a set of discrete equations of motion is derived. These equations may be solved in the time domain using finite difference techniques. Small effects of material damping, bending and torsional moments are ignored.
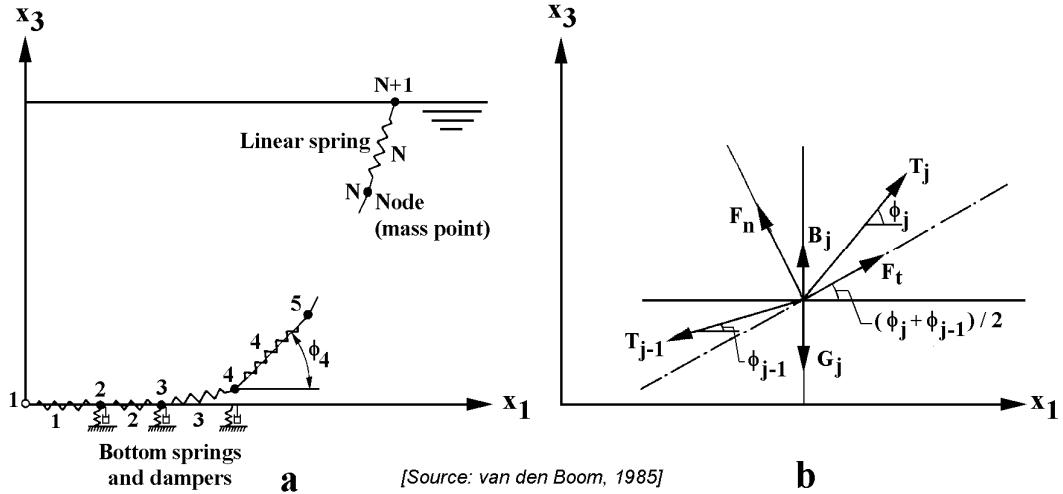
Figure 10.5: Discretization and Definitions for Lump Mass Method

Following the paper of [Van den Boom, 1985], the discretization of the mooring line can be obtained by lumping all forces to a finite number of nodes - so-called 'lumped masses' - as given in figure 10.5-a. The finite segments connecting the nodes are considered as massless springs accounting for the tangential elasticity of the line. The line is assumed to be fully flexible in bending directions. The hydrodynamic forces are defined in a local system of coordinates (tangential and normal direction) at each mass, as given in figure 10.5-b.

In order to derive the equations of motion of the j-th lumped mass, Newton's law is written in global coordinates:

$$([M_j] + [m_j(\tau)]) \cdot \ddot{\vec{x}}_j(\tau) = \vec{F}_j(\tau) \tag{10.24}$$

where $[M_j]$ is the inertia matrix, $[m_j(\tau)]$ is the hydrodynamic inertia matrix, τ is the time, $\vec{x}_j(\tau)$ is the displacement vector and $\vec{F}_j(\tau)$ is the external force vector.

The hydrodynamic inertia matrix, $[m_j(\tau)]$ can be obtained from the normal and tangential fluid forces by directional transformations:

$$[m_j(\tau)] = a_j^n \cdot [\Lambda_j^n(\tau)] + a_j^t \cdot [\Lambda_j^t(\tau)] \tag{10.25}$$

where a_j^n and a_j^t represent the normal (superscript n) and tangential (superscript t) hydrodynamic mass:

$$
\begin{aligned}
a_j^n &= \rho \cdot C_M^n \cdot \frac{\pi}{4} \cdot D_j^2 \cdot l_j \\
a_j^t &= \rho \cdot C_M^t \cdot \frac{\pi}{4} \cdot D_j^2 \cdot l_j
\end{aligned}
\tag{10.26}
$$

In here, C_M^n and C_M^t are the non-dimensional normal and tangential hydrodynamic mass coefficients.

$[\Lambda_j^n]$ and $[\Lambda_j^t]$ are directional matrices given below for the two-dimensional case:

$$[\Lambda_j^n] = \begin{pmatrix} \sin^2 \vec{\phi}_j & -\sin \vec{\phi}_j \cos \vec{\phi}_j \\ -\sin \vec{\phi}_j \cos \vec{\phi}_j & \cos^2 \vec{\phi}_j \end{pmatrix}$$

$$\left[\Lambda_j^t\right] \;\; = \;\; \begin{pmatrix} \cos^2 \vec{\phi}_j & \sin \vec{\phi}_j \cos \vec{\phi}_j \\ \sin \vec{\phi}_j \cos \vec{\phi}_j & \sin^2 \vec{\phi}_j \end{pmatrix}$$

$$\vec{\phi}_j \;\; = \;\; \frac{\vec{\phi}_j + \vec{\phi}_{j-1}}{2} \tag{10.27}$$

The nodal force vector, $\vec{F}$, contains contributions from the segment tension, T, the drag force, $\vec{F}_D$, buoyancy and weight, $\vec{F}_W$, and soil forces, $\vec{F}_S$:

$$\vec{F}_j(\tau) = T_j(\tau) \cdot \overrightarrow{\Delta x}_j(\tau) - T_{j-1}(\tau) \cdot \overrightarrow{\Delta x}_{j-1}(\tau) + \vec{F}_{D_j}(\tau) + \vec{F}_{W_j}(\tau) + \vec{F}_{S_j}(\tau) \tag{10.28}$$

where $\overrightarrow{\Delta x}_j(\tau)$ is the segment basis vector $(\vec{x}_{j+1} - \vec{x}_j)/l_j$, in which l_j is the original segment length.

The drag force, $\vec{F}_D$, (see chapter 4) may be derived from the normal and tangential force components:

$$\vec{F}_{D_j}(\tau) \;\; = \;\; [\ (\tau)] \cdot \vec{f}_{D_j}(\tau)$$

$$f_{D_j}^n(\tau) \;\; = \;\; \frac{1}{2}\rho \cdot C_D^n \cdot D_j \cdot l_j \cdot u_j^n(\tau) \cdot \left|u_j^n(\tau)\right|$$

$$f_{D_j}^t(\tau) \;\; = \;\; \frac{1}{2}\rho \cdot C_D^t \cdot D_j \cdot l_j \cdot u_j^t(\tau) \cdot \left|u_j^t(\tau)\right|$$

$$\vec{u}_j(\tau) \;\; = \;\; [\Gamma_j(\tau)] \cdot \left(c_j - \dot{\vec{x}}_j(\tau)\right) \tag{10.29}$$

where

$\vec{f}_{D_j}$	$=$	drag force in local coordinates
$\vec{u}_j$	$=$	relative fluid velocity in local coordinates
c_j	$=$	current vector in global coordinates
ρ	$=$	fluid density
D	$=$	characteristic segment diameter
l	$=$	segment length
C_D	$=$	non-linear (quadratic) 2-D damping (or drag) coefficient
C_D^n	$=$	normal drag coefficient
C_D^t	$=$	tangential drag coefficient

The directional matrices $[\ _j(\tau)]$ and $[\Gamma_j(\tau)]$ are used to transform the global drag forces and velocities into local drag forces and velocities:

$$[\ _j] = [\Gamma_j] = \begin{pmatrix} -\sin\vec{\phi}_j & \cos\vec{\phi}_j \\ \cos\vec{\phi}_j & \sin\vec{\phi}_j \end{pmatrix} \tag{10.30}$$

C_M is a 2-D non-dimensional hydrodynamic mass coefficient. The 2-D quadratic drag coefficient C_D has been discussed in chapter 4. The hydrodynamic mass and drag coefficients C_M and C_D - as they are used in the so-called Morison equations - will be discussed in more detail in chapter 12.

[Van den Boom, 1985] has derived the fluid reactive force coefficients a^n, a^t, C_D^n and C_D^t from forced oscillation tests and free hanging tension tests with model chain and wire

sections. A volumetric diameter, defined by $d_c = 2\sqrt{\nabla/\pi l}$ (with ∇ is segment volume and l is segment length), proved to be an accurate parameter in the dimensionless hydrodynamic coefficients. From the model tests it was concluded that frequency-independent coefficients can be used for normal mooring chains and wires.

Dynamic sea bed reaction forces do not affect the behavior of the line and can be modelled as critical damped springs to prevent numerical instabilities. Tangential soil friction forces may be of importance when the line part on the bottom is extremely long and transverse soil reactive forces may be of importance for 3-D problems. Both soil effects are neglected here, thus the vertical force component, F_{S3_j}, equals:

$$
\begin{aligned}
F_{S3_j} &= -b_j \cdot \dot{x}_{3_j} - c_j \cdot x_{3_j} & \text{for: } x_{3_j} < 0 \\
F_{S3_j} &= 0 & \text{for: } x_{3_j} > 0
\end{aligned}
\tag{10.31}
$$

The time domain relations between nodal displacements, velocities and accelerations are approximated by finite difference methods such as the Houbolt scheme which is described by [Bathe and Wilson, 1976]:

$$
\begin{aligned}
\dot{\vec{x}}_j(\tau + \Delta\tau) &= \frac{1}{6\Delta\tau} \cdot \{11\vec{x}_j(\tau + \Delta\tau) - 18\vec{x}_j(\tau) + 9\vec{x}_j(\tau - \Delta\tau) + 2\vec{x}_j(\tau - 2\Delta\tau)\} \\
\ddot{\vec{x}}_j(\tau + \Delta\tau) &= \frac{1}{\Delta\tau^2} \cdot \{2\vec{x}_j(\tau + \Delta\tau) - 5\vec{x}_j(\tau) + 4\vec{x}_j(\tau - \Delta\tau) - \vec{x}_j(\tau - 2\Delta\tau)\}
\end{aligned}
$$

or:

$$
\vec{x}_j(\tau + \Delta\tau) = \frac{5}{2}\vec{x}_j(\tau) - 2\vec{x}_j(\tau - \Delta\tau) + \frac{1}{2}\vec{x}_j(\tau - 2\Delta\tau) + \frac{1}{2}\Delta\tau^2\, \ddot{\vec{x}}_j(\tau + \Delta\tau)
\tag{10.32}
$$

The segment tension $T_j(\tau + \Delta\tau)$ is derived from the node positions by a Newton-Raphson iteration using the additional equation for the constitutive stress-strain relation:

$$
\vec{\psi}_j(\tau) = l_j^2 \cdot \left\{ \overrightarrow{\Delta x}_j(\tau) - \left(1 + \frac{T_j(\tau)}{E_j \cdot A_j}\right)^2 \right\}
\tag{10.33}
$$

$$
\vec{T}^{k+1}(\tau + \Delta\tau) = \vec{T}^k(\tau + \Delta\tau) - \left[\Delta\psi^k(\tau)\right]^{-1} \cdot \vec{\psi}^k(\tau)
\tag{10.34}
$$

where $\vec{\psi} = (\psi_1, ..., \psi_j, ..., \psi_N)$ is segment length error vector, $\vec{T}^k = (T_1, ..., T_j, ..., T_N)$ is tentative segment tension vector at the k-th iteration and $\Delta\psi = \partial\psi/\partial T$ is the length error derivative matrix obtained from equations 10.32 and 10.33.

For each time step the system of equation 10.34 should be solved until acceptable convergence of $T^k(\tau + \Delta\tau)$ is obtained. The initial tentative tension can be taken equal to the tension in the previous step. Each node j is connected to the adjacent nodes $j - 1$ and $j + 1$, hence equation 10.34 represents a three-diagonal ($N \times 3$) system. Such equations may be efficiently solved by the so-called Thomas algorithm.

[Van den Boom, 1985] claims that - certainly for engineering applications - the Lumped Mass Method (LMM) does provide efficient and accurate predictions of dynamic line motions and tensions.

10.2.4   Experimental Results

[Kwan, 1990] checked results of calculations in the time domain - which include dynamic effects - against results of measurements. First, he carried out model tests. Then, - to eliminate potential questions about the scale effects of model tests - a full scale measurement was carried out in 1984 on a drill ship.. Some of his results are shown in figure 10.6.
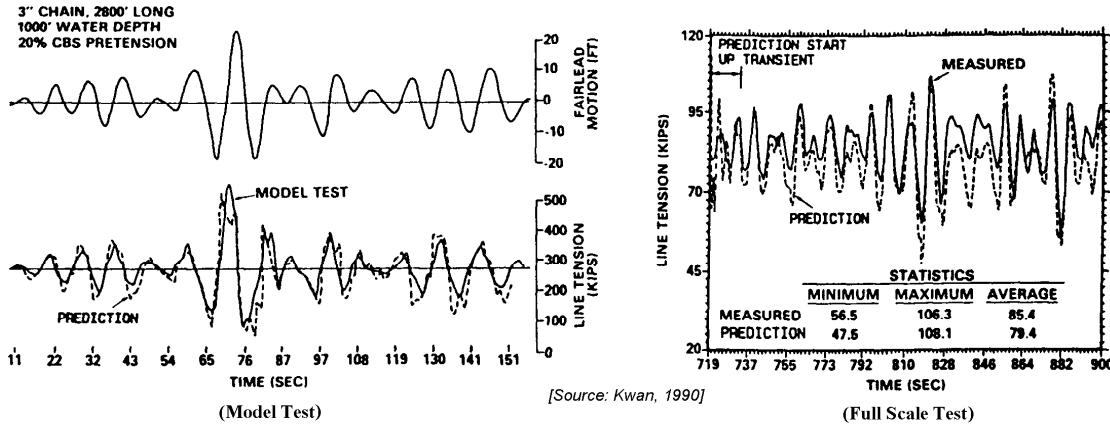
Figure 10.6: Comparison of Predicted and Measured Line Tensions

[Kwan, 1990] concluded that - in general - the predicted line tensions compare well with the model test and full scale measurement results.

10.2.5   Suspension Point Loads

Now, the components of the cable forces in the suspension point, B, in the vertical plane through the cable line are known; they can be derived in the earth-bound (X_1, X_2, X_3)-system of axes by:

$$
\begin{aligned}
T_{X_{1B}} &= +T_B \cdot \cos\phi_B \cdot \cos\alpha \\
T_{X_{2B}} &= +T_B \cdot \cos\phi_B \cdot \sin\alpha \\
T_{X_{3B}} &= -T_B \cdot \sin\phi_B
\end{aligned}
\tag{10.35}
$$

where T_B, ϕ_B and α are defined in figure 10.1.

The angle of the cable forces in the horizontal plane in the (X_1, X_2, X_3)-system of axes is given by:

$$
\alpha = \arctan\left\{\frac{X_{3B} - X_{3A}}{X_{1B} - X_{1A}}\right\} \qquad \text{with: } 0 \leqslant \alpha \leqslant 2\pi
\tag{10.36}
$$

Then, the forces and moments on the structure in the steadily translating axes system G-(x_1, x_2, x_3) are:

$$
\begin{aligned}
F_{x_{1CABLE}} &= +T_{X_{1B}} \cdot \cos x_6 + T_{X_{2B}} \cdot \sin x_6 \\
F_{x_{2CABLE}} &= -T_{X_{1B}} \cdot \sin x_6 + T_{X_{2B}} \cdot \cos x_6 \\
F_{x_{3CABLE}} &= +T_{X_{3B}} \\
F_{x_{4CABLE}} &= +T_{X_{2B}} \cdot (X_{3B} - X_{3G}) + T_{X_{3B}} \cdot (X_{2B} - X_{2G}) \\
F_{x_{5CABLE}} &= +T_{X_{1B}} \cdot (X_{3B} - X_{3G}) - T_{X_{3B}} \cdot (X_{1B} - X_{1G}) \\
F_{x_{6CABLE}} &= -T_{X_{3B}} \cdot (X_{2B} - X_{2G}) + T_{X_{2B}} \cdot (X_{1B} - X_{1G})
\end{aligned}
\tag{10.37}
$$

10.3 Thrusters

Thrusters may be used - in combination with a mooring system or alone - to keep the vessel in its desired position.

10.3.1 Characteristics

From open water propeller tests - see chapter 4 - with fixed pitch propellers (FPP) and controllable pitch propellers (CPP), one can get a first estimate of the thruster characteristics. An FPP prevails, from an energy efficiency point of view. An example of the difference in power consumption of an FPP versus a CPP is shown in figure 10.7.
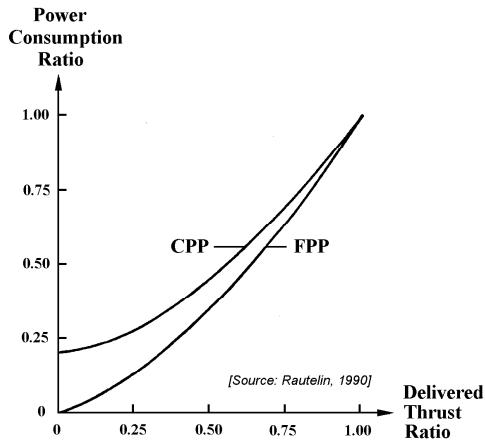
Figure 10.7: Power Consumption of FPP Versus CPP

In typical marine applications, there is always first the question of whether to use direct drive by diesel engine or an electrical drive but in offshore DP applications the diesel drive is rarely considered. For electrical drive, the three main solutions are:
- a constant speed AC motor drive (1- or 2-speed), which requires a CPP,
- a variable speed DC motor drive, which works with an FPP and
- a variable speed frequency converter and AC motor drive, with an FPP.
It derives from the CPP curve that there is a need to improve the efficiency of the thruster performance at part loads from that of a single speed drive. The 2-speed drive already looks much better - on paper - but due to its limited thrust developing capacity at the lower speed, the higher speed tends to be used more for safety's sake in practise. So that, when the energy efficiency at typical DP load area is of prime importance, variable speed (rpm) with an FPP is the ideal solution. This requirement has been mostly met by DC drives so far.
To make an AC motor speed variable, the supply frequency to the motor must be varied, hence the name of the frequency converter. There are basically three types of converters (see figure 10.8):
- the current source converter, which supplies current from the DC link in step form,
- the voltage source, which supplies stepped voltage and
- the pulse width modulated (PMW) type, which simulates the output waveform by supplying a number of pulses of varying width.
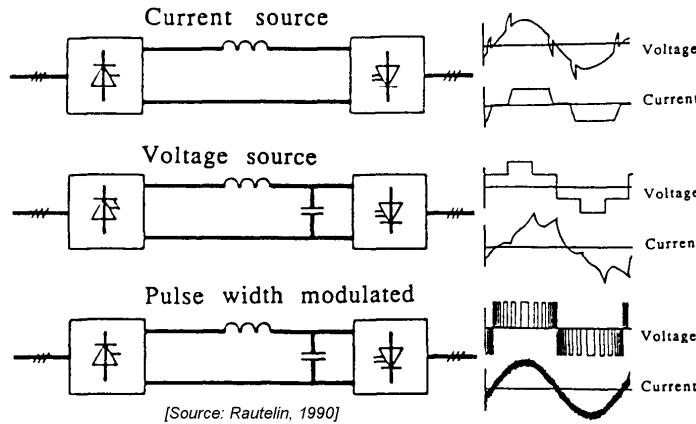
Figure 10.8: Frequency Converter Principles

Frequency converter drives are good solutions for industrial variable speed drives. Pipelaying vessel 'Lorelay' - operated since 1986 by Allseas Marine Contractors S.A. - was the first DP offshore vessel fully designed around AC variable speed FPP propulsion and thruster drives of PMW type. These drives may offer in many ways a solution which can improve the performance of station keeping and the drive system reliability.

10.3.2   Loss of Efficiency

A thruster in isolation will lose efficiency due to an interaction the hull and by the presence of current and waves. Also thruster-thruster interaction can play a significant role.

Coanda Effect

An important thruster-hull interaction effect is the **Coanda effect**. This phenomenon and its effect on the efficiency of the thruster is clearly explained by [Faltinsen, 1990] as follows.
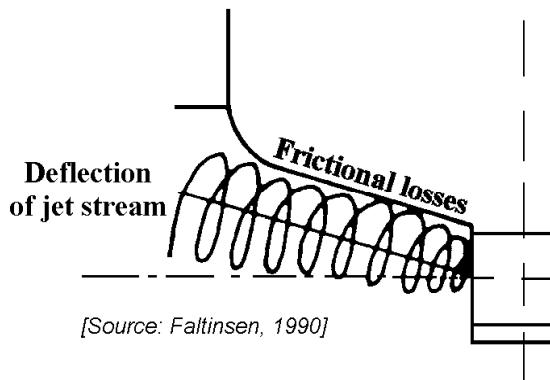
Figure 10.9: Coanda Effect of a Stern Skeg Tunnel Thruster

The thruster slip stream will be attracted by the hull - as shown in figure 10.9 - with loss of thrust as a consequence. This propeller slip stream can be represented by a circular jet, which acts like a line of sinks This means that water is entrained in the jet from
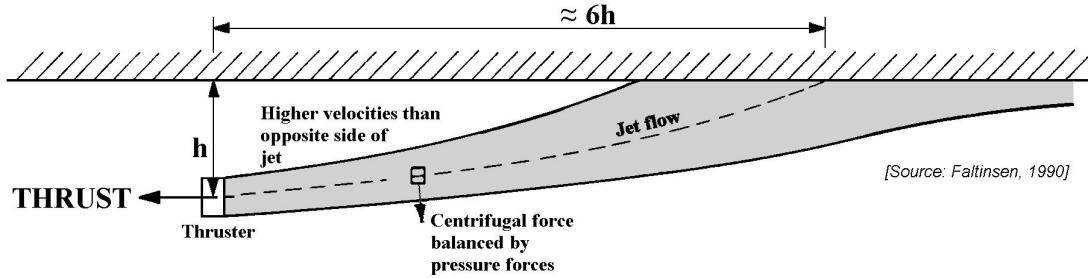
Figure 10.10: Coanda Effect in a Propeller Slip Stream

outside the jet. If the boundary had not been there, the entrained velocity would have been directed radially toward the center of the jet; the entrained velocity is only a function of the radius. If a boundary is present, the velocity will be at a maximum between the jet and the boundary. High velocity means low pressure. This means a pressure difference across the jet with a resultant force towards the boundary. This force will attract the jet towards the wall. The attraction force has to be in balance with the centrifugal force of the jet flow and this balance determines the position of the jet relative to the wall. This principle is shown in figure 10.10.

For a thin jet - initially at a distance h from an infinitely long parallel wall - it takes roughly $6h$ to hit the wall. This information can be used as a rough tool for avoiding the propeller slip stream coming into contact with the hull.

However, one should realize that this approximation of the propeller slip stream by a thin jet is a strong idealization. The jet must have a radius comparable to the propeller radius. Close to the propeller the flow is not jet-like. It actually takes a distance from the thruster of about $6D$ (6 times the diameter of the propeller) before the propeller slip stream develops into a fully turbulent jet-like flow. The jet will spread as a function of the distance from the thruster. If we consider a free jet - so a jet not in presence of a boundary - the points in a jet where the velocity is half the maximum velocity will spread with an angle of about $5°$. This spreading may cause the propeller slip stream to be in contact with the hull before the above attraction effect has fully developed. When the propeller stream clings to the hull, it behaves like a wall jet. The wall jet may very well separate from the hull again. This depends on the local radius of curvature of the hull. If a sharp corner is present the propeller stream will separate and there will be no significant thrust loss.

It is to difficult to estimate theoretically what the loss due to the Coanda effect is. According to [Faltinsen, 1990], limited full scale experience from a supply ship indicates that the Coanda effect may cause a 30-40 % loss of thrust for a given power. In that case the propeller stream followed the ship hull all the way up to the free surface. If the propeller stream had been separated from some point on the hull surface, it is expected that this would have caused a smaller loss.

For semi-submersibles, the Coanda effect for a thruster on one pontoon, may cause the propeller stream to hit another pontoon. The loss due to this can roughly be estimated by considering the propeller stream to be an incident current on the other pontoon.

Another case for a semi-submersible would be if the thruster is aligned longitudinally along the pontoon. Due to the long distance, the propeller slip stream is likely to be completely attracted to the pontoon. The boundary flow between the wall jet and the pontoon will cause shear forces. According to [Faltinsen, 1990], this may amount to 10-15 % loss of

power.

A practical solution to avoid the Coanda effect can be found in tilting the thruster nozzle over about 5 degrees in a downwards direction. Then, the propeller slip stream will not be attracted by the hull in that amount and - in the case of a semi-submersible- hitting the other pontoon by the propeller slip stream can be avoided. As a consequence of this, a decrease of the loss of thrust for a given power can be expected.

Thruster-Thruster Interaction

For vessels where it is impossible to avoid placing the thrusters where the inflow and outflow fields may interfere, physical model tests are the only reliable way to define the effects. [English and Wilde, 1976] describe a series of experiments wherein thruster interaction effects were derived from physical model tests.

In some cases, tilting the thruster nozzle over about 5 degrees in a downwards direction can avoid or decrease thruster-truster interaction.

Current Effects

For tunnel thrusters, the thruster forces are affected by the flow of a current past the inlet and outlet. The loss of thrust is caused by deflection of the jet stream and by interactions between the jet stream and the hull which give rise to suction forces on the tunnel outlet of the vessel.

[Chislett and Bjorheden, 1966] studied the influence of forward speed of a 232 meter length ship on the effectiveness of a lateral-thrust device in turning the hull, which appeared to be of considerable magnitude. They showed results of model experiments on the percentage lost of side force and yaw moment of the thruster as a function of the velocity ratio: the forward ship speed - thruster jet speed ratio.

The thruster jet speed, V_{jet}, has been evaluated by the conservation of momentum in the fluid:

$$T_{\text{jet}} = \rho V_{\text{jet}}^2 \cdot \frac{\pi}{4} D_{\text{jet}}^2 \qquad \text{or:} \qquad V_{\text{jet}} = \sqrt{\frac{T_{\text{jet}}}{\rho \cdot \frac{\pi}{4} D_{\text{jet}}^2}} \qquad (10.38)$$

where the thrust, T_{jet}, is that measured at zero forward speed. With known diameter, D_{jet}, this equation provides the jet speed, V_{jet}. This jet exit velocity was assumed to be independent of the forward ship speed; an assumption supported by additional torque measurements.

The measured forces, Y, and moments, N, on the ship are made dimensionless the jet exit velocity too:

$$Y' = \frac{Y}{\rho V_{\text{jet}}^2 \cdot \frac{\pi}{4} D_{\text{jet}}^2} \qquad \text{and} \qquad N' = \frac{N}{\rho V_{\text{jet}}^2 \cdot \frac{\pi}{4} D_{\text{jet}}^2 \cdot x_T} \qquad (10.39)$$

where x_T is the distance of the tunnel center from amidships.

Figure 10.11-a and 10.11-b and presents, for a number of propeller rates, these non-dimensional loads on the ship as a function of the velocity ratio.

Figure 10.11-a provides the loss of efficiency of the thruster due to the forward ship speed. At ship speeds less than about 3 knots, the lever arm of the moment, calculated from N/Y, appeared to be similar to x_T. At higher speeds this value increases, so the estimated
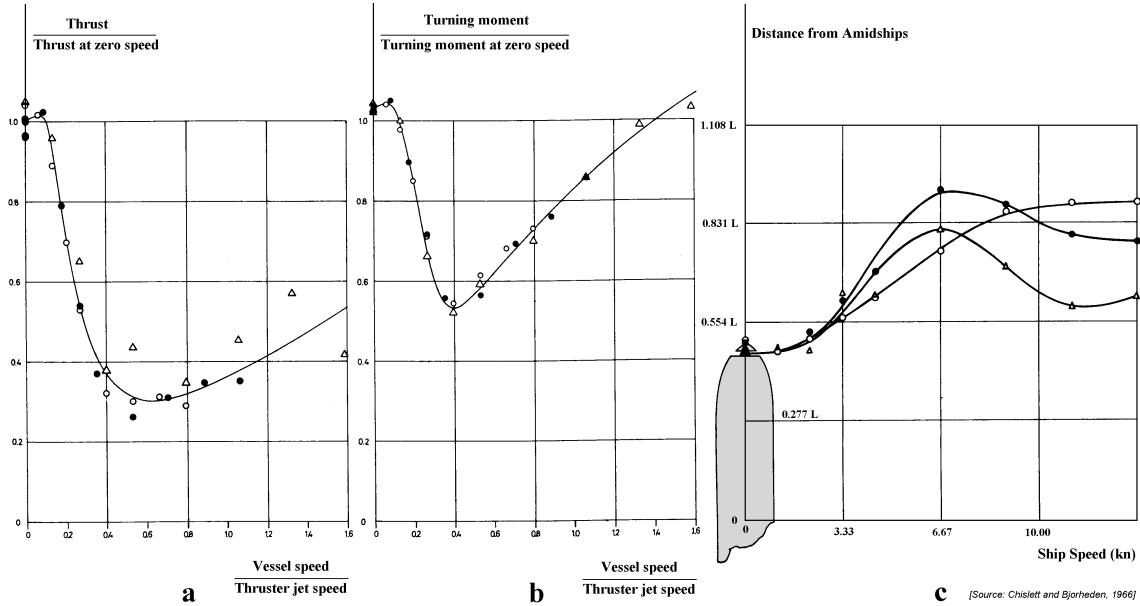
Figure 10.11: Effect of Forward Ship Speed on Bow Thruster Performance

moment will be conservative when using the measured forces from figure 10.11-a and x_T as the lever arm, see figure 10.11-c.

[Faltinsen, 1990] used these thrust reduction results of [Chislett and Bjorheden, 1966] to estimate the loss of efficiency of thrusters by currents. Together with the current velocity, figure 10.11-a provides the loss of efficiency of the thruster due to a current and the moment can be found with the lever arm x_T.

It has been found by [Edwards, 1985] that thrusters and particularly main propulsion units in the vicinity of the after body can create markedly different reaction forces and moments on vessels at oblique angles, particularly at high current speeds.
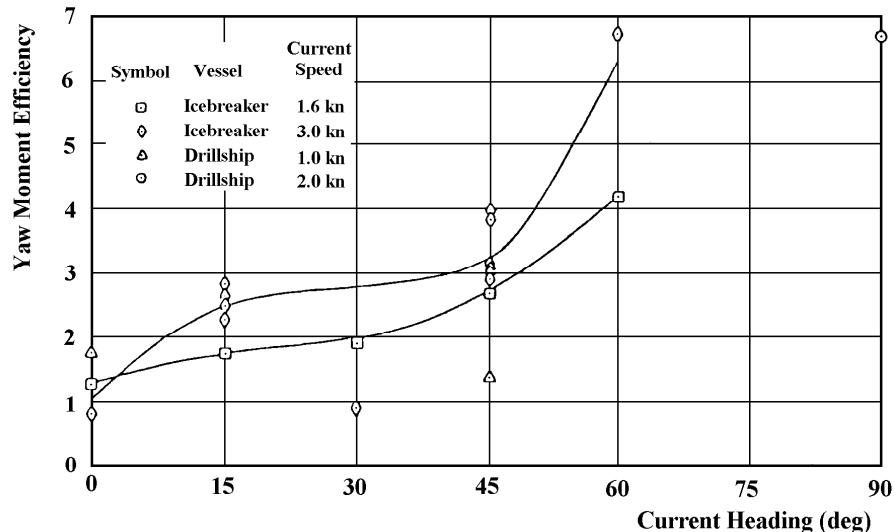
Figure 10.12: Starboard Main Propulsion Unit Yaw Moment Efficiency

This is illustrated in figure 10.12, where the effectiveness of a single main propulsion unit in producing yaw moment is plotted versus heading with respect to current direction. An effectiveness of 1.0 indicates a measured reaction moment equivalent to the calculated thrust times the moment arm, taking into account the observed advance ratio. It can be seen that the measured reaction moment is many times the ideal value. In essence the propeller operation has drastically changed the pressure distribution around the vessel, aligned obliquely to the flow from that with no propeller in operation. To a lower extent, this may be seen for through-hull thrusters placed at the extremity of the vessel. The only way to asses effects such as this is with physical model tests.

Wave Effects

[Minsaas et al., 1986] have argued that a similar effect to this must be present in waves. They did experiments with a fictitious bow thruster system in head waves. The ship sides were simulated by vertical plates parallel to the incident regular waves. The whole system was restrained from oscillating.

As treated in chapter 5, the wave velocity amplitude, V_p, at the propeller centre ($z = -h_p$) can be written as:

$$V_p = \zeta_a \omega \cdot e^{-kh_p} \tag{10.40}$$

By interpreting V_p as a current velocity they were able to predict trends in their experimental results. If a ship is moving in waves the problem becomes more complicated. The velocity across the propeller jet at the tunnel entrance is no longer V_p. This problem requires further research.

The presence of waves causes - even for a thruster with a constant propeller pitch or propeller speed setting - oscillating thrust and torque performances. Similar effects appear in the case of vertical and horizontal oscillations of the ship itself.

Free Surface Effects

When a thruster comes close to the free surface other problems appear. Depending on the thruster loading this may cause air ventilation with a serious loss of propeller thrust and torque.

Tests in still water were performed by [Minsaas et al., 1986], in order to study the effects of waves based on a quasi-steady assumption. As long as the thruster is not ventilating, this is legitimate, since the wave-induced motions occur with a much lower frequency than the propeller rotation. However, when the propeller is in a transient ventilating condition, there is also a frequency connected with the development of the ventilated area on the propeller blades. this wave-induced effect can not be simulated by means of results in calm water.

The tests in calm water were performed with different propeller axis submerges, h_p, relative to the free surface. By the quasi-steady assumption one can interpret h_p as the submergence of the instantaneous position of the wave surface, see figure 10.13. By averaging the propeller thrust and torque in time one can find the effect of the wave induced motions of the ship on the thruster characteristics.
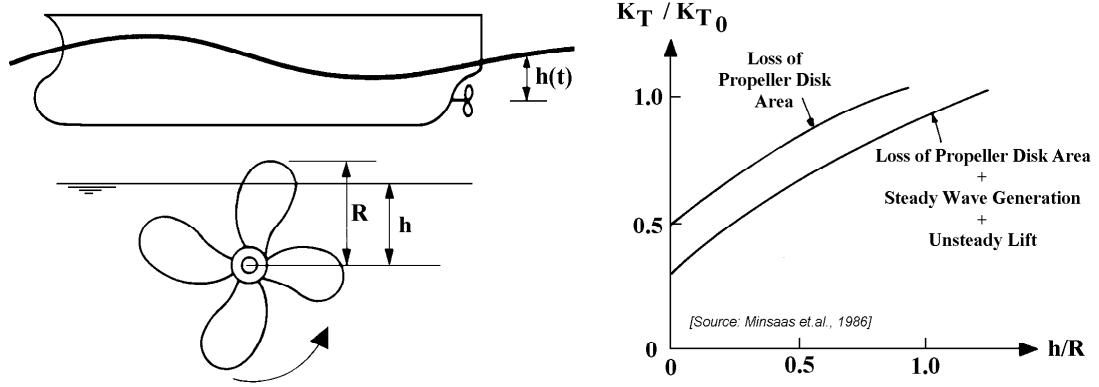
Figure 10.13: Effect of Waves on a Propeller, a Quasi-Steady Approximation
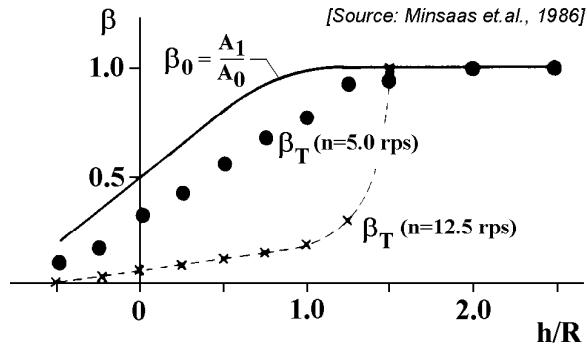
Figure 10.14: Lost of Thrust due to Bow Immersion in Calm Water

Typical model test results from calm water are shown in figure 10.14 where thrust is presented as a fraction of the thrust for a fully immersed propeller, $\beta_T = K_{T_{h/R}}/K_{T_0}$, and for different number of revolutions, n.

It is observed that the number of revolutions has a marked influence on the results. The effect of loss of effective propeller area is important. When $h/R < 1.0$ the ratio of the immersed disk area, A_1, and the total disk area, A_0, of the propeller is $\beta_0 = A_1/A_0$. If we assume that the thrust is proportional to A_1, β_0 gives the thrust reduction for small n-values as illustrated in figure 10.14. For large n-values we see that the thrust is very low for the small h/R-values. This is due to propeller ventilation. Qualitatively it can be explained as follows. Increased n means increased loading. This means large suction pressures on the propeller. The lower pressure is, the more likely it is that ventilation occurs. For $h/R = 1.0$-1.5 there is a very rapid variation in thrust. This is when ventilation starts. The behavior of β in waves is not quasi-steady when the propeller is in a transient ventilating state. The maximum thrust is reached later in time than maximum immersion. In most cases maximum thrust never reaches the same thrust value as when the propeller was fully immersed in static conditions.

[Minsaas et al., 1986] have tried to apply their experimental results for a ducted propeller and bow thruster in regular waves to thrust loss for different ships and sea states. An example for a 250 meter long ship is presented in figure 10.15.

The results will depend on propeller shaft submergence, h, propeller diameter, D, propeller
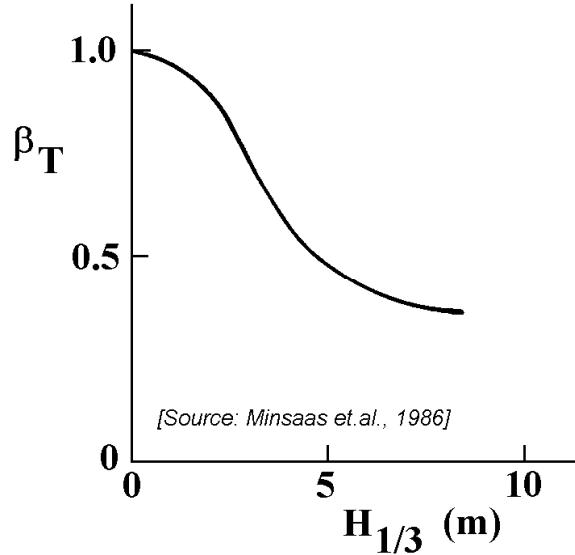
Figure 10.15: Thrust Reduction in Head Waves

pitch, propeller revolution, n, and hull form. The results in figure 10.15 show that even a large ship experiences considerable thrust losses in rough seas.

10.4   Dynamic Positioning

The 'Eureka' was the world's first automatically controlled dynamically positioned vessel. This semi-submersible was built by Shell Oil Company for exploration core drilling and began operation in the spring of 1961. With one thruster power for each of its 400 tons of displacement, it was very successful in taking cores up to 150 m in the sea floor. Averaging over two locations per day, it drilled as many as nine in a single day in water depths out to 1200 m. Comparably sized anchored vessels at the time could get one location in two to four days and were limited to only about 100 m of water.

Since this first operation of a dynamic position system, they have come a long way. Much larger thrusters are stationing much larger vessels in much deeper water. Taut wire position measurements has been given way to satellite positioning by Global Positioning Systems (GPS). The old single-thread analog systems are gone and the digital computers are provided in dual and now triple redundancy. Failure rates have gone from several per month and over 20 percent downtime in the first year to a present day Mean Time Between Failure (MTBF) of about three years for the best systems.

Development of a successful dynamic positioning system requires a means of checking out the performance of the entire system from the controls to the reaction of the vessel to the environmental and thruster forces on the hull. A complete simulation will yield the performance of the system by means of mathematical analysis before any hardware has been acquired. Then by means of the detailed system simulator, one can vary parameters on the control of the system, hardware characteristics, propeller design or even hull design to obtain the desired performance in the changing environment and also in response to sudden failure of a component of the system.

10.4.1 Control Systems

The brain of the dynamically positioned system is the **controller**. Basically, it measures the position of the vessel with respect to the intended position and directs power to the various thrusters to correct any position error.

In its simplest form, the controller will call for thrust in the direct opposite to the position error. Without some modulation of the thrust and provisioning of a 'dead band', the system would continually overshoot. Probably the simplest practical system consists of thrust and moment commands **proportional (P)** to the amount of position and heading error:

$$\vec{T} = f\ (X_1, X_2, X_6) \quad \text{(P-controller)} \tag{10.41}$$

The axes system is given in figure 10.16, with the origin, S, of the earth-bound axes system in the still water surface. Notify the right-handed axes system here, with the vertical axis, X_3, positive downwards, as it is often used by manoeuvreing researchers.
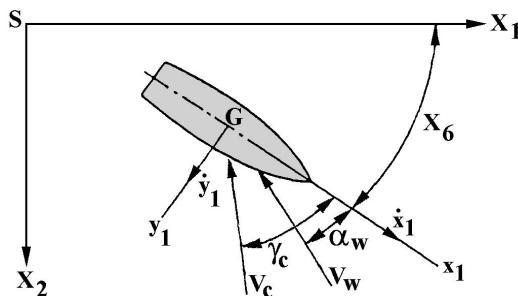
Figure 10.16: Dynamic Positioning Axes System

Even this simple controller needs one more level of complexity. In the event the thruster system is saturated, the controller must assign priority to heading control or position control. Usually heading priority is called for since the proper heading will minimize the relevant motions and thus the translational thrust requirements.

Using successive positioning error signals, one can determine the step-wise velocity of the vessel. System performance is greatly improved by adding velocity terms, the **derivative (D)** of the excursion, to the thrust equations:

$$\vec{T} = f\ \left(X_1, X_2, X_6,\ \dot{X}_1, \dot{X}_2, \dot{X}_6 \right) \quad \text{(PD-controller)} \tag{10.42}$$

Finally in order to bring the vessel back to the zero position, the thrust must take into account the time over which external forces have been acted. A term is added to; the **integral (I)** of the excursion with time:

$$\vec{T} = f\ \left(X_1, X_2, X_6,\ \int (X_1, X_2, X_6)\, dt,\ \dot{X}_1, \dot{X}_2, \dot{X}_6 \right) \quad \text{(PID-controller)}$$

The foregoing systems are all **feed-back** systems. A further refinement in performance can be achieved by adding a predictive or feed-forward component. This is particularly vital where significant time delays may be encountered. Examples of time delays are diesel-generator set power build-up, or even starting an additional thruster. The **feed-forward** elements may be wind velocity, V_w, and direction, α_w:

$$\vec{T} = f\left(X_1, X_2, X_6, \int (X_1, X_2, X_6)\, dt,\, \dot{X}_1, \dot{X}_2, \dot{X}_6,\, V_w, \alpha_w\right)$$

(PID-controller with

wind-feed-forward)

(10.43)

[Pinkster, 1978] suggested to extend the wind-feed-forward system with an intriguing wave-feed-forward system. He carried out model experiments in bow-quartering irregular waves ($H_{1/3} = 4.9$ m and $T_2 = 10.2$ s) and a stern-quartering current (1 knot). The wave-feed-forward system consisted of 8 ship-mounted wave probes. He showed that a wave-feed-forward system is capable to reduce the low-frequency part of the sway motion by about 70 % and the surge motion by about 50 %. The DP simulation procedure can be extended to include this factor, but the value of the simulation would depend primarily on the degree to which the simulated wave data represents possible actual wave measurements. So far, wave-feed-forward has not yet been incorporated in DP simulations.

The possibilities for evaluating the generalized function of eleven variables in equation 10.43 are limitless, hence the need for mathematical simulation.

10.4.2   Mathematical Model

For a dynamically positioned floating structure, only the horizontal low-frequency motions for surge ($k = 1$), sway ($k = 2$) and yaw ($k = 6$) are of interest. The thruster forces have to balance the mean wave, current and wind loads. Further, $\ddot{x}_k$, $\dot{x}_k$ and x_k are the slowly varying motions of the structure. It are the high-frequency motions of the waves that are neglected or filtered out, because it is generally impossible to have a system that can react to these high-frequency wave forces.

A general form of the three nonlinear coupled (Euler) equations of motion in the horizontal plane for surge, sway and yaw of a DP vessel - with an axes system as given in figure 10.16 - is given by:

$$(\rho\nabla + a_{11})\cdot \ddot{x}_1(t) + b_{11}\cdot \dot{x}_1(t) + b_1^V \cdot \dot{x}_1(t)\cdot |\dot{x}_1(t)| - (\rho\nabla + a_{22})\cdot \dot{x}_2(t)\cdot \dot{x}_6(t) =$$
$$= F_1^W(t) + F_1^C(t) + F_1^{WD}(t) + F_1^R(t) + T_1(t)$$

$$(\rho\nabla + a_{22})\cdot \ddot{x}_2(t) + b_{22}\cdot \dot{x}_2(t) + b_2^V \cdot \dot{x}_2(t)\cdot |\dot{x}_2(t)| + (\rho\nabla + a_{11})\cdot \dot{x}_1(t)\cdot \dot{x}_6(t) =$$
$$= F_2^W(t) + F_2^C(t) + F_2^{WD}(t) + F_2^R(t) + T_2(t)$$

$$(I_{66} + a_{66})\cdot \ddot{x}_6(t) + b_{66}\cdot \dot{x}_6(t) + b_6^V \cdot \dot{x}_6(t)\cdot |\dot{x}_6(t)| - (a_{11} - a_{22})\cdot \dot{x}_1(t)\cdot \dot{x}_2(t) =$$
$$= F_6^W(t) + F_6^C(t) + F_6^{WD}(t) + F_6^R(t) + T_6(t)$$

(10.44)

where $\rho\nabla$ is the solid mass of the ship, I_{66} is the mass moment of inertia of the ship, a_{kk} is the hydrodynamic mass or inertia, b_{kk} is the hydrodynamic damping coefficient, b_k^V is the quadratic viscous drag force or moment coefficient, F_k^W is the wind force or moment, F_k^C is the current force or moment F_k^{WD} is the slow-drift wave excitation force or moment, $F_k^R(t)$ is the force or moment due to the riser and T_k is the thruster force or moment.

Notice the appearance here of a sway-yaw velocity coupling term in the surge equation, a surge-yaw velocity coupling term in the sway equation and a surge-sway velocity coupling term in the yaw equation. These three mass terms follow from a proper derivation of the nonlinear Euler equations of motion in the horizontal plane, which has been treated plentiful in the literature on manoeuvering, guidance and control of ships; for instance [Fossen, 1994].

The relative water velocity and direction - see figure 10.16 - are:

$$
\begin{aligned}
V_{C_R} &= \sqrt{(\dot{x}_1 + V_C \cos\gamma_C)^2 + (\dot{x}_2 + V_C \sin\gamma_C)^2} \\
\gamma_{C_R} &= \arctan\left(\frac{\dot{x}_2 + V_C \sin\gamma_C}{\dot{x}_1 + V_C \cos\gamma_C}\right)
\end{aligned}
\tag{10.45}
$$

Then the current forces and moments can be obtained by:

$$
F_k^C = R_k'\left(\gamma_{C_R}\right) \cdot V_{C_R}^2 \qquad \text{for}: \ k = 1, 2, 6
\tag{10.46}
$$

where $R_k'\left(\gamma_{C_R}\right)$ is the resistance coefficient in the x_k-direction due to the relative water velocity in the γ_{C_R}-direction.

The vessel velocities along the fixed (global) axes (X_1, X_2) are related to the velocities along the local axes by the following transformation relations:

$$
\begin{aligned}
\dot{X}_1 &= \dot{x}_1 \cos x_6 - \dot{x}_2 \sin x_6 \\
\dot{X}_2 &= \dot{x}_2 \sin x_6 + \dot{x}_2 \cos x_6 \\
\dot{X}_6 &= \dot{x}_6
\end{aligned}
\tag{10.47}
$$

In addition, the excursions in surge sway and yaw are obtained from:

$$
X_1 = \int \dot{X}_1 \cdot dt \qquad X_2 = \int \dot{X}_2 \cdot dt \qquad X_6 = \int \dot{X}_6 \cdot dt
\tag{10.48}
$$

The first-order differential equations governing thrust build-up with time of a DP system with a PID-controller can be written in the form:

$$
\begin{aligned}
T_1 + \tau_1 \cdot \frac{dT_1}{dt} &= -K_1^P \cdot X_1 - K_1^I \cdot \int_0^t X_1 \cdot dt - K_1^D \cdot \dot{X}_1 \\
T_2 + \tau_2 \cdot \frac{dT_2}{dt} &= -K_2^P \cdot X_2 - K_2^I \cdot \int_0^t X_2 \cdot dt - K_2^D \cdot \dot{X}_2 \\
T_6 + \tau_6 \cdot \frac{dT_6}{dt} &= -K_6^P \cdot X_6 - K_6^I \cdot \int_0^t X_6 \cdot dt - K_6^D \cdot \dot{X}_6
\end{aligned}
\tag{10.49}
$$

where τ_k are **time constants** and the right hand term and K_k^P, K_k^I and K_k^D are **gain constants** of the PID-controller.

Sometimes, a low-pass filter is used in the last term, $K_i^D \cdot \dot{X}_i$, which avoids undesirable effects of high frequencies.

10.4.3 Wind Feed-Forward

[McClure et al., 1990] give a practical example of the utility of a simulation with wind feed-forward for the response of a 189 meter length ship to a sudden squall. Their equations of motion are comparable to those given in 10.44. In each of their simulation runs, the ship was in equilibrium in 29 knots wind, half a knot current and a sea with a significant wave height of 4.5 meter. The squall is of 600 seconds duration with wind velocities of about 35 to 60 knots, see figure 10.17-a.
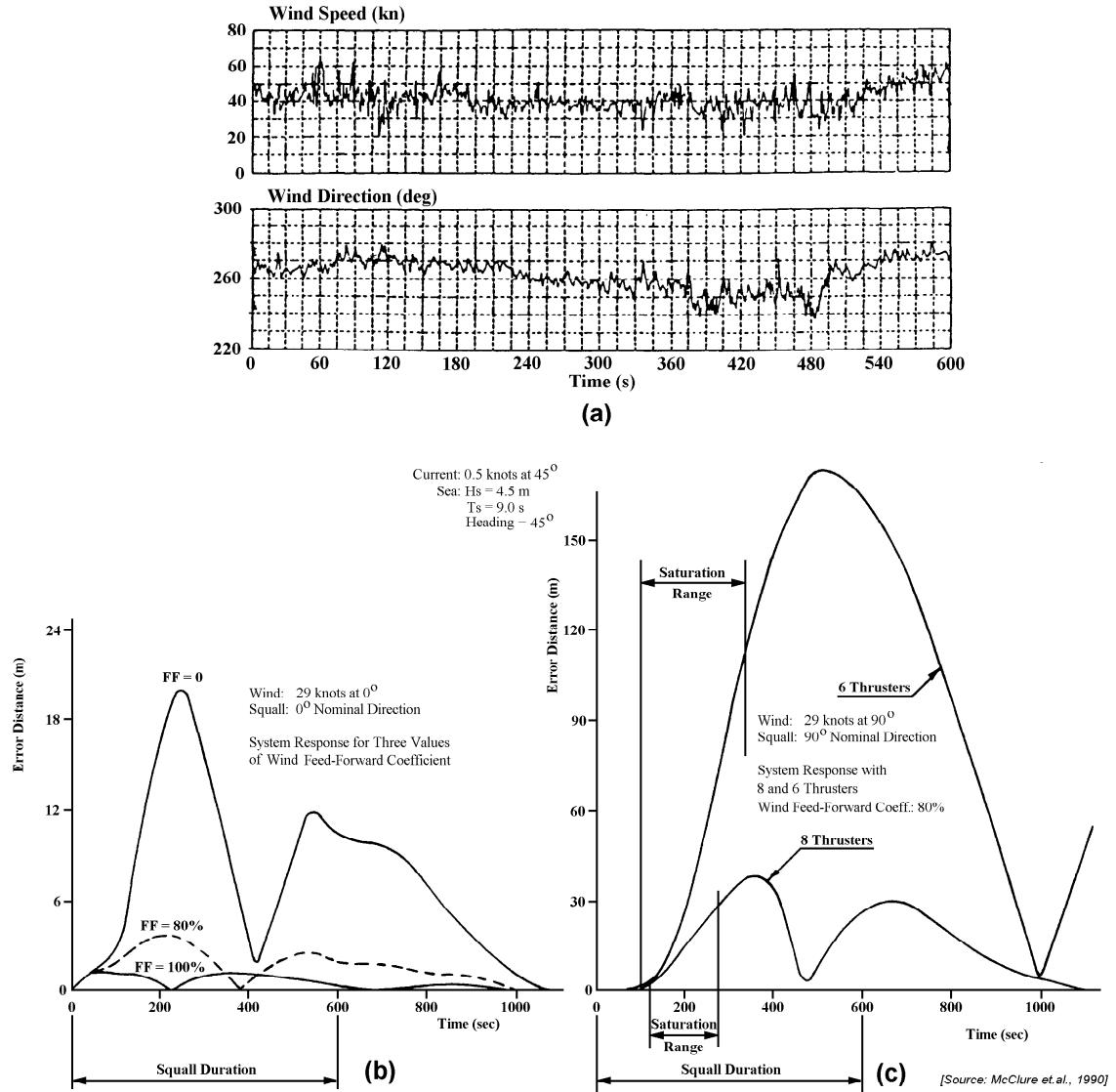
Figure 10.17: Squall Simulation with Head and Beam Wind

With the squall from directly ahead, the thrusters have sufficient capacity and the system behaves satisfactory. The benefit of wind feed-forward is illustrated in figure 10.17-b. Without wind feed-forward, the vessel moves 20 meter off station and overshoots 12 meter before setting down. Feed-forward can never be 100 % effective, so performance at 80 % effectiveness - which is a reasonable expectation - is also shown in this figure.

When the squall is imposed from the beam direction, the thrusters are momentarily loaded

to capacity and the system is 'saturated'. Figure 10.17-c illustrates the necessity of providing thrust in excess of the static balance. The curves shown represent in one case 3 thrusters available, 10,300 kWh, and in the other case 6 thrusters totalling 7725 kWh. Either system has more than enough thrust to exceed the equilibrium loading. Both cases include wind feed-forward at 80 % effectiveness. Note that the time during which the system is saturated is relatively brief, yet the system allows large drift and overshoot.

10.4.4 Gain Constants Estimate

For a DP system there has to be an allocation system that tells how the power should be distributed among the individual thruster units. If the thrusters are a part of a DP system with a PD-controller, an idealized simplification of the total thruster forces - with time constant $\tau \to 0$ - can be written as:

$$T_k = -K_k^P \cdot X_k - K_k^D \cdot \dot{X}_k \qquad \text{for: } k = 1, 2, 6 \qquad (10.50)$$

[Faltinsen, 1990] proposes a simple method to get a feeling for the magnitude of the gain constants, K_k^D and K_k^P of the PD-controller of a dynamically positioned ship. An example is given here for surge, of which the simplified uncoupled equation of the slow-drift motion is given by:

$$(m_{11} + a_{11}) \cdot \ddot{x}_1 + b_{11} \cdot \dot{x}_1 = F_1^{SW} + F_1^W + T_1 \qquad (10.51)$$

A substitution of equation 10.50 (with $x_1 = X_1$ and $\dot{x}_1 = \dot{X}_1$) in equation 10.51 provides equation 10.52 for surge of the DP vessel:

$$(m_{11} + a_{11}) \cdot \ddot{x}_1 + \left(b_{11} + K_1^D\right) \cdot \dot{x}_1 + K_1^P \cdot x_1 = F_1^{SW} + F_1^W \qquad (10.52)$$

where m_{11} is the mass of the ship, a_{11} is the hydrodynamic mass, b_{11} is the hydrodynamic damping, F_1^{SW} is the slow-drift wave excitation force and F_1^W the gust force. The mean values of F_1^{SW} and F_1^W are supposed to be zero.

The gain constant K_1^P will be chosen so that the natural period in surge of the slowly oscillating ship is from 100-200 seconds. The damping coefficient, b_{11}, has been neglected by Faltinsen at this very low frequency and the gain constant K_1^D was set equal to about 60 % of the critical damping; so $\kappa = 0.60$, see chapter 6. The final real values will be decided after full scale sea tests with the DP system.

Thus, as a first estimate:

$$
\begin{aligned}
K_1^P &= \omega_0^2 \cdot (m_{11} + a_{11}) \qquad \text{where } \omega_0 = \frac{150}{2\pi}, \text{ for instance} \\
K_1^D &= 1.20 \cdot \sqrt{(m_{11} + a_{11}) \cdot K_1^P} \qquad\qquad\qquad (10.53)
\end{aligned}
$$

With these equations, the variance of the slow-drift surge motion can be calculated in a way as has been done in chapter 6 for motions with frequencies in the wave-frequency range. Finally, the variance of the total thruster forces follow from equation 10.50.

For ships, the potential mass for surge can be approximated by 5-8 % of the ship's solid mass. The damping coefficient, b_{11}, has assumed to be zero here. This assumption is true for the potential damping but viscous effects can have some influence. In some papers, the use of a surge damping coefficient of about 5 % of the critical damping of a soft spring system is recommended.

10.4.5   Motion Reference Filtering

Suppose a simple uncoupled equation of motion for sway of a DP vessel, given by:

$$(m_{22} + a_{22}) \cdot \ddot{x}_2(t) + b_{22} \cdot \dot{x}_2(t) = F_2^D(t) + T_2(t) \tag{10.54}$$

where $F_2^D(t)$ is the total sway drift force and $T_2(t)$ is the total sway thruster force.
The use of a PD-controller means that the thruster force contains a part which is proportional (P) to the position error, $x_2(t)$, and a part which is proportional to the derivative (D) to time of this position error, the velocity $\dot{x}_2(t)$. To obtain 'smooth' input signals $x_2(t)$ and $\dot{x}_2(t)$, the measured reference signal, $x_2(t)$ - being obtained by systems such as Loran, GPS, a taut wire system or an acoustic system - has to be filtered; the wave frequency motions and the high frequency disturbances are filtered out. But, filtering - for instance by using a Kalman filter - necessarily introduces a time lag, τ. Due to this time lag, the thruster force is applied 'later':

$$T_2(t) = -K_2^P \cdot X(t - \tau) - K_2^D \cdot \dot{X}_2(t - \tau) \tag{10.55}$$

where τ is the time lag of the DP system between the filtered motion signals and the thruster reaction.
However, thruster forces are affected by the presence of waves. This holds that - in spite of filtering out of wave frequent motions - via the actual thruster forces wave frequent contributions will be introduced again in the system.
The displacement and velocity can be expanded in series:

$$
\begin{aligned}
X_2(t - \tau) &= X_2(t) - \frac{\partial \{X_2(t)\}}{\partial t} \cdot \tau + \ldots\ldots \\
\dot{X}_2(t - \tau) &= \dot{X}_2(t) - \frac{\partial \{\dot{X}_2(t)\}}{\partial t} \cdot \tau + \ldots\ldots
\end{aligned} \tag{10.56}
$$

These series can be simplified by assuming τ to be small relative to the natural period of the sway motion; thus a linearization is permitted:

$$
\begin{aligned}
X_2(t - \tau) &= X_2(t) - \dot{X}_2(t) \cdot \tau \\
\dot{X}_2(t - \tau) &= \dot{X}_2(t) - \ddot{X}_2(t) \cdot \tau
\end{aligned} \tag{10.57}
$$

so:

$$T_2(t) = +K_2^D \cdot \ddot{X}_2(t) \cdot \tau + \left\{ -K_2^D + K_2^P \cdot \tau \right\} \cdot \dot{X}_2(t) - K_2^P \cdot X_2(t) \tag{10.58}$$

With $\ddot{x}_2 = \ddot{X}_2$, $\dot{x}_2 = \dot{X}_2$ and $x_2 = X_2$, the following expression is found from equation 10.54:

$$\left(m_{22} + a_{22} - K_2^D \cdot \tau\right) \cdot \ddot{x}_2(t) + \left(b_{22} + K_2^D - K_2^P \cdot \tau\right) \cdot \dot{x}_2(t) + K_2^P \cdot x_2(t) = F_2^D(t) \tag{10.59}$$

This equation shows that the effect of a time lag in the DP system is to reduce the mass term in the equation of motion and also to reduce the damping term.
Assuming that the total sway drift force, $F_2^D(t)$, can be characterized as a low frequency 'white noise' process with mean value $\overline{F_2^D}$ and the spectral density, S_f, the above equation

of motion can be solved in the frequency domain, as has been discussed at the end of chapter 9.

The results with respect to the variance of the sway velocity are as follows:

$$\sigma_{x_2}^2 \quad = \quad \frac{\pi}{2 \cdot (b_{22} + K_2^D - K_2^P \cdot \tau) \cdot K_2^P} \cdot S_f \tag{10.60}$$

$$\sigma_{\dot{x}_2}^2 \quad = \quad \frac{\pi}{2 \cdot (b_{22} + K_2^D - K_2^P \cdot \tau) \cdot (m_{22} + a_{22} - K_2^D \cdot \tau)} \cdot S_f \tag{10.61}$$

Since the sway motion and the sway velocity are not-correlated processes, the variance of the total thruster force is found to be as follows:

$$\sigma_{F_{2_T}}^2 = \left(K_2^P \cdot \sigma_{x_2}\right)^2 + \left(K_2^D \cdot \sigma_{\dot{x}_2}\right)^2 \tag{10.62}$$

The mean thruster force follows from:

$$\overline{T_2} = -\overline{F_2^D} \tag{10.63}$$

Because τ is in the nominator of equations 10.60, 10.61 and 10.62, it is obvious that an increased time lag, τ, results in increased variances, σ, of the motions together with also increased required thruster forces. This means that attention has to be paid to a careful choice and a proper use of the filtering technique.

10.4.6   Role of Model Tests

The role of model tests in the design process of a DP control system for a vessel is well described by [McClure et al., 1990]. Their view on this subject is summarized below.

Clearly, the availability of today's computing power and sophisticated graphics engines render the use of digital time domain, non-linear dynamic simulation programs the best alternative for validating band optimizing the design of modern DP systems. These simulation programs require reliable functional relationships between environmental parameters such as current speed, wind speed, wave height and period - together with their directions to the ships heading - and longitudinal force, side force and yaw moment. In addition to these environmental 'forcing functions' the performance of thrusters, rudders and main propulsors in providing reaction forces and moments in opposition to the environmental forces is required in terms of applied power, thruster orientation and proximity to other propulsion devices.

Despite the advancement of numerical models for the prediction of hydro- and aerodynamic forces on floating structures, they still do not posses sufficient precision for providing an adequate function for use in the dynamic simulators, particularly as the requirements to analyze the station keeping of permanent systems for deep water and hostile environments emerge.

The role of physical model experiments in DP system design, validation and optimization is analogous to their role in supporting maneuvering simulators for surface ships and submarines. This role can be viewed in comparison with the full physical simulation of a DP system at model scale in a similar way that the use of model tests and maneuvering simulators are compared with free-running maneuvering experiments. Both of these 'full physical simulations' are expensive, require physical reproduction of the controller and all

of its strategies and suffer from hydrodynamic and time scale effects. Large models are required to minimize scale effects on control appendage effectiveness and a thorough examination of the sensitivity to overall response to subtle changes in control algorithms is so time consuming as to be virtually impossible.

Nonetheless, some tests facilities have conducted experiments, where a 'complete' physical simulation of a DP system was undertaken. However, the opinion of [McClure et al., 1990] is that such simulations are useful, only to validate numerical codes and are not a viable design or optimization tool.

Nowadays, the efficient use of model tests to provide inputs required by numerical simulators are mainly restricted to the following aspects:

- Wind Forces and Moments
  The use of wind tunnel models to establish the longitudinal and lateral wind force coefficients for mono-hulls and semi-submersibles we well-known. Scale effects due to Reynolds number disparity between model and full scale are mitigated somewhat due to the bluffness of the elements of the above water portion of these vessels. While there exists published data for some classes of vessels, [OCIMF, 1977], it is advisable to conduct experiments to determine the aerodynamic coefficients when the configuration of the above water portion of the vessel departs significantly from that for which published data is available.

- Current Forces and Moments
  If it were possible to always maintain a nearly zero heading with respect to the current, such information would not be terribly important. However, the likelihood of misalignment between the direction of sea, wind and current can be high in tidal seas and estuaries and during squalls. So, in order to accurately analyze the response of a dynamically positioned vessel, it is necessary to understand the relationship between the coefficients of longitudinal and lateral forces and yaw moment and heading.
  Again, it would be useful to use existing systematic series data to determine these coefficients. Indeed, some data has been assembled for tankers by the Oil Company International Marine Forum, [OCIMF, 1977]. However, this data is for a limited class of hull forms. Changes in many hull form parameters such as length to draft ration and fore and aft body fineness, as well as the distribution and size of appendages, can change these coefficients.
  The foregoing is no less true for column stabilized floating platforms. Physical model tests are the best tool today for quantifying these important inputs to the simulator. Nonetheless, the scale of the model must be chosen carefully. It has been shown by [Edwards, 1985] that Reynolds number (based upon beam) of approximately 500,000 are required to produce reliable results for the current force and moment coefficients. This implied model scales on the order of 1:20 to 1:30.

- Wave Induced Forces and Moments
  The forces exerted on a floating body by waves at wave-frequency are ignored in current DP system designs, because it is recognized that response times for the systems cannot approach that necessary to effectively control position at wave-frequency and because wave-frequency oscillations in the horizontal plane are not usually large enough to limit operations. On the other hand, the steady component of wave inducted longitudinal and lateral force and yaw moment must be reacted out by a the

positioning system. The slowly varying component of these forces and moments must be at least be attenuated.

Numerical models have been developed which provide estimates of the steady and slowly varying components of the wave drift forces and moments. Nonetheless, to confirm these estimates for new designs, it is advisable to obtain a semi-empirical relationship between the steady force and moment coefficients and wave period in regular waves. Estimates of the slowly varying drift force and moment coefficients can also be derived from experiments in regular wave 'beats' and from irregular wave tests using cross bi-spectral analysis techniques to derive quadratic transfer functions for second order wave forces. These model tests can be conducted using relative small and inexpensive models, on the order of 1:50, because viscous effects are relatively unimportant in physical simulation of wave drift.

- Thruster Effectiveness

  The effectiveness of thrusters in producing forces and moments to react out the environmental forces and moments is necessary information for the simulator. It is not adequate to consider the thruster in isolation, as done in a foregoing section, because depending upon the proximity of thrusters, their inflow and outflow fields can interact, producing deviations in effectiveness from that which would be expected if the thrusters' force and moment applied to the vessel were calculated taking inflow velocity (free stream current), propeller angular speed and pitch into account and using performance curves for the isolated thruster. For vessels where it is impossible to avoid placing the thrusters where the inflow and outflow fields may interfere, physical model tests are the only reliable way to define the effects.

  These experiments are carried out best with a large captive model. The model is restrained in surge, sway and yaw. The model is towed at various speeds and headings and various thruster operating conditions are prescribed. The resulting residual forces and moments are measured. This data base is used in conjunction with a similar data base obtained from towed tests without the thrusters and propulsors operating to derive the effectiveness and interaction polar plots for the thrusters and propulsors.

.

Chapter 11

OPERABILITY

Ship motions and sea loads can influence the behavior and operability of the ship significantly. The ship's speed will be reduced due to an involuntary speed reduction and it can be reduced voluntarily as well. Involuntary speed reduction is the result of added resistance of the ship due to wind and waves and changes in the propeller efficiency due to the waves and the loading of the propeller. Voluntary speed reduction means that the ship's master reduces the speed due to (green) water on deck or heavy slamming or to reduce large accelerations. Environmental conditions can even lead to an involuntary change of the ship's course.

This chapter discusses ship operability in a variety of contexts, but first some necessary theory on statistics is reviewed.

11.1 Statistics

11.1.1 Short Term Predictions

The basis for calculating a response - such as for instance the pressure at a specified point - is the transfer function of that response. As has been shown in chapter 6, the response spectrum is calculated by multiplying transfer function, $|H_{R\zeta}(\omega)| = R_a/\zeta_a(\omega)$, squared by the incident wave spectrum, $S_\zeta(\omega)$:

$$S_{R\zeta} = |H_{R\zeta}(\omega)|^2 \cdot S_\zeta(\omega) \tag{11.1}$$

Assuming stationary Gaussian incoming waves and a narrow banded response spectrum, the response amplitudes are Rayleigh distributed.

Then the Rayleigh short term probability density function of the response is given as:

$$\boxed{f_{ST}(R_a) = \frac{R_a}{m_{0R}} \cdot \exp\left\{-\frac{R_a^2}{2m_{0R}}\right\}} \tag{11.2}$$

in which m_{0R} is defined as the area under the response spectrum.

11.1.2   Long Term Predictions

This short term probability density function, $f_{ST}(R_a)$, has to be calculated for all wave direction intervals, μ_i, and sea state intervals, defined by (H_j, T_k), in order to determine the long term probability density function, $f_{LT}(R_a)$, which can be calculated as the weighted sum of all short term results:

$$\left| f_{LT}(R_a) = \sum_{i=1}^{N_\mu} \sum_{j=1}^{N_H} \sum_{k=1}^{N_T} f_{ST}(R_a)_{i,j,k} \cdot f_i \cdot f_{j,k} \right| \tag{11.3}$$

in which:

$$
\begin{aligned}
N_\mu &= \quad \text{number of wave direction intervals, } \mu_i \\
N_H &= \quad \text{number of wave height intervals, } H_j \\
N_T &= \quad \text{number of wave period intervals, } T_k \\
f_i &= \quad \text{long term probability of wave direction interval } \mu_i \\
f_{j,k} &= \quad \text{long term probability of wave height and period interval } (H_j, T_k) \\
&\qquad \text{within the wave direction interval } \mu_i
\end{aligned}
$$

The long term sea state probabilities f_i and $f_{j,k}$ can be obtained from wave scatter diagrams. Diagrams for $f_{j,k}$ have been given in chapter 5 for the North Atlantic Ocean and the northern North Sea for all wave directions together; then: $N_\mu = 1$ and $f_i = f_{N_\mu} = 1$.
The long term probability density function, $f_{LT}(x)$, can be integrated to obtain the long term cumulative distribution function, $F_{LT}(R_a)$:

$$F_{LT}(R_a) = \int_0^{R_a} f_{LT}(x) \cdot dx \tag{11.4}$$

When carrying this out numerically, it is advised to integrate in an opposite direction: from the upper tail (high response amplitudes) to zero. This actually computes $\{1 - F_{LT}(R_a)\}$, which can represent the upper tail part more accurately by minimizing numerical errors.
The zero-crossing period of the response in a certain sea state is given by the spectral moments as $T_{2R} = 2\pi\sqrt{m_{0R}/m_{2R}}$ and the mean period over a number of years can be determined by weighting these periods - using the wave scatter diagram - over the wave directions and sea states.
Then the number of observations or cycles, n, during Y years is thus calculated as:

$$n_{Y \text{ years}} = \frac{Y \cdot 365 \cdot 24 \cdot 60 \cdot 60}{\sum_{i=1}^{N_\mu} \sum_{j=1}^{N_H} \sum_{k=1}^{N_T} f_i \cdot f_{j,k} \cdot T_{2R}(i,j,k)} \tag{11.5}$$

This analysis assumes that the observer is continuously exposed to this one wave climate at that particular location.

11.1.3   Extreme Values

There is a relation between the distribution of the maxima or peaks in one sea state (short term) and the distribution of the extremes in a number of equal sea states (long term).
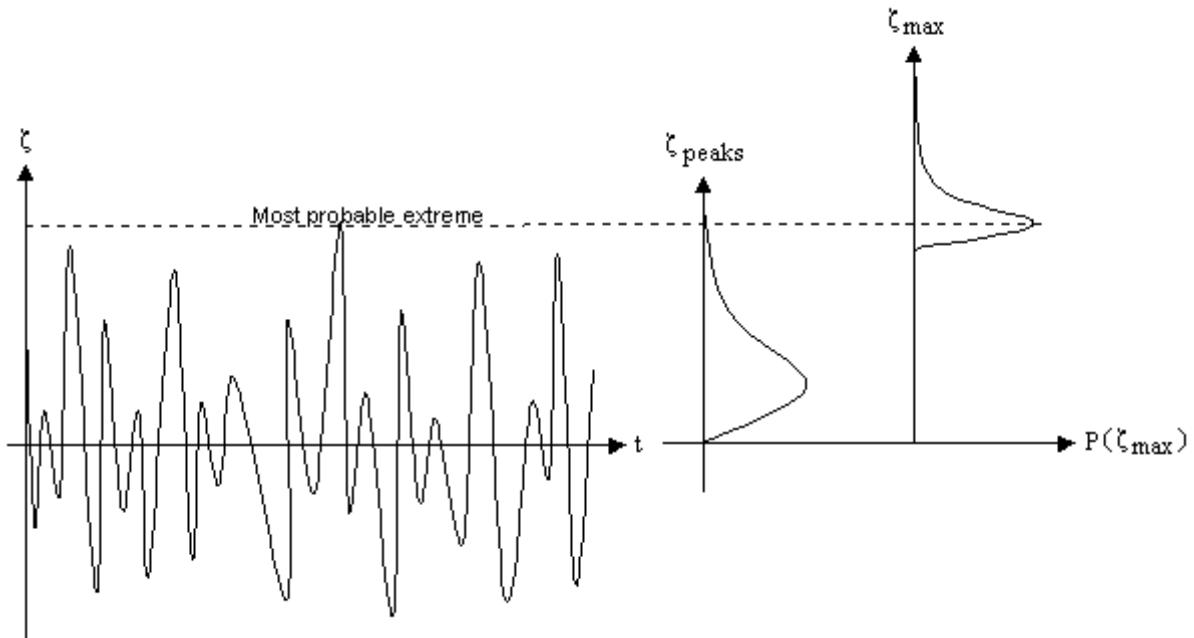
Figure 11.1: Probability Distributions of Maxima and Extremes in an Irregular Sea

Figure 11.1 shows this relation. The short term distribution of the maxima or peaks is the left distribution in this figure and the distribution of the extremes during a long period is the right distribution. This will be discussed in more detail now.

In general the response of a ship to irregular waves is a random variable with an initial probability density function, $f(x)$, and an initial cumulative distribution function, $F(x)$. The extreme value of this irregular response is defined as the largest value expected to occur in a certain number of observations or during a certain period of time.
Let a set of observed (absolute) crest and trough values $(x_1, x_2, x_3, ..., x_n)$ of an irregular response be a random sample of n observations. The elements of this random sample are arranged in an ascending order of magnitude such that $x_1 < x_2 < x_3 < ...... < x_n$; thus the largest value - expected to occur in n observations - is named x_n. This x_n is a random variable as well with its own extreme value probability density function, $g(x_n)$, and extreme value cumulative distribution function, $G(x_n)$.
It is subject of considerable interest in statistics to find the asymptotic behavior of the extreme value cumulative distribution function, $G(x_n)$, for a large sample size n. In other words the question arises: "Do these functions give us the opportunity to determine important phenomena such as the expected maximum response amplitude of a ship during for instance its lifetime or the expected maximum wave height being encountered in for instance a 50-years period, the so-called 50-years wave?" The answer is yes; the probability functions $f(x)$, $F(x)$, $g(x_n)$ and $G(x_n)$ have mathematical relationships which enable us to solve these problems, as will be shown here. The extreme values can be evaluated precisely from the knowledge of the initial probability density function.
From the definition of the cumulative distribution function follows:

$$f(x) = \frac{dF(x)}{dx} \qquad \text{and} \qquad g(x_n) = \frac{dG(x_n)}{dx_n} \tag{11.6}$$

As has been shown in chapter 5 for irregular waves, the probability that an arbitrary response amplitude in irregular waves, R_a, does not exceed a value A is given by:

$$P\{R_a < A\} = \int_0^A f(x) \cdot dx = F(A) \tag{11.7}$$

Thus, the probability that *one* response amplitude in irregular waves does not exceed a value x_n is given by:

$$P\{x < x_n\} \quad \text{in 1 observation} = F(x_n) \tag{11.8}$$

The probability that n response amplitudes in irregular waves does not exceed a value x_n follows from a multiplication of the individual probabilities - assuming independence of the individual response amplitudes - by:

$$P\{x < x_n\} \quad \text{in } n \text{ observations} = (P\{x < x_n\})^n$$
$$= \{F(x_n)\}^n \tag{11.9}$$

Thus, the extreme value cumulative distribution function, $G(x_n)$, in n observations can be formulated as:

$$G(x_n) = \{F(x_n)\}^n \tag{11.10}$$

The extreme value probability density function, $g(x_n)$, in n observations is the derivative of the function $G(x_n)$:

$$
\begin{aligned}
g(x_n) &= \frac{dG(x_n)}{dx_n} \\
&= n \cdot \{F(x_n)\}^{n-1} \cdot \frac{dF(x_n)}{dx_n} \\
&= n \cdot \{F(x_n)\}^{n-1} \cdot f(x_n) \tag{11.11}
\end{aligned}
$$

The probability density functions $g(x_n)$ for various n values are shown in figure 11.2.
An explanatory sketch - illustrating the relationship between the probability density functions $f(x)$ and $g(x_n)$ - is shown in figure 11.3.
Figure 11.3 also shows that - following the so-called modal value approach - the extreme value is defined as the value having the highest probability of occurrence. At that point:

$$\frac{dg(x_n)}{dx_n} = 0 \tag{11.12}$$

so that:

$$\frac{df(x_n)}{dx_n} \cdot F(x_n) + (n-1) \cdot \{f(x_n)\}^2 = 0 \tag{11.13}$$

Rewriting this equation and dividing it by $1 - F(x_n)$ results in:

$$\frac{1}{1 - F(x_n)} = -\frac{n-1}{F(x_n)} \cdot \frac{f(x_n)}{1 - F(x_n)} \cdot \frac{f(x_n)}{\frac{df(x_n)}{dx_n}} \tag{11.14}$$
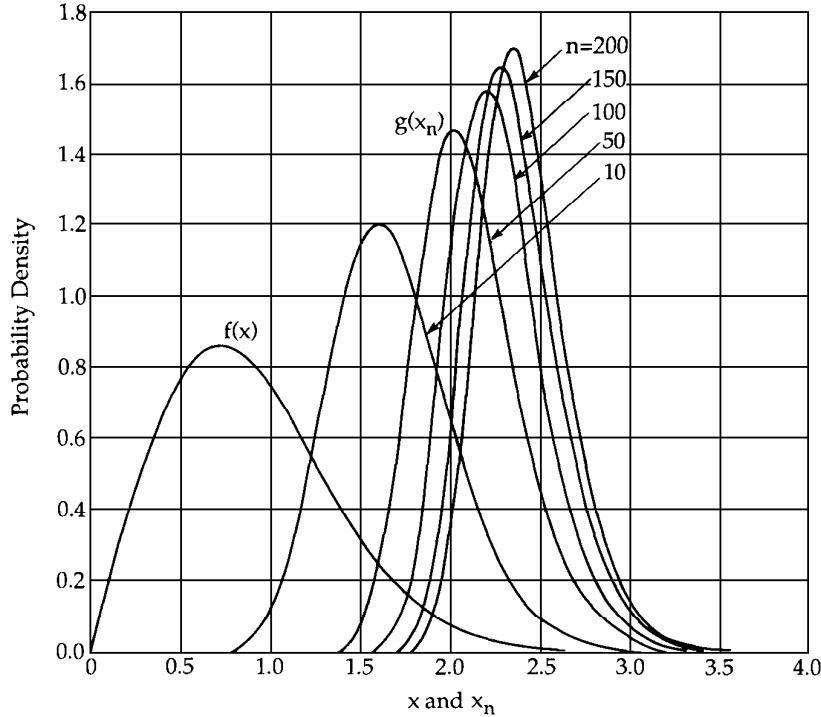
Figure 11.2: Extreme Value Function $g(x_n)$ from Rayleigh Distribution for Various n-Values

Applying the L'Hopital rule:

$$\frac{f\left(x_n\right)}{1 - F\left(x_n\right)} = -\frac{\frac{df(x_n)}{dx_n}}{f\left(x_n\right)} \qquad \text{for large } x_n \tag{11.15}$$

results in:

$$\frac{1}{1 - F\left(x_n\right)} = \frac{n-1}{F\left(x_n\right)} \approx n \qquad \text{for large } n \text{ and } x_n \tag{11.16}$$

or:

$$\frac{df\left(x_n\right)}{dx_n} \approx \frac{-1}{n} \quad \text{and} \quad F\left(x_n\right) \approx 1 - \frac{1}{n} \qquad \text{for large } n \text{ and } x_n \tag{11.17}$$

This last formula 11.17 states that the most probable extreme value expected to occur in n observations, x_n, can be evaluated from the initial cumulative distribution function, $F\left(x_n\right)$, as the value for which the **return period** is equal to n or the probability of exceeding this value is $1/n$. The return period, here, is nothing more than reciprocal frequency. It should not be interpreted directly in terms of an actual time interval between occurrences

Now the extreme wave or response amplitude with an expected average return period of - for instance - 50 years can be determined. Also extreme significant amplitudes - and the most probable extreme amplitude within this response spectrum - can be determined.
For the sake of clearness and simplicity, the examples given here are for the waves only. By using transfer functions, R_a/ζ_a, with an amplitude of 1.0 all previous equations reduce to equations for the probabilities of the irregular waves themselves. This is picked up again later.
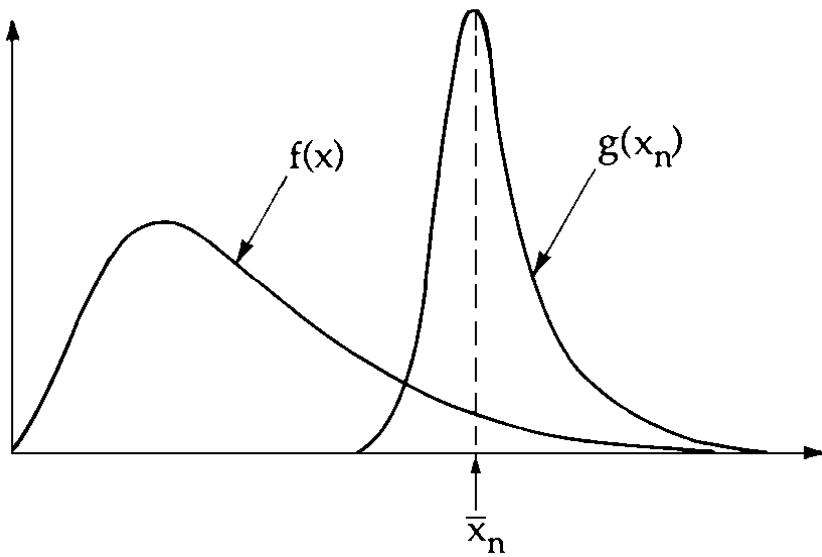
Figure 11.3: Functions $f(x)$ and $g(x_n)$ and Most Probable Extreme Value $\overline{x}_n$

Extreme Wave Amplitude

The wave scatter diagram for the Forties Field - an oil field in the Central North Sea - has been used in this example. This diagram with $126,007$ observations of the significant wave height and the mean zero-crossing period during 21.5 years - so one observation every $1\frac{1}{2}$ hours - is given below.

Wave Scatter Diagram of Forties Field													
Total	549	11284	32993	39460	26353	11109	3293	789	149	25	3		126007
12.75													
12.25									1				1
11.75													
11.25									2	1			3
10.75								2	5	2			9
10.25							1	3	7	5			16
9.75							1	9	11	6			27
9.25							4	30	16	6			56
8.75							16	40	16				72
8.25						2	29	61	8	1			101
7.75						2	104	84	2				192
7.25						8	175	72	3				258
6.75					1	71	313	74	4				463
6.25					3	222	401	47	2	1			676
5.75				1	7	621	431	42	2				1104
5.25				2	114	1228	321	29	5				1699
4.75				3	681	1885	243	19					2831
4.25			3	26	2530	1885	237	35	3				4719
3.75			2	407	4892	1371	221	35	9				6937
3.25			14	2827	5604	1019	205	41	8				9718
2.75		3	233	7972	4588	901	184	33	1				13915
2.25		7	2771	11367	3336	766	129	28	9				18143
1.75		315	9872	8688	2133	446	80	21	6		1		21562
1.25	14	3522	12850	5628	1626	351	79	38	7	2	1		24118
0.75	376	6785	6765	2299	732	277	95	29	10	1	1		17370
0.25	159	652	483	240	106	54	24	17	12				1747
$H_{1/3}$ (m)													Total
T_2 (s)	2.5	3.5	4.5	5.5	6.5	7.5	8.5	9.5	10.5	11.5	12.5	13.5	

The resulting cumulative probability distribution functions can be plotted on Weibull paper; see figure 11.4.
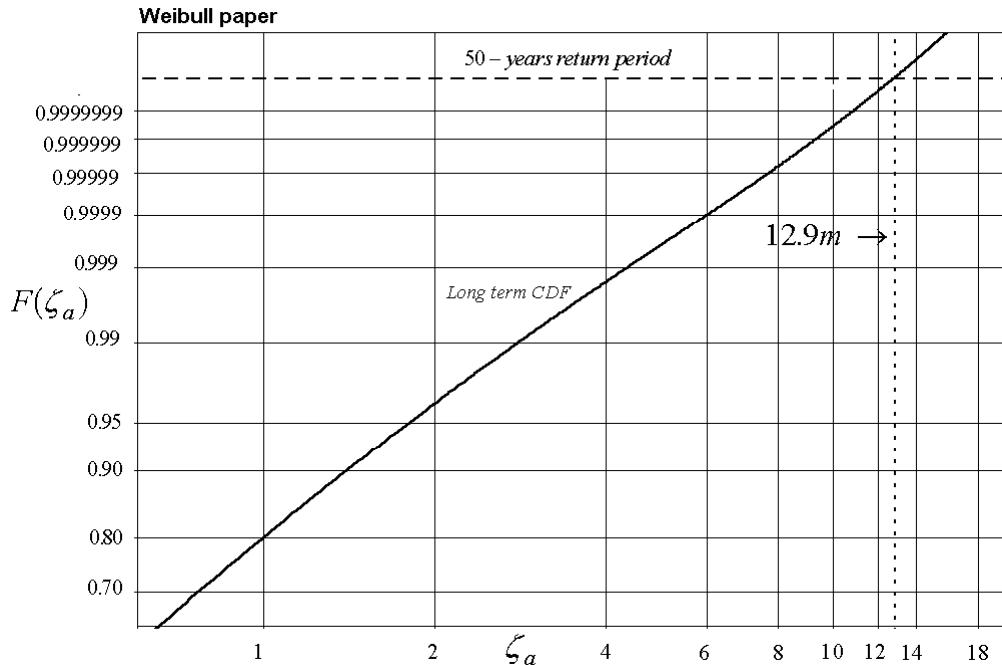
Figure 11.4: Weibull Distribution of Extreme Wave Amplitudes

Long term probability density functions, $f_{LT}(\zeta_a)$, as given in equation 11.3, can be obtained by using the wave scatter diagram of the considered sea area. These functions are integrated, using equation 11.4, to obtain the long term cumulative distribution function, $F_{LT}(\zeta_a)$, - marked by CDF in figure 11.4. So this long term CDF-curve is fully calculated here.

The number of wave cycles during 50 years, $n_{50\ years}$, can be obtained by putting $Y = 50$ in equation 11.5 and using the wave scatter diagram. Equation 11.17 provides the value of the cumulative probability distribution function: $F(\zeta_a) = 1 - 1/n_{50\ years}$. This $F(\zeta_a)$ and the CDF-curve in figure 11.4 provide the **extreme wave amplitude with an expected return period of 50 years**; in this example: $\zeta_a = 12.90$ meter or wave height is 25.80 meter.

Significant Wave Height of an Extreme Sea State

From the wave scatter diagram the probabilities for the significant wave height are known, $F(H_{1/3})$; these can be obtained from the most right column. By plotting these probabilities for the significant wave height on Weibull paper - see the Weibull distribution in chapter 5 - the extreme sea state once every 50 years can be determined. Since the total number of observations is 126,007 over 21.5 years the total number of observations in 50 years is $N = 126007 \cdot 50\ /\ 12.5$. Thus $F(H_{1/3})_{50\ years} = 1 - 1/N$. Because the plotted data of the scatter diagram is often not accurate for the higher sea states - the connecting (dotted) line is curved and twisted - a fit has to be carried out. In figure 11.5, the 3-parameter Weibull plot is fitted on all data (dotted line = data).

$$F\left(H_{1/3}\right) = 1 - \exp\left\{-\left(\frac{H_{1/3} - a}{c}\right)^b\right\} \qquad \text{(Weibull)} \qquad (11.18)$$
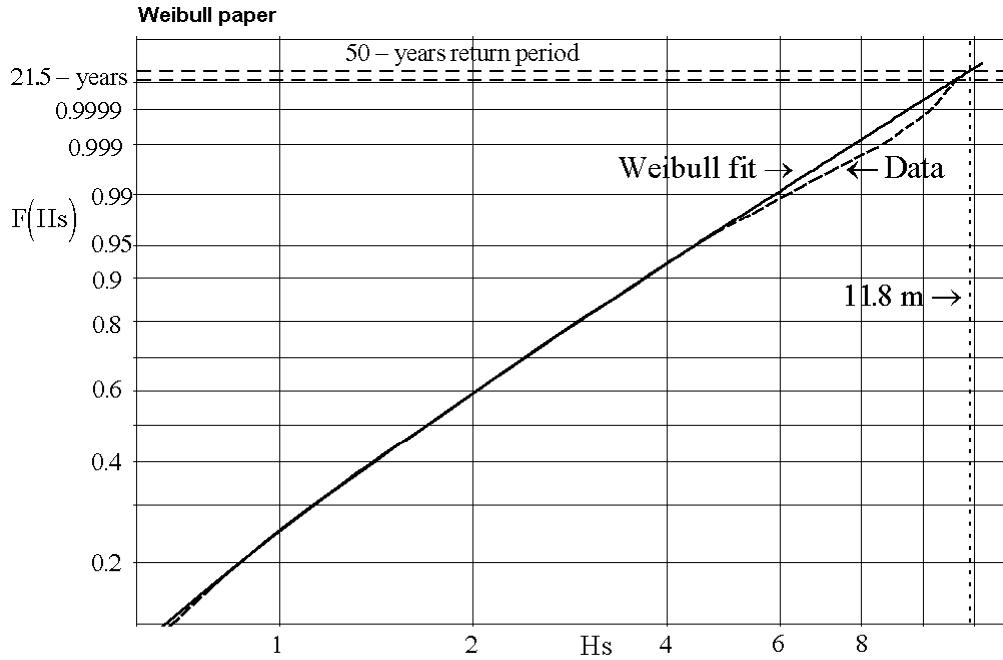
Figure 11.5: Probability Distribution of Significant Wave Heights

This plot gives a straight curve for higher sea states and is then used to determine the extreme significant wave height. From the figure follows that the **extreme significant wave height with a return period of 50 years** is 11.80 meter.

Obviously, the type of fitting is important. How to weigh the importance of the tail? In this case, paying more attention to the upper tail would lead to a fit with a higher extreme significant wave height than a simple extrapolation of the data curve.

Extreme Wave Amplitude in an Extreme Sea State

Consider now this extreme sea state with a return period of 50 years - lasting 3 hours, as generally done in offshore calculations. Using the formulation for the most probable maximum, $F\left(\zeta_a\right) = 1 - 1/N$, the extreme wave amplitude in this sea state can be calculated from the Rayleigh distribution:

$$P\left\{\zeta_a > \zeta_{a \text{ max (50 years storm)}}\right\} = \exp\left\{-\frac{\zeta_{a \text{ max (50 years storm)}}^2}{2 \cdot m_{0\zeta}}\right\} = \frac{1}{N} \qquad (11.19)$$

or:

$$\zeta_{a \text{ max (50 years storm)}} = \sqrt{2 \cdot m_{0\zeta} \cdot \ln\left(N\right)} \qquad (11.20)$$

The number of cycles, N, can be determined by using a wave period $T_2 = 12.0$ seconds. This is the average (central) period belonging to the extreme significant wave height of 11.80 meter, as obtained from the wave scatter diagram.

The spectral area, $m_{0\zeta}$, is determined by:

$$H_{1/3} = 4 \cdot \sqrt{m_{0\zeta}} \qquad \text{or} \qquad m_{0\zeta} = \frac{1}{4} \cdot H_{1/3}^2 \qquad (11.21)$$

in which $H_{1/3}$ is the significant wave height of the extreme sea state with an expected return period of 50 years (11.80 meter in this example).
The resulting **extreme wave amplitude in the extreme sea state** is then 10.90 meter, which is about 1.85 times the significant wave amplitude.
This extreme amplitude is lower than the extreme wave amplitude with an expected return period of 50 years (12.90 meter in this example). It is left to the reader to explain why.

11.2 Operating Limits of Ships

For various types of vessels, some typical phenomena and general operability limiting criteria are given in this section.

11.2.1 Personnel Safety

Some general operability limiting criteria for ships, partially taken from [Faltinsen, 1990], are given below.

General Operability Limiting Criteria for Ships (NORDFORSK, 1987)			
Description	Merchant ships	Naval vessels	Fast small craft
RMS of vertical acceleration at F.P.P.	0.275 g ($L \leq 100$ m) 0.050 g ($L \geq 330$ m)	0.275 g	0.65 g
RMS of vertical acceleration at bridge	0.15 g	0.20 g	0.275 g
RMS of lateral acceleration at bridge	0.12 g	0.10 g	0.10 g
RMS of roll	6.0 deg	4.0 deg	4.0 deg
Probability on slamming	0.03 ($L \leq 100$ m) 0.01 ($L \geq 300$ m)	0.03	0.03
Probability on deck wetness	0.05	0.05	0.05

For intermediate lengths in the criteria for the vertical acceleration forward and the criteria for slamming, a linear interpolation can be used.
The limiting criteria for fast small craft are only indicative of trends. A fast craft is defined as a vessel under about 35 meters in length with a speed in excess of 30 knots. A reason why the vertical acceleration level for fast small craft is set higher than for merchant ships and

naval vessels, is that personnel can tolerate higher vertical acceleration when the frequency of oscillation is high.

Criteria for accelerations and roll for various types of work and for passenger comfort are given in the following table.

Criteria for Accelerations and Roll (NORDFORSK, 1987)			
Description	RMS vertical acceleration	RMS lateral acceleration	RMS roll
Light manual work	0.20 g	0.10 g	6.0 deg
Heavy manual work	0.15 g	0.07 g	4.0 deg
Intellectual work	0.10 g	0.05 g	3.0 deg
Transit passengers	0.05 g	0.04 g	2.5 deg
Cruise liner	0.02 g	0.03 g	2.0 deg

11.2.2 Shipping Water

The relative motions between the ship and the water surface are generally largest at the ends of the ship. In high waves the motions may be so large that the forefoot and propeller are exposed and the deck submerged. This occurs most frequently at high speed in head waves, although it is not unknown in other conditions. The effective dynamic freeboard will differ from the results obtained from the geometric freeboard at zero forward speed in still water and the calculated vertical relative motions of a sailing ship in waves.

When sailing in still water, sinkage, trim and the ship's wave system will effect the local geometric freeboard. A static swell up should be taken into account.

An empirical formula - based on model experiments - for the static swell up at the forward perpendicular is given by [Tasaki, 1963]:

$$f_e = f - \zeta_B \qquad \text{with:} \qquad \zeta_B = 0.75 B \cdot \frac{L}{L_E} \cdot F_n^2 \qquad (11.22)$$

with:

$$
\begin{array}{rcl}
f_e & = & \text{effective freeboard at the forward perpendicular} \\
f & = & \text{geometric freeboard at the forward perpendicular} \\
\zeta_B & = & \text{bow wave} \\
L & = & \text{length of the ship} \\
B & = & \text{breadth of the ship} \\
L_E & = & \text{length of entrance of the waterline} \\
F_n & = & \text{Froude number}
\end{array}
$$
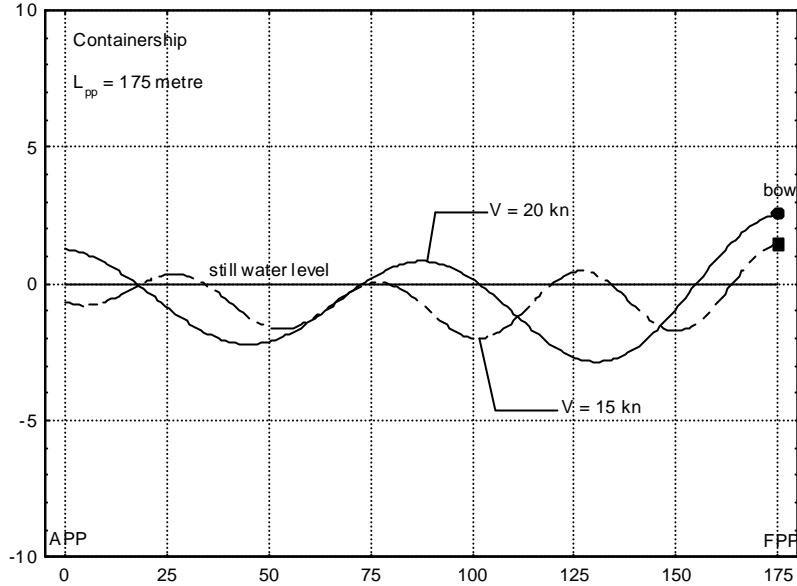
Figure 11.6: Distribution of Static Swell-Up

A very moderate approximation of the disturbance of the still water surface by the bow wave over the ship length can be obtained with:

$$
\begin{aligned}
\zeta_x \;=\;\; & \zeta_B \cdot \cos\left(2\pi \cdot \frac{\xi - 1}{0.78 - 7.2F_n}\right) \cdot e^{0.35(\xi-1)} \\
& -(0.0050 + 0.0025F_n) \cdot L_{pp}\cos\left(\pi\frac{\xi}{2}\right)
\end{aligned}
\tag{11.23}
$$

with Fn is the Froude number, L_{pp} is the length between perpendiculars and $\xi = 2x/L_{pp}$, where $x = -L_{pp}/2$ is the aft perpendicular and $x = +L_{pp}/2$ is the forward perpendicular, so: $-1.0 \leq \xi \leq +1.0$.

An example of the results of the use of formulas 11.22 and 11.23 for a containervessel is given in figure 11.6.

The amplitude of the vertical relative motion, s_a, of an oscillating ship in undisturbed waves can be calculated from the heave, pitch and wave motions. However, an oscillating ship will produce waves itself and this influences the amplitude of the relative motion.

A dynamic swell up, $\Delta\zeta_a$, should be taken into account so that the actual amplitude of the relative motions becomes:

$$
s_a^* = s_a + \Delta\zeta_a
\tag{11.24}
$$

Then, shipping green water is defined by:

$$
s_a^* > f_e \qquad \text{at the bow}
\tag{11.25}
$$

The spectral density of the vertical relative motion at the forward perpendicular is given by:

$$
S_{s^*}(\omega) = \left(\frac{s_a^*}{\zeta_a}\right)^2 \cdot S_\zeta(\omega)
\tag{11.26}
$$

and the moments are given by:

$$m_{ns^*} = \int\limits_0^\infty S_{s^*}(\omega) \cdot \omega_e^n \cdot d\omega \qquad \text{with: } n = 0, 1, 2, ... \qquad (11.27)$$

Using the Rayleigh distribution, the short term probability of shipping green water in a given storm condition is:

$$\boxed{P\left\{s_a^* > f_e\right\} = \exp\left(\frac{-f_e^2}{2m_{0s^*}}\right)} \qquad (11.28)$$

The number of times per hour that green water will be shipped in a certain sea state follows from the short term probability on shipping green water and the number of oscillations per hour:

$$\boxed{N_{\text{shipping/hour}} = \frac{3600}{T_{2s^*}} \cdot P\left\{s_a^* > f_e\right\}} \qquad (11.29)$$

in which $T_{2s^*} = 2\pi\sqrt{m_{0s^*}/m_{2s^*}}$ is the average zero-crossing period.

11.2.3   Slamming

Slamming is a two-node vibration of the ship caused by suddenly pushing the ship by the waves. This occurs when the bow of the ship comes completely out of the water and then "crashes down" with an impact against the next wave. Slamming influences the local pressures on the hull plating and a local damage can be the result. The impulse nature of the impact also causes internal vibrations which can contribute to structural fatigue in the ship. Slamming does not necessarily influence the overall vertical displacements of the ship significantly. Slamming forces can be very large, but they act on the ship during a very short time.

A complete prediction of slamming phenomena is a very complex task, which is beyond the scope of any existing theory. Slamming impact pressures are affected by the local hull section shape, the relative velocity between ship and wave at impact, the relative angle between the keel and the water surface, the local flexibility of the ship's bottom plating and the overall flexibility of the ship's structure.

Ochi Criterium

[Ochi, 1964] has translated slamming phenomena into requirements for the vertical relative motions of the ship; he defined slamming by:

 - an emergence of the bow of the ship at 10 per cent of the length aft of the forward perpendiculars and

 - at the instant of impact the exceedance of a certain critical vertical relative velocity, without forward speed effect, between the wave surface and the bow of the ship.

Ochi defines the vertical relative displacement and velocity of the water particles with respect to the keel point of the ship by:

$$\begin{aligned} s &= \zeta_{x_b} - z + x_b \cdot \theta \\ \dot{s} &= \dot{\zeta}_{x_b} - \dot{z} + x_b \cdot \dot{\theta} \end{aligned} \qquad (11.30)$$

with:

$$\zeta_{x_b} = \zeta_a \cdot \cos(\omega_e t - k x_b \cos \mu)$$
$$\dot{\zeta}_{x_b} = -\omega_e \zeta_a \cdot \sin(\omega_e t - k x_b \cos \mu) \tag{11.31}$$

which means that a forward speed effect is not included in his definition of the vertical relative velocity.

The spectral moments of the vertical relative displacements and velocities are defined by m_{0s} and $m_{0\dot{s}}$. Emergence of the bow of the ship happens when the vertical relative displacement amplitude, s_a, at $0.90 \cdot L$ is larger than the ship's draft, d, at this location. The probability of emergence of the bow follows from:

$$P\{s_a > d\} = \exp\left(\frac{-d^2}{2m_{0s}}\right) \tag{11.32}$$

Ochi's second requirement states that the vertical relative velocity exceeds a threshold value. He used - based on model and full scale experiments with frigates - 12 feet per second as a threshold value for a ship with a length of 520 feet.

Froude scaling of this threshold value results in:

$$\dot{s}_{cr} = 0.093 \cdot \sqrt{g \cdot L} \tag{11.33}$$

The probability of exceeding this threshold value is:

$$P\{\dot{s}_a > \dot{s}_{cr}\} = \exp\left(\frac{-\dot{s}_{cr}^2}{2m_{0\dot{s}}}\right) \tag{11.34}$$

Both occurrences - emergence of the bow and exceeding the threshold velocity - are statistically independent. In case of slamming both occurrences have to appear at the same time.

Thus the probability on a slam is the product of the two independent probabilities:

$$\boxed{P\{\text{slamming}\} = P\{s_a > d\} \cdot P\{\dot{s}_a > \dot{s}_{cr}\}} \tag{11.35}$$

or, using the Rayleigh distribution for each of these:

$$\boxed{P\{\text{slamming}\} = \exp\left(\frac{-d^2}{2m_{0s}} + \frac{-\dot{s}_{cr}^2}{2m_{0\dot{s}}}\right)} \tag{11.36}$$

Conolly Criterium

[Conolly, 1974] has translated slamming phenomena into requirements for the peak impact pressure of the ship; he defined slamming by:
- an emergence of the bow of the ship and
- an exceedance of a certain critical value, p_{cr}, by the peak impact pressure, p, at this location.

The peak impact pressure, p, is defined by:

$$p = C_p \cdot \frac{1}{2}\rho \dot{s}^2 \tag{11.37}$$
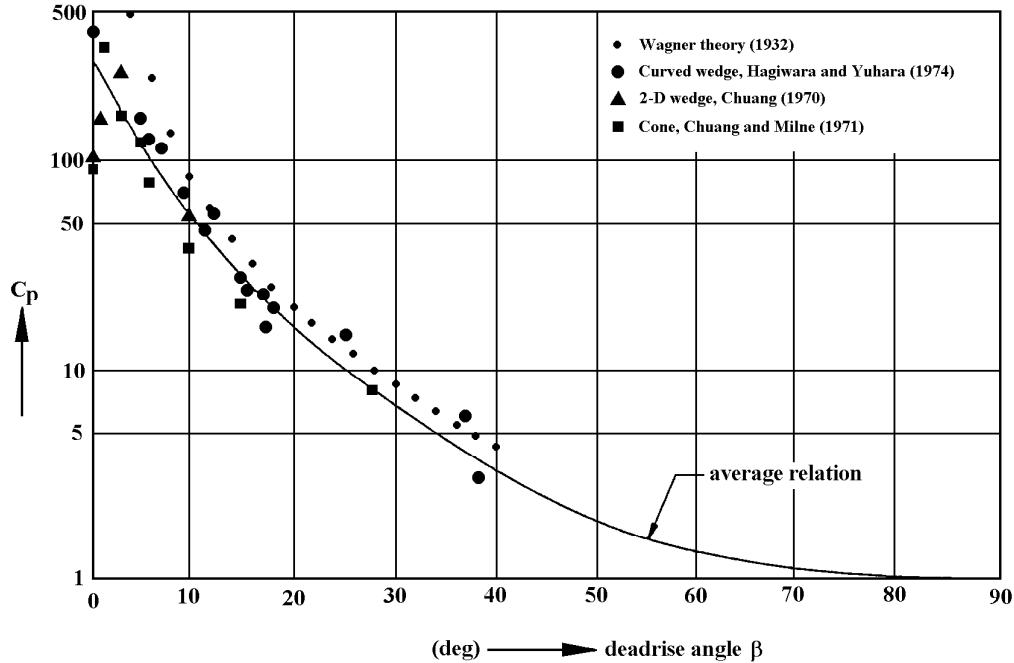
Figure 11.7: Peak Impact Pressure Coefficients

in which $\dot{s}$ is the vertical relative velocity between the ship and the wave.

The pressure coefficient C_p has been taken from experimental slamming drop tests data with wedges and cones, as given in the literature. Some of these data, as presented by [Lloyd, 1989] as a function of the deadrise β, are illustrated in figure 11.7.

The deadrise is the angle of the inclination at the keel of the contour of a cross section. This angle does not remain constant outside the center line. An equivalent deadrise β is defined here by an engineers solution: the deadrise of an equivalent wedge. The contour of the cross section inside 10 percentile of the half breadth $B/2$ of the ship has been used to define an equivalent wedge with a half breadth: $b = 0.10 \cdot B/2$. The accessory draft t of the wedge follows from the section contour. This draft can be larger than 10 percentile of the amidships draft d in the fore body of the ship. If so, the section contour below $0.10 \cdot d$ has to be used to define an equivalent wedge: $t = 0.10 \cdot d$. When this draft, t, is larger than the local draft, d, then the local draft has to be used. The accessory half breadth, b, of the wedge follows from the section contour.

Then the sectional area, A_s, below local draft, t, has to be calculated and the equivalent deadrise angle β (see figure 11.8) follows from:

$$\beta = \arctan\left(\frac{a}{b}\right) \qquad 0 \leq \beta \leq \frac{1}{2}\pi$$

$$a = \frac{2(b \cdot t - A_s)}{b} \tag{11.38}$$

Critical peak impact pressures, p_{cr}, can be taken from [Conolly, 1974]. He gives measured impact pressures over 30 per cent of the ship length from forward for a ship with a length of 112 meters. From this, a boundary of p_{cr} between slamming and no slamming can be assumed. This boundary is presented in figure 11.9.
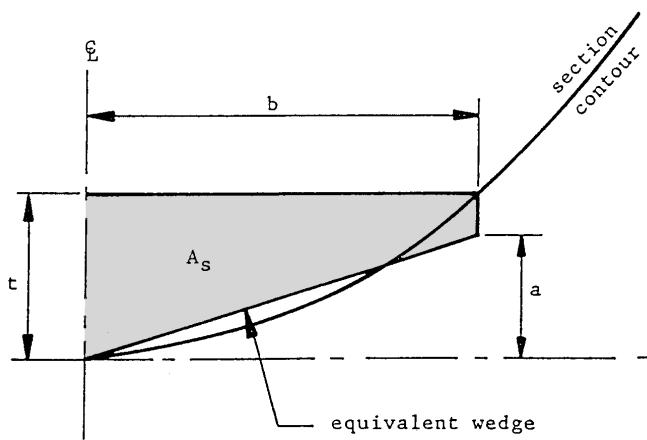
Figure 11.8: Deadrise of an Equivalent Wedge
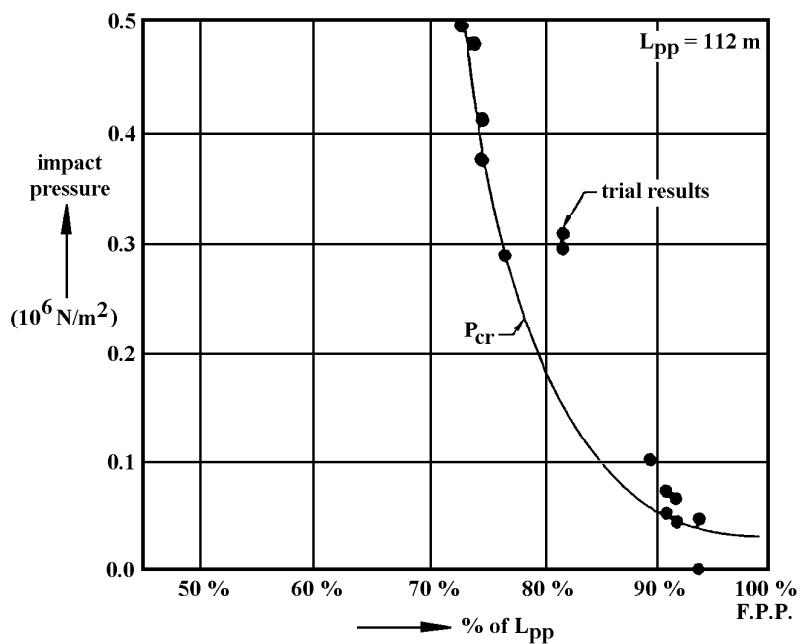
Figure 11.9: Measured Impact Pressures and Lower Limits

These values have to be scaled by Froude's law to the actual ship size. Bow emergence and exceedance of this limit is supposed to cause slamming. This approach can be translated into local hull-shape-dependent threshold values, $\dot{s}_{cr}$, of the vertical relative velocity as well:

$$\dot{s}_{cr} = \sqrt{\frac{2p_{cr}}{\rho C_p}} \qquad (11.39)$$

The vertical relative velocity - including a forward speed effect - of the water particles with respect to the keel point of the ship is defined by:

$$\dot{s} = \frac{D}{Dt} \left(\zeta_{x_b} - \dot{z} + x_b \cdot \theta \right)$$
$$= \dot{\zeta}_{x_b} - \dot{z} + x_b \cdot \dot{\theta} - V \cdot \theta \qquad (11.40)$$

with:

$$\zeta_{x_b} = \zeta_a \cos(\omega_e t - k x_b \cos \mu)$$
$$\dot{\zeta}_{x_b} = -\omega \zeta_a \sin(\omega_e t - k x_b \cos \mu) \qquad (11.41)$$

Then:

$$P\{\text{slamming}\} = \exp \left(\frac{-D_s^2}{2m_{0s}} + \frac{-\dot{s}_{cr}^2}{2m_{0\dot{s}}} \right) \qquad (11.42)$$

Note that - because the forward speed effect is included here - the spectral moment of the velocities does not follow directly from the spectral density of the relative displacement as used by Ochi.

The average period of the relative displacement is found by:

$$T_{2s} = 2\pi \sqrt{\frac{m_{0s}}{m_{2s}}} = 2\pi \sqrt{\frac{m_{0s}}{m_{0\dot{s}}}} \qquad (11.43)$$

Then the number of times per hour that a slam will occur follows from:

$$N_{\text{slams/hour}} = \frac{3600}{T_{2s}} \cdot P\{\text{slamming}\} \qquad (11.44)$$

11.2.4   Sustained Sea Speed

In the last half century ship's officers can obtain routing advice from weather routing offices on shore, often connected with meteorological institutes. With a known or expected rough weather pattern on the ocean, an optimum ship's route with respect to minimum travelling time, minimum fuel consumption or minimum risk of damage can be found.

Wind and wave forecasting is a meteorological problem.

The prediction of the ship's reaction to wind and waves - in particular the ship's speed - is based on predictions and/or routing experience with the ship under consideration or with similar ships. The so-called sustained sea speed depends on the ship's resistance, the characteristics of propeller and engine and the behavior of the ship in waves. In determining the sustained sea speed two factors are considered: the **natural speed reduction** due to added resistance - mainly caused by wind and waves - and the **voluntary speed reduction** by the ships captain, in order to avoid severe motions or their consequences such as damage to ship and cargo or crew and passenger seasickness.

Ship's Resistance

The total resistance of a ship in a seaway can divided in several parts and contributions; the most important of which follow below:

- Still Water Resistance
  Until now it is not possible to make pure theoretical calculations of the ship's resistance in still water. To estimate the required power in a design stage, use must be made of model experiments carried out in a towing tank. These experimental results are extrapolated to full scale by techniques based on physical laws and experience, as has been treated in chapter 4. Numerous empirical methods can be found to estimate the still water resistance, based on model experiments and trial data. Best known is the method of [Holtrop, 1984], which has the advantage that the results are presented in empirical formulas suitable for computer use.

- Wind Resistance
  The wind resistance for ships with high superstructures or with a lot of cargo on deck - such as container ships - can be considerable. A reliable method for estimating the wind resistance of ships was published by [Isherwood, 1973]; see chapter 4.
  The following relation between the absolute wind speed V_w and the significant wave height $H_{1/3}$ - obtained from ITTC recommendations - can be used for a quick analysis:

$$V_w = 10 \cdot {H_{1/3}}^{2/3} \tag{11.45}$$

  in which the wind velocity, V_w, is in knots and the significant wave height, $H_{1/3}$, is in meters.

- Added Resistance due to Waves
  The relative motions of a ship with respect to the water surface cause an added resistance. This has been shown in chapter 8, where two methods are given:
  - the radiated energy method of [Gerritsma and Beukelman, 1972], suitable for head to beam waves and
  - the integrated pressure method of [Boese, 1970], suitable for all wave directions.
  These methods are based on the assumption of the linearity of the ship's response; thus the added resistance varies with the wave amplitude squared.

- Added Resistance due to Steering
  In a seaway, the ship's heading will be disturbed by wind and waves. The beam waves cause sway and yaw motions. To maintain a heading in a sea with a beam wind, rudder angles are necessary to counteract the wind and wave moment at any instant. For instance, a Beaufort 9 sea caused by beam wind can require oscillating rudder angles with an amplitude of 15 degrees or more. All of this results in an increase of the ship's resistance.
  In these beam waves, the ship will sail with yaw motions caused by the sea and by the correcting autopilot. These yaw motions cause centrifugal forces, of which the longitudinal components introduce a resistance; see figure 11.10. Assuming a fixed position of the pivot point (fictive rotation point of the ship) at 10 % from the forward perpendicular and an additional hydrodynamic mass for sway of 80 % of the ship's
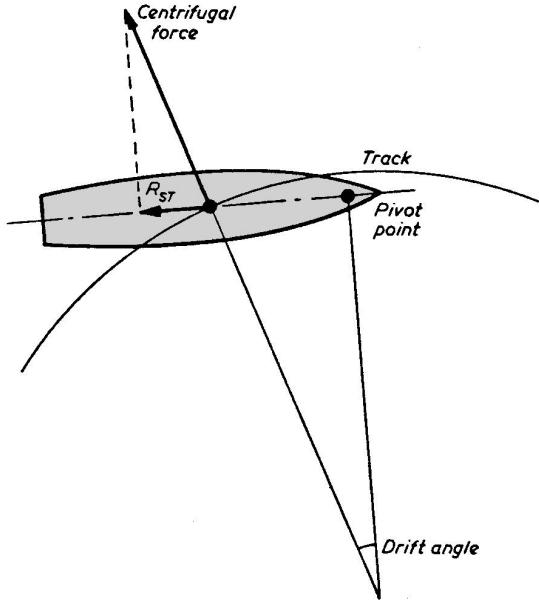
Figure 11.10: Resistance due to Steering

solid mass, the mean added resistance during a harmonic yaw motion will be in the order of:

$$R_{ST} = 0.030 \cdot \nabla L \dot{\psi}_a{}^2 \qquad\qquad (11.46)$$

with:

$$
\begin{array}{rcl}
R_{ST} & = & \text{steering resistance in kN} \\
\nabla & = & \text{volume of displacement in m}^3 \\
L & = & \text{length of the ship in m} \\
\dot{\psi}_a & = & \text{rate of turn amplitude in deg/min}
\end{array}
$$

This means for a 200 meter container vessel - with rate of turn amplitudes of 30 degrees per minute at the service speed in following waves - a resistance increase of 20 % of the still water value. The course deviations in this example are only about 2 degrees. This shows that the setting of the autopilot is important.

Sway motions also increase the total sailed distance and - as a result - a reduced average speed along the given track.

- Added Resistance due to Fouling

  Fouling of the ship's hull can cause a considerable increase in the ship's resistance. The extent of fouling depends on the sailing routes and the time during which the ship will sail in areas with large fouling effects. As fouling is a biological process - depending on the paint used - it is not easy to give accurate mean values for all ships, seasons and areas. Moreover, the effect of fouling depends on the docking period and the time since the last docking of the ship.

  Fouling will only affect the friction part, R_f, of the ship's resistance. Aertssen carried out full scale experiments to investigate the problem of fouling. From his extensive results of full scale measurements it appeared that - for a ship sailing on the Atlantic

route - the effect of fouling on the frictional resistance will be in the order of:

$$\frac{\Delta R_f}{R_f} \cdot 100\% \; = \; 3.6 \cdot y_a + \frac{40 \cdot y_d}{1 + 2 \cdot y_d} \tag{11.47}$$

in which y_a is the age of the ship in years and y_d is the year since the last docking. This means for instance, an increase of the frictional resistance by about 30 % for a ship with an age of five years and a last docking one year previously.

However, the overall effect on the total resistance is smaller and depends on speed and ship type. With low speeds and full ship forms - e.g. tankers - the frictional resistance is the major part of the total resistance, whereas the wave-making resistance dominates in the case of high speed container ships. This means that the effect of fouling is much larger for tankers than for container ships.

An investigation by [Journée, 1976b] of log data of a 200,000 tdw tanker, sailing from Europe to the Persian Gulf, showed an increase of the still water resistance for full load and ballast condition as 26 to 29 % one year after the last docking and 47 to 52 % two years after the last docking. After the oil crisis in the early seventies these ships reduced power by 50 %, resulting in a speed reduction for the clean hull from 16 to 13 knots. To maintain this speed two years after the last docking the power of a fully loaded ship had to be increased from 50 to over 80 %. This behavior is visualized in figure 11.11 as an example to show that fouling is a factor which should not be neglected in sustained sea speed calculations.
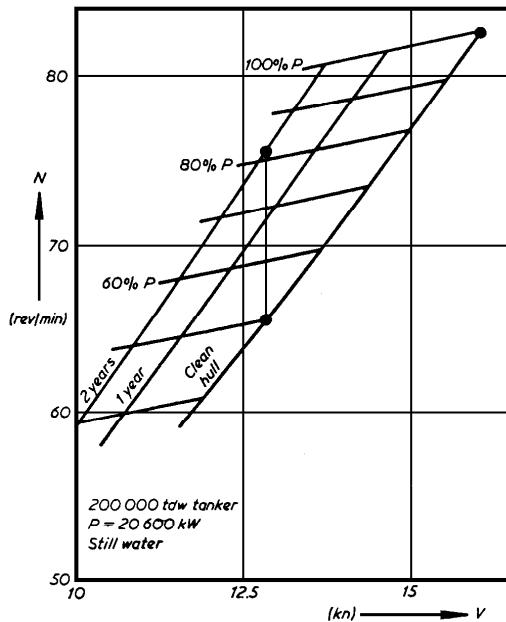
Figure 11.11: Increase of Required Propulsion Power due to Fouling

The sum of these contributions provides the total resistance of the ship under operational conditions.

Propulsion

The propeller behind a ship can be considered as an energy transformer: torque with engine speed will be transformed into thrust with a speed of advance of the propeller, relative to the mean velocity of the incoming water. At a constant engine setting there should be an equilibrium between the engine speed and the ship's speed in such a way that two conditions are fulfilled: the torque required by the propeller must be in equilibrium with the torque delivered by the engine and the thrust delivered by the propeller must be in equilibrium with the total resistance of the ship in the self-propelled condition. This has been treated in chapter 4.

- Propeller
  The characteristics of an open water propeller in its normal operating range are usually expressed in its thrust coefficient, K_T, and torque coefficient, K_Q, as a function of the speed (or advance) ratio, J:

$$K_T = \frac{T}{\rho D^4 n^2} \qquad\qquad K_Q = \frac{Q}{\rho D^5 n^2} \qquad\qquad J = \frac{V_e}{nD} \qquad (11.48)$$

  with T is thrust, Q is torque, ρ is density of water, D is propeller diameter, n is number of propeller revolutions per second and V_e is relative speed of advance.

  These characteristics depend on the number of propeller blades, the pitch ratio and the expanded blade area ratio and can be obtained by means of open water model experiments. Results of such experiments with systematically varied propeller series can be found in various publications.

  One of the best known is the Wageningen B-propeller series of MARIN. Over 120 systematically varied propeller models have been tested and the results are given in polynomials, together with a correction for scale effect. These results are valid for the open water condition.

  For the "behind the ship condition" the open water torque must be multiplied by the relative rotative efficiency η_R:

$$\eta_R = \frac{Q_{\text{open water}}}{Q_{\text{behind ship}}} \qquad (11.49)$$

  which varies from about $\eta_R = 1.04$ for single screw ships to about $\eta_R = 0.97$ for twin screw ships. This efficiency reflects the difference in torque in the wake and in open water at the same thrust.

  The relative speed of the water, V_e, into the propeller disc is not equal to the forward ship speed, V. A wake fraction, w, should be taken into account:

$$V_e = V \cdot (1 - w) \qquad (11.50)$$

  This wake fraction varies from 0.2 to 0.4 and can be obtained directly from model experiments - taking into account the scale effect - or from empirical formulas given in the literature.

  From model experiments it appears that the wake fraction is hardly affected by an increase of the propeller loading due to a resistance increase, caused by - for instance - towing a barge, motions in waves, etc.

  As discussed in chapter 4, the thrust of the propeller, T, is not equal to the ship's

resistance, R, found from resistance tests. A thrust deduction fraction, t, should be taken into account:

$$R = T \cdot (1 - t) \tag{11.51}$$

The thrust deduction fraction in still water is usually about 60 to 80 % of the wake fraction and can be obtained from model experiments or by empirical formulae.

This fraction however, will decrease with an increased loading of the propeller; in the bollard condition - at zero forward ship speed - this fraction will be about 0.03 to 0.05. From model experiments it appears that, at a constant propeller rotation rate, the thrust deduction fraction decreases - at an increasing loading of the propeller - quadratically with the forward ship speed. It can drop down to a value of about 0.03 to 0.05 in the bollard condition (zero speed).

The influence on the efficiency of oscillations of the propeller behind a ship in waves can be neglected for practical purposes.

- Engine
  The relation between the delivered torque of an engine and the engine speed at a constant setting and an increased loading in a seaway is also important. In this connection two different types of engines are distinguished: a turbine and a diesel engine.

  - Turbine
    As a first approximation, it is often accepted that - for an increasing loading of the engine at a constant engine setting - the delivered power remains constant; this means a hyperbolic relation between the torque at the propeller and the engine speed:

    $$Q = c \cdot \eta_m \cdot \frac{Q_0 \cdot n_0}{n} \qquad \text{for a turbine} \tag{11.52}$$

    in which c is the engine setting, η_m is the mechanical efficiency of the shaft bearings and $2\pi Q_0 n_0$ is the maximum continuous rating power with n_0 in rev/sec. More precisely however, there is a linear relation between torque and engine speed:

    $$Q = c \cdot \eta_m \cdot Q_0 \cdot \left(a - (a - 1) \cdot \frac{n}{n_0} \right) \qquad \text{for a turbine} \tag{11.53}$$

    in which the coefficient a depends on the type of the turbine $(2 \leq a \leq 3)$.
    If one takes into account that - at a constant setting - the turbine speed will not be reduced by more than 15 %; the assumption of constant power is sufficiently accurate for practical purposes such as the calculation of the ship's speed.

  - Diesel Engine
    For a diesel engine it is usually accepted that the torque remains constant for an increasing loading of the engine at a constant engine setting:

    $$Q = c \cdot \eta_m \cdot Q_0 \qquad \text{for a diesel engine} \tag{11.54}$$

    This yields that the coefficient a in equation 11.53 is equal to1.0.
    In practice, there are some deviations from this assumption. At a constant engine setting and an increasing loading of the engine the torque will first increase

to a maximum value and will then decrease again. This can be approximated by a linear relation between torque and engine speed, provided that the number of revolutions per minute does not reduce more than about 15 %. Then the linear relation in equation 11.53 can be used for a diesel engine, too, with for instance $a = 1.0 - 1.5$.

Often the engine speed will be kept constant. This means that the coefficient a goes to infinity and the engine setting c has no meaning anymore; n will be equal to n_0.

Speed Calculation

[Journée, 1976b] describes a method to calculate the ship's speed in seaway at a given engine setting. Comparisons with published full scale data have shown a reasonable agreement between 'theory' and results of full scale experiments.

The principle of the calculation method is shown in figure 11.12. For a number of ship speeds, the relation between the torque required by the propeller and the number of revolutions per minute are calculated from the torque characteristics of the assumed B-series propeller behind the ship and a wake fraction. The relation between the torque delivered by the engine to the propeller and the number of revolutions per minute is known from engine characteristics and shaft losses. These relations give an equilibrium relation for speed and number of revolutions per minute, which - together with the thrust deduction faction - results in a resistance that can be overcome by propeller and engine as a function of the speed. This is the right hand part of figure 11.12. The actual total resistance of the ship in a seaway as a function of the speed is known by adding up its components; the required equilibrium yields the ship's speed.

If greater speed-accuracy is required, speed, propeller rate and power data, for instance derived at the ship's trial, can be used to adjust the resistance curve and the propeller characteristics.

Figure 11.13 shows the sustained sea speed (or speed loss) of a ship in relation to its course with respect to the waves in various sea states. The circular curves in this figure are curves of constant ship speeds in knots; the non-circular curves are the sustained sea speeds of the ship, each at a constant sea state defined by a significant wave height - ranging from 2 until 8 meters - only. Note that head waves are indicated here by 0^0; a convention often used in ship navigation.

Often, a fixed relation between the significant wave height and the mean wave period will be used in these speed graphs. Figure 11.14-a gives the results of speed loss calculations in head waves of a 200,000 tdw tanker at a range of wave heights and wave periods. It shows a striking influence of the wave period on the ship's speed.

Voluntary Speed Reduction

When a ship enters a severe storm the ship's captain can reduce speed or change course in order to reduce motions. Phenomena that are important for the decision to reduce speed are shipping of green water and slamming as discussed before, but also heavy vertical accelerations forward and sometimes propeller racing (if it comes partially out of the water).

Accelerations forward - exceeding certain limits - can damage ship or cargo and are therefore often a reason for voluntary speed reduction. This can be too simple; figure 11.14-b shows
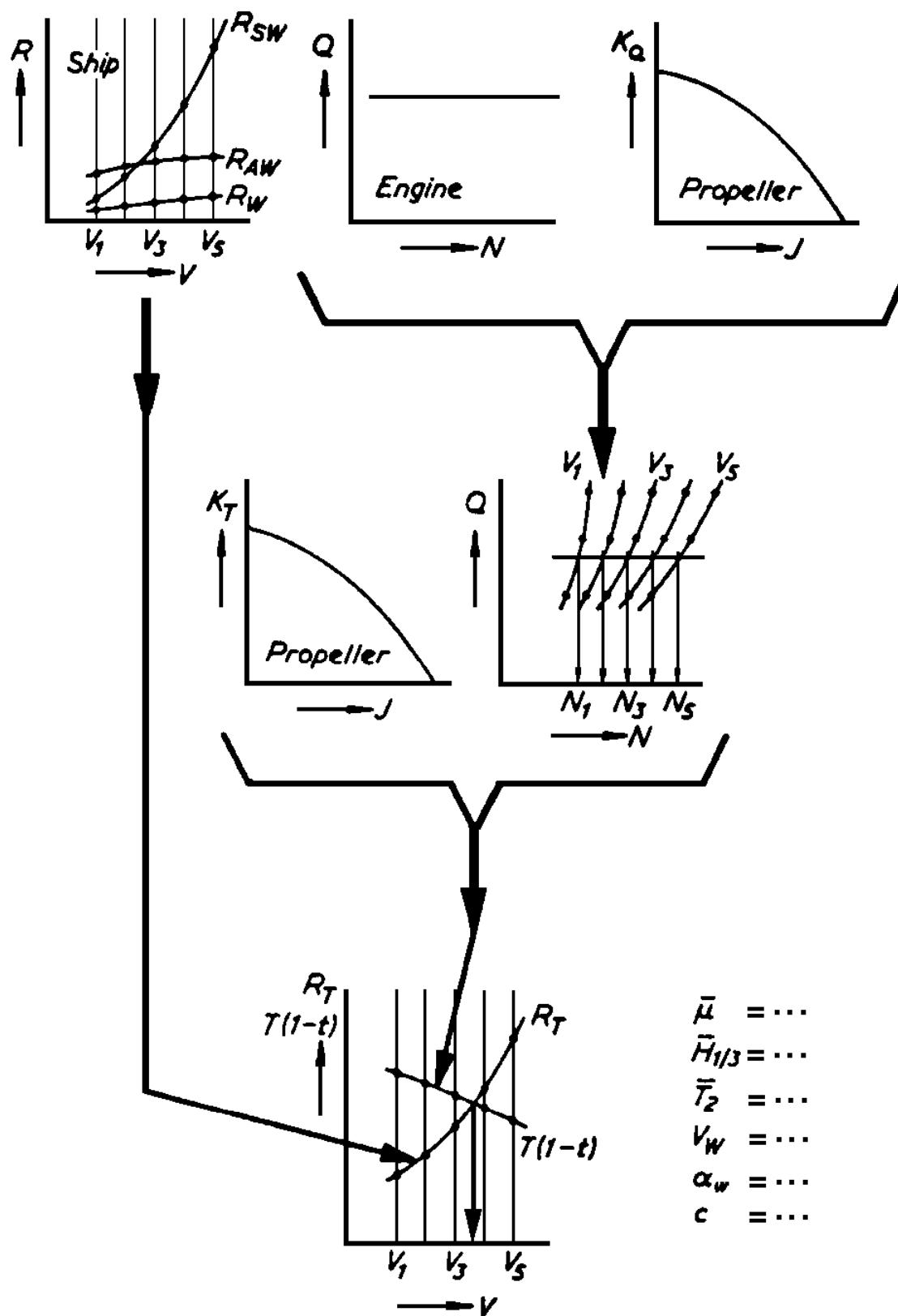
Figure 11.12: Scheme of Forward Speed Calculation
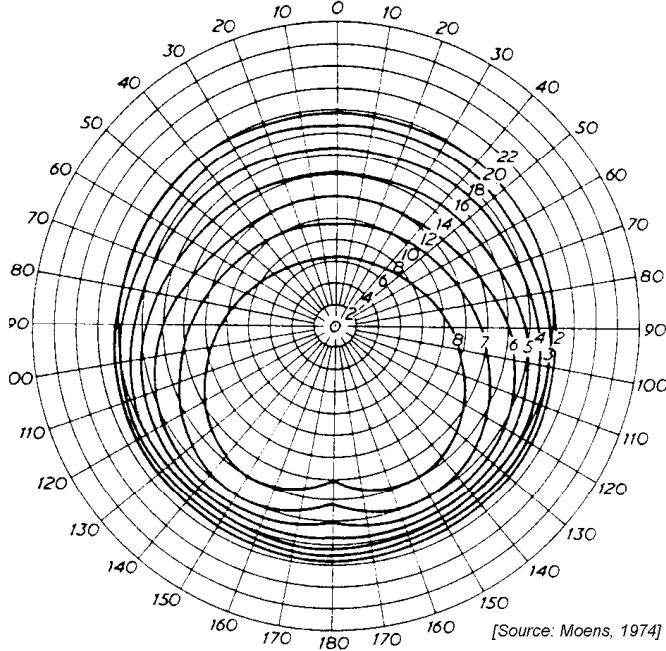
Figure 11.13: Speed Loss Graph with Sustained Sea Speeds

the considerable influence of the forward ship speed on the vertical accelerations forward for a container vessel.

Propeller racing is the rapid increase of the rate of turn due to a lack of loading, because of propeller emergence; it is largely prevented nowadays by rpm-governors on the engine. However, large thrust and torque fluctuations occur in waves, even at a constant number of revolutions per minute. This is reason why propeller racing is sometimes defined as an emergence of the propeller which causes a decrease of torque in excess of 25 %. However, often a more simple definition is used which defines propeller racing as an emergence of the propeller by more than one third of the propeller diameter.

Criteria for reducing speed can be found in various publications. They are commonly expressed as probability limits for the accelerations forward and probability limits for the occurrence of shipping water at the bow and slamming. In some cases, probability limits for propeller racing are included too.

Well-known voluntary speed reduction criteria are those of [Ochi and Motter, 1974]. They give probability limits below which no voluntary speed reduction should be expected. These criteria distinguish between two typical loading conditions of the ship:

- **Fully laden condition:**

$$P\left\{\text{bowdeck wetness}\quad\text{and/or}\quad \ddot{z}_{a_{1/3}}(\text{bow}) \geq 0.4 \text{ g}\right\} \leq 0.07 \qquad (11.55)$$

  This probability criterium of Ochi and Motter can be rewritten as:

$$P\left\{\text{bowdeck wetness}\quad\text{and/or}\quad \ddot{z}_a(\text{bow}) \geq 0.46 \text{ g}\right\} \leq 0.07 \qquad (11.56)$$

  or:

$$\begin{aligned} P\left\{\text{bowdeck wetness}\right\} + P\left\{\ddot{z}_a(\text{bow}) \geq 0.46 \text{ g}\right\} \\ -P\left\{\text{bowdeck wetness}\right\} \cdot P\left\{\ddot{z}_a(\text{bow}) \geq 0.46 \text{ g}\right\} &\leq 0.07 \end{aligned} \qquad (11.57)$$
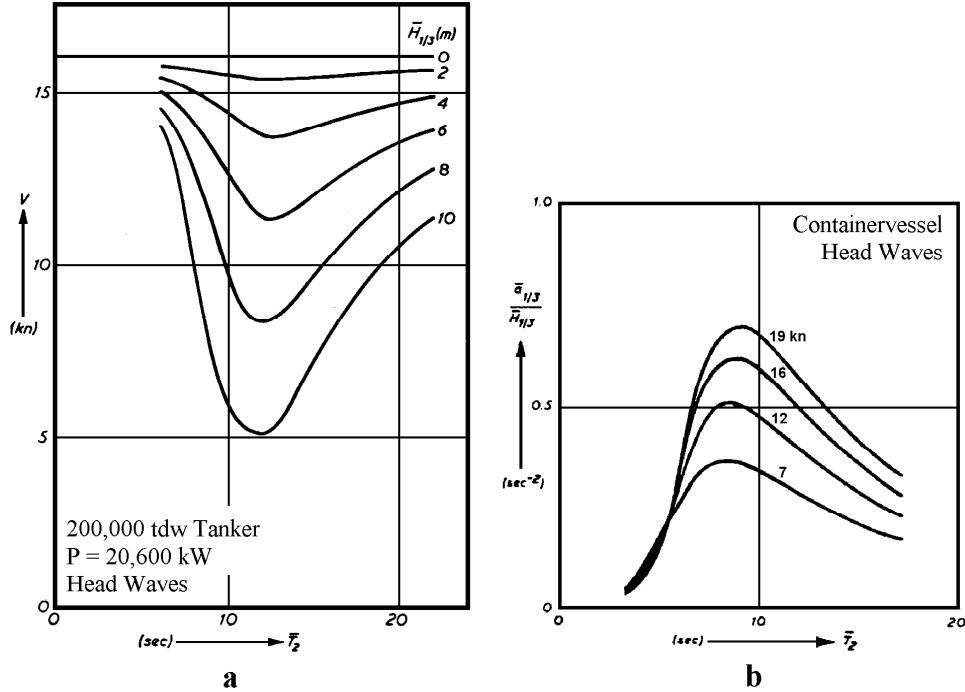
Figure 11.14: Effect of Wave Period on Sustained Sea Speed and on Accelerations Forward

- **Light laden condition:**

$$P\left\{\text{slamming} \quad \text{and/or} \quad \ddot{z}_{a_{1/3}}(\text{bow}) \geq 0.4 \text{ g}\right\} \leq 0.03 \qquad (11.58)$$

This probability criterium of Ochi and Motter can be rewritten as:

$$P\left\{\text{slamming} \quad \text{and/or} \quad \ddot{z}_a(\text{bow}) \geq 0.53 \text{ g}\right\} \leq 0.03 \qquad (11.59)$$

or:

$$\begin{aligned} P\left\{\text{slamming}\right\} + P\left\{\ddot{z}_a(\text{bow}) \geq 0.53 \text{ g}\right\} \\ -P\left\{\text{slamming}\right\} \cdot P\left\{\ddot{z}_a(\text{bow}) \geq 0.53 \text{ g}\right\} \quad \leq \quad 0.03 \qquad (11.60) \end{aligned}$$

Use has been made here of the following probability relation, valid for two **statistically independent events** A and B:

$$\begin{aligned} P\left\{A \text{ and/or } B\right\} &= P\left\{A\right\} + P\left\{B\right\} - P\left\{A \text{ and } B\right\} \\ &= P\left\{A\right\} + P\left\{B\right\} - P\left\{A\right\} \cdot P\left\{B\right\} \qquad (11.61) \end{aligned}$$

In these criteria, bowdeck wetness has to be determined at FPP (forward perpendicular), slamming at $0.90 \cdot L_{pp}$ and the vertical accelerations of the bow at FPP.
Note that these criteria are rather moderate; in fact they should also depend on the type of the ship and its cargo.

Figure 11.15 shows an example of the sustained sea speed as a function of the Beaufort scale for Victory Class ships. In order to avoid severe motions, these ships have to reduce power already in rough weather conditions defined by Beaufort 6, approximately.

[Source: Principles of Naval Architecture]
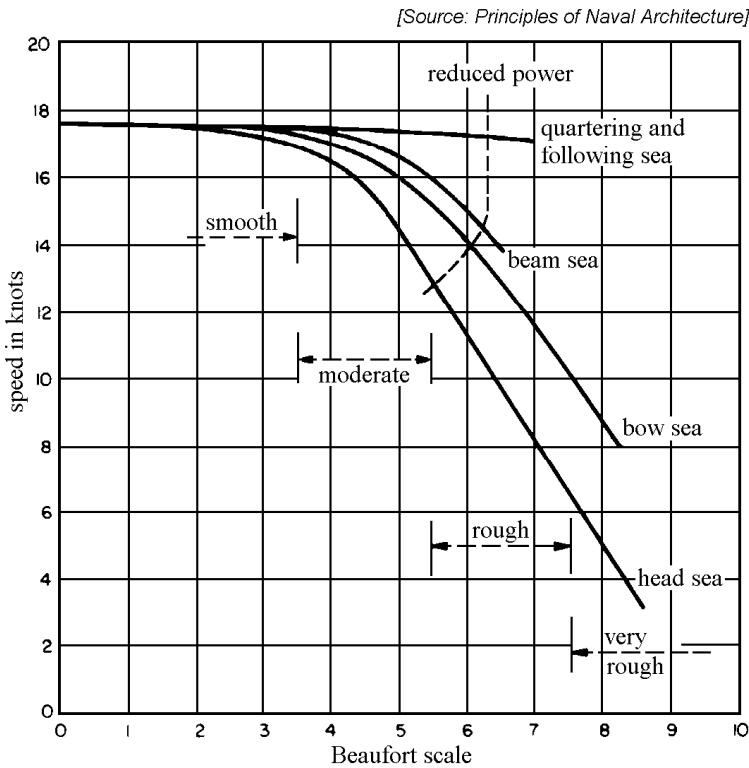
Figure 11.15: Speed Loss of Victory Class Ships

Applications

When designing a ship, much attention is paid to the still water resistance with respect to hull form, expensive bulbous bows and propeller design. On the North Atlantic Ocean however, a sea state of Beaufort 6 is exceeded 70 % of the time during the winter season and 45 % during the summer season. Depending on the ship's size, the added resistance - caused by vertical ship motions - can be considerable. In head waves in this sea state, a ship with a length of about 135 meters and a service speed of 16 knots in still water will have an added resistance equal to its still water resistance at about 12 knots. Thus, it is worthwhile to pay attention to this added resistance, caused by vertical ship motions in a seaway.

Speed and power calculations of a ship in a seaway can be used to support the work of routing officers. Together with the meteorological information, accurate speed loss graphs will help them to give well-founded routing advice to the ship's captain. This is of importance from an economic point of view as well as from the ship's safety point of view. Ship motions can be calculated with a fair accuracy but the limits with respect to the voluntary speed reduction are less certain. Computations use moderate limits, derived from the available literature. However, these limits can be adjusted at sea to correspond to those permitted by the ship's captain.

This kind of calculation can also be used in developing operational performance systems on board of ships. The calculated speed, power, fuel consumption and motion data can be used in these systems with respect to decisions for course deviations or speed reductions. Another application of these calculations can be found in economical studies of the

operation of these ships with respect to travelling time, fuel consumption, etc. This brings one to a very interesting economic calculation which should include such factors as safety limits in relation to insurance costs, the total transit time for both the ship and its cargo (think of the lost production from a jack-up drilling rig being moved on a heavy-transport ship), fuel consumption and its costs and personnel costs.

11.3 Dredger Limitations

Dredging masters tend to be experienced-based rather than theoretical. Since they often spend a significant part of their career on one ship, they can circumvent the response computations and thus express operational limits directly in terms of the conditions (wind, waves and currents) which cause the limit conditions. Note that this experienced-based direct approach can have significant errors from an economic point of view (stopping operations too soon or continuing too long). It is also difficult to use for special dredgers of an extreme size or with a non-standard form.

11.3.1 Dredger Wave Limitations

With these limitations, the following are considered to be general operating limits - in terms of significant wave height - in short waves (sea) or longer waves (swell) for each of the given dredging operations.

Floating Object	Maximum $H_{1/3}$ (m) in short waves	Maximum $H_{1/3}$ (m) in long waves
Small equipment discharging into barges	0.30 - 0.50	0.20 - 0.40
Large equipment discharging into barges	0.50 - 1.00	0.40 - 0.80
Small equipment with floating pipeline	0.20 - 0.50	0.20 - 0.50
Large equipment with floating pipeline	0.50 - 1.00	0.30 - 0.60
Self-propelled barges with suction pipe	0.60 - 1.00	0.40 - 0.80
Trailer with swell compensator	2.00 - 4.00	2.00 - 4.00

This is not the whole story however. Consider the case when a trailing suction dredge (with swell compensator) is being used to pick up sand, bring it near shore, and discharge it into a pipeline (at an exposed location), for instance to restore a beach. Even though the ship may be able to dredge (pick up sand) in 2 to 4 meter waves, it will likely not be appropriate to come into shallow water (where the discharge pipeline starts) or even to use a small boat to assist in connecting to this line. The proper analysis of such a dredging cycle must account for these differences as well as the sequence and duration of each component step. This can be a very interesting topic, but one which is beyond the scope of this text.

11.3.2   Dredger Current Limitations

If the anchors hold sufficiently, it makes a considerable difference as to whether the ship can work with the current or whether it has to work at an angle to the current, as for instance a cutter suction dredger. For a cutter suction dredger the situation is particularly dangerous when the current is directed against the ladder side. The current direction in this figure approaches from the ladder side, which is convenient in that it helps supply material to the suction mouth in the cutter. On the other hand, when the current is too strong or the deviation angle gets too large the anchoring system on the ladder can fail. When this happens, the dredge will swing around her spud pile which can result in a broken discharge pipe, a broken (or bent) spud pile, a broken ladder when it hits the channel side or even a capsized dredger, if the spud pile and/or the ladder do not fail.

Here, again, dredging masters are experience-based. For most of the larger cutter suction dredgers the safe limit can be estimated at about 2 knots velocity of the current. For bucket dredgers and stationary dredgers the limit is about 3 knots provided the anchorage and freeboard of the ship are sufficient. Self-propelled barges are preferable when working in strong currents; this avoids the need for moorings between the dredge and transportation barge.

Chapter 12

WAVE FORCES ON SLENDER CYLINDERS

12.1 Introduction

Chapters 6 through 11 have handled the hydromechanics of large (floating) bodies in the sea. Attention now switches to the hydromechanics of slender cylinders. Examples of such cylinders include the leg or brace of an offshore space truss structure, a pipeline or even an umbilical cable extending down to some form of remotely controlled vehicle.

12.2 Basic Assumptions and Definitions

A slender cylinder in this discussion implies that its diameter is small relative to the wave length. The cylinder diameter, D, should be much less than the wave length, λ; the methods to be discussed here are often usable as long as $\frac{D}{\lambda} <$ about 0.1 to 0.2.

Derivations are done for a unit length of cylinder. Force relationships will yield a force per unit length. This relationship must then be integrated over the cylinder length to yield a total force. The implications of this unit length approach combined with the restriction to slender cylinders is that the ambient water motions in the immediate vicinity of the cylinder are all about the same at any instant in time. This is (assumed to be) true both vertically and horizontally; the spatial variation in the undisturbed flow near a unit length of cylinder is simply neglected. A similar assumption was made for the heaving cylinder in chapter 6, but this is not usually the case with a ship or other large structure as discussed in the previous chapters.

The absence of a spatial variation in the ambient flow as one moves from place to place near the cylinder, makes it possible to characterize the flow in the entire region of the cylinder by the ambient flow at one characteristic location. The axis of the cylinder is chosen as that location; this simplifies the bookkeeping.

The flow around this cylinder segment will be considered to be two-dimensional - quite analogous to strip theory for ships except that the axis of the infinitely long cylinder is not generally horizontal as it was for a ship. Flow components and any resulting forces parallel

---

to the cylinder axis are neglected; all forces are caused by the flow - and later cylinder motion - components perpendicular to the cylinder axis.

The axis system used here is identical to that used for the waves in chapter 5, see figure 5.2. The origin lies at the still water level with the positive z-axis directed upward. The wave moves along the x-axis in the positive direction.

The resulting water motions come directly from chapter 5 as well:

$$u = \frac{\partial \Phi_w}{\partial x} = \frac{dx}{dt} = \zeta_a \omega \cdot \frac{\cosh k\,(h+z)}{\sinh kh} \cdot \cos\,(kx - \omega t) \tag{12.1}$$

$$w = \frac{\partial \Phi_w}{\partial z} = \frac{dz}{dt} = \zeta_a \omega \cdot \frac{\sinh k\,(h+z)}{\sinh kh} \cdot \sin\,(kx - \omega t) \tag{12.2}$$

These can be simplified for the following discussions, however. Since the location, x, of the cylinder element is more or less fixed, the kx term in the above equations can be dropped. For the moment, it is simplest to consider a vertical cylinder so that equation 12.1 will yield the desired flow velocity. All of this yields an undisturbed horizontal flow velocity given by:

$$u(z,t) = \zeta_a \omega \cdot \frac{\cosh k\,(h+z)}{\sinh kh} \cdot \cos\,(-\omega t) \tag{12.3}$$

or at any chosen elevation, z:

$$u(t) = u_a \cos(-\omega t) \tag{12.4}$$

and since $\cos(-\omega t) = \cos(\omega t)$ the sign is often dropped so that:

$$u(t) = u_a \cos(\omega t) \tag{12.5}$$

in which:

$$
\begin{aligned}
u_a \quad &= \quad \text{amplitude the wave-generated horizontal} \\
&\qquad \text{water velocity at elevation } z \text{ (m/s)} \\
\omega \quad &= \quad \text{wave frequency (rad/s)}
\end{aligned}
$$

Note that the elevation dependence in equation 12.3 has been included in u_a in 12.4; this dependence is not included specifically in the most of the following discussion.

Since the flow is time dependent, it will have a horizontal acceleration as well. This can be worked out to be:

$$\dot{u}(t) = -\omega\ u_a \sin\,(\omega t) \tag{12.6}$$

The acceleration amplitude is thus given by:

$$\dot{u}_a = \omega\ u_a \tag{12.7}$$

Since potential theory describes waves so well, the above relations are assumed to hold for any undisturbed wave flow - even when viscosity is involved.

12.3   Force Components in Oscillating Flows

It is convenient to derive the relationships in this section for a smooth-surfaced vertical cylinder. This restriction will be relaxed later in this chapter, however. Since potential flows are so convenient for computations, this discussion of forces in oscillating flows starts with this idealization. The unit length of cylinder being considered is thus vertical and submerged at some convenient depth below the water surface.

12.3.1 Inertia Forces

Remember from chapter 3 that D'Alembert proved that there is no resultant drag force when a **time-independent** potential flow is present. Here, it is the effect of the **flow accelerations** that is of concern.

Consider first the undisturbed ambient (surrounding) flow without any cylinder in it. According to Newton's second law of motion, accelerations result from forces; this is universally true. Thus, the horizontal acceleration of the ambient flow must be driven by a force in the water which, in turn, must come from a horizontal pressure gradient. This pressure gradient is present, even when there is no cylinder in the flow. By examining the pressure gradient force on a differential 'block' of fluid, one discovers that:

$$\begin{aligned} \frac{dp}{dx} &= \rho\frac{du}{dt} \\ &= \rho \cdot \dot{u} \end{aligned} \tag{12.8}$$

which is nothing more than Newton's second law applied to a fluid.

Given this information, what happens when a cylinder is inserted into this pressure and flow field? This question is answered using an approach which has the advantage of physically explaining the separate contributions of two separate inertia force components; a faster, but less 'transparent' derivation will be given later.

Pressure Gradient Force

One must 'drill a hole' in the ambient pressure gradient field in order to 'insert' the cylinder. For now, the fact that the cylinder wall is impervious is neglected completely; the flow is still undisturbed. Any force which this undisturbed pressure field exerts on the cylinder can be computed by integrating this pressure around the perimeter of the circular hole.

This integral yields, knowing that the cylinder is symmetrical with respect to the x-axis and has a unit length:

$$F_{x1}(t) = 2 \cdot \int_0^\pi p(R, \theta, t) \ R \ \cos\theta \cdot 1 \cdot d\theta \tag{12.9}$$

in which $p(R, \theta, t)$ is the undisturbed pressure (N/m^2) on the perimeter of the circle and R is the cylinder radius (m).

The resulting force is computed just as was done in chapter 3, using figure 3.16.

Since the pressure difference across the cylinder at any distance, y, away from the x-axis is:

$$\Delta p = \rho \cdot \dot{u} \cdot \Delta x \tag{12.10}$$

where Δx is the width of the cylinder at distance y from its axis. The integral can be simplified again so that:

$$F_{x1}(t) = 2 \cdot \int_0^{\frac{\pi}{2}} \Delta p(R, \theta, t) \cdot R \cdot \cos\theta \cdot d\theta \tag{12.11}$$

After integrating one gets:

$$F_{x1}(t) = \rho \ \pi \ R^2 \cdot \dot{u}(t) \tag{12.12}$$

In which one should recognize $\pi R^2 \rho$ as the mass, M_1, of fluid displaced by the unit length of cylinder - the mass of fluid one would have 'removed' when 'drilling the hole' in the pressure gradient field.

This inertia force term stems from the pressure gradient already present in the accelerating flow - even before the cylinder was installed. It is equal to the product of the mass of water displaced by the cylinder and the acceleration already present in the undisturbed flow. This force component is fully equivalent to the Froude Krilov force mentioned in chapter 6.

Disturbance Force

The cylinder was not allowed to disturb the flow when F_{x1} was computed; this error is now corrected. Obviously, the cylinder is impermeable; fluid cannot actually flow through the cylinder wall. The cylinder geometry forces the fluid to go around it modifying all the local velocities and thus accelerations. This can only occur if a force is exerted on the fluid, and this force can only come from the cylinder.

Figure 3.12, which can be found in chapter 3, shows how the streamlines diverge and converge around a cylinder in a potential flow. One way to evaluate the extra force causing this total disturbance field is to examine the kinetic energy change caused by the cylinder as was done by [Lamb, 1932]. He evaluated the kinetic energy represented by the entire (disturbed) flow field around the cylinder and subtracted from that value the kinetic energy of the undisturbed flow in the same - theoretically infinite - region. This yields in equation form:

$$E = \iint\limits_{cyl.\ wall}^{\infty} \frac{1}{2}\rho \cdot [u(x,y,t)]^2\, dx \cdot dy - \iint\limits_{cyl.\ wall}^{\infty} \frac{1}{2}\rho \cdot u_\infty^2(t) \cdot dx \cdot dy \qquad (12.13)$$

It is convenient to associate this energy with some sort of equivalent mass, M_2, moving with the ambient (undisturbed flow) velocity, u_∞, so that:

$$E = \frac{1}{2}M_2\, u_\infty^2 \qquad (12.14)$$

Lamb discovered that:

$$M_2 = \pi\ R^2\ \rho \qquad (12.15)$$

or that M_2 is simply the mass of fluid displaced by the cylinder segment (just as was M_1) so that:

$$F_{x2} = \pi\ R^2\ \rho \cdot \dot{u}(t) \qquad (12.16)$$

Note that F_{x2} has the same form as F_{x1} and that they both have the same phase as well. F_{x2} is analogous to the part of the diffraction force which was in phase with the ship acceleration in chapter 6.

A thoughtful reader may wonder why this second force component, F_{x2} , was not present in a constant current; after all, that cylinder was then impervious to the flow, too. The answer to this question lies in the fact that F_{x2} does not result from the pattern itself, but rather from its continuous build-up and break-down which occurs only in a time-dependent flow. In a constant current there is no time dependent change and thus no F_{x2}.

Resultant Inertia Force

Potential theory indicates that the resultant force on a fixed cylinder in an oscillating flow is the sum of two terms:

$$F_{x1}(t) = \rho\,\pi\,R^2 \cdot \dot{u}_\infty(t) \quad \text{from the 'hole' in the undisturbed pressure gradient in the ambient flow. This is also know as the Froude-Krilov force.}$$

$$F_{x2}(t) = \rho\,\pi\,R^2\ \cdot \dot{u}_\infty(t) \quad \text{from the flow disturbance caused by the impervious cylinder.}$$

The resultant force is then:

$$\begin{aligned} F_I(t) &= F_{x1}(t) + F_{x2}(t) \\ &= 2 \cdot \pi\,R^2\,\rho \cdot \dot{u}(t) \end{aligned} \tag{12.17}$$

Note that because this is still a potential flow, there is no drag force. Also, since there is no circulation, there is no lift, either.

Alternate Direct Calculation Approach

Another, possibly faster way to calculate the flow disturbance force coefficient starts with the potential function for an oscillating cylinder in still water. This approach is completely analogous to that used in chapter 6 to determine the added mass of a floating body. One starts directly with the potential function just as was done there, and uses the Bernoulli equation to calculate the pressure on the cylinder surface and then integrate this as was done in chapter 3 to determine the resultant force.

Experimental Inertia Coefficients

The theoretical value of 2 in equation 12.17, above, is usually replaced by an experimental coefficient, C_M - often called the **inertia coefficient**. Remember that the theoretical value of 2 is made up of 1 from F_{x1} (the ambient pressure field) and 1 from F_{x2}, the flow disturbance caused by the cylinder. In practice the 1 from the ambient pressure field is usually considered to be acceptable; potential theory predicts the water motion in undisturbed waves well. The coefficient from F_{x2} is much less certain; the vortices in the wake (in a real, [not potential!] flow) disturb the theoretical flow pattern used to determine F_{x2}. This is taken into account by using a value C_a - a '**coefficient of added mass**' - instead. Usually $C_a < 1$. Note that C_a is quite analogous to the hydrodynamic mass used in chapter 6. This is all summarize in the table below.

Force Component	Force Term	Experimental Coefficient	Theoretical Value	Experimental Value
Froude-Krylov	F_{x1}	1	1	1
Disturbance	F_{x2}	C_a	1	Usually < 1
Inertia	F_I	C_M	2	Usually 1 to 2

Remember that:

$$\boxed{C_M = 1 + C_a}$$ (12.18)

and that C_a is associated with flow disturbance.

The phrase '**added mass**' has just been used above, much like it is often used in ship hydromechanics as in chapters 6 through 9. C_a is often interpreted as 'hydrodynamic mass' - some mysterious mass of surrounding fluid; this interpretation can be very misleading and dangerous, however. Consider the following true situation taken from ship hydromechanics. An investigator was carrying out tests to determine the hydrodynamic coefficients for a flat-bottomed barge in shallow water. Attention was focussed on its heave motion and the influence of the barge's (relatively small) keel clearance on the hydrodynamic mass. Tests were carried out with various (average) keel clearances so that C_a could be determined as a function of (average) keel clearance value. Figure 12.1 shows a cross-section sketch of the set-up.
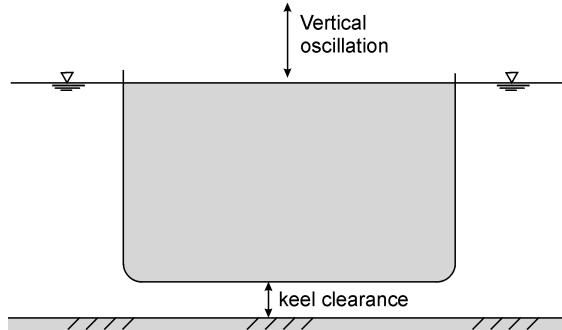
Figure 12.1: Cross Section of Barge Showing Keel Clearance

Since the relatively deeply loaded barge had vertical sides, these caused no waves or other disturbance as the barge oscillated vertically; the only water that is initially really disturbed by the vertical motions is the layer of water directly under the barge. The researcher who carried out these tests then reasoned somewhat as follows: "The mass of water under the ship is directly proportional to the average keel clearance. This mass becomes less and less as the keel clearance becomes smaller; it is therefore logical to expect C_a to approach zero as the keel clearance becomes less and less." His experiments proved however that C_a values became larger and larger as the keel clearance decreased.

The error here is the interpretation of C_a as if it represents a physical mass. It is not this! Instead, C_a (or even C_M for that matter) should be interpreted as force per unit acceleration or $\frac{Force}{Acceleration}$. Returning to the experiments and the researcher above, C_a only represents an 'extra' (in comparison the situation in air!) force needed to given the barge a unit acceleration in the vertical direction. Thinking in this way, one can easily reason that as the layer of water under the barge became thinner, it became more difficult for it to 'get out of the way' by being accelerated horizontally as the barge accelerated downward. Conversely, it therefore took a larger force to give the barge its unit of vertical acceleration as the keel clearance became smaller. With this reasoning, one gets the correct answer: In the limit, $C_a \rightarrow \infty$ as the keel clearance $\rightarrow 0$.

Fixed Cylinder in Waves

For a fixed cylinder in waves, one is confronted with both F_{x1} and F_{x2} so that equation 12.17 becomes:

$$
\begin{aligned}
F_I(t) &= F_{x1}(t) + F_{x2}(t) \\
&= \rho\,\frac{\pi}{4} C_M\, D^2 \cdot \dot{u}(t)
\end{aligned}
\tag{12.19}
$$

in which:

$$
\begin{aligned}
F_I(t) &= \text{inertia force per unit cylinder length (N/m)} \\
\rho &= \text{mass density of the fluid (kg/m}^3\text{)} \\
C_M &= \text{dimensionless inertia coefficient (-)} \\
\dot{u}(t) &= \text{time dependent undisturbed flow acceleration (m/s}^2\text{)}
\end{aligned}
$$

C_M has a theoretical value of 2 in a potential flow.

Oscillating Cylinder in Still Water

One might reason that the flow around an oscillating cylinder in still water would be kinematically identical to that of an oscillating flow past a fixed cylinder and that the resulting forces would be identical. This is not the case, however.
There is no ambient dynamic pressure gradient present in still water so that the first inertia force term above, F_{x1} the Froude-Krilov force, is now identically equal to zero. Thus, if the cylinder is oscillating such that its velocity is given by:

$$
\dot{X}(t) = a\cos(\omega t)
\tag{12.20}
$$

then the resultant hydrodynamic inertia force on the cylinder will be:

$$
F_I(t) = -F_{x2}(t) = -C_a \cdot \pi\, R^2\, \rho \cdot \ddot{X}(t)
\tag{12.21}
$$

The minus sign indicates that the hydrodynamic resisting force is opposite to the direction of cylinder acceleration. The value of C_a will generally not be larger than its theoretical value of 1. Note as well that if one is measuring forces within an instrumented pile on a segment of this oscillating (accelerating) cylinder, one will usually also measure a force component proportional to the mass times acceleration of the (solid) cylinder element itself. Force measurements in the lab are often corrected for this by first measuring forces while oscillating the cylinder in air before the basin is filled with water. This force is usually considered to be the inertia force of the measuring element itself. Only a slight error is made here by neglecting the aerodynamic resistance caused by the accelerating flow pattern in the still air.

12.3.2   Drag Forces

Experiments have shown (see chapter 4) that a drag force proportional to U^2 and the cylinder diameter, D, is caused by a constant current; it is only reasonable to expect a similar force to be present in a time-dependent real flow as well. Since the drag force is in the same direction - has the same sign - as the velocity in an oscillating flow, the constant

current, U^2, is commonly replaced by its time-dependent counterpart, $u(t)\,|u(t)|$ in order to maintain a proper sign. Substituting relationships for $u(t)$ and working this out yields:

$$F_D(t) = \frac{1}{2}\,\rho\,C_D\,D\,u_a^2 \cdot \cos(\omega t)\,|\cos(\omega t)| \qquad (12.22)$$

in which:

$$
\begin{aligned}
F_D(t) &= \text{drag force per unit length of cylinder (N/m)}\\
C_D &= \text{dimensionless drag coefficient (-)}\\
D &= \text{cylinder diameter (m)}\\
u_a &= \text{water velocity amplitude (m/s)}\\
\omega &= \text{circular water oscillation frequency (rad/s)}\\
t &= \text{time (s)}
\end{aligned}
$$

One should not, however, expect the values of C_D for an oscillating flow to correspond with those found in chapter 4 for a constant flow. Instead, they will have to be determined again in a time-dependent flow.

12.4   Morison Equation

J.E. Morison, a graduate student at the University of California at the time, wanted to predict wave forces on an exposed vertical pile; see [Morison et al., 1950]. He simply superimposed the linear inertia force (from potential theory and oscillating flows) and the adapted quadratic drag force (from real flows and constant currents) to get the following resultant force (per unit length):

$$F(t) =\ F_{inertia}(t) + F_{drag}(t) \qquad (12.23)$$

or:

$$\boxed{F(t) = \frac{\pi}{4}\,\rho\,C_M D^2 \cdot \dot{u}(t) + \frac{1}{2}\,\rho\,C_D D\ \cdot u(t)\,|u(t)|} \qquad (12.24)$$

in which the first of these two terms is the inertia force and the second represents the drag force.

Note that in equations 12.24 the drag and inertia force components are 90° out of phase with each other when seen as functions of time. This is a direct consequence of the phase shift between velocity and acceleration in an oscillatory motion; check equations 12.4 and 12.6 if necessary. Examples of this will be shown during the discussion of coefficients and their determination below; see figure 12.2 later in this chapter as well.

12.4.1   Experimental Discovery Path

Morison formulated his equation simply by hypothesizing that the superposition of two separate and well know phenomena (drag in a current and hydrodynamic inertia in an accelerating flow) would yield a viable solution for a vertical pile in waves. This section explains how one comes to the same equation via experiments much like those for ships.
Readers should know from earlier chapters that a common technique in marine hydrodynamics is to oscillate a body with a chosen displacement amplitude in still water and to

record its displacement and the force, $F(t)$ acting on it as functions of time. Further, the force record is resolved into two components: one in phase with the acceleration and one in phase with the velocity.

The first is determined by multiplying $F(t)$ by $-\cos(\omega t)$ and integrating the result to get an inertia force; the second comes from the integral of the product of $F(t)$ and $\sin(\omega t)$ to yield a component in phase with velocity.

One single test might not tell too much, but if testing were done with different excitation amplitudes, but at constant frequency (or period), then a plot of the amplitude of the inertia force component versus the oscillation acceleleration amplitude would be linear; the plot of the drag force amplitude as a function of velocity amplitude would be quadratic. Similarly, comparison of test results carried out with cylinders of different diameter would show that the inertia force component was proportional to D^2, while the drag force would be linearly proportional to D.

Putting all this together would indicate that the force on a cylinder was of the form:

$$F(t) = A \cdot D^2 \cdot \dot{u}(t) + B \cdot D \cdot [u(t) \cdot |u(t)|] \tag{12.25}$$

in which A and B are constants. It is then simple enough to use dimensional analysis and common sense to express the unknown coefficients, A and B as:

$$A = \frac{\pi}{4} \, \rho \cdot C_a \qquad \text{and} \qquad B = \frac{1}{2} \, \rho \cdot C_D \tag{12.26}$$

12.4.2 Morison Equation Coefficient Determination

In this section, a vertical cylinder is assumed to be fixed in a horizontal sinusoidal oscillatory flow. The force per unit length acting on the cylinder can be predicted using the Morison equation with two empirical coefficients:

$$\boxed{F(t) = +\frac{\pi}{4} \, \rho \, C_M \, D^2 \cdot \dot{u}(t) + \frac{1}{2} \, \rho \, C_D \, D \cdot u(t) \, |u(t)|} \tag{12.27}$$

The values of the dimensionless force coefficients C_D and C_M can be determined experimentally in a variety of ways. The first step, however, is always to get a recording of the force, F, as a function of time, t. A characteristic of the flow - usually the velocity - will form the second time function.

Experimental Setup

These measurements can be made in a variety of test set-ups.

1. Oscillating flows can be generated in a large U-tube. Unfortunately the flow can only oscillate with a limited frequency range - the natural oscillation frequency for the installation - unless an expensive driving system is installed. An advantage of a U-tube, on the other hand, is that its oscillating flow is relatively 'pure' and turbulence-free. A discussion continues about the applicability of results from such idealized tests in field situations, however. This topic will come up again later in this chapter.

2. A second method is to impose forced oscillations to a cylinder in still water. The flow - when seen from the perspective of the cylinder - appears similar to that in a U-tube but the inertia force is not the same. Review the material above about C_a to understand why this is so.

3. A third possibility is to place a vertical cylinder in regular waves. The waves are generated by a wave maker located at one end of the experimental tank; they are absorbed on an artificial beach at the other end. In this case it is often the wave height (actually the water surface elevation) which is measured as a function of time. The horizontal water velocity and acceleration at the location of the cylinder are in this latter case determined using linear wave theory - see chapter 5:

$$
\begin{aligned}
u(z,t) &= \frac{\omega\,H}{2}\cdot\frac{\cosh\left[k\,(z+h)\right]}{\sinh\left(k\cdot h\right)}\cdot\cos\left(\omega t\right) \\
&= u_a(z)\cdot\cos\left(\omega t\right) \qquad\qquad (12.28) \\
\dot{u}(z,t) &= -\frac{\omega^2\,H}{2}\cdot\frac{\cosh\left[k\,(z+h)\right]}{\sinh\left(k\cdot h\right)}\cdot\sin\left(\omega t\right) \\
&= -\,\omega\cdot u_a(z)\cdot\sin\left(\omega t\right) \qquad\qquad (12.29)
\end{aligned}
$$

in which:

$\omega = 2\pi/T$ = wave frequency (rad/s)
$k = 2\pi/\lambda$ = wave number (rad/m)
z = elevation (+ is upward) from the still water level (m)
H = wave height (m)
h = water depth (m)
T = wave period (s)
λ = wave length (m)
$u_a(z)$ = amplitude of horizontal water velocity component (m/s)

Note that even though u_a is now a function of z, this will not really complicate matters when studying the forces on a short segment of a cylinder. The change in u_a over such a short distance can be neglected.

With any of these methods, the resultant force on a section of the cylinder is often measured by mounting that section on a set of leaf springs which are equipped with strain gauges. These - via a Wheatstone bridge circuit and a proper calibration - provide the force record, $F(t)$ to use in conjunction with the measured or computed $u(t)$ and $\dot{u}(t)$.

Data Processing

Once the necessary data time series have been obtained, one is still faced with the problem of determining the appropriate C_D and C_M values. Here, again, one has several options dependent upon the computer facilities available.

Several methods are presented here, primarily for reference purposes:

1. **Morison's Method**
   Morison, himself, suggested a simple method to determine the two unknown coefficients, see [Morison et al., 1950]. His method was elegant in that it was possible to

determine the coefficients without the use of computers. (Computers - if available at all - were prohibitively expensive when he did his work.) His approach was suitable for hand processing and depended upon the realization that when:

u is maximum, $\dot{u}$ is zero so that at that instant, t_1, $F(t_1) = F_D$ and

$\dot{u}$ is maximum, u is zero so that at that instant, t_2, $F(t_2) = F_I$.

Figure 12.2 shows a sample of an idealized measurement record. Under each of the above specific conditions, equation 12.27 can be re-arranged to yield:

$$C_D = \frac{2F}{\rho D \cdot u_a |u_a|} \qquad \text{at an instant } t_1 \text{ when } \dot{u} = 0$$

$$C_M = \frac{4F}{\pi \, \rho \, D^2 \cdot \omega \, u_a} \qquad \text{at an instant } t_2 \text{ when } u = 0 \qquad (12.30)$$

The method is simple, but it lacks accuracy because:
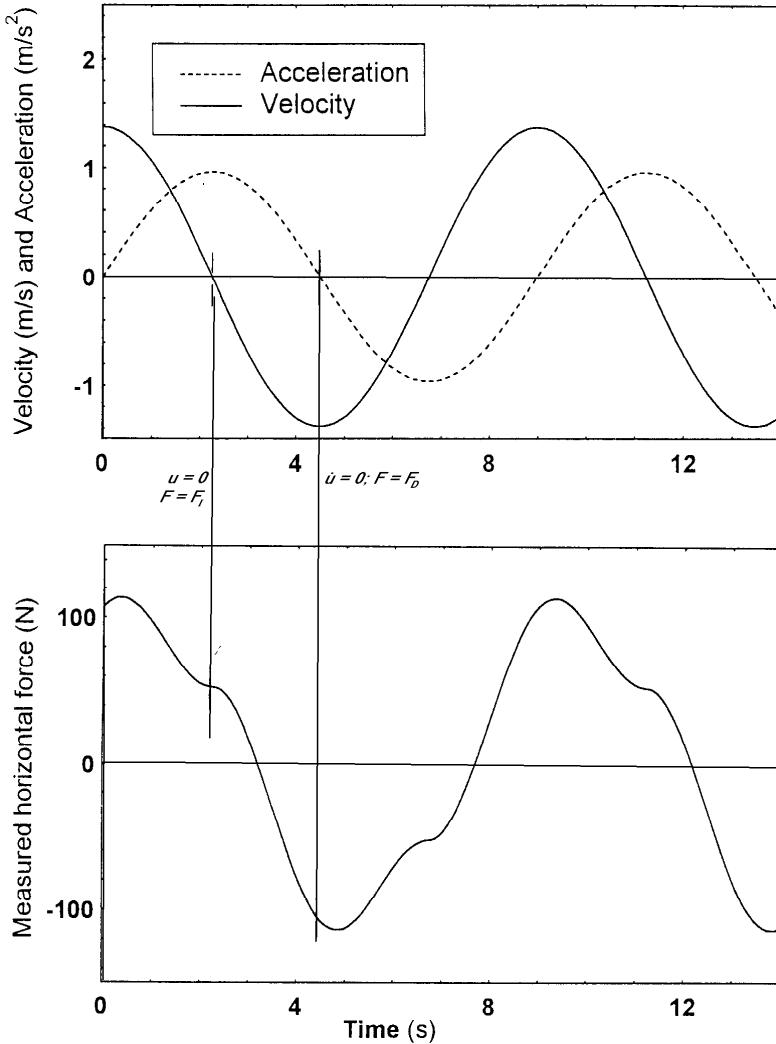
Figure 12.2: Measured Force and Velocity Record

- A small error in the velocity record can cause a significant phase error. Since the

curve of $F(t)$ can be steep (especially when determining C_D in figure 12.2), this can cause quite some error in this coefficient. The effect on C_M is usually smaller.
- Information from only two instants in the time record is used to determine the coefficients; the rest is thrown away.
Morison reduced errors by averaging the coefficients over a large number of measurements (wave periods).
One might try to use this same approach at other time instants in the record. The only difficulty, however, is that one is then confronted with a single equation (for F at that instant) but with two unknown coefficients. This cannot be solved uniquely. A second equation could be created by examining the situation at a second, independent time instant. A generalization of this would be to use the data pairs at every instant with a least squares fitting technique. This is discussed below, but only after another approach using Fourier series has been presented.

2. **Fourier Series Approach**
An entirely different method for determining the drag and inertia coefficients is based upon the comparison of similar terms in each of two Fourier series: One for the water motion and one for the force. Appendix C summarizes the theory behind Fourier series.
Since modern laboratory data records are stored at discrete time steps (instead of as continuous signals), the integrals needed to evaluate the Fourier coefficients are replaced by equivalent sums.
Looking at this in a bit more detail, the water velocity and acceleration is already in a nice form as given in equation 12.28. A single Fourier series term is sufficient to schematize this quite exactly. Since the inertia force, F_I, is also well behaved, it can be 'captured' with a single Fourier series term as well.

The only remaining problem is the series development of the drag term; this requires the development of a function of form:

$$f(t) = A \cos(\omega t) \cdot |\cos(\omega t)| \tag{12.31}$$

This has been worked out in Appendix C as well. The resulting coefficients (given there as well) for the first harmonic development of the quadratic drag turn out to be:

Fourier Coefficient	Value
Constant, a_0	0
Cosine, a_1	$\frac{8}{3\pi} \cdot A = 0.849 \cdot A$
Sine, b_1	0

As shown in Appendix C, the drag force, dependent upon $u\,|u|$, develops into a series of odd-numbered harmonics in a Fourier series; only the first harmonic terms are used here. Since this has an amplitude of $\frac{8}{3\pi}$ times the original signal, one must multiply the first order harmonic of the force in phase with the velocity by a factor $\frac{3\,\pi}{8}$ to get the amplitude of the quadratic drag force.
Once this has been done, then the determination of C_D and C_M from the analysis of the compete force signal, $F(t)$ is completely straightforward. Since the inertia force component shows up now in the b_1 term of the series development, the results are:

$$C_D = \frac{3\,\pi}{4\,\rho\,D} \cdot a_1 \qquad \text{and} \qquad C_M = \frac{4}{\pi\,D^2\,\rho} \cdot \frac{b_1}{\omega\,u_a} \tag{12.32}$$

in which the following amplitudes are found:

$$a_1 \quad = \quad \text{velocity-dependent Fourier amplitude (kg/m}^2)$$
$$b_1 \quad = \quad \text{acceleration-dependent Fourier amplitude (N m)}$$

Notice that with this method one has used data from the entire time record in the determination of the Fourier series components and thus for the determination of C_D and C_M. This should be an improvement over the method used originally by Morison, but on the other hand, it is still only as accurate as the linearization can be.

3. **Least Squares Method**
A third approach treats the basic Morison equation, (12.27) as a computational approximation, $F(t, C_D, C_M)_{computed}$, for the measured force record, $F(t)_{measured}$. One is now faced with only the problem of determining the (linear) unknown coefficients, C_D and C_M. This is done by minimizing some residual difference (or fit criterion) function. The method of least squares uses a residual function of the form:

$$R(C_D, C_M) = \int_0^T \left[F(t)_{measured} - F(t, C_D, C_M)_{computed} \right]^2 dt \qquad (12.33)$$

in which T is now the length of the measurement record.
Now one only needs to iteratively evaluate equation 12.33 for various values of C_D and C_M until the residual function, $R(C_D, C_M)$ is minimized. If one were to plot this function in three dimensions - with C_D and C_M on the two orthogonal horizontal axes and $R(C_D, C_M)$ on the vertical axis, then one would find a sort of 'bowl-shaped' function. It doesn't take too much thought to realize that if the shape of the bottom of this 'bowl' is rather flat, then there are many combinations of C_D and C_M which give about the same $R(C_D, C_M)$ function value. The consequence of this is that it is quite difficult to determine the 'best' C_D and C_M values exactly in a numerical way. On the other hand, it is theoretically possible to determine the minimum of the function $.R(C_D, C_M)$ by setting both of its partial derivatives, $\frac{\partial R}{\partial C_D}$ and $\frac{\partial R}{\partial C_M}$ equal to zero analytically.

4. **Weighted Least Squares Method**
The least squares method, above, uses the entire time record for the determination of C_D and C_M ; it shares that advantage with the Fourier series approach. On the other hand, one can reason that for offshore design purposes, it is more important that the Morison equation **predict the force peaks accurately** than to be as precise at moments when the force is nearly zero. One way to improve the fitting near the peak forces is to weight the difference found above in equation 12.33 with - for example - the measured or computed force value. Equation 12.33 can then become something like:

$$R_w(C_D, C_M) = \int_0^T \left[F(t)_{measured} \right]^2 \cdot \left[F(t)_{measured} - F(t, C_D, C_M)_{computed} \right]^2 dt$$

Of course the shape of the residual function - the shape of the 'bowl' - will now be different and hopefully steeper and deeper (not so flat on its bottom). Even if this

is not the case, however, one can expect that a Morison equation fitted in this way will give a more accurate prediction of the force peaks.

Note that most any researcher can dream up his own residual or criterion function to use in this approach. Residual values are usually **not dimensionless quantities**; **the absolute (numerical) value** of R or R_w (or any other criterion function for that matter) **is quite irrelevant**; only relative values are of interest. There is certainly no point in comparing them by, for example, comparing values of R with those of R_w. The only important matter is that of finding the C_D and C_M associated with the minimum value of the criterion function chosen.

5. **Alternative Approach**

This method illustrates an entirely different approach to the problem. It was used by Massie some years ago - in an age when digital computers were still slow enough to make numerical integrations a cumbersome process. Instead, integrations were carried out using an analog computer; this could carry out these nearly instantly and painlessly. The analog computer was coupled to a digital computer which read the results of the integration and adjusted the coefficients accordingly for the next try. Such a computer was called a hybrid computer.

The solution was based upon the following approach: First the Morison equation, 12.27, was written in the following form:

$$F(t) = +P \cdot C_M \cdot \dot{u}(t) + Q \cdot C_D \cdot u(t) \cdot |u(t)| \qquad (12.34)$$

in which P and Q are simply known constants. Both $u(t)$ and $F(t)$ had been measured and were known functions of time.

The special approach feature was to re-arrange equation 12.34 by solving it for $\dot{u}(t)$ yielding:

$$\dot{u}(t) = \frac{1}{P} \cdot \frac{1}{C_M} \, F(t) - \frac{Q}{P} \cdot \frac{C_D}{C_M} \cdot u(t) \cdot |u(t)| \qquad (12.35)$$

Equation 12.35 is, thus, a first order nonlinear ordinary differential equation in $u(t)$ which has a given solution - the measured $u(t)$ - but two unknown coefficients: $1/C_M$ and C_D/C_M. Values for the unknown coefficients were set by the digital portion of the computer; the analog portion integrated the differential equation to generate a computed $u_c(t)$ and simultaneously subtract it from the measured $u(t)$ to give a residual which was also integrated over a time period in the analog portion. This integral value was the residual function to be minimized using a numerical routine in the attached digital computer. Notice that the criterion function is now based upon the velocity record instead of the force record! Of course, various weighting functions were tried as well.

Five different methods of determining C_D and C_M (or C_a) coefficient values from a single time record of water motion and force have been presented here. The frustrating result of all this is that if one time record were to be analyzed with each of these methods, each method would yield a different pair of C_D and C_M coefficient values! One can conclude - correctly! - from this that it is impossible to determine exact values for these coefficients; a tolerance of several percent is the very best one can expect.

It can also happen that one finds widely varying values for C_D or C_M when comparing results from two different time series with very similar test conditions. This can happen

with the drag coefficient, for example, when $F(t)$ is **inertia dominated** as it is called. Inertia dominated implies that the drag force is relatively unimportant so that since the rest of the information used to compute F_D is relatively small, this small value times any coefficient value is still small. The converse is obviously also true: The inertia coefficient value is unimportant if the force is **drag dominated**. More about the conditions which can lead to this will be presented below in the discussion of the relative amplitudes of the drag and inertia forces.

Cylinder Roughness

All of the above discussion has been for a smooth-surfaced (vertical) cylinder. Since offshore structures accumulate marine growth very easily in at least the warmer seas, this modifies the hydrodynamic force computation in two ways: First, the cylinder can become larger - a marine growth layer of 10 centimeters thickness will increase the cylinder's diameter by 0.2 meters. This can be accounted for quite easily in the Morison equation. The second influence is that the roughness will influence the boundary layer and vortex separation near the cylinder. The drag and inertia coefficient values are generally adjusted to account for this as will be seen later in this chapter.

Presentation Parameters

Now that C_D and C_M values have been found for a given flow condition, it is logical to want to present these results via a graph in which C_D and C_M are the dependent variables plotted along the vertical axis. One must still choose a proper independent variable for the horizontal axis, however. This would (ideally) include information on the wave (H, T or something related to these), the fluid (ρ, ν for example) and the cylinder (D is most obvious choice for this, but it might include the roughness, too). Several possibilities for making dimensionless combinations are discussed in this section.

1. **Reynolds number**
   The Reynolds number for a constant current was given in chapter 4. This is modified here for unsteady flow by replacing the constant current by the amplitude of the oscillation velocity yielding:
   $$Rn = \frac{u_a \cdot D}{\nu} \tag{12.36}$$

   in which:
   Rn = Reynolds number (-)
   u_a = flow velocity amplitude (m/s)
   D = cylinder diameter (m)
   ν = kinematic viscosity (m^2/s)

2. **Froude Number**
   The Froude number can now be expressed using the velocity amplitude as well as:
   $$Fn = \frac{u_a}{\sqrt{g \cdot D}} \tag{12.37}$$

   in which:
   Fn = Froude number (-)
   g = acceleration of gravity (m/s^2)

The Froude number is associated primarily with free surface effects while wave forces can be exerted on cylinder elements which are so far below the sea surface that no surface disturbance is generated. The Froude number is not really suitable for the present purpose, therefore.

3. **Keulegan Carpenter Number**
[Keulegan and Carpenter, 1958] determined C_D and C_M values for various cylinders in an oscillating flow. They discovered that their data could be plotted reasonably as a function of the dimensionless Keulegan Carpenter number:

$$\boxed{KC = \frac{u_a \cdot T}{D}} \tag{12.38}$$

in which:
KC = Keulegan Carpenter number (-)
T = oscillating flow period (s)
This number can be defined in alternate ways. In a sinusoidal wave, $u_a = \omega \cdot x_a$, in which x_a is the (horizontal) water displacement amplitude. A bit of substitution then yields:

$$KC = 2\pi \cdot \frac{\text{water displacement amplitude}}{\text{cylinder diameter}} = 2\pi \frac{x_a}{D} \tag{12.39}$$

which is very likely an important characteristic for the wake formation in the flow as well.
In **deep water**, the water displacement amplitude x_a **at the sea surface** is identical to the wave amplitude. This allows still another form in this specific situation:

$$KC = \pi \cdot \frac{H}{D} = 2\pi \cdot \frac{\zeta_a}{D} \quad \text{(deep water only)} \tag{12.40}$$

4. **Iversen Modulus**
Even before Keulegan and Carpenter did their work, [Iversen and Balent, 1951] suggested:

$$Iv = \frac{\dot{u}_a \cdot D}{u_a^2} \tag{12.41}$$

in which:
Iv = Iversen modulus (-)
$\dot{u}_a$ = flow acceleration amplitude (m/s^2)
Knowing that in a sinusoidal wave $\dot{u}_a = \frac{2\pi}{T} u_a$, and by doing a bit of algebra, one can discover that:
$$Iv = \frac{2\pi}{KC} \tag{12.42}$$

KC is more convenient to use in practice, however.

5. **Sarpkaya Beta**
[Sarpkaya and Isaacson, 1981] carried out numerous experiments using a U-tube to generate an oscillating flow. He found that the ratio:

$$\beta = \frac{D^2}{\nu \cdot T} \tag{12.43}$$

was convenient for plotting his data.

Just as with the Iversen modulus, this can be 'processed' a bit to reveal that:

$$\beta = \frac{Rn}{KC} \qquad (12.44)$$

so that this is not really anything new, either.

6. **Dimensionless Roughness**

Cylinder roughness is generally made dimensionless by dividing it by the diameter, yielding:

$$\frac{\varepsilon}{D} = \frac{\text{roughness height}}{\text{cylinder diameter}} \qquad (12.45)$$

The Keulegan Carpenter number has survived as the most realistic and useful primary independent parameter for plotting C_D and C_M. This is sometimes augmented by using Rn , β or $\frac{\varepsilon}{D}$ to label specific curves, thus introducing additional independent information.

12.4.3   Typical Coefficient Values

Hundreds (at least) of researchers have conducted laboratory tests to determine C_D and C_M coefficients in one way or another and often for very specific situations. In many cases, their objective and/or experimental set-up limited their range of test conditions so that their results are quite restricted, too. Typical results are listed in this section.

The results of Sarpkaya's experiments with smooth cylinders in U-tubes are presented as graphs of the coefficients C_D and C_M as functions of β and KC. Note that in figure 12.3 the horizontal (KC) axis is logarithmic. Individual curves on each graph are labeled with appropriate values of β.

[Clauss, 1992] for example suggests drag and inertia coefficient values given in the following table:

	$Rn < 10^5$		$Rn > 10^5$	
KC	$\mathbf{C}_D$	$\mathbf{C}_M$	$\mathbf{C}_D$	$\mathbf{C}_M$
< 10	1.2	2.0	0.6	2.0
$\geqslant 10$	1.2	1.5	0.6	1.5

Morison Coefficients Suggested by [Clauss, 1992]

Various design codes or rules also specify (or suggest) appropriate values for C_D and C_M. Those published by [DetNorskeVeritas, 1989] or the American Petroleum Institute (API) are the most widely accepted; the DNV suggestions for design purposes are shown in figure 12.4.

The API as well as the SNAME have the simplest approach as listed in the table below:
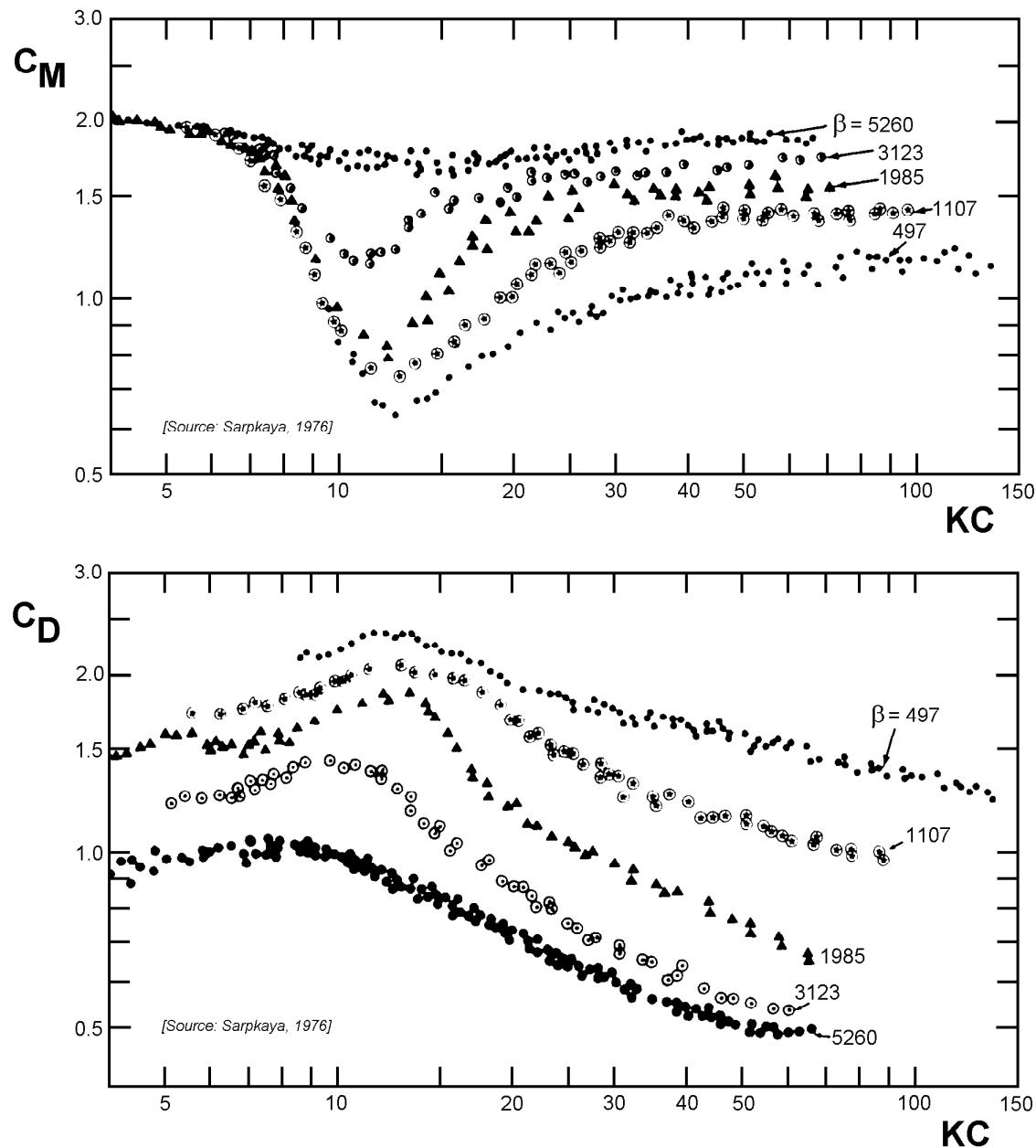
Figure 12.3: Typical Laboratory Measurement Results from Sarpkaya
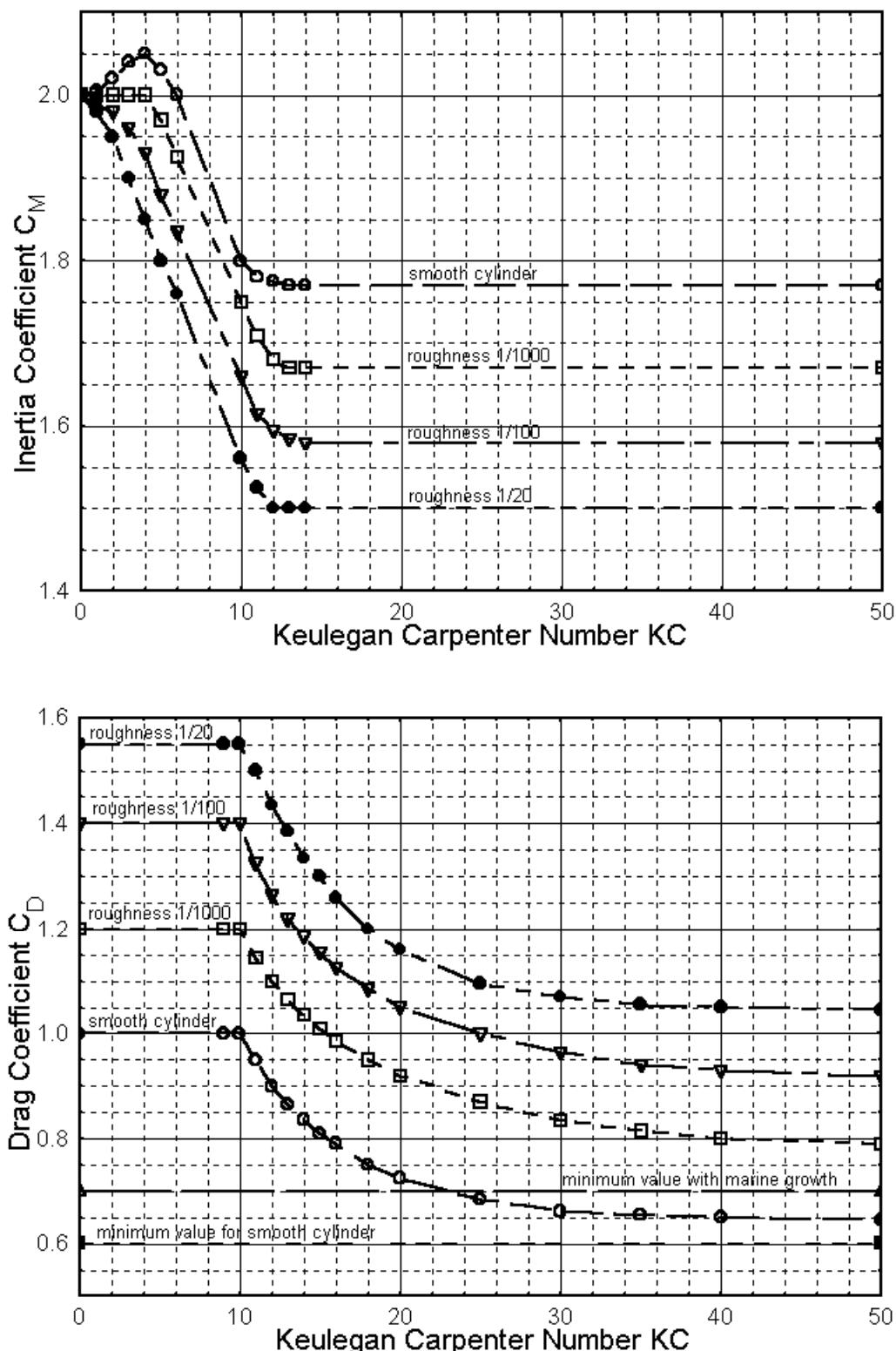
Figure 12.4: Suggested Drag and Inertia Coefficient Values from DNV

	Smooth		Rough	
	$\mathbf{C}_D$	$\mathbf{C}_M$	$\mathbf{C}_D$	$\mathbf{C}_M$
API	0.65	1.6	1.05	1.2
SNAME	0.65	2.0	1.0	1.8

The following observations can be made from the above information:

- For low values of KC, the inertia coefficient C_M is almost equal to its theoretical value of 2 - at least if the KC value is used as a selection parameter. Also, one can notice that the drag coefficient C_D generally increases or stays rather constant till a value of KC near 10 is reached.

- One sees as well from figure 12.3 that the C_D value gets lower as β increases. This is just the opposite of the trend observed with C_M.

- Comparison of Sarpkaya's curves (figure 12.3) with those from DNV (figure 12.4) show that there can be quite some discrepancy in the value of C_D or C_M to choose.

- The DNV curves (figure 12.4) as well as the other design and assessment codes include roughness - that can easily result from marine growth, especially near the sea surface. The roughness in figure 12.4 is an $\frac{\epsilon}{D}$ ratio.

- The API and SNAME recommendations seem rather simple in that they neglect the KC number; Clauss adds that effect, but in a more simple way that suggested by DNV.

Comparisons

Examination and comparison of the various drag and inertia coefficient values presented above shows that there is little agreement on exact values. This is true for smooth cylinder values and even more so when a rough cylinder is involved. Differences of up to roughly 40% can be found when comparing the drag or inertia coefficients suggested by the various sources for a specific flow situation.

This direct comparison of coefficient values can be misleading, however. In some cases a low drag coefficient value can be at least partially compensated by a larger inertia coefficient. After choosing a typical cylinder diameter and wave conditions, one can select appropriate coefficients from each of the sources and compute the actual maximum force per unit length upon which to base a comparison. Such an exercise can still lead to differences of up to about 30%. Luckily for survival design of offshore structures, the differences found for extreme wave conditions are generally less than this!

Even this comparison need not be correct. The 'purest' approach is to select a typical structure, and place it (in one's mind) at a given location in the sea. Given this, one should follow the entire procedure (given in each particular design or analysis code) to select wave and current conditions and to translate these into forces on that structure. These resulting forces should be compared. Carrying out such a comparison operation is beyond the scope of this text, however.

One additional discovery that one will make when computing forces under field conditions is that Sarpkaya's data is a bit restricted for this. Indeed, the Reynolds numbers - needed for his β parameter - are much too low in nearly all laboratory situations.

12.4.4 Inertia or Drag Dominance

Now that C_D and C_M values have been presented, one should further reflect upon their use and importance. The Keulegan Carpenter number can be a very important parameter for this. Indeed, it can be used as an indication of the relative importance of drag versus inertia forces in a particular situation. To prove this, one must work out the ratio of the amplitudes of the drag and inertia forces. The 90° phase difference between the force components is completely neglected now; only the force component amplitudes are compared.

$$\frac{F_{drag_a}}{F_{inertia_a}} = \frac{\frac{1}{2} \rho C_D D u_a |u_a|}{\frac{\pi}{4} \rho C_M D^2 \omega u_a}$$
$$= \frac{2 C_D |u_a|}{\pi C_M D \omega} \tag{12.46}$$

Note that the maximum value of $|u_a|$ is the same as that of u_a.
Since $\omega = 2\pi/T$, then this can be reduced a bit to:

$$\frac{F_{drag_a}}{F_{inertia_a}} = \frac{1}{\pi^2} \cdot \frac{C_D}{C_M} \cdot \frac{u_a \cdot T}{D}$$
$$= \frac{1}{\pi^2} \cdot \frac{C_D}{C_M} \cdot KC \tag{12.47}$$

Since $1/\pi^2 \approx 1/10$ and the value of C_D is often a bit more than half the C_M value, the two force component amplitudes are about equal when KC is in the range of roughly 15 to 20.
Remembering the earlier definition of KC from equation 12.39:

$$KC = \frac{2\pi x_a}{D} \tag{12.48}$$

then this means that x_a/D will be about 3; this is big enough to generate a very respectable set of vortices.

The Morison equation includes a nonlinear (quadratic drag) term which is 90° out of phase with the inertia force. Many offshore engineers want to avoid using the entire Morison equation (and the quadratic drag computation especially) unless it is absolutely necessary. It would be convenient to have a simple way to justify neglecting either the drag term or the inertia term in that equation. The Keulegan Carpenter number is an excellent help with this:

- For low values of KC ($KC < 3$), the **inertia force is dominant**. The flow 'does not travel far enough' relative to the cylinder diameter to generate much of a boundary layer not to mention vortices; potential flow theory is still applicable. **Drag can simply be neglected**.

- For the next range until drag becomes significant ($3 < KC < 15$), one will often **linearize the drag** as has been explained earlier in this chapter.

- There is a range of KC ($15 < KC < 45$) in which one cannot really avoid using the **full Morison equation** with its nonlinear drag.

- For high values of KC ($KC > 45$), the **drag force is dominant**. The vortex shedding frequency becomes high compared to the wave frequency so the flow tends to behave more and more like a uniform flow. **Inertia can be neglected**. Indeed, the limit $KC \to \infty$ corresponds to a constant current.

12.5 Forces on A Fixed Cylinder in Various Flows

This section describes the forces acting on a fixed cylinder in currents and/or waves. While parts of it may seem like repetition of earlier work, its objective is to clarify the underlying principles.

12.5.1 Current Alone

A fixed cylinder in a current alone will experience only a quadratic drag force (per unit length) as already indicated in chapter 4. This force is assumed to be caused by the flow component:

$$U_p = U \sin \kappa$$

acting perpendicular to the cylinder axis so that the force can be expressed as:

$$F_c = \frac{1}{2} \, \rho \, U^2 D \, C_D \sin^2 \kappa \tag{12.49}$$

In these equations:

$$
\begin{array}{rcl}
U & = & \text{Total velocity vector (m/s)} \\
U_p & = & \text{Perpendicular velocity component (m/s)} \\
C_D & = & \text{Drag coefficient for constant current (-)} \\
\kappa & = & \text{Cone angle between the velocity vector, } U, \\
& & \text{and the cylinder axis.} \\
F_c & = & \text{Current force per unit cylinder length (N/m)}
\end{array}
$$

See figure 12.5 for a sketch showing the cone angle. The force, F_c, will act in the direction of U_p of course; this is perpendicular to the cylinder axis and in the plane defined by the cylinder axis and the approaching velocity vector, U.
Note that only the so-called cone angle, κ, is important in this computation. This is sufficient to describe the orientation of the cylinder relative to the current vector. It makes no difference whether the cylinder is in a vertical, horizontal or any other plane; it is only the angle between the cylinder axis and total velocity vector which is important. (This will be generalized to include inertia forces in waves below.)

12.5.2 Waves Alone

The time dependent flow associated with waves requires the inclusion of inertia force components into a force computation. Indeed, the basic Morison equation - derived for a unit length of a fixed, vertical cylinder in waves is re-stated here for reference:

$$\left| F = \frac{1}{4} \, \pi \, \rho \, D^2 \, C_M \, \dot{u}(t) + \frac{1}{2} \, \rho \, C_D \, D \, u(t) \, |u(t)| \right| \tag{12.50}$$
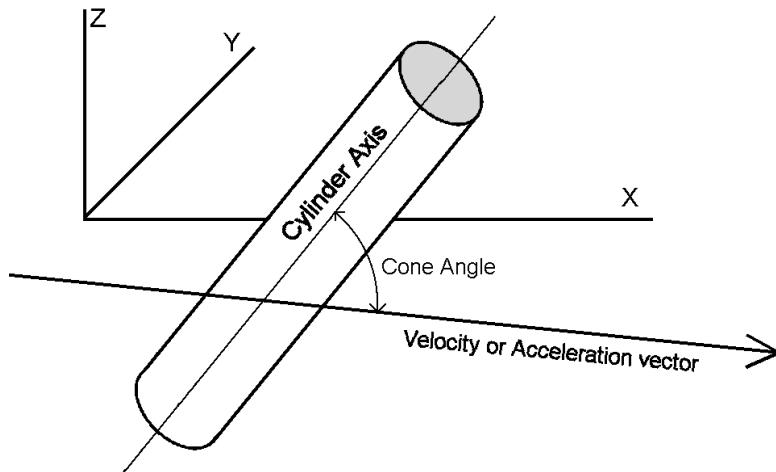
Figure 12.5: Cone Angle Definition

in which:

F	=	Force per unit length of cylinder (N/m)
D	=	Cylinder diameter (m)
$u(t)$	=	Horizontal velocity component (m/s)
$\dot{u}(t)$	=	Horizontal acceleration component (m/s^2)

How can this be generalized in the light of the above information on currents for a cylinder having a non-vertical orientation? The following steps are suggested in which the inertia force and the drag force are considered to be separate entities until the end. The following sequence of steps must be carried out sequentially and at each time step for which results are desired::

1. Determine the instantaneous water kinematics: velocity and acceleration (magnitudes as well as directions) in a fixed x, y, z axis system. Relate their phase to that of a reference such as the wave profile.

2. Knowing the cylinder axis orientation (in that same x, y, z axis system), determine the instantaneous cone angles, κ_I and κ_D for the acceleration and velocity respectively.

3. Determine the instantaneous perpendicular components of acceleration and velocity - $\dot{u}_p$ and u_p - as well as their directions. Use the results from the two previous steps to do this. These two vectors will not generally be co-linear; they are both in the plane perpendicular to the cylinder axis, however.

4. Evaluate the inertia and drag force components at each instant. Don't forget that the drag is quadratic! The direction of each force component will correspond to that of its associated kinematics found in the previous step.

5. If the force on an entire member is needed, then now is the time to integrate these separate force components over the length of the member in order to determine each resultant at that time. The member support forces - and thus the equivalent loads to be applied at the structure nodes - can be found by treating each member as a simple beam.

6. Since the inertia and drag force components are not generally colinear, they can be combined (if desired) via vector addition to yield the resulting force magnitude and its direction (still in a plane perpendicular to the cylinder axis). This step is not absolutely necessary for the computation of resulting forces on a large structure, however.

Note that these five or six steps must be repeated at each instant in time. These steps are not difficult in principle, but very careful bookkeeping is essential!

In many simple cases, each of the quantities needed for this methodology will be expressible in terms of nicely behaved and convenient functions so that the resulting force can be described as one or another continuous time function. On the other hand, if the wave is irregular and thus composed of many frequency and direction components, then the necessary bookkeeping becomes too cumbersome for a hand calculation. The only requirement for the force computation is that the water acceleration and velocity be known at any time.

Special Orientations

One can check his or her understanding of the above by evaluating the forces acting on two special cases of a horizontal cylinder in a regular wave. These are in addition to the vertical cylinder used during the Morison equation derivation.

If the **horizontal cylinder** segment is oriented with its axis **parallel to the direction of wave propagation** (and thus perpendicular to the wave crests), then it will experience a vertical force which has a time trace which looks much like that for a vertical cylinder - see figure 12.2. This force record will be shifted 90° in phase relative to a similar record for a vertical cylinder, however. The relative phases of the resulting drag and inertial force components on consecutive segments of the cylinder will correspond - with some constant shift - to that of the wave profile on the sea surface.

The second case has the **horizontal cylinder** turned **parallel to the wave crests** (and thus perpendicular to the direction of wave propagation). If the cylinder is situated in a deep water wave (in which the horizontal and vertical kinematic components have the same magnitudes) then one will find a resultant force of constant magnitude which sweeps around the cylinder once per wave period. It may seem strange, but the horizontal component of this force will have a purely sinusoidal form (except for a possible phase shift) independent of the fact that quadratic drag is involved. Force components on consecutive segments of this cylinder will have identical phases in this case as compared to the previous one.

12.5.3   Currents plus Waves

It is generally accepted practice to vectorially superpose the current velocity on the velocity resulting from the waves before calculating the drag force. In a general case the wave and current directions will not be co-linear making a vector sum necessary. Once this has been carried out, however, one simply has to use the sequential steps given above to determine the resulting force at any instant.

Why is it not acceptable to compute the wave force and the current force separately? The current has no effect at all on the flow accelerations so that the inertia force is unchanged by the current. The difficulty lies with the quadratic drag force. Since:

$$U_p^2 + u_p^2 < (U_p + u_p)^2 \tag{12.51}$$

then a segregated treatment of the current drag and wave drag - which are superposed only at the end of the computation - will lead to an underestimation of the forces involved.

12.6 Forces on An Oscillating Cylinder in Various Flows

Now that the hydrodynamic interaction of a fixed cylinder in a variety of flows has been explained, it is appropriate to discuss the hydrodynamic interaction of a moving cylinder - again in a variety of flow conditions.

A distinction will now have to be made between the (external) force exerted by the cylinder on the surrounding water and the (internal, structural) force needed to cause the cylinder (segment) to oscillate. In general, the internal force will often be one that is measured - especially in a laboratory setting. This force includes the external hydrodynamic force but also includes a force needed to accelerate the cylinder itself. Also, one should remember that the hydrodynamic interaction force components will generally be in a direction opposite to the actual velocity and acceleration of the cylinder.

12.6.1 Still Water

As indicated much earlier in this chapter, the Froude-Krilov force will be absent since there are no ambient pressure gradients in water which is at rest. The inertia force will be associated with a C_a value and there will be a drag force - associated with C_D as well. Analogous to the assumption made for a fixed cylinder, these forces will be associated with the cylinder kinematics components (velocity and acceleration) which are perpendicular to the cylinder's axis.

The five steps used for determining the forces on a fixed cylinder can used here too, albeit that the kinematics now is that of the cylinder instead of the water.

12.6.2 Current Alone

This interaction situation has already been discussed to some extent in chapter 4. One should remember that the direction of cylinder oscillation and the current direction may be quite different. Indeed, a vortex-induced vibration usually has its largest component more or less perpendicular to the current direction. This results from the lift force - the most important dynamic force in this flow situation - which was discussed in chapter 4.

The drag component of the hydrodynamic interaction was quite well described in section 6 of that chapter too; there is no need to repeat that here.

Inertia forces will - in principle - now be present, too. They will be associated with a C_a value since there is still no ambient time-dependent pressure gradient. These forces will be opposite to the acceleration component which results exclusively from the cylinder oscillation in this case.

In many realistic cases the approaching flow velocity will be considerably larger than the cylinder's oscillation velocity. Also, since most oscillating cylinders are rather slender (an umbilical cable to a ROV is an excellent example) the KC number will be large so that inertia forces will be small anyway. In many practical situations, then, one considers only a drag force as if it were exerted on a fixed cylinder. The drag coefficient is sometimes a bit larger to account for the wider wake resulting from the cylinder oscillation.

12.6.3   Waves Alone

The inertia and drag forces are treated entirely separately here for clarity.

Inertia Forces

Waves will contribute both a Froude-Krilov force (from the ambient, time-dependent pressure gradient) as well as a disturbance force from the encounter with the solid cylinder. The cylinder oscillation, on the other hand, plays no role in the Froude-Krilov force but it does contribute to the disturbance term. (It is implicitly assumed here that the motion of the cylinder is small relative to the wave length so that no phase changes result from this displacement. It is hard to conceive of a practical situation for which this assumption does not hold.) When one keeps in mind that the direction of cylinder oscillation need not coincide with the wave direction, then careful bookkeeping is called for.
One finds the following inertia terms in the equation of motion:

$$M \ \ddot{X}(t) \boxminus C_M \ M_D \ \dot{u}_p(t) - C_a \ M_D \ \ddot{X}(t) \tag{12.52}$$

in which:

M	=	Mass of the cylinder segment (kg/m)
M_D	=	Displaced water mass $= \frac{\pi}{4}D^2\rho$ (kg/m)
$\dot{u}_p(t)$	=	Perpendicular acceleration component from the waves (m/s^2)
$\ddot{X}(t)$	=	Cylinder acceleration (m/s^2)

The symbol $\boxminus$ has been used to segregate terms from the left hand side of the full equation of motion from those on the right. Since only selected terms are included, true equality cannot be guaranteed. The above relationship can be re-arranged by splitting the wave force term into its two components so that:

$$M \ \ddot{X}(t) \boxminus 1 \ M_D \ \dot{u}_p(t) + C_a \ M_D \ \dot{u}_p(t) - C_a \ M_D \ \ddot{X}(t) \tag{12.53}$$

If the cylinder acceleration corresponds exactly - in both magnitude and direction - to that of the waves, then the last two terms in this latter equation cancel. This is logical; there is then no disturbance at all and only the Froude-Krilov force remains.
In the more general case, all three hydrodynamic force components in equation 12.53 will be present. It is often convenient to move all the force terms involving the cylinder motion to the left hand side of the equation so that it becomes:

$$(M + C_a \ M_D) \ \ddot{X}(t) \boxminus C_M \ M_D \ \dot{u}_p(t) \tag{12.54}$$

This isolates the (unknown) cylinder motion on the left hand side of the equation and places the time-dependent external exciting force on the right. This right hand side can be evaluated (without knowing the cylinder motion) as a pure time function before the differential equation of the cylinder motion is evaluated.

Drag Forces

Drag forces result from the flow disturbance and wake near the cylinder. Two quite different approaches to the description of hydrodynamic drag are used. They are discussed separately here.

Relative Velocity Approach It is reasonably simple to postulate that this wake depends upon the motion of the water relative to the (moving) cylinder - the relative velocity: $u - \dot{X}$. It results in a drag force proportional to the square of this relative velocity so that one finds the following velocity-dependent terms in the equation of motion:

$$c \, \dot{X}(t) \boxminus \frac{1}{2}\rho \, C_D \, D \, (u_p(t) - \dot{X}(t)) \, \left|u_p(t) - \dot{X}(t)\right| \qquad (12.55)$$

in which:

c	=	Material damping coefficient $(\text{N} \cdot \text{s/m})$
$u_p(t)$	=	Time-dependent perpendicular water velocity (m/s)
$\dot{X}(t)$	=	Time-dependent cylinder velocity (m/s)

The linear damping term on the left hand side of relation 12.55 involves the internal material damping of the cylinder itself. This has nothing to do with hydrodynamic interaction which is concentrated on the right hand side of the relation.

Notice that the quadratic nature of the drag force makes it impossible to segregate the (unknown) cylinder velocity from the ambient water velocity when computing this exciting force in this way. It is not possible compute this time-dependent excitation force component from the water motion independent of the (also time-dependent) dynamic response of the cylinder. This requires simultaneous step-by-step solution of the differential equation in the time domain. Additionally, an extra iterative loop must be included **within each time step** in order to successively approximate values of $\dot{X}$ until the entire differential equation is satisfied at each time step. This makes such time-domain computations rather time-consuming - even with modern computers.

Absolute Velocity Approach A strict interpretation of this approach uses the principles of superposition in much the same way as they are used in the hydrodynamics of larger structures. The forces resulting from the combined motion of the cylinder in waves plus currents is treated as if it were made up of two independent phenomena: A force caused by the waves plus current on a stationary cylinder proportional to $u_p \, |u_p|$ plus a separate force exerted on a cylinder oscillating in still water which is proportional to $\dot{X}^2$. This approach inherently 'fails to see' the cross product $(-2 \, u_p \, \dot{X})$ term included automatically in the relative velocity approach. Further, since the motions of the cylinder will usually be considerably less that those of the surrounding water, the largest contribution to the (external) drag force will therefore come from the $u_p \, |u_p|$ term. This can be left alone on the right hand side of the equation; it can be evaluated quite easily. The relatively small $\dot{X}^2$ term can be linearized and moved to the left hand side of the equation of motion. This linearized drag force now behaves in the same way as a linear damping; it has the same effect as increasing the structural damping which one normally includes in such computations.

Alternatively, one can use an even more pragmatic approach by noticing that the latter two terms of the time-dependent product in the expanded version of relation 12.55 involving u are both smaller than the first term and are often of opposite sign; their combined effect will be small. One now linearizes this small effect and associates it entirely with the cylinder velocity, $\dot{X}$, and treats it as above.

Even if the structure's damping coefficient is not modified, the result of either of these approaches can be that the full differential equation of motion for the cylinder has been

linearized and that the wave-caused excitation force has been isolated on its right hand side. Each motion is treated as if it is in a fixed axis system. It is for this reason that this approach is often referred to as the absolute motion approach.

Comparison   Designers tend to be conservative in practice. As a result of this, they tend not to modify the linearized damping when using the absolute motion approach. Since a dynamic system with a lower damping will often have a larger response, the absolute motion approach most usually leads to higher predicted structural responses (internal stresses or even displacements, for example) than does the relative velocity approach. This is indeed a strong motivation to use the absolute velocity approach when evaluating the performance of a proposed design. The additional advantage of having a straightforward and simple computational procedure comes as an added bonus.

12.6.4   Currents Plus Waves

Just as with the fixed cylinder, all hydrodynamic velocity components are generally superposed before starting a force computation. Once this has been done, the further treatment is identical to that for an oscillating cylinder in waves alone as discussed above.

12.7   Force Integration over A Structure

The discussion above has concentrated on the forces on a unit length of cylinder or at least no more than a single member of a large truss structure. It is now time to integrate these forces over the length of the cylinder in order to determine loads which are relevant for structural analysis and design evaluation.

Since many space truss analysis computer programs work with externally applied joint loads, the goal should be to transform the distributed hydrodynamic load on each member of the structure to equivalent concentrated loads at the structure's nodes. Generally, this procedure will have to be followed during a whole series of discrete time steps in order to generate time-dependent loadings which may be needed for a dynamic analysis.

Many computer programs for this purpose work somewhat as follows:

As preparation,

- The nodes of the structure are numbered sequentially.

- Each node is assigned a set of X, Y, Z coordinates corresponding to the intersection point of the member axes at that joint. (Any member eccentricity at the joint is neglected in the hydromechanics.)

- Each member is specified by its diameter and the numbers of the two nodes which it joins. Each member's geometric position and length is now defined.

Once this has been completed the following steps will be carried out for the dynamic loads at each desired time step:

1. The water kinematics - both combined velocities and accelerations - will be computed at each node location. It makes no difference now whether the waves are regular or irregular; there can even be directional spreading or additional currents involved.

The result in all cases is known water kinematics at each node and at every chosen time.

2. If a dynamic calculation is included, and relative velocity drag is used, then the structure's velocity and acceleration at each node will have to be estimated as well. This is usually done by incrementally integrating the structure's equations of motion by working from the previous time step.

3. The results of the above two steps along with the known geometry allow the computation of the force per unit length (for inertia and drag forces separately) at each end of each member. These load intensities will have to be computed separately for each member and at each of its end joints.

4. Most programs now consider each member to be a simple beam carrying a distributed load which is assumed to vary linearly from one end to the other. Note that both the intensity of the loading as well as the vector direction of the loading (about the axis of the cylinder) may vary along its length. (Direction variation can be present when the waves and current are not co-linear. It is also present when wave directional spreading is involved.)

5. Basic mechanics yields the two reaction force components (relative to each member's axis!) at each of its ends.

6. It is now only a matter of bookkeeping to transform these individual member reaction forces into equivalent X, Y, Z force components at each joint.

7. The above X, Y, Z components at each joint are summed to determine the total equivalent applied dynamic load at that joint at the chosen moment. This is the desired result.

8. If relative velocity hydrodynamics is being used this result must be checked. The equations of motion of the structure must be integrated now to determine its new velocity and acceleration at the end of the time step. If these values do no correspond (within a chosen tolerance) with those estimated in step 2, then the above steps must be repeated for another iteration cycle - within this same time step - until the estimated and computed values appropriately coincide.

It is the extra iteration loop discussed in the last of the above steps that makes the relative velocity approach to hydromechanics so computationally inefficient relative to other approaches.

Constant static loads, such as member weight and buoyant forces, can be included in the above computation, but can be computed more efficiently separately before starting on the dynamic computations. The computation principle is analogous to that for the dynamic loads, by the way.

.

Chapter 13

SURVIVAL LOADS ON TOWER STRUCTURES

13.1 Introduction

Chapter 12 has discussed how to compute the hydrodynamic forces on an element (of unit length) of a single (slender) cylinder; a simplified means of estimating the largest hydrodynamic forces on an offshore tower structure will be handled in this chapter.

Figure 13.1 shows an isometric drawing of one of the larger offshore structures. The annotations in that figure will become clear in the course of this chapter.

Some refer to such a structure as a space frame, others see it as a space truss, some just call it a tower. The terms 'frame' and 'truss' have quite different structural engineering connotations which are not at all relevant to the hydrodynamic discussion in this chapter. Another structural distinction is that a jacket is supported from the top by piles driven through its legs while a tower is generally supported from below by piles driven through sleeves - usually at the sea bed. This distinction is also irrelevant for the hydrodynamics being discussed here; the term tower will be used more generically in this chapter to refer to any three-dimensional structure made up from slender elements.

Imagine the bookkeeping and computational effort needed to compute the total hydrodynamic forces on the structure shown in figure 13.1 if this were to be done using the elemental methods of chapter 12. Such a rigorous computation for a 'real' tower structure (with all its members: chords, braces, risers, etc.) is a very cumbersome undertaking, indeed.

Many design engineers have no need for the computational accuracy suggested by a detailed schematization of such a complex offshore structure - at least not during the preliminary design phase. Instead, one more often needs a fast method of making a rough and preferably conservative estimate of the hydrodynamic forces on a complex offshore structure. Such a method can serve two purposes: Give a rough estimate for preliminary design or assure that a detailed model is not making a major error. The objective of this chapter is to outline a 'quick and dirty' method to estimate the horizontal loads on a tower structure. These loads generally yield the largest overall bending moments in the structure and thus axial leg forces as well as the largest horizontal shear forces. These forces and moments are also important for the foundation design. Maximum in-service bracing loads result from
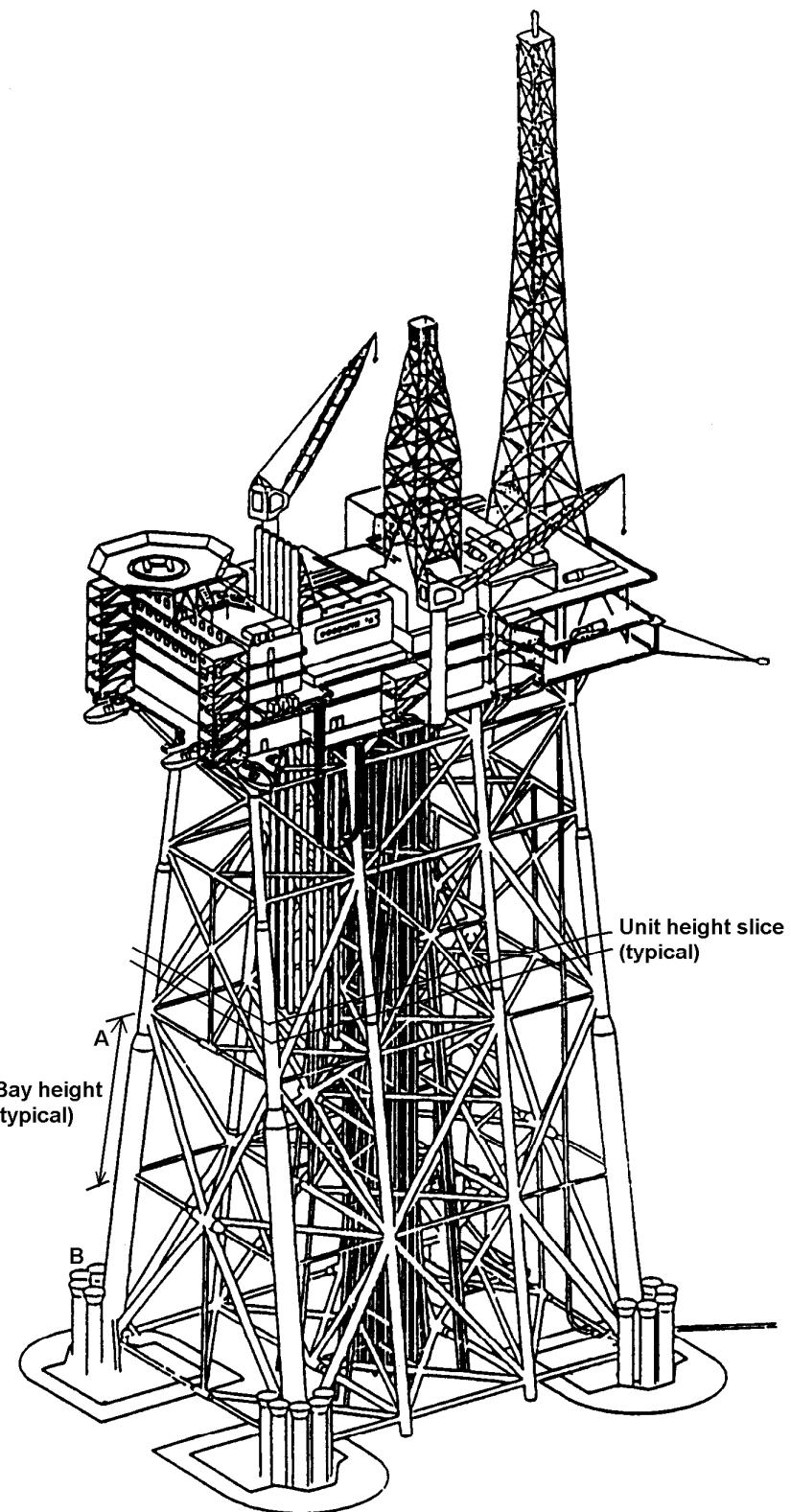
Figure 13.1: Typical Larger Offshore Tower Structure

the horizontal wave and current loads as well.

13.1.1 Method Requirements

The results obtained with any approximation need not be exact - especially if one can reasonably predict whether the 'real' loads will be smaller (or larger) than the estimates. Generally - and for preliminary design in particular - it is handy if the hydrodynamic loads resulting from the approximation are larger than those which would follow from a more sophisticated analysis.

When a preliminary design is based upon loads which are overestimated, it is most likely that the resulting structure will be 'over-designed'; it will be a bit too big, or heavy, or strong and thus probably too costly. Given this fact, then one would not expect the costs of a structure resulting from a more detailed design to come out too high. Said in another way, if the preliminary design survives an economic analysis, then the final design has a good chance of surviving this too - at least to the extent that its total cost is determined by hydrodynamics. An additional factor in practice is that topsides tend to become heavier (as more equipment is added) rather than lighter during the design process. (Whether one likes it or not, topside structures usually tend to get larger and heavier in the course of their detailed design. This can result from equipment or throughput changes as well as from modified environmental or safety requirements.) To the extent that the tower design is dictated by topside weight (if the water is not all that deep depending upon the sea conditions), a bit of initial tower overdesign can prove to be handy during the later, more detailed design analysis phase.

The objective of this chapter, therefore, is to come up with a computational procedure to conservatively predict the hydrodynamic forces on a complex offshore tower structure.

13.1.2 Analysis Steps

Any hydrodynamic analysis of an offshore structure involves the following steps:
1. Selection of environmental conditions (raw data).
2. Schematization of the ambient hydrodynamics.
3. Schematization of the structure.
4. Computation of resulting (survival) forces and overturning moments.

These steps will be followed in the remainder of this chapter.

13.2 Environmental Conditions to Choose

Since one is looking for a maximum external load condition, it is common that this will be caused by a maximum environmental input condition. (A significant dynamic response - which via resonance can lead to enhanced internal loads - can lead to internal response maxima (leg forces, for example) which are caused by more moderate external sea conditions. This is not considered here; it is not that common with tower structures, anyway.) All of this means that extreme wind, wave and current conditions should be chosen for this first design. Each of these involves at least two independent variables: Speed (in some form) and direction. All of environmental inputs can be represented as vectors, but their scalar magnitudes and directions are discussed separately here.

Wind Speed

Wind loads on offshore structures often play a relatively minor role in comparison to the hydrodynamic loads. For an offshore wind turbine, even - on which one would expect to have a relatively high wind load - the wind load is seldom greater than the combined wave and current load unless the structure is placed in water somewhat less than about 20 meters deep (in the North Sea). This implies that the selection of design wind conditions is often not all that important. When one *does* want to estimate wind loads, a maximum one-minute wind gust is often chosen. This wind speed is usually measured at a 'standard' elevation of 10 meters above the sea surface.

Current Speed

Maximum current speeds are usually chosen for survival design purposes as well. One could select a speed corresponding to a maximum spring tide current, for example. In some cases a velocity profile giving the current as a function of depth will be available, too. If not, it is of course conservative to assume that the maximum current acts over the entire depth.

Wave Height and Period

One should choose wave height and period values such that a maximum wave force or overturning moment is obtained. A high wave is obviously needed. If one assumes that the worst part of a storm will have a duration of about 3 to 6 hours and that an extreme wave - if seen as a single wave - will have a period of in the order of 15 to 20 seconds, then one can expect an exposure to something in the order of 1000 waves during the peak of the storm. The highest wave in a series of 1000 would have a chance of exceedance of $\frac{1}{1000}$. Substituting this in a Rayleigh wave height distribution yield a design wave height of 1.86 times the design significant wave height chosen. (If one works out these limits more exactly, one should expect something more than 540 waves and less than 1440 of them; one thousand is pretty close to the average - by chance. If $\frac{1}{540}$ and $\frac{1}{1440}$ are used instead, the wave height ratio is in the range 1.77 to 1.91; this makes no more than 5% difference.) Selecting the shortest wave period consistent with the chosen wave height will yield maximum water velocities and accelerations - at least near the water surface. On the other hand, the hydrodynamics of waves with shorter periods 'die out' faster at deeper locations; a proper balance must be found between these two requirements. Wave breaking will, of course, put a lower limit on the wave period for a given wave height; a very high and very short wave will break so that one should also check any chosen combination of these to be sure that the wave is not broken. The necessary relationships (for deep water and a quick estimate) include:

$$\lambda = 1.56 \cdot T^2 \qquad \text{and} \qquad \frac{H}{\lambda} < \frac{1}{7} \tag{13.1}$$

in which λ is the wave length (m), H is the wave height (m) and T is the wave period (s). The above relations - which come directly from regular wave theory of chapter 5 - are less dependable for larger and irregular waves at sea, however.

Since H will generally be rather large, λ will not be small, either. The significance of this will show up below.
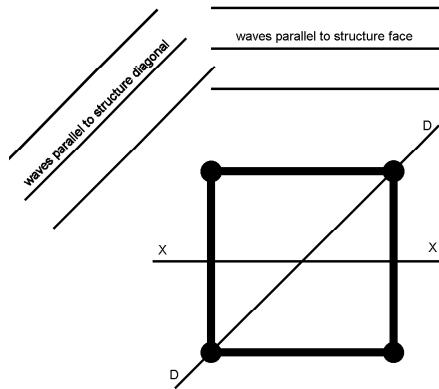
Figure 13.2: Schematic Plan of Tower and Approaching Wave Crests

Wind, Current and Wave Directions

In general, each of these independent physical phenomena will have its own direction, independent - at least to some extent - from that of others. This is most obvious for the relation between the tidal current direction and the wave direction. These seldom have much correlation. The wind direction and the wave direction - in a major storm at least - is usually rather well (but not perfectly) correlated of course.
The conservative choice (which is easy to work with too!) is to simply assume that all three of these phenomena are colinear; they all come from the same direction.
Be sure to keep the direction bookkeeping correct. The wind direction is specified usually as the direction from which it comes, while a current direction is most commonly stated as the direction to which it goes. It sounds inconsistent, but a northwest wind and southeast current go in the same vector direction.

An independent direction consideration involves the orientation of the structure (about its vertical axis) relative to the environmental conditions. Consider a simplified situation as shown in plan in figure 13.2. The solid circles represent the legs of the tower as seen from above. Two possible wave and current approach directions (indicated by the wave crests) are shown: One with crests parallel to a face of the structure (and its X axis) and one with crests parallel to its diagonal - the D axis in the figure. If one assumes for simplicity (for now) that the total external horizontal force as well as the overturning moment about an axis at the sea bed is independent of the approach direction, one will still find larger axial pile forces when the wave crests are parallel to a diagonal. On the other hand, since the horizontal shear forces within the structure are carried primarily by the bracings, waves approaching parallel to one side of the tower will generally lead to maximum forces in these members.This is because the entire shear load is carried by only half of the braces then; braces parallel to the wave crests carry essentially no load.

Phasing

All of the independent environmental phenomena - wind, waves and tides - are time dependent. Do all of the maxima selected above then occur at one and the same instant? Formally, the answer to this lies in a comparison of the periods of the various phenomena. Since the tidal period (12 h 24 min) is long relative to the wind gusts and waves, it is

almost certain that a high wave or strong wind gust can occur when the tidal current is
high.

Looking next at the wind gust relative to the wave, its duration (1 minute) would be a
few wave periods long. Here, again, there is at least some finite chance that a major wave
peak will coincide with this in time. On the other hand, many more waves will occur at
times when the design wind gust is *not* present!

Of course, assuming that the maxima of wind, waves and current *do* occur simultaneously
will lead to a conservative result; this is chosen here.

Implications

The choices made above already have significant implications for the computations to be
carried out. For example, the wave length, λ , chosen above will be rather large relative to
the horizontal dimensions of (most) offshore structures being considered. This means that
there will be relatively little phase difference between the 'upstream' and 'downstream'
sides of the entire structure at any instant in time.

In chapter 12 the phase shift from one side to the other side (of a single cylinder) was
neglected. Now, with an extreme wave, the same reasoning is being applied to an en-
tire tower structure. Since phase differences only tend to reduce the horizontal loads on
the structure, neglecting these will be conservative. Additionally, neglecting this phase
difference will simplify the formulation of the structural model enormously.

Since the wave is relatively high, the Keulegan Carpenter number $KC = \frac{\pi \cdot H}{D}$ (at the sea
surface and in deep water) will tend to be high as well. This indicates that the wave forces
will tend to be drag dominated - at least at the sea surface where they are largest.

Note that if the structure is not in deep water, the actual KC value will be even higher
than that estimated above; this can be checked by using the complete equations - rather
than deep water approximations - to describe the water motion. When the current is added
to the water velocity caused by the wave, then this drag dominance becomes even more
pronounced, of course. In all cases, the water velocity will decrease with depth so that the
KC value will decrease as well. One can expect the inertia force to increase in importance
as one moves down along the structure. A significant current can prevent it from ever
playing much role, however.

Remember too from wave kinematics that the maximum horizontal water velocity in a
wave occurs under that wave crest or trough. The total resulting force (integrated over
the structure) will be greatest when the wave crest passes by, simply because more of the
structure is then exposed to the wave. Wave kinematics will have to be predicted over the
entire height from the sea bed to the wave crest in order to carry out such a computation.

13.3   Ambient Flow Schematizations

This section discusses the numerical models needed to translate the raw data on environ-
mental conditions into input data for a force model.

Wind

Wind velocity distributions have been discussed in chapter 4. If - as is standard meteoro-
logical practice - the wind is given at a standard elevation of 10 meters above mean sea

level, then wind speeds at other elevations are often predicted from this value by using:

$$\frac{V_{tw}(z)}{V_{tw}(10)} = \left(\frac{z}{10}\right)^{0.11} \quad \text{(at sea)} \tag{13.2}$$

in which:

$$
\begin{array}{lll}
z & = & \text{desired elevation (m)} \\
V_{tw}(z) & = & \text{true wind speed at elevation } z \text{ (m/s)} \\
V_{tw}(10) & = & \text{true wind speed at 10 meters elevation (m/s)}
\end{array}
$$

The exponent 0.11 in equation 13.2 is for sea conditions only; see chapter 4.

Some designers often reason that since wind loads on many offshore structures are often relatively unimportant and hydrodynamic loads tend to be over-estimated, they can just neglect wind loads altogether. This is certainly the very simplest approach that can be chosen. On the other hand, the wind load has the longest moment arm when one is studying the overturning moments about the structure's base. It is best not to neglect them in the overturning moment computation at least.

Waves

A maximum wave at sea results from the superposition of a large number of wave spectrum components. The objective here is to replace this multi-component wave with a single regular wave for computation purposes. Linear wave theory is certainly convenient for predicting the water kinematics within such a wave, but it has one important drawback: It predicts water motions only in the zone below mean sea level. As has been indicated above, the water motions right up to the wave crest will have to be predicted. Methods for doing this have been given in chapter 5. Of these, the use of a constant velocity - the same as the velocity at $z = 0$ - or Wheeler stretching are the most popular.
Remember from chapter 5 that the (extreme) wave crest will be higher than $H/2$ above the still water level as well. A common rule of thumb is that:

$$\zeta_{\max} = +\frac{2}{3}\,H \qquad \text{and} \qquad \zeta_{\min} = -\frac{1}{3}\,H \tag{13.3}$$

With this, one can use either constant extension or Wheeler stretching along with the complete equations for the water motion in order to calculate the horizontal components of water particle acceleration and velocity at all elevations between the sea bed and wave crest. All details of this can be found in chapter 5.

One should note the following about the waves formulas to be used:

1. If only a maximum velocity is needed, the time function in the wave can be neglected.
2. Since the wave length is usually considerably larger than the horizontal dimensions of the total structure being considered, the phase relation, kx can be dropped too.
3. If the wave crest is involved, then the maximum crest elevation will follow from equation 13.3.
4. The full equations (and not deep or shallow water approximations) must be used when evaluating the horizontal kinematics in the wave. This is then valid for any water depth and at any point under a wave profile.

Use of deep water wave theory - with its simplifications - can lead to less than conservative results as the water depth decreases; this is the reason that use of the full theory is recommended above.

The wave height used should be the correct one for the actual water depth, h. Include the shoaling influence, if appropriate; see chapter 5. Use this same actual water depth when computing λ as well.

Current

Since the current is constant and in the same direction as the wave propagation, it can simply be added to the velocity component amplitude, $u_a(z)$, computed for the wave. If the current velocity is given by $V(z)$, then the total horizontal velocity will become:

$$U_a(z) = V(z) + u_a(z) \tag{13.4}$$

Of course, $V(z) = 0$ for $z > 0$.

Remark

Upon reflection, one can conclude that the computational effort needed to describe the environmental hydrodynamics and aerodynamics has been simplified considerably in comparison to the most general case:
  - Only conditions under the wave crest are considered.
  - Only hydrodynamic drag is considered.
  - All spatial phase differences are neglected.

These all reduce the computational effort. On the other hand, one is forced to add a limited amount of complication in order to:
  - extend hydrodynamics up to the wave crest and
  - have a solution valid for all water depths.

Even so, the overall result of all this is that the hydrodynamics has been considerably simplified. A simplified schematization of the offshore structure will be discussed in the following section.

13.4   Structure Schematization

The objective of this section is to replace the actual truss-like marine structure - with all of its members and nodes - with a much simpler and computationally efficient equivalent one for the purpose of estimating its external hydrodynamic drag loads. The formulations derived in this section are valid only when all velocity or acceleration components are co-linear. This means that the all waves and all currents come from the same direction. This is completely in agreement with the schematization of the environment made above, but it will not be true in a more general case. The formulations in this section will be incorrect, however, if the current comes from another direction than the waves or even if only directional spreading of the waves must be included.

The drag term in the Morison equation (for a vertical cylinder) is of the form:

$$F_{drag_a} = \frac{1}{2}\rho \ C_D \ D \cdot U_a^2 \tag{13.5}$$

in which:

$$
\begin{array}{rcl}
F_{drag_a} & = & \text{drag force amplitude per unit length of vertical cylinder (N/m)} \\
C_D & = & \text{drag coefficient, to be discussed later (-)} \\
D & = & \text{cylinder diameter (m)} \\
U_a & = & \text{horizontal velocity amplitude at the chosen elevation (m/s)}
\end{array}
$$

Since U_a will be positive in this case, $U_a \cdot |U_a|$ has been replaced by U_a^2.

Consider now a horizontal 'slice' of the entire structure having a unit height; see figure 13.1. What happens as one sums the drag forces across all the members found at that level? $\frac{1}{2}\rho, C_D$, and U_a in equation 13.5 remain constant. The remaining quantity, D times a unit height, is simply an area. Since attention focuses on the horizontal forces on the structure, this is an area projected on to a vertical plane, perpendicular to the 'slicing' planes; it is the area one would be able to measure on a side view photograph of the structure (if no members were hidden behind others in that photo!). The 'photo' should be made looking in the direction of wave propagation, of course.

Continuing for now with a 'horizontal slice' (of unit height) of the structure at a given elevation, then the equivalent diameter, D_e, which must be used in the Morison equation drag term (in order to get the total drag force) is simply that total area (as seen on the projection or photo) divided by the unit height.

Upon reflection, one will discover that at each elevation, z, one finds the following contributions to D_e:

- Leg chords (nearly vertical) each contribute their actual diameter, D.

- Horizontal braces (if present at the chosen elevation) at an angle θ relative to the plane of water motion contribute:

$$
D_e = L \sin\theta \tag{13.6}
$$

in which:

$$
\begin{array}{rcl}
L & = & \text{brace length (to the centerline of its nodes) (m)} \\
\theta & = & \text{brace azimuth relative to the water motion plane (rad)}
\end{array}
$$

but only over the limited height, D.

- Sloping braces in the plane of the picture contribute:

$$
D_e = \frac{D \cdot L}{H_B} = \frac{D}{\sin\alpha} = D \ \csc\alpha \tag{13.7}
$$

in which:

$$
\begin{array}{rcl}
H_B & = & \text{height of the bracing bay (m); see fig. 13.1} \\
\alpha & = & \text{slope of brace relative to the horizontal (rad)}
\end{array}
$$

- Sloping braces in a vertical plane perpendicular to the plane of the picture (in the plane of the water motion) contribute D.

- Sloping members with other spatial orientations - think of sloping braces when waves approach a tower in a diagonal direction - require a bit more geometry and book-keeping. Letting:

$$\ell = \frac{1}{2}\left(\frac{L}{H_B} - 1\right) = \frac{1}{2}\left(\csc\alpha - 1\right) \tag{13.8}$$

then:

$$D_e = D \cdot \{1 + \ell \cdot [1 - \cos(2\theta)]\} \tag{13.9}$$

in which θ is the bracing azimuth relative to the wave direction (rad).

This angle θ could alternatively be referred to as the angle between the (vertical) plane which includes the brace and the vertical plane in which the flow takes place. One might note that equation 13.9 is quite general; it even works (in a degenerate way) for a vertical cylinder.

One can argue that measuring each brace length to the centerline of each of its end nodes, includes too much length; more than one member is being counted within each joint's volume. This is true, but it is often seen as a compensation for the fact that the flow will actually be more complex in the joint vicinity. This will - in turn - likely lead to higher forces than would be predicted for a single straight member.

Since the diameter is a linear factor in the drag force relation, one can simply sum the above diameters at any given elevation to come to a total equivalent diameter, $D_e(z)$, to use at that elevation. This procedure reduces the 'forest' of truss and other members at each elevation, z, to a single vertical cylinder segment.

For most structures, the resulting vertical cylinder will look rather 'lumpy' in that its diameter will not be constant over its length. Indeed, whenever horizontal members are encountered, D_e will abruptly bulge out and become larger. It can also be larger where the leg chords become larger or near the sea bed where extra legs or pile sleeves are often included in the structure. Locations A and B in figure 13.1 are such elevations.

Some may wish to simplify this schematization even more by 'smoothing out' these diameter bulges. This can be a dangerous operation, because the hydrodynamic forces are quite elevation-dependent (and structure overturning moments are even more so) - especially in the zone just below the sea surface. This is at best an operation which must be based upon broad experience.

13.5   Force Computation

Now that the environment as well as the structure have been schematized, one is well on his or her way to computing the hydrodynamic forces and associated overturning moment. One remaining preparatory task is to select an appropriate drag coefficient. Usually a single value is chosen for the entire structure.

How should the drag coefficient be selected? One wrong approach is to use the diameter of the schematized pile, D_e, and u_a to compute the Keulegan Carpenter number, KC, and then to select C_D based upon these values. This is wrong because the equivalent cylinder diameter, D_e cannot be found in the sea at all.

The diameter selected for determining C_D should be more representative of those found in the real structure which is being schematized. If one also discovers that C_D is then rather independent of the exact value of KC, then one is extra fortunate; the precise choice of diameter used in this determination is not critical then anyway.

Should u_a or the total velocity, U, be used to compute KC? Usually only the wave-caused velocity component, u_a, is used, but this can be a very interesting discussion topic.

Once a proper C_D value has been selected, then the (peak value of) the drag force per unit elevation can be computed directly:

$$F_{drag_a}(z) = \frac{1}{2}\rho \; C_D \; D_e(z) \cdot U_a^2(z) \tag{13.10}$$

for the waves plus current, and:

$$F_{wind_a}(z) = \frac{1}{2}\rho_{air} \; C_d \; A_w(z) \cdot V_{tw}(z) \tag{13.11}$$

in which $A(z)$ is the projected area exposed to the wind.

13.6 Force and Moment Integration

The drag forces caused by the wind as well as waves and currents are known as a function of elevation. All the necessary information is now available to compute the resulting horizontal force and overturning moment on the (schematized) structure.

13.6.1 Horizontal Force Integration

The resulting horizontal force can now be computed by integrating F_{drag_a} and F_{wind_a} over the appropriate height segment of the structure. This integration can most efficiently be done using a spreadsheet program. This integration usually proceeds by computing the forces (per unit length) at chosen elevations and then linearly interpolating the loading between these values. The elevations to choose for this evaluation should be chosen based upon the following criteria:

- If D_e or A_w changes abruptly, then one should evaluate the loading for each value - just above and just below the transition.

- Additional successive elevations should be chosen close enough together so that linear interpolation between elevations still provides a reasonable approximation of the exponential curve of the actual elevation function associated with the drag force.

The linear interpolation procedure suggested here replaces some form of elevation dependent exponential decay function by a straight line. This is generally conservative and quite in accordance with the objective of overestimating - if anything - the results. In order to prevent this overestimation from becoming too great, one must be sure that the linear function used for a segment of elevation does not diverge too much from the actual elevation decay function. This implies that finer integration steps - shorter (in height) tower slices - should be selected where conditions change rapidly. Sensitive locations can be found near the water surface and wherever the structure changes abruptly.

13.6.2 Overturning Moment Integration

Overall structure overturning moments are usually computed about a horizontal axis at the sea bed (mudline). The computation proceeds quite analogously to that used to compute the horizontal force, but now one must include the appropriate moment arm with each integration step. This is simply the elevation of that segment relative to the sea bed.

Alert readers can (correctly, in theory) point out that when a real structure - with 'real' horizontal dimensions - includes horizontal members (this is usually the case, by the way!), then the *vertical* water motions *also* induce overturning moments about the mudline. Luckily, one only has to sketch the water motion as a wave progresses through the structure to conclude that the vertical velocity components near the wave crest are small and that this additional (small) moment acts counter (in the opposite sense) to that just computed above. Once again, the objective of predicting an upper bound for the overturning moment is achieved by neglecting this small (and very time-consuming!) detail.

13.7   Comparative Example

The 'proof of any pudding is in the eating'; this section demonstrates the results of computations carried out using the various alternative computation procedures. This is illustrated here by working with an arbitrarily chosen standard case and then by varying one a single variable (while keeping all the others constant) in order to observe its influence.
The standard case involves:

Input Item	Value
Wave Ht. H	15 m
Wave Per. T	12 s

as a wave whose crest extends 10 meters above the still water level. This yields a q parameter for the Wheeler Stretching of 0.80. Further, in order to focus the comparisons on the hydromechanics and to avoid a discussion of the structure or the drag coefficient, the following quantity is keep constant from the wave crest elevation (+10 m) to the sea bed.

$$\frac{1}{2}\rho C_D D = 1000 \tag{13.12}$$

Further, only the drag force is considered here.
Computations have been carried out for each of the four treatments of the splash zone discussed in chapter 5:

- Linear Theory - nothing above the still water level

- Extrapolated Linear Theory - linear theory functions are continued to the wave crest.

- Constant Extrapolation - the linear theory value as $z = 0$ is used for all positive z values

- Wheeler Stretching - the profile is stretched to the wave crest.

Since the water motion in waves is more or less concentrated near the sea surface, one would expect that the total horizontal force on a structure would increase more and more slowly as the water depth continues to increase; each additional increment of structure height (added at the bottom) adds less and less total horizontal force.
As the water depth approaches zero - at the other end of the range - one might reason that the total horizontal force there should also approach zero as the tower height exposed to the waves becomes less and less.

Figure 13.3 shows the total static horizontal shear force at the base of the structure (the integral of the drag force from the wave crest to the sea bed) versus water depth.

The behavior of the curves on the right-hand side of the figure is as expected; the behavior on the left is not - although the curves do not extend completely to a zero water depth. As the water depth decreases, the water motion in the wave becomes more and more like that of a shallow water wave; the horizontal water velocities increase. This increased water velocity - especially when used in a quadratic drag force formula - causes the force per unit height of the structure to increase so rapidly that it more than compensates for the corresponding loss of total tower height. The curves are not extended to zero depth because wave breaking would limit the wave height. Neither wave breaking nor wave height changes resulting from shoaling outside the breaker zone are included in this analysis.

The four curves on the figure are located more or less as one would expect. It is no surprise that extrapolated linear theory yields the largest force and that 'plain' linear theory the lowest.

Figure 13.4 shows the resulting moments. As would be expected, the overturning moment increases significantly with water depth. The relative positions of the four curves is logical as well in view of the results above.
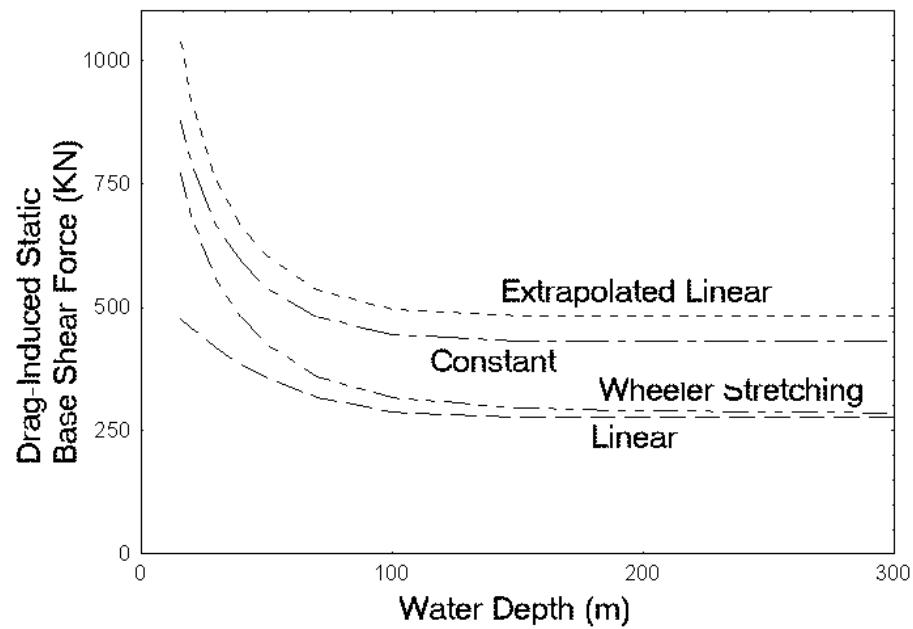
Figure 13.3: Horizontal Force versus Water Depth
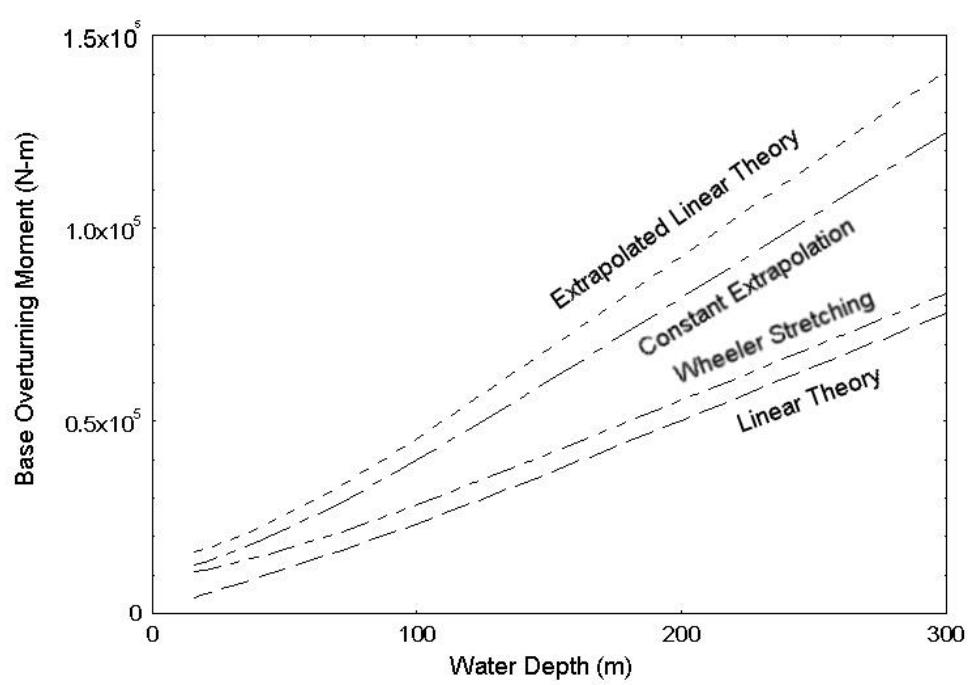
Figure 13.4: Base Overturning Moment versus Water Depth

Chapter 14

SEA BED BOUNDARY EFFECTS

14.1 Introduction

So far, attention has focussed on flows near and forces on man-made objects in the sea. Now, attention is shifted to the largest object in the sea: the sea bed, itself. Along the way, a few topics concerning forces on small man-made structures placed on or near the sea bed will be discussed as well.

These are all cases in which the flow of sea water over the sea bed is markedly influenced by the sea bed boundary layer; an exposed pipeline is an excellent example as is an item of ship's cargo that has been lost overboard and has sunk.

The influence of the flow boundary layer on the sea bed itself becomes important when one considers the erosion or deposition of sea bed material near a man-made object. Erosion around the piles of an offshore platform can leave a segment of the piles without lateral support. It is harder to find and recover a valuable piece of ship's cargo that has become covered by the natural action of the sea bed.

The approach used in this chapter is not, in principle, really any different from that used already. First attention is paid to the flow - in the vicinity of the sea bed, in this case. This is followed by a discussion of forces on objects (including the sea bed itself!) and the consequences which these forces can have.
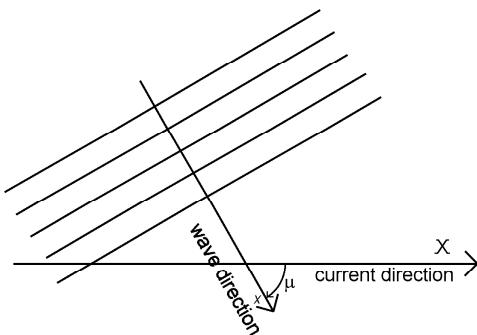
Figure 14.1: Axis System (plan view)

The axis system shown in figure 5.2 in chapter 5 and here in figure 14.1 remains consistent with that used in offshore engineering:

- A current (if present) will flow in the $+X$ direction.
- The waves propagate in the $+x$ direction.
- The positive wave direction $(+x)$ makes an angle μ with the X-axis.
- The $+z$-axis is upward from the still water level.

Note that this last convention, especially, can be in contrast to that used by coastal engineers (who often place the vertical coordinate origin at the sea bed). Their approach leads to numerical computational difficulties in deeper water.

The notation for some variables used in this chapter may not agree with that often used by coastal engineers; these changes have been made to make the notation within this book more consistent.

14.2 Boundary Layer under Currents and Waves

One should remember the following facts about boundary layers from basic fluid mechanics courses or the earlier chapters of this book:

- They result from a velocity difference between the ambient flow and an object.
- They need time - or equivalently distance - to develop.
- Surface roughness plays an important role in their development.

The second of these items is more obvious if one remembers that distance is an integration of velocity with respect to time.

What currents are important for this analysis? Tidal currents are driven by the gravitational attraction of the sun and the moon. These attraction forces act essentially uniformly over the entire depth of the sea, irrespective of the water depth at the given location. (This is in sharp contrast to the situation with large scale oceanographic currents - which are generally less than a kilometer deep - and the water motion caused by wind waves - which are even more 'surface-bound'.) Since the tidal current driving force is uniformly distributed over the depth, one would expect that this current would also be uniformly distributed, too. This is not the case, however - at least not in the vicinity of the sea bed. Here, the current is influenced by a friction force resulting from the water motion over the sea bed. The Prandtl-Von Kármán logarithmic velocity distribution shown in figure 14.2 results in this case. Such a velocity distribution has its maximum at the sea surface and the velocity reduces very slowly at first, but more and more rapidly as one gets nearer - in the profile - to the sea bed. The exact shape of the profile depends upon the bed roughness.

Since the logarithm of small numbers is negative, the logarithmic velocity distribution yields - strictly speaking - negative velocities in the immediate vicinity of the sea bed; this is obviously unrealistic. This shortcoming is 'patched' by using a linear (straight line) velocity profile in the area nearest to the sea bed. This line has a velocity of zero at the sea bed, and is tangent to the curve of the logarithmic velocity profile. The velocity at this elevation of tangency is often referred to as V_t. Obviously, this linear velocity profile has a constant slope, $\frac{dV}{dz}$; if the elevation of the tangency, z_t, is known and fixed, then $\frac{dV}{dz}$ is simply proportional to V_t.

The sea bed roughness (a length), which determines the details of the velocity profile can be defined in either of two ways:

- If the sea bed is essentially flat, the roughness is defined in terms of the grain size of the sea bed material.
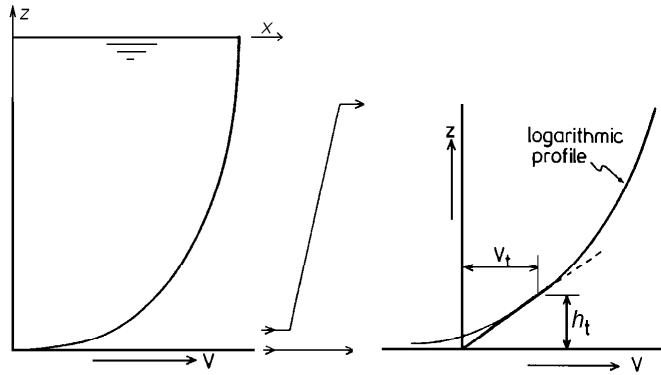
Figure 14.2: Logarithmic Velocity Distribution

- Sandy sea beds especially, are often covered with small ripples which are perhaps a centimeter or so high - much larger than a sand grain, in any case. The height of these ripples then determines the bed roughness. Such ripples are often found on the sea bed where ocean waves are present.

In both cases, the height z_t is usually of the same order of magnitude as this roughness, by the way.

14.2.1 Bed Shear Stress With Currents Alone

Newton postulated a friction model for two plates separated by a fluid - see chapter 4. It resulted in a shear stress - to use the notation of this chapter:

$$\tau = \eta \cdot \frac{dV}{dz} \tag{14.1}$$

in which:

$$
\begin{array}{lll}
\tau & = & \text{shear stress at bed (N/m}^2) \\
\eta & = & \text{dynamic viscosity (kg/m/s)} \\
dV/dz & = & \text{velocity gradient near bed (1/s)}
\end{array}
$$

Since the time scale in which a tidal current varies is so long, it can be treated as a constant current for the purposes of this chapter; it flows long enough for a well-developed boundary layer to develop. This means that the shear stress, τ, (caused now by the current) will also be essentially constant with respect to a time interval of several minutes or perhaps even an hour.

Constant current shear stresses also occur in rivers. If one considers a unit length (and width) of a river section, one finds that the energy input or driving force for the flow comes from the decrease in elevation (potential energy loss) over that length; the flow resistance comes from the shear stress between the river bed and flow. This yields, in an equation form:

$$\tau = \rho \; g \; h \; i \tag{14.2}$$

in which:

$$
\begin{aligned}
\tau &= \text{bed shear stress (N/m}^2) \\
\rho &= \text{mass density of water (kg/m}^3) \\
g &= \text{acceleration of gravity (m/s}^2) \\
h &= \text{water depth (m)} \\
i &= \text{river surface slope } dz/dx \text{ in the direction of flow (-)}
\end{aligned}
$$

In the eighteenth century, the French hydraulic engineer, Antoine Chézy, developed an empirical relationship for the depth-averaged velocity in a river. The earliest know record of its publication is 1775. It is quite certainly the first uniform flow formula for open channels; it is still used today. It is a formula:

$$V = C\sqrt{h\,i} \tag{14.3}$$

in which C is an empirical coefficient which is *not dimensionless;* it has units of $m^{1/2}/s$. It also has an inverse relation to the bed roughness: the rougher the bed, the lower the value of C.

It can be convenient to combine equations 14.2 and 14.3. Since there is essentially no constant water surface slope offshore, one simply eliminates the slope term, i, from the above two equations. This yields:

$$\tau = \rho\,g\,\frac{V^2}{C^2} \tag{14.4}$$

Notice that the water depth falls out of this equation, too, but C must still be estimated. This can be done for a constant current (at least) using:

$$C = 18\ \log\frac{12\,h}{r} \tag{14.5}$$

in which:

$$
\begin{aligned}
C &= \text{Chézy Coefficient (m}^{\frac{1}{2}}/\text{s)} \\
h &= \text{water depth (m)} \\
r &= \text{bed roughness (m)}
\end{aligned}
$$

All of this brings up an interesting question: Since V_t - the current velocity at the elevation of the point of tangency - is directly proportional to the average velocity, V, how does one explain that Newton's approach relates τ to V, while at the same time, Chézy (see [Herschel, 1897]) relates τ to V^2? One of these must be wrong, or there may be another explanation.

One is not sure that C (or even η for that matter) remains constant for a wide variety of flow conditions. Indeed, every river engineer knows that C is *not* constant. In practice, there is generally more faith in Chézy than in Newton in this case, however, so that τ is usually associated with a higher power of V or dV/dz.

The shear stress, τ, discussed so far has been the shear stress which the sea bed exerts on the flow. Newton's Third Law of motion indicates, however, that this is also the shear stress which the flow exerts on the sea bed.

Before proceeding with this development, the discussion backtracks to discuss the boundary layer and shear stress under waves.

14.2.2 Boundary Layer Under Waves

Wind waves are generally present at sea, but our river engineering colleagues did not need to consider them when they came up with their velocity profile and bed shear stress expressions. Potential theory - which by definition considers no friction - predicts that the horizontal water motion velocity caused by surface waves decreases in some negative exponential way as one proceeds deeper in the sea; see chapter 5. It is sometimes a misnomer to assume that the water motion had completely died out at the sea bed; a storm wave of 30 meters height and a period of 20 seconds still has a horizontal water motion velocity amplitude of $0,23$ m/s at the bottom - in this case in 300 meters of water! Even with more modest waves in shallower water, one can expect to have a wave-caused water motion near the bed which cannot be neglected.

Since there is a motion of the water relative to the sea bed, one might expect a boundary layer to be present. This motion is only the first of the three necessary conditions for a boundary layer stipulated above, however. One can reasonably expect bed roughness to be present, too; the third requirement is satisfied. Concern centers on the second requirement: That there is enough time (or distance) for the boundary layer to develop. Indeed, the flow in the example wave reverses every 10 seconds. There is no hope that a well-developed boundary layer can be built up. Instead, a boundary layer of very limited thickness develops in the immediate vicinity of the sea bed; the flow above this layer remains 'ignorant' of the fact that the bottom (with its roughness) is present. This neglects the diffusion of turbulence originating at the sea bed.

Analogous to the treatment of the lowest part of logarithmic velocity profile, it is convenient to assume that this wave boundary layer also will have a linear velocity profile. Continuing the analogy, this means as well that the linear velocity gradient can be characterized by a velocity at some chosen, known elevation above the sea bed; it is convenient to choose the elevation z_t for this, too. (One assumes that the boundary layer under the waves will be at least this thick; this is safe in practice.) Since the boundary layer retards the flow, it is logical that the characteristic velocity for this shear stress determination will be less than that predicted from wave theory. One generally assumes that:

$$u_t = p \cdot u_b \tag{14.6}$$

in which:

$\quad u_b \quad = \quad$ sea bed water velocity predicted by wave potential theory (m/s)
$\quad u_t \quad = \quad$ characteristic water velocity for shear stress computations (m/s)
$\quad p \quad = \quad$ dimensionless constant with a value between zero and one (-)

The above relationship is true for all times during the wave period, but it is most often used with velocity amplitudes.

14.2.3 Shear Stress Under Waves Alone

The characteristic velocity for waves, u_t, can be used in place of V_t in a shear stress relation just as was done for constant currents. One should now, however, be aware that since u_t is a periodic function with zero mean (at least to a first order approximation), the resultant shear stress - when averaged over at least a wave period - will now be zero; there is no time-averaged resultant shear stress, even though it has non-zero instantaneous values. The importance of this will become obvious later.

14.2.4   Shear Stress Under Waves Plus Currents

To combine the influences of waves and current a way must be found to combine the influences of the two boundary layers considered separately above. This is done via a careful superposition. Note that at an offshore location, the wave can propagate in any direction, μ, relative to the (tidal) current. (This is in contrast to the Coastal Engineering situation where the waves are usually nearly perpendicular to ($\mu \approx 90°$) the current direction.) Because the sea bed portions of each of the velocity profiles - one caused by the current and one caused by the waves - are linear, the resulting profile can be expected to be linear in the near-bed zone as well. Since the current boundary layer was characterized by a velocity V_t acting at the elevation of the tangency point, it can be convenient to choose this same elevation for the wave boundary layer as well. Figure 14.3 shows a plan view (one is looking down from above) of the velocity vectors at elevation z_t above the bed.
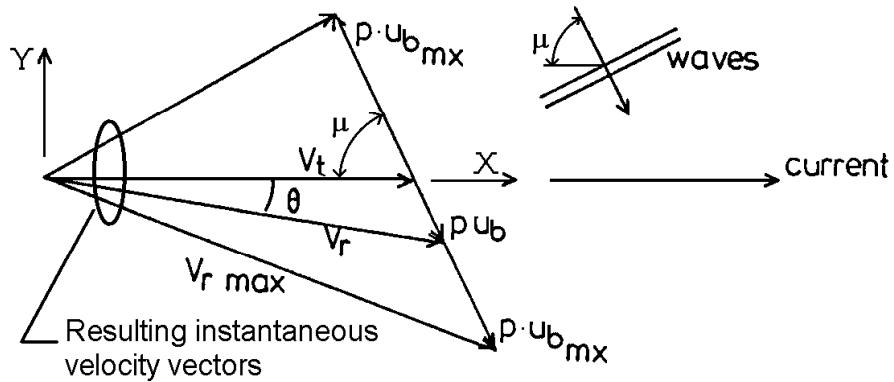
Figure 14.3: Plan View of Flow Components Just Above the Sea Bed

In this figure, V_t has been normalized to 1 m/s. The wave velocity vector has an amplitude of 0.5 m/s and makes an angle, μ, of a bit over 60° with the X-axis which coincides with the constant current velocity vector. The currents are added as vectors in this figure. The resultant velocity vector sweeps back and forth a bit in direction from one side of the axis to the other. Its magnitude changes continually, too, from a maximum of 1.30 m/s to a minimum of 0.90 m/s in this case.

The instantaneous shear stress will be proportional to the square of the instantaneous velocity and its direction will correspond to that of the instantaneous velocity. (See figure 14.4.)

This shear stress can be worked out a bit as follows.

The X and Y components of the wave current velocity will be of the form:

$$
\begin{aligned}
u_X(t) &= u_a \sin(\omega t) \cdot \cos \mu \\
u_Y(t) &= u_a \sin(\omega t) \cdot \sin \mu
\end{aligned}
\tag{14.7}
$$

The constant current velocity, V_t (acting along the X-axis) will be added to $u_X(t)$.

The resulting bed shear stress magnitude at any instant is proportional to the square of this resultant velocity so that:
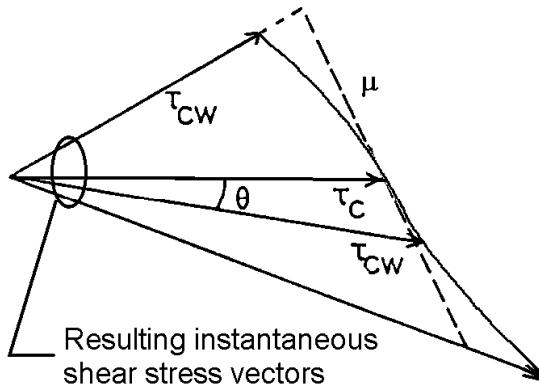
Figure 14.4: Instantaneous Shear Stresses Under Waves Plus Currents

$$
\begin{aligned}
|V_r^2| &= (V_t + u_X(t))^2 + (u_Y(t))^2 \\
&= \left(V_t^2 + 2\,V_t \cdot u_a \sin(\omega t) \cdot \cos\mu + u_a^2 \sin^2(\omega t) \cdot \cos^2\mu\right) \quad (14.8) \\
&\quad + u_a^2 \sin^2(\omega t) \cdot \sin^2\mu \quad\quad\quad\quad\quad\quad\quad\quad\quad\quad\quad\quad (14.9)
\end{aligned}
$$

The instantaneous magnitude of the resulting shear stress, τ, is directly proportional to this.

Time Averaged Shear Stress Magnitude

The magnitude of τ can be averaged over a wave period as well so that:

$$
\tau_{cw} = \overline{|\tau|} \quad \alpha \quad V_t^2 + 0 + \frac{1}{2}\,u_a^2 \cdot \cos^2\mu + \frac{1}{2}\,u_a^2 \cdot \sin^2\mu \quad (14.10)
$$

Noting that: $\cos^2\mu + \sin^2\mu = 1$, one comes to the final conclusion that:

$$
\tau_{cw} = \overline{|\tau|} \quad \alpha \quad V_t^2 + \frac{1}{2}\,u_a^2 \quad (14.11)
$$

which happens to be completely independent of μ ! In these equations (with all velocities at height $z = z_t$):

$$
\begin{aligned}
\tau_{cw} &= \text{time averaged bed shear stress (N/m}^2) \\
V_t &= \text{current velocity (m/s)} \\
u_a &= \text{amplitude of the wave motion (includes the factor, } p) \text{ (m/s)} \\
\mu &= \text{angle between the wave propagation and current directions (rad)}
\end{aligned}
$$

This average magnitude of the bed shear stress (independent of its direction) will be found later to be important for the determination of sediment transport. Equation 14.11 makes very clear that both the current and the waves contribute to the bed shear stress; waves, if present, generally increase the average bed shear stress - in spite of the fact that the average shear stress under the waves alone is identically zero as indicated earlier in this chapter.

Time Averaged Shear Stress Components

Applying Newton's third law again, the current reacts to the time averages of the X and Y components of instantaneous shear stress. The corresponding flow velocity components responsible for each shear stress component are proportional to:

$$|V_{rX}^2(t)| \;=\; (V_t + u_X(t))^2 \tag{14.12}$$

$$|V_{rY}^2(t)| \;=\; u_a^2 \sin^2(\omega t) \cdot \sin^2 \mu \tag{14.13}$$

in which the subscript r denotes resultant.

It has been assumed in equation 14.12 that $V_t > u_X$ to guarantee that V_{rX}^2 is never negative. With this knowledge, then the time averaged shear stress in the X direction becomes:

$$\overline{\tau_x} \; \alpha \; \left(V_t^2 + 0 + \frac{1}{2} u_a^2 \; \cos^2 \mu \right) \tag{14.14}$$

This indicates that the average bed shear stress in the direction of the current is increased unless $\mu = \pi/2$.

The average shear stress in the Y direction is even more interesting. It is proportional to the time average of $V_{rY}\,|V_{rY}|$ since τ is always in the direction of the current. The result is, then:

$$\overline{\tau_y} = \frac{1}{2} \; u_a^2 \sin^2 \mu \tag{14.15}$$

which is zero only when $\mu = \pi/2$. This means that if $\mu \neq \pi/2$, $\overline{\tau_y} \neq 0$, and the resultant bed shear stress is not co-linear with the constant current. This implies in turn that there will be a resultant force acting on the water flow which is perpendicular to the original constant current direction. This force tends to divert the current so that μ does approach $\pi/2$; the current tries to turn to become parallel with the wave crests.

On the one hand, this shift in the current direction can actually take place more easily offshore than it can near the coast where other boundary conditions such as the impermeability of the beach itself also contribute to the current's behavior. On the other hand, these boundary conditions have a much smaller influence on the currents offshore; these currents tend to be stronger in deeper water and the wave influence near the bed is less than it would be in shallower water, too.

This concludes our discussion of how the sea bed influences the flow - at least for now. Results from above will be utilized in later steps, however. For now, the next step is to look at the bed shear stress in the opposite sense - to examine how the bed shear stress affects the sea bed itself.

14.3　Bed Material Stability

This section discusses the forces on and stability of cohesionless grains of bed material.

14.3.1 Force Balance

The limit of stability of (cohesionless) bed material grains can be studied via a detailed examination by an equilibrium of horizontal forces: A tiny wake - with low pressure - forms just downstream of a soil grain on the bed surface; this yields a miniature drag force, F_D, as indicated in figure 14.5.
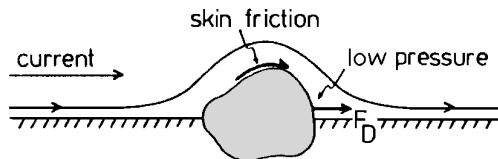
Figure 14.5: Sea Bed Grain with Drag Force

This is resisted by a horizontal inter-granular friction force which is dependent in turn on the vertical intergranular normal force. This latter force depends upon the net submerged weight (weight minus buoyant force) of the grain and the vertical resultant of the hydrodynamic pressure force distribution around that grain; see figure 14.6. (The working of this latter under-pressure or lift has been described in chapters 3 and 4. It will come up as well when pipelines are discussed in a later section of this chapter.)
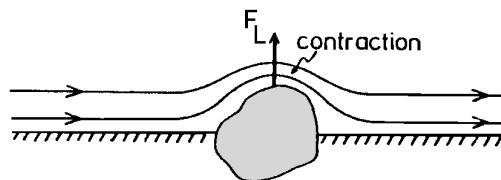
Figure 14.6: Sea Bed Grain with Lift Force

The total force 'picture' is shown in figure 14.7.
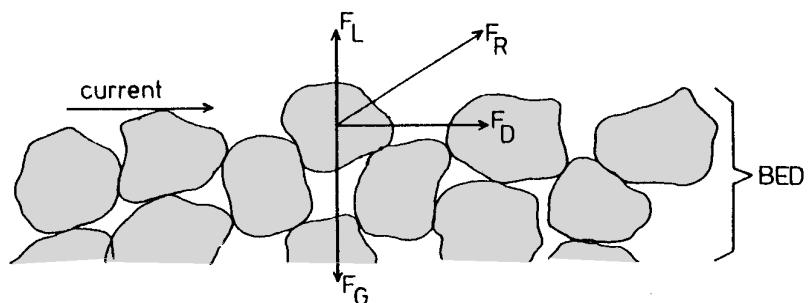
Figure 14.7: Schematic of Forces on A Sea Bed Surface Grain

One can see from figure 14.7 that a complete force balance - including the quite irregular intergranular forces - would be cumbersome to carry out at best. An alternative more global approach is therefore used instead.

14.3.2   Shields Shear Stress Approach

This alternative approach simply relates the time-average bed shear stress, $\bar{\tau}$ or τ_{cw}, to a stability parameter for the soil grains. This was first done by [Shields, 1936] for rivers. He (as well as most others!) assumed that the river bed was so nearly horizontal that its slope had no effect on the stability of the bed grains.
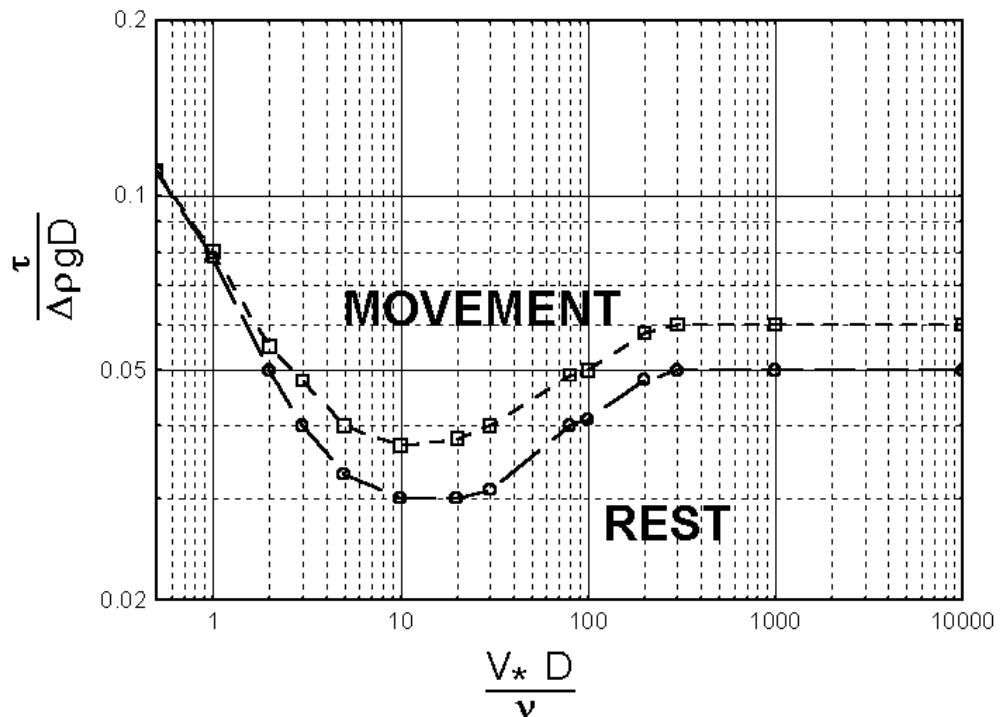
Figure 14.8: Shields Grain Stability Curve

Figure 14.8 shows the Shields relationship. The dimensionless bed shear stress,

$$\frac{\tau}{\Delta\rho \cdot g \cdot D} \tag{14.16}$$

is plotted along the logarithmic vertical axis; a grain Reynolds number,

$$\frac{V_* \cdot D}{\nu} \tag{14.17}$$

is plotted horizontally - again with a logarithmic scale.

In this figure and these formulas:

$$
\begin{array}{rcl}
g & = & \text{acceleration of gravity (m/s}^2) \\
\tau & = & \text{bed shear stress (N/m}^2) \\
\Delta\rho & = & \rho_s - \rho_w \text{ is density difference (kg/m}^3) \\
\rho_s & = & \text{mass density of bed grains (kg/m}^3) \\
\rho_w & = & \text{mass density of (sea) water (kg/m}^3) \\
D & = & \text{diameter of the bed grains (m)} \\
V_* & = & V\sqrt{g}/C \text{ is the so-called shear velocity (m/s)} \\
C & = & \text{Chézy coefficient (m}^{1/2}/\text{s)} \\
V & = & \text{depth-averaged flow velocity (m/s)} \\
\nu & = & \text{kinematic viscosity of (sea) water (m}^2/\text{s)}
\end{array}
$$

The zone between the two curves in figure 14.8 is the area of uncertainty between stability below the band, and movement above. The fact that this boundary is a bit unclear, stems from the fact that bed particles can interlock, etc., to some extent.

14.3.3   Link to Sediment Transport

One should be careful to note that bed material instability in a Shields sense is not sufficient for material actually to be transported; instability simply indicates that the particle 'cannot sit still'. Two criteria must be met simultaneously for there to be net bed material transport:

- Particles must be loosened from the sea bed; this is indicated by the Shields criterion, and
- There must be a resultant current to provide a net transport of those particles.

Since a wave, alone, provides no net current or mass transport, it fails to satisfy this latter criterion; it can only cause particles to 'cha-cha' back and forth. On the other hand, if the waves are intense enough to 'stir up' the sea bed material, then only a very small resultant current superposed on the waves can cause a very significant bed material transport. Note that this is true even when the current - if acting alone without the waves - would be too weak to cause sea bed particle instability and thus transport.

14.4   Sediment Transport Process

Now that the stability of bed material grains has been discussed, attention switches to the mechanisms by which such material is transported.

14.4.1   Time and Distance Scales

The work to be described here was first carried out for rivers. It was generally assumed that the flow conditions were not changing rapidly; a quasi-static or steady state solution was found. This means then, that accelerations could be neglected and that conditions remained essentially constant along a streamline. [Rijn, 1990] indicates that steady state conditions - in terms of sediment transport - are restored within about 80 to 100 water depths downstream from a major disturbance - such as a dam - in a river. With a typical river depth of 5 meters, this means that conditions become stable after about half a kilometer. In other words, there is still a lot of river left (usually) in which a sediment transport predicted by a steady state solution can be utilized.

For offshore conditions - in water ten times as deep, for example - this distance to regain sediment transport equilibrium becomes 5 km - a distance which far exceeds the dimensions of most offshore structures! This means that a completely stable sediment transport condition will never be achieved near an offshore structure as a result of its (local!) disturbance. Offshore engineers are continually confronted by the transient situation; this is in contrast to the situation for coastal or river engineers. Even so, it is convenient for the explanation to start with the stable or steady state situation - at least for now; the transient will be picked up in a later section.

14.4.2   Mechanisms

How is bed material transported in a river? In principle there are three ways in which it can be moved:
  - solution,
  - suspension and
  - moving along the bed - sometimes called saltation.
Most minerals which make up the earth dissolve slowly in water and come out of solution slowly, too. Transport via **solution** is of a molecular nature throughout the water; it is not at all important for cases being considered here.

Particles in **suspension** tend to be relatively fine; they move along with the water which surrounds them. This transport can take place at any elevation in the flow. It is suspended transport which often makes water look turbid or 'hard to see through'.

Saltation, or **bed load transport** 'never really gets off the ground' - to put it popularly; it rolls and bounces along the bed with a speed which is less than that of the adjacent flow in the sea bed boundary layer.

These latter two transports are discussed a bit more below.

Suspended Transport

It will later become obvious that suspended transport is only occasionally important for offshore engineering applications. The following discussion is given for completeness and to provide a basis of understanding for some other phenomena.

What mechanism keeps bed materials in suspension? Suspended sediment particles fall back toward the sea bed with their fall velocity. (This was discussed in chapter 4.) Material is moved back upward as a result of turbulent diffusion and the fact that the water exchanged upward has a higher sediment concentration than the water swapped downward at the same time. This is illustrated in figure 14.9.

Further, there is usually a free exchange of material between the flow and the sea bed. Generally, no suspended material is lost at the sea surface. This can all be put together to yield a classical ordinary differential equation for an equilibrium situation:

$$V_f \; c(z) + \epsilon(z) \; \frac{dc(z)}{dz} = 0 \tag{14.18}$$

in which:

$$
\begin{array}{rcl}
V_f & = & \text{particle fall velocity in water (m/s)} \\
c(z) & = & \text{sediment concentration at elevation } z \\
\epsilon(z) & = & \text{turbulent eddy viscosity at elevation } z
\end{array}
$$

$$V_f \cdot c(z) \qquad \varepsilon(z) \frac{dc(z)}{dz}$$
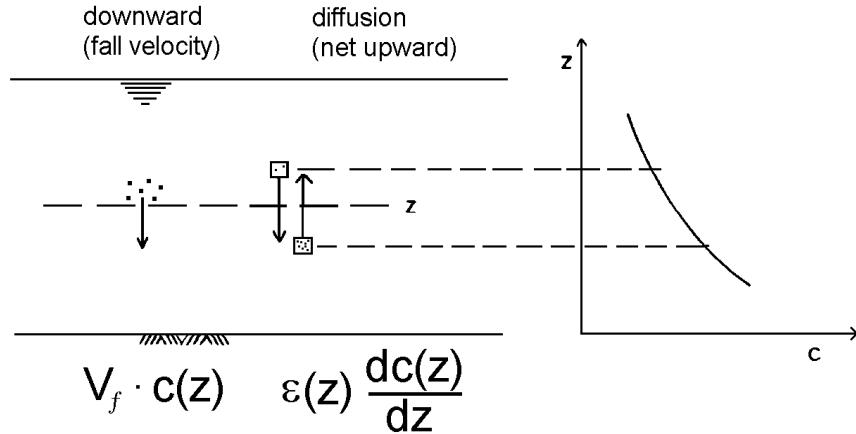
Figure 14.9: Vertical Suspended Sediment Transport Balance

ϵ is a measure of the scale of turbulence in the flow. By assuming a distribution for $\epsilon_s(z)$, one can work out the solution to equation 14.18. After a bit of mathematical manipulation (which is not really important for our insight here) the coastal engineers get a solution which looks like:

$$c(z) = c_a \cdot \left(\frac{-z}{z+h} \cdot \frac{a}{h-a} \right)^{z^*} \tag{14.19}$$

in which:

$$
\begin{array}{rcl}
c(z) & = & \text{sediment concentration at elevation } z \\
c_a & = & \text{sediment concentration at a chosen elevation } a > 0 \text{ above the bed} \\
h & = & \text{water depth (m)} \\
z & = & \text{vertical coordinate, + upward from the water surface (m)} \\
z^* & = & \text{dimensionless parameter (-), dependent upon } \tau, \rho \text{ and } V_f \\
& & \text{(The exact background of z}^* \text{ is not important here)} \\
V_f & = & \text{the particle fall velocity (m/s)}
\end{array}
$$

The sediment concentration at some chosen elevation, a, must be known in order to determine the quantitative solution of equation 14.19. One will discover below that this comes from the bed transport to be discussed in the next section.

Once $c(z)$ is known, the total rate of suspended material transport follows directly from the following integral:

$$S_s = \int_{bed}^{sea\ surface} U(z,t) \cdot c(z) \cdot dz \tag{14.20}$$

in which:

$$
\begin{array}{rcl}
S_s & = & \text{suspended sediment transport (m}^3\text{/s per meter width)} \\
U(z,t) & = & \text{velocity (from any cause) at elevation } z \text{ and time } t \text{ (m/s)}
\end{array}
$$

This is usually simplified a bit if waves are involved; one is not interested in a truly instantaneous sediment transport. Its time average (over a wave period) is much more relevant. This allows $U(z,t)$ to be replaced in 14.20 by its time averaged value, $\bar{U}(z)$.

Bed Load Transport

Bed load transport 'never gets off the ground'; it stays near the bed in a thin layer below
the suspended sediment transport. The same forces which determine particle stability also
govern bed load transport. In contrast to the situation with suspended transport, the bed
load moves more slowly than the water near the bed; most formulas for predicting the rate
of bed load transport, S_b, express this rate directly instead of via a concentration times
a velocity as was done with suspended transport. Indeed, the water velocity is changing
rapidly as a function of elevation here and the sediment concentration is hard to define in
this region, too.

On the other hand, a sediment concentration - at some elevation - is needed in order to
determine the actual suspended sediment concentration profile as explained above. It is
convenient to perform this coupling near the sea bed - more specifically at an elevation
h_t above the bed - the height at which the linear near-bed velocity profile is tangent to
the logarithmic Prandtl-Von Kármán profile. It is being assumed (quite arbitrarily) that
transport above this level takes place in suspension and that only bed load transport is
found below.

Hydraulic engineers have taken the very pragmatic step of converting the bed load transport
into a (form of) concentration by assuming that S_b takes place in a layer of thickness h_t
and with a velocity equal to V_t. This equivalent 'concentration' is then:

$$c_a = \frac{S_b}{h_t \cdot V_t} \tag{14.21}$$

Using this link, one can relate the entire steady state sediment transport, $S = S_b + S_s$,
to one quantity: The bed transport, S_b. Attention can be concentrated on determining
this value. Before doing so, however, the relative importance of S_b and S_s for offshore
applications will be examined in this next section.

14.4.3   Relative Importance of Bed versus Suspended Load

Many comparisons can be included under this heading. River engineers are often interested
in the ratio of suspended load transport to bed load transport, S_s/S_b. This value can vary
widely in rivers, by the way; it can be high (thousands) for a muddy river such as the
Amazon or Mississippi, and very low ($\ll 1$) for a sparkling clear mountain stream tumbling
over rocks.

In offshore engineering on the other hand, one is wise to first consider the relative time
(or distance) scales within which S_b or S_s change. Consider what happens to each of these
quantities when - for example - the near-bed flow is locally disturbed by a partially exposed
submarine pipeline, for example. Such a pipeline will typically be no more than a meter in
diameter and it may protrude 50 centimeters or so above the sea bed. At the same time,
the water depth can easily be in the order of 100 meters.

Using potential theory from chapter 3 to estimate the order of magnitude of the disturbance
caused by the half-buried pipe, one finds that at a distance of at little as 1 meter above
the sea bed (above the pipe) the velocity has only been increased by 25%. At 2 meters
height this increase is only a bit more than 6%. The conclusion must be that the pipe only
disturbs the velocity field in its immediate vicinity. Consequently, the velocity gradients
and thus the local bed shear stresses and vertical diffusion of sediment will be disturbed
only locally as well.

One can expect the bed transport, S_b, to react quickly to these changes. Indeed, each bed transport particle can stop any time it hits the bottom and this happens almost continuously. The bed transport can adjust or adapt itself several times within a distance of a few meters.

The material making up the suspended transport, S_s, on the other hand, does not frequently come in contact with the bottom; it gets little opportunity to stop. Except that flow in the immediate vicinity of the pipe - especially in its wake - may be a bit more turbulent, the rest of the (tidal current) flow does not even 'notice' that the pipe is there; the major part of the flow as well as the suspended transport it carries is essentially undisturbed by such small scale changes.

Some may argue that whenever S_b changes, S_s will change as well. Their reasoning follows from the link established above between suspended and bed load transports. What they fail to realize is that this theoretical 'link' was established for an equilibrium situation and that a change in S_s must take place via changes in its sediment concentration profile. The driving forces for determining that profile - the turbulent diffusion and the particle fall velocity - are not (or only very locally) changed. It is indeed because of S_s that [Rijn, 1990] concluded that a distance of 80 to 100 water depths is needed for an equilibrium sediment transport to be reached in a river.

The conclusion to all this is that bed load transport reacts very quickly to flow changes which occur on a scale typical of offshore engineering objects, but that suspended transport does not. Offshore engineers seldom have to worry about the transport of suspended material. S_b is almost always the most important transport component in an offshore situation. Conversely, S_s is seldom important in an offshore situation!

14.5 Sea Bed Changes

14.5.1 Sediment Transport Not Sufficient for Bed Changes

Having bed material instability (in the Shields sense) and having a resulting current to transport that material is not usually sufficient to cause a real morphological problem (erosion or deposition). The presence of sediment transport past a point only indicates that the bed material grains now present at that location will (probably) be replaced by others within a very short time; a dynamic equilibrium can exist.

In order to have (or reveal) morphological changes as a result of sediment transport, one must examine dS/dX, the change in sediment transport along a (resulting) streamline. If S increases as the flow proceeds from point A to point B, as shown in schematic cross section in figure 14.10, then the extra material transported past point B (if dS/dX is positive) can only have come from the bed segment between A and B; a positive value of dS/dX leads to erosion. Conversely, a negative value must lead to sedimentation or deposition of material in the segment between A and B.

How does a time dependence affect the situation? When the current changes slowly as a function of time - such as with a tidal current - this makes no difference. This variation only introduces a dS/dt which is pretty much the same in the entire vicinity; this does not - of itself - yield either a significant erosion or deposition.
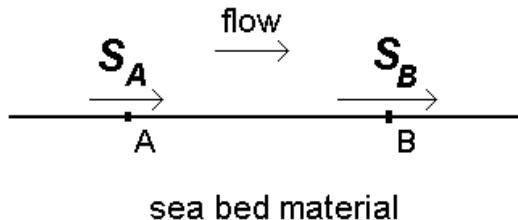
Figure 14.10: Longitudinal Bed Section Along Flow Line

14.5.2   Bed Change Time Scale

Coastal engineers work on a large scale. They are typically concerned with a beach which can be hundreds of meters wide and many kilometers long. Hundreds or even thousands of cubic meters of bed material must be removed or deposited in order to make a significant impact. This can take so long that the beach never really 'comes to rest'; it keeps on changing continuously. Because of this, coastal engineers invest a major portion of their efforts in determining the speed with which (coastal) conditions change. They need to predict how much a given coastline will change in - for example - the coming decade as a result of natural accretion and erosion resulting from waves and currents along the coast.

Typical objects for which sea bed morphology is important to offshore engineers include a pipeline, the base of a jack-up platform leg or even an entire steel tower structure. Smaller objects can include equipment lost overboard, an anchor or a communications cable. Offshore engineering morphological phenomena take place within a distance of no more than some tens of meters. As a consequence of this, only a relatively very small amount - very often less than a hundred cubic meters - of bed material needs to be removed (or deposited) in order to reach a new equilibrium. One can intuitively feel (correctly) that this can occur much faster. Indeed, morphological changes significant for offshore engineering often occur during a single tide period - usually when there is a storm going on. This enhances the wave action and thus the magnitude of the bed shear stress. This in turn stirs additional bed material loose from the sea bottom so that the resulting current - locally influenced by the pipeline or other object present - can transport it.

14.6   Laboratory Modeling

Before discussing applications, our attention will be temporarily diverted to the topic of physical modeling of local morphological changes.

14.6.1   Theoretical Background and Scaling

Imagine the physical problem of modeling the morphology of a the area around a pipeline in say 100 meters of water. Since waves are involved, one uses Froude scaling; see chapter 4 or appendix B. If the wave and current flume has a maximum depth of 1 meter, one would be forced to use a geometric scale of 1 : 100. At this scale, a cylinder with a diameter comparable to that of a pencil would be a reasonable pipeline model. This is too small; The Reynolds number, etc. become too distorted.

A more inspired physical model is possible, however. Since offshore morphological problems are dominated by bed load transport, there is no real need to model the suspended transport correctly - or even at all for that matter. Since the bed load moves along in a thin layer near the bed, why, then, is it necessary to model the entire ocean depth? Indeed, this is no longer necessary at all!

With this knowledge, one can modify the laboratory model so that only some meters (in height) of the near-bed flow is reproduced as is shown in figure 14.11.
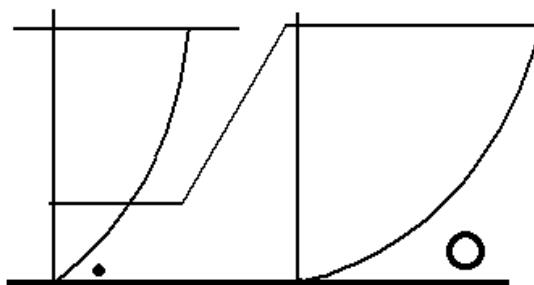
Figure 14.11: Schematic Longitudinal Section of Field and Model Conditions

The height chosen must be such that the pipeline - which is now larger, too - does not significantly 'block' the entire flow; this would introduce extra influences not found in nature. A good rule of thumb is that the object being studied should not block more than 1/10 (or 1/6 at the very worst!) of the flow cross section. With this, an exposed model pipeline about 80 mm in diameter would require a water depth of about 800 mm, leaving a freeboard in the flume of 200 mm for waves or any other disturbances.

It should be realized as well, that this model no longer represents the entire flow depth; it only includes the lower meters of the prototype situation. What is the consequence of this? What current velocity should now be used in the (new) model? It is no longer correct just to scale the depth-averaged velocity from the prototype for use in the model. Instead, the depth average of the current in the (lower) portion of the velocity profile - the part actually being modeled - should be reproduced (to an appropriate scale, of course); this has already been suggested in figure 14.11.

What about waves, then, one can ask? The surface waves from the field will be much too near the sea bed in the 'cut down' model! Here again, it is the velocities near the bed caused by the waves that must be reproduced to scale.

Since it will be generally necessary to reproduce the spatial effects - in the horizontal direction - it will be necessary to scale the wave length according to the geometric scale; this - with the water depth - sets the wave period relationship in accordance with Froude scaling. One obtains the proper bed velocity amplitude by adjusting the wave height; this compensates for the fact that the water depth is not scaled in the same way as the rest of the model.

One would probably not choose the actual current velocity to be used until this step was completed by the way - in spite of the discussion above! One (alternate?) approach is to scale the current velocity using the same ratio as was found for the wave motion velocities.

The key to successful physical modeling of sea bed sediment transport is to properly scale the bed shear stresses in relation to the stability (in the Shields sense) of the bed material. This fact may require that both water motion components be adjusted to achieve the

proper match of the sea bed flow conditions to the stability of the bed material used in the model. Indeed - to complicate matters even more - one may be using a different bed material in the model than one finds in the field.

14.6.2 A Modeling Experience

This relates to a modeling situation actually encountered by a thesis student in the mid nineties. He was conducting lab experiments to check the stability of stone berms occasionally used to cover otherwise exposed subsea pipelines. The tests were being carried out in a wave and current flume with wave propagation in the same direction as the current. On the fateful day, a berm of loose stone had been built across the bottom of the flume; it had a slope of 1 : 5 on both the upstream and downstream sides; the crest height was such that the water depth on top of the berm was about 90% of that in the rest of the flume. This was in accordance with all the criteria stated above. Figure 14.12 shows a (distorted) cross-section of the berm and thus also a longitudinal profile of part of the flume. The water surface is well above the top of the figure and only the surface layer of berm gravel is represented in the sketch.
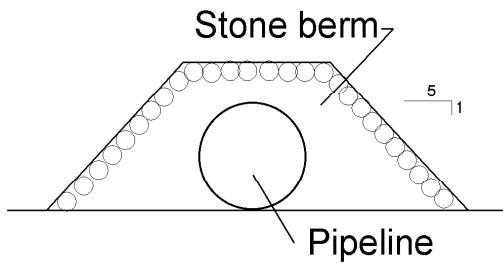
Figure 14.12: Longitudinal Section of Berm Model

As a check, the first tests of the day were carried out with just a current. After the current had been increased in a few steps, the bed shear stress on the crest of the berm became high enough to cause instability of the stones; quite a rapid erosion started - with the stones being deposited downstream at the toe of the berm.

Remembering from the theory that waves, if present, increase the bed shear stress and thus the sediment transport rate, the student hastened to start the wave generator in order to be able to observe a really spectacular erosion process. Can you imagine his dismay when - after the waves had been added - the stones in the berm remained stable! What was wrong with the experiment? Is the theory wrong?

After recovering from the initial shock, he investigated the matter systematically as follows: The distorted berm profile was fixed in place (by sprinkling fine cement into its pores and letting it set) and a series of local velocity profiles were measured at various locations around the berm using a laser anemometer. Since bed load sediment transport is governed by the bed shear stress, the laser beams were set close to the berm surface to make measurements in the boundary layer in order to determine the velocity gradients and thus infer the bed shear stresses from the local flow parameters.

Just as in the seemingly ill-fated experiments, tests were carried out both with a current alone and with waves superposed on the current. To everyone's surprise, the velocity profile

measurements revealed that the velocity gradients (and thus the shear stress on the stones) above the berm crest were greatest when just the current was present!

Apparently, when the waves were added to the current, they interacted with that current and with the berm, and possibly other parts of the flume itself, in such a way that the gradients in the velocity profiles above the berm crest were reduced instead of enhanced by the waves. This confirmed that the experiments still agreed with the basic theory; the experiment was just a bit different that had been expected!

The morals of this whole experience are that the bed shear stress is important for determining bed load sediment transport and that such experiments must be carried out very carefully. Persons trying to predict stability or erosion or deposition of bed material can best do this by evaluating - only in a qualitative way if necessary - the local bed shear stress and the changes which it undergoes as the flow progresses along the streamline.

14.7 Vertical Pile in Current

The first application involves a somewhat isolated vertical pile which penetrates well into the sea bed and protrudes above the bed to a height of at least several diameters. The discussion which follows includes both the hydrodynamics and the resulting morphology - both now in three dimensions.

14.7.1 Two Dimensional Approach

Remembering the 2-dimensional hydrodynamics (in a plan view, now) of the flow around a circular cylinder, one knows that there is a stagnation point at the most upstream side of the cylinder and a wake behind the cylinder. Also, theoretically at least, the velocity on each side immediately adjacent to the cylinder is twice that of the undisturbed ambient flow.

Since there is no velocity at a stagnation point, one would expect little to happen to the bed on the most upstream or 'leading' part of the pile; at the sides where the velocity is locally doubled, one might very reasonably expect an increased shear stress, too, yielding a positive dS/dX and thus a local erosion. The extra turbulence caused by the wake could enhance erosion on the lee side of the cylinder, too. This would leave the cylinder standing in a 'pit' (except on the upstream side).

One of the world's greatest tragedies is the murder of a beautiful theory by a brutal set of facts: One observes - in nature or even in a lab experiment - that there is a significant erosion hole on the entire upstream side of the cylinder. This extends along the sides (where it is already expected) and 'fades out' in the wake area. Apparently, the two-dimensional approach is insufficient to explain what happens.

14.7.2 Three Dimensional Flow

The three-dimensional flow pattern includes the velocity profile (in the vertical) caused by bed friction in the ambient current. Figure 14.13 shows a longitudinal vertical section with the approaching velocity profile shown on the left. The current shown here is quasi-constant such as a tidal current. Waves are not needed for this explanation; they just complicate the discussion in this case.

Consider now horizontal cross sections at two different elevations, A and B, in that figure. Because of its higher location, the approaching current at elevation A will be faster than at location B.

$$V(A) > V(B) \tag{14.22}$$
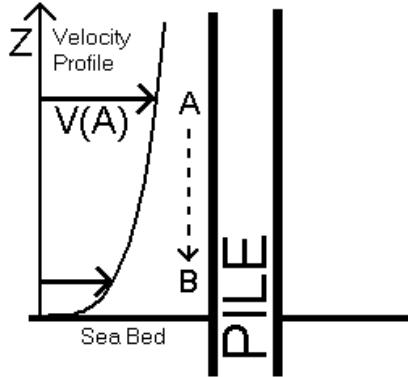
Figure 14.13: Pile with Approaching Velocity Profile

This implies, in turn, that the stagnation pressure at A, $\frac{1}{2} \rho V^2(A)$, will be greater than the stagnation pressure farther down along the pile at point B. Along the vertical line of stagnation points on the upstream side of the pile one will find a dynamic pressure gradient which is steeper than the hydrostatic gradient, ρg; there will be a residual quasi-static downward pressure gradient along the upstream side of the pile! This pressure gradient will result in a downward flow along these stagnation points as indicated by the dashed arrow in figure 14.13. What happens to this flow when it hits the sea bed?

Horseshoe Vortex

After colliding with the bed, the flow turns upstream, along the bed against the approaching flow (where the approaching velocity is lowest) as shown very schematically in figure 14.14. This flow can turn upstream here along the bed because the kinetic energy of the
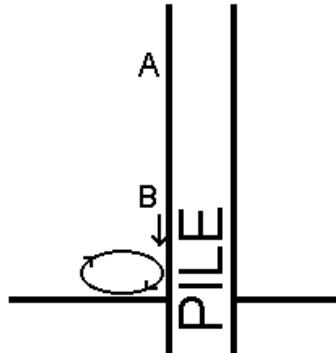
Figure 14.14: Schematic Detail of Horseshoe Vortex just Upstream from the Pile

approaching flow is low here, anyway. After progressing a short distance - think in terms

of a pile diameter - it bends up and is swept back to the cylinder to form a vortex. This vortex grows in length on each side; its ends (or tails) get swept around the cylinder by the flow so that this vortex takes on a U-shape resembling a horseshoe when viewed from above.

A common feature of vortices is that they are local and have higher flow speeds than one would otherwise expect in the vicinity. A vortex has a relatively thin boundary layer adjacent to an object or the sea bed so that relatively high velocity gradients and turbulence (in their radial direction) result. Given this - and remembering that shear stresses are dependent upon velocity gradients - it is not surprising at all that an erosion pit develops on the entire front and sides of the pile.

What prevents this erosion from going on 'forever' and making a pit of unlimited depth? After all, the horseshoe vortex is not time limited. As the erosion pit gets deeper, the slopes at its sides become steeper. This upward slope - as seen in the direction of local flow - makes it more difficult for bed material to be transported. (Remember that slopes have been neglected in sediment transport discussions.) In practice with a nice sandy bed, one can expect this erosion pit to develop to an ultimate depth of in the order of 1.5 pile diameters. All of these phenomena are illustrated in figure 14.15.
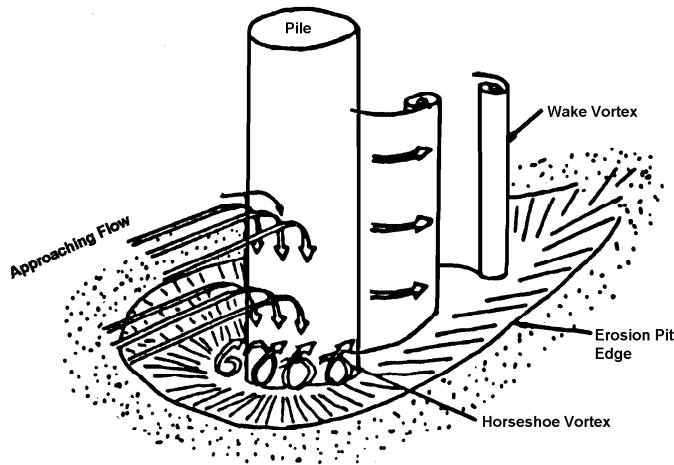
Figure 14.15: Final Overall Bed Situation Near Pile

What happens to the material eroded from the pit, and what happens on the downstream side of the pile? Here the vortices in the pile wake cause increased turbulence. Also, the story about stagnation pressures can be repeated here, but it now works in the opposite sense. A small secondary flow of water coming from the sea bed - and even from the horseshoe vortex - will be drawn upward into the wake. Is it surprising that this flow also carries sediment in suspension? Its (temporarily) increased turbulence makes this possible. However, once the flow is swept downstream past the pile, no new turbulence is added and the vortices in the wake gradually die out. The sediment that had been picked up in the immediate vicinity of the pile now falls out on a relatively extensive area downstream.

Flow Reversal

What happens when the tidal current reverses direction and - to make this discussion clearer - flows from north to south instead of from south to north? It has just been explained that the 'original' erosion pit generated by the south to north current was formed on the east, south and west sides of the pile. Now, after the current reverses, the pit will form on the east, north and west sides. The existing pit on the south side which is now in the wake will most likely fill up a bit with very loose material.

Final Erosion Pit

As a consequence of tidal action, therefore, one can expect - for design purposes - an erosion pit to be formed completely around any slender vertical pile. The depth and width of this pit will be in the order of 1.5 pile diameters. This, in turn, means that the lateral support of the pile begins only 1.5 pile diameters below the sea bed; this can have consequences for the design of the foundation (in a geotechnical sense) as well as the pile (in a structural engineering sense).

Using the above rule of thumb for a pile 2 meters in diameter as an example, one finds that roughly 50 m^3 of bed material will be removed to form the stable state erosion pit. In onshore terms, this is not even two truckloads of earth - relatively little, indeed. One can indeed expect this erosion pit to form quite rapidly - usually within a single tide period.

14.7.3 Drag Force Changes

Even though hydrodynamic forces on a pile are not of primary interest in this chapter, it is convenient to discuss drag forces on the cylinder here, too - at least to the extent that they are influenced by the velocity gradient caused by bed friction.

One will already know that the drag force acting on a vertical cylinder in a constant current of velocity, V, will be given by:

$$F_D(z) = \frac{1}{2} \rho C_D D V^2(z) \tag{14.23}$$

in which:

$$
\begin{array}{lll}
F_D(z) & = & \text{drag force per unit length at elevation } z \quad \text{(N/m)} \\
\rho & = & \text{mass density of the fluid (kg/m}^3) \\
V(z) & = & \text{approaching velocity at elevation } z \quad \text{(m/s)} \\
D & = & \text{pile diameter (m)} \\
C_D & = & \text{cylinder drag coefficient (m)}
\end{array}
$$

Does $F_D(z)$ change because the velocity profile is present or because of other factors not accounted for by the strictly two-dimensional flow pattern assumed in the earlier discussion of forces in chapter 4? There are two additional effects discussed so far: One at the sea bed and one at the water surface.

Secondary Flow Effect at Sea Bed

The secondary downward flow on the upstream side of the pile leads to the horseshoe vortex formation at the bed, but it also supplies an extra volume of water which flows around

the cylinder at the bed elevation. Looked at in another way, the flow past the cylinder near the bed is actually greater than one would expect to find based upon the undisturbed approach velocity at that level.

Since the (measured) force is generally related to a velocity which in fact is smaller than one would associate with that actually present, one will find a slightly larger value for the drag coefficient, C_D. A plot of C_D versus depth will increase a few percent near the sea bed.

Water Surface Effect

The pile will cause what looks like a standing wave at the water surface. It is in fact a travelling wave which propagates upstream at a speed identical to that of the flow at that level. In this way, the wave stays synchronized with the pile location. This small wave generates a dynamic pressure field which dies out exponentially with depth (just like that of any other short wave). Since the wave crest (with higher pressure) is near the upstream part of the pile and the wave trough (with lower pressure) is on the downstream side, this wave will cause a net (additional) force component in the direction of the flow.

When the total drag force at this level (including this additional component) is related to the undisturbed near-surface flow velocity, it is only logical that the associated C_D value will be a few percent higher at this elevation.

Free End Effect

A third effect is more often encountered in the lab. One simple way to measure drag forces in a towing tank is to extend a cylinder vertically downward into a towing tank and to tow it while measuring its total resistance as a function of towing velocity. The force is then assumed to be uniformly distributed over the submerged length of the cylinder in order to ultimately arrive at a C_D value. Is this correct?

This will not be precisely correct for the following two reasons: The force will be disturbed (slightly) by the surface wave already discussed above, and there will be a three-dimensional flow pattern near the free, submerged end of the cylinder. This end effect will reduce the force there.

None of these force disturbances are significant enough for one to have to worry about them when predicting loads on an offshore structure. The situation can be quite different if one is determining a drag coefficient value from experiments in the lab, however.

These end effects - as all three of these phenomena are sometimes collectively called - can be eliminated for tests with currents only by adding thin but rigid horizontal plates to the cylinder: One just below the water surface and one near its free end. The upper plate should be larger than the wave length of the surface disturbance wave; the top of this plate will absorb the wave's dynamic pressure, thus preventing it from disturbing the pressure field lower down in the water. The lower plate will force the flow around the cylinder above it to remain two-dimensional.

Obviously, it would be best if the drag force was measured now only on some segment - located between the two guiding plates - of the total cylinder length. If this is done, however, and the measuring section is far enough from the water surface and the free end anyway, then it is not necessary to install the flow-guiding plates in the first place.

If measurements are to be made in waves, it is impossible from the start to use plates to guide the flow around anything except a cylinder submerged horizontally with its axis parallel to the wave crests.

14.8   Small Objects on The Sea Bed

There is a whole variety of small objects that can be found on or in the sea bed. In some cases the objects are intentionally deployed; anchors, subsea positioning beacons, or even mines and military listening devices fall into this category. Cargo items which fall overboard are generally not intentionally deployed on the sea bed - think of an automobile from a ferry or a small container being lifted to an offshore platform. The total list of objects one can find on the sea bed is nearly endless.

In some cases it is necessary that an object remain exposed on top of the bed; the functionality of a subsea beacon can depend upon this, for example. In other cases prompt self-burial is desired as a means of reducing the chance of detection of certain military devices. Here, again, the range of possibilities is broad.

14.8.1   Burial Mechanisms

How can an object which falls overboard become buried? There are several mechanisms conceivable:

- It can hit hard enough to create its own crater which is then re-filled by 'conventional' sediment transport. The chance that this occurs is small, however. Most objects don't fall fast enough to have enough impact energy. Indeed, as indicated in chapter 4, the fall velocity of most objects in the sea is modest. The pile dropped vertically was a striking (no pun intended) exception to this, however; see chapter 4.

- The object sinks into the soil under its own weight. This implies that there will be a soil bearing failure under the object. For this to happen, either the object will have to generate a high normal stress on the sea bed, or the bed material will have to be relatively weak - think of a very soft mud in this latter case. Such self-burial will often require a heavy and specially shaped object.

- An object can become buried as a result of local erosion and deposition. This is 'our' type of problem which will be discussed more below.

- The object may be covered or exposed as a result of large scale bed form mobility. Many of the large sand banks or shoals along the Dutch coast migrate slowly northward as a result of material being eroded on one side and re-deposited on the other.

- Sudden large scale sea bed movements can take place, triggered by very high storm waves or even by an earthquake. These can expose, cover, or even sweep away an object in their path. This has happened from time on the continental slopes. This was detected when transatlantic communication cables were suddenly broken and swept away. The time lapse between the failures of successive cables even yielded insight into the propagation speed of such slides.

- A last mechanism results from the possible slow build-up of excess pore pressure in the soil - usually an initially loosely-packed fine sand. This will be discussed below, too.

Local Morphology

The morphology near the (small) object on the sea bed has much in common with the pile. The object will generally stick up a bit but not have a nicely streamlined form. Since it is sticking up into an ambient velocity profile, it is logical that a downward secondary flow develops on the upstream side; this will result in some form of horseshoe vortex on the upstream side at the sea bed, just as near the pile. This vortex will again start creating an erosion pit immediately upstream of and beside the object as shown (as a longitudinal section) in figure 14.16.
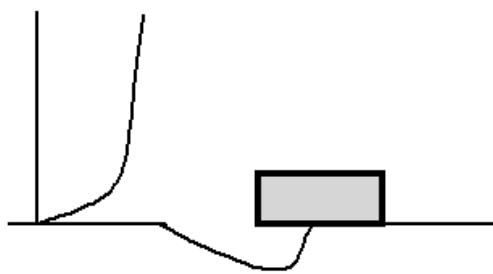
Figure 14.16: Small Object with Approaching Velocity Profile and Upstream Erosion Pit

Now, however, since the object does not penetrate significantly into the sea bed, material from under the object will fall into the pit; the object's support is eroded on the 'upstream' side, too. The result of this is often that the object ultimately tips forward into its 'own' erosion pit. Depending on the exact shape of the object, this can then change the local flow geometry significantly as well.

Such a fate is common for small irregular objects such as odd cargo items no bigger than a meter or so in maximum dimension. Short, stubby concrete cylinders - often used as inexpensive moorings for navigation buoys, etc. are another excellent example of this.

Pore Pressure Buildup and Bed Instability

Pressure changes on the surface of the sea bed which result from surface (storm) wave action can cause minute cyclic soil deformations. Loosely packed soil will 'try' to consolidate, thus reducing its void volume. Since the soil is saturated, water will have to escape during this consolidation process. Fine soils - even fine sand - can have a low permeability; this in combination with the oversupply of pore water, leads to an increase in pore pressure. Since Terzaghi's rule that:

$$\text{Total Stress} = \text{Grain (or Effective) Stress} + \text{Pore Pressure} \qquad (14.24)$$

is valid, the increased pore pressure results in a reduction of effective grain stress. In the limit, a quicksand condition occurs in which the effective stress has become too small to withstand the applied loads. Such a soil then behaves more like a high density fluid instead of a solid.

If the density of an object is less than that of quicksand (in the order of 1800 kg/m^3), it will 'float' in the quicksand and move slowly and incrementally to the bed surface; a heavier item sinks, instead. Pipelines - when filled with air (just after installation) or even with gas

often have an overall density of about 1300 kg/m^3; they have been known to 'float' upward through a beach and become re-exposed. At the opposite end of the scale, electric and some communications cables buried in the ground or sea bed will have an overall density of more like 4000 kg/m^3; they will indeed sink.

Note that it is not absolutely necessary for the quicksand condition to become 'fully developed'. The soil's effective intergranular stress and thus its shear strength is reduced as soon as the pore pressure increases. Since the net vertical force exerted by the buried object - it does not matter if it is positive or negative - will also cause shear stresses in the surrounding soil, it is only necessary that the soil's shear strength be reduced below the imposed stress level for failure to occur. Actual failure usually occurs slowly, the cyclic wave action stimulates cyclic variations in the pore pressure so that the failure is intermittent rather than continuous.

Relatively large pressure cycles are needed in order to build up sufficient pore pressure for this whole process to take place; this makes it essentially a shallow water phenomenon in the marine environment. At leas one newly-installed pipeline has floated up after being buried across a beach in The Netherlands. Luckily the problem became apparent before the pipeline was put into service.

In an onshore situation, electric cables laid in poor soil have been 'lost' in that they have sunk deeper - except where they are held in place in a junction house! In this case, the vibration source was the traffic on the adjacent highway.

What can be done to prevent this problem - at least in the marine situation? There are two possible solution approaches:

1. Consolidate the sand artificially as the pipeline or cable trench is being backfilled. While this is theoretically possible, it is probably a pretty expensive solution for a pipeline - even when one can work from the beach! Hydraulic engineers have used this approach however during the construction of the dam in the mouth of the Eastern Schelde. There, they feared that vibrations of the barrier support structures could lead to pore pressure build-up and subsequent failure of the deeper sand layers.

2. Backfill the pipeline trench with coarser material, providing sufficient soil permeability to prevent pore pressure build-up. This is the most commonly chosen preventative measure - at least for offshore situations.

14.9   Pipelines

This section discusses forces on exposed pipelines as well as the sea bed morphology in their vicinity. The discussion of hydrodynamic forces on pipelines has been delayed till this point because the presence of the current velocity profile caused by bed friction plays such an important role in the hydrodynamics.

A pipeline seems like a small object when seen in cross-section; in the third dimension it is very much a one-dimensional or line-like object. Much of what was discussed about small objects on the sea bed turns out to be applicable to pipeline cross-sections as well. The reader must be careful, however; since differences do exist. The following discussion will be for a pipeline which is initially laying on the sea bed with only a minimum of penetration into that bed (caused by its own weight). The current will flow more or less perpendicular to the pipeline route. The sea bed material is sand.

14.9.1 Flow and Forces

Because the pipeline is bedded slightly in the sand, it will not allow flow to pass under it; the entire approaching flow will have to pass over the pipeline. This flow pattern is obviously quite distorted relative to that for an isolated cylinder far away from any flow-constraining walls.

Drag Force

The drag coefficient for the pipeline will be somewhat higher than that for the cylinder in the unrestricted flow. This higher drag coefficient is then used in conjunction with the undisturbed current at the elevation of the pipeline center line. Remember that there is a strong velocity profile gradient here! Continuing the discussion of the horizontal equilibrium, first, the drag force is resisted by a friction force which, in turn, depends upon the contact force between the pipeline and the sea bed; horizontal stability depends upon the vertical force balance, too. These forces are all illustrated schematically in figure 14.17. There will be something similar to a stagnation area - with an associated relatively high quasi-static pressure - on the upstream side of the pipe near the bed.
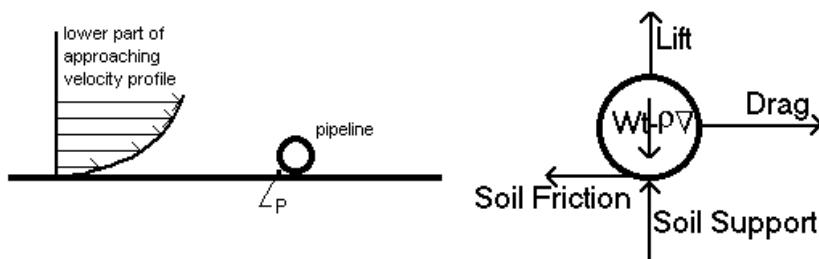
Figure 14.17: Flow Situation and Forces on a Cross Section of Exposed Pipe

Lift Force

Because of the approaching velocity profile and the fact that all of the flow must pass over the pipe, the velocities on top of the pipe will be even higher than those predicted by potential theory for an isolated cylinder. The concept of reflection was used in chapter 3 to model a potential flow around a cylinder near (or in contact with) a flat bed, but this still neglects the influence of the velocity profile in the approaching flow.

A high velocity along the top of the pipe implies low pressure there, while the water on the underside of the pipe - near point P in figure 14.17 - is nearly stagnant.

Conceptually, this begins to resemble the net flow effect of an isolated cylinder in a uniform current and surrounded by a circulation; the net force effect will be a lift directed perpendicular to the current - upward in this case. This force will have to be counteracted by pipe weight.

Looking for a moment at the total vertical equilibrium, this lift force reduces the soil contact force and thus, indirectly, the sliding friction resistance from the bed. Unless the pipe is constrained somewhere else along its length, it will slide sideways before it lifts off the bottom.

It is usually most economical to provide sufficient pipeline weight (for larger lines) by adding a high-density concrete coating; for smaller lines it can be more economical just to increase the steel wall thickness a bit. In either case, however, the added weight increases the pipe's outside diameter. One can quickly realize that as the outside diameter is increased, the drag and lift forces are increased, too! One is 'chasing one's tail' so to speak. Even so, an iterative solution can be found so that a stable design can be achieved.

Morphology

What about the morphology? The approaching velocity profile will collide with the pipe and cause the generation of a vortex on the upstream (or luff) side just as has been the case for piles and small objects. Since the horizontal pipeline presents a less streamlined shape to the flow (compared to the vertical pile), the upstream vortex may not be as nicely defined as the horseshoe vortex near a vertical pile. On the other hand, this vortex will be (theoretically) as long as the segment of exposed pipe.

Because the flow past the pipe cross-section is very unsymmetrical now, a larger and stronger (in comparison to that for a free-standing cylinder) vortex will be formed on the downstream (or lee) side of the pipe. It will be 'one-sided', too, in that it will rotate in only one direction: Clockwise if the flow is from left to right as shown in figure 14.17. For those who are not sailors, the terms luff and lee originally referred to the windward and leeward side (or edge) of a sailboat sail.

Luff and Lee Erosion   The upstream vortex, with its high turbulence and sharp velocity gradients, will cause what is called **luff erosion** - a bit of a trench, often wider and shallower than that near a pile - on the upstream side of the pipe.

The downstream vortex, too, will cause erosion - now called **lee erosion** - resulting in another trench, now (obviously) on the downstream side. The resulting trenches are shown somewhat schematically in image 2 of figure 14.18. The series of images in this figure depict a whole series of pipeline self-burial steps.

As these two trenches develop, one can imagine that sand under the pipe becomes unstable and falls gradually into the trenches. This loose sand is easily washed away.

Tunnel Erosion   Ultimately the remaining ridge of sand under the pipe can no longer support the pipe's weight and resist the hydrodynamic pressure differential between the upstream and downstream sides of the pipe as well; it fails, letting water flow under the pipe. This flow is initially squeezed between the pipe and the sea bed, restricting the formation of the boundary layer; see figure 14.18 part 3. Velocity gradients are then very high on the bed under the pipe so that there is also a very large bed shear stress. **Tunnel erosion** of material directly below the pipe can go quite fast! The high velocity flow now present under the pipe reduces the original upward lift force for two reasons: Less water flows over the pipe now, and the pressure on the bottom side of the pipe is reduced as a result of the high velocity now present there.

Pipeline Sag   Looking at the pipeline as a structural element for a moment, the pipe segment loses its vertical support as soon as the soil under it fails and tunnel erosion starts. Shear forces in the pipe convey the weight of the suspended pipeline segment to adjacent segments increasing their load on the intact sea bed and stimulating their failure
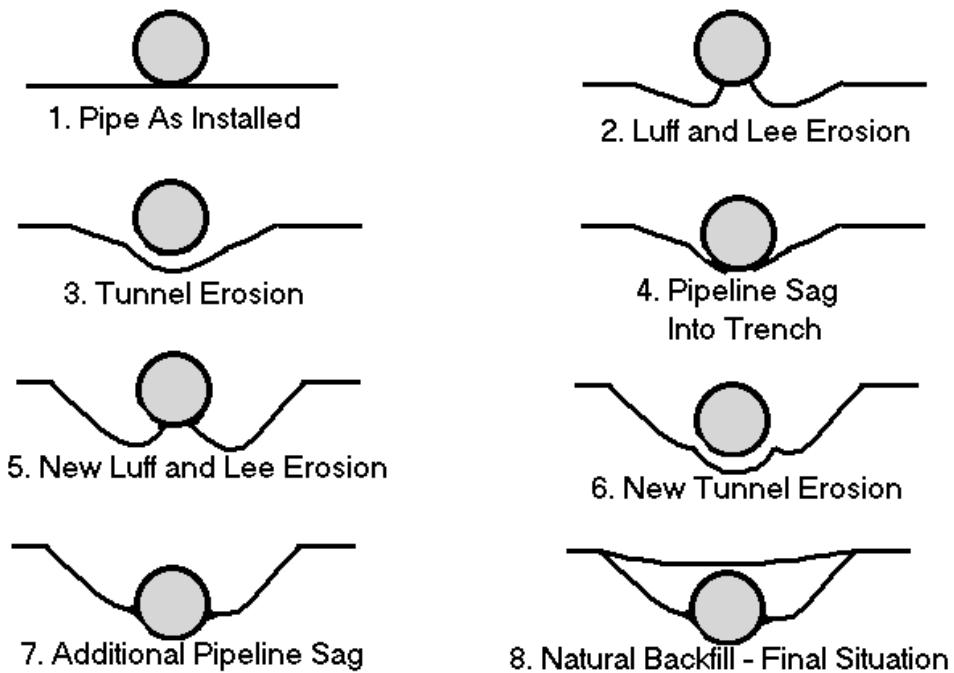
Figure 14.18: Pipeline Cross-Sections showing Progressive Self-Burial Steps

as well. The erosion tunnel can extend thus itself along the pipe axis crosswise to the flow. Obviously the pipe will start acting as beam, and as the erosion tunnel extends, the pipe will sag under its own weight into its own trench formed by the tunnel erosion.

In some cases the pipeline axis is nearly down to the original sea bed level (but still sticking up above the luff and lee erosion trenches) while a narrow tunnel still exists under the pipe. Ultimately, as the pipe continues to sink, it blocks less of the original flow thus reducing the driving force for the flow in the tunnel under the pipe. At the same time, the tunnel and streamlines under the pipe are getting longer, thus increasing the frictional resistance. At some point in this development, the current under the pipe will become too weak to transport (enough) sediment and the tunnel will become plugged with sand.

Repeated Cycle What happens next depends upon the extent to which the pipeline still projects above the sea bed. If the pipeline is high enough, luff and lee erosion will start again so that the entire cycle including a new tunnel erosion phase is repeated. Of course each repetition of this cycle leaves the pipeline a little lower relative to the original sea bed. If the pipe gets deep enough - often its crown is then even below the original sea bed level. Its disturbance to the flow will be so slight then that local erosion will stop and any remaining trenches will be re-filled by the ambient sediment transport. The final situation can be one in which the pipeline is completely buried and is even covered by a few decimeters of sand!

Tunnel Erosion Stimulation It is of course financially lucrative for a pipeline owner if this natural erosion process takes place; no costs are involved in this burial method! Since the costs of trenching and covering a pipeline can easily amount to several hundred guilders per meter of pipeline length, owners can be thankful for nature in this case! Dutch
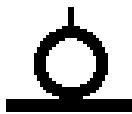
Figure 14.19: Pipeline with Spoiler

regulatory authorities are cooperative, too: They require that pipelines with diameters of 16 inches (406 mm) or less be buried only within a year after their installation. Since one good storm is often sufficient to completely bury a pipe line in Dutch waters, there is a good chance that this will occur - or, seen the other way, if it has not occurred within a year it probably won't occur at all. Then the owner will have to take action. The action that will have to be taken is discussed in a later section.

Why are owners only required to bury smaller lines? The reasoning is that smaller lines are weaker and can be more easily damaged by whatever may hit them - such as fishing gear, an anchor or something which has fallen overboard. Larger lines are considered to be strong enough. Also, since larger lines have a greater bending stiffness, they don't sag into their own erosion trenches as easily, either.

Do not get the impression that burial of a pipeline will actually provide that much protection against dragged anchors; anchors - especially those used in the offshore industry - usually dig in a bit too deep to pass over a pipeline. Expressed another way, most pipelines are not deep enough to escape a dragged anchor. On the other hand, pipelines are often buried more deeply - using artificial means - when their exposure to anchors is abnormally high - such as can be the case when a pipeline crosses a designated shipping channel.

Returning now to the main topic, how can the self-burial of a pipeline be stimulated? One obvious way would be to stimulate tunnel erosion by increasing the natural flow of water under the pipe. This can be done by blocking the flow of water over the pipe using what is often called a spoiler.

A pipeline **spoiler** is a vane, which typically sticks upright from the pipeline crown or top see figure 14.19. It usually projects about a quarter of the pipe diameter above the crown. The spoiler can be made of stiff but flexible plastic and it is held in place by plastic bands placed at intervals around the pipe. It is installed just before the pipeline leaves the laying ship during the installation process.

If the exposed pipeline and spoiler is hit by a towed object, it is designed to fold down temporarily and then spring back into its upright position.

Obviously the presence of the spoiler increases the drag force on the pipeline, but - once tunnel erosion has started - it makes the lift force even more negative so that the pipe is 'pulled' down toward the sea bed by the lift forces. This enhances its overall stability against sliding by increasing its normal on the soil elsewhere along the pipe.

14.9.2   Cover Layers

It has just been shown that natural processes can cause a pipeline or other small object to become buried in the sea bed. There are other situations in which it is desirable or even required that artificial means be used to cover or otherwise protect an object on the sea bed. Applications can be quite diverse:

- Cover an exposed pipeline or back-fill its trench,

- Locally cover a pipeline so that a new pipeline can cross it,
- Cover a long distance power or communications cable to protect it,
- Build up intermittent supports to prevent a pipeline from sagging too much into a deep 'valley' in the sea bed.

Most of these applications should be obvious. The last one has been used when crossing areas with hard and rough sea beds. The pipeline then tends to span from sea bed peak to sea bed peak. If this results in too long a span, internal pipeline forces can exceed allowable limits; an extra support is then needed. Such a support can be provided by a mound of coarse (stable) material installed at an intermediate location along the span. Of course the base of the support - up to the desired pipeline level - must be in place before the pipe is installed. Its top will be 10 meters or so square to allow some tolerance for the pipeline laying. After pipeline installation it is common practice to cover the pipe on top of the support mound in order to guarantee that it remains fixed at that location.

Two separate problems should become obvious to the reader from this discussion:

- How to guarantee the stability of a cover layer or intermediate support?
- How to install the necessary materials efficiently - especially in water depths of a few hundred meters?

These items will be discussed separately below.

Stability

In principle, the stability of any placed stone or gravel can be evaluated using the Shields criterion. A detailed review of the offshore situation, however, shows that conditions are not quite the same as in a river: The roughness of the dumped material will generally be different from that of the natural sea bed. Figure 14.20 shows such a situation rather schematically.   This means that - at least at the upstream side - the approaching flow
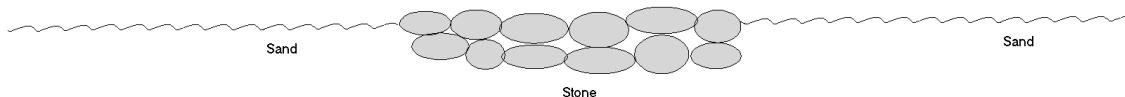
Figure 14.20: Cover Layer with Adjacent Sea Bed

velocity profile will be the one associated with the original sea bed roughness instead of the one that could be expected to develop above a bed of the dumped gravel or crushed stone. This velocity profile will probably generate a different shear stress as well. It should be obvious that at least the first part of the cover layer will have to remain stable under the influence of this latter (ambient) flow profile and resulting shear stress.

If the material placed on the sea bed distorts the general flow pattern as well - think of a berm or ridge of material covering an exposed pipeline - then the local influence of this flow distortion will have to be included in the analysis as well. Theory is often considered to be a bit too crude - still - for this sort of prediction; model tests are still popular for this. This has been (and can still be) an interesting experimental research area.

It has been pointed out that the stability of the first cover stones on the luff side can be critical. Is this the only concern? What about the start of the natural bed on the lee side? This bed is exposed to a velocity profile which has adapted (at least for the lower

few meters) to the roughness of the cover material. Assuming that the cover material is rougher than the sea bed - as will usually be the case - this flow may at least be a bit more turbulent than it would otherwise be. Local erosion of sea bed material on the lee side can often be expected. This means that the 'trailing edge' of the cover layer can be lost; it falls into the downstream erosion pit. This can be compensated very pragmatically by making the cover layer a bit wider. Then this loss will not be detrimental to the functionality of the cover layer.

Installation

It is one thing to design a local cover layer; one must still install it efficiently in a water depth of sometimes a several hundred meters. The hydraulic engineer's approach of just pushing gravel or stone overboard from a ship is fine for building a breakwater in shallow (from an offshore engineering point of view) water; it is not at all effective in deep water! In water deeper than a few tens of meters, cover layer material is often 'guided' toward the sea bed by a **fallpipe**. This is a long, more or less vertical pipe which extends from the work ship to a point just a few meters above where the material is to be deposited. The gravel or stone is then dumped into the top of the pipe; it will then come out the bottom a while later.

The fall pipe, itself, only really needs to contain the stone or gravel being dumped. It can be made up in at least three ways using either:
- 'Conventional' pipe sections - often made from plastic to save weight. This makes a closed pipe.
- A series of loosely coupled 'funnels' such as those used onshore to guide building renovation waste down into a container. Such a fallpipe allows water to enter at each joint.
- A 'loosely braided hose' made of chain links which contains the flow of solids. This is porous (to water) over its entire length.

Whatever type of fallpipe is used, it should be obvious (from chapter 12) that it will not simply hang straight down from the workship. Indeed, the combined action of the ship's forward speed plus any currents will exert quasi-static drag forces on the pipe, causing it to swing from the vertical. It may even respond to excitation coming from the ship's motion in waves as well. In order to be more certain that the lower end of the fall pipe is exactly in the desired position, that end is often equipped with a remote controlled vehicle or **spider**. This spider will have thrusters to compensate for small positioning errors.
The computation of the external hydrodynamic forces on a fallpipe is relatively straightforward. Even so, the prediction of its more complete static and dynamic behavior is not a trivial task. Attention, here, however, focuses on its internal hydraulics.

Internal Fallpipe Hydraulics   Since the pipe is open at the bottom, it will fill with water as it is initially deployed from the work ship. It is convenient at first to consider an impermeable pipe and to keep its top end above the sea surface. The pipe will be filled to sea level with still water when material dumping starts.
The hydrostatic pressure in the surrounding sea water will match the static pressure resulting from the column of clear water or later even the mixture of water and gravel in the pipe. This is shown in figure 14.21. Since the stone or gravel dumped into the pipe will increase the overall density of the mixture in the pipe, this dumping will cause the
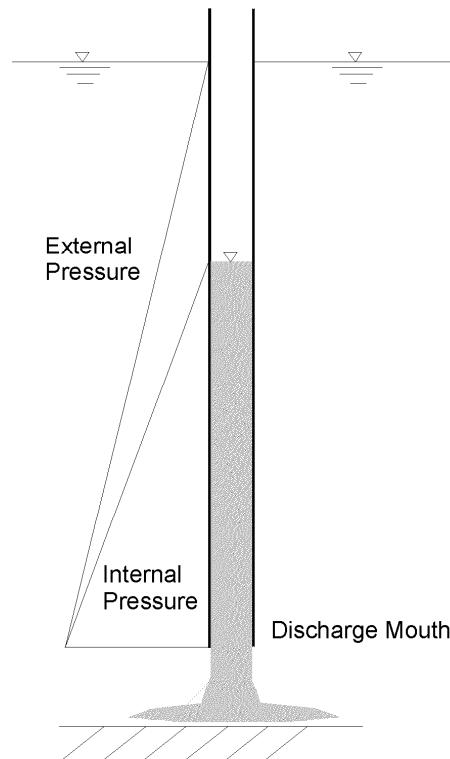
Figure 14.21: Pressure Distribution in and Around a Fallpipe (not to scale!)

liquid (mixture) level in the pipe to drop. The faster material is dumped into the pipe, the higher the concentration of solids in the water in the pipe. Thus, the overall density of the mixture will become higher, too. To compensate for this, the mixture level in the pipe will drop even more.

The upper segment of the pipe - at least - will be subjected to a substantial net external pressure as shown schematically in figure 14.21. This pressure difference forms a structural engineering problem for the pipe, but this may not be the biggest problem, however. With a constant rate of material dumping, the density of the mixture in the pipe will become constant and the *water* in the pipe will come to rest. This means that the stone or gravel dumped in the pipe will move downward in the pipe through essentially still water; it will move with its fall velocity - which is not especially high! The table below summarizes some typical soil grain fall velocity values (in water). This data can be found in chapter 4 as well.

Particle Type	Sand Grain	Gravel	Stone
Diameter (mm)	0, 2	20	100
Fall Velocity (m/s)	0, 02	1, 0	2, 35

The particles will fall relatively freely (and much faster) through the air in the pipe above the water; they will be abruptly decelerated by their impact with the water (lower) surface in the pipe. The only way the total mass transport of stone can be maintained with the sudden lower velocity is for there to be many more particles per unit length of pipe. If this 'concentration' becomes too high, the stone or gravel can bridge across the pipe and block

it so that nothing more gets through; this is a disaster for the productivity of the entire operation and embarrassing for the supervisor as well!

Even when this is working properly, the particles move relatively slowly - only with their fall velocity - through the still water in the fallpipe. It would be attractive to increase the productivity in terms of tons or cubic meters of solid material placed per hour using the same fallpipe.

One way to increase the productivity of the entire system is to let water flow down the fallpipe along with the stones. Since at any elevation the external hydrostatic pressure is greater than that in the pipe - see figure 14.21 - one has only to provide an opening to allow surrounding water to enter. This can be done at chosen intermediate elevations, at the top only, or even continuously along the pipe. One way to let the water enter is to use a porous pipe - such as the chain links hose - or simply to lower the top end of the pipe below sea level so that water overflows into it at the top.

Now, the particles sink through the moving water and a flow of water plus particles is discharged from the bottom end of the pipe. For the same rate of material supply as was used with the closed pipe, the concentration of particles discharged will be relatively lower and the discharge velocity will be higher when water is also moving downward through the fallpipe. Adding water is certainly a simple way to increase the productivity of the system, but how far can one go with this?

Discharge Morphology   What can happen when too much water is allowed to enter the fall pipe? The discharge velocity gets so high that a vertical jet (of a mixture of water and solids) collides with the sea bed and spreads out. It has even happened that this local spreading current - with its higher density and thin boundary layer! - generates too much local bed shear stress for the material being deposited.. Discharged stone will be swept away from the place where it is wanted taking the reputation of the contractor with it!

Another interesting question involves the effect of the grain size distribution of the material. If all of the particles are essentially of the same size and density, then their fall velocities will be more or less the same, too. For some applications, such as insulating a hot flow line between a subsea well and a production platform, it is desirable to use a well graded gravel to cover the pipe. This reduces the permeability of the cover, thus reducing the heat loss from the pipe via convected sea water in its vicinity. (Some crude oils become semi-solid if they are cooled below their so-called pour point temperature; it can be very important for the pipeline operator to keep things warm!)

When a well graded mixture of gravel sizes is dumped into a fallpipe, then the coarse material will fall faster than the fines. This means that when a discharging operation is started, first only coarse material will be discharged; there will be a 'tail' of fines at the end of the run as well. This need not be important - of itself - for a long pipeline, but it can make a mess of an attempt to form a neat supporting mound of material by passing slowly back and forth to build it up.

A second complication when discharging a well graded mixture of gravel is that the finest material must remain stable on the sea bed in the discharge jet. Segregation of the particles can take place so that coarse material is left near the pipeline with the finer fractions deposited more to the sides. This can mean disaster for the insulation function of the cover layer. It has led to litigation between the pipeline owner and covering contractor in the past.

Appendix A

TABLES

A.1   Greek Symbols

Classic Greek symbols			
name	letter	capital letter	English pronounciation
alpha	α	A	'alpha'
beta	β	B	'vita'
gamma	γ	Γ	'gama'
delta	δ	Δ	'delta'
epsilon	ϵ , ε	E	'epsilon'
zeta	ζ	Z	'zita'
eta	η	H	'ita'
theta	ϑ , θ	Θ	'thita'
iota	ι	I	'giota'
kappa	κ	K	'kapa'
lambda	λ	Λ	'lambda'
mu	μ	M	'mi'
nu	ν	N	'ni'
xi ("ksi")	ξ	Ξ	'xi'
omikron	o	O	'onikron'
pi	ϖ , π	Π	'pi'
rho	ρ	P	'ro'
sigma	σ	Σ	'sigma'
tau	τ	Υ	'taph'
upsilon	υ	Y	'ipsilon'
phi	φ , ϕ	Φ	'phi'
chi	χ	X	'chi'
psi	ψ	Ψ	'psi'
omega	ω		'omega'

Greek symbols used here		
name	letter	capital letter
alpha	α	
beta	β	
gamma	γ	Γ
delta	δ	Δ
epsilon	ε	
zeta	ζ	
eta	η	
theta	θ	
iota		
kappa	κ	
lambda	λ	Λ
mu	μ	
nu	ν	
xi ("ksi")	ξ	
omikron		
pi	π	Π
rho	ρ	
sigma	σ	Σ
tau	τ	Υ
upsilon		
phi	φ , ϕ	Φ
chi	χ	
psi	ψ	Ψ
omega	ω	

A.2 Water Constants

Temp.	Density Fresh Water	Density Salt Water	Kinematic Viscosity Fresh Water	Kinematic Viscosity Salt Water	Vapor Pressure Water
t	ρ_{fresh}	ρ_{salt}	ν_{fresh}	ν_{salt}	p_v
(°C)	(kg/m^3)	(kg/m^3)	(m^{2}s $\cdot 10^{-6}$)	(m^{2}s $\cdot 10^{-6}$)	(N/m^2)
0	999.8	1028.0	1.78667	1.82844	608
1	999.8	1027.9	1.72701	1.76915	
2	999.9	1027.8	1.67040	1.71306	706
3	999.9	1027.8	1.61665	1.65988	
4	999.9	1027.7	1.56557	1.60940	814
5	999.9	1027.6	1.51698	1.56142	
6	999.9	1027.4	1.47070	1.51584	932
7	999.8	1027.3	1.42667	1.47242	
8	999.8	1027.1	1.38471	1.43102	1069
9	999.7	1027.0	1.34463	1.39152	
10	999.6	1026.9	1.30641	1.35383	1226
11	999.5	1026.7	1.26988	1.31773	
12	999.4	1026.6	1.23495	1.28324	1402
13	999.3	1026.3	1.20159	1.25028	
14	999.1	1026.1	1.16964	1.21862	1598
15	999.0	1025.9	1.13902	1.18831	1706
16	998.9	1025.7	1.10966	1.15916	1814
17	998.7	1025.4	1.08155	1.13125	
18	998.5	1025.2	1.05456	1.10438	2059
19	998.3	1025.0	1.02865	1.07854	
20	998.1	1024.7	1.00374	1.05372	2334
21	997.9	1024.4	0.97984	1.02981	
22	997.7	1024.1	0.95682	1.00678	2638
23	997.4	1023.8	0.93471	0.98457	
24	997.2	1023.5	0.91340	0.96315	2981
25	996.9	1023.2	0.89292	0.94252	
26	996.7	1022.9	0.87313	0.92255	3364
27	996.4	1022.6	0.85409	0.90331	
28	996.2	1022.3	0.83572	0.88470	3785
29	995.9	1022.0	0.81798	0.86671	
30	995.6	1021.7	0.80091	0.84931	4236

Appendix B

MODELING AND MODEL SCALES

B.1   Introduction and Motivations

This appendix provides a rather complete discussion of the design of various sorts of models used in offshore engineering. Certain specific elements - such as Reynolds or Froude scaling, for example - are also summarized in the various chapters of the main text. In its most abstract sense, a model is some form of representation of an object. In a few cases, it is the object itself, but it is usually a more convenient representation (in some form) of an actual or proposed situation.

Models are used for many purposes; the main reasons for using models include the facts that they are:

- easier,
- faster,
- safer,
- cheaper.

It is generally easier, faster, safer, and cheaper to work with a model than to make all discoveries when a 'real thing' is used. For example, in the days before Computer Aided Design (CAD) software became trustworthy, it was common practice to build a plastic model of an offshore platform topsides - from the design drawings - in order to make sure that the piping all fits - or even worse - a major structural element conflicts with the piping or something else. While such a model may have cost tens of thousands of guilders, it was obviously much less expensive to correct errors in the design phase rather having to correct them in the field.

B.2   Model Types

There are many types of models that can be used.

CAD models in which the form of an object is modeled in a computer have been mentioned in the example above. Such models are used as well to generate the form of a ship or floating structure, for example. Since volumes and weights can easily be calculated, such systems can conveniently be extended to interface with hydrodynamic models or to check floating stability, for example.

Computer Simulations are a special category within the group of Computer Models. These represent the dynamic behavior of an object - such as a ship in waves or even the spreading of an oil spill - effectively by solving the related differential equations.

Computer models - of whatever type - have several advantages, especially in relation to their alternatives:

- They are reasonably inexpensive to use, although their initial development costs may be significant.

- Computers are so universally available today that they can be used most anywhere.

- A computer model is safe; they present not danger to humans or the environment.

- All included phenomena can be represented at full scale. (The signifcance of this will become apparent below.)

On the other hand, a computer model and especially a simulation has one important drawback: it is only as good as the mathematics which is used to (approximately) describe the phenomena which actually take place. In the mid nineteen-eighties, Petroski reported on the comparison of measured and computed loads in a large transmission line tower.

> "Computer predicitions of structural behavior were within only sixty percent of the actual measured values only ninety-five percent of the time, ..."

Computer users should never allow blind trust to replace reasonable engineering thinking!

Of course it is possible to carry out testing using a 'real thing': a full-sized and complete prototype. Such testing can be expensive - certainly if it leads to required changes. Even without that, measuring a ship's behavior in waves at sea requires a significant mobilization of test equipment and personnel and one has no control over the input - the weather-dependent waves - either. Many field test programs have been unsuccessful because nature provided the wrong (either too much or too little) input! In some cases it can even be downright dangerous to carry out measurements on a full-scale basis.

This is not to say that prototype testing is always bad; indeed not. Such measurements can be very valuable as well for diagnostic purposes such as to determine why relatively many persons on a particular platform complain of motion sickness. Field measurements are often used as well to verify the correctness of a different model - of whatever type. Indeed, all physical phenomena are (obviously) properly modeled in a full-scale prototype situation.

One way to avoid the disadvantages of a (series of) prototype(s) is to use a small scaled model and test it in a laboratory instead. Such a model is obviously cheaper than a prototype and the laboratory conditions under which it is tested can be carefully controlled. There is seldom risk to life and limb involved either!

Compared to a computer model, a physical model is slower in use but it has at least the potential to work with a more accurate representation of nature. Indeed, more of the actual physical phenomena are inherently included in a physical model.

A disadvantage of a physical model, however, is that a specialized (and therefore scarce and expensive) test faciltiy is often needed in order to carry out its testing.

B.3 Basic Phenomena and Scales

Given that one wants to work with a model (any type will do, but it is conceptually easier to think in terms of a physical model for now), one must decide what phenomena to include in the model. These are discussed in this section.

Geometric

The first requirement of any model is that it reproduce the geometry of the situation in some consistent way. This usually means that all physical dimensions of the model are represented at the same length scale, α_L. An exception to this will be mentioned in section 9, however.

Kinematic

Secondly, it is convenient if the kinematics (velocities and accelerations) are reproduced in the model at consistent scales. The velocity scale is denoted by α_V and since the acceleration of gravity is an acceleration, this scale is denoted by α_g.

Dynamic or Kinetic

Additionally, it is even handy if the dynamics - the forces - are also modeled consistently to some scale, α_F. Fluid density is usually scaled by a factor α_ρ, and kinematic viscosity is scaled by a factor α_ν.

The following table summarizes the scale factors found so far. Each factor relates a prototype phenomena (subscript, p) and a model phenomena (subscript, m):

Unit	Scale	Relationship
Length:	α_L,	$L_p = \alpha_L \cdot L_m$
Velocity:	α_V,	$V_p = \alpha_V \cdot V_m$
Acceleration of gravity:	α_g,	$g_p = \alpha_g \cdot g_m$
Density:	α_ρ,	$\rho_p = \alpha_\rho \cdot \rho_m$
Fluid kinematic viscosity:	α_ν,	$\nu_p = \alpha_v \cdot \nu_m$
Fluid dynamic viscosity	α_η,	$\eta_p = \alpha_\eta \cdot \eta_m$

Note that all α values in this table are greater than or equal to 1.0 .

B.4 Derived Scales

With these, the scale factors for the areas S, the volumes ∇, the masses M and the mass moments of inertia I, respectively, are then found easily:

$$\alpha_S = \alpha_L^2 \qquad \alpha_\nabla = \alpha_L^3 \tag{B.1}$$

$$\alpha_M = \alpha_\rho \cdot \alpha_\nabla = \alpha_\rho \cdot \alpha_L^3 \tag{B.2}$$

$$\alpha_I = \alpha_\rho \cdot \alpha_L^5 \tag{B.3}$$

The velocity of a body or a (water) particle is defined as a displacement per unit of time, so the scale factor for the time becomes:

$$\alpha_T = \frac{\alpha_L}{\alpha_V} \tag{B.4}$$

The acceleration of a body or a (water) particle is defined as an increase of the velocity per unit of time, so the scale factor for the acceleration becomes:

$$\alpha_A = \frac{\alpha_V}{\alpha_T} = \frac{\alpha_V^2}{\alpha_L} \tag{B.5}$$

This should be same, by the way, as the scale factor for the acceleration of gravity, α_g. According to Newton's law, inertia forces are defined as a product of mass and acceleration, so the scale factor for the inertia forces (and also the resulting pressure forces) is:

$$\alpha_F \;=\; \alpha_M \cdot \alpha_A = \left(\alpha_\rho \cdot \alpha_L^3\right) \cdot \left(\frac{\alpha_V^2}{\alpha_L}\right) = \tag{B.6}$$

$$\;=\; \alpha_\rho \cdot \alpha_V^2 \cdot \alpha_L^2 \tag{B.7}$$

Then, the relation beteen the forces F_p on the prototype and the forces F_m on the model are:

$$F_p = \alpha_\rho \cdot \alpha_V^2 \cdot \alpha_L^2 \cdot F_m \tag{B.8}$$

or:

$$\alpha_F = \frac{F_p}{F_m} = \frac{\rho_p \cdot V_p^2 \cdot L_p^2}{\rho_m \cdot V_m^2 \cdot L_m^2} \tag{B.9}$$

From this, it is obvious that these forces can be expressed as:

$$F_p = C \cdot \frac{1}{2}\rho_p V_p^2 \cdot L_p^2 \quad \text{and} \quad F_m = C \cdot \frac{1}{2}\rho_m V_m^2 \cdot L_m^2 \tag{B.10}$$

in which the coefficient or constant C does not depend on the scale. Further, one recognizes the term $\frac{1}{2}\rho V^2$ as the **stagnation pressure**.

B.5   Forces to Model

Since forces and kinetic similarity are so important in offshore engineering, extra attention to specific forces is given in this section.

Inertia

Whenever velocities and accelerations are involved - and that is the usual case in offshore engineering - modeling will involve inertia forces.

Gravity

Gravity forces are important for problems involving buoyancy and more generally for flow situations in which a free water surface is involved. Gravity forces are therefore important for waves and for all sorts of open channel flow. They also play an important part in soil mechanics as well. They are not usually very important, on the other hand, for pipeline flow.

Viscous or Damping

Viscous forces are important when friction is significantly involved. Pipeline pressure losses are an example of this. Damping forces in structural dynamics are a different example; they only become important when a structure has a near-resonant response.

Surface Tension

Surface tension forces are important when capillary action - between a fluid and a wall - or other deformations of a fluid surface are involved. It is only occasionally that surface tension forces become very important in offshore engineering. One example involves the later phases of the spreading of an oil on water; this is driven by surface tension forces.

Internal Stresses

Internal stresses can often be as important as the external shape in a design. Indeed, a sleek and fast ship which breaks when it encounters its first wave is of little practical use.

B.6 Force Scaling

A casual reader can conclude that there are no real problems with physical modeling yet. This impression may change if we compare the ways in which the various forces are scaled in a model.

Force	Scale
Inertia	$\alpha_\rho \cdot \alpha_V^2 \cdot \alpha_L^2$
Gravity	$\alpha_\rho \cdot \alpha_g \cdot \alpha_L^3$
Viscous	$\alpha_\eta \cdot \alpha_V \cdot \alpha_L$
Surface Tension	$\alpha_\sigma \cdot \alpha_L$
Internal Stresses	$\frac{\alpha_\rho \cdot \alpha_g \cdot \alpha_L^3 \cdot \alpha_L \cdot \alpha_L}{\alpha_L^4} = \alpha_\rho \cdot \alpha_g \cdot \alpha_L$
Bulk Strain	$\alpha_K \cdot \alpha_L^2$

in which the following scale factors are used:

$$
\begin{aligned}
\alpha_g &= \text{gravitational acceleration} \\
\alpha_K &= \text{bulk modulus of the fluid} \\
\alpha_L &= \text{length} \\
\alpha_V &= \text{velocity} \\
\alpha_\eta &= \text{dynamic viscosity} \\
\alpha_\rho &= \text{mass density} \\
\alpha_\sigma &= \text{surface tension}
\end{aligned}
$$

One can see from this table that not all forces are scaled equally; this is unfortunate. As stated above, only a computer model has the potential to include all forces in their proper relative scales.

The fact that not all of the above forces are identically reproduced in a physical scale model of a prototype, means that some forces will become (relatively) more important in the model than they actually are in the prototype. What must the model designer do? The

most common way to minimize the effects of this problem is to keep the **ratio of the two most important forces** - such as inertia and gravity (or possibly some other important phenomena) for example - the same in the model as they are in the prototype. Such ratios are dimensionless and many have special names as outlined in the following section.

B.7 Dimensionless Ratios

The following ratios - not all of which are strictly defined in terms of forces, by the way - are relatively common:

Name	Symbol	Ratio
Froude	Fn	$\sqrt{\dfrac{\text{Inertia Force}}{\text{Gravity Force}}}$
Reynolds	Rn	$\dfrac{\text{Inertia Force}}{\text{Viscous Force}}$
Keulegan-Carpenter	KC	$2\pi \cdot \dfrac{\text{Water Displacement Amplitude}}{\text{Cylinder Diameter}}$ *
Sarpkaya Beta	β	$\dfrac{\text{Re}}{\text{KC}}$
Reduced Velocity	V_r	$\dfrac{\text{Steady Flow Velocity}}{\text{Oscillating Flow Velocity Amplitude}}$
Strouhal	St	$2\pi \cdot \dfrac{\text{Cylinder Diameter}}{\text{Water Displacement Amplitude}}$ *
Kenn	Ke	$\dfrac{\text{Viscous Forces}}{\text{Surface Tension Forces}}$
Weber	We	$\dfrac{\text{Inertia Forces}}{\text{Surface Tension Forces}}$

*While St and KC look quite similar, they are associated with entirely different phenomena and are therefore quite different.

One sees from this table that:

- Not all dimensionless ratios involve forces directly.

- Some ratios - such as β above - can be expressed in terms of others.

If one includes additional engineering fields, then one can compile what seems like an endless list containing several hundred entries.

Scaling Consequences

Once one has chosen to use a given dimensionless ratio as the basis for a model, then this provides additional information for use in modeling in many practical situations.

It is usually impractical to replace water with another liquid in a physical model. Indeed, one author knows of cases when water has replaced other more exotic fluids - such as supercritical steam or even molten sodium - for very special testing or modeling purposes. Generally in offshore engineering however, one is confronted with water in both the model and prototype - even though one will usually be saltier than they other! A consequence of this is that the densities and other fluid properties will have a scale which is quite close to unity. This means that: $\alpha_K, \alpha_\eta, \alpha_\rho,$ and α_σ are all very close to unity.

Similarly, except in modern soil mechanics, it is seldom convenient to change the acceleration of gravity; α_g will be identically equal to 1. (Centrifuges are often used in soil mechanics to create an artifically higher 'gravitational' acceleration.) The only other know way to change the acceleration of gravity is to work in a space lab or on the moon; both of these alternatives are (still) too expensive for routine use!

This information can now be used in combination with a scaling law to derive additional relations.

Froude Scaling

Given that the Froude Number in the model must be same as that in the prototype, and that the Froude Number is the ratio of inertia to gravity forces, one may conclude that - using information from the tables above:

$$\alpha_\rho \cdot \alpha_V^2 \cdot \alpha_L^2 = \alpha_\rho \cdot \alpha_g \cdot \alpha_L^3 \qquad (B.11)$$

and since:

$$\alpha_V = \frac{\alpha_L}{\alpha_T} \text{ and } \alpha_g = 1. \qquad (B.12)$$

then equation B.11 can be re-written as so that:

$$\frac{\alpha_L}{\alpha_T^2} = 1. \qquad (B.13)$$

Time One can conclude from this that the time scale, $\alpha_T = \sqrt{\alpha_L}$. Thus if a model is built with a length scale of 100 (1 meter in the prototype is 1 centimeter in the model) then one second in the model will correspond to 10 seconds in the prototype when Froude scaling is used.

Velocity A quick check will show, too, that velocities in the model will also be scaled with $\sqrt{\alpha_L}$; a prototype current of 1 m/s will correspond to 10 cm/s in the model.

Reynolds Number and Viscous Forces Since viscous forces may also be involved in a physical model designed to Froude Scale, it can be interesting to check how the Reynolds Number is scaled.
Since Re is the ratio of inertia to viscous forces, then:

$$\alpha_{\mathrm{Re}} = \frac{\alpha_\rho \cdot \alpha_V \cdot \alpha_L}{\alpha_\eta} \qquad (B.14)$$

Since α_ρ and α_η are both equal to 1, then $\alpha_{\mathrm{Re}} = \alpha_L^{1.5}$. This means that the Reynolds Number in the model will be $\frac{1}{100^{1.5}}$ or 1000 times too small. In other words, the viscous forces in the model will be 1000 times more important in the model than in the field.

Keulegan Carpenter Number The Keulegan Carpenter number, $KC = \frac{\hat{u}T}{D}$, is scaled according to:

$$\alpha_{KC} = \frac{\alpha_V \cdot \alpha_T}{\alpha_L} = \frac{\sqrt{\alpha_L} \cdot \sqrt{\alpha_L}}{\alpha_L} \equiv 1 \qquad (B.15)$$

KC is not changed when Froude scaling is used.

Internal Forces Internal forces - such as bending stresses in the hull of a ship - are scaled according to:
$\alpha_\rho \cdot \alpha_g \cdot \alpha_L$ - from the table above. Since α_ρ and α_g are both equal to 1 , then internal stresses are scaled in the same way as the length. Now the example model will be (relatively) 100 times as strong as the prototype. Failure to recognize this scaling little detail has led to

the failure (in the field) of concrete armor units for rubble mound breakwaters. Concrete units used in the model were strong enough, but the prototype scale units in the field did not have a significantly higher allowable stress than in the model. As a consequence, the concrete units in the sea broke up in a storm and the whole breakwater - as well as the infrastructure it was protecting - was severely damaged.

Reynolds Scaling

One way to avoid the distortion of the viscous forces in a Froude Scale Model is to use Reynolds Scaling, instead. Now the ratio of inertia to viscous forces is kept constant. This means that:

$$\alpha_\rho \cdot \alpha_V^2 \cdot \alpha_L^2 = \alpha_\eta \cdot \alpha_V \cdot \alpha_L \qquad (B.16)$$

Since α_ρ and α_η are still equal to 1, then $\alpha_V \cdot \alpha_L = 1$. so that $\alpha_V = \frac{1}{\alpha_L}$. This means that if the model has a scale (as above) of 100, then the velocities in the model will have to be 100 times larger than in the prototype. This is essentially impossible to achieve in practice!

Other Scaling Laws

Most any of the dimensionless ratios listed in the table above can be used as a basis for a scaling law. Froude Scaling is the most common in offshore engineering hydromechanics simply because gravity plays a dominant role in the behavior of the free surface of the ocean. Reynolds scaling is often used for pipe flows (under pressure) such as can be found in the topsides of an offshore production platform.

The following figure compares a variety of scaling laws.

B.8   Practical Compromises

Consider for the moment a physical model of the entire North Sea (to stay offshore!) or even of a few kilometers of a broad river. Since the free water surface is important, Froude scaling would be most appropriate, but one quickly becomes concerned about the strongly increased influence of the viscous forces. Indeed, the model can become so shallow that boundary layer effects become too dominant.

Distorted Scale

One way to reduce the viscous influence in an open channel model is to use a smaller length scale for vertical dimensions than that used for horizontal dimensions. One author has worked on such a model with a vertical scale of 40 and a horizontal scale of 60. This makes the model relatively 1.5 times as deep as would be indicated from the field. This keeps the Reynolds numbers 1.5 times as large (relative to the undistorted model); they are still small relative to the prototype or field situation, however.

Added Roughness

A quite opposite problem occurs with ship models towed in a towing tank. Because the models are relatively smooth, the laminar boundary layer which forms near the bow extends
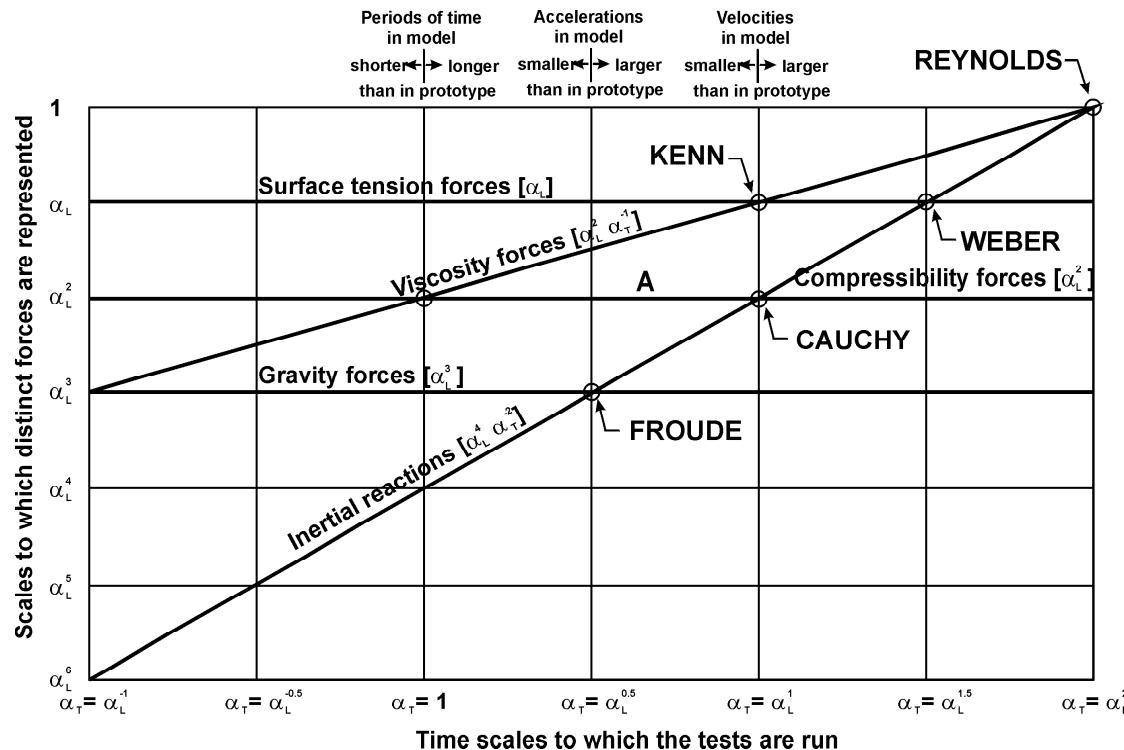
Figure B.1: Graphical Comparison of Scaling Laws

much too far aft (in the model) and thus distorts its skin friction resistance. In this case, this laminar boundary layer is forcefully broken up by attaching strips of rough material (It looks like coarse sandpaper.) to the model hulls a bit aft of the bow.

Adjust Gravity

The use of centrifuges has already been mentioned above in connection with geotechnical work. By artificially increasing g, one can use a relatively thin soil layer to model a much thicker one. Such models have been used - for example - to study the behavior of deeply penetrating offshore anchors in soft clay soils.

Adjusting gravity is never inexpensive! It can run into a number of very practical problems associated with carrying out the test, too - especially when free surfaces of liquids are involved.

Distort All Scales

Some have suggested that instead of keeping one dimensionless ratio constant, experiments might be designed so that all (more than one) important dimensionless ratios are distorted more or less equally. This idea may be better in theory than in practice, however. The author is aware of no specific examples of its application. This could mean, for example, that one would choose scaling corresponding to point A in the above figure.

B.9 Conclusion

Any physical scale model will distort the relative importance of various forces and other physical phenomena involved. On the other hand, a physical model **does include** all these physical phenomena.

The only way to avoid the distortions associated with physical models is to use a computer model or simulation. This has the disadvantage, however, that its representation of the physical situation is only as good as the mathematician has been able to make it.

Appendix C

FOURIER SERIES APPROXIMATIONS

C.1 Basic Form

Baron Jean Baptiste Jouseph Fourier, a French mathematician who died in 1830, concluded in that any time dependent signal, $F(t)$, which repeats itself with period, T, can be expressed as:

$$F(t) = a_0 + \sum_{n=1}^{\infty} \left[a_n \cos(n\omega t) + b_n \sin(n\omega t) \right] \tag{C.1}$$

in which:

$$
\begin{array}{rcl}
F(t) & = & \text{Arbitray periodic function} \\
a_n & = & \text{Coefficients; } n = 0, 1, 2, \ldots \\
b_n & = & \text{Coefficients; } n = \quad 1, 2, \ldots \\
n & = & \text{An integer} \\
t & = & \text{Time} \\
\omega = 2\pi/T & = & \text{Frequency} \\
T & = & \text{Period of the function}
\end{array}
$$

Further, the coefficients a_n and b_n can be computed from $F(t)$ using:

$$a_0 = \frac{1}{T} \int_0^T F(t)\, dt \tag{C.2}$$

$$a_n = \frac{2}{T} \int_0^T F(t) \cdot \cos(n\omega t)\, dt \quad \text{with: } n > 0 \tag{C.3}$$

$$b_n = \frac{2}{T} \int_0^T F(t) \cdot \sin(n\omega t)\, dt \tag{C.4}$$

These equations express a Fourier series in its basic form.

The above integrals must be carried out over one period, T, of the measured signal. It does not matter when, exactly, that period begins or ends. The limits of 0 and T above (as well as in the rest of this appendix) can be replaced by t and $t+T$ respectively if desired. The basic version will be used in this appendix, however.

C.2 Derived Form

Equation C.1 can be expressed in another way as well:

$$F(t) = a_0 + \sum_{n=1}^{\infty} c_n \cos(n\omega t + \phi_n) \tag{C.5}$$

in which:

$$c_n = \sqrt{a_n^2 + b_n^2} \tag{C.6}$$

and:

$$\phi_n = \arctan\left(\frac{b_n}{a_n}\right) \tag{C.7}$$

(The arctan function denotes the angle whose tangent is ....)

C.3 Limits

Fourier's theory indicates explicitly that his series includes an infinite number of terms; this is never practical, however.

One approach is to bluntly limit the order of the Fourier Series to $n = 1$. This is often used as a means of linearizing a peridoic signal, by the way. If one wants to average this linearization over several periods of the signal, one can do this by treating some integer, k number of periods of that signal and then computing only the $n = k^{th}$ harmonic.

While use of a single periodic Fourier Series component is very attractive from both a computational and linearization points of view, one can become worried about whether such a simplification is really justified.

Fourier showed that the following relation also holds:

$$\frac{2}{T} \int_0^T [F(t)]^2 = \frac{a_0^2}{2} + \sum_{n=1}^{\infty} c_n^2 \tag{C.8}$$

so that in practice the error, E_N (represented by all of the terms of order higher than N) is given by:

$$E_N = \frac{2}{T} \int_0^T [F(t)]^2 - \frac{a_0^2}{2} - \sum_{n=1}^{N} c_n^2 \tag{C.9}$$

This can evaluated readily, and if one is lucky, E_N will decrease rapidly as N increases.

C.4 Application Example

One function for which a Fourier Series linearization is commonly used that for quadratic drag in the Morison equation. This means that one wants to express a function of the form:

$$F(t) = A\cos(\omega t) \cdot |\cos(\omega t)| \tag{C.10}$$

as a Fourier series. (See chapter 12 for a discussion of the Morison Equation.)
Using equations C.3 and C.4 one finds that:

$$
\begin{aligned}
a_0 &\equiv 0 \\
a_1 &= \tfrac{8}{3\pi} = 0.849A \\
b_n &\equiv 0 \quad \text{for all } n \\
a_n &\equiv 0 \quad \text{for all even } n \\
a_3 &= \tfrac{8}{15\pi} = 0.170A = \tfrac{a_1}{5} \\
a_5 &= \tfrac{8}{105\pi} = 0.024A = \tfrac{a_1}{35} \\
&\quad \text{etcetera}
\end{aligned}
$$

If a linearization is used in this particular case, then the amplitude of the linear equivalent component should be chosen equal to a_1. Note, however, that even though the second harmonic is absent, the amplitude of the third harmonic, a_3, is still 20% of the amplitude of the first harmonic; linearization may not be all that precise in this case.

.

Bibliography

[Bales, 1983] Bales, S. L. (1983). Wind and Wave Data for Seakeeping Performance Assessment. Technical report, Prepared for Seakeeping Committee ITTC, Athens, Greece.

[Bathe and Wilson, 1976] Bathe, K. and Wilson, E. L. (1976). Numerical Methods in Finite Element Analysis. Technical report, Prentice Hall, Englewood Cliffs, 1976.

[Boese, 1970] Boese, P. (1970). Eine Einfache Methode zur Berechnung der Wiederstandserhöhung eines Schiffes in Seegang. Technical Report 258, Institüt für Schiffbau der Universität Hamburg, BRD.

[Bosch and Vugts, 1966] Bosch, J. J. v. d. and Vugts, J. H. (1966). Roll Damping by Free Surface Tanks. Technical Report 83-S, Netherlands Ship Research Centre TNO, Shipbuilding Department, Delft, The Netherlands.

[Bowers, 1975] Bowers, E. C. (1975). Long Period Oscillations of Moored Ships Subject to Short Wave Seas. *Trans. Royal Institution of Naval Architects*.

[Chislett and Bjorheden, 1966] Chislett, M. S. and Bjorheden, O. (1966). Influence of Ship Speed on the Effectiveness of a Lateral-Thrust Unit. Technical Report Hy-8, Hydro- Og Aerodynamisk Laboratorium, Lyngby, Denmark.

[Clauss, 1992] Clauss, G. (1992). *Offshore Structures, Volume 1, Conceptual Design and Hydromechanics*. Springer, London, UK.

[Conolly, 1974] Conolly, J. E. (1974). Standards of Good Seakeeping for Destroyers and Frigates in Head Seas. In *International Symposium on the Dynamics of Marine Vehicles and Structures in Waves, London, UK*, number 8.

[Cramer and et.al., 1993] Cramer, E. and et.al. (1993). Fatigue in Side Shell Longitudinals due to External Wave Pressure. *OMAE*, II:267–272.

[Cummins, 1962] Cummins, W. E. (1962). The Impulse Response Function and Ship Motions. In *International Symposium on Ship Theory, Hamburg, Germany*, number 8.

[Dalzell, 1976] Dalzell, J. F. (1976). Application of the Fundamental Polynomial Model to the Added Resistance Problem. In *Eleventh Symposium on Naval Hydrodynamics, London*, University College, London, UK.

[Delany and Sorensen, 1970] Delany, N. K. and Sorensen, N. E. (1970). Low Speed Drag of Cylinders of Various Shapes. Technical Report 3038, NACA.

[DetNorskeVeritas, 1989] DetNorskeVeritas (1989). Rules for the Classification of Fixed Offshore Installations. Technical report, DNV, Hovik, Norway.

[Dev, 1996] Dev, A. (1996). *Viscous Effects in Drift Forces on Semi-Submersibles*. PhD thesis, Delft University of Technology, The Netherlands.

[Edwards, 1985] Edwards, R. Y. (1985). Hydrodynamic Forces on Vessels Stationed in a Current. In *OTC 1985, Paper No. 5032, Houston, Texas, USA*.

[English and Wilde, 1976] English, J. W. and Wilde, D. A. (1976). Hydrodynamic Positioning. In *NECIES, Presented at a Joint Meeting with RINA, December 8, 1976*.

[Faltinsen, 1990] Faltinsen, O. M. (1990). *Sea Loads on Offshore Structures*. Number ISBN 0-521-37285-2, 1990 / ISBN 0-521-45870-6, 1993. University Press, Cambridge, UK.

[Faltinsen and Loken, 1978a] Faltinsen, O. M. and Loken, E. A. (1978a). Drift Forces and Slowly Varying Forces on Ships abd Offshore Structures. Technical Report 1, Norwegian Maritime Research.

[Faltinsen and Loken, 1978b] Faltinsen, O. M. and Loken, E. A. (1978b). Drift Forces and Slowly Varying Horizontal Forces on a Ship in Waves. In *Timman Symposium on Applied Mathematics*, Delft, The Netherlands.

[Faltinsen and Loken, 1979] Faltinsen, O. M. and Loken, E. A. (1979). Slow Drift Oscillations On a Ship in Irregular Waves. *Journal of Applied Research*, (1).

[Fang, 1985] Fang, Z. (1985). A New Method for Calculating the Fundamental Potential Functions Induced by a Source/Dipole Polygon. *Applied Mathematics and Mechanics*, 6(7).

[Fossen, 1994] Fossen, T. I. (1994). *Guidance and Control of Ocean Vehicles*. John Wiley and Sons, Chichester, England.

[Frank, 1967] Frank, W. (1967). Oscillation of Cylinders in or below the Free Surface of Deep Fluids. Technical Report 2375, Naval Ship Research and Development Centre, Washington DC, USA.

[Franzen, 1962] Franzen, A. (1962). Ghost from the Depths: the Warship Vasa. *National Geographic*, pages 42–57.

[Gerritsma and Beukelman, 1972] Gerritsma, J. and Beukelman, W. (1972). Analysis of the Resistance Increase in Waves of a Fast Cargo-ship. *International Shipbuilding Progress*, 18(217).

[Haskind, 1957] Haskind, M. (1957). The Exciting Forces and Wetting of Ships in Waves (in Russian). *Izvestia Akademii Nauk SSSR, Otdelenie Tskhnicheshikh Nauk*, (7):65–79.

[Herschel, 1897] Herschel, C. (1897). On the Origin of the Chezy Formula. *Journal of the Association of Engineering Societies*, 18.

[Hoerner, 1965] Hoerner, S. F. (1965). *Fluid Dynamic Drag*.

[Holtrop, 1977] Holtrop, J. (1977). A Statistical Analysis of Performance Results. *International Shipbuilding Progress*, 24.

[Holtrop, 1984] Holtrop, J. (1984). A Statistical Reanalysis of Resistance and Propulsion data. *International Shipbuilding Progress*, 31.

[Holtrop and Mennen, 1982] Holtrop, J. and Mennen, G. (1982). An Approximate Power Prediction Method. *International Shipbuilding Progress*, 89.

[Hooft, 1970] Hooft, J. P. (1970). *Aspects of Semi-Submersible Platforms, MARIN publication 400*. PhD thesis, Delft University of Technology, The Netherlands.

[Hsu and Blenkarn, 1970] Hsu, F. H. and Blenkarn, K. A. (1970). Analysis of peak mooring forces caused by slow vessel drift oscillations in random seas. In *Offshore Technology Conference*, number 1159, Houston, USA.

[Huijsmans, 1996] Huijsmans, R. H. M. (1996). *Motions and Drift Forces on Moored Vessels in Current*. PhD thesis, Delft University of Technology, The Netherlands.

[Ikeda et al., 1978] Ikeda, Y., Himeno, Y., and Tanaka, N. (1978). A Prediction Method for Ship Rolling. Technical Report 00405, Department of Naval Architecture, University of Osaka Prefecture, Japan.

[Isherwood, 1973] Isherwood, M. A. (1973). Wind Resistance of Merchant Ships. *Trans. Royal Institution of Naval Architects*.

[Iversen and Balent, 1951] Iversen, H. W. and Balent, R. (1951). A Correlating Modulus for the Fluid Resistance in Accelerated Motion. *Journal of Applied Physics*, 22(3):324–328.

[John, 1949] John, F. (1949). On the Motions of Floating Bodies, Part I. *Comm. on Pure and Applied Mathematics*, pages 13–57.

[Joseph, 1973] Joseph, D. D. (1973). Domain Perbutations: The Higher Order Theory of Infinitesimal Water Waves. *Arch. Rational Mech. Anal.*, 51:295–303.

[Journée, 1976a] Journée, J. M. J. (1976a). Motions, Resistance and Propulsion of a Ship in Longitudinal Regular Waves. Technical Report 428, Delft University of Technology, Ship Hydromechanics Laboratory, The Netherlands. (Internet: http://dutw189.wbmt.tudelft.nl/~johan or http://www.shipmotions.nl).

[Journée, 1976b] Journée, J. M. J. (1976b). Prediction of Speed and Behaviour of a Ship in a Seaway. *International Shipbuilding Progress*, 23(265):285–313. (Internet: http://dutw189.wbmt.tudelft.nl/~johan or http://www.shipmotions.nl).

[Journée, 1991] Journée, J. M. J. (1991). Motions of Rectangular Barges. In *Proceedings 10th International Conference on Offshore Mechanics and Arctic Engineering*, Stavanger, Norway.

[Journée, 1992] Journée, J. M. J. (1992). Strip Theory Algorithms, Revised Report 1992. Technical Report 912, Delft University of Technology, Ship Hydromechanics Laboratory, The Netherlands.

[Journée, 1997] Journée, J. M. J. (1997). Liquid Cargo and Its Effect on Ship Motions. In *STAB'97 Conference*, Varna, Bulgaria. (Internet: http://dutw189.wbmt.tudelft.nl/~johan or http://www.shipmotions.nl).

[Journée, 1999] Journée, J. M. J. (1999). User Manual of SEAWAY, Release 4.18 (09-10-1999). Technical Report 1212, Delft University of Technology, Ship Hydromechanics Laboratory, The Netherlands. (Internet: http://dutw189.wbmt.tudelft.nl/~johan or http://www.shipmotions.nl).

[Journée, 2000] Journée, J. M. J. (2000). Theoretical Manual of SEAWAY (Release 4.18). Technical Report 1216, Delft University of Technology, Ship Hydromechanics Laboratory, The Netherlands. (Internet: http://dutw189.wbmt.tudelft.nl/~johan or http://www.shipmotions.nl).

[Journée and van 't Veer, 1995] Journée, J. M. J. and van 't Veer, A. P. (1995). First Order Wave Loads in Beam Waves. In *Proceedings 5th International Offshore and Polar Engineering Conference*, The Hague. (Internet: http://dutw189.wbmt.tudelft.nl/~johan or http://www.shipmotions.nl).

[Keulegan and Carpenter, 1958] Keulegan, G. H. and Carpenter, L. H. (1958). Forces on Cylinders and Plates in an Oscillating Fluid. *Journal of Research of the National Bureau of Standards*, 60(Research Paper 2857).

[Kim and Breslin, 1976] Kim, C. H. and Breslin, J. P. (1976). Prediction of slow drift oscillations of a moored ship in head seas. In *Proceedings BOSS Conference*.

[Korkut and Hebert, 1970] Korkut, M. and Hebert, E. (1970). Some Notes on Static Anchor Chain Curve. In *Offshore Technology Conference, 1970, Dallas, Texas, USA.*, number OTC 1160, Dallas, Texas, USA.

[Korvin-Kroukovsky and Jacobs, 1957] Korvin-Kroukovsky, B. V. and Jacobs, W. R. (1957). Pitching and Heaving Motions of a Ship in Regular Waves. *Transactions* SNAME, 65:590–632.

[Kudou, 1977] Kudou, K. (1977). The Drifting Force Acting on a Three-Dimensional Body in Waves. *Journal of the Society of Naval Architects of Japan*, 141.

[Kuiper, 1992] Kuiper, G. (1992). The Wageningen Propeller Series. Technical Report 92-001, MARIN, Wageningen.

[Kuiper, 1997] Kuiper, G. (1997). Resistance and Propulsion of Ships, Lecture Notes. Technical Report 847-K, Delft University of Technology.

[Kwan, 1990] Kwan, C. T. (1990). Design Practice for Mooring of Floating Production Systems. *The Society of Naval Architects and Marine Engineers, Offshore Station Keeping Symposium, Houston, Texas USA*.

[Lamb, 1932] Lamb, H. (1932). *Hydrodynamics*. Dover Publications, Inc., New York, 6 edition.

[Lewis, 1929] Lewis, F. M. (1929). The Inertia of Water Surrounding a Vibrating Ship. In *Transactions* SNAME.

[Lienhard, 1966] Lienhard, J. H. (1966). Synopsis of Lift, Drag, and Vortex Frequency Data for Rigid Circular Cylinders. Technical Report 300, Washington State University, College of Engineering, Research Division.

[Lloyd, 1989] Lloyd, A. R. J. M. (1989). *Seakeeping, Ship Behaviour in Rough Weather.* Number ISBN 0-7458-0230-3. Ellis Horwood Limited, Market Cross House, Cooper Street, Chichester, West Sussex, P019 1EB England.

[Maruo, 1960] Maruo, H. (1960). The Drift of a Body Floating in Waves. *Journal of Ship Research*, 4(3).

[Massie, 1997] Massie, W. W. (1997). Offshore Moorings. Technical Report OT-4661, Delft University of Technology, Civil Engineering Department.

[McClure et al., 1990] McClure, A. C., McClure, S., and Edwards, R. (1990). Dynamic Positioning Dynamics. In *The Society of Naval Architects and Marine Engineers, Offshore Station Keeping Symposium 1990, Houston, Texas, USA*, number 8.

[Minsaas et al., 1986] Minsaas, K. J., Thon, H., and Kauczynski, W. (1986). Influence of Ocean Environment on Thruster Performance. In *International Symposium on Propeller and Cavitation, Supplementary Volume, Editorial Office of Shipbuilding China, Shanghai, China.*

[Morison et al., 1950] Morison, J. R., O'Brien, M., Johnson, J., and Schaaf, S. (1950). The Forces Exerted by Surface Waves on Piles. In *Petroleum Transactions, AIME 1950*, volume 189, pages 149–157.

[Newman, 1962] Newman, J. N. (1962). The Exciting Forces on Fixed Bodies in Waves. *Journal of Ship Research*, 6(4):10–17.

[Newman, 1977] Newman, J. N. (1977). *Marine Hydrodynamics.* MIT Press, Cambridge, UK.

[Newman, 1985] Newman, J. N. (1985). Algorithms for the Free-Surface Green Function. *Journal of Engineering Mathematics*, 19:57–67.

[Newman, 1993] Newman, J. N. (1993). Wave-Drift Damping of Floating Bodies. *Journal of Fluid Mechanics*, 249:241–259.

[Ochi, 1964] Ochi, M. K. (1964). Prediction of Occurence and Severity of Ship Slamming at Sea. In *Proceedings of 5th O.N.R. Symposium, Bergen, Norway.*

[Ochi and Motter, 1974] Ochi, M. K. and Motter, E. (1974). Prediction of Extreme Ship Responses in Rough Seas in the North Atlantic. In *Proceedings of the International Symposium on the Dynamics of Marine Vehicles and Structures in Waves London, UK, Paper 20*, number 20.

[OCIMF, 1977] OCIMF (1977). Prediction of Wind and Current Loads on VLCCs. In *TOil Companies International Marine Forum, London, UK, 1977.*

[Ogilvie, 1964] Ogilvie, T. (1964). Recent progress towards the understanding and prediction of ship motions. In *Proc. 5th Symposium on Naval Hydrodynamics.*

[Ogilvie, 1963] Ogilvie, T. F. (1963). First and Second Order Forces on a Cylinder Submerged under a Free Surface. *Journal of Fluid Mechanics*, pages 451–472.

[Oortmerssen, 1976a] Oortmerssen, G. v. (1976a). The Motions of a Moored Ship in Waves. *Journal of Ship Research*, 4(3).

[Oortmerssen, 1976b] Oortmerssen, G. v. (1976b). The Motions of a Moored Ship in Waves. Technical Report 510, MARIN.

[Oortmerssen et al., 1984] Oortmerssen, G. v., van den Boom, H. J. J., and Pinkster, J. A. (1984). Mathematical Simulation of the Behaviour of Ships Moored to Offshore Jetties. *ASCE*.

[Pastoor, 1997a] Pastoor, L. (1997a). Combination of Local and Global Wave Induced Loads on Side Shell Longitudinals of FPSO 'Glas Dowr' (Master Thesis, Part II). Technical report, Delft University of Technology, Ship Hydromechanics Laboratory, The Netherlands.

[Pastoor, 1997b] Pastoor, L. (1997b). External Wave Pressure Loading of Side Shell Longitudinals of FPSO 'Glas Dowr'(Master Thesis, Part I). Technical report, Delft University of Technology, Ship Hydromechanics Laboratory, The Netherlands.

[Pinkster, 1976] Pinkster, J. A. (1976). Low-Frequency Second Order Forces on Vessels Moored at Sea. In *Eleventh Symposium on Naval Hydrodynamics, London*, University College, London, UK.

[Pinkster, 1977] Pinkster, J. A. (1977). Computations of the First and Second Order Wave Forces on Bodies oscillating in Regular Waves. In *Second International Conference on Numerical Ship Hydrodynamics*, Berkeley, USA.

[Pinkster, 1978] Pinkster, J. A. (1978). Wave feed-forward as a means to improve dynamic positioning. In *Offshore Technology Conference*, number OTC 3057, Houston, USA.

[Pinkster, 1979] Pinkster, J. A. (1979). Mean and Low Frequency Wave Drifting Forces on Floating Structures. *Ocean Engineering*.

[Pinkster, 1980] Pinkster, J. A. (1980). *Low Frequency Second Order Wave Exciting Forces on Floating Structures*. PhD thesis, Delft University of Technology, The Netherlands.

[Pinkster and Hooft, 1978] Pinkster, J. A. and Hooft, J. P. (1978). Computations of the First and Second Order Wave Forces on Bodies oscillating in Regular Waves. In *First International Ocean Development Conference*, Tokyo, Japan.

[Remery and Hermans, 1971] Remery, G. F. M. and Hermans, J. A. (1971). The slow drift oscillations of a moored object in random seas. In *Offshore Technology Conference*, number OTC 1500, Houston, USA.

[Remery and Hermans, 1972] Remery, G. F. M. and Hermans, J. A. (1972). The slow drift oscillation of a moored object in random seas. *Journal of the Society of Petroleum Engineers*.

[Remery and van Oortmerssen, 1973] Remery, G. F. M. and van Oortmerssen, G. (1973). The mean wave, wind and current forces on offshore structures and their role in the design of mooring systems. In *Offshore Technology Conference*, number OTC 1741, Houston, USA.

[Rijn, 1990] Rijn, L. V. (1990). *Principles of Sediment Transport i98n Rivers, Estuaries and Coastal Areas*. Number ISSN 90-8000356-2-9 bound, NUGI 186/831. Amsterdam Aqua Publications - I11.

[Sarpkaya and Isaacson, 1981] Sarpkaya, T. and Isaacson, M. (1981). *Mechanics of Wave Forces on Offshore Structures*. Number ISBN 0-442-25402-4. Van Nostrand Reinhold Company Inc., New York.

[Schlichting, 1951] Schlichting, H. (1951). *Grenzschicht-Theorie*. G. Braunsche Hofbuchdruckerei und Verlag, GmbH, Karlsruhe.

[Shields, 1936] Shields, A. (1936). Anwendung der aehnlichkeitsmechanik un turbulenzforschung auf die geschiebebewegung. *Mitt. Preuss Versuchanstalt fur Wasserbau und Schiffbau, Berlin*, (26).

[St. Denis and Pierson, 1953] St. Denis, M. and Pierson, W. J. (1953). On the Motion of Ships in Confused Seas. *Transactions* SNAME, 61:1–53.

[Suyehiro, 1924] Suyehiro, K. (1924). The Drift of Ships Caused by Rolling Among Waves. In *Transactions of INA*, volume 66, pages 60–76.

[Tasai, 1959] Tasai, F. (1959). On the Damping Force and Added Mass of Ships Heaving and Pitching. Technical report, Research Institute for Applied Mechanics, Kyushu University, Japan. Vol. VII, No 26.

[Tasai, 1969] Tasai, F. (1969). Improvements in the Theory of Ship Motions in Longitudinal Waves. In *Proceedings 12th I.T.T.C.*

[Tasaki, 1963] Tasaki, R. (1963). Researches on Seakeeping Qualities of Ships in Japan, Model Experiments in Waves, On the Shipment of Water in Head Waves. *Journal of the Society of Naval Architects of Japan*, 8.

[Timman and Newman, 1962] Timman, R. and Newman, J. N. (1962). The Coupled Damping Coefficients of a Symmetric Ship. *Journal of Ship Research*, 5(4):1–7.

[Tuck, 1970] Tuck, E. O. (1970). Ship Motions in Shallow Water. *Journal of Ship Research*, 14(4):317–328.

[Ursell, 1949] Ursell, F. (1949). On the Heaving Motion of a Circular Cylinder on the Surface of a Fluid. *Quarterly Journal of Mechanics and Applied Mathematics*, II.

[Van den Boom, 1985] Van den Boom, H. (1985). Dynamic behaviour of mooring lines. In *Behaviour of Offshore Structures*, Elsevier Science Publishers, B.V., Amsterdam.

[Verhagen and van Wijngaarden, 1965] Verhagen, J. and van Wijngaarden, L. (1965). Non-linear oscillations of fluid in a container. *Journal of Fluid Mechanics*, 22(4):737–751.

[Vugts, 1970] Vugts, J. H. (1970). *The Hydrodynamic Forces and Ship Motions in Waves*. PhD thesis, Delft University of Technology, The Netherlands.

[Wehausen and Laitone, 1960] Wehausen, J. V. and Laitone, E. V. (1960). *Handbuch der Physik*. Springer Verlag, Berlin.

[Wheeler, 1970] Wheeler, J. D. (1970). Method for calculating forces produced by irregular waves. *Journal of Petroleum Technology*.

[Wichers, 1979] Wichers, J. E. W. (1979). On the slow motions of tankers moored to single point mooring systems. In *Proceedings BOSS Conference*, London, UK.

[Wichers, 1988] Wichers, J. E. W. (1988). *A Simulation Model for a Single Point Moored Tanker*. PhD thesis, Delft University of Technology, The Netherlands.

[Wichers, 1992] Wichers, J. E. W. (1992). Lecture notes on ocean engineering. In *IHEE Delft 1992, Part I: Introduction*, number IHEE 1992, Delft.